New Generation Foam to Revolutionise the Building Industry

Lee Michael Price, M.Sc.

Submitted to Swansea University in Fulfilment of the Requirements for the Degree of Doctor of Engineering (EngD)

Swansea University

2023

Declarations

Statement 1

This work has not previously been submitted in substance for any degree and is not being concurrently submitted in candidature for any degree.

Signed Lee Price

16/02/2024

Statement 2

This thesis is the result of my own investigations, except where otherwise stated. Where correction services have been used, the extent and nature of the correction is clearly marked in footnote(s).

Other sources are acknowledged by footnotes giving explicit references. A full bibliography is appended to each chapter of this thesis.

Signed Lee Price

16/02/2024

Statement 3

I hereby give my consent for this thesis, if accepted, to be made available for electronic sharing **after expiry of a bar on access approved by Swansea University**.

Signed Lee Price

16/02/2024

Statement 4

The University's ethical procedures have been followed, and, where appropriate, ethical approval has been granted.

16/02/2024

Acknowledgments

I would like to give the greatest of thanks to my academic supervisor, Professor Peter Holliman, for his patient guidance, encouragement, and advice and for his whole-hearted support in the completion of this thesis. I could not have wished for a better mentor. Further thanks to Dr. Eurig Jones, Dr. Christopher Kershaw, Dr. Diana Meza-Rojas, Emily Thomas and the rest of the CEMEG group for the role their collective experience and knowledge has played in my studies. Finally, to everyone in the Swansea University research community who has assisted or supported me in any way.

I would also like to thank my industrial supervisor Julia Lloyd and everyone at Building Systems UK for their assistance in facilitating my research.

I wish to express an infinity of gratitude to my partner, Sara Nieto Calo, for her love, patience, and understanding, and for helping me keep perspective through the most trying times in this journey. This has been a truly shared endeavour and I could not have done it without you. Also, to all the friends who have supported us both, especially to Lluis Amengual Cabanellas, Adam Godfrey and Maf Nunes. Thanks also to the members of Bridgend Board Gamers.

To Aloia the Greatest and Alfred the Great, who are unable to read this on account of being cats and whose efforts at clerical assistance have been no help whatsoever but whose presence has been a source of great joy and comfort.

To my father Michael, my brothers Kyle, Adam and Simon, and my grandmother Barbara for the countless ways you have helped me reach this point.

In loving memory of my mother Christine and my grandfather Howard. To Mum, for teaching by example the importance of kindness and making me strive to always do better. To Gramp, for fostering my curiosity about the world. Your loss is keenly felt, and my deepest regret is that you could not be here for this. I know you both would have been immensely proud.

COVID-19 Impact Statement

The primary research work presented in this thesis was conducted during the COVID-19 pandemic and the author would like to take this opportunity to highlight the impacts of this unprecedented public health crisis on the work herein.

A combination of an eight-month loss of access to research facilities due to lockdown and remote working measures instituted to protect public health and the longer-term aftereffects occurring at a critical period in this research required a substantial restructuring of this thesis.

The most significant impact was a required change of focus from the planned investigation and development of a broader range of alternative fire-retardant systems to the characterisation of a more focused set of trial samples produced by the project industrial sponsor.

Furthermore, it was necessary, owing to the reduction in time available to conduct primary data collection and problems with equipment due to prolonged shutdowns, to omit certain aspects of analysis that were planned for inclusion in this thesis. These included imaging techniques, fixed gas analysis, and the development of larger scale fire testing, which were intended to be included in chapter 5 of this thesis. These methods would have allowed for a yet more comprehensive characterisation of polyisocyanurate degradation and fire behaviour to be presented within this work.

Abstract

With the ongoing focus on improving energy efficiency and reducing carbon emissions to mitigate the effects of anthropogenic climate change, the demand for effective building insulation is likely to increase in the coming years. Polyisocyanurate foams are widely used insulation materials due to their excellent thermal insulation performance, but a number of fire incidents involving building cladding comprising these materials, notably the Grenfell Tower tragedy, have raised questions over the safety of such materials. In addition, the long-term effects of fire retardants on human health and the environment have also come under increased scrutiny.

In this thesis, a detailed analysis of the high-temperature degradation of polyisocyanurate foams has been conducted, bringing together a range of thermal analysis techniques to produce a more comprehensive picture of the behaviour of these materials at extreme temperatures.

Comparative thermal analysis of a range of polyisocyanurate formulations has been conducted and a number of non-halogenated fire retardants, being ammonium polyphosphate, expandable graphite and a proprietary phosphorus-based reactive flame retardant, have been evaluated for their efficacy in polyisocyanurate foam systems during the pyrolytic preignition phase of foam degradation. These agents have been found to induce a substantial decrease in the pyrolytic mass loss of polyisocyanurate foams and indicate the potential for the development of polyisocyanurate insulation systems with improved fire safety characteristics. The findings of this thesis strongly support further research in this subject area, as the availability of safe and effective insulation materials offers clear social, environmental and economic benefits.

Table of Contents

Glossary of Abbreviations and Acronyms

AV	Acid value
DEG	Diethylene glycol
DSC	Differential scanning calorimetry
dTG	Derivative thermogravimetric analysis
EPS	Expanded polystyrene
HRR	Heat release rate
HV	Hydroxyl value
LOI	Limiting oxygen index
(4,4)-MDI	(4,4)-Methylene diphenyl diisocyanate
NCO	Isocyanate
PhF	Phenolic formaldehyde
PIR	Polyisocyanurate
PPG	Polypropylene glycol
PUR	Polyurethane
RPUF	Rigid polyurethane foam
TCPP	Tris(1-chloro-2-isopropyl) phosphate
TEP	Triethyl phosphate
TGA	Thermogravimetric analysis
XPS	Extruded polystyrene

1 Introduction

1.1 Aims and Objectives

This thesis aims to present a comprehensive analysis of the high-temperature thermal behaviour of pentane-blown polyisocyanurate (PIR) insulation foams, with a particular focus upon their thermal degradation under pyrolytic and thermo-oxidative conditions. To this end, an array of thermal analysis techniques will be applied to such foams and brought together with the aim of developing a robust and novel methodology for characterising this behaviour and its underlying mechanisms at laboratory-scale while capturing bulk effects that would be outside of scope of traditional laboratory-scale thermal analysis.

The inherent combustibility of polyisocyanurates and other polymeric insulation materials may contribute to fire load and provide a route for the spread of fire. Furthermore, the breakdown and combustion of insulation materials under fire conditions may increase the toxicity of fire products. It is therefore a central objective of this thesis to examine the implications of foam thermal behaviour on fire safety.

Fire retardants are widely used in insulating foams to improve fire performance, with members of the ‘chlorinated tris’ family of compounds having entered widespread use following the phasing out of the previous generation of brominated fire retardants. Like their predecessors, concern exists over the potential toxicity of such fire retardants. The effects of one member of this family, being tris-1-chloro-2-isopropyl phosphate, will be analysed herein, providing evidence of both efficacy and potential for toxicity. The industrial sponsor of this research, Building Systems UK, seeks to eliminate the use of this agents and several alternative fire-retardant systems will be extensively evaluated using the methods developed to assess their suitability as replacements within PIR foam systems.

1.2 Context

This thesis addresses thermal insulation foams for the building envelope. These are important either to prevent heat dissipating from a building in cooler climates (thus saving heating costs) or preventing heat entering a building in warmer climates (thus saving air conditioning costs. Rigid polymer foams are widely used in the construction industry as thermal insulation materials (1). However, there are issues with the potential flammability of polymer foams as shown by the Grenfell tragedy (2)(3) and also in understanding and improving thermal insulation values.

Rigid polymer foams are materials which have a low density closed-cell structure. Such a structure consists of a gaseous blowing agent confined to discrete cells within a polymer matrix, contrasting with open-cell foams in which the gaseous phase can move throughout the polymer matrix and is often in direct communication with the external environment. As the thermal conductivity of the blowing agents is very low and the closed-cell structure of the foam prevents convective heat transfer, the resulting material possesses very low specific thermal conductivity (λ). For the insulation foams discussed in this thesis, the ability of a material to transmit heat can be measured in watts per square metre of surface area for a temperature gradient of 1 K per unit thickness of 1 m (4). This is given by the following expression:

$$\lambda\ (thermal\ conductivity\ (\frac{W}{mK})) = \frac{P(heat\ flow(W))x\ t(thickness(m))}{A\ (surface\ area(m^2))\ x\ \Delta T\ (temperature\ gradient(K))} \quad (1.1)$$

The insulation performance of materials can also be expressed using the reciprocal of this quantity, referred to as thermal resistivity, $R_\lambda = 1/\lambda$.

Insulating materials have typical λ of 0.020-0.044 W/mK. The λ of foamed polymer materials ranges from ~0.02 W/mK in the case of some phenolic foams to ~0.038 W/mK for some polystyrenes.

Improving thermal insulators reduces heat transfer between building interiors and the surroundings, reducing energy expenditure. It follows from the definition of thermal conductivity given above that the required thickness of the insulation layer decreases proportionally with thermal conductivity. More effective insulation materials may therefore deliver reduced material costs and embodied energy in addition to the benefits of improved energy efficiency.

Despite their sector leading insulation performance, the flammability of synthetic polymers presents a considerable drawback. The safety of building occupants is a crucial consideration for construction projects, and a key aspect is mitigating the risk of serious injury or death due to fire. To this moral duty is added legislative force by fire safety regulations seeking to reduce this risk to tolerable levels. Combustible materials are often treated with flame retardants to comply with safety standards.

The widespread use of flame retardants is not without controversy, and some have been phased out due to concerns over health and environmental effects (5,6). Furthermore, certain fire retardants may exacerbate the release of noxious fire effluents (7) from combusting materials potentially increasing the risk of lethal injury in some fire scenarios.

The fire safety of foamed polymer insulation, particularly polymer foams like the PIR foams considered in this thesis, has been subject to increased public scrutiny in the aftermath of the 2017 Grenfell Tower disaster, a catastrophic fire in a 24-storey building in London which resulted in 72 deaths (2). The fire occurred after the installation of an insulation and cladding system consisting of aluminium-coated PIR insulation blocks (8) affixed to the external faces of the building and an outer layer of aluminium-coated polyethylene rain cladding separated from the insulation layer by an air gap. The public inquiry into the disaster identified this cladding system as a principal contributor to the rapid spread of the fire with combustion of the cladding materials driven by a chimney effect overcoming passive fire containment measures. Such incidents have led to calls from some for a total ban on the use of combustible insulation materials including PIR.

1.3 Fire Behaviour of Construction Materials

In the 2016/17 period, fire brigades in England attended 68,871 primary fire incidents (9). These are serious fires that meet one or more of the following criteria:

a) the fire occurred in a non-derelict building, vehicle, or outdoor structure.
b) the fire involved a fatality, casualty, or rescue.
c) the fire was attended by five or more pumping appliances.

This number included 28,470 primary dwelling fires, occurring predominantly in houses and flats, causing a total of 191 fatalities (81% of all fire-related deaths) and 7,021 non-fatal casualties (9). Casualties were defined as any persons involved in a fire incident who were at a minimum advised to seek precautionary medical attention and of these, 43% (3,026) received treatment in hospital (9). Figures for the past decade show a sustained decrease in both the number of serious fire incidents and associated fatalities and casualties, but there can be no acceptable number of preventable deaths or serious injuries. Even in the absence of injury to persons, losses due to fire represent a significant socioeconomic burden (10). The choice of materials and methods of construction should therefore assign high priority to the reduction of fire risk.

It is generally unrealistic to avoid the use of all combustible materials in construction. Materials such as wood and plastics are inherently combustible but possess useful physical properties that are not readily obtained from other materials. Likewise, the characteristics of polymer foams make them highly attractive options for improving building energy efficiency through their insulation performance.

The fire behaviour of materials encompasses multiple characteristics. The resistance of a material to ignition will determine whether a fire will occur, and how readily an existing fire will spread to that material. Combustible materials contribute to fire loading depending on their heating value. Materials may also contribute to either the spread or containment of fire, depending on their ability to sustain a flame, the production of flammable droplets or vapours, and how well they are able to resist heat transfer and maintain integrity in fire conditions. As most fire-related deaths are caused by smoke inhalation injuries, it is also crucial to understand the thermal decomposition and combustion by-products of materials, especially asphyxiant, toxic, or irritant gases. These include carbon monoxide, which binds with haemoglobin reducing blood oxygen capacity (11). Lethal levels of carboxyhaemoglobin have been found to be present in at least half of autopsied fire victims, constituting the chief primary cause of fire-

related mortality (12). Other significant noxious agents in fire effluents include hydrogen cyanide, an inhibitor of cellular respiration; and irritant gases, which may incapacitate fire victims (13).

1.4 Combustibility of Insulating Materials

A basic parameter of fire behaviour is the categorisation of materials as either combustible or non-combustible. Relevant standards include BS 476-4:1970 (UK), ASTM E136 (US) and CAN/ULC-S114/05 (Canada). Such standards involve the insertion of a sample into a furnace preheated to a specified temperature. Non-combustible materials are typically defined as those that do not undergo sustained flaming, cause a specified increase in temperature measured at the sample or lose more than a specified proportion of their mass during the duration of testing. The BS 476-4:1970 standard specifies inserting three dry samples of dimensions 50 mm x 40 mm x 40 mm into tube furnace at a temperature of 750 ^{o}C. A thermocouple is positioned near the sample to record the temperature change and materials are deemed non-combustible if the following conditions are met for each sample:

- The ΔT at the thermocouple does not exceed +50 ^{o}C.
- Continuous flaming is absent or occurs for a period of <10 s.

If either threshold is exceeded, the material is deemed to be combustible (14).

Among insulating materials, only mineral wools typically meet these criteria for being classified as non-combustible. Such materials are composed of inherently non-flammable metallic or silicon oxides such as silicon dioxide and aluminium oxide with only a small quantity of organic binding agents to contribute to fuel load.

However, these tests give little information about the fire behaviour of individual materials. The methods specified expose the entire bulk of combustible materials to ambient temperatures far above their autoignition point. While this condition may arise within large, well-established fires, it can be argued that these test conditions do not very accurately reflect the likely behaviour of materials in response to common point sources of ignition. It cannot be stated that materials deemed combustible are inherently unsafe for use in all building applications, only that these materials have the potential to combust and contribute to fuel load in certain conditions. To accurately assess the fire performance of these materials, it is necessary to understand the broader mechanisms of building fires, and the specific behaviour of materials in response to high temperatures.

Limiting oxygen index (LOI) is another bench-scale test used to provide a measure of flammability in polymeric materials. The sample is exposed to a mixture of nitrogen and oxygen with the LOI of a material being the minimum concentration of oxygen supporting candle-like burning. PIR foams are generally found to have a higher limiting oxygen index than polyurethane (PU) foams. For example, for foams with no added fire retardant, Du et al. (15) provide LOI values of 22 % for PIR and 19 % for PU. Thus, the concentration of oxygen necessary to support stable burning in PIR foam is slightly higher than atmospheric oxygen concentration (21 %) which helps limit its combustibility. Materials with an LOI greater than 26 % are generally considered to exhibit high flame-retardancy, as such materials will tend to exhibit self-extinguishing behaviour under normal atmospheric oxygen concentrations.

1.5 Mechanisms of Combustion Reactions and the Dynamics of Compartment Fires

Fire is a complex and dynamic interaction of physical and chemical phenomena. In characterising the fire behaviour of organic materials, and ultimately in improving their resistance to fire, it is necessary to understand the mechanisms by which combustion occurs. The overall process of combustion in solid fuel sources consists of three distinct, overlapping phases. In the pyrolysis phase, the cleavage of bonds is induced by thermal energy. Large macromolecular structures are thus broken down into smaller fragments. Some of these smaller fragments are volatile enough to enter the gas phase, while other may undergo secondary fragmentation, polymerise to form solid carbonaceous chars or condense as tar, a liquid mixture of heavy hydrocarbons. Pure pyrolysis does not require oxygen to proceed but is not self-sustaining, requiring an external supply of heat. The specific products of pyrolysis depend upon the chemical structure and composition of the material and may comprise a vast range of organic species (16).

For most solid materials, the gaseous phase of combustion begins when gases released from the material mix with atmospheric oxygen and undergo ignition (17). Ignition is the transition to a self-sustaining reactive state and can be either piloted or spontaneous (18). The combustion chain in organic materials is typically initiated by the thermal cleavage of a C-H bond and abstraction of the resultant hydrogen radical from a fuel molecule through the action of molecular oxygen at high temperature (19). This produces radical pairs consisting of a fuel and perhydroxyl ($^{\bullet}$OOH) radical. Such free radicals possess unpaired valence electrons and as a result are highly reactive as they will attempt to either donate or acquire valence electrons.

These radicals can propagate a chain of further radical generating reactions. Even in the case of simple hydrocarbon combustion, this comprises a large set of possible reactions which ultimately terminate in either radical recombination or complete combustion of the fuel to simple fully-oxidised products (20). These reactions are typically exothermic thereby driving further decomposition of the solid and sustaining combustion while the oxygen concentration and diffusion of flammable species into the gas phase remains sufficient. These combustion reactions occur entirely within a thin layer at the interface between fuel and air.

Certain materials, including PU and PIR foams exhibit a propensity to undergo smouldering combustion (21) where oxygen directly attacks the solid fuel in the condensed phase and may be observed as a glowing flameless condition (22). Smouldering may occur after flaming combustion when the production of volatiles has slowed and can no longer support flaming combustion or may precede it. Smouldering may be more easily initiated than flaming combustion requiring only a relatively cool ignition source and produces a higher proportional yield of gases such as carbon monoxide (7)(23) which are both toxic and flammable and may create the conditions for initiation or reignition of flaming combustion.

For a given material critical temperatures will exist at which components in the vapour phase are able to ignite in the presence of an ignition source or spontaneously and at which the diffusion of flammable gases into the reaction zone will be sufficient to maintain combustion. In this context, a comparison of polystyrene, polyurethane, and polyisocyanurate foams found that pyrolysis started at 170 ^{o}C, 200 ^{o}C, and 300 ^{o}C, respectively. The respective flash points for each material were found to be around 280 ^{o}C, 330 ^{o}C, and 370 ^{o}C. Autoignition occurred for all materials at temperatures between 430 ^{o}C and 550 ^{o}C, with PIR in this case having the lowest autoignition point, followed by EPS and PUR (24). Despite its lower autoignition point, PIR is generally considered to be more resistant to ignition than other polymeric foams (25). This is because most ignition events do not occur under conditions where the bulk of the material is exposed to ambient conditions above its autoignition point, but rather occur at lower ambient temperature due to contact with a point source of ignition. All polymeric foams have a relatively high potential influence on fire load when compared to mineral-based insulation materials, exhibiting a higher peak heat release rate and total heating value (26).

The behaviour of enclosed compartment fires, such as those occurring inside buildings differs from those in open air (27). When materials combust in an enclosed compartment, heated air and combustion gases form a hot layer beneath the ceiling. Heat from this layer is lost via the

egress of hot gases through vents and thermal conduction through the walls of the compartment. Ingress of air is dependent upon the degree of ventilation of the compartment. A small fire originating at a point of ignition will exist initially in a well-ventilated (i.e., fuel-controlled) state and grow larger primarily through direct contact of volatile pyrolysis products with the flame front, increasing the rate of heat release and the temperature of the hot layer. Conductive heat losses will increase proportionally with the temperature gradient between the interior and exterior of the compartment but will also be limited by the thermal resistance of the boundaries of the compartment.

In this scenario, thermal radiation emitted by hot layer at the ceiling is absorbed by combustible materials, increasing the release of hot gases as these reach their pyrolysis temperatures. This may be exacerbated by rollover in which the smoke layer undergoes flaming combustion as the concentration of combustible gases reaches the flammability range and is ignited by contact with the flame plume or airborne embers (28). For a given fire system, the rate of heat release can eventually exceed the loss of thermal energy, establishing an unstable feedback condition. Once the radiative flux from the hot layer reaches a critical value, flashover may occur, in which all remaining combustible material undergoes autoignition. In conditions where flaming combustion has ceased due to oxygen depletion, a dangerous backdraft event may be triggered by the reintroduction of air to the compartment, such as may occur by the opening or breaching of a door or window.

Insulation materials interact with these processes in several ways. As the loss of heat from the compartment is partially dependent upon the conduction of heat through the enclosure, the presence of low λ materials reduces the rate of heat loss and so may lower the heat release threshold necessary to initiate flashover conditions (29). Although insulation foams have a relatively high specific heat capacity, their low density and thermal conductivity results in low thermal inertia such that the surface temperature of the material will rapidly rise with high external temperature, driving the pyrolysis of the material. In addition, because insulation materials are often integrated into the building enclosure in the form of structural insulated panels, consisting of an insulating core bonded to structural metal facings and are fitted together to form the enclosure, combustion of the core may be delayed as the facings isolate flammable gases produced by pyrolysis from the fire compartment. The degradation of the core material and bonding adhesive, pressure from hot gases, and buckling due to thermal expansion may create gaps at panel joins, with flaring of gases as they are released into the fire compartment

and come into contact with sources of ignition and exposing insulation material to combustion (25)(30).

1.6 Chemistry of Polyisocyanurate Foams

Polyisocyanurate (PIR) is a thermosetting polymer of 4,4-methylene diphenyl diisocyanate (4,4-MDI) (Figure 1.1) and a polyester polyol, commonly based on phthalic acid isomers. PIR comprises a heterogeneous structure of linear polyurethane/urea domains, resulting from the reaction of isocyanates with hydroxy and amine groups, extensively cross-linked by isocyanurate groups from the trimerisation of isocyanates. PIR has similar monomer components to rigid polyurethane but differs in its higher ratio of isocyanate to hydroxy groups (isocyanate index). This index depends upon the mass proportion, molecular weight, and average functionality of the monomers, and a high index indicates that excess isocyanate is present, encouraging the formation of isocyanurate structures.

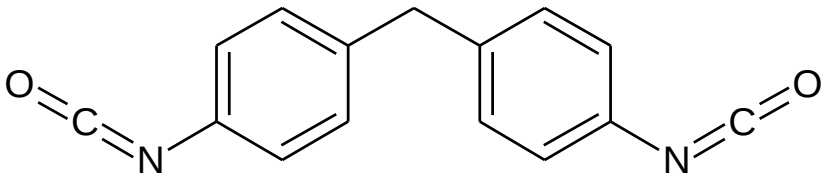

***Figure 1.1**. Structural formula of 4,4-methylene diphenyl diisocyanate.*

Pure 4,4-MDI is a white or pale-yellow solid with a melting point around 40 ^{o}C, but commercial preparations of MDI consist of a dark amber liquid containing around 50 % 4,4-MDI and smaller quantities (<5 % combined) of the 2,4 and 2,2 isomers with the remaining fraction made up of oligomeric MDI, consisting typically of three to six phenyl isocyanate monomeric units bridged by methylene groups. The presence of the oligomer accounts for the physical state and appearance of the commercial preparations, and results in a reduction of free isocyanate groups compared to the pure monomeric MDI.

Three principal types of isocyanate reaction occur in the formation of PIR foam, primarily resulting from the interaction of the electrophilic isocyanate carbon with various nucleophiles. The first of these is the gelling reaction between the isocyanate group of 4,4-MDI and terminal hydroxy groups on the polyol or diol chain extender to form a urethane linkage. Two overall mechanisms for this reaction are proposed **(Figures 1.2 and 1.3).**

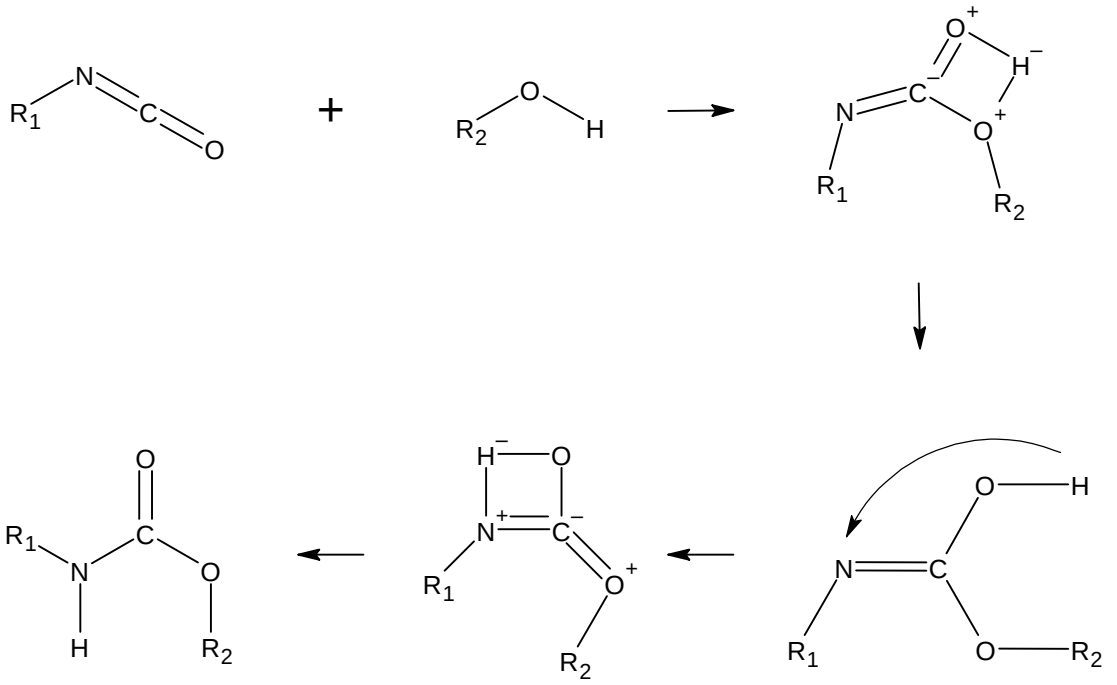

Figure 1.2. *Reaction mechanism of isocyanate and hydroxy across C=O bond with 1,3-hydride shift.*

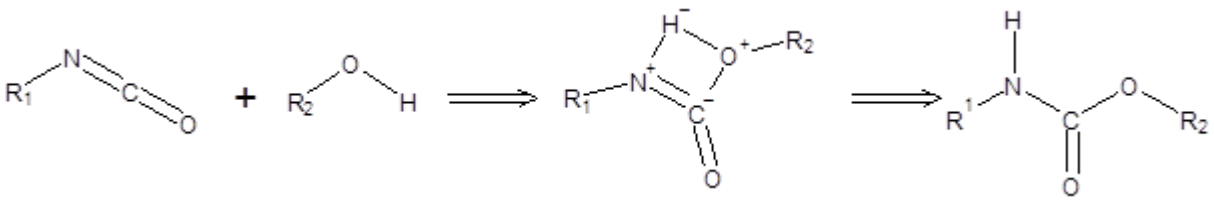

Figure 1.3*. Reaction mechanism of isocyanate and hydroxy across N=C bond.*

In industrial production of polyurethane, a gelling catalyst will typically be used in the reaction mix. Common catalysts are tertiary amine compounds and metallic carboxylates. Tertiary amines exhibit strong nucleophilic activity due to the presence of a lone electron pair on the amine nitrogen along with the high electronegativity of this site. The precise mechanism by which tertiary amines catalyse the gelling reaction is not definitively known. A hydrogen bond is readily formed between a hydroxy group and the catalyst, and the catalyst may in fact deprotonate the hydroxy group. This is corroborated by the observation that catalytic activity of amines increases with their basicity, as this would favour protonation to form [R_3NH^+] and [RO^-]. If a negatively charged oxygen centre is produced on the polyol, then the nucleophilicity of this site, and therefore its affinity for the isocyanate carbon, will be increased. In this mechanism the catalyst is regenerated by protonation of the isocyanate nitrogen, effectively

acting to transfer a proton between the hydroxy and isocyanate group (31). The alternative proposed mechanism is the formation of a tertiary amine-isocyanate complex by coordinate covalent bonding between the tertiary amine nitrogen and the isocyanate carbon, increasing the δ+ polarisation of the isocyanate carbon and rendering it more vulnerable to nucleophilic attack (32). In this case, regeneration of the catalyst occurs by the dissociation of this complex and the reformation of the C=O bond in the urethane group. It is likely that both catalytic mechanisms occur to some extent, but modelling of the reactions suggest that the catalyst primarily interacts with the hydroxy group of the polyol. Metal-based catalysts such as the metallic carboxylates predominantly interact with the oxygen of the isocyanate group. Acting as Lewis acids, these can accept a pair of electrons from the oxygen, resulting in a positive charge which is transferred to the isocyanate carbon through bond reorganisation. This enhances the electrophilic nature of this site, increasing the susceptibility to nucleophilic attack.

The second important reaction is the blowing reaction between the isocyanate group of 4,4-MDI and water. Water can be regarded as a hydroxy compound and can interact with the isocyanate carbon producing an unstable carbamic acid functional group. This dissociates producing a primary amine and carbon dioxide which contributes to the formation of the cellular structure alongside the thermal evaporation of physical blowing agents such as pentane isomers and hydrofluoroalkanes. The resulting amine groups react with isocyanate analogously to hydroxy groups, forming disubstituted ureas (Figure 1.4).

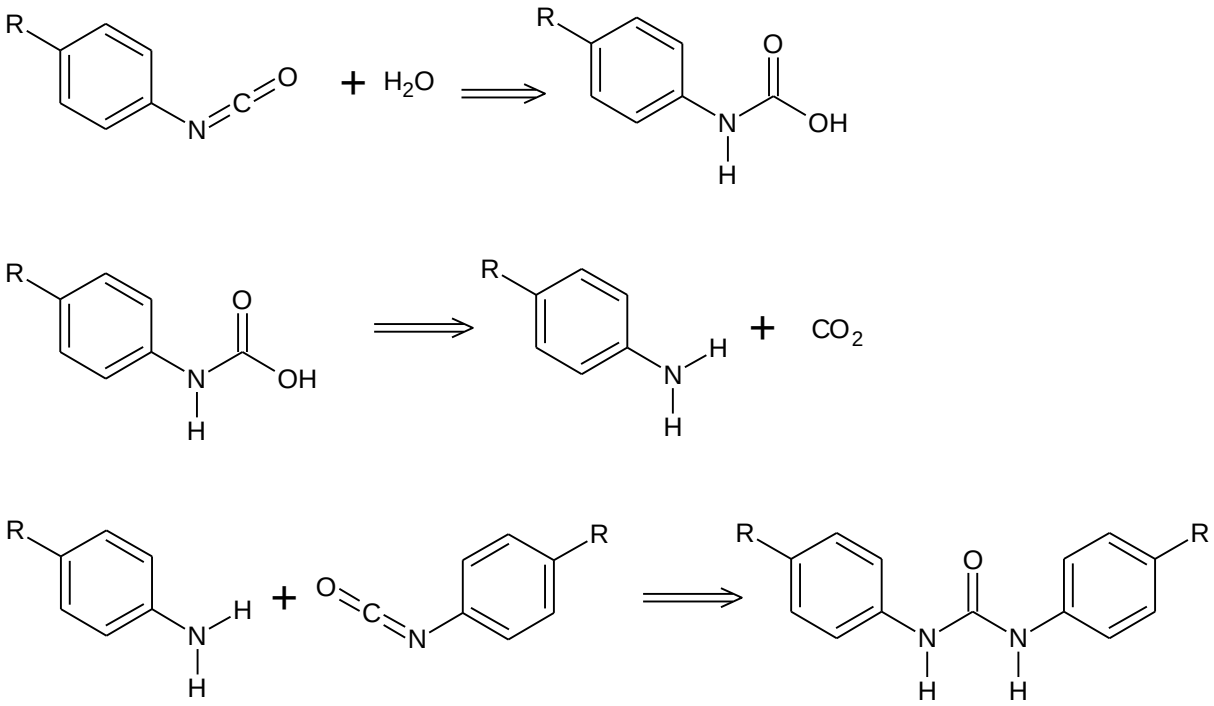

Figure 1.4. *Reaction of isocyanate with water to produce carbamic acid group (top); dissociation of carbamic acid group to primary amine and carbon dioxide (middle); reaction of amine and isocyanate to form disubstituted urea (bottom).*

These reactions result in the production of linear polymer chains containing a mixture of hard segments, predominantly consisting of diisocyanate moieties, and soft segments consisting of the longer polyester polyol chain. The formation of disubstituted ureas increases the hard segment content, resulting in a more brittle and friable material. The extensive cross-linking in PIR results from the presence of groups a functional greater than 2. Such groups can form linear chains with their terminal functional groups while retaining free reactive groups to form cross-links. While the oligomeric MDI content of the isocyanate component contributes to this, the key cross-linking reaction is the trimerization of isocyanates (Figure 1.5). Here, a 3-dimensional polymerisation effect is facilitated by three isocyanate groups reacting together to form an isocyanurate group (32). Trimerization can occur through the stepwise addition of three isocyanate moieties or by the reaction of isocyanate with allophanate, itself formed by the reaction of isocyanate with urethane (33).

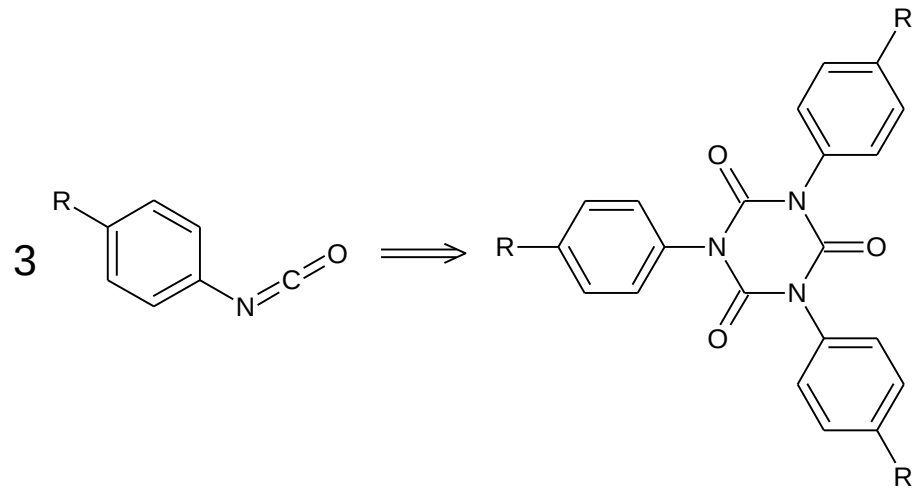

***Figure 1.5**. Trimerisation reaction of isocyanate forming isocyanurate.*

In Figure 1.5, as the R-groups terminate in reactive isocyanates, alcohols, or amines, the trimerization product is also trifunctional along those axes, allowing the formation of complex non-linear networks within the polymer matrix. A further degree of cross-linking may also occur from side reactions occurring between isocyanate and urethane/urea reaction products to form trifunctional allophanates and biurets (34). The allophanate reaction is shown in Figure 1.6 below. The biuret-forming reaction is nearly identical, with the urethane group being replaced by a disubstituted urea. In both cases, there resultant product will have three reactive groups capable of polymer forming reactions.

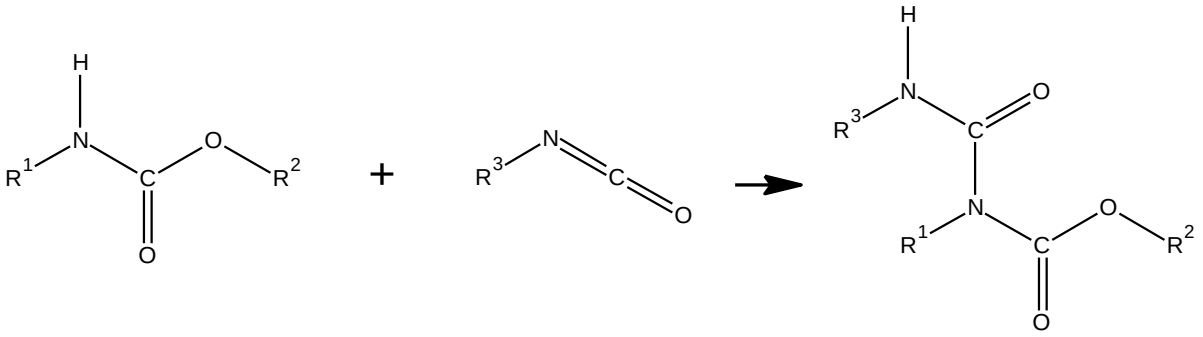

***Figure 1.6.** Reaction of isocyanate with urethane to form allophanate.*

In industrial production, the rates of these competing reactions must be tightly controlled to produce foam materials with the desired physical properties. The relative rates of blowing and gelling activity affect the size and geometry of the cellular structure and ultimately influence multiple physical characteristics of the produced foam. Control of these parameters is achieved using appropriate catalysts, primarily tertiary amines and metal carboxylates, and the correct loading of physical blowing agents in the reaction mixture.

1.7 Thermal Behaviour of Polyisocyanurate Foams

The previous section is intended to provide the reader with a broad insight into the chemical and physical mechanisms leading to and sustaining combustion in almost any solid organic fuel source. Understanding of these mechanisms can be applied to the thermal behaviour of PIR foams. In this section, the specific processes occurring during the pyrolysis and combustion of PIR foams are described, along with methods for the characterisation and analysis of thermal behaviour and the findings of experimental studies in this field.

1.7.1 Non-oxidative Pyrolysis

As previously outlined, the ignition and combustion of a solid material is often preceded by the generation of flammable substances in the gaseous phase by non-oxidative pyrolysis. Characterisation of this process can provide an insight into the likely behaviour of materials under fire conditions, and several analytical techniques can be applied for this purpose. These techniques and their relevant findings are described below.

Firstly, thermogravimetric analysis (TGA) is a common technique for characterising and quantifying the thermal behaviour of materials. A thermogravimetric analyser consists of a high-precision microbalance holding a small sample of the analyte (typically <10 mg) within an enclosed furnace. The mass of the sample is recorded over time either at a constant temperature (isothermal TGA) or as the temperature changes at a controlled rate (dynamic TGA). Thermogravimetry data is commonly presented as a plot of sample mass as a function temperature or time, or as the first-order derivative of this function with respect to time. The latter is termed differential thermogravimetry (dTG) and gives the rate of mass change as the dependent variable. The use of an inert purge gas such as nitrogen prevents oxidative reactions and allows for the isolation of purely thermal processes.

Extensive application of thermogravimetric analysis to PIR-based materials is reported in the literature. The improved thermal stability of hybrid polyisocyanurate-polyurethane insulation compared to standard polyurethane was observed using this method at least as early as 1971 (35). Typical TGA profiles for polyisocyanurate-based materials are reported widely in the scientific literature (21–27) and consistently exhibit a characteristic reverse sigmoidal shape.

Dick *et al.* investigated the effect of isocyanate index on thermal stability foam materials based on 4,4-MDI and polypropylene glycol (PPG), a polyether polyol. All the samples reported in

this work had the same mass ratio of 4,4-MDI to PPG, but their PPG components were of different molecular masses with the isocyanate indices of the resulting foams ranging from 219 to 2078. The isocyanate index is the ratio of the actual amount of isocyanate present at the start of the reaction to the theoretical amount of isocyanate that would be required for a 1:1 equivalence between isocyanate and hydroxyl groups, multiplied by 100. An index of 200 therefore represents starting reaction conditions where two isocyanate groups are present for each hydroxyl group. Since isocyanates can undergo trimerization reactions to form isocyanurate, this number is indicative of the relative prevalence of urethane and isocyanurate domains within the PIR structure.

The foam samples with the highest and lowest indices were then subjected to TGA under nitrogen over a temperature range of 0-600 ^{o}C. In both cases, the TGA curves were of approximate reverse sigmoid form with the high index foam being markedly more stable across the entire temperature range. The onset of mass loss in the low index foam occurred just above 100^{o}C and was near-linear until 250 ^{o}C, whereas almost no mass loss was observed in this range for the high index foam. The temperature ranges over which the most rapid mass loss occurs were around 300-375 ^{o}C and 315-425 ^{o}C in the lowest and highest index foams respectively (36). The retained char fraction at 600 ^{o}C was 10% higher in the high index foam than the low index foam (48 % vs 38 %) The behaviour of the low index foam, where urethane bonding would be expected to be more prevalent, is very similar to that of rigid polyurethane foam (43)(44).

A continuation of this work by Dominguez-Rosado *et al.* further characterised the influence of different polyol components on thermal stability, incorporating TGA data for aliphatic and aromatic polyester polyols added into the foams along with data for the PPG-200 and PPG-2000 polyols from the previous analysis. The isocyanate indices of these foams were 340 for the aliphatic polyester polyol and 490 for the aromatic polyester polyol. The foams containing polyester polyols were initially more similar in behaviour to the PPG-200 foam but became noticeably more stable above 250 ^{o}C in the case of the aliphatic polyester, and above 350 ^{o}C in the case of the aromatic polyester, exhibiting similar behaviour to the PPG-2000 foam above these temperatures. Despite its initial low stability, the aromatic polyester foam has a final retained char fraction at 610 ^{o}C almost identical to that of the PPG-2000 polyether foam (37) at 44 % and 45 %, respectively. This may reflect differences in the resistance of the polyol component itself to thermal degradation due to the higher thermal stability of the ester group

(39). The influence of isocyanate index and the type of polyol component have also been investigated elsewhere (41).

Similar degradation behaviour under TGA in inert atmosphere is reported elsewhere in the literature and dTG thermograms indicate that the peak mass loss rate in most PUR/PIR materials under pyrolysis conditions occurs at temperatures around 320-340 ^{o}C (39)(41)(42) indicating that this is a critical temperature range for these types of material regarding their fire behaviour as this may represent a rapid release of flammable volatiles.

Typical samples sizes for TGA are between 10 mg and 100 mg, and larger scale testing may more closely model conditions that occur in realistic fire scenarios. The basic operating principle of TGA can be readily scaled up using a mass balance within a temperature-controlled furnace, and this technique has been used to compare the stability of common insulation materials (30). Here, the mass loss of steel-faced, foam-cored samples in the range of 20-30 g was measured during heating in a convection furnace. Sample were placed in the middle of the furnace in a steel sample cradle which was suspended by means of a cable running through the roof of the furnace to an overhead balance. Heat was provided radiatively from below using a brass heating element. The data obtained showed that both PUR and PIR foams exhibited similar thermal stability at 150^{o}C, losing 5.6-5.7 % of their core mass under isothermal conditions at 150 ^{o}C for 20 minutes. This temperature was selected as it was expected that the degradation of adhesive binders would begin at around this temperature. The difference in thermal stability between PUR and PIR became apparent at 250^{o}C, with respective mass losses of 18.1 % and 7.7 % over 20 minutes of heating. At the highest temperature of 350 ^{o}C, chosen to represent a temperature corresponding to pre-flashover conditions, 83 % of the PU core mass was lost over 20 minutes of heating, compared to 29 % of the PIR indicating a significantly greater thermal stability for PIR compared to PU.

Differential scanning calorimetry (DSC) is a common technique for characterising thermal processes which is often used in conjunction with TGA. DSC measures the difference in the amount of heat required to maintain temperature parity between the analyte and a reference as the temperature of both is increased linearly with time. This enables the detection of endothermic and exothermic processes occurring in the sample, as these will either increase or decrease the amount of supplied energy required to raise its temperature. Non-oxidative pyrolysis is often described as an endothermic process, since bond cleavage requires thermal energy, but secondary, exothermic reactions may affect also the net heat flow by releasing

energy within a sample. This can be studied by changing the ramp rate to help resolve individual thermal processes.

The application of DSC to PIR foams is reported in the previously referenced experimental work by Dominguez-Rosado *et al.* (37) with distinctive sharp endotherms observed at 300-350 ^{o}C in two of the four foams, those based on PPG-200 and aromatic polyester polyol, but not in those based on aliphatic polyester polyol or PPG-2000. The presence of an endotherm appears to be correlated with lower thermal stability over this temperature range. Some degree of endothermic activity is a common DSC finding under nitrogen in PIR materials but the intensity of this activity appears to vary considerably (40).

1.7.1.1 Pyrolysis Mechanisms of PIR/PUR Foams

The thermogravimetry results reported previously provide valuable information about the thermal stability of PIRs, but these techniques do not provide a detailed characterisation of the specific processes associated with thermal degradation. The chemical structure of typical PIR-based materials is relatively complex, with different structural elements varying in their susceptibility to thermal degradation. The overall mechanism of pyrolysis depends upon the distribution of each of these groups and their differing thermal stability, and it is expected that pyrolysis will occur as a series of temperature-specific processes.

Previous work has shown that specific thermal degradation reactions can be predicted from the behaviour of model compounds and *in* situ characterisation can be performed through the application of analytical techniques to foams and their pyrolysates. Characterisation of pyrolysates may comprise both evolved gas analysis using FTIR and GC/MS and the analysis of solid residues through FTIR and other methods. The availability of literature suggests that the pyrolysis of PIRs has been less comprehensively studied than that of pure polyurethanes, but similarities are expected based on shared structural features.

Reports show that the low temperature mass loss observed under thermogravimetry in some PIR materials may be attributed to the release of trapped volatiles such as the evaporation of adsorbed water and unreacted isocyanates, and the outgassing of blowing agents possibly assisted by increased cellular pressure and diffusion rates through the polymer matrix (45). The presence of blowing agent in evolved gas samples at low temperatures has been confirmed by both mass spectrometry and FTIR spectroscopy (46). This may be significant due to the high flammability of some common blowing agents such as pentane isomers. FTIR of the solid

foams and their pyrolysates obtained after heating confirms initial loss of water and free isocyanate after heating to lower temperatures (<200 ^{o}C).

The release of trapped volatiles overlaps to some extent with the dissociation of weaker linkages within the polymer matrix. For example, allophanate and biuret cross-linking groups are the least stable linkages within the polymer structure (47) and may begin to dissociate at temperatures as low as 90 ^{o}C (48)(49). Calculated dissociation rates of allophanates have been found to increase more than four-fold with an increase in temperature from 130-150 ^{o}C. The review by Singh and Jain reports values of 100-120 ^{o}C for allophanates and 115-125 ^{o}C for biurets (50).

Dissociation of allophanate and biuret groups has been reported to occur by depolymerisation to the initial urethane/urea and isocyanate groups. These side-reaction products are minor contributors to cross-linking in typical PIR materials and their dissociation may cause a minor weakening of the polymer structure, but these reactions do not produce small molecule products, and so are not associated with a significant release of volatile fragments.

It has been reported that the first major stage in the degradation of the PIR structure involves the cleavage of bonds within the linear regions of the polymer. Excluding the ester bonds within the polyol, these regions are dominated by urethane linkages between 4,4-MDI and diols. Some urea linkages are also present, primarily between directly neighbouring 4,4-MDI-derived structures.

Evolved gas analysis of rigid polyurethane carried out by Park *et al.* indicates four stages of decomposition as measured by the total abundance of volatile products under evolved gas analysis-mass spectrometry (EGA-MS). These peaks correspond to temperatures of 236 ^{o}C, 293 ^{o}C, 337 ^{o}C, and 383 ^{o}C (51), confirming that mass loss under TGA is the result of a series of processes occurring in succession. The first peak at is attributed to the cleavage of urethane bonds occurring in the polyurethane hard segments.

It has been reported that urethane groups exhibit greater thermal stability than allophanates and biurets, influenced by the aryl or alkyl nature of the monomers. For example, Bayer (1947) reported upper stability temperatures for a variety of urethanes ranging from 120-250 ^{o}C, with a temperature of 200 ^{o}C for aryl-alkyl urethanes (52). This structure is typical of urethane groups found in PIR-PUR materials based on 4,4-MDI. Although slow depolymerisation of urethane groups may occur from 150 ^{o}C (53), significant decomposition is associated with

temperatures in the 200-250 ^{o}C interval. This may account for the mass loss observed in this range under thermogravimetric analysis. Studies of model urethane compounds by Dyer *et al.* (54) indicated three possible mechanisms of degradation:

1. Depolymerisation forming isocyanate and alcohol.
2. Dissociation forming primary amine, CO_2 and alkene.
3. Decarboxylation forming secondary amine and CO_2.

Dyer *et al*. (54) reported that mechanisms 1 and 2 result in the production of free diisocyanate or its diamine and aminoisocyanate derivatives via the cleavage of the flanking urethane bonds and these products have been detected as low abundance peaks in the mass spectra of the evolved gases from rigid polyurethanes in the 200-250 ^{o}C temperature range along with significant releases of CO_2 and products resulting from the liberation of the small molecule chain extenders (55).

The low abundance of 4,4-MDI and its derivatives in the evolved gases indicate limited volatilisation of these compounds between 200-250 ^{o}C. This may reflect the low volatility of these compounds but it has been reported that it may also be reduced by the products undergoing secondary polymerisation reactions (56). For example, it is known that isocyanate groups dimerise to carbodiimides (-N=C=N-) (57)(58) with further release of CO_2. FTIR and NMR analysis of residues obtained before and after heat treatment indicates a mechanism in which free isocyanate groups form carbodiimides which react further with water and alcohols to form disubstituted ureas, with some of these reaction forming cross-links (56). Both groups are reported to be more stable than urethanes, with dissociation temperatures of 235-250 ^{o}C and 250-280 ^{o}C, respectively. The increased detection of 4,4-methylenedianiline from the pyrolysis of rigid polyurethanes between 250-300 ^{o}C has been attributed to the degradation occurring at the interface between the hard and soft segments but may also indicate the breakdown of the stabilised polyurea structures.

Even more recalcitrant structures may be formed by the direct trimerization of isocyanate (56) or through the reaction of isocyanate groups with previously formed carbodiimides. Carbodiimides themselves may also undergo trimerization to form a similar structure to isocyanurate (59). The thermal stability of isocyanurate groups is high, and the dissociation temperature for these groups is typically reported as at least 300 ^{o}C.

Previous work has also shown that the degradation of PIR foams below 300 °C primarily entails the breakdown of allophanate, biuret and urethane groups, with secondary polymerisation forming a thermally resistant residue of carbodiimide and isocyanurate-derived structures and large polyol and olefin fragments. Mass losses in this temperature range primarily result from the release of CO_2, with some depolymerised isocyanate products and other low-molecular weight fragments such as small diol chain extenders and their derivatives (45)(55) along with products derived from the first stages of polyol decomposition.

At temperatures of 300-350 °C, GC-MS characterisation by Kim *et al*. of the evolved gases from rigid polyurethane foams detects several mass peaks matching those detected from the pure polyol component, confirming the breakdown of the polyol segment at this temperature. The GC-MS profile of the rigid polyurethane foam also contains peaks corresponding to several compounds closely-related to 4,4-methylenedianiline (55). This is strongly suggestive of the decomposition of stabilised polyurea structures resulting from the earlier degradation. The specific breakdown products will depend largely upon the structure of the polyol component, but it is generally observed that the maximum rate of mass loss from rigid polyurethanes correlates with the detection of polyol-derived fragments (60)(61)(55).

Above 400 °C the degradation products of RPUFs are predominantly structurally related to 4,4-methylenedianiline and this may reflect the breakdown of isocyanurate rings and similar structural groups, whether these were present as part of the initial polymer structure, as is extensively the case for PIR, or were formed as secondary products during decomposition. A kinetic study of model isocyanurate compounds with cyclohexyl and phenyl R-groups calculated dissociation temperatures of 417 °C and 380 °C, respectively (62), with the difference in stability being influenced by that of the R-group. Pure isocyanurate polymers have demonstrated stability to temperatures >400 °C (63).

It is known that the risk of ignition is a dependent upon the inherent flammability of the gases produced by the thermal breakdown of the material. Fuel materials dispersed in air will tend to burn only when the concentration is within a critical range. Flammability limits have been established for polystyrene, polyurethane and polyisocyanurate foams. Pyrolysis gases produced by PIR were found to have a lower flammability limit of 29.2 % by mass, compared to 9.1 % and 3.1 % for polyurethane and polystyrene respectively (30).

1.7.2 Oxidative Degradation of PIR/PUR Foam

Outside of controlled laboratory settings, the thermal degradation of insulation materials almost always occurs under oxidative conditions and this is much closer to fire conditions. When characterising the thermal stability and combustion behaviour of polymer foams it is therefore crucial to understand the influence of oxygen on these behaviours. The impact of the presence of oxygen on thermal stability can be very clearly observed through thermogravimetric analysis when a side-by-side comparison of identical materials is performed under inert and oxidative conditions.

A kinetic study by Li *et al.* directly comparing the oxidative and non-oxidative thermal degradation of water-blown rigid polyurethane foams provides a clear illustration of the differences in behaviour under these two sets of conditions (64). As discussed earlier, under an inert atmosphere, the TGA and dTG thermograms exhibit a single major mass loss step, with an onset temperature of 280-292 ^{o}C and maximal mass loss rate at 309-331 ^{o}C, depending on heating rate, sometimes with a shoulder at the higher temperature end and a long tail at high heating rates. In all cases, relatively little mass loss is seen at temperatures >500 ^{o}C. Final char yield was positively correlated with heating rate, ranging from 16.5-22.0 %. This is likely the result of the lower overall time to which the material was exposed to higher temperatures when the heating rate was higher. Under oxidative conditions the onset of degradation and the peak mass loss temperature in this stage have been reported to shift to slightly lower temperatures of 263-277 ^{o}C and 294-318 ^{o}C, respectively while the rate of mass loss in this region is actually slightly lower in air than nitrogen. This report suggests that this may indicate solid-state oxidation occurring in the polymer, reducing the net mass loss. The most obvious differences in behaviour compared to anaerobic conditions occur at temperatures above 350 ^{o}C. In contrast to the gradual tailing off observed under inert conditions, mass loss decreases sharply in air between 350-500 ^{o}C under air, before again increasing, producing a second major mass loss stage with its maximum at 523-575 ^{o}C, again depending on heating rate. This results in an almost total degradation of the sample, which is completed at 600-700 ^{o}C. Char yield in these conditions is less than 2.5 % and is zero in two of the samples.

This pattern of behaviour, in which degradation occurs in two major stages is widely reported throughout the literature. Since this second stage is only observed in the presence of oxygen, it can be reasonably inferred that this second stage represents a combustion reaction, resulting in

almost complete consumption conversion of the sample to smoke consisting of gaseous combustion products and airborne particulates.

Oxidative reactions are typically strongly exothermic and would therefore be expected to be associated with significant heat release from the sample and this is reflected in differential scanning calorimetry results. In inert conditions, the degradation of PUR and PIR foams is generally slightly endothermic. In the presence of oxygen two exotherms are observed coinciding with the mass loss peaks, with the first being of significantly lower intensity than the second, and possibly reflecting solid-state oxidation of the polymer residue. The second peak almost certainly indicates a combustion reaction. The overall heat flow of a polyurethane foam under nitrogen was measured at -156.42 J/g, compared to +7201.53 J/g under air, where a positive sign indicates net release of heat (61).

The heat release from combusting materials can be measured using cone calorimetry. In contrast to DSC, where samples are typically in the milligram mass range, cone calorimetry allows for such measurements to be conducted on much larger samples, on the order of several grams.

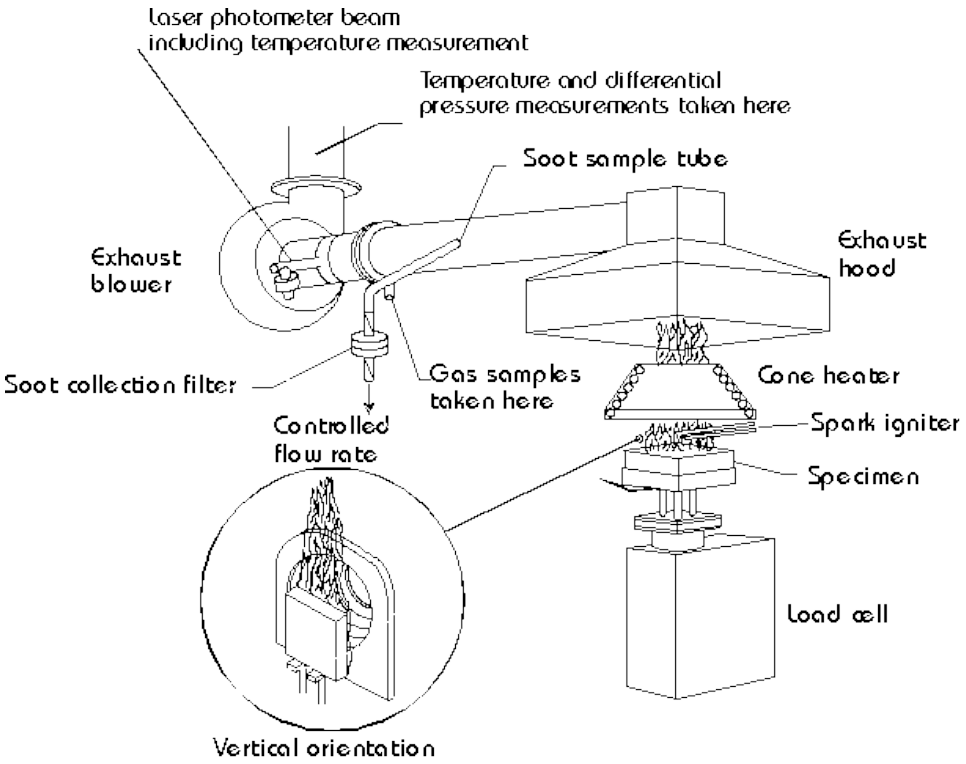

Figure 1.7 Schematic diagram of a typical cone calorimeter, reproduced from *Heat Release and Fire Hazard, Vol. 1*

In a cone calorimeter setup (Figure 1.7), a sample with typical exposed top surface area of 100 mm x 100 mm is placed on a mass balance and exposed to a constant radiative flux from the cone heater. A radiative flux value of 35 kW/m^2 is common, although more intense heating may be used for heat resistant materials. The purpose of this extrinsic heating is to induce pyrolysis of the sample with the resultant pyrolysis products being ignited by a spark. It has also been reported that increasing the incident heat flux also tends to increase the peak heat release rate, as fuel is added to the vapour phase at a higher rate, and the amount of external flux necessary to support sustained combustion is indicative of fire retardance (65). Fire effluents are extracted through the exhaust for analysis. This method provides data on a broad range of parameters using an actively combusting sample. These include ignition time, mass loss, heat release and smoke production rates, total heat release, and characterisation of fire effluent composition. Heat release rate is estimated by Huggett's principle, which states that the gross heat of combustion for organic material is directly related to the amount of oxygen required for combustion (66).

Cone calorimetry has shown that the peak heat release rate of PIR foams is found to be lower than that of PURs. For example, the peak heat release rate of a polyurethane based on 4,4-MDI and a diethylene glycol/phthalic anhydride polyester was found to be 279.8 kW/m^2, with the main peak being sustained for around 50 seconds, while the peak HRR for a PIR foam based on the same components was 143.6 kW/m^2 with the PIR also releasing less total heat than the polyurethane (15). The degree of isocyanurate conversion has been shown under cone calorimetry testing to be directly related to peak heat release rate (67), with isocyanurate-modified foams consistently outperforming pure polyurethanes. These and similar results from the literature suggests that PIR foams are more resistant to ignition and inherently contribute less to the growth of fire and fire load than other polymeric foams, with the exception of phenolic foams, which perform similarly to PIR (65).

The potential fire load of polymers can also be calculated through bomb calorimetry. This measures the total heat released during the complete combustion of a sample in pure oxygen pressurised to around 2.5 MPa. Total heat of combustion is calculated from the increase in temperature of a volume of deionised water surrounding the pressure vessel. A broad range of high-temperature polymers have been characterised using this method (68), and the technique has been specifically applied to insulation foams. Consistent with the results obtained from

cone calorimetry, bomb calorimetry found a modest improvement for PIR over PUR, with respective heating values of 29.8 MJ/kg and 32.1 MJ/kg respectively, with a carbodiimide-modified PIR having a lower heating value still of 26.6 MJ/kg (69).

1.8 Toxicity of Fire Effluents

A critical parameter of fire behaviour is the composition of the effluent produced during thermal degradation and combustion. This impacts on flammability, but also upon the risk posed to human life by exposure to these effluents, which often contain toxic gases such as carbon monoxide and hydrogen cyanide. Important characteristics to consider are the volume of smoke produced during combustion and the chemical composition of both pre- and post-combustion effluents. In bench-scale testing, the quantification of smoke produced during flaming combustion is usually carried out as part of the cone calorimeter test. This is achieved by measuring the density of solid particulates present in the flue gases based on the attenuation or scattering of a light beam. Time-resolved measurement of smoke density from the effluent passing over the sensor can be integrated to find the total volume of smoke released from the sample.

It has been reported that smoke release of PUR and PIR foams through this method follows a similar pattern to that of heat release rate where increased isocyanurate conversion is directly related to a lower volume and rate of smoke release, and a higher proportion of residual char (67)(15). There is a positive correlation between the rates of mass loss, heat release, and smoke production for commonly used insulation materials, with PIR and phenolic foams performing similarly to each other and better than polyurethane and polystyrene foams on these parameters (65). This can be explained by the production of soot resulting from incomplete combustion, which is commonly the result of fuel-rich conditions, where there is insufficient available oxygen for a stoichiometric conversion to fully oxidised products. This is significant to fire toxicity as incomplete combustion is associated with the production of carbon monoxide. The equivalence ratio, φ, is defined as the quotient of the actual fuel-to-air ratio within an enclosed fire and the stoichiometric fuel-to-air ratio. A fuel-rich simple hydrocarbon fire with $\varphi = 1.5$ may produce 0.20 g of CO for each gram of CO_2, compared to 0.05 g when $\varphi = 1$ (70). In real-world fire situations, this corresponds to the conditions that would typically be encountered in a well-developed building fire, where high ambient temperatures produced by rapid heat release will sustain combustion even in depleted-oxygen environments.

This model for carbon monoxide production can be shown to hold true for commonly used insulation foams. Insulation foams combusting in a tube furnace according to the ISO/TS 19700 standard (71) produce low CO yields in the well-ventilated conditions typically of early-stage flaming combustion, while CO_2 yields are high. However, as the fire progresses and the conditions become increasingly under-ventilated, CO_2 yield decreases, while CO yield increases. The performance of PIR and PUR foams is near identical under these conditions, and is similar to phenolic formaldehyde (PhF) foam (23).

However, unlike PhF and polystyrene foams, PUR and PIR foams contain nitrogen due to their isocyanate content. This raises the possibility of the release of toxic nitrogen compounds in fire effluent. These include HCN, NO, NO_2, and NH_3, as well as unburnt fuel containing the isocyanate monomer and its derivatives. These compounds have been detected in fire residues from rigid PUR and PIR foams using an impinger system that was subsequently subject to analysis by LC-MS and gas analysis by FTIR (72). GC-MS analysis of the decomposition products of PIR foams identify a large number of nitrogenous organic compounds that are liable to lead to the production of HCN and NO_2 during the combustion reaction (73). In the above tube furnace tests, both PIR and PUR were found to produce increasingly large quantities of hydrogen cyanide as φ increased, with PIR generating ~0.017 g/g of HCN in the most poorly ventilated conditions. The composition of the effluent under these conditions was such that the human LC_{50} (the concentration that will be lethal to 50 % of exposed individuals) corresponded to the combustion of 8.3 g/m^3 of PIR foam (23), compared to 11.4 g/m^3 for PUR and 21.0 g/m^3 for PhF.

1.9 Improving the Fire Performance of PIR Foams

Improving the inherent thermal stability of polymeric materials may prevent or delay combustion by limiting the production of flammable products through pyrolysis. PIR itself is an example of a chemical modification of polyurethane where the isocyanurate group improves thermal stability (35). In addition to this, several other structural modifications are mentioned in the literature. One such modification is the use of the carbodiimide group as a thermally stable chain extender to improve stability (74). Both pure carbodiimide foams and hybrid carbodiimide-PIR foams have been demonstrated to have a higher temperature at onset of thermal decomposition under N_2 (75) and tend to produce a greater quantity of char and less

smoke than conventional formulations (74). Amide-modified PIR, in which some of the urethane bonds are replaced by more stable amide bonds have also been show to retain a greater proportion of their mass than unmodified foams under chimney tests and have lower surface friability (75). Low friability reduces the tendency of foams to produce dust pollution and improves the bonding of the foam to other materials, for example the facings of structural insulated panels. Other linkages that have been evaluated for use in thermally stable foams include oxazolidones and imides (76)

As the initial mass losses from the thermal decomposition of polymers foams are likely to come from the decomposition of the polyurethane hard segments, stabilising this part of the structure may delay the onset of thermal decomposition and therefore increase the flash ignition temperature of foams (77). It has been demonstrated that foams produced with diamine and dithiol chain extenders are more thermally stable than those with diols (78)(79). Aliphatic chain extenders, especially those with branched chains, have been found to negatively contribute to stability (80), while aromatic chain extenders may result in increased mass retention as the degree of aromaticity within foam structures appears directly related to retained mass fraction (81). Parameters of the foam such as cross-link density and the molecular weight and composition of the polyol monomer can also be altered to improve the thermal stability of foams.

1.9.1 Fire Retardant Additives

1.9.1.1 Halogenated Fire Retardants

Halogenated fire retardants encompass a range of organic compounds containing either bromine or chlorine and entered widespread use in the 1970s as a response to fire safety regulations, offering a relatively inexpensive approach to reducing the ignition risk in flammable materials. Such agents include polybrominated diphenyl ethers (PBDEs), hexabromocyclododecane (α-HBCD), and tetrabromobisphenol-A(5). Combined halogenated organophosphorus fire retardants such as tris(1-chloroisopropyl) phosphate (TCPP) are also commonly used, exerting effects of both halogen and phosphorus mechanisms. TCPP is one of the fire retardants studied in this thesis.

Halogenated agents exert their fire-retardant effects through the reaction of their hydrogen halide decomposition products with radical species including hydroxyl and hydroxyperoxyl radicals generated during a fire event. These reactions quench the free radicals and produce inactive molecules and less reactive •Cl or •Br radicals, inhibiting the propagation of the combustion chain. This mechanism of action tends to promote incomplete combustion and is associated with greater yields of carbon monoxide and hydrogen cyanide from polymeric materials compared to those not treated with these fire retardants (7). Furthermore, the irritant hydrogen halides may incapacitate those exposed to them during fire (82).

Halogenated flame retardants are typically non-reactive additives meaning that they can have long environmental lifetimes so, if released, they do not easily degrade (83)(84). Their potential for toxicity has received attention, leading to several such agents being banned or restricted in some jurisdictions. In 2004, pentabromodiphenyl ether and octabromodiphenyl ether were banned in Europe, followed by decabromodiphenyl ether in 2008(85). Pbromodiphenyl ethers are highly hydrophobic and resistant to degradation predisposing them to bioaccumulation, and since the 1980s studies have detected these compounds in river sediments and aquatic organisms (86), and along with α-HBCD in the eggs of peregrine falcons (87). As apex predators, birds of prey are vulnerable to bioaccumulation, and halogenated pollutants have in the past been strongly linked with severe population declines in several such species.

A substantive body of evidence for the chronic toxicity of halogenated fire retardants has been found in animal models (5). Many of these effects are associated with developmental exposure, and include effects on liver enzyme function, endocrine disruption, reproductive damage, immunotoxicity and neurotoxicity. The phasing out of chemicals in this class has tended to lead to their replacement with analogous compounds, of unknown, but plausibly similar toxicity, and several agents still in active use are listed as chemicals of very high concern under the European Union's REACH regulatory framework, which seeks to provide a high level of protection to public health and the environment from the use of chemicals.

1.9.1.2 Alternative Fire Retardants

As alluded to in the previous section, fire retardants exert their effects by interfering with one or more processes involved in fire. Fire retardants may act both in the gas and solid phases. A common mechanism of action is the quenching of radicals in the gas phase. This mode of action is prominently associated with halogenated fire retardants but also occurs with some organophosphate FRs such as triethyl phosphate (TEP) through the production of phosphorus

oxide radicals. An alternative mode of action in the gas phase occurs through the production of inert gases, chiefly water and carbon dioxide from the decomposition of hydroxides or carbonates (88). Such inert products reduce the concentration of reactive species in the gas phase, slowing the combustion reaction and reducing the flame temperature. This may be sufficient to prevent sustained combustion (88) and this mechanism may be less prone to exacerbating the release of toxic products of incomplete combustion and does not result in the production of irritant halides from the decomposition of the fire retardant.

The decomposition of some fire retardants has been reported to be strongly endothermic. The required thermal energy is absorbed from the surrounding material, effectively acting as a heat sink and delaying its pyrolysis or ignition. Such decompositions contribute to the potential fire retarding action of hydroxides and carbonates alongside diluent gas production. This effect is also associated with the decomposition of melamine, requiring the absorption of around 1600 kJ/mol of energy during its decomposition which is also accompanied by the release of ammonia.

Another important mode of solid-phase fire retardant action is the formation of a physical barrier layer where the action of the fire retardant during thermal degradation of the polymer-FR system produces a protective structure at the surface. For such a barrier layer to be effective, it should possess low thermal conductivity, reducing the heating of the underlying virgin material and be relatively impermeable to oxygen. The barrier layer must also resist crack formation, as any breach of the layer will expose undegraded material, negating the protective effect.

Barrier formation may be achieved in several ways, with the barrier layer consisting of mixture of carbonaceous material derived from the degraded polymer and some decomposition product from the fire retardant. Ammonium pentaborate (APB) is currently used as a fire retardant in some polymer systems such as thermoplastic polyurethanes. The decomposition of APB and its interaction with the polymer produces a glassy char structure containing boron trioxide which resists degradation and insulates the unburnt material beneath (89). Other glass-forming inorganic agents may exert similar effects (90).

Condensed-phase fire retardants may act on the polymer to catalyse the charring reaction. This accelerates the initial degradation of the surface but may also result in a resistant barrier at the surface. This occurs in phosphorus-based fire retardants such as red phosphorus and ammonium polyphosphate (APP), where the initial decomposition of the fire retardant

produces condensed polyphosphoric acid. This acts both as the charring catalyst and physically stabilises the char layer.

Gases arising from the decomposition of the fire retardant may become trapped within the char layer, imparting a low-density cellular structure – known as an intumescent char. This intumesced char layer has very low thermal conductivity and enhances the protective effect. Intumescence plays a role in the action of several solid phase fire retardants, such as in APP due to the ammonia gas also produced during its decomposition. Expandable graphite, consisting of graphite layers with intercalated sulphuric acid, also acts as a fire retardant primarily through intumescence. When heated, the graphite layers are forced apart, greatly increasing the volume of the flakes, and producing a low-density layer containing vermiform graphitic structures. Melamine may provide an intumescent effect through the production of ammonia in combination with carbonaceous condensation products. Intumescent systems can also consist of multiple components comprising a carbonific, which may be the polymer itself or a carbon donor such as pentaerythritol, along with a gas forming agent and a charring catalyst (91).

Solid-phase mechanisms as detailed above may avoid the exacerbation of toxic effluent release associated with radical quenching mechanisms but may require high loadings that are undesirable for some applications and are often more substrate-specific than halogenated FRs, being effective in a narrower range of polymer systems.

1.10 Conclusion

The chemical composition and structure of foamed PIR polymers provides a reasonable level of resistance to pyrolytic and oxidative decomposition at high temperatures when compared to similar materials. The combustion of PIR foam is a predominantly vapour-phase process and is preceded by the production of flammable species via the thermal decomposition of polymer in the solid continuous phase of the foam.

The temperature of onset of decomposition and the rate at which mass loss occurs provides are reasonable predictors of ease of ignition, heat release rate, and smoke production rate, and are linked to the spread of fire. PIRs exhibit improved fire performance over polyurethane and polystyrene foams but in contrast to mineral-based insulation materials all polymer-based foams are inherently combustible to some degree, and fire retardants must be added to mitigate the risk of sustained combustion.

In addition, fire effluents produced by the combustion of PIR contain significantly greater quantities of toxic gases, primarily carbon monoxide and hydrogen cyanide, than similar materials, and common fire retardants have been found to amplify this toxicity by preventing the oxidation of these toxic products of incomplete combustion into less harmful ones. These fire retardants are also associated with the production of irritant gases, which may incapacitate fire victims. This effect is balanced with the effects of fire spread on the volume of toxic effluents produced, but toxicity studies have found that even small masses of combusting PIR are able to produce lethal concentrations of toxic gases. Furthermore, halogenated fire retardants may have adverse effects on the environment and human health, and chemicals of concern in this class have previously been phased out only to be replaced by similar or analogous compounds which have later been found to have similar toxicity concerns.

Alternative non-halogenated fire retardants are referenced in the scientific and technical literature, but relatively few of these have received extensive analysis specific to their use in PIR-based foam materials, and the halogenated fire retardant TCPP is still frequently used in industrial formulations. There remains significant scope for more comprehensive and integrated work comparing alternative fire-retardant systems with those currently in widespread use, understanding their mechanisms of action, and examining the challenges to scaling these up to commercial production. Improving the fire safety of these materials while reducing the reliance on halogenated fire retardants presents clear human, environmental, and economic benefits.

Chapter 1 Bibliography

1. Gama N V., Ferreira A, Barros-Timmons A. Polyurethane foams: Past, present, and future. Materials. 2018;11(10):1841.

2. Moore-Bick M. Grenfell Tower Inquiry: Phase 1 Report Overview. 2019. 2–4 p.

3. Yuen ACY, Chen TBY, Li A, Cachinho Cordero IM de, Liu L, Liu H, et al. Evaluating the fire risk associated with cladding panels: An overview of fire incidents, policies, and future perspective in fire standards. Fire Mater. 2021;45(5):663–89.

4. Bird RB, Stewart WE, Lightfoot EN. Transport Phenomena. 2006. 266–267 p.

5. Shaw SD, Blum A, Weber R, Kannan K, Rich D, Lucas D, et al. Halogenated flame retardants: do the fire safety benefits justify the risks? Rev Environ Health. 2010;25(4):261–305.

6. Sjödin A, Carlsson H, Thuresson K, Sjölin S, Bergman Å, Östman C. Flame retardants in indoor air at an electronics recycling plant and at other work environments. Environ Sci Technol. 2001;35(3):448–54.

7. Mckenna ST, Birtles R, Dickens K, Walker RG, Spearpoint MJ, Stec AA, et al. Flame retardants in UK furniture increase smoke toxicity more than they reduce fire growth rate. Chemosphere. 2018;196:429–39.

8. Mitchener G. Impact of Grenfell Tower fire disaster on polyisocyanurate industry. Polimery/Polymers. 2018;63(10):716–22.

9. Home Office. Fire and Rescue Incident Statistics : England , April 2016 to March 2017. 2017.

10. Salter C, Ramachandran G, Emmitt S, Bouchlaghem N. Economic cost of fire: Exploring UK fire incident data to develop a design tool. Fire Saf J. 2013;62(PART C):256–63.

11. Gorman D, Drewry A, Huang YL, Sames C. The clinical toxicology of carbon monoxide. Toxicology. 2003;187(1):25–38.

12. Gormsen H, Jeppesen N, Lund A. The causes of death in fire victims. Forensic Sci Int. 1984;

13. Stec AA. Fire toxicity – The elephant in the room? Fire Saf J. 2017;

14. British Standards Institution. BS 476-4-1970--[2020-05-21--11-51-11 AM].pdf. British Standards Institution; 1970.

15. Du M, He C, Zhou C. Flame Retardant Effect of Isocyanate Trimer on Polyisocyanurate Foam. 2017;1–7.

16. Wentrup C. Flash Vacuum Pyrolysis : Techniques and Reactions Angewandte. Angewandte Chemie. 2017;56(47):14808–35.

17. Quintiere JG. Ignition of Solids. In: Fundamentals of Fire Phenomena. John Wiley & Sons; 2006. p. 159–90.

18. Atreya BA. Ignition of fires. 1998;(i):2787–813.

19. Zhou C wen, Simmie JM, Somers KP, Goldsmith CF, Curran HJ. Chemical Kinetics of Hydrogen Atom Abstraction from Allylic Sites by 3O2 ; Implications for Combustion Modeling and Simulation. Journal of Physical Chemistry A. 2017;121(9):1890–9.

20. Petrova M V., Williams FA. A small detailed chemical-kinetic mechanism for hydrocarbon combustion. Combust Flame. 2006;144(3):526–44.

21. Hidalgo JP, Torero JL, Welch S. Fire performance of charring closed-cell polymeric insulation materials: Polyisocyanurate and phenolic foam. Fire Mater. 2018;42(4):358–73.

22. Rein G. Smouldering Combustion Phenomena in Science and Technology. International Review of Chemical Engineering. 2009;1:3–18.

23. Stec AA, Hull TR. Assessment of the fire toxicity of building insulation materials. Energy Build. 2011;43(2–3):498–506.

24. Cooke G. Resisting collapse of steel-faced sandwich panel walls and ceilings exposed to fire. Journal of Fire Protection Engineering. 2008;(18):275–90.

25. Cooke G. Sandwich panels for external cladding – fire safety issues and implications for the risk assessment process . 2000.

26. McKenna ST, Jones N, Peck G, Dickens K, Pawelec W, Oradei S, et al. Fire behaviour of modern façade materials – Understanding the Grenfell Tower fire. J Hazard Mater. 2019;368:115–23.

27. Liang FM, Chow WK, Liu SD. Preliminary studies on flashover mechanism in compartment fires. J Fire Sci. 2002;20(2):87–112.

28. Quintiere JG. Some Observations on Building Corridor Fires. Symposium (International) on Combustion. 1975;15(1):163–74.

29. Manescau B, Wang H ying, Coudour B, Garo JP. Influence of Heat Tightness of an Enclosure Fire on Ignition Risk of Unburnt Gases in a Connected Exhaust System – An Experimental Study. Fire Saf J. 2019;109(1):102867.

30. Giunta AW, Kluiver LL De, Korte ACJ De, Herpen RAP Van. Mass loss and flammability of insulation materials used in sandwich panels during the pre-flashover phase of fire. Fire Mater. 2017;41(6):779–96.

31. Schwetlick K, Noack R, Stebner F. Three fundamental mechanisms of base-catalysed reactions of isocyanate. Journal of the Chemical Society, Perkin Transactions II. 1994;(3):599–608.

32. Van Maris R, Tamano Y, Yoshimura H, Gay KM. Polyurethane catalysis by tertiary amines. Journal of Cellular Plastics. 2005;41(4):305–22.

33. Cheikh W, Rózsa ZB, López COC, Mizsey P, Viskolcz B, Szori M, et al. Urethane formation with an excess of isocyanate or alcohol: Experimental and Ab initio study. Polymers (Basel). 2019;

34. Dušek K, Špirková M, Havliček I. Network formation of polyurethanes due to side reactions. Macromolecules. 1990;23(6):1774–81.

35. Riccitiello SR, Fish RH, Parker JA, Gustafson EJ. Development and Evaluation of Modified Polyisocyanurate Foams for Low-Heating-Rate Thermal Protection. Journal of Cellular Plastics. 1971;7(2):91–6.

36. Dick C, Dominguez-rosado E, Eling B, Liggat JJ, Lindsay CI, Martin SC. The Flammability of urethane-modified polyisocyanurates and its relationship to thermal degradation chemistry. Polymer (Guildf). 2001;42(3):913–23.

37. Dominguez-Rosado E, Liggat JJ, Snape CE, Eling B, Pichtel J. Thermal degradation of urethane modified polyisocyanurate foams based on aliphatic and aromatic polyester polyol. Polym Degrad Stab. 2002;78(1):1–5.

38. Hu X, Wang D, Wang S. Synergistic effects of expandable graphite and dimethyl methyl phosphonate on the mechanical properties, fire behavior, and thermal stability of a polyisocyanurate–polyurethane foam. Int J Min Sci Technol. 2013;23(1):13–20.

39. Vitkauskiene I, Makuška R, Stirna U, Cabulis U. Thermal properties of polyurethane-polyisocyanurate foams based on poly(ethylene terephthalate) waste. Medziagotyra. 2011;17(3):249–53.

40. Liszkowska J, Czupryński B. Thermal Properties of Polyurethane-Polyisocyanurate (PUR-PIR) Foams Modified with Tris(5-Hydroxypenthyl) Citrate. Journal of Advanced Chemical Engineering. 2016;06(02).

41. Cabulis U, Kirpluks M. Rapeseed oil as main component in synthesis of bio-polyurethane-polyisocyanurate porous materials modified with carbon fibers. Polym Test. 2017;59:478–86.

42. Cabulis U, Augu M, Kura M, Prociak A. Bio-based polyurethane-polyisocyanurate composites with an intumescent flame retardant. Polym Degrad Stab. 2016;127:11–9.

43. Lefebvre J, Duquesne S, Mamleev V, Le Bras M, Delobel R. Study of the kinetics of pyrolysis of a rigid polyurethane foam: Use of the invariant kinetics parameters method. Polym Adv Technol. 2003;14(11–12):796–801.

44. Wang C, Wu Y, Li Y, Shao Q, Yan X, Han C, et al. Flame-retardant rigid polyurethane foam with a phosphorus-nitrogen single intumescent flame retardant. Polym Adv Technol. 2018;29(1):668–76.

45. Chattopadhyay DK, Webster DC. Thermal stability and flame retardancy of polyurethanes. Progress in Polymer Science (Oxford). 2009;34(10):1068–133.

46. Jiao L, Xiao H, Wang Q, Sun J. Thermal degradation characteristics of rigid polyurethane foam and the volatile products analysis with TG-FTIR-MS. Polym Degrad Stab. 2013;98(12):2687–96.

47. Kogon I. Chemistry of Aryl Isocyanates: Rate of Decomposition of Some Arylalkyl Biurets and Ethyl α,γ-Diphenylallophanate. Journal of Organic Chemistry. 1958;23(10):1984.

48. Lapprand A, Boisson F, Delolme F, Méchin F, Pascault JP. Reactivity of isocyanates with urethanes: Conditions for allophanate formation. Polym Degrad Stab. 2005;90(2 SPEC. ISS.):363–73.

49. Dusek K. Side Reactions in the Formation of Polyurethanes : Stability of Reaction Products of Phenyl Isocyanate. Journal of Macromolecular Science: Chemistry. 1990;27(4):509–22.

50. Singh H, Jain AK. Ignition , Combustion , Toxicity , and Fire Retardancy of Polyurethane Foams : A Comprehensive Review. J Appl Polym Sci. 2008;111(2):1115–43.

51. Park DH, Park GP, Kim SH, Kim WN. Effects of isocyanate index and environmentally-friendly blowing agents on the morphological, mechanical, and thermal insulating properties of polyisocyanurate-polyurethane foams. Macromol Res. 2013;21(8):852–9.

52. Bayer O. Das Di-Isocyanat-Polyadditionsverfahren (Polyurethane). Angewandte Chemie. 1947;59(9):257–72.

53. Fabris HJ. Thermal and Oxidative Stability of Urethanes. Advances in Urethane Science and Technology. 1976;4:89–111.

54. Dyer E, Newborn GE. Thermal Degradation of Carbamates of Methylenebis-(4-phenyl Isocyanate). J Am Chem Soc. 1958;80(20):5495–8.

55. Kim B hyoun, Yoon K, Cheul D. Thermal degradation behavior of rigid and soft polyurethanes based on methylene diphenyl diisocyanate using evolved gas analysis- (gas chromatography)– mass spectrometry. J Anal Appl Pyrolysis. 2012;98:236–41.

56. Berta M, Lindsay C, Pans G, Camino G. Effect of chemical structure on combustion and thermal behaviour of polyurethane elastomer layered silicate nanocomposites. Polym Degrad Stab. 2006;91(5):1179–91.

57. Chambers J, Jiricny J, Reese CB. The thermal decomposition of polyurethanes and polyisocyanurates. Fire Mater. 1981;

58. Duquesne S, Le Bras M, Bourbigot S, Delobel R, Camino G, Eling B, et al. Thermal degradation of polyurethane and polyurethane/expandable graphite coatings. Polym Degrad Stab. 2001;74(3):493–9.

59. Sonnenschein MF. Polyurethanes: Science, Technology, Markets, and Trends. Polyurethanes: Science, Technology, Markets, and Trends. 2014;1–417.

60. He JJ, Jiang L, Sun JH, Lo S. Thermal degradation study of pure rigid polyurethane in oxidative and non-oxidative atmospheres. J Anal Appl Pyrolysis. 2016;120:269–83.

61. Jiao L, Xiao H, Wang Q, Sun J. Thermal degradation characteristics of rigid polyurethane foam and the volatile products analysis with TG-FTIR-MS. Polym Degrad Stab. 2013;98(12):2687–96.

62. Kordomenos PI, Kresta JE. Thermal Stability of Isocyanate-Based Polymers. 1. Kinetics of the Thermal Dissociation of Urethane, Oxazolidone, and Isocyanurate Groups. Macromolecules. 1981;14(5):1434–7.

63. Kordomenos PI, Kresta JE, Frisch KC. Thermal Stability of Isocyanate-Based Polymers. 2. Kinetics of the Thermal Dissociation of Model Urethane, Oxazolidone, and Isocyanurate Block Copolymers. Macromolecules. 1987;20(9):2077–83.

64. Li X bin, Cao H bin, Zhang Y. Thermal Degradation Kinetics of Rigid Polyurethane Foams Blown with Water. J Appl Polym Sci. 2006;102(5):4149–56.

65. Thomas G. Cleary JGQ. Flammability Characterization of Foam Plastics. 1991;

66. Huggett C. Estimation of rate of heat release by means of oxygen consumption measurements. Fire Mater. 1980;4(2):61–5.

67. Xu Q, Hong T, Zhou Z, Gao J, Xue L. The effect of the trimerization catalyst on the thermal stability and the fire performance of the polyisocyanurate-polyurethane foam. Fire Mater. 2018;42(1):119–27.

68. Walters RN, Hackett SM, Lyon RE. Heats of combustion of high temperature polymers. Fire Mater. 2000;24(5):245–52.

69. Zatorski W, Brzozowski ZK, Kolbrecki A. New developments in chemical modification of fire-safe rigid polyurethane foams. Polym Degrad Stab. 2008;93(11):2071–6.

70. Pitts W. The global equivalence ratio concept and the formation mechanisms of carbon monoxide in enclosure fires, . Prog Energy Combust Sci. 1995;21(3):197–237.

71. International Organisation for Standardisation. ISO/TS 19700 Controlled Equivalence Ratio Method for the Determination of Hazardous Components of Fire Effluent. 1997.

72. Blomqvist P, Hertzberg T, Dalene M, Skarping G. Isocyanates, aminoisocyanates and amines from fires - a screening of common materials found in buildings. Fire Mater. 2003;27(6):275–94.

73. Cornu A, Massot R. Compilation of Mass Spectral Data. 1966.

74. Bernard DL, Doheny AJ. US3657161A Polycarbodiimide-polyisocyanurate foam. 1972.

75. Kemani KC. Polyisocyanurate foams modified by thermally stable linkages. In: Polymeric foams: science and technology. 1997. p. 81–100.

76. Sendijarevic A, Sendijarevic V, Frisch KC, Vlajic M. Novel heat-resistant isocyanate-based polymers. Journal of Elastomers and Plastics. 1991;23(3):192–217.

77. Grassie N, Zulfiqar M, Guy MI. Thermal degradation of a series of polyester polyurethanes. J Polym Sci Polym Chem Ed 1980;18:265–74. [164]. Journal of Polymer Science and Polymer Chemistry. 1980;18(265–74).

78. Chattopadhyay DK, Sreedhar B, Raju KVSN. Influence of varying hard segments on the properties of chemically crosslinked moisture-cured polyurethane-urea. J Polym Sci B Polym Phys. 2006;44(1):102–18.

79. Kultys A, Puszka A. Transparent poly(thiourethane-urethane)s based on dithiol chain extender: Synthesis and characterization. J Therm Anal Calorim. 2014;117(3):1427–39.

80. Zulfiqar S, Zulfiqar M, Kausar T, McNeill IC. Thermal degradation of phenyl methacrylate-methyl methacrylate copolymers. Polym Degrad Stab. 1987;17(4):327–39.

81. Bruck SD. Thermally Stable Polymeric Materials. J Chem Educ. 1965;42(1):18–24.

82. Hirschler M. Fire Retardants and the Associated Toxicity. Fire Protection Engineering. 2015;

83. Michałowicz J, Włuka A, Bukowska B. A review on environmental occurrence, toxic effects and transformation of man-made bromophenols. Science of the Total Environment. 2022;811.

84. Hsu YC, Arcega RAD, Gou YY, Tayo LL, Lin YH, Lin SL, et al. Levels of non-PBDE halogenated fire retardants and brominated dioxins and their toxicological effects in indoor environments-A review. Aerosol Air Qual Res. 2018;18(8):2047–63.

85. Betts KS. New thinking on flame retardants. Environ Health Perspect. 2008;116(5).

86. Watanabe I, Kashimoto T, Tatsukawa R. Polybrominated diphenyl ethers in marine fish, shellfish and river sediments in Japan. Chemosphere. 1987;16(10–12):2389–96.

87. Lindberg P, Sellstrom U, Haggberg L, de Wit C. Higher Brominated Diphenyl Ethers and Hexabromocyclododecane Found in Eggs of Peregrine Falcons (Falco peregrinus) Breeding in Sweden. Environ Sci Technol. 2004;38(1):93–6.

88. Hull TR, Witkowski A, Hollingbery L. Fire Retardant Action of Mineral Fillers. Polym Degrad Stab. 2011;96:1462–9.

89. Myers RE, Dickens ED, Licursi E, Evans RE. Ammonium pentaborate: An intumescent flame retardant for thermoplastic polyurethanes. J Fire Sci. 1985;

90. Myers RE, Licursi E. Inorganic glass forming systems as intumescent flame retardants for organic polymers. J Fire Sci. 1985;

91. Wang J, Chen Y. Flame-retardant mechanism resulting from an intumescent system. J Fire Sci. 2005;

2 Materials and Methods

In line with the aims and objectives detailed in the introduction to this thesis, a programme of experimental techniques has been developed with a view to carrying out a detailed analysis of the behaviour of PIR foams at high temperatures and the influence of various flame-retardant agents. This section details the production of hand-mixed foam samples that were subjected to testing and the methods used for their analysis, as well as the techniques used for the processing of acquired data.

Thermogravimetric analysis has been applied extensively to identify the stages comprising the thermolytic degradation of PIR foams and the temperature ranges over which these occur. As related to fire scenarios, this is intended to provide information about the potential contribution of foam insulation to fuel loading and production of potentially hazardous volatile fragments.

The furnace treatment detailed herein, and applied to gram-scale samples, were developed to extend the principles of TGA to samples on a larger scale and to provide information which could not be obtained by TGA. This includes measurements of the volumetric changes occurring during degradation.

FT-IR spectroscopy and Pyrolysis GC-MS have been applied to elucidate the chemical changes occurring in foams during their thermal degradation and to characterise the chemical species present within the pyrolysis gases. These methods were selected to identify the reaction mechanisms underlying the overall degradation of PIR foams at high temperatures, and the ultimately the ways in which PIR-based insulation materials may contribute to fire risk, for example by the release of flammable or toxic breakdown products in reaction to fire.

2.1 Production of Hand-mixed PIR Foam

2.1.1 Materials

Unless stated otherwise, all chemicals used in the foaming reaction were provided by Tata Steel Building Systems UK. The primary polymer components consisted of a commercial polymeric MDI formulation (Huntsman Suprasec 2085) with an isocyanate content of 30.5 % and average functionality 2.9, and an aromatic polyester polyol blend (Stepanpol PS-2412) composed primarily of a diethylene glycol-phthalic anhydride copolymer (70-85% wt.). The polyol blend also contained diethylene glycol as a chain extender (10-20 % wt.) and the halogenated organophosphate flame-retardant TCPP (5-10 % wt.). This was foamed using a physical

blowing agent mix consisting of a 70:30 volumetric mixture of cyclopentane and 2-methylbutane both obtained from Sigma-Aldrich.

The flame-retardant additives used in the stock formulation were TCPP and TEP. Dimethylcyclohexamine (DMCHA, Huntsman Polyurethanes) and potassium octanoate (Evonik Kosmos 75) were used to catalyse the blowing and gelling reactions. A polyether polydimethylsiloxane copolymer (Evonik Tegostab 1048) was added as a stabilising agent.

Mixing was performed using a mechanical overhead stirrer suitable for high viscosity fluids (Caframo UltraSpeed 6015) and materials were measured using an analytical balance and micropipette.

2.1.2 Procedure

2.1.2.1 Safety Measures

DMCHA and pentane mixtures are volatile and flammable. DMCHA is also acutely toxic, and inhalation of vapours may cause irritation of the lungs and respiratory tract with inhalation of large quantities being potential fatal. The mixing process also has the potential to aerosolise reagents. Mixing and handling of all foaming chemicals was carried out under vapour extraction in a fume-hood. Appropriate gloves were worn.

2.1.2.2 General Procedure

Foams produced at the university laboratory were produced in an open container and allowed to freely rise until the reaction was completed and allowed to cure at room temperature. The reagents were separated into two mixtures as follows:

Mixture A: Polymeric MDI.

Mixture B: Polyester polyol, stabiliser, flame retardants, catalysts, water, blowing agent.

These mixtures were then combined and mixed to initiate the reaction.

2.1.2.3 Measurement of MDI

Due to the relatively high viscosity of polymeric MDI, a significant amount of residual reagent remained in the container when poured out. To account for this 75 g of polymeric MDI was decanted into clean container A and then poured back into the sample bottle for 10 seconds. The mass of the container plus the residual MDI was taken as the tare weight for the purposes of measuring the MDI. With the container on a mass balance, 75.90 g of polymeric MDI was then poured into the container.

2.1.2.4 Measurement of B Components

Clean container ‘B’ was placed on the mass balance and the components were added in the following order and amounts, taring the balance between each addition. Where the viscosity of reagents would allow, clean plastic syringes were used during the measurement of chemicals to maximise measurement accuracy. Deionised water and DMCHA were measured volumetrically using a micropipette.

PS-2412	36.80 g
TCPP	7.36 g
TEP	1.84 g
Tegostab	0.92 g
Water	0.2 g (200 µL)
Kosmos 75 (Potassium octanoate)	0.65 g
DMCHA	0.18 g (210 µL)

After measurement of components, the B mixture was stirred for one minute at 2000rpm before the addition of the blowing agent.

2.1.2.5 Measurement of Blowing Agent

To limit the evaporation of the blowing agent during processing, the pentane mixture was refrigerated before use. The target mass of blowing agent was 6.16 g, but due to its volatility, around 7.00 g was added to the B mixture initially. This was then stirred at 2500 RPM for one minute. During this process the mixture emulsified, becoming ‘creamy’ in appearance. Following this mixing step, the container was weighed again, to measure the evaporation of pentane. Additional blowing agent was then added back to the target mass and was not mixed further.

2.1.2.6 Initiation of Foaming Reaction

Immediately following the final addition of blowing agent, the contents of the A container were poured into the B container for 10 seconds, and then mixed at 3000 RPM for 8 seconds. The container was then placed down in the fume hood, and the foaming reaction was observed. At the end of the rise, the container was allowed to stand until the top of the foam bun no longer felt tacky when touched with the back of a spatula.

Figure 2.1. *Free-rise PIR foam bun.*

2.1.2.7 Curing of Foam

Foams were allowed to cure at room temperature for a minimum of 48 hours before any analysis was carried out.

2.1.3 Block Mould Foams

A large set of hand-mixed foam samples were prepared by the project industrial sponsor (Tata Building Systems UK) at their industrial laboratory in Shotton Works, Deeside. These samples were produced using the same basic method as detailed above but were poured into a block mould during the foaming reaction to produce a large cuboidal slab. A total of 30 formulations containing a range of different polyol components were produced in triplicate for a total of 90 sample batches.

2.2 Thermal Stability Analysis

2.2.1 Background

The mechanisms leading to and supporting combustion are outlined in the introduction to this thesis. Combustion of polymeric materials is preceded by a pyrolytic phase in which heating of the material leads to fragmentation of the polymer structure and the production of volatilised compounds. These fuel species react with oxidising species in the vapour phase triggering an

exothermic chain reaction and leading to combustion at the interface layer between the solid material and the surrounding atmosphere.

Based on this, it can be inferred that the loss of mass from the sample is indicative of the transfer of potentially flammable products to the combustion zone, and since mass (m) is conserved then:

$$m_{total} = m_{(s)} + m_{(l)} + m_{(g)} \tag{2.1}$$

The three right-hand side terms indicate the mass of solid, liquid and gaseous components respectively, noting that the $m_{(g)}$ component encompasses both the gaseous components of pyrolysis and combustion and particulate matter emitted as smoke and therefore may contain airborne solid particles and liquid droplets.

In a non-enclosed system, gaseous products escape and no longer exert weight, therefore:

$$m_{residual} = m_{total} - m_{(g)}$$

$$m_{total} - m_{residual} = m_{(g)}$$

$$\Delta m_{residual} = -\Delta m_{(g)} \tag{2.2}$$

The rate of mass loss is of interest because combustion can only be sustained if there is a sufficient flow of fuel products into the combustion zone.

2.2.2 Thermogravimetric Analysis

2.2.2.1 Operating Principle

Thermogravimetric analysis (TGA) is a common method for quantifying mass loss and mass loss rate with respect to temperature and time. A thermogravimetric analyser consists of a high-precision mass balance enclosed within a temperature-controlled furnace chamber. In the most common application, the sample placed on the balance and the mass is constantly measured as

the temperature increases at a programmed rate (dynamic TG). The mass can also be measured over time at a constant temperature (static/isothermal TG).

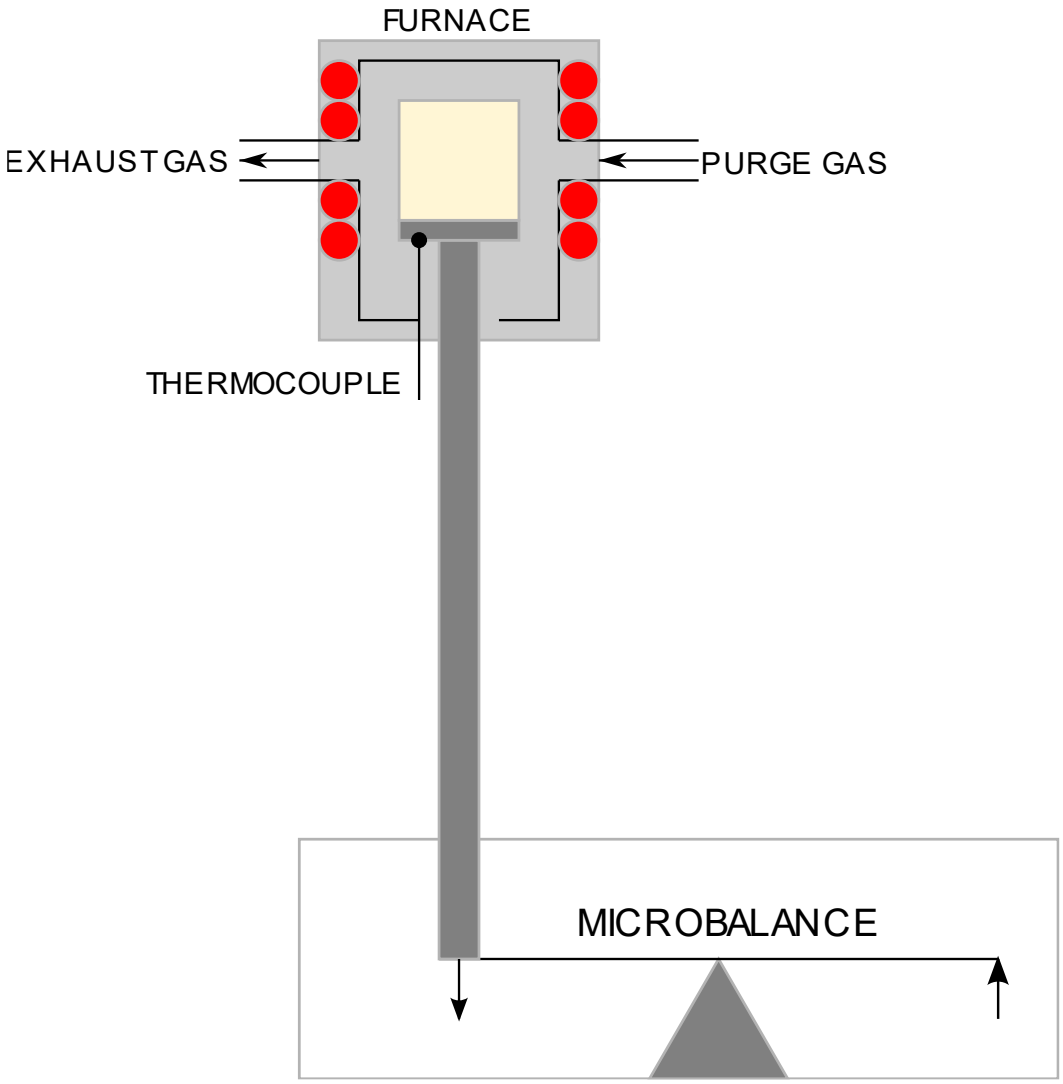

Figure 2.2. *Schematic illustration of thermogravimetric analyser.*

2.2.2.2 Baseline Curves

In the absence of other forces, the mass indicated by the TG sample balance would indicate the actual mass of the sample based on the weight exerted. In practice this is not the case as the indicated mass is affected by the buoyant force exerted on the balance and sample by the displaced gas inside the furnace chamber. This force occurs in reaction to the displacement of air within the furnace chamber by the sample and pan and will act directly upwards against the hydrostatic pressure gradient within the furnace chamber. This buoyant force is not constant with respect to temperature as the density of gases decreases with increasing temperature. The density of air at standard ambient temperature and pressure (25 ^{o}C, 1 atm) is 1.168 kg/m^3 but this decreases to 0.277 kg/m^3 at 1000^{o}C and 1 atm.

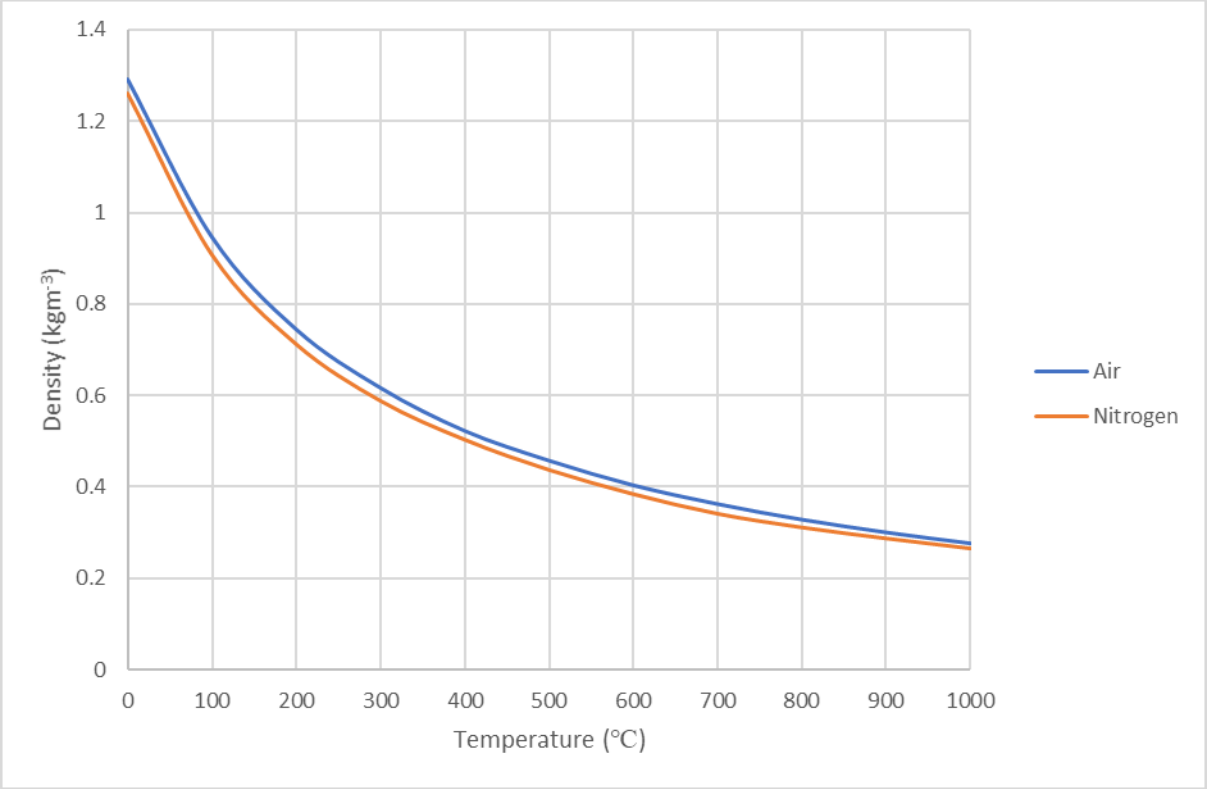

***Figure 2.3**. Density curves of air and nitrogen from 0-1000°C at 1atm (101.325kPa) plotted from data in NIST WebBook*

The magnitude of the buoyant force, F_b is calculated as follows, where ρ is the fluid density, g is the acceleration due to gravity, and V is the displaced fluid volume.

$$F_b = -\rho g V \tag{2.3}$$

Since the acceleration due to gravity is constant for a given location and the volume of the sample pan and balance assembly is also largely constant, gV can be treated as a constant term so:

$$F_b \propto -\rho \tag{2.4}$$

The magnitude of the buoyant force is 4.2 times greater at room temperature than at 1000 °C. The decrease in buoyant force will be observed as an increase in weight as temperature increases since buoyancy acts in opposition to gravity.

Resultantly, the indicated sample mass at a given temperature is:

$$m_{indicated} = m_{actual} - \rho V \tag{2.5}$$

As TGA samples are usually on the order of tens of milligrams, the effect of buoyancy changes may exert a non-negligible influence on the accuracy of sample mass measurements. For this reason, it is necessary to correct for buoyancy effects. This can be achieved by producing a baseline curve.

A baseline curve was produced for each temperature program by running the program with an empty sample pan with the mass at the starting temperature recorded as zero and measuring the deviation throughout. The measured deviation could then be subtracted from the obtained experimental data for samples.

The baseline curve below was obtained for a nitrogen atmosphere over a temperature range of 30-900 ^{o}C at a constant temperature ramp rate of 10 ^{o}C per minute with a purging nitrogen flow of 20 cm^3 per minute.

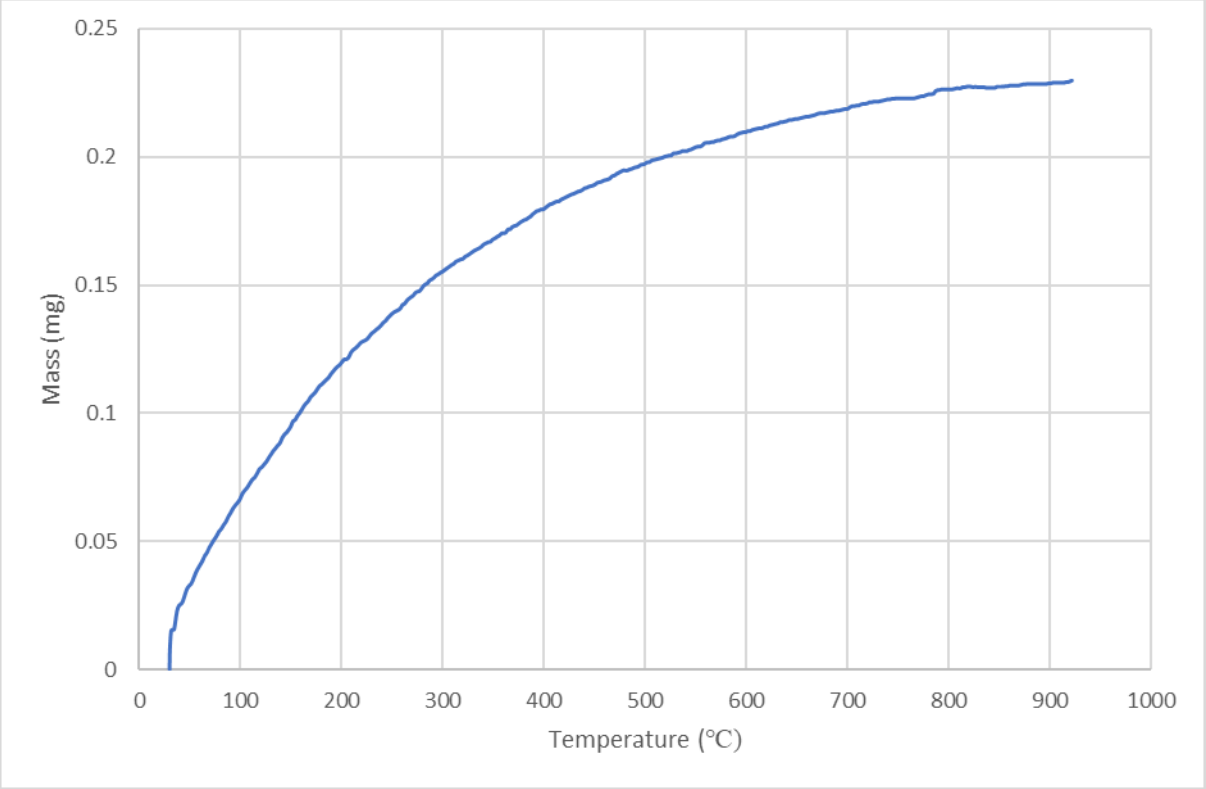

Figure 2.4. *Baseline TGA curve obtained under nitrogen atmosphere at heating rate of 10^{o}C per minute.*

A mass increase of 0.23 mg was observed at 900 ^{o}C and the overall shape of the baseline curve was broadly similar to that expected based on the theoretical changes to the magnitude of the buoyant force with temperature. As the typical mass of TG samples is on the order of 10-20 mg, the observed baseline drift was equivalent to 1.25 % to 2.5 % of initial sample mass. The baseline drift likely also captures additional effects such as convection currents within the purge gas and the influence of heating on the balance assembly.

2.2.2.3 Sample Preparation

Thermogravimetric analysis of foam samples in this work was carried out on both whole and pulverised foams as described below.

For whole foams, these were simply cut from sample blocks and then shaped into roughly cylindrical sections of appropriate size to fit snugly in the TGA sample pan. In the case of samples taken from free-rise foams produced on-site, these were taken from the core region of the foam bun, at the approximate centre, avoiding the material at and within 2 centimetres of the surface of the bun.

Pulverised foam samples were hand-ground using a pestle and mortar. Liquid nitrogen was used to cool the samples to assist with grinding. It was expected that pulverised foam samples would largely lose their blowing agent content due to the destruction of the cellular structure.

2.2.2.4 Data Acquisition

Two thermogravimetry instruments were used for data acquisition. These were a PerkinElmer STA6000 and a Setaram LabSys Evo. Both instruments are simultaneous thermal analysers equipped to provide both thermogravimetric and heat flow data but were predominantly used in this work for TGA.

Except where stated otherwise the following temperature program was used:

1. Hold at initial temperature (30 ^{o}C) for five minutes.
2. Heat from 30 ^{o}C to 900 ^{o}C at a constant temperature ramp rate of 10 ^{o}Cmin^{-1}.
3. Hold at final temperature (900 ^{o}C) for two minutes.

The above was used for both inert (nitrogen) and oxidative (dry air) atmospheres. A sample purge rate of 20 cm^{3}/min was used for all samples.

Where possible TG data acquisition was done at least in duplicate and preferably in triplicate for a given sample formulation and experimental conditions.

2.2.3 Data Processing

Instrument data was exported in the *.csv* file format and processed in Microsoft Excel. Some simple statistical analyses were carried out using GraphPad. The key data extracted from the .csv files were time, program and sample temperatures, and unsubtracted mass. Where duplicate or triplicate data existed for a particular formulation and set of experimental conditions, thermograms and other analyses were carried out on both individual sample data and mean data produced from the replicates.

2.2.3.1 Production of TGA Thermograms

TGA thermograms were produced using the following method. Firstly, the mass data for the relevant baseline curve for the temperature program were subtracted from the unsubtracted mass data to produce a corrected mass. The corrected mass was then converted into a percentage of the initial mass at the start of the temperature ramp. Data from the isothermal regions in the first five and last two minutes of the temperature program were not included in this part of the data processing. Time-filtering was applied to the data to reduce the number of data points to be plotted and reduce noise while accurately retaining the overall shape of the curve. The selection of this filtering is discussed in further detail in the following section on derivative thermogravimetry. Thermograms in this thesis have been produced by plotting the percentage mass against the measured sample temperature.

2.2.3.2 Production of dTG Thermograms

Following the initial thermogravimetric analysis, derivative (dTG) thermograms were produced to allow for further characterisation of mass loss events. Derivative thermogravimetry measures the rate of change of mass against time or temperature during heating, taking the first-order derivative of the thermogravimetric curve. Derivative thermogravimetry highlights mass loss events that are not easily discerned from TG curves, e.g., the exact temperature at which the highest rate of mass loss occurs, or when mass loss occurs in multiple phases that can be difficult to distinguish from TG data (1). This technique is widely used throughout the literature on PIRs and other insulation materials (2–4), and is of particular value when comparing materials as it allows relatively small changes in thermal stability and decomposition behaviour to be identified. The mass loss rate at each time interval is calculated using the following method:

$$\frac{dm}{dt} = \frac{m\ at\ (t + \delta t) - Mass\ at\ t}{t + \delta t - t} = \frac{m\ at\ (t + \delta t) - Mass\ at\ t}{\delta t} \qquad (2.6)$$

Where:

$$\frac{dm}{dt} = rate\ of\ change\ in\ mass$$

$$m = mass\ of\ sample$$

$$t = time$$

$$\delta t = change\ in\ time$$

The TGA instrument used in this thesis can directly provide data for the derivative mass. However, the instrument is set up to capture the current mass of the sample at time point separated by 0.125 s. This interval corresponds to the value of δt in the above equation. When this value is small the effects of high-frequency noise are amplified.

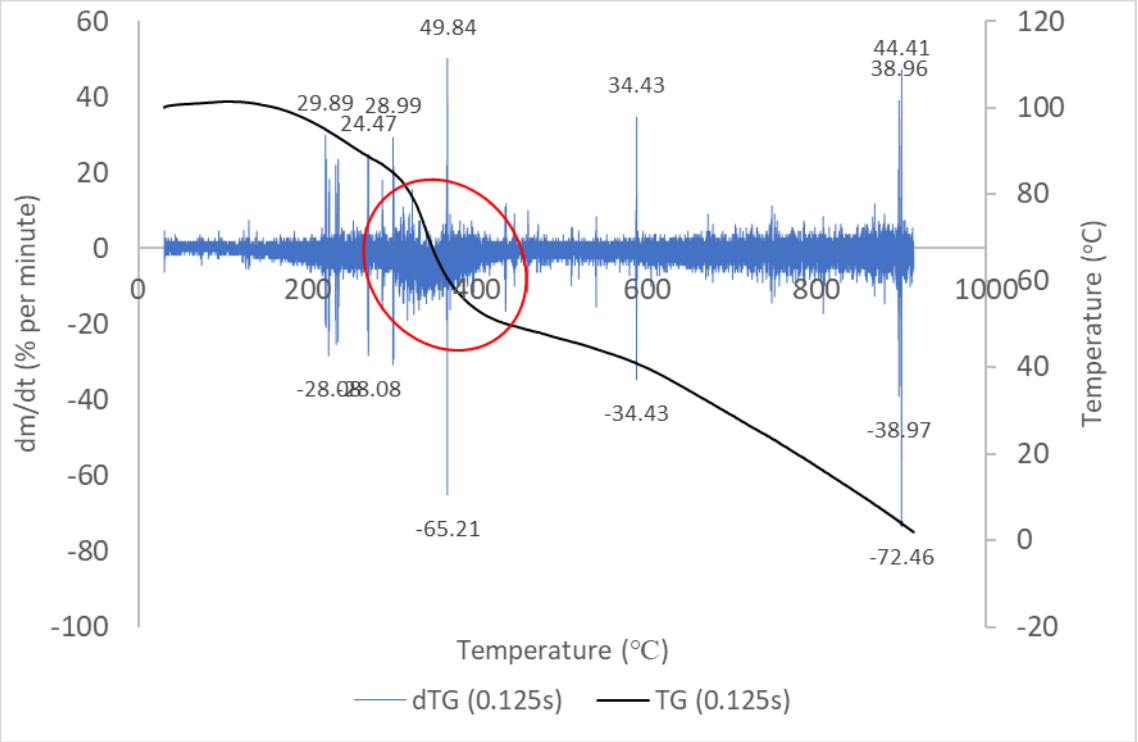

Figure 2.5. *Unfiltered TG (black) and dTG curve (blue) from sample LF1 over a temperature range of 30-900 °C at 10 °C/min under N_2 showing high amplitude instantaneous peaks present at measurement interval of 0.125 seconds.*

Figure 2.5 shows a dTG thermogram produced from the raw dTG data taken directly from the STA6000 instrument LF1. This sample has been selected for illustrative purposes, but similar features were observed for samples LF2 and LF3. Visual inspection indicates a poor signal-to-noise ratio, due to the presence of numerous high amplitude, short duration peaks. While these

peaks are very prominent features of the dTG curve, it is obvious from inspection that they do not correspond to similarly prominent features in the TG curve. Conversely, mass loss events that are clearly visible on the overlaid TG thermogram are largely obscured in most cases due to their low relative amplitude. This can be seen by examination of the red circled area in the figure. Here, the TG curve clearly shows a sustained mass loss, which is seen much less clearly in the dTG thermogram. The amplitude of some of these high-frequency peaks were highlighted on the thermograms and were in the range tens to hundreds of percent per minute across the three samples. It is clearly the case that these features do not correspond to sustained thermogravimetric events, as again seen in the circled area. The presence of similar noise artefacts in raw dTG data is reported elsewhere in the literature (5)

The appearance of the unfiltered dTG curve can be explained mathematically. Recalling that:

$$\frac{dm}{dt} = \frac{m \text{ at } (t + \delta t) - m \text{ at } t}{\delta t} \tag{2.7}$$

Then it can be demonstrated that even very small instabilities in measured mass will produce relatively large values for $\frac{dm}{dt}$ when δt, the measurement interval, is small. The largest absolute value of $\frac{dm}{dt}$ in Figure 2.5 indicates a rate of mass loss of 72.5 % per minute (1.21 % per second):

$$1.21 = \frac{m\ at\ (t + \delta t) - m\ at\ t}{0.125} \tag{2.8}$$

$$m\ at\ (t + \delta t) - m\ at\ t = 1.21 \times 0.125 = 0.15125\%$$

It is found that this large high-frequency peak represents a change in measured mass of only 0.15 % of the sample mass, equivalent to 0.02 mg and it is therefore demonstrated that small momentary variations in measured mass, resulting from balance instability and vibration, can result in spurious *dm/dt* values when these occur across small time intervals. Even fluctuations on the magnitude of 1 µg (1/10000th of the average sample mass) will produce *dm/dt* values of around ± 5 % per minute for a 10 mg sample.

The following section will demonstrate that the application of simple numerical methods is able to produce smoothed first-order derivative thermogravimetric curves that accurately reflect the underlying thermogravimetric data. Example curves presented in this section have been derived from three samples of line-produced PIR foam, labelled LF1, LF2, and LF3.

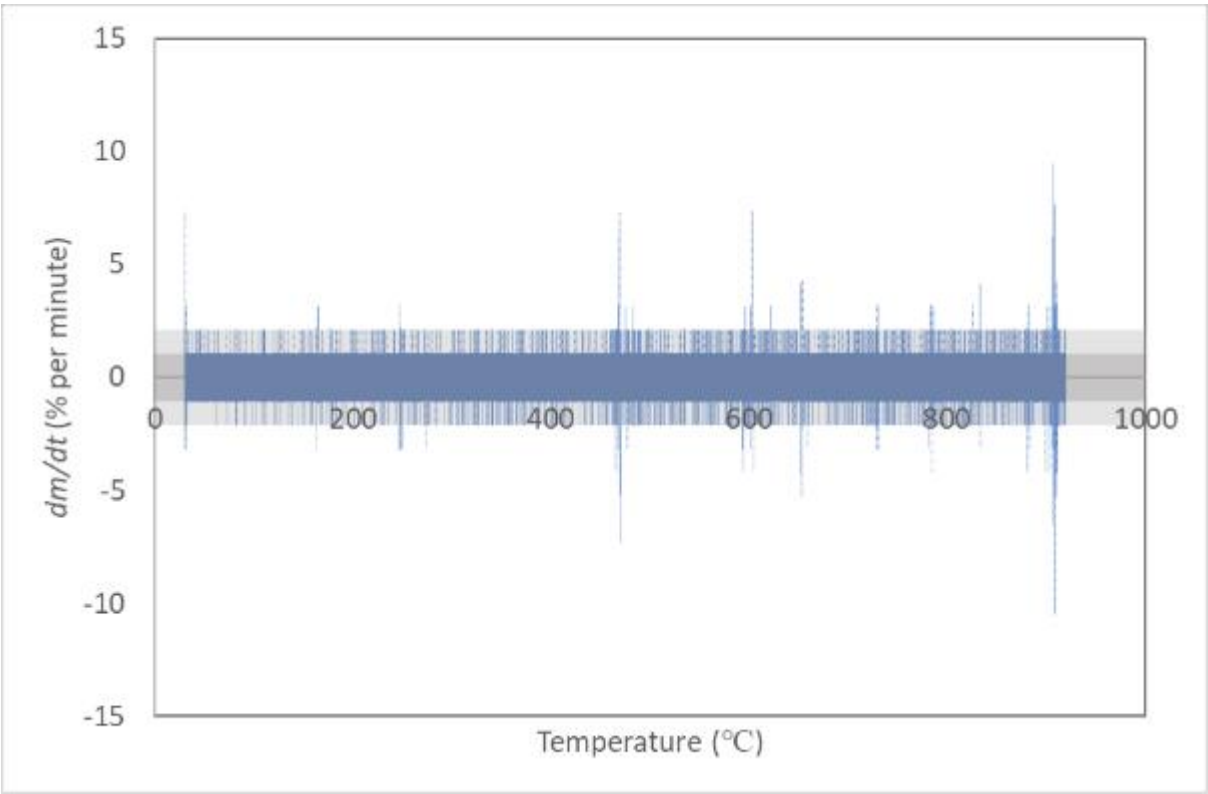

Figure 2.6. *Unfiltered dTG curve produced for blank pan. Grey shading has been added to show extent of regular oscillations around baseline.*

Figure 2.6 displays a dTG curve produced for a control experiment (i.e., an empty sample pan run at the same ramp rate etc.). A fixed value of 10mg has been added to the measured mass values to scale the percentage mass values to a similar magnitude as seen for actual sample runs, as these were also in the range of 10 mg. The absence of a sample was expected to have relatively little impact on the effect of non-sample induced fluctuations, as the samples themselves accounted for only around 3-4 % of the total mass of the initial load placed on the balance, with the remainder consisting of the much heavier ceramic sample pan. The impact of differences in balance stability resulting from such changes in the total load placed on the balance are therefore assumed to be negligible.

As no sample was present, it can be determined that some of the noise observed in the previous dTG thermograms is unrelated to any effects arising from the sample. Several potential sources of noise have been identified and are categorised here.

1. Baseline Fluctuation

The rescaled dTG for the empty sample pan exhibits a remarkably consistent high-frequency fluctuation around the baseline. Two grey bands have been added to the figure to illustrate this fluctuation indicating consistent oscillation of ±1.05 % (≈0.2 µg) with a secondary larger amplitude band of ±2.1 % (≈0.4 µg). These bands likely represent a continuous regular fluctuation of the microbalance around an idealised, perfectly stable baseline. The absolute magnitude of this oscillation indicates a very high degree of balance stability as the relative size of this oscillation is around 1/50000th of the actual mass of a typical sample. The large effect size is, as previously stated, a function of the short measurement interval, and this was demonstrated by re-sampling the data over longer time periods, where it was found that increasing the time interval by a factor of *n* decreased the amplitude of the primary and secondary fluctuation bands by a factor of *1/n*. This is represented in Figure 2.7 below.

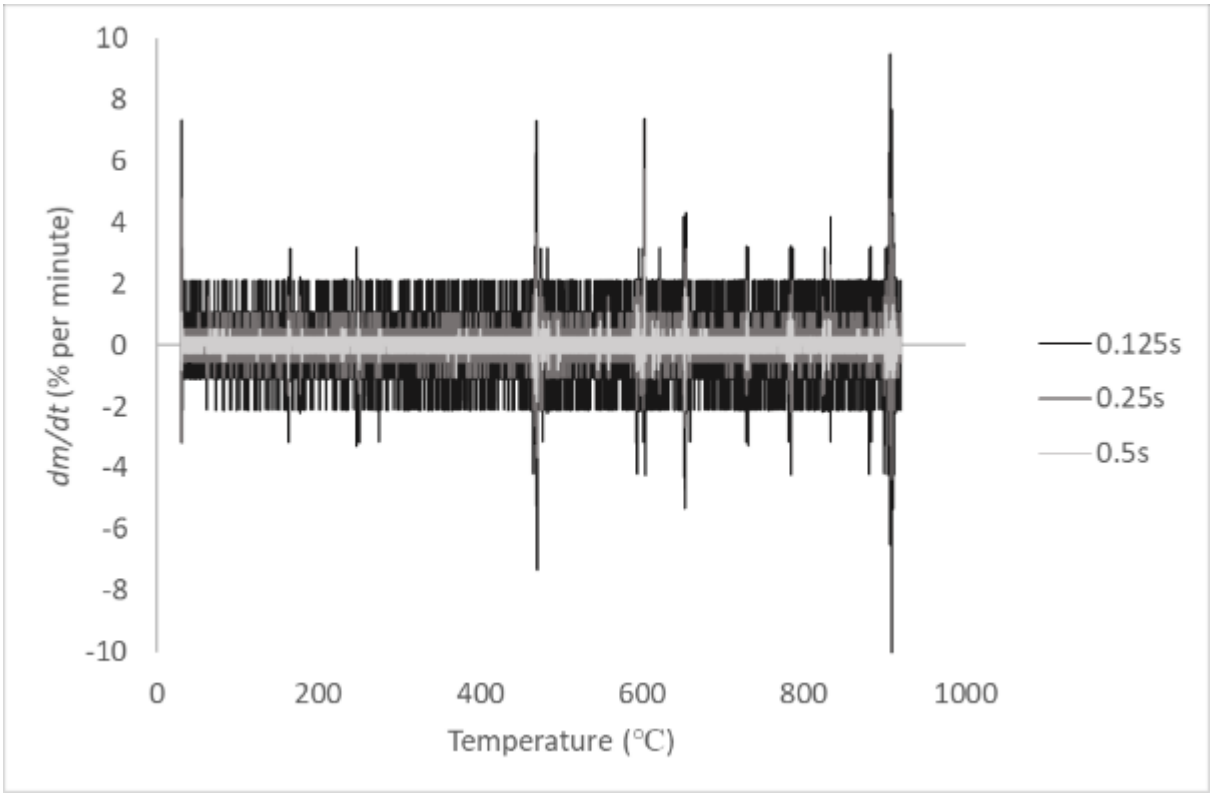

Figure 2.7. *The effects of increasing values of δt on deviation about baseline.*

As the value of δt was sequentially doubled from 0.125 s → 0.25 s → 0.5 s, the width of the inner band decreased from ±1.05 % → ±0.53 % → ±0.26 %. The amplitude of the outer band also decreased by the same factor, with the peaks in this band also become more sporadic. These results indicate that the degree of noise in the dTG curve is in large part an inverse function of δt.

2. Extrinsic Vibration

In addition to the regular bands observed on the empty pan dTG, sporadic higher amplitude peaks are also observed. It is known that due to the sub-microgram sensitivity of the TGA balance, vibration arising from the internal and external environment of the balance can affect the measured mass. Hence, the instrument should be set up in such a way as to isolate the balance assembly from external vibration as much as possible, for example by placing the instrument on a highly stable, flat surface (6). In practice, it is very difficult to eliminate this source of noise entirely, and the balance may be affected by a wide range of vibration sources. These may occur within the instrument set up, for example from vibration transmitted through the cooling system arising from the pump to external vibrations in the local environment arising from other equipment and human activity in the vicinity, to longer-range natural and artificial seismic and atmospheric vibrations. Such external sources of interference may account for the presence of the sporadic high amplitude artefacts observed in unfiltered dTG data seen in Figure 2.5. This indicates that the thermogravimetric instruments used in this work are susceptible to external vibration, but it will be demonstrated that such effects are distinguishable from true changes in sample mass and that these can be corrected for by the application of suitable data analysis methods.

These sources of noise can produce artifacts in the raw dTG data that are of similar or greater magnitude than true sample mass effects but occur over a time span that is two to three orders of magnitude shorter, and this difference in frequency can be exploited to separate sample behaviour from the effects of baseline fluctuation and other sources of noise. As these artifact-derived fluctuations occur at a higher frequency than true changes in sample mass, it should be possible to eliminate or strongly reduce their impact by effectively applying a low-pass filtering procedure to the data. This can be achieved by calculating *dm/dt* over larger time increments. As such, Fig. 3.10 has already demonstrated in the case of the empty pan that increasing the

sampling interval decreases the calculated amplitude of baseline fluctuation in inverse proportion to the length of the sampling interval.

As this process reduces the total number of data points used to construct the dTG curve, some resolution is necessarily sacrificed to reduce noise, as the temperature change between data points will be larger. It is therefore important to establish a degree of filtering sufficient to maximise signal-noise ratio while avoiding unacceptable loss of accuracy. The approach taken for the data in this thesis is described as follows.

An empirical method was employed to identify a suitable degree of filtering. For each of the three line-produced foam samples previously described, *dm/dt* was recalculated across a range of intervals, starting at every 10^{th} point (1.25 s) and doubling the interval up to every 1280^{th} point (160 s). At a ramp rate of 10 ^{o}C/min, these intervals correspond to temperature changes of 0.21 ^{o}C at the bottom end of the range, and 26.67 ^{o}C at the top end. This range was selected as it was predicted that the lower extreme would provide insufficient filtering to achieve an acceptable signal-noise ratio, while the upper extreme would demonstrate a loss of resolution that would not allow for accurate differentiation of the TG curve. The optimum degree of filtering was therefore expected to be located somewhere within this range, at an interval that reduced the impact of noise while accurately reflecting key data features observed in the corresponding TG curves.

$$\frac{dm}{dt} = \frac{m\ at\ t - m\ at\ (t - i)}{i} \tag{2.9}$$

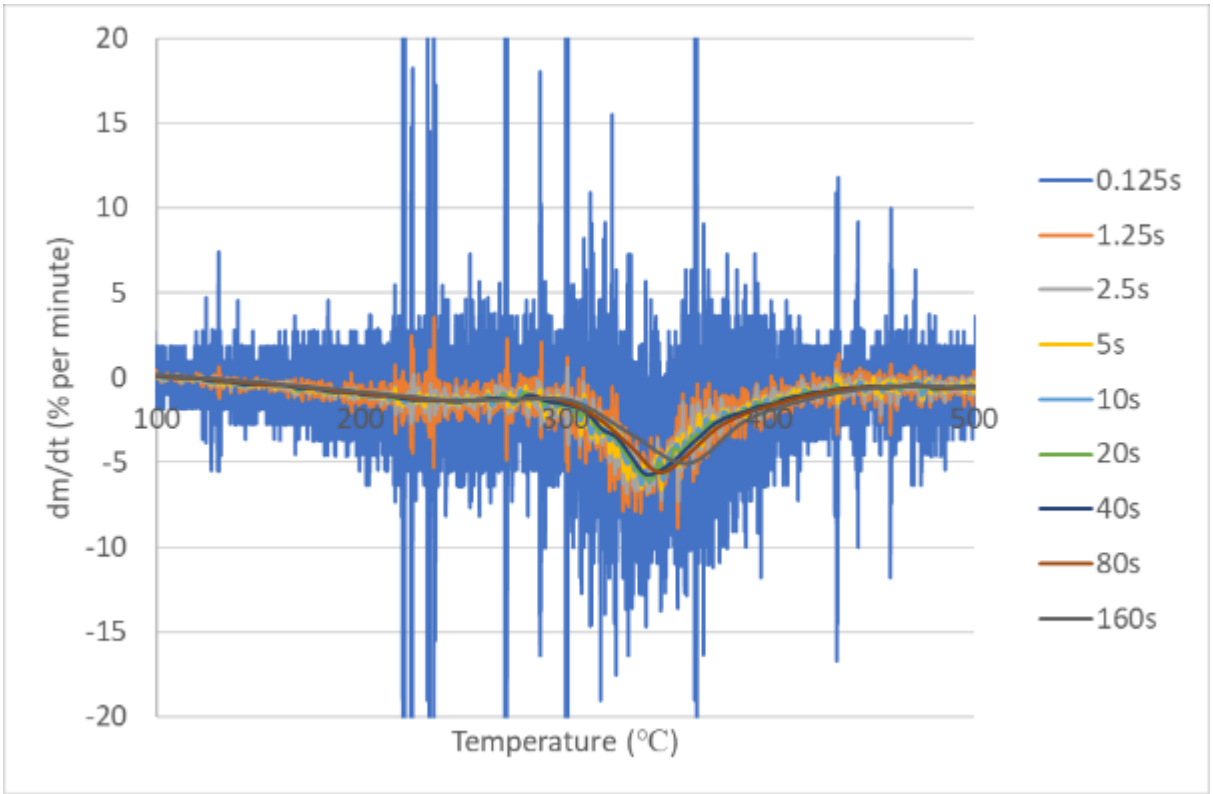

Figure 2.8. *dTG curves for line LF1 across a range of intervals from 0.125s to 160s.*

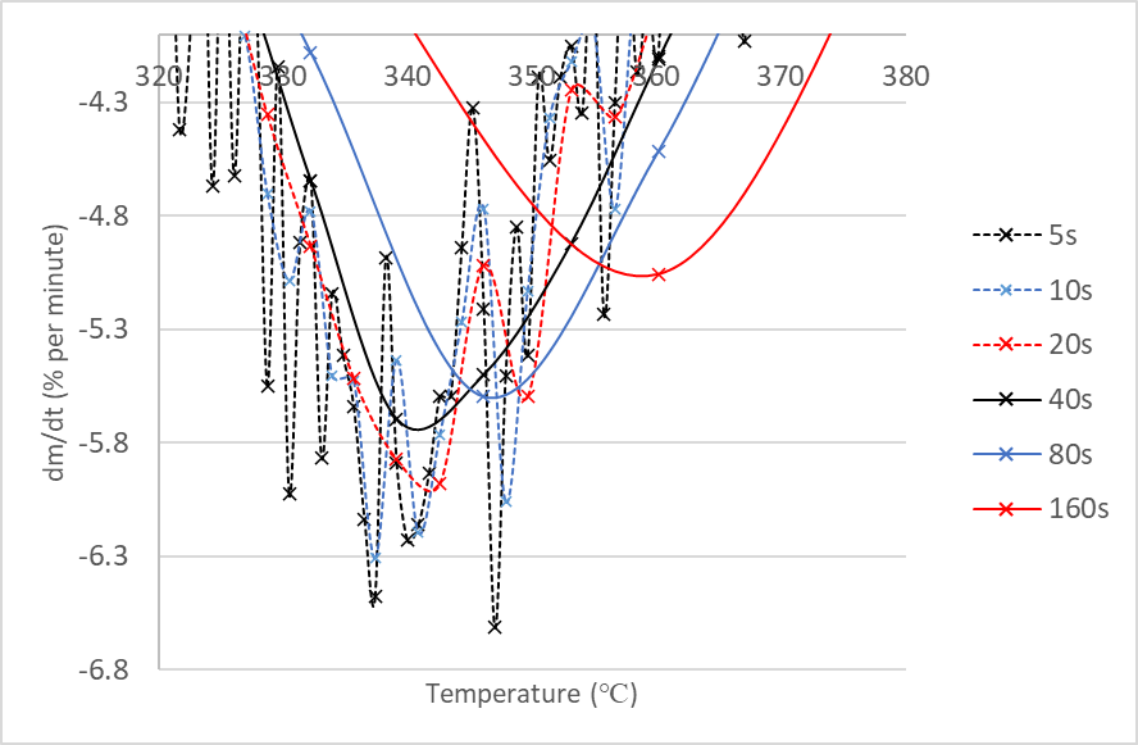

Figure 2.9. *Detail view of main peak of sample LF1 at intervals from 5s to 160s, with individual data points marked.*

Figure 2.8 shows the dTG curves for LF1 for each of the calculated time intervals from 100-500 ℃. The vertical axis has been restricted to ±20 % to improve visualisation. It is seen that when δt = 1.25 s, the degree of noise is reduced by around one order of magnitude, consistent with the results from Figure 2.8, which indicates that the amplitude of noise artifacts is proportional to $\frac{1}{\delta t}$. The inset view, shown in Figure 2.9 more clearly depicts the smoothing of the curve as the value of δt increases.

By visual inspection, the position of the peak is preserved at intervals up to 40 seconds (programmed temperature change 6.66 ^{o}C). At 80 seconds and 160 seconds, there is a progressive shift of the peak upwards in temperature with concurrent flattening, and as such these intervals are too broad to accurately differentiate the TG curve. When filtering using only this method, the optimum interval appears to be around 40 seconds, as this almost eliminates high-frequency oscillation, while preserving data integrity. However, as mentioned above, this value of δt corresponds to a change in temperature of 6.66 ^{o}C, and therefore is likely to limit the ability to resolve small differences in temperature dependent behaviour due to loss of resolution.

It may be possible to further optimise the production of dTG curves by applying a secondary smoothing method to the calculated dm/dt values. Numerical methods based on taking a moving average across a so-called window of data points have previously been found to be capable of producing smoothed dTG curves while preserving key features of underlying thermogravimetric data (5)(7)(8). Two variations of this approach are discussed here.

1. *Simple Moving Average Filtering*

   This method replaces each point in the dTG series with the arithmetic mean of that point and several preceding and subsequent points across a given interval, which is referred to herein as the window.

   In general, this is given by the following for a window size of w.

$$x_n \rightarrow \frac{x_{n-p} + \cdots + x_{n-1} + x_n + x_{n+1} + \cdots + x_{n+p}}{w}, where\ p = \frac{w-1}{2} \tag{2.10}$$

For example, the process for $w = 5$ is as follows.

$$x_n \rightarrow \frac{x_{n-2} + x_{n-1} + x_n + x_{n+1} + x_{n+2}}{5}, since\ p = \frac{5-1}{2} = 2 \tag{2.11}$$

2. *Savitsky-Golay Filtering*

Savitsky-Golay filtering is a numerical method that functions as an extension of the moving average but applies a weighting to each point in the interval and effectively fits a polynomial curve to small intervals of the data (9). In the simplest case, $w = 3$, this takes the following form:

$$x_n \rightarrow \frac{(x_{n-1} + 2x_n + x_{n+1})}{4} \tag{2.12}$$

This can be extended to larger windows by altering the coefficients and denominator.

$$x_n \rightarrow \frac{(-3x_{n-2} + 12x_{n-1} + 17x_n + 12x_{n+1} - 3x_{n+2})}{35} \tag{2.13}$$

$$x_n \rightarrow \frac{(-2x_{n-3} + 3x_{n-2} + 6x_{n-1} + 7x + 6x_{n+1} + 3x_{n+2} - 2x_{n+3})}{21} \tag{2.14}$$

The mathematically equivalent first-order derivative method can be directly applied to the filter thermogravimetric data to produce a very similar dTG curve as shown below for $w = 3$, $w = 5$, and $w = 7$.

$$\frac{dx}{dt} = \frac{-x_{n-1} + x_{n+1}}{2\delta t} \tag{2.15}$$

$$\frac{dx}{dt} = \frac{-2x_{n-2} - x_{n-1} + x_{n+1} + 2x_{n+2}}{10\delta t} \tag{2.16}$$

$$\frac{dx}{dt} = \frac{-3x_{n-3} - 2x_{n-2} - x_{n-1} + x_{n+1} + 2x_{n+2} + 3x_{n+3}}{28\delta t} \tag{2.17}$$

It was thought that it may be preferable for maintaining the data integrity of dTG curves to use an intermediate time-filtering interval of 10 seconds and apply a secondary smoothing method to this data (8)(5). The use of shorter time interval increases the total number of data points available for plotting the curve and reduces the change in temperature between consecutive point, allowing greater resolution of temperature-dependents events, while the smoothing filter normalises these points, bringing them closer to a theoretical line of best fit. To test this assumption and establish the most optimised method for producing dTG curves from the data, a series of smoothing processes were applied to one of the TG data sets at an interval of 10 seconds (1.67 ^{o}C).

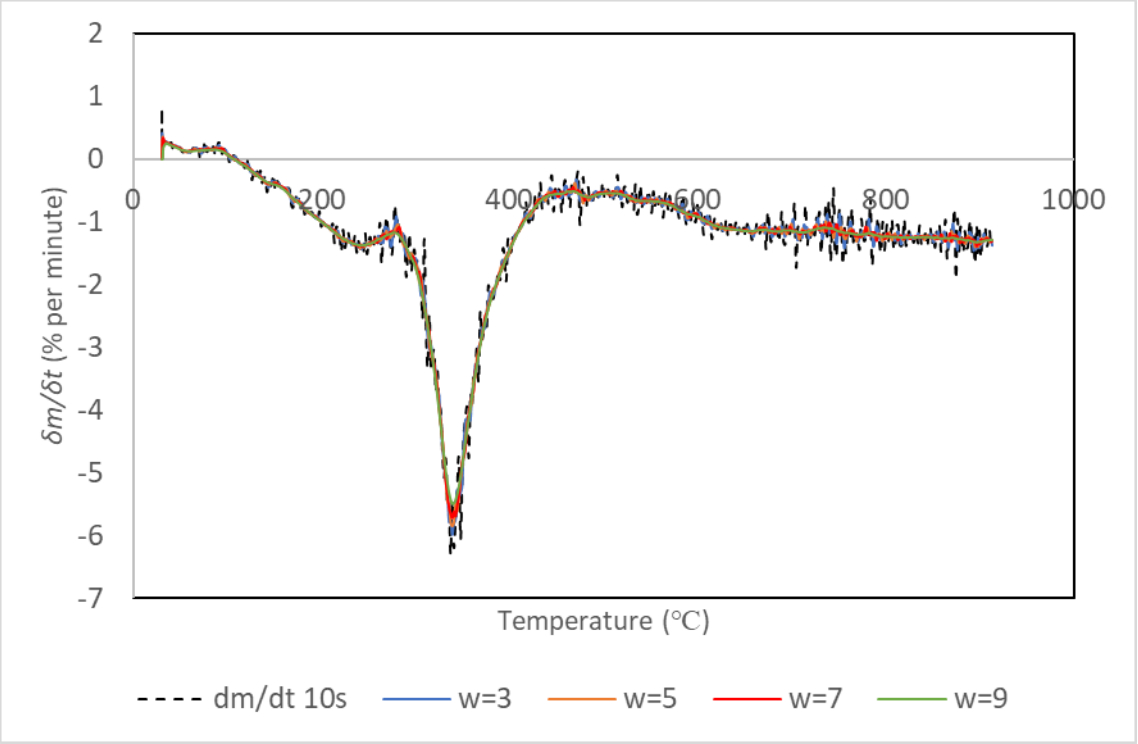

Figure 2.10. *dTG curves for line sample 1 at a filtering interval of 10 s – unsmoothed (grey) and after application of a moving average filter of interval 5 (black)*

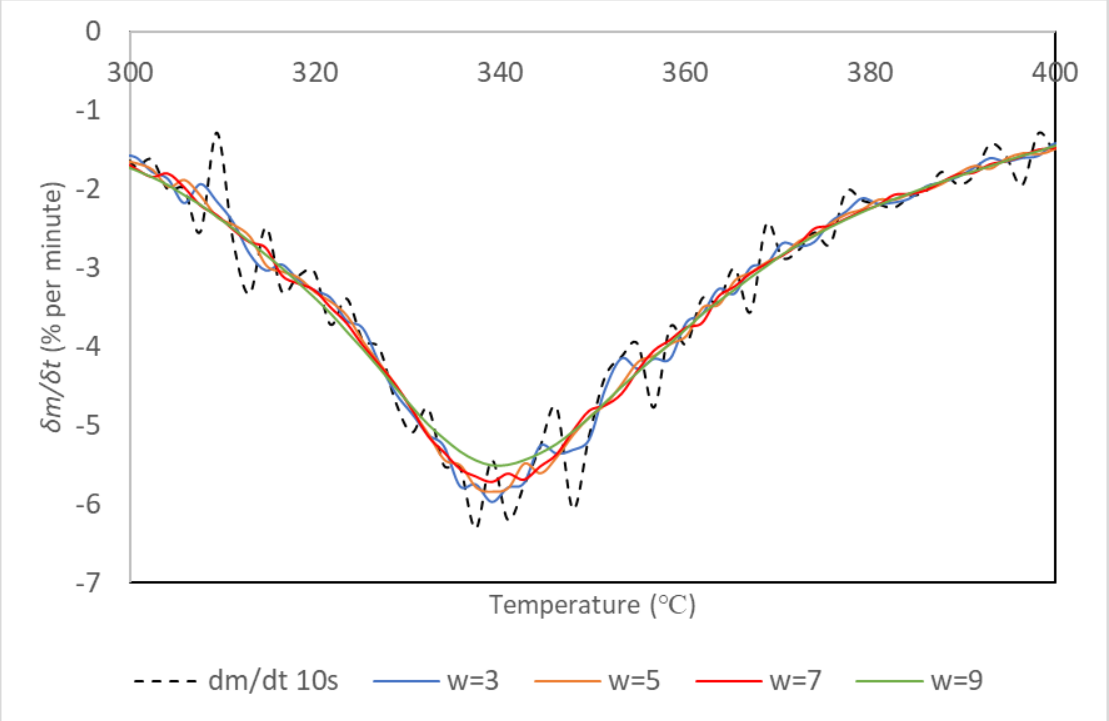

Figure 2.11. *Detail view of largest mass loss peak from line sample 1, unsmoothed (black) and following application of moving average filter at window sizes of 3, 5, 7, and 9*

Inspection of Figures 2.10 and 2.11 demonstrates a reduction in the degree of high frequency noise observed. This effect increased as the size of *w* increased. Table 2.1 shows the position of the mass loss peak in the resulting dTG thermograms.

Table 2.1 Maximum mass loss rate and corresponding temperature for line sample LF-1 following application of moving average smoothing at different window sizes.

Window Size	**T(°C)**	***dm/dt* (% per minute)**
1	337.4	-6.3
3	339.1	-6.0
5	339.1	-5.8
7	339.1	-5.7
9	339.1	-5.5

The position of the peak is preserved using the moving average method, with a value of 339.12 ºC for all *w* between three and nine points in width. A progressive decrease in the calculated maximum value of dm/dt was observed. While the curves generally appear to conform well to the underlying unsmoothed data, it is noted that there was a progressive flattening at the peak as the value of *w* increased.

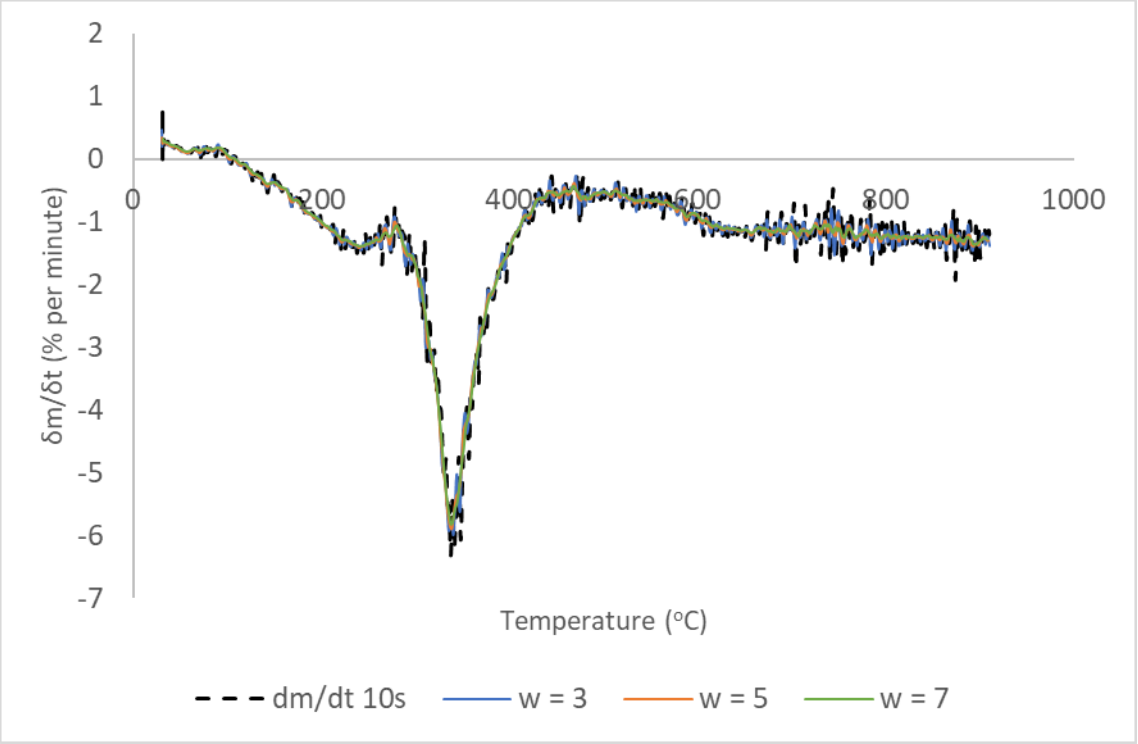

Figure 2.12. *dTG curves for line sample LF1 at a filtering interval of 10s – unsmoothed (black) and after application of Savitsky-Golay filtering at increasing windows size of 3, 5, and 7.*

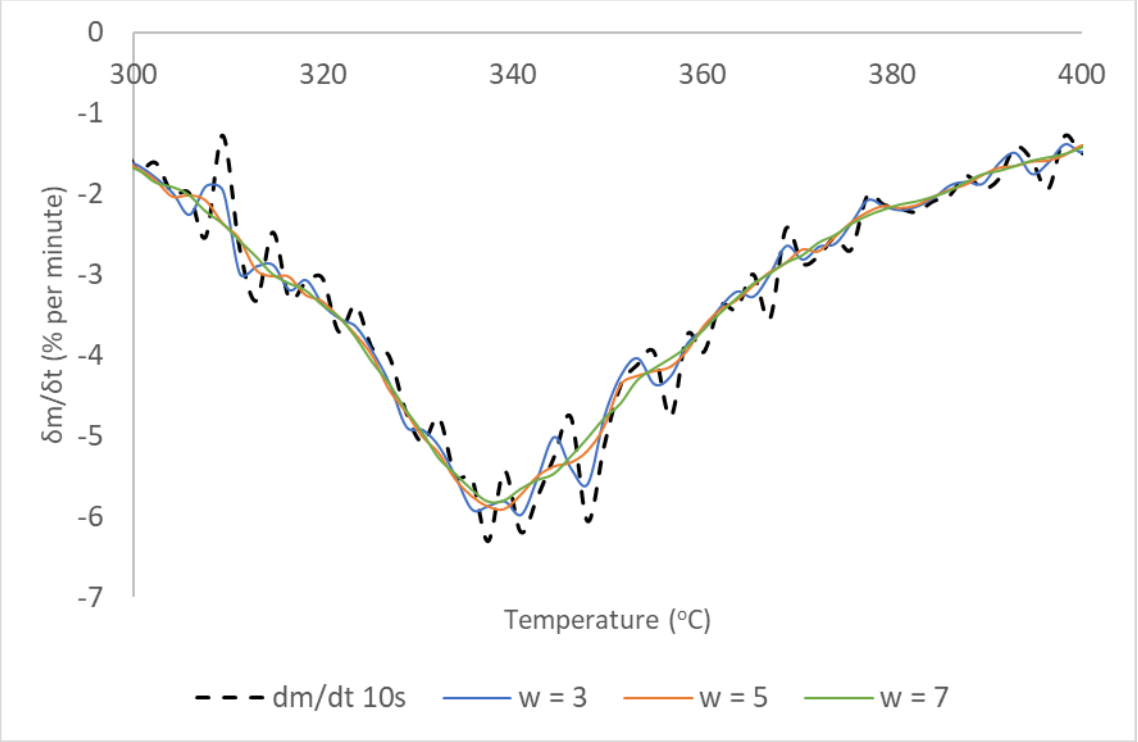

Figure 2.13. *Detail view of largest mass loss peak from line sample 1, unsmoothed (black) and following application of Savitsky-Golay filtering at window sizes of 3, 5, and 7.*

The first-order derivative Savitsky-Golay method was used to produce smoothed dTG curves at intervals of 3, 5, and 7 points. This method produces similar results to the moving average method, but results in less distortion of individual points as a greater weighting is given to the central point of the interval (10). As with the previously applied method, the effect size increases as a wider interval is used, but with relatively less smoothing than a moving average taken over the same interval. At $w = 3$, the apparent noise reduction using a Savitsky-Golay mask is relatively mild and does not produce a sufficient degree of smoothing to clearly visualise features. Noise reduction is significantly improved at window sizes of five and seven. Figure 2.13 shows an inset view of the region around the peak, and it can be seen that the smoothed curves conform well to the shape of the unfiltered data, with fluctuations appearing to be centred around the smoothed curve. Notably, the Savitsky-Golay method results a smaller decrease in the absolute value of $\frac{dm}{dt}$ at the peak than the simple moving average method.

Table 2.2 Maximum mass loss rate and corresponding temperature for sample LF1 following application of Savitsky-Golay filtering at window sizes of 3, 5, and 7.

	T(°C)	**dm/dt (% per minute)**
Unsmoothed (10s)	337.4	-6.3
Savitsky-Golay 3	340.9	-6.0
Savitsky-Golay 5	339.1	-6.0
Savitsky-Golay 7	337.4	-5.8

From Table 2.2, it can be seen that the position of the peak is reasonably well-preserved across the different intervals and when compared to the maximum from the unsmoothed values, falling within 3.5 ^{o}C and exactly matching with a window size of seven. It is also noted that it is somewhat difficult to accurately identify the centre of the peak in unsmoothed data, and that the temperature assigned to the maximum value of $\frac{dm}{dt}$ will tend to capture the most negative noise artifact in the vicinity of the underlying peak. Furthermore, the application of larger window sizes does not induce a progressive shift of the peak further away from the value in the unsmoothed data. However, possible errors resulting from smoothing should be taken into account in comparisons between data sets, and some uncertainty will exist if measured values differ by only a small value.

Further error analysis was carried in an attempt to quantify the accuracy of the smoothed curves. The first step in this process was to produce a deviation value in the y-axis for each point on the smoothed curves as below.

$$Point\ Deviation\ at\ T = (Unsmoothed - Smoothed)\ at\ T \tag{2.18}$$

Where T denotes the temperature. Taking the mass loss peak at 337.39 ^{o}C as an example in the unsmoothed curve and the curve smoothed using a Savitsky-Golay filter with $w = 7$, gives the deviation below.

$$Point\ deviation\ at\ 337.4^{o}C = \frac{dm}{dt}(unsmoothed - smoothed)\ at\ 337.4^{o}C \tag{2.19}$$

$$Point\ deviation\ at\ 337.4 = -6.3\ \% - (-5.8\ \%) = -0.5\ \%$$

A main selection criterion for selecting a smoothing method is that it should not exhibit a significant bias towards the positive or negative direction in the dependent variable (dm/dt). If this is true, then it would be expected that the mean and median of the error values will be close to zero. A significant positive or negative deviation from zero will indicate the direction of any induced bias in the opposite direction. To test this, the point deviations were used to draw box-and-whisker plots for each smoothing method and the data are shown in Figures 3.16.

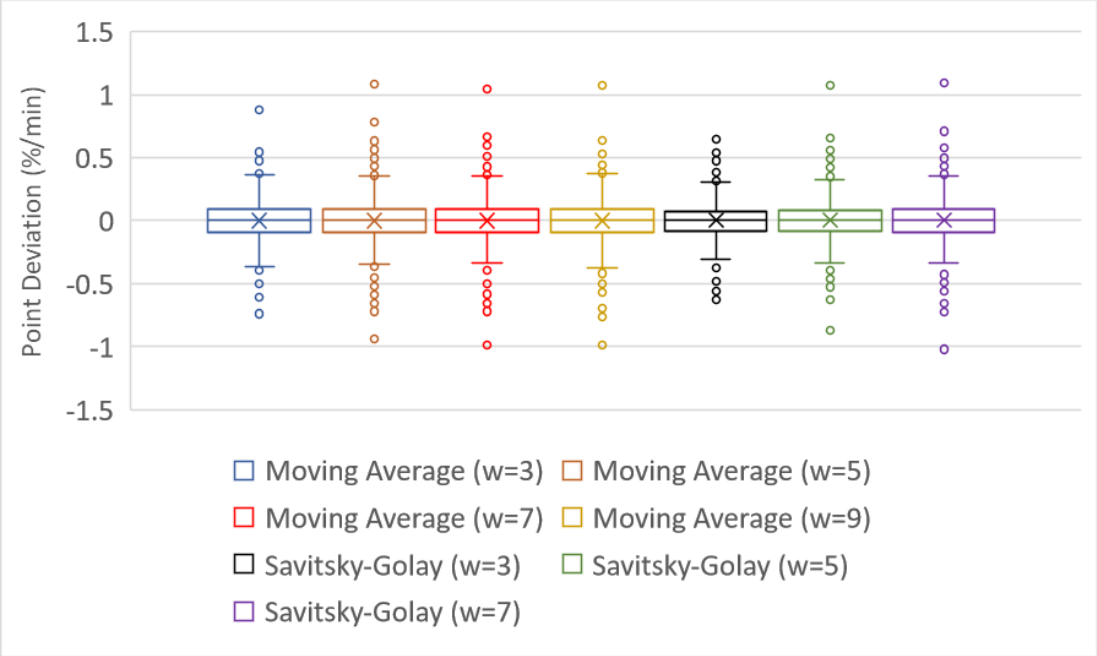

Figure 2.14. *Box-and-whisker plots for point deviations in the y-axis versus unsmoothed data for moving average and Savitsky-Golay filtering methods on line sample LF1*

On inspection, all obtained box plots appear to be near-symmetric with mean and median values close to zero. Table 2.2 below summarises the descriptive statistical values of mean, medium, upper and lower quartiles and skewness derived from each of the box plots in Figure 2.14.

Table 2.3. *Descriptive summary of point deviations from in smoothed dTG curves by smoothing method showing the distribution of distribution of deviations from the unsmoothed curve.*

	Mean	Q_1	Q_2 (Median)	Q_3	Minimum	Maximum	Skewness
3-Mean	0.0005	-0.0943	0.0004	0.0907	-0.3700	0.3624	0.025
5-Mean	-0.0002	-0.0934	0.0001	0.0867	-0.3511	0.3488	-0.016
7-Mean	-0.0002	-0.0906	0.0016	0.0881	-0.3333	0.3510	-0.221
9-Mean	-0.0001	-0.0957	0.0006	0.0918	-0.3738	0.3700	-0.226
S-G 3	0.0021	-0.0835	-0.0002	0.0736	-0.3115	0.3058	0.348
S-G 5	0.0014	-0.0884	0.0029	0.0837	-0.3409	0.3227	0.175
S-G-7	0.0014	-0.0924	0.0041	0.0913	-0.3406	0.3579	-0.098

For all smoothing methods that were employed, the median value for absolute single point deviation was ≤0.0041%. This indicates a close to equal number of positive and negative deviations as, by definition, half of the deviation values will lie to either side of this point. The similar absolute values of the quartile points and minimum and maximum deviations suggest furthermore that the magnitude of positive and negative deviations are alike. This is further supported by mean values in the range -0.0020 to 0.0026, suggesting that there is little bias in the magnitude of deviation and below the smoothed line.

Calculated skewness values all fell within a range of ±0.5, generally taken to indicate a nearly normal distribution (11). For each filtering method, a general trend was observed where skewness became moved from positive to negative as the size of *w* increased. Due to the way in which point deviations were calculated, negative values indicate that, at a given temperature point, the smoothed line was less negative than the unsmoothed line, and this conforms with what was intuitively expected based on visual inspection of the smoothed curves (Figures 3.16-3.17). Since calculated values of *dm/dt* are almost all negative in direction, any smoothing method that involves taking an average across a group of points will tend to induce a shift in the positive direction.

The calculated values summarised in Table 2.3 strongly suggest a pattern that is only likely in the case where the smoothed curve passes near to the centre of the fluctuations in the y-dimension in the unsmoothed curve. Referring back to Figure 2.5, these methods produce a smoothed curve that closely conforms to the x-axis (Figure 2.15).

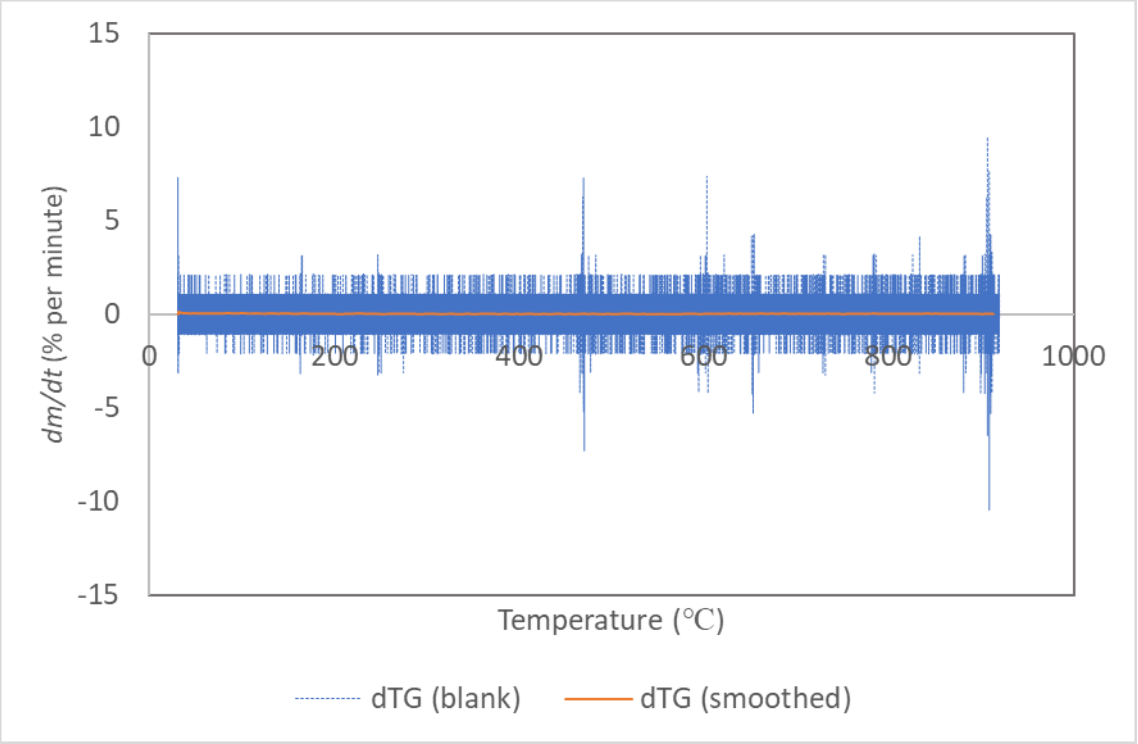

Figure 2.15.. *dTG curve for empty pan reproduced from Figure 2.5 with smoothed curve overlaid produced by applying Savitsky-Golay filter (w=7) over 10 second measurement intervals.*

At the scale of common dTG features, it can be seen that both the quasi-periodic fluctuation around the baseline, and sporadic high-amplitude events are seen to be minimised.

Since both the moving average method at $w = 9$, and the Savitsky-Golay method at $w = 7$ produce a high degree of noise reduction and conform well to the underlying data, the final choice of smoothing method was made based on the preservation of peak features. The analysis carried out for sample 1 suggests that Savitsky-Golay filtering is superior to a simple moving average by this measure, but this has been confirmed by further comparing both methods on samples LF2 and LF3 (Figures 2.16-2.19)

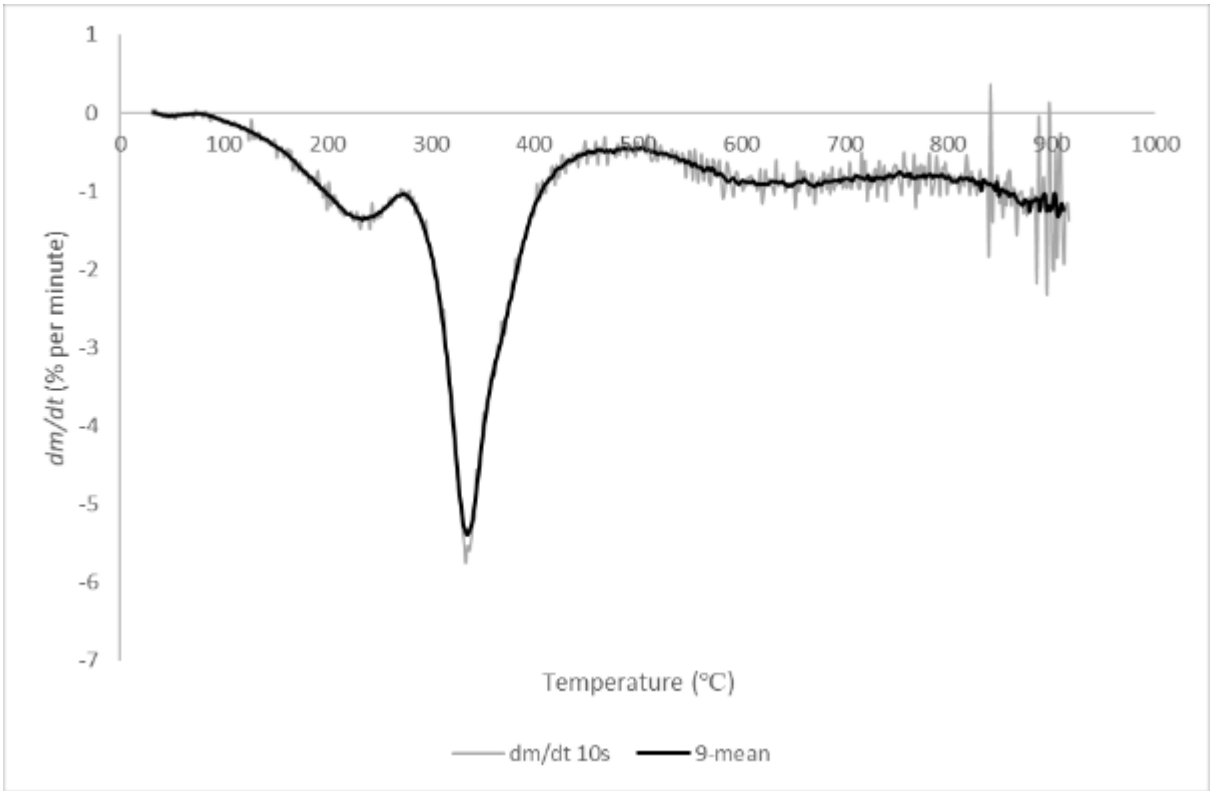

Figure 2.16. *dTG of sample LF2 at filtering interval of 10 seconds with moving average smoothing applied across a window size of nine points.*

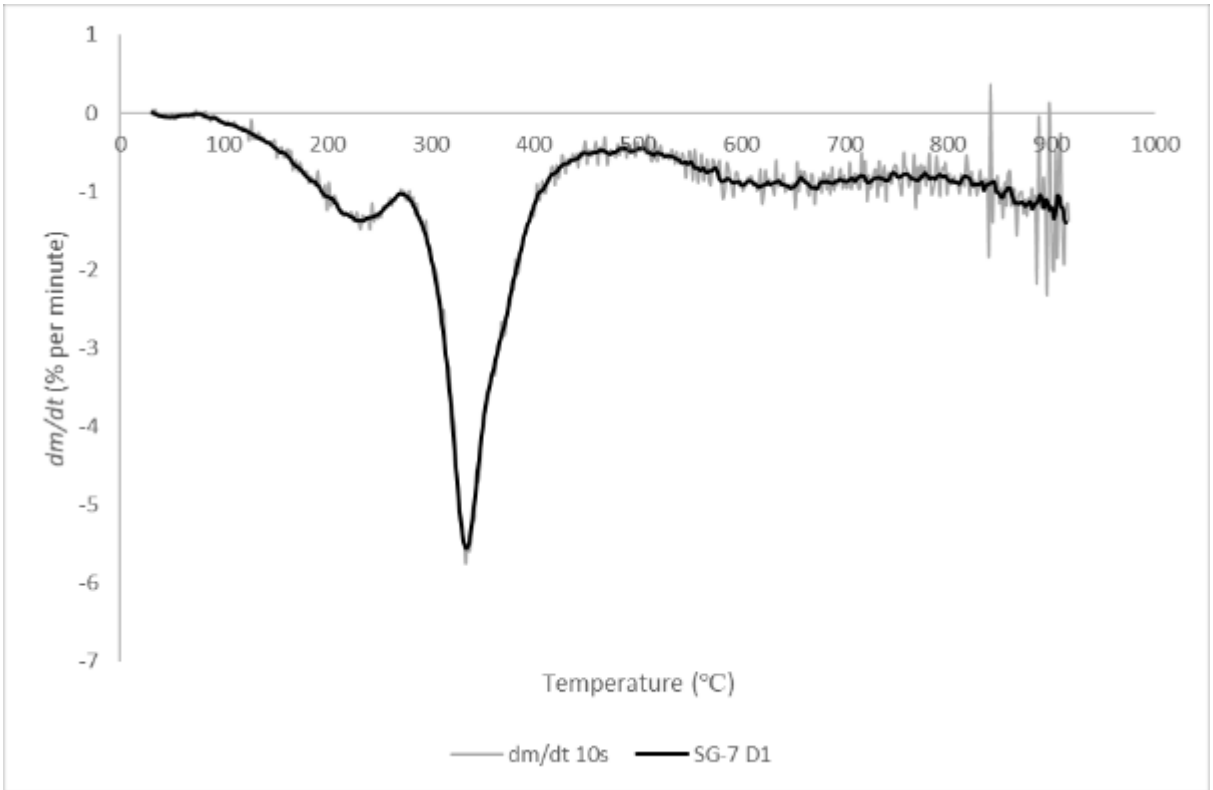

Figure 2.17. *dTG of sample LF2 at a filtering interval of 10 seconds with first-order derivative Savitsky-Golay mask applied with window size of 9.*

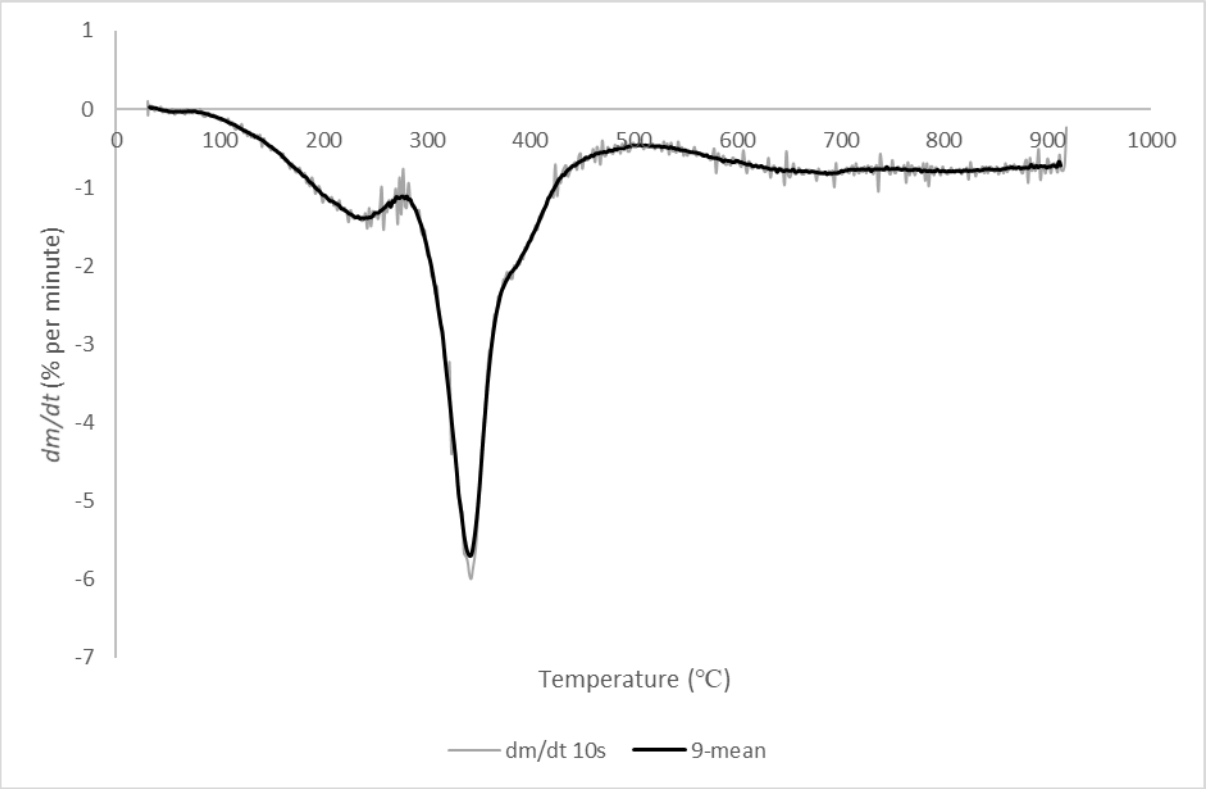

Figure 2.18. *dTG of sample LF3 at filtering interval of 10 seconds with moving average smoothing applied across a window size of nine points.*

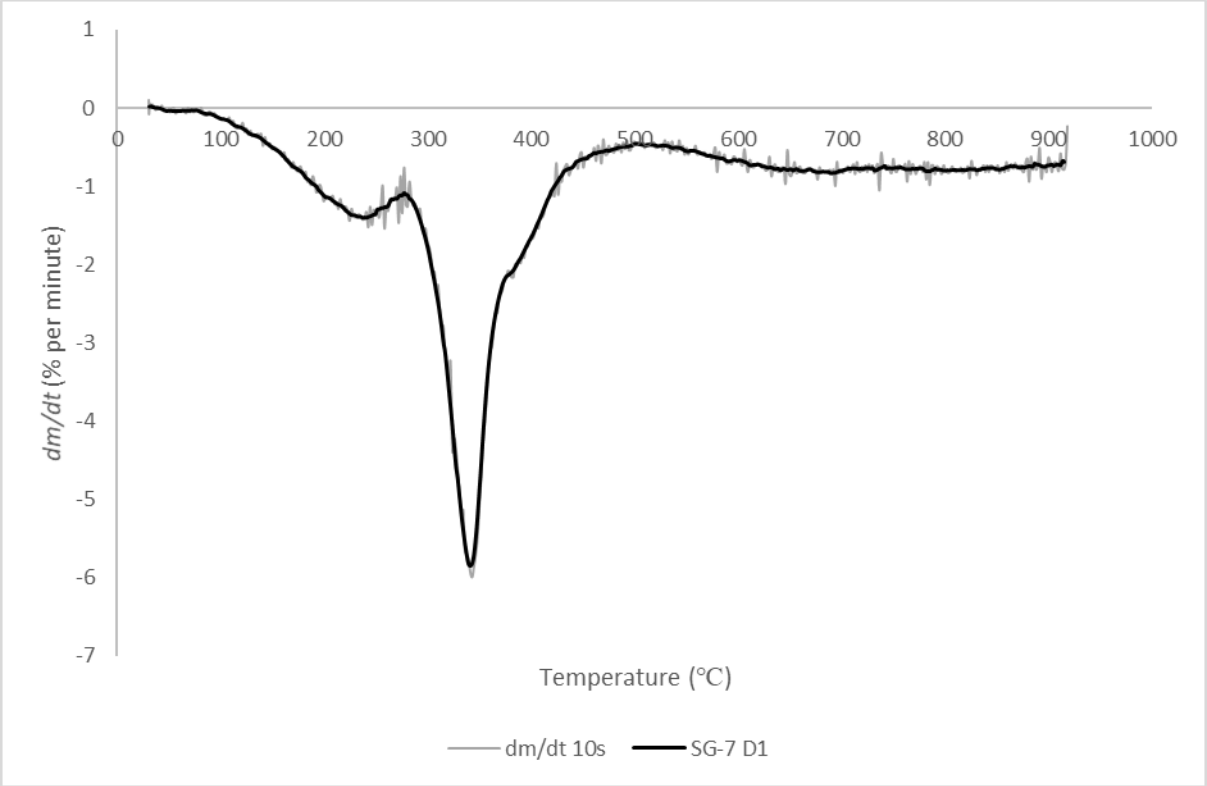

***Figure 2.19**. dTG of sample LF2 at a filtering interval of 10 seconds with first-order derivative Savitsky-Golay mask applied with window size of seven points.*

The unsmoothed dTG curves produced after time-filtering exhibit varying degrees of residual data noise (Figure 2.16-2.19). Sample LF2 overall appears to exhibit less noise than LF1 but the level of noise generally increases above 500 ºC and especially above 850 ºC where particularly large fluctuations are observed. Sample LF3 exhibits relatively little residual noise throughout. At a 10 s time-filtering interval, it is expected that the impact of the regular baseline fluctuation would be reduced by a factor of around 80 based on the previously observed inverse relationship with δt and would therefore be effectively eliminated from the resultant dTG curve. These noise variations therefore likely represent difference in extrinsic sources of vibration within the vicinity of the instrument.

In all cases, the combination of time-filtering over a 10s interval with either Savitsky-Golay or moving average smoothing produced a relatively low-noise curve that appeared, under visual inspection, to closely conform to the underlying unsmoothed data. The only noticeable deviation from this is at the point of the sharp peak in the 333-343 ºC temperature range. Due to the narrowness of this peak, a degree of flattening is induced by the smoothing procedure. This is displayed in the Table 2.4.

Table 2.4. *Mean location and amplitude of largest mass loss peak in samples LF1, LF2 and LF3 in unsmoothed data and after application of Savitsky-Golay filtering (w = 7) and moving average filtering (w = 9) over 10 second measurement intervals.*

	T(°C)	***dm/dt* (% per minute)**
LF 1 Unsmoothed	337.4	-6.3
LF1 Savitsky-Golay	337.4	-5.8
LF1 Moving Average	339.1	-5.5
LF2 Unsmoothed	333.5	-5.8
LF2 Savitsky-Golay	333.5	-5.5
LF2 Moving Average	335.3	-5.4
LF3 Unsmoothed	342.9	-6.0
LF3 Savitsky-Golay	341.2	-5.9
LF3 Moving Average	341.2	-5.7

Based on these findings, it was determined that a combination of time-filtering over an interval of 10 seconds and secondary smoothing using a Savitsky-Golay first-order derivative method would produce smooth dTG curves without introducing significant loss of resolution and would most accurately reflect the position of peaks in the underlying data. All dTG curves in this thesis have therefore been prepared using this method.

Data Analysis

For the purposes of analysis, the onset of significant mass loss was generally taken as occurring at the temperature at which residual corrected mass was <97.5 % of the initial sample mass. This choice of threshold may be regarded as somewhat arbitrary but it provided a consistent data point in the graphs for comparison across multiple samples. In addition, the selection of this value appeared to reduce the impact of variations in the TG baseline, as extrinsic mass drift was more pronounced in the lower temperature regions of the TG curve.

2.3 Furnace Treatment

2.3.1 Background

While thermogravimetric analysis is a powerful tool for investigating thermal stability, the milligram-scale masses of typical TGA samples limits the applicability of these results to larger scales. Bulk effects related to heat transfer, which may be particularly pronounced in materials

with low thermal conductivity, are likely to be less prominent in very small samples. The analysis of larger samples on the gram-scales has been carried out to account for such effects with the intention of providing a closer indication of the typical thermal behaviour of PIR foams as pertains to their use as construction materials.

As an example, increasing the dimensions of a sample results in a smaller surface-area to volume ratio in a square-cube relationship.

$$A_2 = A_1 \left(\frac{l_2}{l_1}\right)^2 \tag{2.20}$$

$$V_2 = V_1 \left(\frac{l_2}{l_1}\right)^3 \tag{2.21}$$

Where V_1/V_2, A_1/A_2, and l_1/l_2 represent the volume, area, and length of two geometrically similar objects.

Therefore, while doubling the dimensions of a sample increases the surface area and therefore heat flow into the surface by a factor of 4, the volume into which this heat is distributed has increased by a factor of 8. Hence, assuming a constant volumetric heat capacity, the overall temperature increase would be halved for the larger sample. However, the very low thermal conductivity and correspondingly high thermal inertia of the materials under investigation in this thesis will have resulted in slow inward heat transfer, with the outside of the material heating more rapidly than the inside. This will have resulted in a steep temperature gradient across the samples. Thus, the absolute surface-to-core temperature differential for TGA samples was limited by their millimetre-scale dimensions but was more pronounced for samples with dimensions of several centimetres. This was especially important in rapid heating experiments.

Furthermore, heating of larger samples allowed for the larger-scale phenomena to be more readily observed. Such phenomena included colour change, swelling and shrinkage, the formation of cracks and fissures, and the gross morphology of surface charring.

2.3.2 Sample Preparation

Samples were measured and hand-cut from foam slabstock to dimensions of 35 x 25 x 20 mm (±2 mm). Swarf resulting from the cutting process was removed from the surface of by means of gentle abrasion. Samples were photographed and weighed on a precision balance. The mass of these samples was typically in the range of 0.6-0.8 g which is 60-80 times greater than typical TGA samples.

2.3.3 Heat Treatment

Heating experiments were carried out in an ashing furnace (CarboliteGero AAF). Samples were arranged on a steel tray and inserted into the centre of the furnace chamber. Two experimental procedures were followed, slow-ramp and flash heating.

2.3.3.1 Slow-ramp Heating

Slow-ramp furnace heating was intended to replicate conditions roughly analogous to those used in TGA experiments. Since mass could not be constantly monitored within the furnace, batches of samples were heated in temperature steps. The heating rate was set at 10 ^{o}C per minute, which was the same heating rate as that used in the TGA measurements. Seven samples were arranged on the sample tray, and this was placed into a furnace at ambient temperature. The samples were then subjected to the heating program shown in Figure 2.20.

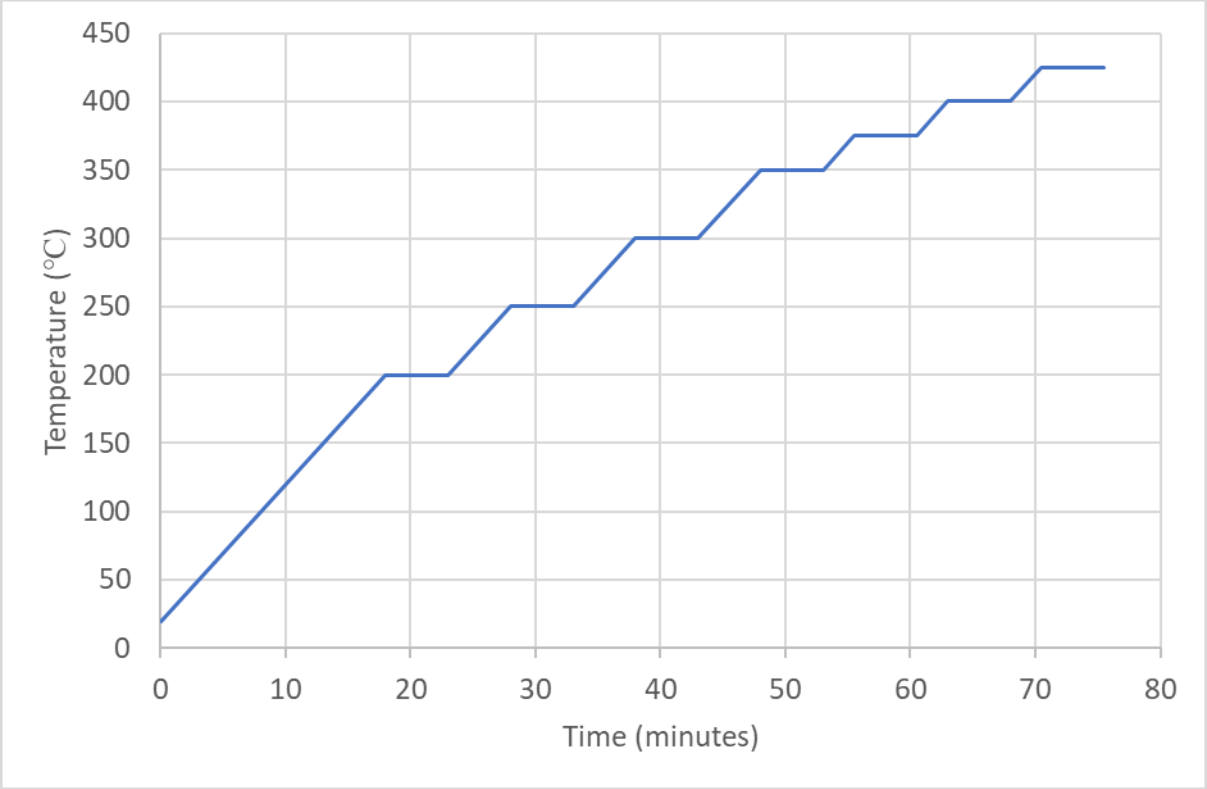

Figure 2.20. *Heating profile for slow-ramp heating furnace experiments showing constant ramp rate of 10 °Cmin^{-1} with intermittent dwells at 200 °C, 250 °C, 300 °C, 350 °C, 375 °C, 400 °C and a final dwell at 425 °C.*

At each of the dwell temperatures (200, 250, 300, 350, 375, 400 and 425 °C) one sample of foam was removed from the oven and allowed to cool to room temperature for future analysis. A five-minute dwell was then performed at each dwell temperature before the ramp rate was resumed.

Figure 2.21. *Photographs of unheated foam samples (left) and after heating (right). Sample numbers from 2-8 correspond to final heating temperatures of 200 °C, 250 °C, 300 °C, 350 °C, 375 °C, 400 °C, and 425 °C in ascending order.*

2.3.3.2 Flash Heating

The flash heating method was used to rapidly heat samples to an elevated temperature by pre-heating the furnace to a specified temperature and rapidly inserting the sample. Flash heated samples were generally exposed to temperatures above 450-600 °C for a period of 30 seconds.

2.3.4 Basic Sample Analysis

Following removal from the furnace samples were photographed, measured and re-weighed to quantify dimensional change and mass loss.

2.4 FT-IR Analyses of Foams and Residues

2.4.1 Background

Thermogravimetric analysis is a powerful technique for locating temperature-dependent processes occurring during the heating of materials but do not provide the molecular information required to characterise the underlying physicochemical processes. Within the

scope of this thesis, TGA has been coupled with molecular spectroscopy techniques to elucidate the chemical changes that occur during the thermolytic and oxidative degradation of PIR foams. The first of these techniques considered here is the application of infrared spectroscopy in the 750-4000 cm^{-1} wavenumber range on unheated foams and the solid residual material obtained during furnace treatment at a range of temperatures from 200-425 ^{o}C.

Attenuated total reflectance (ATR) is a sampling technique which allows FT-IR analysis to be applied to solid samples without the need for additional preparation. In this technique, the sample is brought into intimate contact with the ATR crystal, through which an IR beam is internally reflected. An evanescent wave is generated at the crystal-sample interface, propagating within the surface layer of the sample to a depth of around 1 µm. This limits the analysis of the sample composition to a very thin layer and means that ATR-FTIR is primarily suited to surface analysis or samples of homogeneous composition.

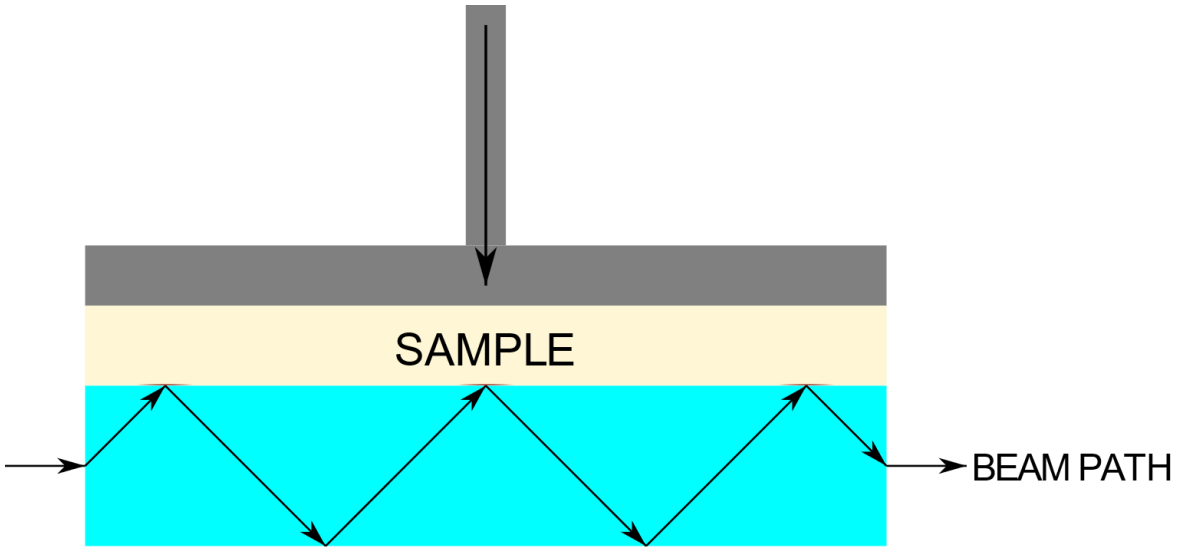

Figure 2.22. *Schematic illustration of ATR-FTIR showing beam path through crystal and evanescent wave propagation from internal reflection of beam at sample surface.*

2.4.2 Sample Preparation

Sections of 5 mm x 5mm x 2 mm were cut from foam samples or from residual material obtained after furnace heating for ATR analysis. Samples were analysed by placing them on the ATR-IR crystal without any further preparation.

2.4.3 Experimental Procedure

ATR-FTIR analyses were carried out using a Perkin-Elmer Spectrum Two IR spectrometer with an ATR accessory. Perkin Elmer Spectrum software was used for data acquisition. Upon initialising the software, the sample retention arm was moved into position and lowered so that it sat around 1 mm from the surface of the crystal and a background scan was carried out. For data acquisition from samples, the sample was placed on the ATR crystal and the instrument was switched into monitoring mode. The sample retention clamp was then tightened until peaks could be clearly distinguished and a minimal amount of noise was observed. Scans were carried out across a wavenumber range of 4000 cm^{-1} to 400 cm^{-1} with a resolution of 1 cm^{-1} and an accumulation number of 8.

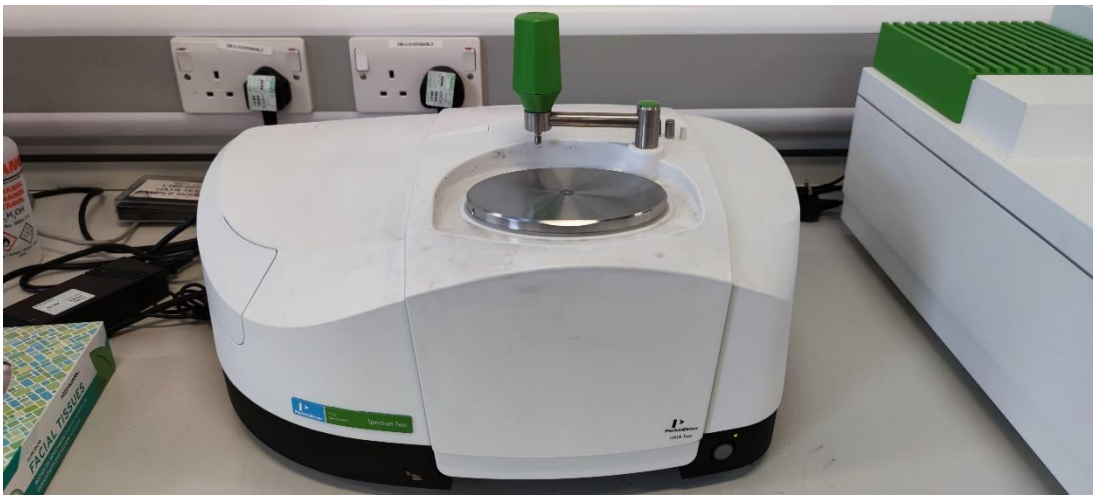

Figure 2.23. *Photograph of Perkin-Elmer Spectrum Two FT-IR spectrometer with ATR accessory.*

Figure 2.24. *Positioning of foam sample in contact with ATR crystal.*

2.4.4 Data Processing

Data was exported from the Perkin Elmer Spectrum software in the *.csv* format and copied into Excel. For unheated foam samples, the absorbance data for each wavenumber were normalised by conversion into relative intensities taking the aromatic C=C stretch at around 1595 cm^{-1} as a value of 1.

$$Relative\ Absorbance = \frac{A_{\bar{\nu}_n}}{A_{\bar{\nu}_{1595}}} \tag{2.22}$$

The C=C stretch was selected as the fixed point since this functional group is already present in 4,4-MDI and the aromatic polyester polyol and is not affected by the blowing, gelling and trimerization reactions which occur during the foaming process.

2.5 Pyrolysis-Gas Chromatography-Mass Spectrometry

2.5.1 Background

Gas chromatography-mass spectrometry (GC-MS) is a common and powerful analytical technique for the identification of chemical species within a sample. Species within a gaseous

sample are separated in the GC column by their interaction with the stationary phase lining the column. Individual species progress through the column at different rates based on their physical and chemical properties and are separated based on their final retention time. These products are then introduced to the MS and fragmented and ionised at the ion source with the resultant ions being separated on the basis of their mass-to-charge (m/z) ratio.

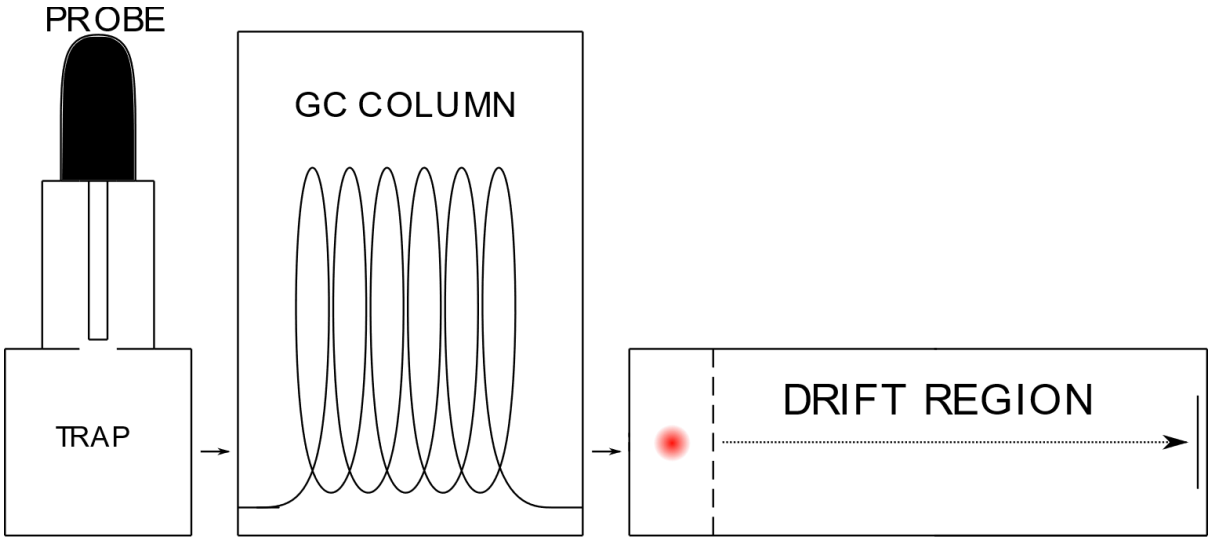

Figure 2.25. *Schematic Illustration of Py-GC/TOF-MS*

In the case of the analysis carried out in this thesis, a time-of-flight mass spectrometer was used. In this type of instrument, separation is achieved by accelerating the ions using an electric field of known strength.

When a charged particle is exposed to an electric field, its potential energy is the product of the particle's charge and the voltage of the field as below.

$$E_p = qU \tag{2.23}$$

Where E_p is the potential energy, q is the charge and U is the accelerating voltage.

This potential energy is converted to kinetic energy in the time-of-flight tube. The kinetic energy of an object being given by the following:

$$E_k = \frac{1}{2}mv^2 \tag{2.24}$$

By conservation of energy it follows that:

$$E_p = E_k \therefore qU = \frac{1}{2}mv^2 \tag{2.25}$$

Velocity can be substituted for displacement over time, giving the following:

$$qU = \frac{1}{2}m\left(\frac{d^2}{t^2}\right) \tag{2.26}$$

Rearrangement to isolate t^2 on the left-hand side gives the following:

$$t^2 = \frac{d^2 m}{2qU} = \frac{d^2}{2U} \cdot \frac{m}{q} \tag{2.27}$$

Since the length of the time-of-flight tube and the accelerating voltage are fixed quantities within the context of a single instrument set-up, $\frac{d^2}{2U}$ can be treated as a constant and it is therefore shown that:

$$t^2 = k\frac{m}{q} \therefore t \propto \sqrt{\frac{m}{q}} \tag{2.28}$$

Therefore ions possessing a higher mass to charge ratio will take longer to pass through the drift region and will arrive at the detector later, achieving separation and allowing m/q to be quantified.

Of particular interest within the scope of this work are the products resulting from pyrolysis reactions. By coupling a pyrolysis device to the inlet of a GC-MS, pyrolysis reactions can be performed *in situ* with immediate analysis and characterization of their products. Analysis of fixed gases such as CO, CO_2, and H_2 in pyrolysis products can also be achieved be carried out by directing the products through a fixed gas analyser, which is effectively a gas chromatograph with a column optimised for separating low molecular weight compounds, which can be identified based on physical properties such as thermal conductivity.

The pyrolysis device used in this work was the CDS™ Pyroprobe 5150. Flash pyrolysis was carried out by placing the sample tube containing a small sample (~100 µg) within a resistive platinum heating coil. When a current was applied to this coil, heating rates of up to 20,000 $^{o}Cmin^{-1}$ were achieved, heating the sample almost instantaneously to a target temperature. The products were then flushed into a sorbent trap. This trap was then flash heated

to the desired inlet temperature so that all the analytes were desorbed together and from there the analytes were transferred via heated transfer line to either the GC-MS or the FGA. Figure 2.26 shows a schematic illustration of the pyrolyser probe tip.

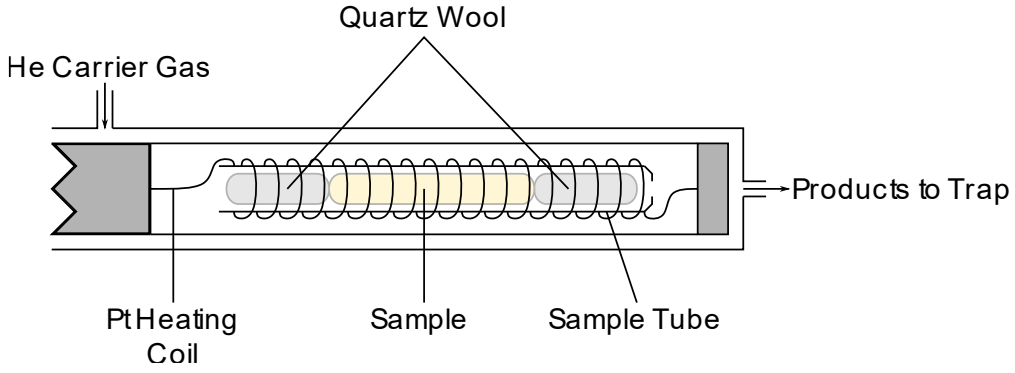

Figure 2.26. *Pyrolyser sample probe detail*

2.5.2 Sample Preparation and Data Collection

Prior to running samples, a trap cleaning method was run on the pyrolyser to remove any residual products held in the trap from previous runs. Empty tubes were run through the GCMS, firstly to remove any residual species from the GC column and then to identify the products passing from the column due to background column bleed.

Foam samples were placed in the sample tube with quartz wool above and below the sample. This was done to ensure that the sample was position roughly in the centre of the heating coil and to prevent any particulates from potentially entering the analysers. Sample mass was captured by weighing the empty tube, the tube with the quartz wool, and the tube with quartz wool and sample. Sample masses were found to be in the region of 100 µg.

The probe was inserted into the pyrolyser and the pyrolyser running method was set in the Pyroprobe software. Heating rate was set to maximum (nominally 20,000 ^{o}C/s) and probe temperature methods were set for 200 ^{o}C, 250 ^{o}C, 300 ^{o}C, 350 ^{o}C, 400 ^{o}C and 800 ^{o}C. The trap temperature was set at 300 ^{o}C.

The GC inlet temperature and pressure were set to 250 ^{o}C and 30 Pa. The GC oven was set to ramp from 40-250 ^{o}C at 10 ^{o}Cmin^{-1}, to trigger on receiving a signal from the pyrolyser. The standard full-scan method was used for the MS. When the ready signal was received from the GCMS, the pyrolyser was manually triggered.

2.5.3 Data Processing

At the end of the sample run, GCMS data was processed using the recommended standard processing method. The total ion chromatogram (TIC) and base peak chromatograms were

exported along with the peak table containing best matches cross-referenced from the NIST MS library.

The TIC chromatograms were plotted in Excel, and the peak table was filtered using the following method. All peaks with an area ≥10 % of the largest peak were identified by calculating a threshold value by applying the following formula to the peak area column:

$$Threshold\ Area = \frac{MAX(Peak\ Area)}{10} \tag{2.29}$$

Conditional formatting was used to highlight all peaks where peak area ≥ threshold area. Peaks identified from blank tube runs as column products were disregarded. The remaining peaks were plotted against retention time in a scatter chart with no line. For visualisation the data points were converted to vertical lines by applying a vertical error bar in the negative direction at 100 %.

Chapter 2 Bibliography

1. Heal GR. Thermogravimetry and Derivative Thermogravimetry. In: Principles of Thermal Analysis and Calorimetry. 2002. p. 10–54.

2. Zhang L, Zhang M, Hu L, Zhou Y. Synthesis of rigid polyurethane foams with castor oil-based flame retardant polyols. Ind Crops Prod. 2014;52:380–8.

3. Chuang FS, Tsi HY, Chow JD, Tsen WC, Shu YC, Jang SC. Thermal degradation of poly(siloxane-urethane) copolymers. Polym Degrad Stab. 2008;93(10):1753–61.

4. Wang C, Wu Y, Li Y, Shao Q, Yan X, Han C, et al. Flame-retardant rigid polyurethane foam with a phosphorus-nitrogen single intumescent flame retardant. Polym Adv Technol. 2018;29(1):668–76.

5. Chen HX, Liu NA, Shu LF, Zong RW. Smoothing and differentiation of thermogravimetric data of biomass materials. J Therm Anal Calorim. 2004;78(3):1029–41.

6. Palmer LD. Sources of error in thermogravimetry: Balance inclination and specimen temperature. J Phys E. 200AD;19(9):919.

7. Junmeng C, Di X, Zhujun D, Xi Y, Yang Y, Banks SW, et al. Processing thermogravimetric analysis data for isoconversional kinetic analysis of lignocellulosic biomass pyrolysis: Case study of corn stalk. Renewable and Sustainable Energy Reviews. 2018;82(3):2705–15.

8. Onsree T, Tippayawong N. Application of Gaussian Smoothing Technique in Evaluation of Biomass Pyrolysis Kinetics in Macro-TGA. Energy Procedia. 2017;138:778–83.

9. Savitsky A, Golay MJE. Smoothing and Differentiation of Data by Simplified Least Squares Procedures. Anal Chem. 1964;36(8):1627–39.

10. Guiñón JL, Ortega E, García-Antón J, Pérez-herranz V. Moving Average and Savitzki-Golay Smoothing Filters Using Mathcad. International Conference on Engineering Education. 2007;(1):1–4.

11. Klima K. Good Data. 2021. p. https://community.gooddata.com/metrics-and-maql-kb Normality Testing: Skewness and Kurtosis.

3 Thermal Analysis of Polyisocyanurate Foams

3.1 Introduction

Polyisocyanurate (PIR) foam is a common insulation material often used as the core material in structural insulated panels (1)(2). The specific thermal conductivity (λ) of PIR foam is typically reported as 0.021-0.028 W/mK (3), indicating that PIR is one of the most effective of common insulation materials per unit thickness.

As is the case for almost all synthetic organic polymers, PIR is inherently combustible, although it is sometimes regarded as being more fire resistant than some other common polymer insulation materials such as polyurethane and polystyrenes (4). It has long-been known that the apparent flaming combustion of most solid and liquid materials occurs in the gas-phase within a turbulent interface layer between the material and the surrounding atmosphere in which gaseous species produced by the thermolysis of the material mix with and undergo exothermic reactions with oxygen (5).

Hence, within this chapter, a comprehensive analysis of the thermal behaviour of an existing commercial PIR foam formulation has been conducted, encompassing both foams produced on an industrial production line and hand-mixed foams produced using the same components. The thermal stability of these foams has been characterised using thermogravimetric analysis.

3.2 Methods Related to this Chapter

Line-produced foam samples were provided by the project industrial sponsor Tata Steel Building Systems UK (Shotton, N. Wales). These foams were produced in situ as part of a steel-faced sandwich panel construction. The usual method of construction of Tata's commercial insulation panels is shown in Figure 3.1. The usual thickness of the core material is 45-135 mm depending on insulation requirements.

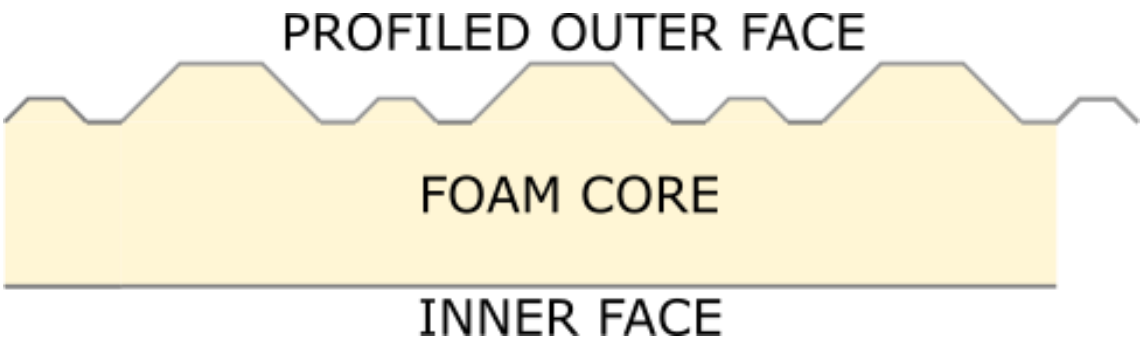

Figure 3.1. *Cross-sectional schematic of typical steel-faced, polyiso-filled sandwich panel.*

The primary reactive components of the PIR foam studied in this chapter were a commercial preparation of oligomeric MDI with a functionality of 2.9 and 30-31 % free isocyanate content, and a polyol blend comprising a phthalic anhydride-diethylene glycol polyester co-polymer and free diethylene glycol. The hydroxyl value of this polyol blend was 240 mgKOH/g. The polyol blend also contained a 5-10 % loading of the non-reactive halogenated fire retardant TCPP. These components were present in a mass ratio of ~2:1. Based on these values an approximate range of isocyanate indices can be calculated as follows.

$$Moles\ of\ NCO\ per\ gram = \frac{Mass\ of\ MDI\ \times NCO\ Content}{Molar\ Mass\ of\ NCO} \tag{3.1}$$

Where NCO is the reactive isocyanate group and MDI is 4,4-methylene diphenyl diisocyanate.

By this, each gram of crude methylene diphenyl diisocyanate contains 0.0071-0.0073 moles of reactive isocyanate groups.

The hydroxyl value is the number of milligrams of KOH required to neutralise the quantity of acetic acid taken up in the acetylation reaction between acetic acid and one gram of the polyol and serves as a measure of the quantity of free hydroxyl groups. The standard method involves the acetylation of the test material using a specified quantity of acetic anhydride in pyridine solvent under reflux conditions (6)

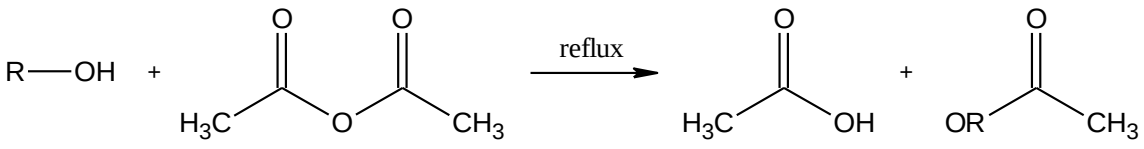

Reaction 3.1. Reaction of polyol hydroxyl group with acetic anhydride producing acetate and acetic acid.

This reaction is run to completion, after which excess acetic anhydride is converted to acetic acid by hydrolysis.

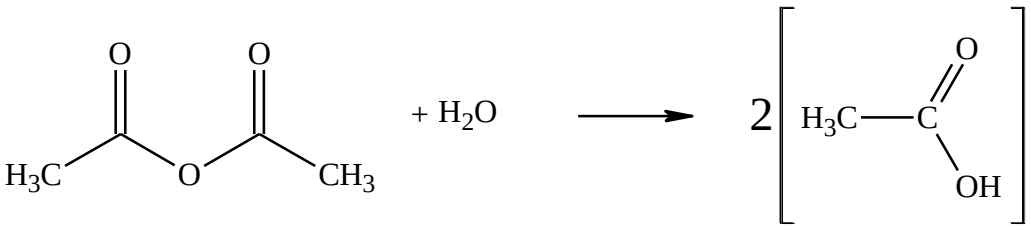

Reaction 3.2. Hydrolysis of acetic anhydride to acetic acid.

The resulting acetic acid in the solution is neutralised by titration with potassium hydroxide, producing potassium acetate and water.

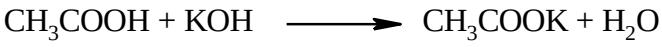

Reaction 3.3. Neutralisation of acetic acid by potassium hydroxide.

The quantity of acid taken up by the acetylation can be calculated by comparing the titre used to neutralise the remaining acid in the test solution against that used in a blank consisting of the same quantity of acetic anhydride pyridine solution as used for the acetylation.

Hydroxyl value, HV, is then calculated using the following:

$$HV = \left[\frac{(56.1)(N)(V_B - V_{acet})}{W_{acet}}\right] + AV \tag{3.2}$$

Where 56.1 g/mol is the molecular weight of KOH, N is the normality of the titrant, V_B and V_{acet} are the volumes of titrant required to neutralise the acetic acid in the blank and test sample respectively, and W_{acet} is the weight of the sample being acetylated, which is typically set to one gram. AV is the acid value of the test substance, representing the presence of carboxylic acid groups in the sample prior to acetylation.

Therefore:

$$Moles[OH/g] = \frac{hydroxyl\ value \div 1000}{molar\ mass\ KOH} = 0.0043$$

The isocyanate index can then be found by calculating the molar ratio of isocyanate to hydroxyl groups as follows.

$$Isocyanate\ Index = \frac{Moles\ NCO}{Moles\ OH + 2 \times Moles(H_2O)} \quad (3.3)$$

Each mole of water consumes two moles of isocyanate since water initially reacts with isocyanate to form a primary amine and CO_2 and this amine can then react with another isocyanate group. Water is added to the reaction at mass ratio of 1:0.005 polyol:water, corresponding to 0.0003 moles at this scaling.

Based on the mass ratio of crude methylene diphenyl diisocyanate and the polyol this gives the lower and upper bounds for isocyanate index of 290 and 298 respectively.

These values indicated that, a maximum of around one-third of the isocyanate content can be consumed through reactions with the polyol and water leaving the remainder available for conversion to isocyanurate and other addition products of isocyanates, and this high isocyanate--hydroxyl ratio is a defining characteristic of PIR materials. An excess of reactive isocyanate groups results in the extensive formation of isocyanurate ring structures, with the high dissociation temperature of these structures contributing the improved inherent thermal stability of PIRs (7)

Initial analysis of line-produced foams was carried out under both inert and oxidative conditions using the standard experimental parameters outlined previously in the methods section. This involved a 5-minute dwell at 30 ^{o}C to allow the sample temperature to stabilise, followed by heating from 30-900 ^{o}C at a constant rate of 10 ^{o}C per minute. This was followed by a final 2-minute dwell at 900 ^{o}C. The dwell regions were included to allow the sample to achieve thermal equilibrium with the surrounding environment and as such were not included in the analysis of the dynamic thermogravimetry.

3.3 Results and Discussion

3.3.1 Thermogravimetric Analysis of Line-produced Foam Samples

3.3.1.1 Determination of TG Baseline

As outlined in the methodology chapter of this work, it is known that the buoyant force of the TG purge gas, along with other factors such as turbulent flow, may exert an influence on the apparent weight of the sample (8). It is therefore essential when considering the validity of results to have first identified the extent and influence of these extrinsic factors. Prior to conducting the initial sample measurements, two blank runs were carried out under nitrogen using an empty sample pan (Figure 3.2).

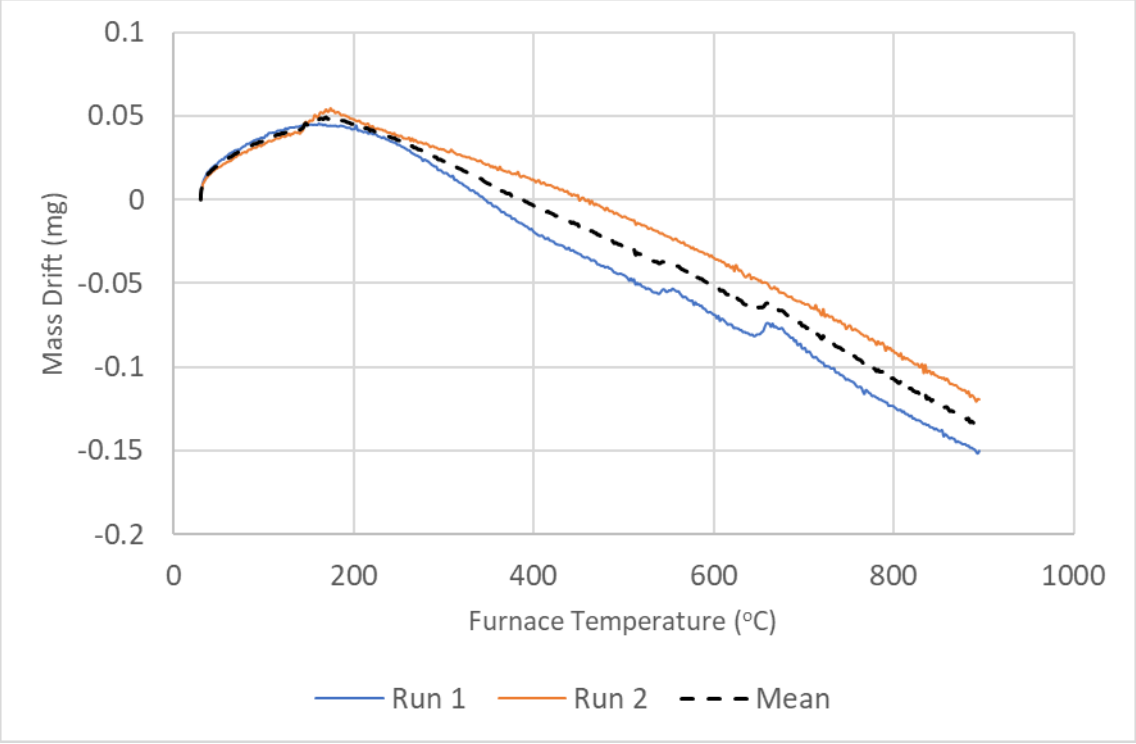

Figure 3.2. *Measured balance drift of empty TG sample pans under nitrogen over 30-900 °C at 10 °C/min*

These curves differed from what would be expected if buoyancy alone was responsible for balance drift, as this would be expected to produce a smooth curve with a quasi-logarithmic form with positive balance drift throughout, conforming to the relationship between the density of the purge gas and its temperature. In these runs, a positive balance drift occurred up to around

150-200 ºC, before reversing in direction. The overall magnitude of the deflection became negative at 360 ºC and 480 ºC in the first and second run, respectively. The complex shape of these curves and the difference between two consecutive runs indicates that this behaviour may be the result of complex and variable interactions between several extrinsic factors and presents a challenge in correcting exactly for baseline fluctuations. However, the overall magnitude of this drift is relatively small, with a maximum value of around -150 µg, less than 2% of a typical initial TG sample mass.

Despite the variations in baseline behaviour, the mean curve produced from these runs has been applied as a correction for mass measurements carried out on this instrument setup, as it still been deemed likely to provide a more accurate baseline than using uncorrected weight data.

3.3.1.2 Thermogravimetric Analysis in Nitrogen

Thermogravimetric analyses for three identical line-produced foam samples are displayed in the Figures 3.3-3.5 below. These samples will be referred to in the text by the identifiers LF1, LF2, and LF3. These samples were taken from a single section of foam core material taken from a panel and were therefore expected to have identical physical and chemical composition to each other due to the homogeneity of the material. These samples should therefore provide a baseline for the typical behaviour of commercial PIR foam and provide an indication of the degree of expected variation in the thermogravimetric behaviour of identical samples.

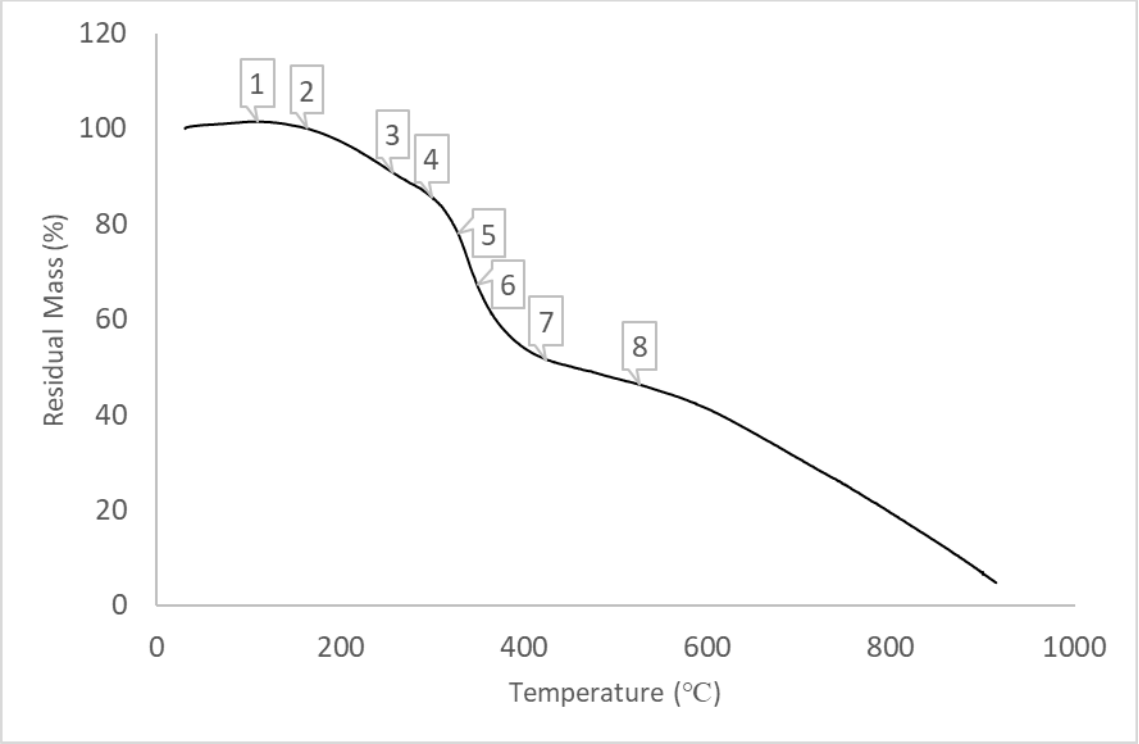

Figure 3.3. *TGA thermogram of line foam sample LF1 under inert atmosphere (initial mass = 11.52mg) with key points labelled. Key points are referenced within the subsequent text using square brackets ([1], [2], etc.)*

For line-produced foam sample LF1, the TGA thermogram exhibits several distinct phases of mass loss occurring across progressive temperature regimes. In the initial phase of heating, from ~30-100 °C a small and gradual increase in mass was observed, reaching a maximum recorded mass increase of 1.49 % (0.17mg) at 109.6 °C [1], before decreasing and returning to initial mass at 160 °C [2]. As per the baseline observations in Figure 3.2, this apparent increase in mass may constitute an artefact arising from buoyancy effects, as these were particularly pronounced in the temperature range 30-200 °C temperature range. From 160-300 °C [2-4], a relatively slow and almost constant rate of mass loss was observed, with a subtle dip in the vicinity of 260 °C [3]. Mass loss in this temperature range is likely to result from the cleavage of urethane linkages (9,10), especially within the hard segments consisting of isocyanates bonded to low molecular weight chain extenders. Overall mass loss in this temperature interval was 15.0 % (1.72 mg) with an average mass loss rate of 1.1 % (0.13 mg) per minute against a heating rate of 10°C per minute. Kinetic studies on pentane-blown rigid polyurethane foams by Pielichowski *et al.* obtained simulated mass losses for these materials of 5-40 % over two hours in isothermal conditions at temperatures ranging from 160-260 °C. Mass loss then accelerates from 300-330 °C [4-5], with a further mass loss of 8.6 % (0.99 mg) occurring across the

interval. The most rapid mass loss occurred from ~330-350 ºC [5-6], with a mean rate of 5.5 % (0.63 mg) per minute and a total mass loss of 10.5 % (1.21 mg). Mass loss slowed markedly from 350-425 ºC [6-7] before remaining linear, accelerating again above 525 ºC [7-8]. Several selected data points were recorded for comparison with other samples, being the sample temperature at which a given total mass loss had occurred. The selection of these thresholds was somewhat discretionary but were more closely spaced at low mass losses to reflect the generally slower mass loss in the early stages of heating. These data have been tabulated in Table 3.1 along with corresponding data for the other samples in the set.

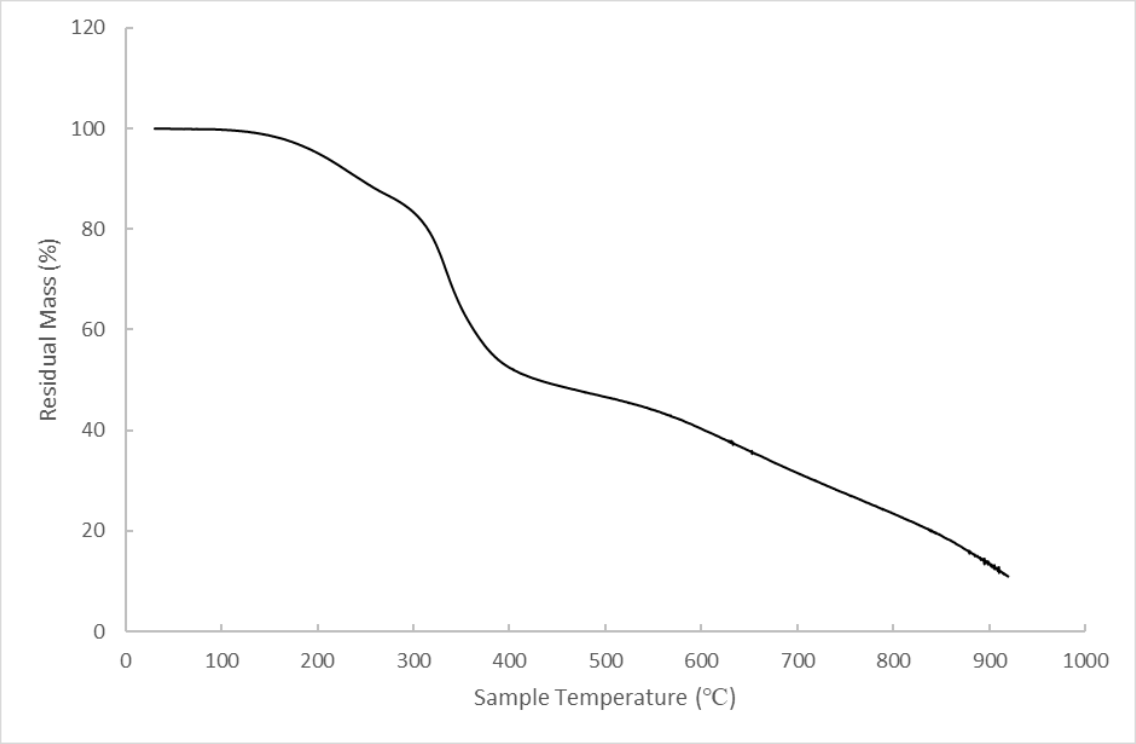

Figure 3.4. *TGA thermogram of line foam sample LF2 under inert atmosphere (initial mass = 11.70mg)*

The TGA thermogram for LF2 exhibited a broadly similar overall shape to that of sample LF1 with mass loss events occurring in the same approximate temperature regimes. However, appreciable discrepancies could also be observed. In contrast to LF1, apparent mass increase over 30-100 ºC was negligible, not exceeding 0.02 % (~2 µg), with mass recorded at 99.8 % at 100 ºC. Above 100 ºC, a decrease in recorded mass was again observed, with a mass loss of 1.6 % (0.22mg) occurring from 100-160 ºC. This is of very similar magnitude to that observed in the same temperature interval for LF1, and strongly suggests that the indicated mass gain occurring from 30-100 ºC reflects variance in the baseline as opposed to a thermophysical or

thermochemical process occurring within the sample. A slow mass loss phase was again observed from 160-300 ºC, with average mass loss of 1.1 % (0.13 mg) per minute, closely matching the rate observed in LF1, with a similar dip being observed around 260 ºC. Mass loss during the accelerating phase from 300-330 ºC was 9.5 % (1.11 mg), similar in magnitude to that in the same interval for LF1. The average mass loss rate in the 330-350 ºC temperature interval was 5.1 % (0.60 mg) per minute. Behaviour above this temperature was similar to LF1 but retained with greater retain mass at the end of heating (11.0 % (1.28 mg) vs 2.1 % (0.24 mg)).

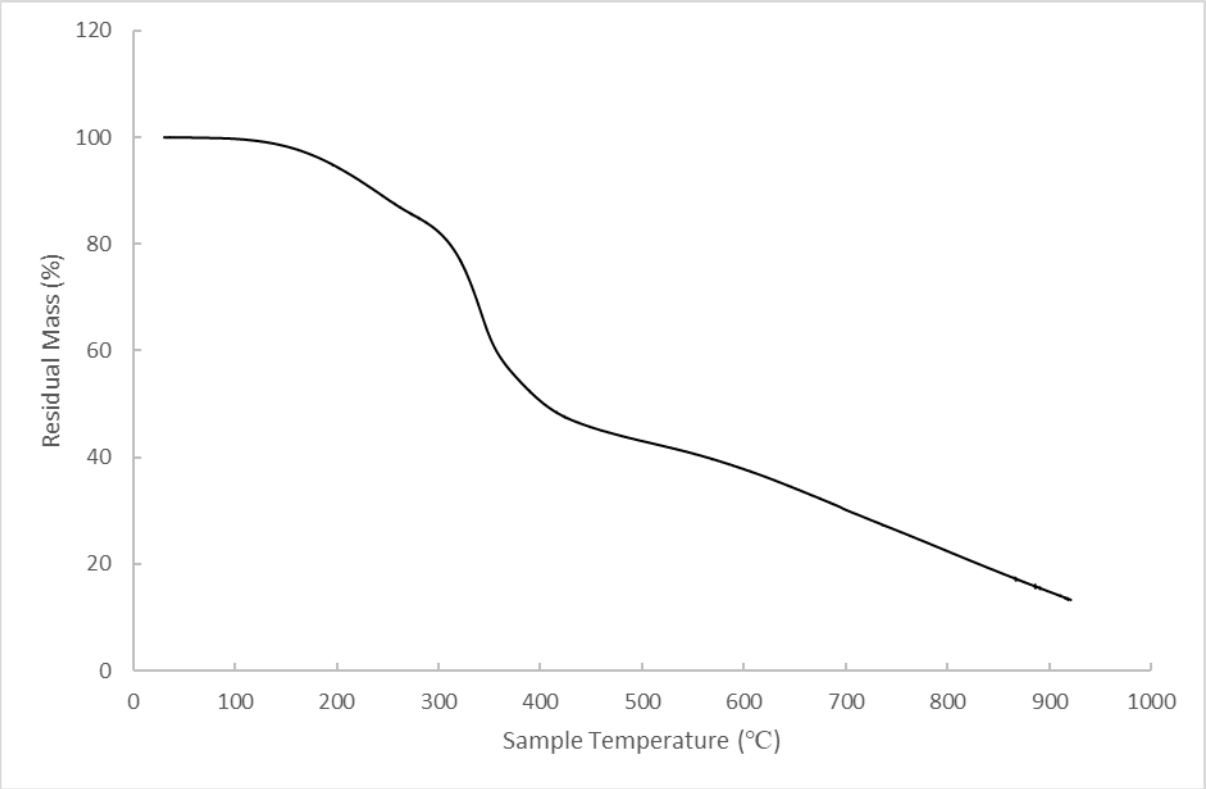

***Figure 3.5**. TGA thermogram of line foam sample LF3 under inert atmosphere (initial mass = 9.41mg)*

Sample LF3 was of substantially lower initial mass than the previous 2 samples. This difference in mass did not appear to have a large impact on the overall form of the TGA thermogram. As in sample LF2, the increase in mass observed from 30-100 ºC in LF1 was again not evident for this sample, with a recorded mass of 99.7 % at 100 ºC. A mass loss of 1.9 % (0.18 mg) was observed from 100-160 ºC. Relatively slow mass loss was again observed from 160-300 ºC, occurring at a mean rate of 1.2 % (0.11 mg) per minute. This rate was therefore very consistent across all three samples, and all three samples also exhibited a dip in this region around 260 ºC. Mass loss from 300-330 ºC was 9 % (0.85 mg), consistent with previous samples. The rate of

mass loss from 330-350 ^{o}C was similar consistent, being 5.5 % (0.52 mg) per minute, as was the behaviour beyond this temperature. Among the three samples, LF3 exhibited the highest proportion of retained mass at the end of heating, 13.3 % (1.2 mg). Retained mass was slightly lower (11.0 %) in sample LF2, and substantially lower (2.1 %) in sample LF1. The very low mass retention in LF1 could not be readily explained, and appeared to be a significant outlier, as similar behaviour was not encountered in other foam samples analysed in this thesis.

Table 3.1 Temperatures at which key % mass losses occur for three replicate line foam samples (LF1-3) taken from TGA data.

Mass Loss (%)	**LF1**	**LF2**	**LF3**	**Mean**
1	177.9	140.1	133.6	150.5
2.5	196.1	171.2	164.7	177.3
5	220.7	201.7	195.0	205.8
7.5	241.0	223.9	217.8	227.6
10	260.4	244.1	237.8	247.4
15	300.4	289.1	279.4	289.6
20	321.3	314.9	311.0	315.7
30	342.0	337.4	336.6	338.7
40	366.5	362.8	356.8	362.0
50	434.3	430.6	403.8	422.9

From the above data it was seen that there were some substantial differences in thermal stability in the line foam (LF1-3) sample set, and that these differences were more pronounced at lower temperatures. The temperature at which a total mass loss of 1% had occurred ranged from 133.6 ^{o}C to 177.9 ^{o}C (44.3 ^{o}C difference). The variance in temperature decreased for higher values of mass loss, reaching a minimum at the 30 % mass loss threshold, where values ranged from 336.6-342.0 ^{o}C (5.4 ^{o}C difference), before the variance again increased at higher mass loss values.

Table 3.2 Residual mass (%) at selected temperature points for line foam samples LF1-3

Temp (°C)	LF1	LF2	LF3	Mean
100	101.4	99.8	99.7	100.3
125	101.2	99.4	99.3	100.0
150	100.5	98.6	98.3	99.1
175	99.2	97.2	96.8	97.7
200	97.1	95.1	94.5	95.6
250	91.3	89.3	88.4	89.7
300	85.1	83.4	82.3	83.6
350	66.0	64.3	62.7	64.3
400	53.2	52.5	50.6	52.1
500	46.5	46.6	43.1	45.4
900	2.1	11.0	13.3	8.8

When comparing samples on the basis of mass loss at a given temperature, the differences between samples appear smaller than those indicated by Table 3.1, which is generally a function of the gradient of the curves, since when the gradient is relatively low, an offset between curves will have a greater impact in the x-direction than in the y-direction and the opposite effect in regions where the gradient is relatively high.

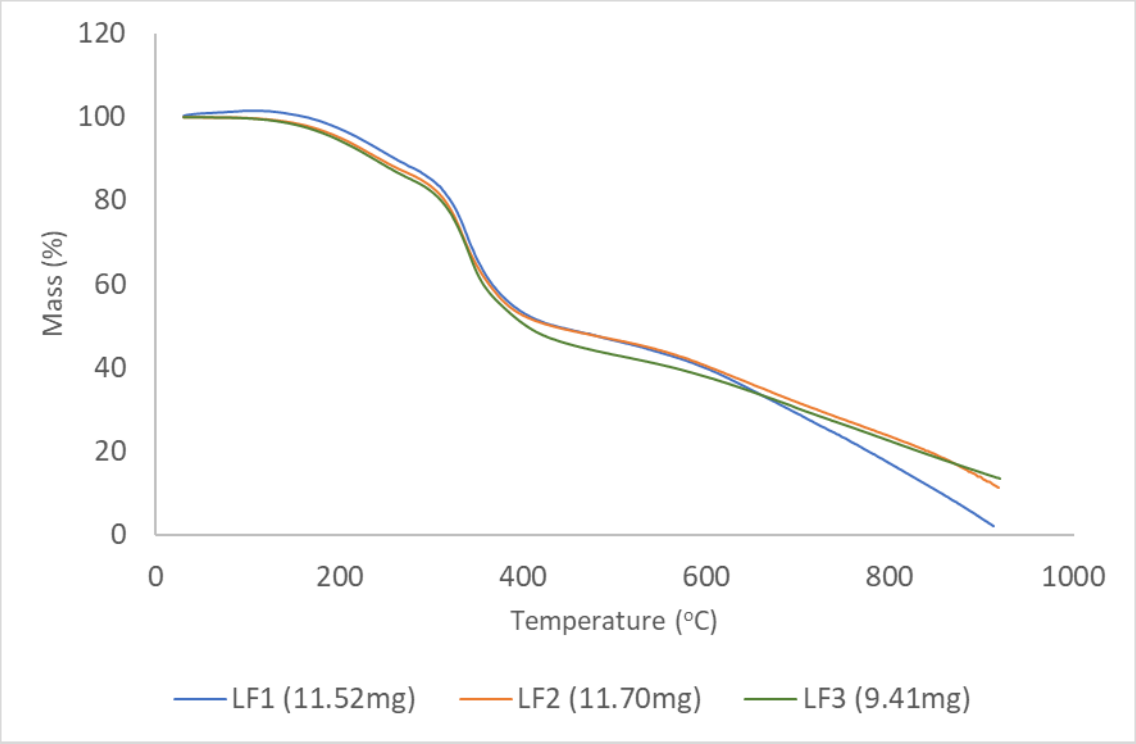

***Figure 3.6**. TGA thermogram comparisons of samples LF1-3 under nitrogen.*

From Figure 3.6, it is seen that the curves appear to converge around the region corresponding to the second apparent phase of mass loss (~300-350 °C), with less consistent behaviour beyond this at temperatures above 400 °C. A possible explanation for this is here posited that since the second phase of mass loss is thought to be predominantly due to the breakdown of isocyanurate structures, this process reflects the degree of isocyanate conversion, thought to be largely consistent across the sample set.

In spite of the variance between samples in this set, the general temperature and mass trends are broadly consistent and clearly demonstrate the presence of two substantial mass loss events in the temperature region below 400 °C as a consistent feature of the LF sample set.

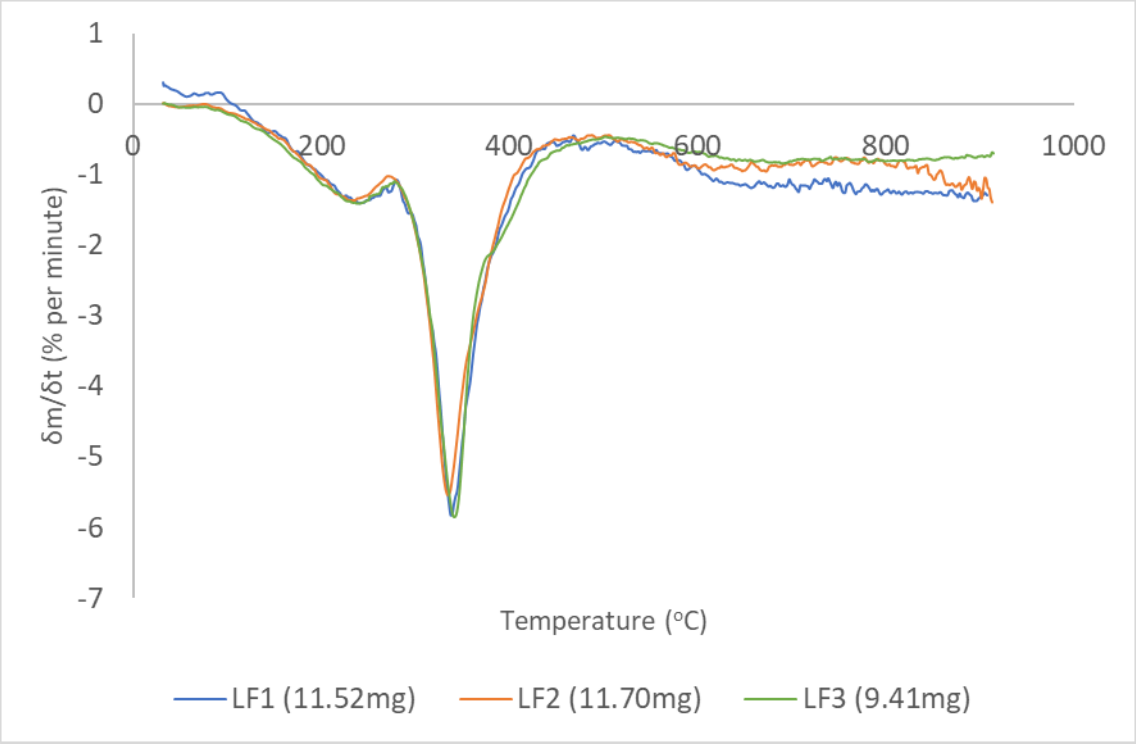

Figure 3.7. *Filtered dTG thermograms for foam samples LF1-3 under inert atmosphere (N_2) at 10 °C/min produced using first-order derivative Savitsky-Golay method with a window size of 7*

Both the TG and dTG curves produced for each of the three samples were broadly similar in their overall shapes. The onset of significant mass loss, taken herein to mean the temperature at which residual sample mass first falls below 97.5 % occurred at 198 °C, 174 °C, and 167 °C in line foam samples LF1-3 respectively. The significantly higher value for sample LF1 may reflect a greater degree of positive drift occurring in the <200 °C temperature range as this has been seen to be somewhat variable and sample LF1 exhibited a small increase in mass at the start of heating that did not return to the initial value until around 170 °C even after applying baseline correction.

All three samples exhibit a characteristic a pair of distinct troughs corresponding to the mass loss events observed on TG. The first trough occurs from 100-280 °C with local minima occurring at 239 °C, 229 °C, and 241 °C for samples LF1, LF2, and LF3, respectively with mass loss rates in the range of 1.3-1.4 % per minute. The second trough, constituting the primary mass loss event, spanned a temperature interval between 280 °C and 420 °C. The highest rate of mass loss occurred in this temperature region at temperatures of 339 °C (LF1), 335 °C (LF2) and 341 °C (LF3). The mass loss rate at this point was 5.8 %, 5.5 % and 5.8 % per minute for line foam samples LF1, LF2 and LF3, respectively. The thermogram for line

foam sample LF3 displays a pronounced shoulder on the high temperature side of the primary trough. Subtle shouldering in this region was also observed for line foam sample LF2.

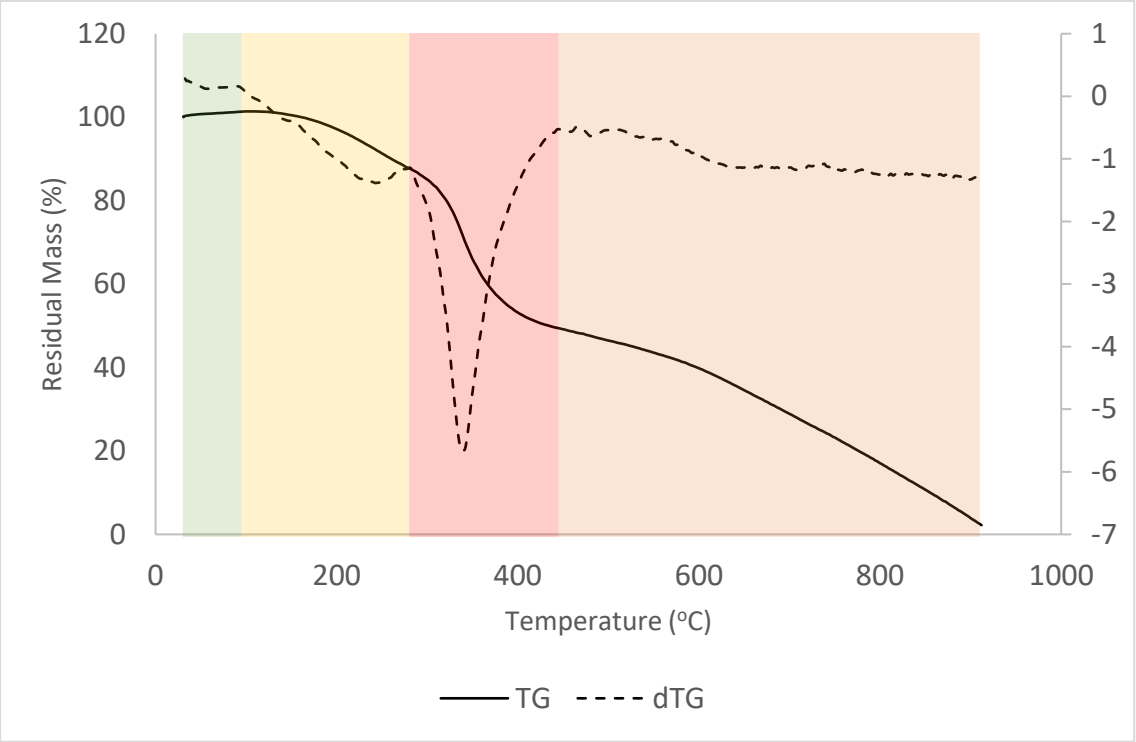

Figure 3.8. *TG/dTG thermograms based on the arithmetic mean of samples LF1-3 colourised to identify key temperature regions.*

The data for the three-line foam samples were combined by taking the mean of the sample temperature and mass data at each time point. Residual mass % and dm/dt were recalculated from the mean data. The maximum point of the first mass loss event here appears at 239 °C with an instantaneous mass loss rate of 1.4 % per minute. The maximum of the second mass loss event appears at 336 °C with an instantaneous mass loss rate of 5.6 % per minute.

The dTG thermograms can be divided into four separate temperature regimes based on the observed behaviour. These are highlighted in Figure 3.8.

The existence of clearly distinct temperature zones supports the existing theory that the breakdown of PIRs is a phased process where each zone corresponds to the temperature range over which a different breakdown process dominates (11–13). In Figure 3.8, the zone highlighted in green occurs across a temperature range from 30-92 °C. This region is characterised by negligible mass loss. While the precise endpoint of this region varied somewhat between samples, none of the three samples lost more than 0.3 % of their initial sample mass at sample temperatures ≤100°C.

The start-point of the second region, highlighted in yellow, is clearly demarcated by the start of a sustained period of increasingly negative values of dm/dt, indicating the onset of mass loss, although this is not readily detected by visual examination of the TG curve until ~120 ^{o}C. Mass loss exceeds 1 % between at ~155 ^{o}C and 2.5 % at ~178 ^{o}C. Throughout this region, mass loss continues to accelerate until the previously described minimum at 239 ^{o}C and 1.38 % per minute before decelerating through to the inflexion point at 279 ^{o}C, where $dm/dt = -1.08$ % per minute. Total mass loss to the end of this region is 13.6 % of the initial sample mass. The slowing of mass loss at temperatures above 239 ^{o}C is inferred to correspond to the slowing of these processes as they approach completion.

The third region, highlighted in red, extended from 279-468 ^{o}C and encompassed the main peak observed on the dTG. This region is characterised by generally high rates of mass loss throughout most of its range. Total mass loss in this temperature range was around three times greater than in the preceding region (39.4 %).

With reference to the previously existing literature on PU and PIR, the small mass losses in the green region are most likely to represent the evaporation of physisorbed moisture (8). While some loss of blowing agent is possible, the low amount of mass loss suggests that most of the blowing agent is retained within the closed-cell structure at this stage, as this accounts for around 5 % of the total mass.

Within the yellow region, mass losses are inferred to result from a combination of physical and chemical processes. Previous characterisation of the evolved gas products arising from the pyrolysis of rigid polyurethane foams have detected the presence of blowing agents (14) at temperatures as low as 165 ^{o}C (15), and therefore it is proposed that the off-gassing of pentane-based blowing agent mixtures will be a contributing factor to low temperature mass losses from PIR foams. When pentane is heated either the volume or pressure will increase. Assuming ideal gas behaviour, this relationship can be described by:

$$PV = nRT \tag{3.4}$$

Where P = pressure, V = volume, n = moles of gas, R = the molar gas constant (8.3145 $JK^{-1}mol^{-1}$) and T = temperature (K).

Within a closed-cell structure, the ability of the gas to increase in volume is limited by the containing polymer matrix, and therefore the pressure within the cells can be expected to

increase. An increase in pressure gradient between the internal environment of the cells and the surrounding atmosphere will tend to increase outward diffusion of pentane, limited by the solubility of the blowing agent in the polymer and the permeability of the cell walls. However, as the pressure of the gas increases, the ability of the cell walls to maintain this pressure gradient will necessarily be finite, eventually resulting in cell rupture with accompanying release of blowing agent, or in swelling of the foam in a pyroplastic state, which is corroborated by direct observation of this phenomenon later in this thesis. This suggests that disruption of the cellular structure at the surface of the material may be one of the first processes resulting in mass loss. As stated above, the blowing agent accounts for 4.5-5.0 % of the foam mass at the start of the foaming process. Significant release of pentane may present a fire hazard, since the lower flammability limit of pentane isomers is 1.1-1.5 %. This value is the lowest volume concentration at which a gas or vapour can ignite in air under standard conditions (16) and may result in a risk of deflagration under fire conditions where point ignition sources such as airborne sparks and embers, arising from the combustion of other materials in the vicinity, may be abundant.

It is also known (17,18) that the polymer matrix contains a quantity of weak cross-linking groups that are particularly vulnerable to thermal degradation, notably allophanate and biuret linkages. These have characteristic thermal dissociation temperatures in the range of 100-125 ^{o}C, and while the breakdown of such groups is unlikely to result in the release of significant polymer fragments, it may nonetheless contribute to some weakening of the polymer structure.

As the temperature increases within this region towards the peak, it is expected that the cleavage of more predominant functional groups such as urethane and isocyanurate linkages will start to occur. As previously described in the introduction to this thesis, the chemical structure of PIR consists of a mixture of linear polyurethane domains consisting of a mixture of hard and soft segments and isocyanurate ring structures. The linear domains consist primarily of alternating diisocyanate and polyol residues, with some polyols substituted for low molecular weight chain extenders. These groups are joined together by urethane linkages, with these linkages likely being the first structurally significant bonds within the structure to undergo thermal cleavage. Mass loss arising from this process is likely to correspond to the release of volatilised polymer fragments of relatively low molecular weight, such as chain extenders and their secondary reaction products. While some free 4,4-methylene diphenyl diisocyanate is formed by this process, the proportion of this which becomes volatilised is

likely to be relatively low due to the high boiling point (314 ^{o}C) and low vapour pressure ($6.67x10^{-7}$ kPa at 20 ^{o}C) of 4,4-methylene diphenyl diisocyanate.

The slowing of mass loss at temperatures above 239 ^{o}C is inferred to correspond to the slowing of these processes as they approach completion. Based on the reported composition of the polyol blend included in the manufacturers data sheet, the diethylene glycol chain extender may account for 3-6 % of the total sample mass, and therefore a mass loss of up to ~10 % could be attributed to the total release of blowing agent and diethylene glycol or its secondary reaction products.

Much of the red region corresponds with a temperature range in which free isocyanate resulting from thermal retro-polymerisation (19) can be readily volatilised. However, previous analyses of the breakdown products of polyurethane pyrolysis indicate that the quantity of detectable isocyanates in the vapour phase is actually very low (20). This can be explained if simple retro-polymerisation is not the dominant reaction mechanism involved in the breakdown of urethane bonds, but rather a cleavage of the internal C-N bond, which would favour the formation of 4,4-methylenedianiline, which has previously been detected (21) at relatively high abundance at lower temperatures in the breakdown products of rigid polyurethanes.

There was a rapid increase in the rate of mass loss in this region, from 1.1 % per minute at 279 ^{o}C to 5.6 % per minute at 336 ^{o}C indicating the onset of a critical process. Due to the expected preponderance of heterocyclic isocyanurate rings within the foam, this was likely due to the dissociation of these groups. It has been suggested that this proceeds via the breakdown of the ring structure back to free isocyanates through cleavage of the C-N bonds within the heterocycle.

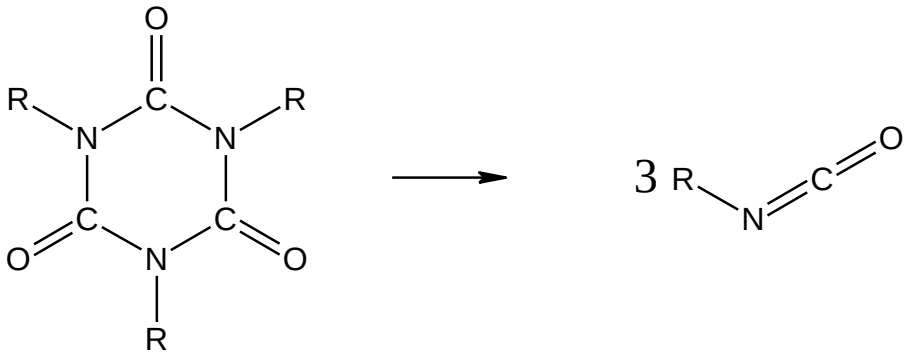

Figure 3.9. *Cleavage of isocyanurate rings to produce free isocyanate.*

This would correlate with an almost complete degradation of the polymer and the transition from a structure dominated by isocyanurate groups into a carbonaceous char.

3.3.2 Thermogravimetric Analysis of Free-Rise Foams

Much of the work within this thesis was carried out on hand-mixed PIR foams. This presents an opportunity to characterise the differences between line-produced and hand-mixed foams. Here, the TG results obtained from the line produced foam samples have been compared with two sets of hand-mixed foams. The first of these sets was produced on-site using an open-cup free-rise method, while the second was produced at Shotton Works using a block-mould method. The free-rise method meant that this foam sample was mixed in an open container using an overhead stirrer and allowed to freely rise *in situ*. When the reaction reached its apparent end-point, the container was transferred to a pre-heated oven at 75 ^{o}C for 5 min to assist with initial curing, and then allowed a further 24 h at ambient temperature before analysis was conducted.

After curing, a cross-sectional slice was taken from the foam bun, starting at the level of the top of the cup and extending two centimetres downwards. Three samples for analysis were cut from the intermediate region of this slice, avoiding the material at the outer edges and the small region of poorly foamed material at the centre. This approach was employed in an attempt to obtain samples of relatively homogeneous composition, mostly on the basis of visual inspection of the material. These samples ranged in initial mass from 8.07-8.75mg.

Time-filtered (10-second interval) TG thermograms for these three samples are shown in Figure 3.10. These three samples exhibited very consistent behaviour broadly similar to that observed for the three line-produced foam samples, LF1-3.

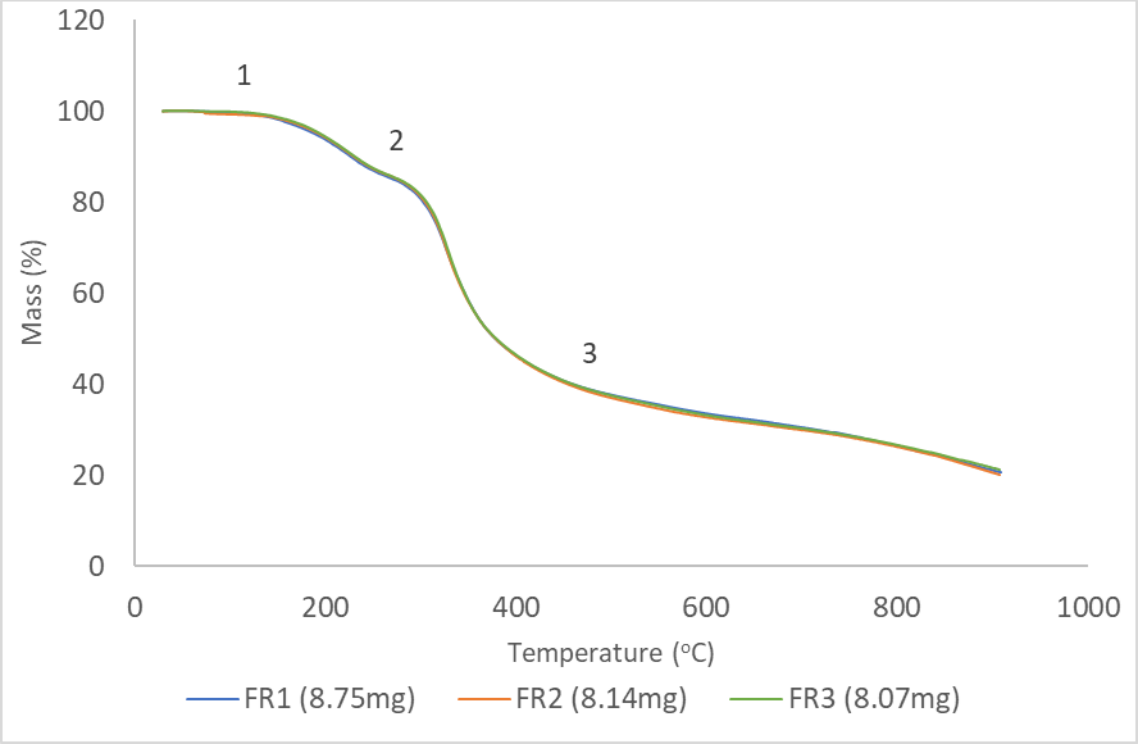

Figure 3.10. *TG thermograms for free-rise foam samples FR1-3 under inert atmosphere of N_2.*

It was seen that all three samples exhibited extremely consistent behaviour, with the three TG curves overlapping almost completely throughout most of the temperature range. Very little mass loss occurred in the 30-120 °C [1] temperature range, corresponding to the initial flat region in the thermograms. Average mass loss in this region was <0.6 % (0.05 mg). This was followed by two distinct mass loss events of 14.9 % from 120-280 °C [1-2] and of 44.7 % from 280-460 °C [2-3]. Mass loss continued gradually to the end of heating with an average retained char fraction of 20.6 % (1.72 mg). The temperature at which mass loss exceeded selected values are given in table 3.8.

Table 3.8. Temperature at which selected mass loss values were recorded for free-rise foam samples (FR1-3) compared against mean value for line foam samples (LF1-3)

Mass Loss (%)	FR1 (°C)	FR2 (°C)	FR3 (°C)	Mean FR	Mean LF	Difference (FR-LF)
1	134.5	138.2	144.7	139.0	150.5	-11.5
2.5	160.2	167.2	170.1	165.8	177.3	-11.5
5	189.5	194.3	195.8	193.2	205.8	-12.6
7.5	210.2	213.7	214.8	212.9	227.6	-14.7
10	227.3	230.7	231.8	229.9	247.4	-17.5
15	272.0	277.2	277.9	275.7	289.6	-13.9
20	303.4	305.2	306.6	305.1	315.7	-10.6
30	326.6	326.9	328.1	327.2	338.7	-11.5
40	346.4	345.8	346.5	346.2	362.0	-15.8
50	378.8	379.0	379.4	379.1	422.9	-43.8

Table 3.9. Retained mass at selected temperatures for free-rise foam samples (FR1-3) compared against mean value for line foams samples (LF1-3)

Temp (°C)	FR1 (%)	FR2 (%)	FR3 (%)	Mean	Mean LF	Difference (FR-LF)
100	99.8	99.4	99.9	99.7	100.3	-0.6
125	99.3	99.1	99.6	99.3	100.0	-0.7
150	98.3	98.5	99.2	98.7	99.1	-0.4
175	96.4	96.9	97.1	96.8	97.7	-0.9
200	93.8	94.4	94.5	94.2	95.6	-1.4
250	87.0	87.5	87.6	87.4	89.7	-2.3
300	80.8	81.4	81.6	81.3	83.6	-2.3
350	58.5	58.3	58.4	58.4	64.3	-5.9
400	46.3	46.3	46.5	46.4	52.1	-5.7
500	37.7	37.1	37.5	37.4	45.4	-8.0
900	20.6	20.1	21.1	20.6	8.8	+11.8

Comparison of mean selected mass loss values between line-produced and hand-mixed free-rise samples indicates lower thermal stability for the hand-mixed foams. For a given percentage mass loss, it is observed that the line-foam 'lags' the hand-mixed foam by between 10.6 % and 17.5 % at temperatures below ~360 ^{o}C, and that a 50 % mass loss is induced in hand-mixed foam samples at a temperature of 40 ^{o}C lower than that required for line-produced samples.

It is also noted that the sample masses of the line-produced foams are greater than those for the hand-mixed samples (mean mass 10.98 mg vs. 8.32 mg), but are of almost identical volume, indicating that the free-rise foams have a significantly reduced density compared to the line-produced samples. This likely represents a larger cell volume due to lack of containment during the blowing reaction, whereas the expansion of line-produced foams is somewhat constrained as the foaming reaction occurs *in situ* between two steel facings. This difference could account for some of the recorded difference in mass loss. A sample of lower mass will have a lower extensive heat capacity, *C*, and will therefore be expected to heat up more rapidly under identical heating conditions. While the reported temperatures correspond to the actual temperature recorded at the sample monitoring thermocouple, rather than the program temperature, a smaller sample may exhibit a shallower temperature gradient from the surface to the core.

In the case of line-foam samples, it can be observed that sample LF3 is of substantially lower mass (9.24 mg) than the samples LF1 and LF2, and closer in mass to the largest of the hand-mixed samples (8.75 mg) than to either of the other line-foam samples. Comparison of these samples indicates far more similar behaviour than suggested by the average of the data sets. However, there remained a significant temperature discrepancy at the 50 % mass loss point (403.8 ^{o}C vs. 378.8 ^{o}C, difference = 25 ^{o}C).

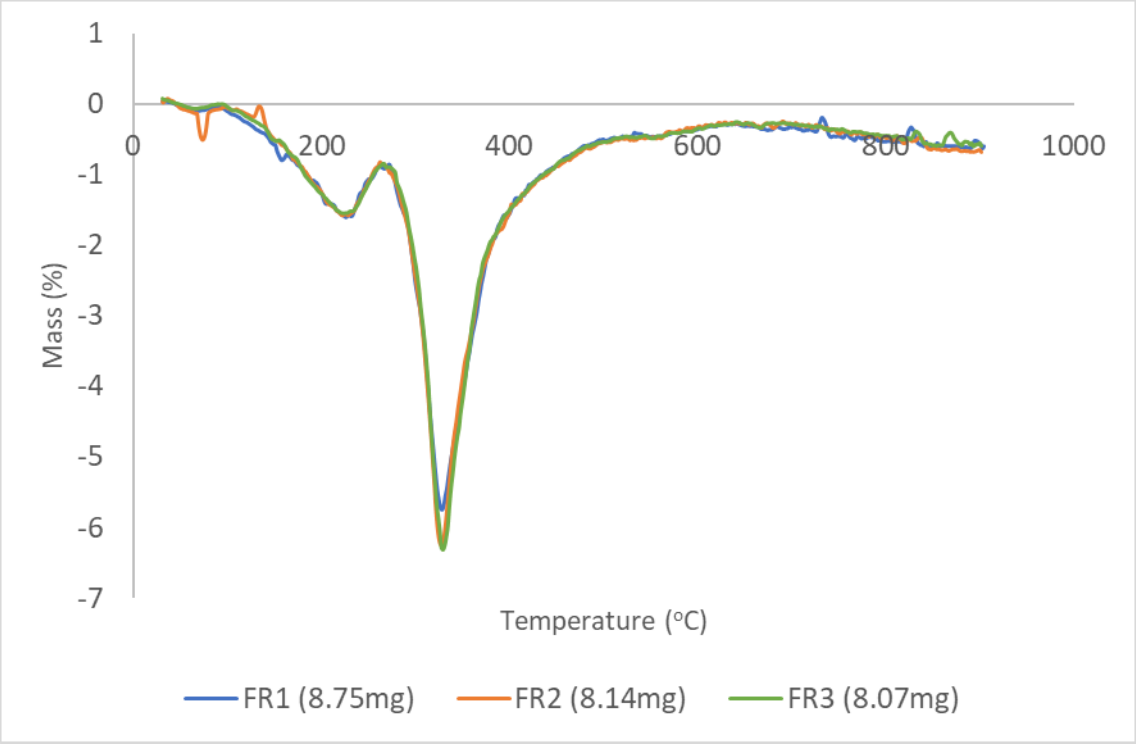

Figure 3.11. *dTG thermograms for free-rise foam samples under inert atmosphere at 10 °C/min.*

Inspection of the dTG thermograms obtained from the open-rise foam samples indicates some variation in behaviour that is not easily observed from the TG data. A similar degree of noise is observed in the raw dTG which as in the previous samples with high-amplitude fluctuations superimposes onto the regular baseline oscillation. The same smoothing process has been applied as previously, with the TG data filtered over a 10 second time interval and the first derivative taken using the direct Savitsky-Golay method with a window size of seven. This resulted in the dTG curves reproduced in Figure 3.11. Even after the smoothing procedure, some noise artifacts are still present, and this is especially noticeable in the region of the sample FR2 curve below 200 °C and within the high-temperature tail region. Despite this, it can easily be seen that the overall curve forms are similar to those observed for the line-produced foams, with two primary mass loss regions readily apparent.

The noise artifacts in the low-temperature range make it difficult to clearly ascertain the onset of mass loss in sample FR2 but this can be estimated to occur within the same 90-95 °C temperature range as in samples FR1 and FR3. Following the onset point, there is an overall trend of accelerating mass loss up to temperatures of 226 °C in sample 1, then 236 °C in sample 2, and then 224°C in sample 3. These peak temperatures are overall lower than those observed for the corresponding event in the line-produced foam samples where the lowest temperature

observed for this peak is 229 ºC, with the remaining samples exhibiting peak breakdown temperatures in this region of 239-241 ºC. Peak mass loss rates are all around 1.6 % per minute, a slightly higher rate of mass loss than occurs in the line-produced foams. Beyond the peak, this region continues upwards to temperatures from 265-271 ºC across the three samples, compared to a mean value of 278 ºC in samples LF1-3. Despite this downward shift, total mass loss in the first mass loss event is very similar in both the line-produced (LF1-3) and free-rise (FR1-3) sample sets on average (13.6 % vs. 13.8 %). If the first mass loss peak largely represents the degradation of urethane bonds, this suggests that the composition of the free-rise and line-produced foam samples are similar, and the difference in stability may result from difference in the physical characteristics of these foams.

Above this temperature, there is a transition into the second and larger mass loss event. There is an acceleration in mass loss to the primary peak, with maximum mass loss rates occurring at 328 ºC, 335 ºC, and 329 ºC in samples FR1-3 with respective peak mass loss rates per minute of 5.7 %, 6.2 %, and 6.3 %. These values maintained the same relationship to those recorded for the line-produced samples as observed for the previous peaks, occurring at slightly lower overall temperatures with greater rates of mass loss. Following the maximum mass loss, the deceleration of mass loss appears to be slower, compared to LF samples, with a gradual 'tailing off' continuing to temperatures above 600 ºC, in contrast to the more distinct endpoint near 500 ºC previously observed. No pronounced curve shouldering is observed for any of the three free-rise foam samples as is observed on the high-temperature side of the second peak for the line-produced samples LF3 (Figure 3.11).

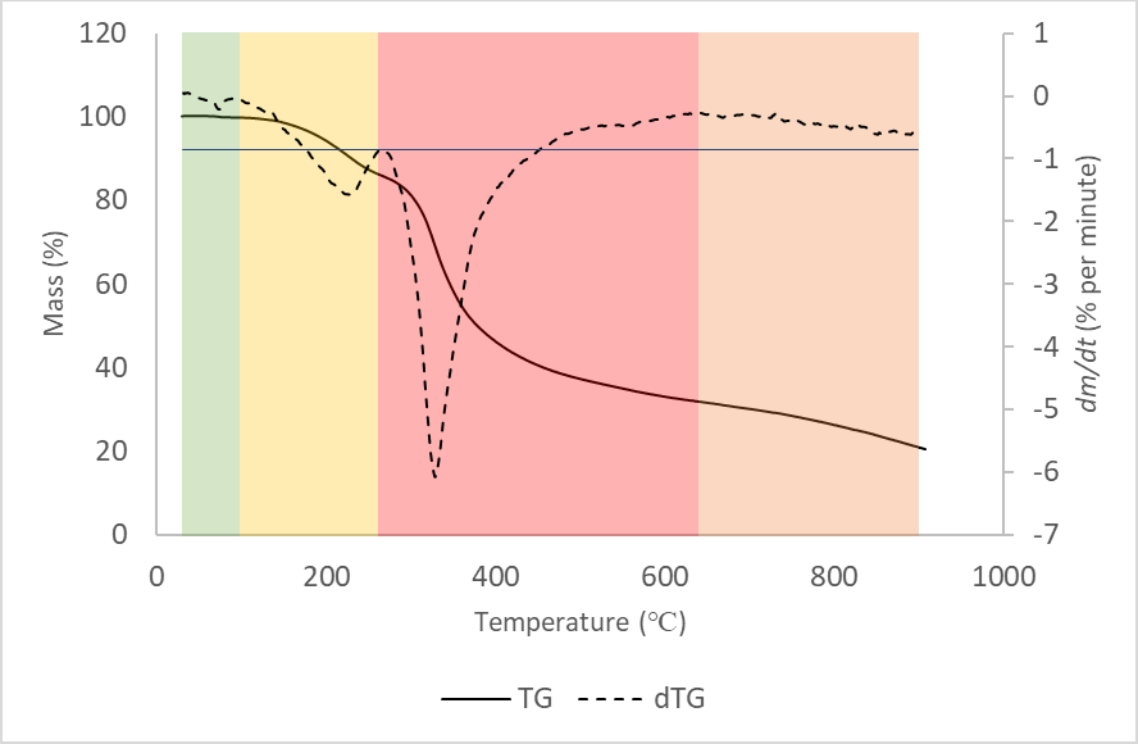

Figure 3.12. *Combined mean TG/dTG thermograms based on average of three samples (FR1-3) of free-rise foams.*

Figure 3.12 has been produced by calculating the arithmetic mean of sample temperature and residual mass for each of the three samples and re-converting to percentage mass. The dTG curve was recalculated using the Savitsky-Golay method outlined in the previous section of this chapter. The previously identified regions have been highlighted. Across the three samples, the first mass loss event begins at a mean temperature of 97 ^{o}C with an approximate mass loss of ~0.3 % below this temperature.

The initial mass loss event, highlighted in yellow, reached a peak rate of 1.6 % per minute at 228 ^{o}C before decelerating, with the endpoint of the region occurring at 261 ^{o}C. Total mass loss for this region was 13.5 %. This is an almost identical value to that observed for the line-produced foams (13.4 %), but the lowest point of the trough is shifted downward in temperature by 11 ^{o}C and the temperature at the endpoint by 18 ^{o}C.

The red-highlighted region encompassed the temperature interval from 261 ^{o}C to the peak at 327 ^{o}C where the mean maximum mass loss rate was 6.1 % per minute and then extending above this temperature. The endpoint for this region was selected as the temperature after the peak at which mass loss stopped decelerating, which occurred at around 640 ^{o}C. Using these boundaries, this region is much broader in the free-rise foams than the line-produced samples,

where the deceleration of mass loss occurred at 468^{o}C. There is a total mass loss in this region of 54.2 %.

While this is significantly greater than the corresponding mass loss for the line-produced foams (39.4 %) this may be expected as a far broader temperature interval has been captured. The lower boundary of this mass loss event could be easily identified by inspection of the dTG curve, due to the relatively sharp transition between the two peaks, but it is far more difficult to locate a precise and consistent upper boundary for this event.

One method for providing more consistent points of comparison may be to consider the mass loss across a particular absolute temperature interval roughly corresponding to the location of the peak, for example 250-500 ^{o}C. Across this interval, average mass loss from the free-rise foam was 50.0 % compared to 44.3 %. An alternative for more accurately characterising the boundaries of the primary mass loss region was to define this region as the area lying below a horizontal line drawn level with the start-point. Applying this method to both sets of samples situates the lower and upper boundaries at 261-450 ^{o}C for the line-produced samples and 279-410 ^{o}C for the free-rise samples. This provides mass loss values of 46 % for the line-produced foams and 36 % for the line-produced samples. All these methods indicate greater proportional mass loss in this region for free-rise foams, and this region is broader, centred at a lower temperature, and reaches a greater peak rate of mass loss.

3.3.3 Thermogravimetric Analysis of Block-mould Foams

Block-mould foams were produced externally at Tata Steel, Shotton by the industrial project co-sponsor. The mixing process for these foams was identical to that used for free-rise foams, but the reaction mixture was poured into a closed steel block mould immediately after the combination of the two pre-reaction mixtures. As the reaction was enclosed on all sides by the mould and top cover, this contained the rising foam and resulted in a foam block of set volume (as describe in the Experimental chapter).

Samples were provided from three separate batches of block-moulded foam produced to the same formulation as the samples LF1-3 and FR1-3, with a fire-retardant system consisting of TEP and TCPP. Samples were prepared for thermogravimetric analysis. Block-mould foams were provided by the industrial sponsor as cuboidal sections with approximate dimensions of 100 mm x 70 mm x 50 mm. Visual inspection of these pieces found a homogeneous

appearance, although some samples appeared to exhibit a film of glossy material on one surface, corresponding to the surface that had been in direct contact with the mould. When producing samples for thermogravimetry, this material, and the underlying 2 cm were avoided. Samples were otherwise prepared using the same methods as for the line-produced and free-rise foams and subjected to identical experimental conditions. Initial sample masses ranged from 10.07 mg to 12.15 mg, being closer in mass to the line-produced foams than was the case for free-rise foams.

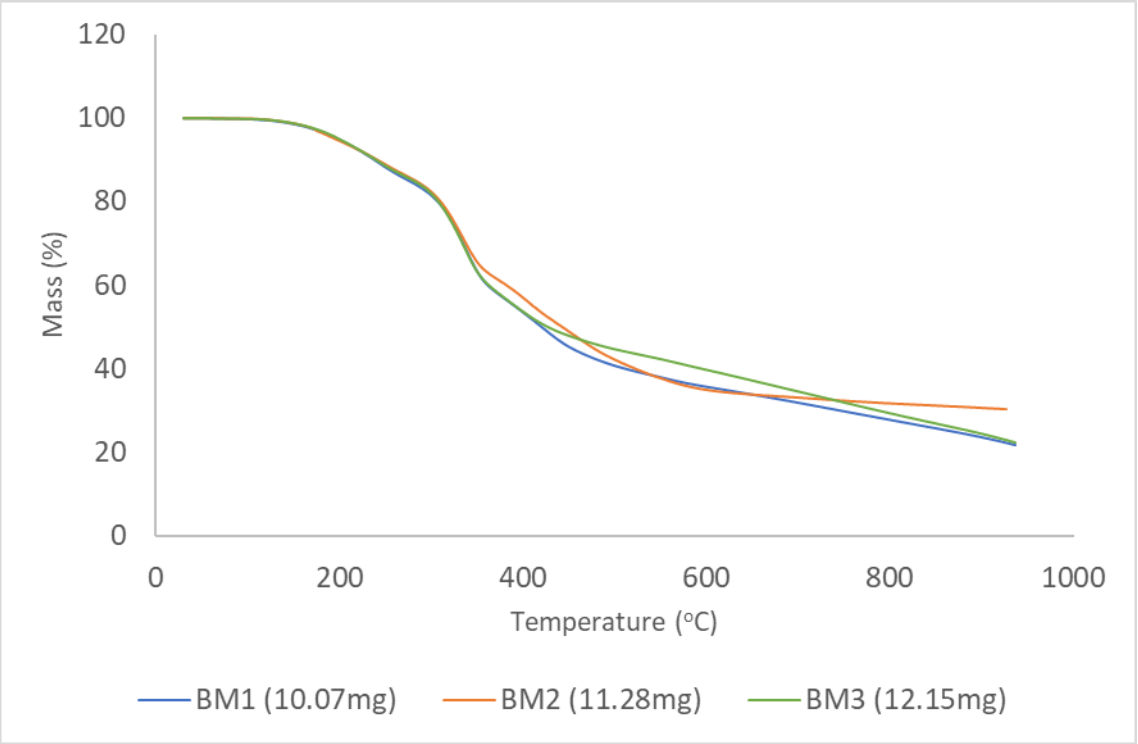

***Figure 3.13**. TG thermograms for block-mould samples (BM1-3) under N_2.*

TG thermograms for three block-mould samples (BM1-3) are displayed in Figure 3.13 above. These samples were taken from three separately produced foam blocks produced by the industrial laboratory at Shotton Works. The formulation of these samples exactly matched the formulation used for the manufacture of line-produced foams.

Inspection of the above thermograms indicates very consistent behaviour of all three samples at temperatures up to 320 °C. An initial flat region can be seen at temperatures from 30-120 °C, with mass loss of less than 0.5 % in all three samples. This was followed by a period of relatively slow and small mass loss over the temperature range from 120-320 °C, with an average retained mass of 76.1 % at this temperature.

At temperatures above 320 ºC, samples BM1 and BM3 continued to exhibit near identical behaviour to around 400 ºC, while BM2 showed reduced mass loss over this range. Selected comparative data points for the three samples are tabulated in Tables 3.11 and 3.12. Above 400 ºC, BM3 exhibited consistently high retained mass than BM1, although the mass of the final retained char was very similar in both samples and was substantially lower than that for sample BM2.

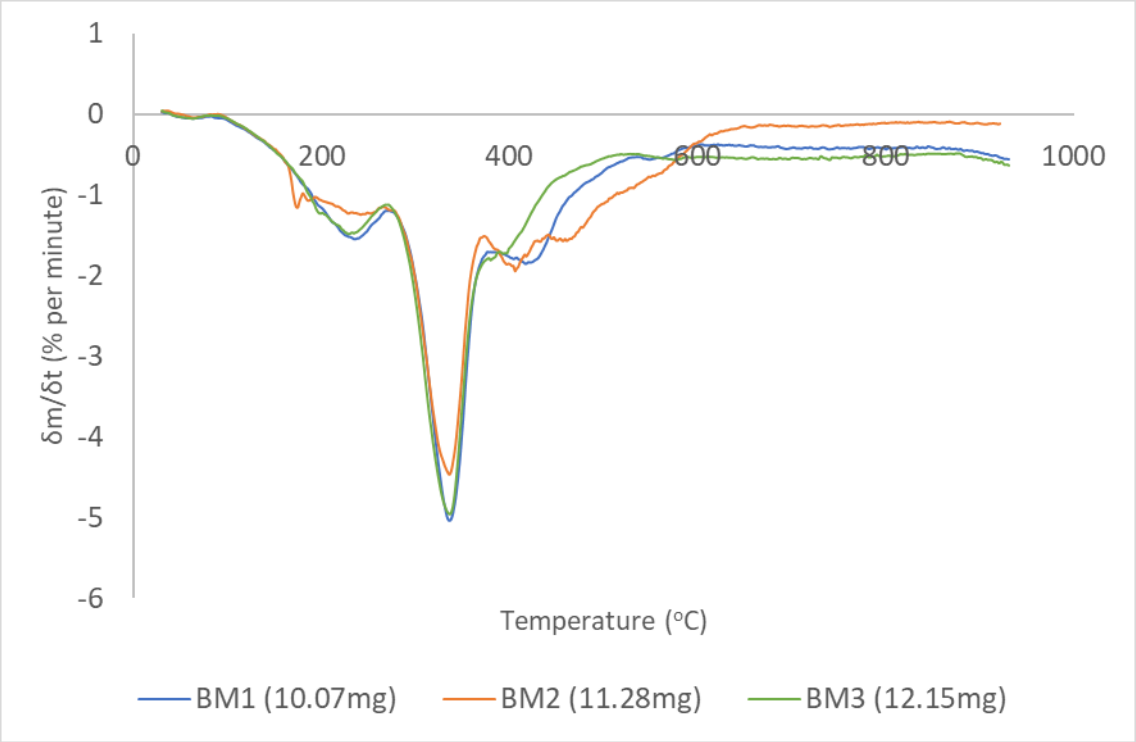

***Figure 3.14**. dTG thermogram of block-mould samples (BM1-3) under N_2*

The dTG thermograms for the BM sample set exhibit several distinctive features. The flat region observed on the TG thermogram corresponds to the region of the dTG thermogram below 95 ºC, corresponding to a similar feature observed in both the LF and FR sample sets. The maximum rate of mass loss within this region was <0.1 % per minute, at a consistent temperature of around 64 ºC.

All three samples exhibited a steady increase in the rate of mass loss above 95 ºC to around 0.6 % per minute at 165ºC. Samples BM1 and BM3 on this trend to respective rates of 1.6 % per minute and 1.5 % per minute at 236 ºC and 229 ºC. A deviation from this behaviour was observed in sample BM2, with a rapid increase in rate to 1.2 % per minute occurring at from 165-175 ºC, followed by a flattened peak with its maximum at 242 ºC. The end point of this

phase also occurred at a lower temperature in sample BM2 (264 ^{o}C) compared to the remaining samples (272 ^{o}C).

The major mass loss peak occurred across at a mean temperature of 336 ^{o}C (range 335-337 ^{o}C) with a mean $\frac{dm}{dt}$ of -4.8 % per minute. Among the three samples, BM2 exhibited a substantially lower rate of mass loss than BM1 and BM3.

Behaviour at temperatures above the primary mass loss exhibited a greater degree of variability than at lower temperatures. BM1 had a discrete third peak with $\frac{dm}{dt}$ of -1.9 % per minute at 417 ^{o}C, while two peaks were observed in this region for BM2 at 406 ^{o}C (-1.9 % per minute) and 457 ^{o}C (-1.6 % per minute). No discrete peaks were observed in BM3, but there was a pronounced shoulder on the upper end of the main mass loss peak that was absent from BM1 and BM2.

Table 3.11. Sample temperature at selected mass loss thresholds for block-mould foam samples BM1-3

Mass Loss (%)	BM1	BM2	BM3	Mean BM	Mean LF	Difference (BM-LF)
1	140.2	144.9	145.2	143.4	150.5	-7.1
2.5	169.8	171.3	173.3	171.5	177.3	-5.8
5	198.6	195.4	200.3	198.1	205.8	-7.7
7.5	220.0	220.0	221.3	220.4	227.6	-7.2
10	238.2	241.0	240.0	239.7	247.4	-7.7
15	275.8	282.7	280.9	279.8	289.6	-9.8
20	307.1	309.8	308.0	308.3	315.7	-7.4
30	334.6	337.3	334.1	335.3	338.7	-3.4
40	361.6	381.1	362.7	368.5	362.0	+6.5
50	420.5	441.7	427.2	429.8	422.9	+6.9

Table 3.12. Retained mass (%) at selected temperatures for block-mould foam samples BM1-3

Temp (°C)	BM1	BM2	BM3	Mean BM	Mean LF	Difference (BM-LF)
100	99.8	99.9	99.9	99.9	100.3	-0.4
125	99.4	99.6	99.6	99.5	100.0	-0.5
150	98.6	98.8	98.8	98.7	99.1	-0.4
175	97.1	97.0	97.4	97.2	97.7	-0.5
200	94.9	94.6	95.0	94.8	95.6	-0.8
250	88.3	88.9	88.6	88.6	89.7	-1.1
300	81.5	82.3	82.0	81.9	83.6	-1.7
350	63.3	65.4	63.3	64.0	64.3	-0.3
400	53.5	56.9	53.7	54.7	52.1	+2.6
500	40.8	42.0	44.7	42.5	45.4	-2.9
900	21.8	30.2	22.3	24.8	8.8	+16.0

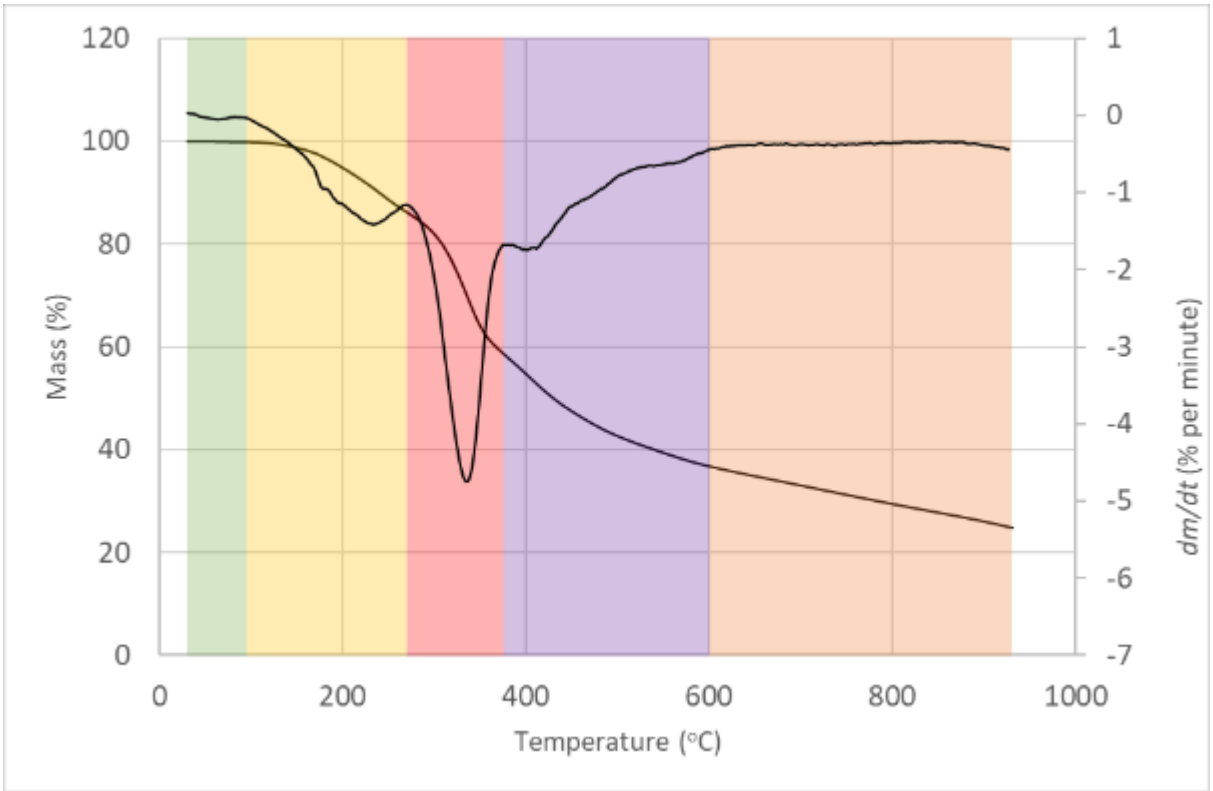

Figure 3.15. *Combined mean TG/dTG thermogram based on three samples of block-mould PIR foams.*

The combined TG/dTG curves were produced by taking the arithmetic mean of sample temperature and residual mass for each time point. The dTG curve was recalculated from the TG data using a Savitsky-Golay filter.

For the block-mould samples, five distinct regions have been identified. The first region, highlighted in green, extends from 30-94 ^{o}C, corresponding to the temperature range in which negligible mass loss occurs and *dm/dt* is close to zero. The maximum rate of mass loss in this region is <0.1 % per minute and likely corresponds to the evaporation of adsorbed volatiles on surfaces exposed to the air. A mass loss of 0.1 % occurs in this region.

The second region, highlighted in yellow, extends from 94-269 ^{o}C, and includes the first significant mass loss event. These lower and upper boundaries correspond quite closely with those observed for the free-rise foam samples and are therefore the upper boundary occurs at lower temperature than for line-produced foams. The maximum rate of mean mass loss was 1.4 % per minute, occurring at 234 ^{o}C. This is 6 ^{o}C higher than that for free-rise foams but 5 ^{o}C lower than for line-produced foams. Mass loss in this temperature range was 13.5 %.

The region highlighted in red comprises the main mass loss event, extending from 269-375 ^{o}C. The highest calculated mass loss is 4.7 % per minute at 336 ^{o}C and the total mass loss across this temperature range was 27.0 %.

At temperatures above the main mass loss event, a fourth region was described that was not well-defined in previous samples. This region is highlighted in purple in the above figure and appears to consist of a sequence of smaller mass loss events occurring in the temperature range from 375-600 ^{o}C, with peak mass loss rate of 1.7 % per minute at 402 ^{o}C. This region accounted on average for 21.8 % mass loss. Above 600 ^{o}C, there is a slow and gradual mass loss, with no clearly defined events.

The greater variability in thermal stability behaviour observed between samples taken from different batches of block-moulded foams suggests that hand-mixing methods may result in inconsistencies in the physical and chemical composition of the resulting foams. In contrast to the free-rise foams, in which all three samples were taken from a single batch, the block-mould samples were taken from three separate batches. Multiple factors may have an impact in this regard. Firstly, the proportions of components in the reaction mixture may have varied due to measurement error, especially in the case of components added in small quantities such as reaction catalysts. It is also conceivable that the quantity of 4,4-methylene diphenyl diisocyanate that remained in the original container when the two mixtures were combined varied to some extent due to changes in viscosity due to ambient temperature. Ambient temperature could also have exerted an impact on the degree of blowing agent evaporation that occurred during the mixing process, resulting in differing amounts of blowing agent being retained within the cellular structure. Furthermore, the hand-mixing method may to result in a less homogeneous mixture, and this is probably the most likely effect to have an impact on the reaction.

3.3.4 Comparison of Line and Hand-mixed Foams

Initial examination of thermogravimetric data obtained from line-produced, free-rise, and block-mould foams indicated differences in thermal stability arising from these production methods. However, there was also a significant degree of variance *within* each sample set, necessitating further analysis.

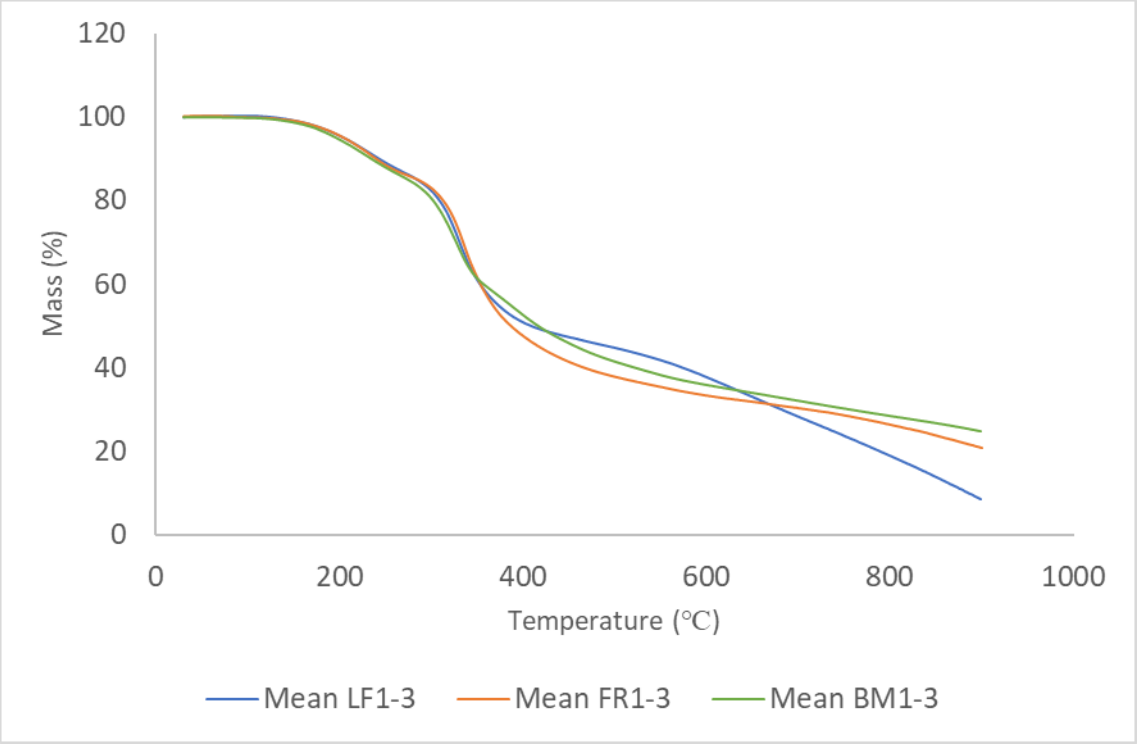

Figure 3.16. *Comparison of TG thermograms for line-produced, free-rise, and block-mould foams under inert atmosphere.*

Figure 3.16 reproduces the averaged TG thermograms for each of three previously analysed sample sets. It can be seen that line-produced foams exhibited greater average thermal stability than either set of hand-mixed samples at all temperatures below 355 °C. Above this temperature, in the 355-400 °C temperature range, block-mould foams exhibited greater thermal stability than line-produced foams with a maximum difference of around 3 % at 400 °C. From 400-650 °C, greater stability was again observed for line-produced foams. Free-rise foams were less stable on average than both line-produced and block-mould foams at all temperatures below 700 °C. The relative stability diverged significantly above 650-700 °C, as the rate of mass loss in line-produced foams above 600 °C was noticeably greater than for the hand-mixed foams, resulting in a retained mass of 9 % at the end-point versus 20 % for free-rise and 25 % for block-mould foams.

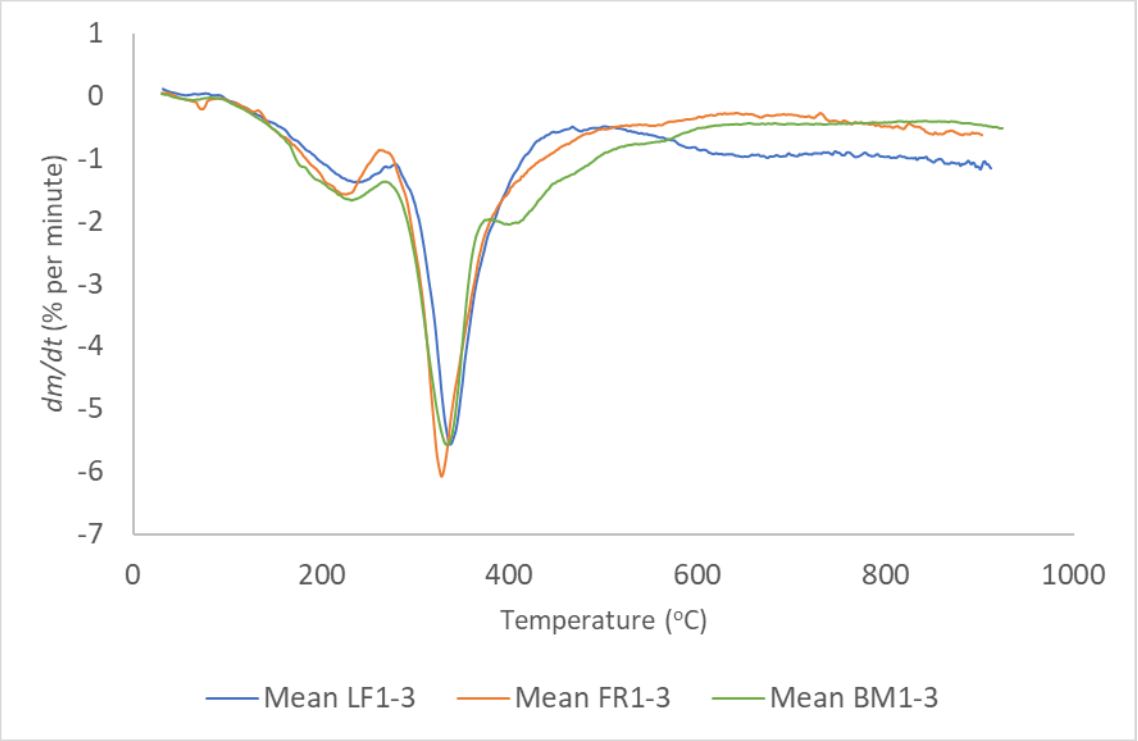

Figure 3.17. *Comparison of dTG thermograms for line-produced, free-rise, and block-mould foams under inert atmosphere.*

The mean dTG thermograms for each of the three sample sets are reproduced in Figure 3.17. These further highlight the appreciable differences in behaviour between these sets. At low temperatures, there was a marked reduction in thermal stability of hand-mixed foams compared to line-produced samples, both in the temperatures at which breakdown occurred and in the calculated rates of mass loss. The temperature at the onset of mass loss is broadly consistent, occurring in all cases with a 10 °C temperature range from 90-100 °C. Above the onset temperature, line-produced foams exhibit a relatively slower acceleration in mass loss, reaching a peak rate of 1.4 % per minute at 239 °C. In contrast, block-mould and free-rise more rapidly accelerated, with block-mould foams reaching their first event maximum of 1.7 % per minute at 233 °C, and free-rise foams reaching 1.6 % per minute at 228 °C.

The relative temperatures at the first peak were also reflected in the temperature at the transition point between the first and second mass loss events. This transition occurs 262 °C in free-rise foams, 271 °C in block-mould foams, and 278 °C in line foams. The smaller difference between the peak and the transition in free-rise foams compared to block-mould and line foams demonstrates a narrowing of the temperature interval over which the first mass loss event occurs in free-rise foams in addition to the negative temperature shift, visually apparent from

the sharper form of the first peak. Beyond the transition point, free-rise foam diverges noticeably from the other sets, accelerating to a peak rate of 6.1 % per minute at 328 ^{o}C.

It appears that the overall pattern is that thermal stability decreases from line-produced > block-mould > free-rise foams. However, simple visual inspection of the mean curves does not take into account the variability between samples within each set, and therefore further statistical analysis was carried out on the sample sets to take this into account.

For each of the sample sets, standard deviation values were calculated for the sample mass at each time point, using the standard formula for sample standard deviation.

$$s = \sqrt{\frac{\Sigma_{i=1}^{n}(x_i - \bar{x})}{N - 1}} \tag{3.5}$$

These values were used to calculate the 95 % confidence interval at each point. For each of the sets of samples, the mean TG curve was plotted, along with lines curves representing the upper and lower bounds of the confidence interval at that point. This effectively functions as a set of continuous error bars, with the bounds demarcating the range of values with a 95 % probability of containing the true mean. Where the confidence intervals do not overlap, it can considered that the difference of true means is statistically significant at a threshold p-value of 0.05.

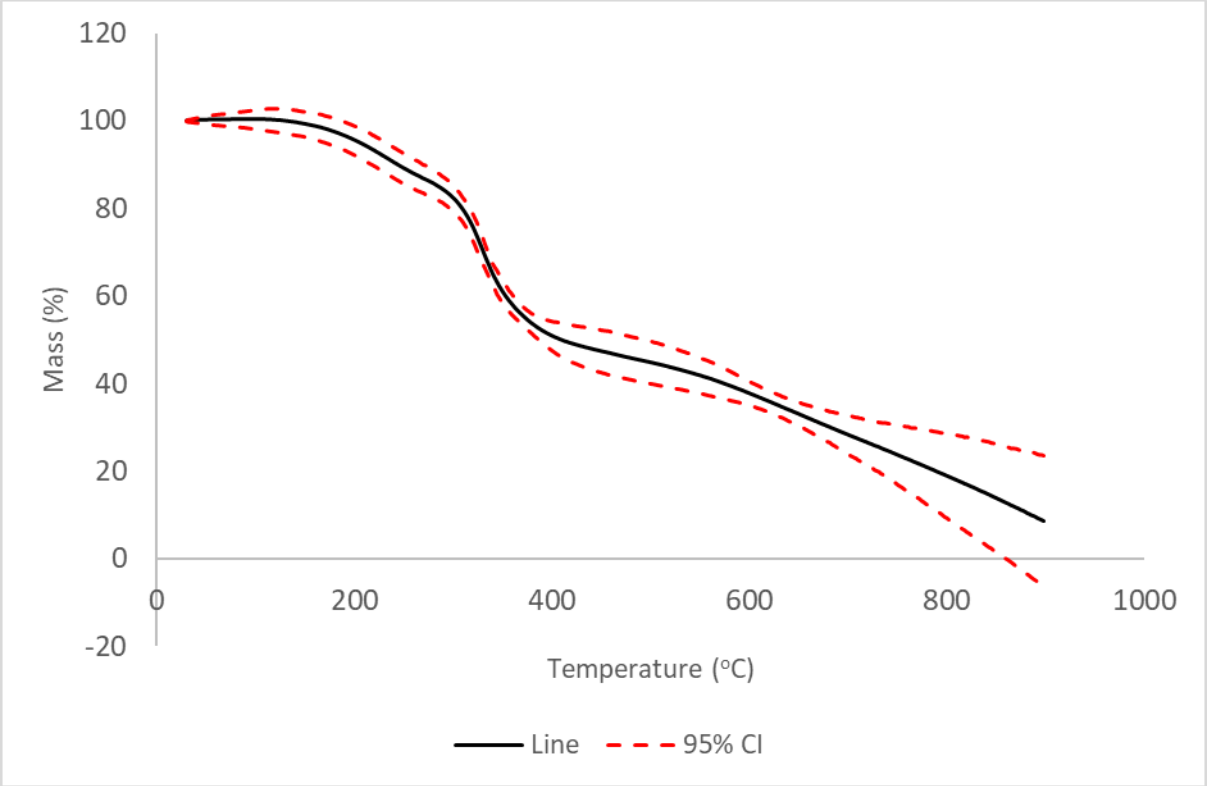

Figure 3.18. *Mean TG and 95% confidence distribution for line-produced foam samples in inert atmosphere.*

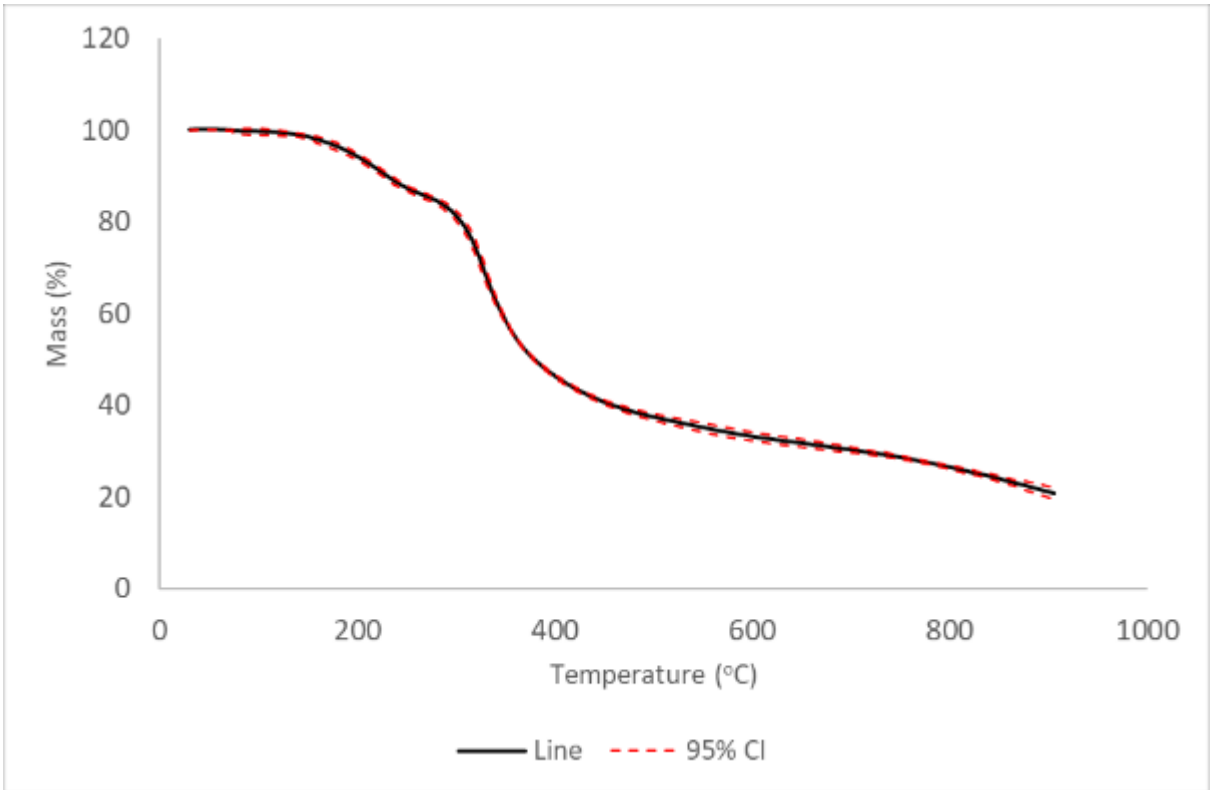

Figure 3.19*. Mean TG and 95% confidence distribution for free-rise foam samples heated in an inert (N_2) atmosphere.*

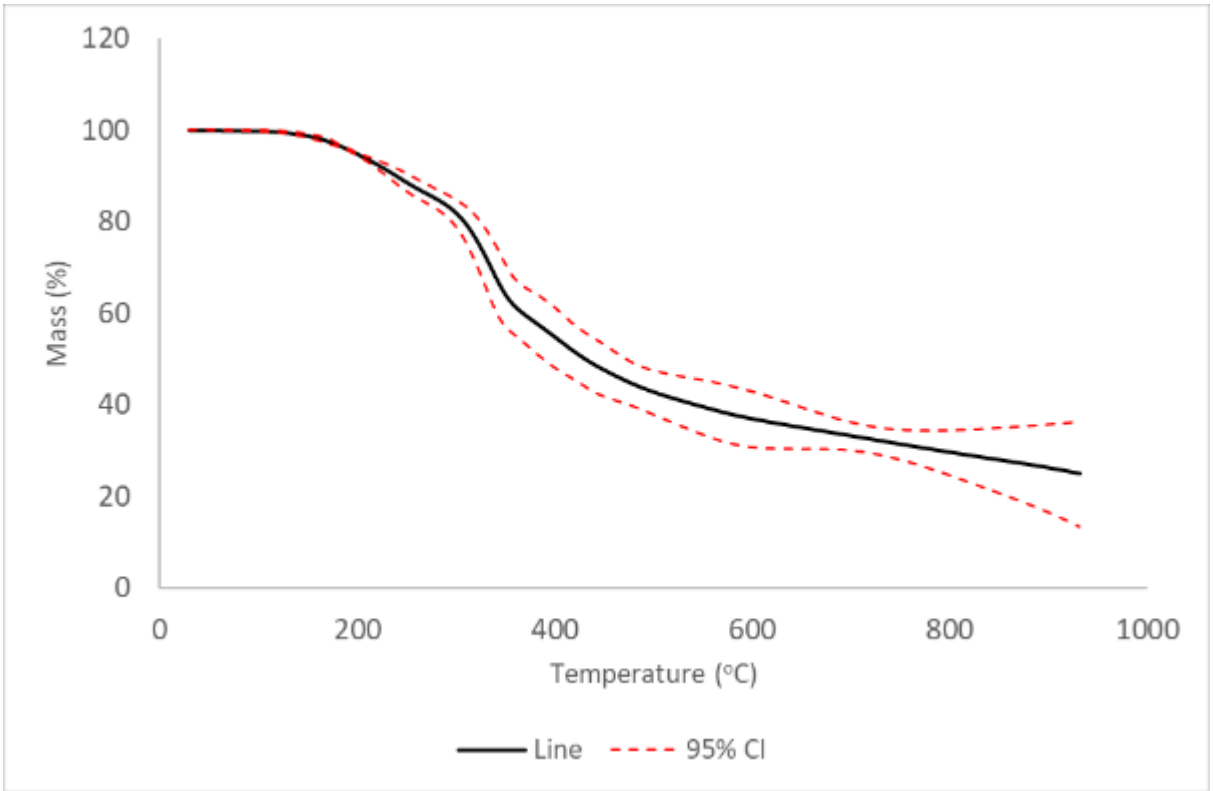

Figure 3.20. *Mean TG and 95% confidence distribution for block-mould foam samples in N_2.*

Figures 3.18-3.20 display the plots obtained by applying the previously described process to the data for each of the three sample sets. At a given temperature, the width of the 95 % confidence interval reflects the variability in thermal stability observed for sample within each set at that temperature. Visual examination of the TG curves obtained for each sample previously indicates that the free-rise foam samples exhibit more consistent behaviour than either line-produced or block-mould foams. It is likely that this is at least in part attributable to the free-rise samples having been drawn from a relatively small volume within a single-batch of foam. However, the line-produced samples were also cut from a single piece of slabstock and exhibited a similar degree of overall variability to the block-mould samples, the latter of which were taken from separately produced batches.

When the confidence distributions are compared, it is found that there is a great deal of overlap with all three intervals overlapping across much of the temperature range. The only temperature regions in which this is not the case, are those between 360-500 ^{o}C, within which there was no overlap between the free-rise foams samples and either of the line and block foams, and 500-650 ^{o}C, in which the free-rise foams overlap with the block foams but not with the line foams. Within these regions, it can be said that free-rise foams exhibit significantly lower thermal stability than one or both other sample sets at a threshold of p = 0.05. However, it is overly

conservative to assume no significant difference based on at this threshold based on the overlap of 95 % confidence intervals(22), with the 84 % confidence interval instead suggested as a more appropriate value.

When this less conservative criterion is applied, it is found that free-rise foams experience significantly greater mass loss than line-produced foams across approximate temperature intervals of 225-260 ^{o}C and 290-680 ^{o}C, but significantly less above temperatures of 760 ^{o}C. Compared to block-mould foams, significantly greater total mass loss is observed from 210-250 ^{o}C and 330-840 ^{o}C. Finally, no significant difference is observed in the thermal stability of line-produced and block-mould foams at temperatures below around 700 ^{o}C, above which block-mould foams show significantly lower total mass loss. The significant difference observed at these temperatures is likely to have been influenced by the high than expected mass loss observed in one of the line foam samples, which represents a significant outlier compared to the observed range for the remaining eight foam samples. It is therefore reasonable to conclude that the behaviour of block-mould foam samples is, on average, a reasonable approximation to the likely behaviour of line-produced samples.

When evaluating the lower observed stability of free-rise foam samples, the effect of initial mass on thermal stability should be considered. For identical materials, a sample of lower mass will have a correspondingly lower total heat capacity, *C*, as given by the following equation:

$$C = mc_p \tag{3.6}$$

Where:

$$C = heat\ capacity\ (JK^{-1})$$

$$m = mass\ (kg)$$

$$c_p = specific\ heat\ capacity(\ Jkg^{-1}K^{-1})$$

The amount of absorbed heat can be calculated by the equation:

$$Q = mc_p\Delta T \tag{3.7}$$

Where:

$$Q = absorbed\ heat, (J)$$

$$\Delta T = change\ in\ absolute\ temperature\ (K)$$

This can be rearranged to derive the following relationships:

$$Q \propto m \tag{3.8}$$

$$\Delta T \propto \frac{1}{m} \tag{3.9}$$

Therefore, a sample of lower mass requires less absorbed heat to undergo a given change in temperature and will undergo a greater increase in temperature for a given heat absorption.

Additionally, for materials of equal density ρ, mass m will be directly proportional to volume V as below.

$$\rho = \frac{m}{V} \tag{3.10}$$
$$m = \rho V$$

The total heat absorbed into an object is a product of the surface area and the incident heat flux. Because of the square-cube relationship between surface area and volume, this implies that an object of smaller mass will tend possess a greater surface area to volume ratio where the objects are of similar shape.

We can consider a simple case of two cubic samples of PIR foam with masses of $\rho = 50$ mg/cm^3 and masses of 15 mg and 10 mg respectively. Calculating the volume (m/ρ) for the samples gives values of 0.3 cm^3 and 0.2 cm^3, with side lengths $(\sqrt[3]{V})$ of 0.669 cm and 0.585 cm respectively. Since the surface area of a cube = $6l^2$, the surface areas of the two samples are 2.69 cm^2 and 2.05 cm^2 with surface area to volume ratios of 8.97 and 10.25, respectively.

The calculation of heat transfer into an object is complex, as conductive, convective and radiative modes will contribute to the total heat transfer, but the rate of heat transfer in all three modes is seen to be directly proportional to surface area as seen below (23).

$$Q(conductive) = \frac{\lambda A(T_2 - T_1)}{\Delta x} \quad (3.11)$$

$$Q(convective) = hA(T_2 - T_1)$$

$$Q(radiative) = \varepsilon\sigma A(T_2^4 - T_1^4)$$

$Q = heat\ transfer\ rate$

$\lambda = thermal\ conductivity$

$\Delta x = thickness$

h

$= convective\ heat\ transfer\ coefficient$

$\varepsilon = emissivity$

$\sigma = Stefan - Boltzmann\ constant$

$A = exposed\ surface\ area$

$T_2 - T_1 = temperature\ difference$

Consequently, a smaller object will absorb a greater amount of heat from its surroundings per unit volume and unit mass, which may manifest itself in a reduced thermal lag between the furnace temperature and the temperature of the sample.

For the foam samples tested, it cannot be assumed that all of the variation in mass is attributable to differences in sample volume. While a small change in sample dimension can have a relatively large impact on volume due to the cubic relationship between them, thermogravimetry samples were prepared as cylindrical sections to ensure a tight fit with the sample pan and would therefore be expected to have volumes approximately equal to that of the pan. Since mass of the nine samples varied considerably, ranging from 8.07 mg to 12.15 mg, a 51 % difference, this indicates substantial variation in the density of the samples. Free-rise foams were considerably lower in mass (mean = 8.32 mg) than both line-produced (mean = 10.88 mg) and block-mould (mean = 11.15 mg) foams.

When no physical constraint is placed on the rise of the foam, it is possible that this results in greater expansion of the blowing agent, leading to a structure with a larger cell size and thinner cell walls as the cells are in effect given more freedom to expand during the foaming reaction. It has been previously demonstrated that a decrease in the density of polyurethane foams results in lower thermal conductivity, and that this relationship is approximately linear.

The absorption of heat into an object is influenced by thermal inertia, also known as thermal effusivity(24), which describes the rate at which a material responds to the temperature of its surroundings and is given by:

$$e = \sqrt{\lambda \rho c_p} \tag{3.12}$$

$e = thermal\ effusivity\ (\frac{W\sqrt{s}}{m^2K})$

$\lambda = specific\ thermal\ conductivity\ (\frac{W}{mK})$

$\rho = density\ (\frac{kg}{m^3})$

$c_p = specific\ heat\ capacity\ (\frac{J}{kgK})$

Effusivity is the ability of a material to exchange heat across an interface and is qualitatively experienced as the difference in perceived warmth or coolness of materials to the touch(24). At an ambient temperature of 20 ^oC copper, with a thermal effusivity of around 37,000 $W\sqrt{s}/m^2K$, feels colder than a plastic with a thermal effusivity of 500-600 $W\sqrt{s}/m^2K$ at the same temperature due to its greater ability to absorb heat. For typical PIR foams, this value is likely to be as low as 25-50 $W\sqrt{s}/m^2K$. The extremely low thermal effusivity of these materials is apparent from the observation that they do not feel appreciably hot to the touch even after periods in excess of 24 hours at ambient temperature in excess of 200 ^oC.

Another important intensive property is thermal diffusivity. Thermal diffusivity is the rate at which heat will transfer across pressure gradient within a material and is given by the thermal conductivity divided by the volumetric heat capacity (25).

$$\alpha = \frac{\lambda}{\rho c_p} \tag{3.13}$$

$\alpha = thermal\ diffusivity\ \left(\frac{m^2}{s}\right)$

$\lambda = specific\ thermal\ conductivity\ (\frac{W}{mK})$

$\rho = density\ (\frac{kg}{m^3})$

$c_p = specific\ heat\ capacity\ (\frac{J}{kgK})$

Thermal diffusivity differs from thermal conductivity, as it applies to transient conduction conditions. A thermal conductor bridging two otherwise thermally isolated regions with a constant ΔT will, given time, reach a steady state in which there is a linear temperature gradient between the hot and cold ends. Under such steady-state conditions, the transfer of heat through the material is wholly dependent upon the thermal conductivity of the material. Steady-state conditions are preceded by a period of transient conduction in which the temperature gradient will vary throughout the material as one end is heated, and the rate at which the gradient equalises throughout will be dependent on thermal diffusivity. In materials with low thermal diffusivity absorbed heat effectively becomes trapped at the boundary layer, leading to a rapid temperature increase near the heated surface as heat is conducted away slowly(25).

It follows that lower thermal conductivity will result in both a slower absorption of heat, and slower distribution of heat throughout the material, but a lower thermal diffusivity may also result in the concentration of absorbed heat near the exposed surfaces of the material, resulting in an increased surface temperature. It is also the case that the volumetric heat capacity, $\rho c_{p,}$ will increase with the proportion of polymer per unit volume. The specific heat capacity of solid PIR is not widely reported due to the polymer being almost exclusively produced as a foam but is likely to be on the same order as that of amorphous polyurethane resin (~2250 J/kgK). At a density of 1200 kg/m^3, this corresponds to a volumetric heat capacity of 2.7 MJ/m^{3}K, of similar order to the volumetric heat capacity of steel (3.7 MJ/m^{3}K). By contrast, pentane isomers have volumetric gas-phase heat capacity under standard laboratory conditions of 3.3-4.9 kJ/m^{3}K, around 3 orders of magnitude lower. In general, the heat capacity of a composite material is approximately equal to that of its constituent parts, multiplied by their proportion. In terms of specific heat capacity, this means that:

$$C_{pmixture} = \left(\frac{m_1}{m_{mixture}}\right) C_{p1} + \left(\frac{m_2}{m_{mixture}}\right) C_{p2} + \cdots + \left(\frac{m_n}{m_{mixture}}\right) C_{pn} \tag{3.14}$$

In the case of volumetric heat capacity:

$$\rho C_{pmixture} = \left(\frac{V_1}{V_{mixture}}\right) \rho C_{p1} + \left(\frac{V_2}{V_{mixture}}\right) \rho C_{p2} + \cdots + \left(\frac{V_n}{V_{mixture}}\right) \rho C_{pn} \tag{3.15}$$

In the specific case of the foam samples under analysis:

$$\rho C_{pfoam} = \left(\frac{V_{matrix}}{V_{foam}}\right)\rho C_{pmatrix} + \left(\frac{V_{pentane}}{V_{foam}}\right)\rho C_{ppentane} \quad (3.16)$$

Assuming a foam density of 50 kg/m^3, matrix density of 1200 kg/m^3 and blowing agent density of 3 kg/m^3, the contribution of the polymer matrix to the total foam volume can be calculated as follows:

$$\rho_{foam} = \frac{V_{matrix}}{V_{foam}}\rho_{matrix} + \frac{V_{pentane}}{V_{foam}}\rho_{pentane} \quad (3.17)$$

$$V_{foam} = V_{matrix} + V_{pentane} \quad (3.18)$$

Setting total foam volume to a unit value:

$$V_{pentane} = 1 - V_{matrix} \quad (3.19)$$

$$\rho_{foam} = (V_{matrix}\rho_{matrix}) + ((1 - V_{matrix})\rho_{pentane})$$

$$\rho_{foam} = 1200V_{matrix} + 3 - (3V_{matrix})$$

$$\frac{\rho_{foam} - 3}{1197} = V_{matrix}$$

$$V_{matrix} = \frac{47cm^3}{1197cm^3} = 0.039$$

The PIR matrix is therefore found to account for 3.9 % of the total volume. Using these values in the above equation gives the following.

$$50C_p = (0.04 \times 2.7 \times 10^6) + (0.96 \times 4.1 \times 10^3) = 1.12 \times 10^5\ Jkg^{-1}K^{-1}$$

Under these assumptions, the volumetric heat capacity of PIR foam is 112 kJ/m^{3}K, while the specific heat capacity is 2200 J/kgK. This value is similar to values of 2359-2996 J/kgK reported in the literature for polyurethane foams (26). While the polymer matrix makes up only around 4 % of the volume of the foam, it accounts for 96 % of the volumetric heat capacity, with the gas accounting for the remainder.

The density of PIR foams is reported in a range from 25-70 kg/m^3. Applying the previously described methods, the relationship between foam density and volumetric heat capacity can be established by substituting different values for the density into the above system of equations.

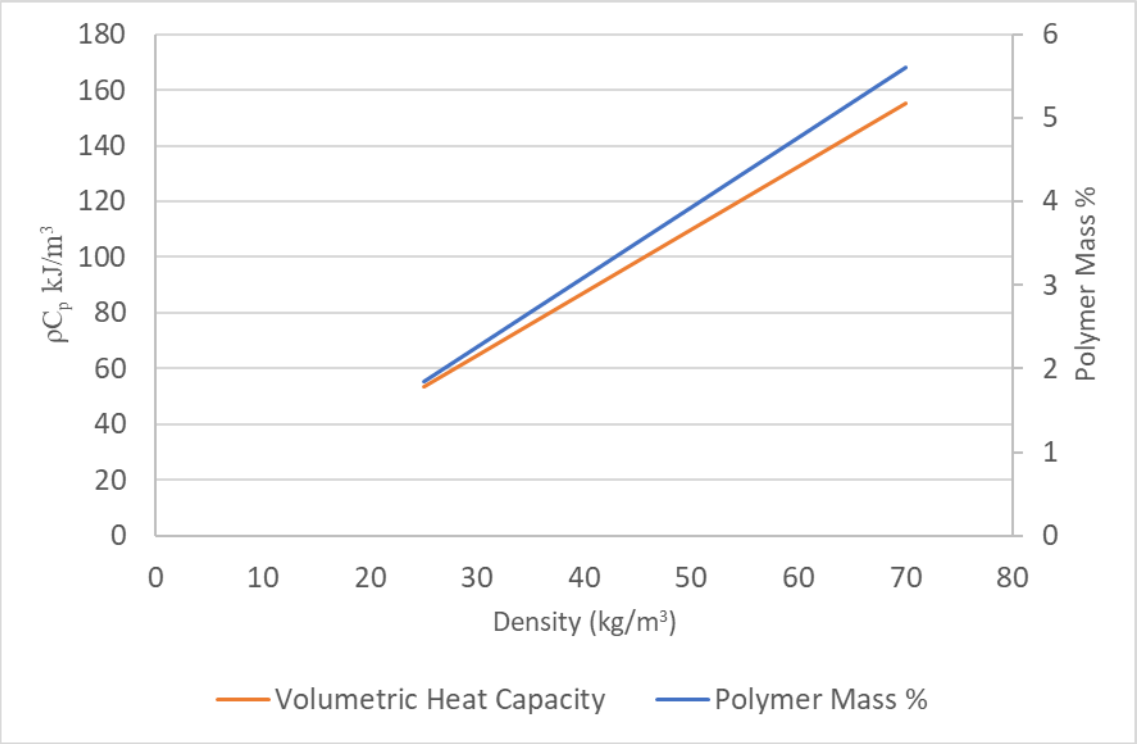

Figure 3.19. *Calculated ρC_p and proportion of mass accounted for by polymer matrix for polyisocyanurate foams having densities from 25-70 kg/m^3 based on values used within this thesis.*

Volumetric heat capacity and the proportion of mass accounted for by the polymer increase linearly with foam density as seen in Figure 3.19 above.

For each of the nine samples, the initial mass has then been plotted against percentage mass loss at 200 ºC, 250 ºC, 300 ºC, 350 ºC and 500 ºC (data shown in Figure 3.20).

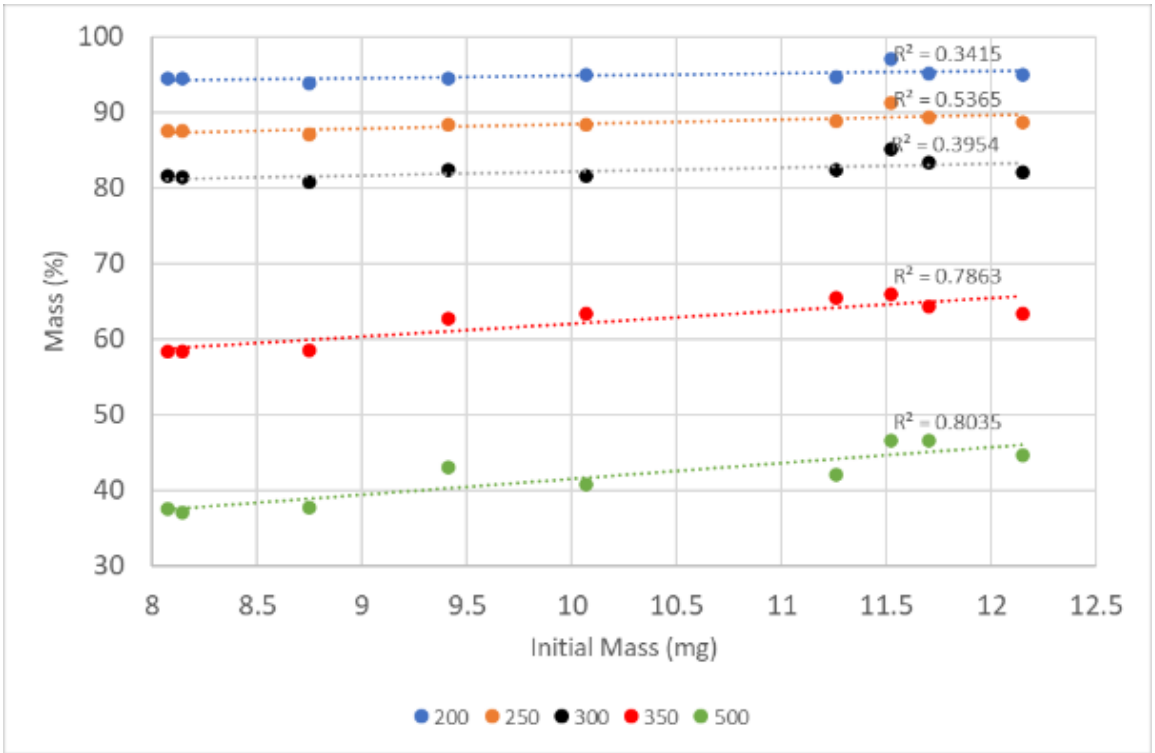

Figure 3.20. *Relationship between initial samples mass and retained mass % at 200 ºC, 250 ºC, 300 ºC, 350 ºC and 500 ºC.*

A positive correlation is observed between initial sample mass and retained mass percentage using a linear regression model across a range of temperatures from 200-500 ºC (Figure 3.20). A positive correlation in this case indicates that retained mass increased with sample mass.

A weak positive correlation is observed between initial sample mass and the sample temperature at the first mass loss peak, while a moderate correlation was observed for the second mass loss peak (Figure 3.21). In this case, most of the variance in the observed temperatures is not explained by the difference in sample mass, and this is also the case for the relationship between mass loss rates at the first and second peaks and initial sample mass (Figure 3.22).

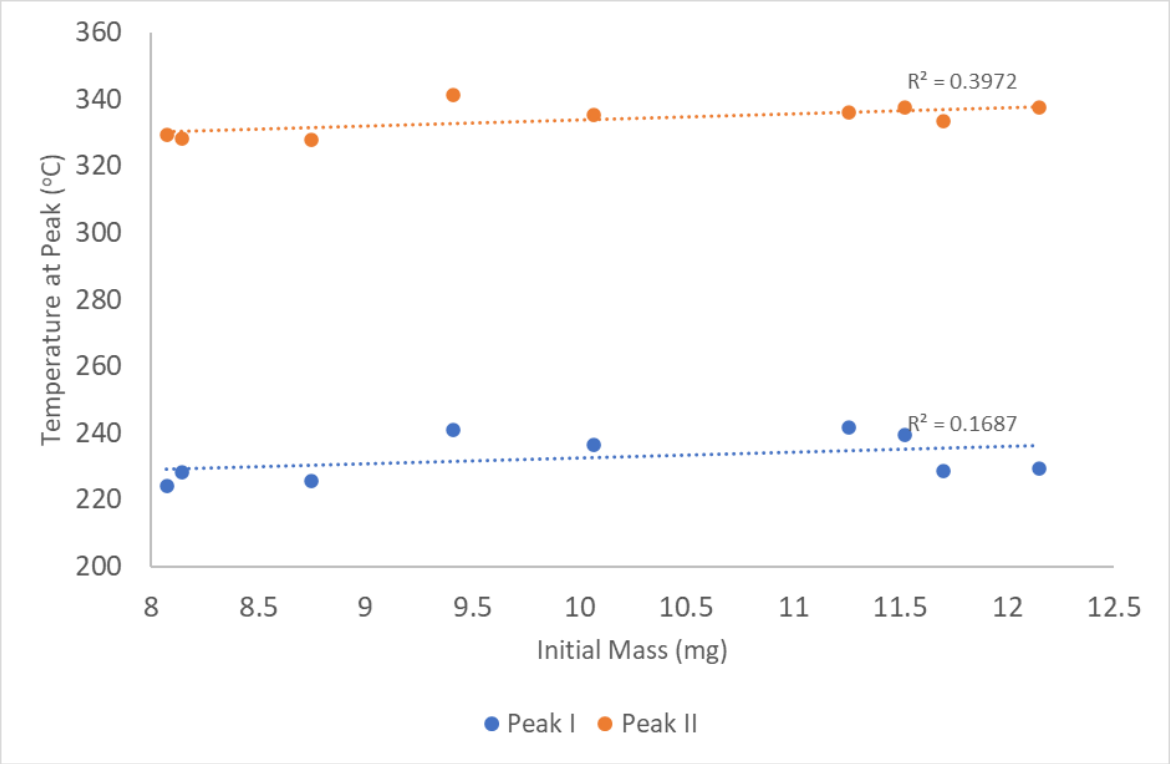

Figure 3.21. *Temperature (°C) at first and second mass loss peak versus sample mass for LF, FR and BM foam samples*

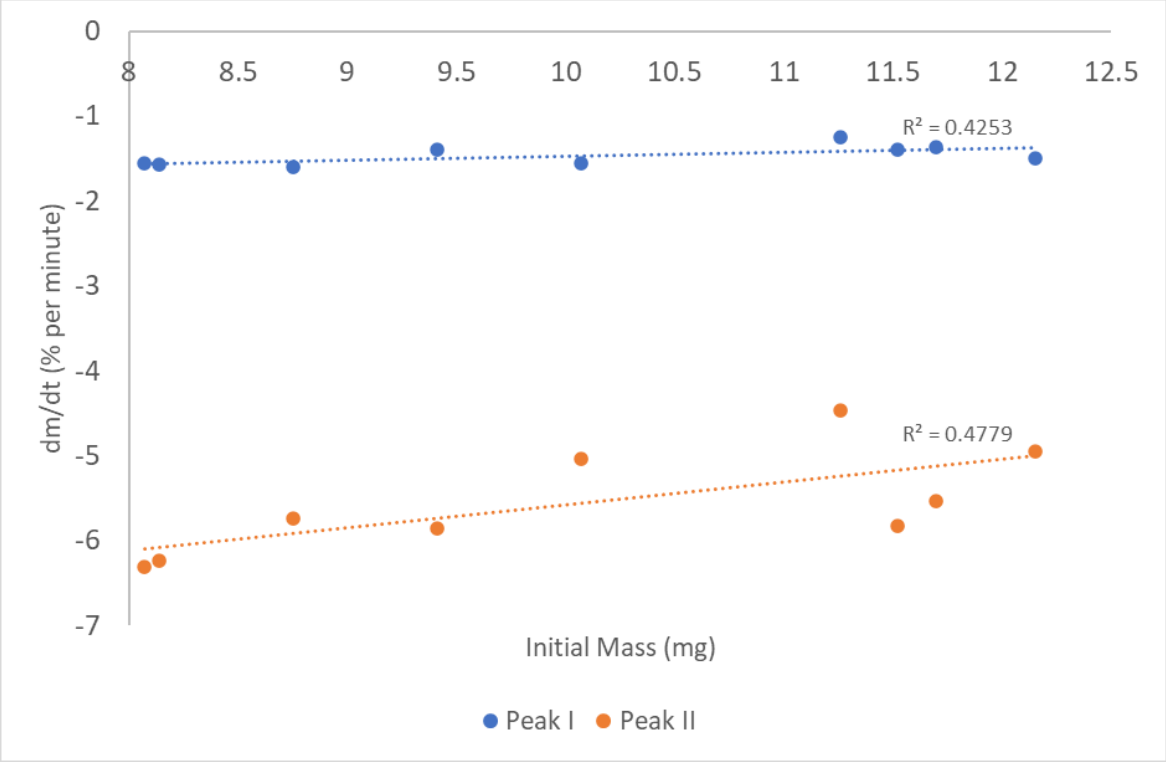

Figure 3.22. *Mass loss rate (% per minute) at first and second mass loss peak versus sample mass for LF, FR and BM foam samples.*

Overall, it is observed that initial sample mass does appear to influence thermal stability even at this scale where mass/bulk effects could be expected to be less dominant. In the context of insulation material as used in construction, these mass and bulk effects are likely to limit the decomposition of the foam further away from the outer surfaces of the material, due to the low rate of heat transfer to these parts of the foam.

3.3.5. Oxidative TG/dTG

Previous thermogravimetric analyses carried out in this work have pertained to PIR foams in an inert atmosphere (i.e., under flowing N_2 gas). Under such conditions, observed behaviour will tend to be largely pyrolytic as oxidative reactions are minimized. Outside of controlled environments, the thermal degradation of materials usually occurs under conditions in which some concentration of ambient oxygen is present (i.e., up to 21 % O_2). Under such conditions, pyrolytic behaviour is a precursor to thermo-oxidative degradation processes, which can favour more exothermic reactions due to the presence of oxygen as a readily available terminal electron acceptor. Figures 3.23 and 3.24 show TG and dTG thermograms obtained for three samples of free-rise foams, designated FR4, FR5 and FR6 under an oxidative atmosphere of dry air. These samples were taken from the same batch of free-rise foam as samples FR1-3 that were analysed in section 3.3.2.

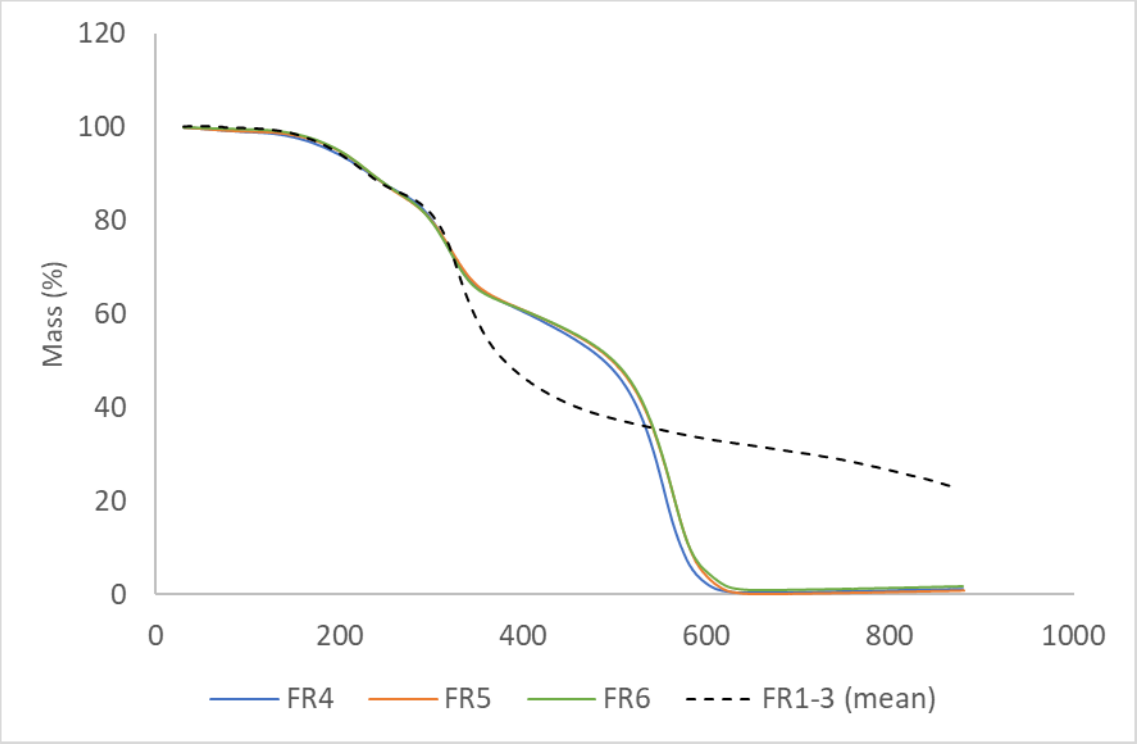

Figure 3.23. *TG thermograms for three free-rise foam samples (FR4-6) under dry air at 10°C/min. Mean TG curve for samples FR1-3 has been overlaid for comparison.*

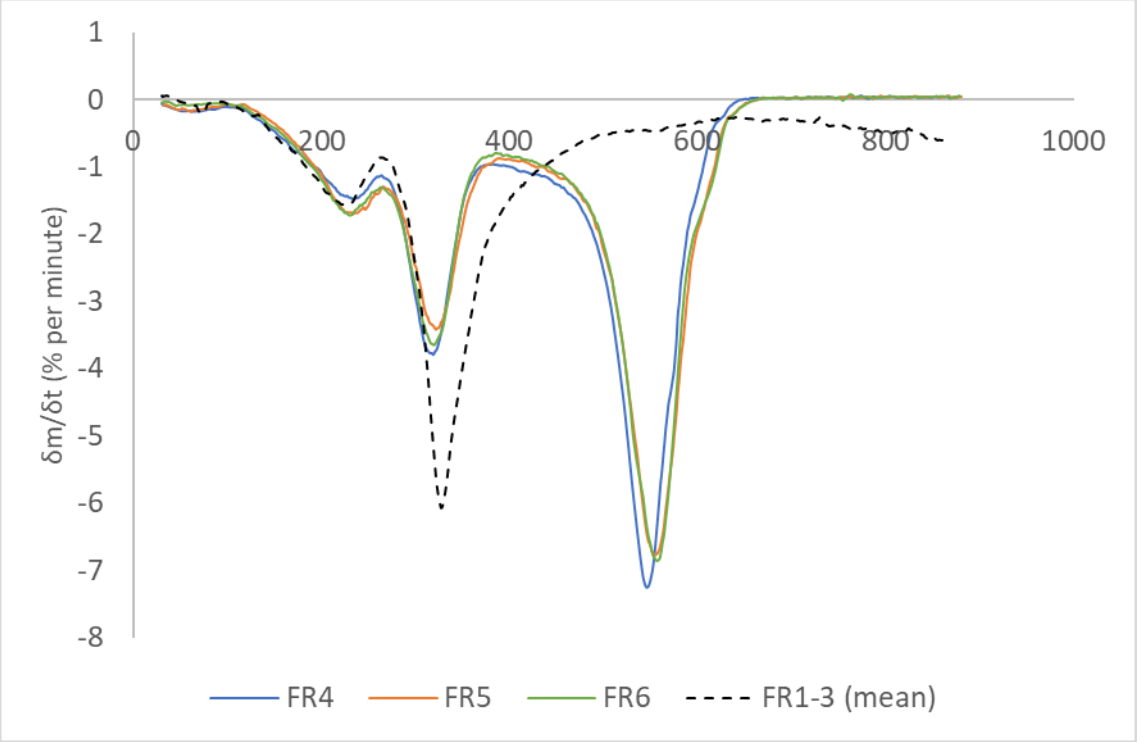

Figure 3.24. *dTG thermograms for three free-rise (FR4-6) foam samples under dry air at 10°C/min. Mean dTG curve for FR1-3 has been overlaid for comparison.*

Dynamic thermogravimetric analysis was carried out on three free-rise PIR foam samples (mean mass = 10.75 mg) under dry air, with otherwise identical experimental conditions to the previous analysis under nitrogen. These samples were produced to an identical formulation as the previous free-rise foam samples analysed under nitrogen, matching the project sponsor's commercial formulation. The overall shapes of the TG and dTG curves are markedly different from those obtained under nitrogen. Under nitrogen, two major mass loss events are observed from 97-261 ^{o}C and 261-450 ^{o}C. But, under oxidative conditions, three distinct mass loss events occur. Samples analysed under oxidative conditions exhibit a negligible rate of mass loss at temperatures below ~104-116 ^{o}C with a maximum observed mass loss at 100 ^{o}C of 0.9 % in sample LF4.

Above this temperature, all three samples undergo an increase in mass loss rate, reaching a peak rate of 1.5-1.7 % per minute at 230-233 ^{o}C. This is generally consistent with the measurements in this temperature range for samples under inert conditions. Based on this, it can be inferred that the presence or absence of oxygen does not exert a strong influence on the thermal degradation processes in this temperature regime. This is compatible with pyrolytic processes such as the thermal dissociation of the weaker bonds in the polymer structure and the volatilisation of light depolymerisation products and the outgassing of blowing agent due to increased intracellular pressure. The first mass loss event extended beyond the peak to a transition point at 266-267 ^{o}C, with total mass loss at this transition point being 14.2-14.4 %.

The second mass loss event consists of a region of accelerating mass loss from the first transition temperature to a peak at 319-321 ^{o}C with calculated mass loss rates of 3.4-3.8 % per minute. This indicates a divergence in the behaviour of foams under inert and oxidative conditions. The temperature at which the second peak is observed is lower under oxidative conditions than under inert conditions, where this peak occurred between 324-336 ^{o}C across the free-rise samples. This is despite the oxidative samples being generally higher in mass, when it was previously observed that there is a moderate positive correlation between initial sample mass and the temperature at which the second mass loss peak occurs. Furthermore, while this peak occurs at a lower temperature, the peak rate of mass loss is lower under oxidative conditions than under inert conditions, where a rate of 5.7-6.3 % per minute was observed at the second peak. Above the peak, the rate of mass loss decelerates to a minimum, occurring at 374-388 ^{o}C. The total mass loss associated with this region ranged from 23.7-24.8 %. This compares to a mass loss of 46 % observed under inert conditions.

It is apparent that the presence of oxygen exerts a substantial effect on the thermogravimetric behaviour of free-rise foams in the second mass loss region, with reduced mass loss in the presence of oxygen compared to under non-oxidative conditions. This is a possible indication of a critical temperature at which solid-state oxidation focused around the methylene bridge of 4,4-MDI (27).

The third mass loss event begins immediately after the second transition point. There is initially a relatively slow increase in the rate of mass loss, with increasing sharply towards a peak at 547-555 °C. The mass loss rate at this peak is 6.7-7.2 % per minute. During this event, an effectively total consumption of the polymer occurs, with the entire residual mass (60-65 %) being lost and dm/dt reaching zero by 630-640 °C.

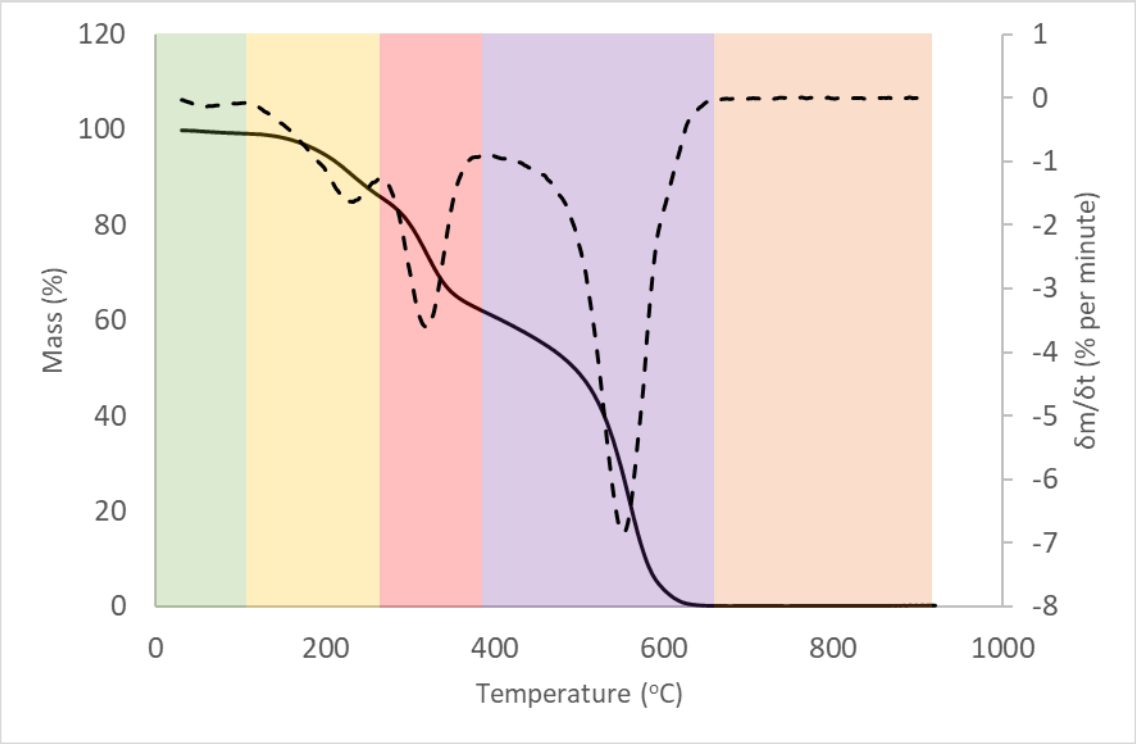

Figure 3.25. *Mean TG (solid) and dTG (dashed) curves of free-rise foams in oxidative atmosphere.*

Taking the mean across the three samples, the initial green pre-pyrolytic region appears to lie between 30-107 °C, with a maximum mass loss rate of 0.13 % per minute and total mass loss of 0.7%. The three consecutive mass loss events are observed above this temperature across ranges of 107-264 °C, 264-386 °C, and 386-660 °C maximum rate of mass loss at 233 °C

(-1.63 % per minute), 321 °C (-3.61 % per minute), and 552 °C (-6.84 % per minute). Mass losses in these regions are 12.4 %, 24.3 %, and 61.2 %, respectively.

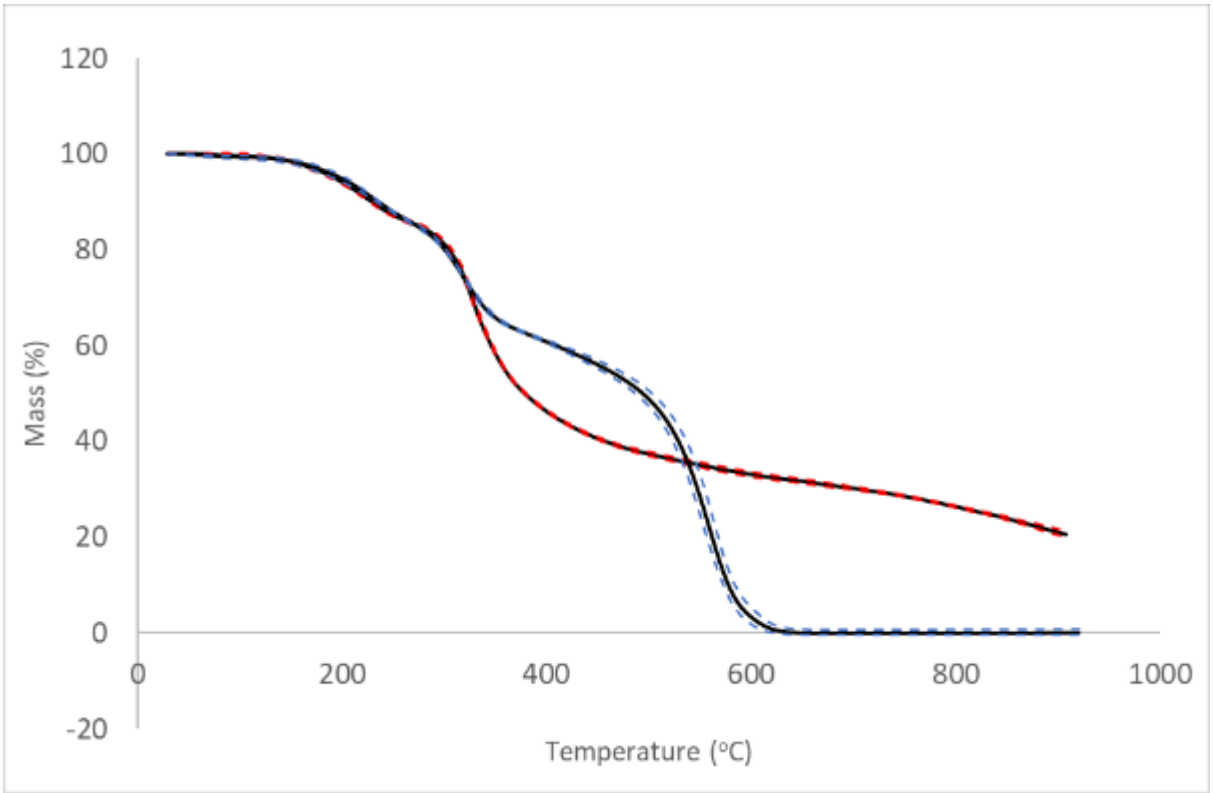

Figure 3.26. *Comparison of mean TG thermograms for free-rise foam samples under inert (red) and oxidative (blue) conditions. Dashed lines indicate the upper and lower boundaries of the 84 percent confidence interval.*

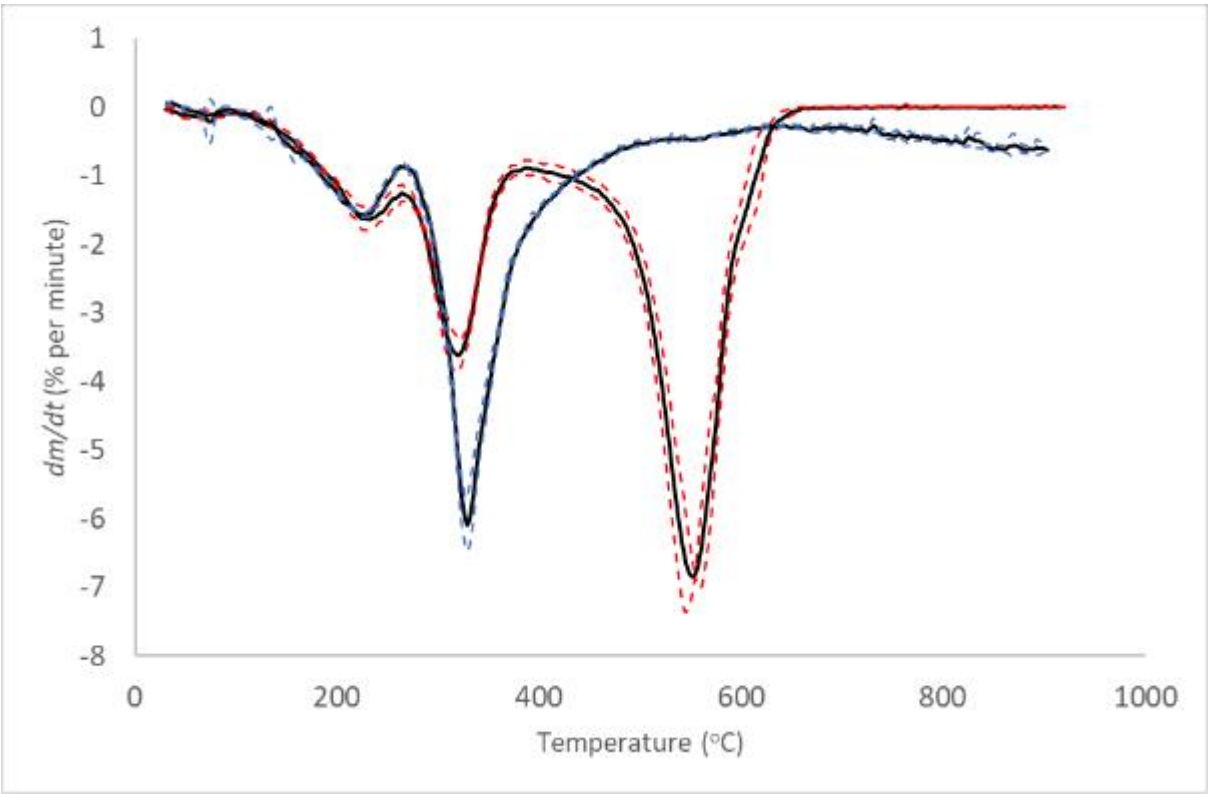

Figure 3.27. *Comparison of mean dTG thermograms for free-rise foam samples under inert (blue) and oxidative (red) conditions. Dashed lines indicate the upper and lower boundaries of the 84 % confidence interval.*

Side-by-side comparison of the TG and dTG curves for free-rise foams in inert and oxidative atmospheres do not exhibit significant differences in behaviour at temperatures below 236 °C. The rate of mass loss in inert conditions is significantly lower than under oxidative conditions at 236-295 °C based on inspection of the dTG curves, significantly higher from 315-425 °C, and once again significantly lower from 445-615 °C. Total mass loss is significantly higher under inert conditions across the 330-520 °C temperature range, and significantly lower above 545 °C. These findings are consistent with previous comparisons of thermolytic and thermo-oxidative degradation in polyisocyanurates and polyurethanes (28,29).

Accounting for the observed behaviour in the first mass loss event of all three sets of foam samples analysed under inert conditions, it appears that the first mass loss event is not significantly influenced by oxygen. This provides a strong inference that the observed behaviour of PIR foams under oxidative conditions remains predominantly pyrolytic at

temperatures below 315 °C. It is likely that mass losses in this region arise primarily from the off gassing of blowing agent from within the foam matrix and from the breakdown of urethane bonds liberating diethylene glycol.

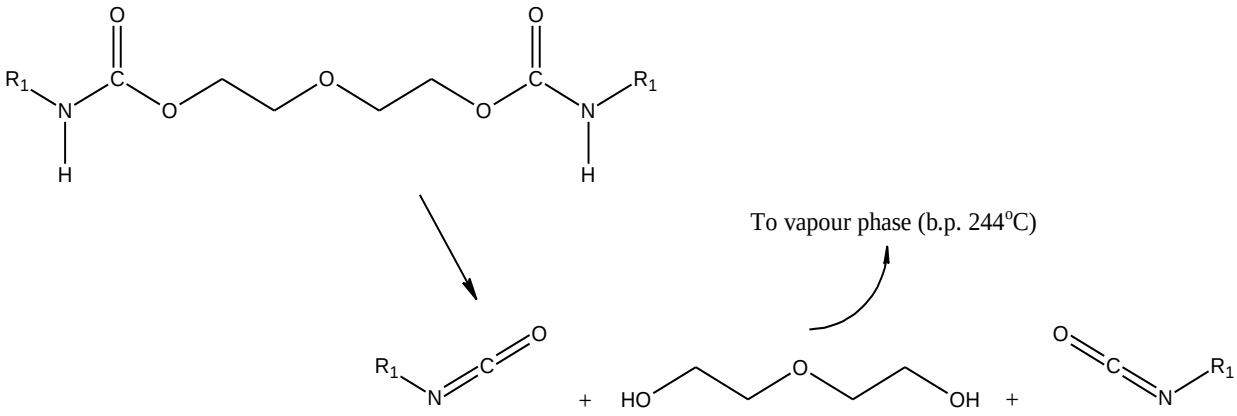

Figure 3.28. *Dissociation of flanking urethane bonds in linear polyurethane segment releasing diethylene glycol into vapour phase*

Above this temperature oxidative processes begin to exert a measurable influence on thermal behaviour. As temperature increases, bond dissociation will tend to become more extensive, so the observed decrease in mass loss rate under oxygen is most likely to result from oxygen reacting with polymer in the condensed phase, resulting in the formation of higher molecular weight compounds. Several solid-state oxidations reactions have been identified in the literature which may account for this observation (27)(30).

One such reaction is the conversion of the diphenylmethane moiety of 4,4-methylenediphenyldiisocyanate to a benzophenone moiety through a radical mechanism. This reaction has been identified as a dominant mechanism in the accelerated oxidative aging of polyurethanes based on 4,4-methylene diphenyl diisocyanate and polyester polyol. When such foams were subjected to a temperature of 150 °C over a 77-day period, over half of the diphenylmethane groups were converted to benzophenone, while the polyester segments remained largely unchanged. This indicates that this group is particularly susceptible to thermal oxidation, and this reaction would be expected to occur at a higher rate at the temperatures encountered here (27).

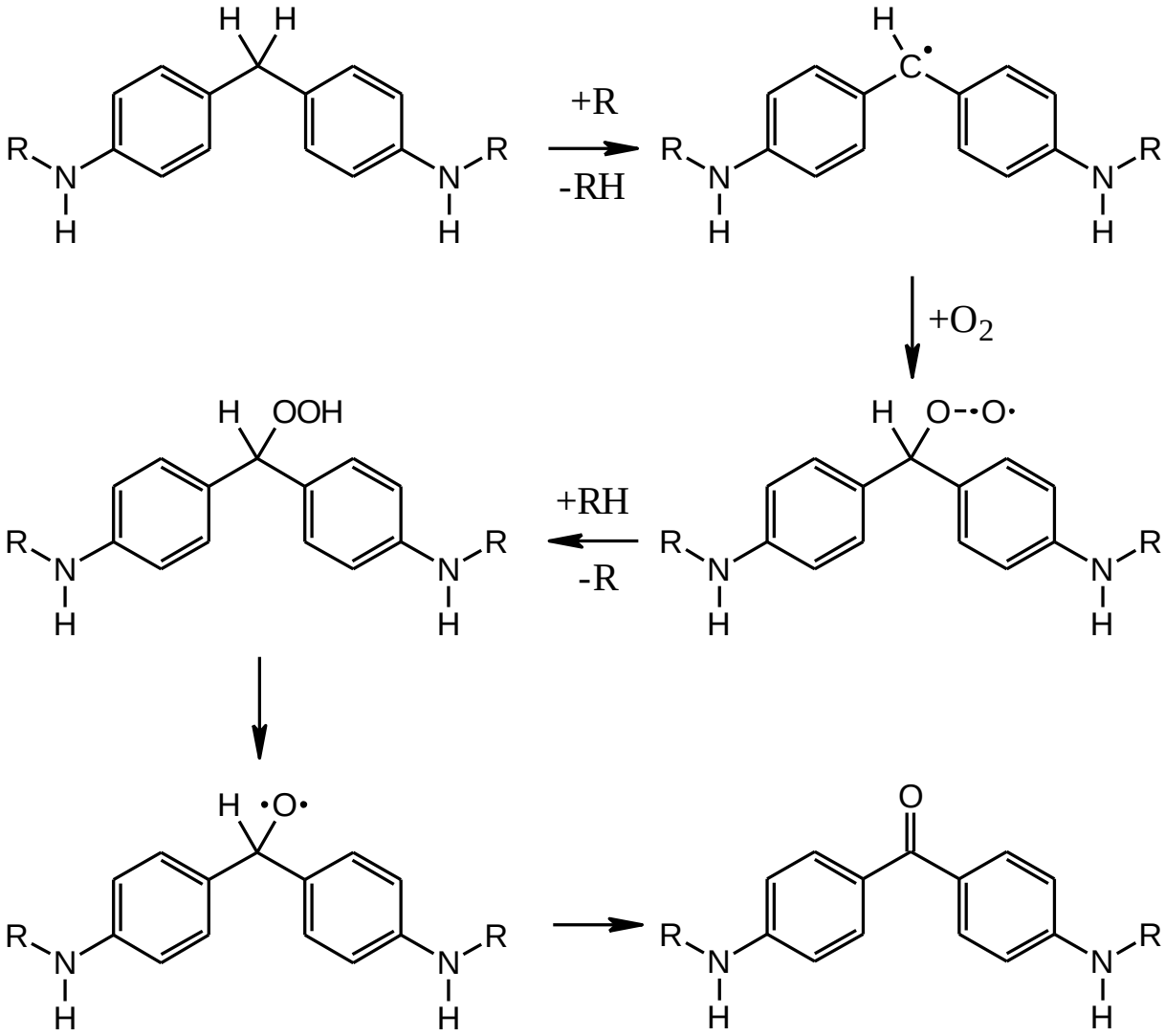

Figure 3.29. *Conversion of diphenylmethane to diaminobenzophenone derivative via radical substitution mechanism under oxidative conditions* (30)

The diphenylmethane group is abundant within the PIR structure and this oxidative conversion would increase the molecular mass of the moiety from 188.18 $gmol^{-1}$ to 203.18 $gmol^{-1}$, an increase of 7.97 %. If widespread, such a reaction might be detectable in the TGA trace as an increased mass retention compared to that which is observed under purely thermolytic conditions. Furthermore, benzophenone and its derivatives tend to have higher phase change temperatures than those of diphenylmethane, potentially reducing the volatilisation of fragmentary products. For example, the melting and boiling points of diphenylmethanediamine are 89 ^{o}C and 398 ^{o}C respectively, while the corresponding of the analogous benzophenone compound, diaminobenzophenone are 245 ^{o}C and 458 ^{o}C. Oxidative conditions may also

initially act to promote charring reactions in the condensed phase, resulting in increased formation of less volatile structures(31).

Marquis *et al.* (28) have proposed that the breakdown of hard and soft segments (Figure 3.30) in the linear segments of the polymer are competing reactions, as evidenced by differences in the evolved gaseous products. Hard segment degradation appears to be insensitive to the presence of O_2, occurring across a temperature range of 217-344 ^oC under both inert and oxidative conditions. In contrast, soft segment degradation is promoted by the presence of oxygen, with a temperature shift from 249-421 ^oC under inert conditions to 238-410 ^oC under oxidative conditions. Under the proposed reaction scheme, hard and soft segment degradation lead to the production of distinct polyol intermediates, which are subsequently converted to a carbodiimide-rich char. Carbodiimide production may occur more readily when soft segment degradation becomes more dominant, accounting for the region of increased stability observed under oxidative conditions.

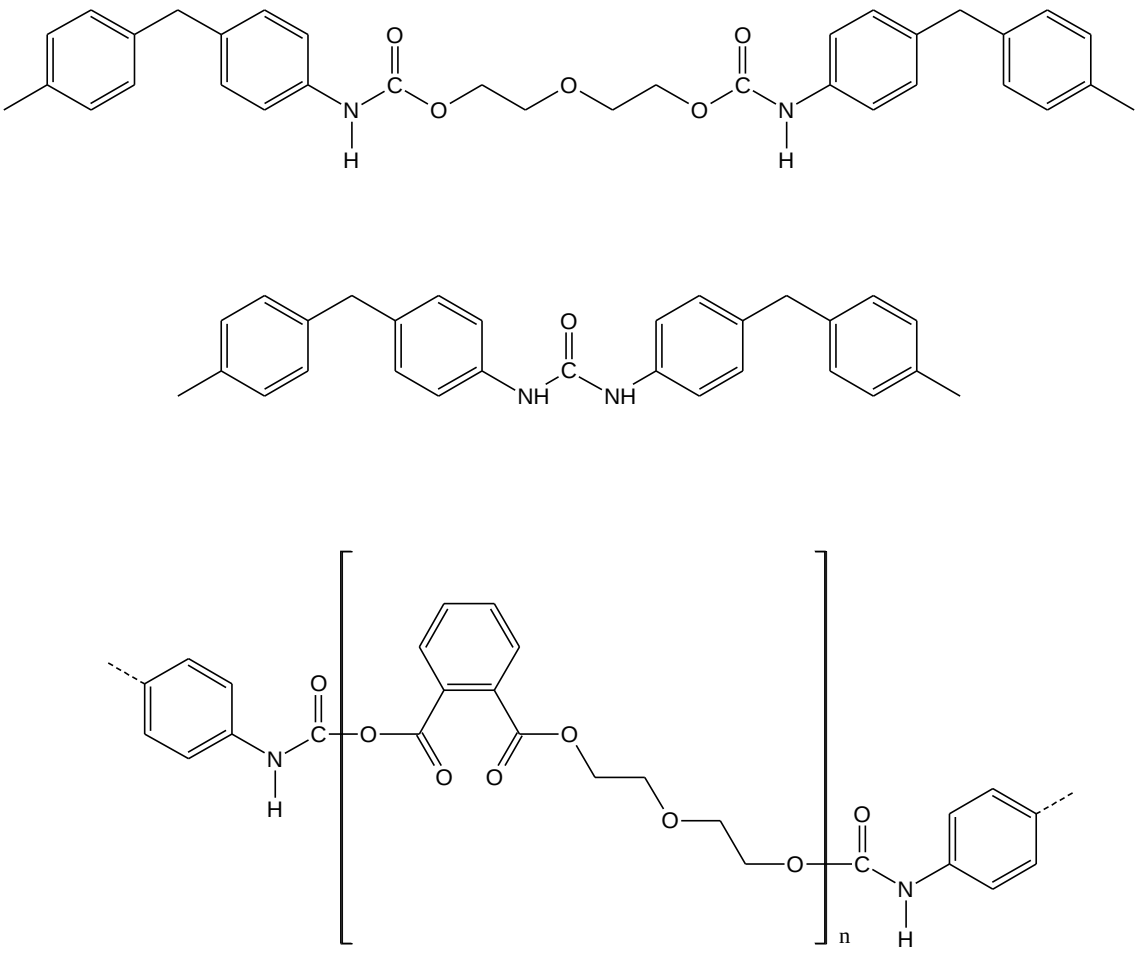

Figure 3.30. *From top to bottom: polyurethane/urea hard segment consisting of two diisocyanate moieties connected via diethylene glycol chain extender; polyurethane/urea hard segment linkage consisting of two diisocyanate moieties connected by disubstituted urea group; polyurethane urea soft segment consisting of two diisocyanate moieties connected by polyester polyol molecule.*

At higher temperatures, the apparent inhibition of mass loss under oxidative conditions is reversed, and at temperatures above 386 ^{o}C, a total breakdown of the polymer residue is initiated as more thermolytically resilient structures are more readily broken down in the presence of reactive oxygen species.

Table 3.13 *Temperature at key mass loss thresholds for free-rise foam samples (FR4-6) under oxidative conditions.*

Mass Loss (%)	**FR4 (ºC)**	**FR5 (ºC)**	**FR6 (ºC)**	**Mean (ºC)**
1	112.9	127.7	144.2	128.3
2.5	159.8	170.4	173.2	167.8
5	192.3	200.2	201.1	197.9
7.5	215.3	219.8	219.8	218.3
10	234.2	235.9	235.9	235.3
15	275.4	271.4	272.6	273.1
20	301.2	300.6	299.6	300.5
30	331.0	333.7	330.6	331.8
40	405.7	411.3	410.9	409.3
50	487.6	497.1	498.4	494.4

Table 3.14 *Retained mass loss at selected temperatures for three free-rise foam samples under oxidative conditions*

Temperature (ºC)	**FR4 (%)**	**FR5 (%)**	**FR6 (%)**	**Mean (%)**
100	99.1	99.2	99.7	99.3
125	98.8	99.0	99.5	99.1
150	98	98.5	98.8	98.4
175	96.5	97.2	97.4	97.0
200	94.2	95.0	95.1	94.8
250	87.9	87.9	87.9	87.9
300	80.4	80.1	79.9	80.1
350	65.7	66.3	65.5	65.8
400	60.6	61.0	60.9	60.8
500	47.5	49.5	49.7	48.9

3.3.6 Effect of Heating Rate on Decomposition of Foam

Four samples of line-produced foam were subjected to dynamic thermogravimetric analysis from 30-900 ^{o}C at heating rates of 10, 15, 20, and 30 ^{o}C/min under an atmosphere of nitrogen at a purging flow rate of 20ml/min. It was expected that, as the heating rate increased, the observed mass loss at a given temperature would decrease. At lower heating rates, the sample temperature should be closer to thermal equilibrium with the furnace and this should be reflected in a smaller difference between the furnace and sample temperatures. Conversely, higher heating rates should generate greater thermal lag. This can be visualised by plotting the furnace set-point temperature against the difference between the set-point and the temperature recorded at the sample monitoring thermocouple.

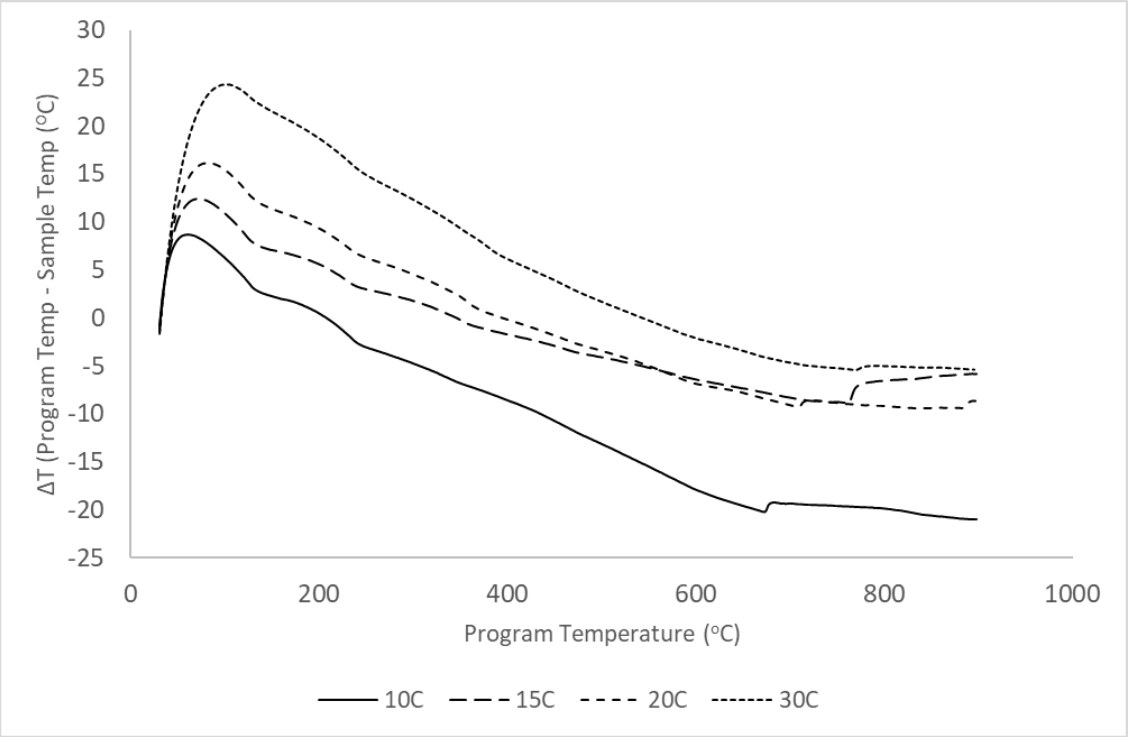

Figure 3.31. *Difference between program temperature and temperature at sample thermocouple during heating program for heating rates from 10-30^{o}C/min.*

A general upward trend is observed in maximum value of ΔT as heating rate increases, from 8.71 ^{o}C at 10^{o}C/min, through 12.48 ^{o}C at 15 ^{o}C/min and 16.16 ^{o}C at 20 ^{o}C/min, to 24.38 ^{o}C at 30 ^{o}C/min. This is an almost perfectly linear relationship within this temperature range. The program temperature at which the maximum ΔT is reached increases in a quadratic relationship from 60 ^{o}C at 10 ^{o}C/min to 70 ^{o}C at 15 ^{o}C/min, 83.3 ^{o}C at 20 ^{o}C/min and 100 ^{o}C at 30 ^{o}C/min. The value of ΔT decreases after this peak, and there is a point at which the difference between

program temperature and sample temperature reaches zero, before becoming negative. This temperature also increases with heating rate, from 207 ^{o}C at 10 ^{o}C/min to 542 ^{o}C at 30 ^{o}C/min.

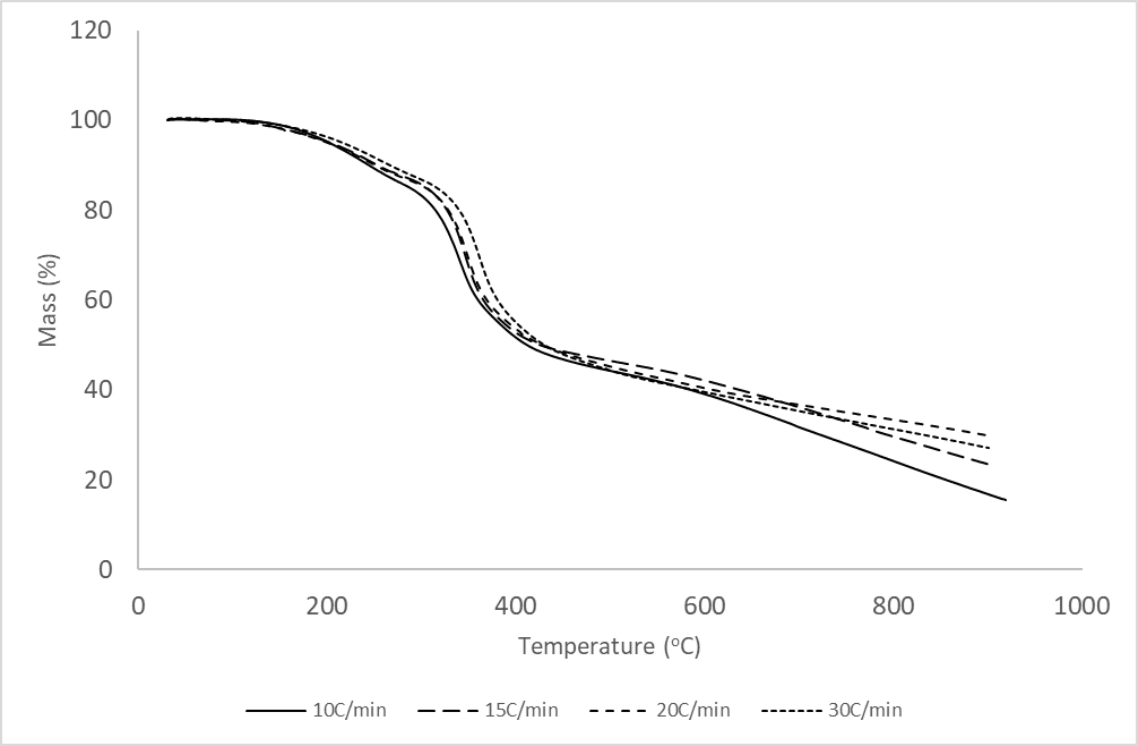

Figure 3.32. *TG thermograms for four line-produced foam samples at heating rates from 10-30^{o}C/min*

The TG curves obtained are of broadly similar shapes, indicating the same patterns of temperature dependent behaviour, but there is an apparent shift towards the right as the heating rate increases. Throughout much of the curve, the total mass loss at a given temperature is lower at higher heating rates, reflecting the lower residence time within that temperature range. The residual mass at a series of selected temperatures has been tabulated below. In the context of real-world fire conditions, heating rates throughout the foam will vary depending upon the proximity to the heat source, with areas in direct contact with the flame front being very rapidly heated. This may predispose these regions to rapid surface charring with limited heat transfer to the core of the material.

Table 3.15. Retained mass proportion (%) at selected temperatures for the four line-produced foam samples in Figure 3.32 at heating rates of 10, 15, 20, and 30 ^{o}C/min

	10^{o}C/min	**15^{o}C/min**	**20^{o}C/min**	**30^{o}C/min**
100^{o}C	100.2	99.9	99.6	100.0
125^{o}C	99.8	99.3	99.1	99.7
150^{o}C	99.8	98.1	98.2	98.8
200^{o}C	95.3	95.2	94.9	96.2
250^{o}C	89.3	90.3	90.0	91.6
300^{o}C	83.3	85.7	85.4	86.6
350^{o}C	63.8	67.5	68.5	75.9
400^{o}C	51.7	52.7	53.4	55.0
500^{o}C	44.2	46.5	45.2	44.3

The positive correlation between retained mass and heating rate is primarily observed in the temperature regime from 200-400 ^{o}C, coinciding with the temperature range in which the main pyrolysis reactions appear to occur. Note that the TG and dTG curves here plot mass loss against the temperature measured at the monitoring thermocouple, and therefore correspond to the temperature at the junction between the balance and the sample pan. This therefore accounts for the previously described lag between furnace and sample temperatures. It has previously been shown that the combination of low specific thermal conductivity and volumetric heat capacity result in a slow response to heating, and therefore it is highly likely that there will be a greater lag between the bulk temperature of the sample and the furnace temperature than is indicated by the sample thermocouple. It was also observed that the behaviour at heating rates of 15 ^{o}C and 20 ^{o}C per minute are more similar relatively similar, with greater differences when increasing the rate from 10-15 ^{o}C per minute and from 20-30 ^{o}C per minute. This may be partly explained by the greater proportional increase in heating rate across these intervals (50 % compared to 33 %).

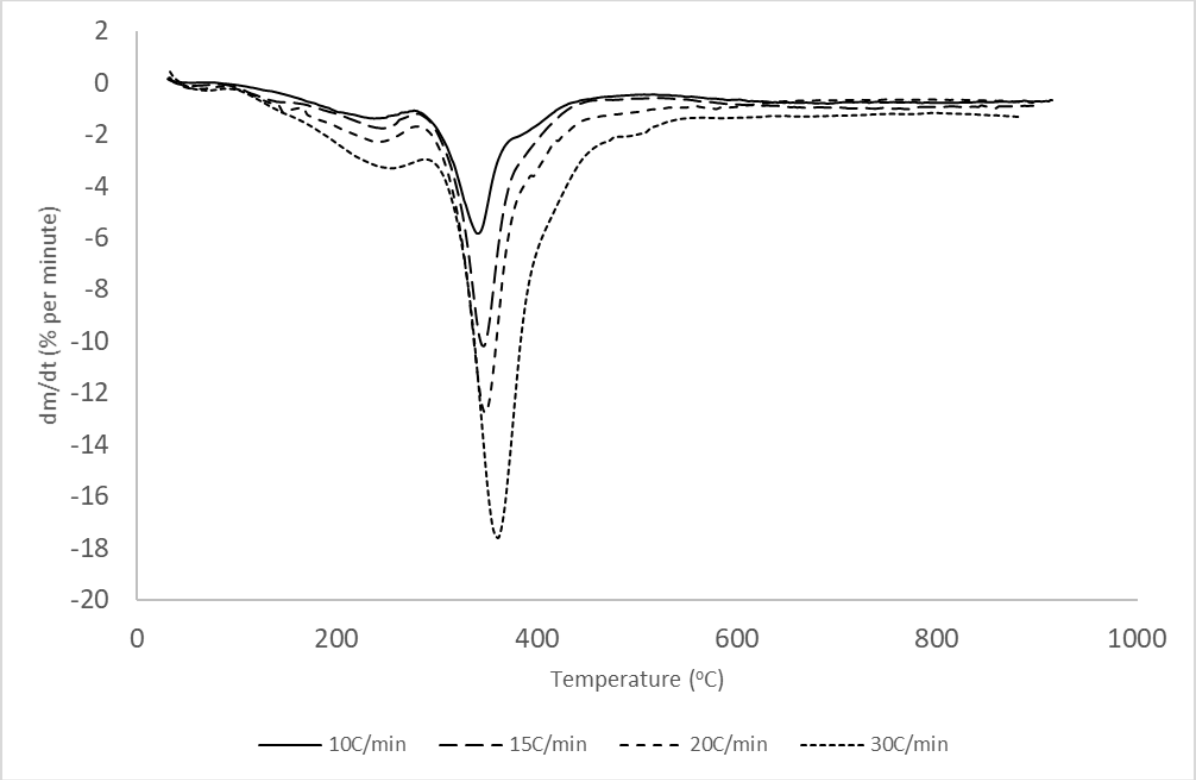

***Figure 3.33**. dTG thermograms for line-produced foam samples at heating rates from 10-30°C/min, corresponding to TG thermograms in figure 3.32*

The dTG curves exhibits a similar shape at all heating rates, with two mass loss events being observed. As expected, the amplitude of peaks increases with heating rate, and this is accompanied by a corresponding upward shift in peak temperatures. At 10 °C/min the first mass loss event occurs over a temperature range of 80-277 °C with a maximum rate of 1.4 % per minute at 237 °C. At 15 °C/min, the temperature range for this event is 81-280 °C, while the peak occurs at 244 °C with a mass loss rate of 1.76 % per minute. At 20 °C/min, the temperature range is 81-281 °C with peak mass loss of 2.30 % per minute at 240 °C. While lower heating rates largely preserve the boundaries of the first mass loss event, at 30 °C/min, a noticeable upward temperature shift is observed to a range of 91-288 °C. At this heating rate, a peak of 3.31 % per minute occurs at 256 °C. This closely conforms to a linear relationship between mass loss and heating rates with a proportionality constant of 0.11 % per °C. A total of 14.2 % mass loss occurs in this region at 10 °C/min, 12.5 % at 15 °C/min, 12.7 % at 20 °C/min and 12.2 % at 30 °C/min.

The temperature at the larger second mass loss peak is also seen to shift upwards in temperature with increasing heating rates. At 10°C/min, the peak occurs at 341 °C, with a positive shift to 348 °C (+7 °C) at both 15 °C/min and 20 °C/min. At 30 °C/min, the peak temperature occurs at

362 ºC (+21 ºC). The value of *dm/dt* at this peak is -5.8 % per minute at 10 ºC/min and increases to -10.2 % per minute at 15 ºC/min, -12.8 ºC/min at 20 ºC/min, and -17.6 %/min at 30 ºC/min. The second mass loss event does not exhibit a consistently clear endpoint. Above the peak temperature, mass loss decreases, but continues at a low rate to the end of the temperature range. For this analysis, the boundaries of the second event have been taken to be the region lying below a straight line passing through the transition point. When applying this method, the following temperature ranges, and total mass loss values have been identified as shown in Table 3.16.

Table 3.16. Temperature range and mass loss in main peak at heating rates from 10-30ºC/min

Heating Rate (ºC/min)	Start point (ºC)	End point (ºC)	Mass Loss (%)
10	277	419	37.0
15	280	422	37.4
20	281	438	38.0
30	287	462	39.5

As heating rate increased, there is a small, but consistent, increase in total mass loss within this region. This trend runs in the opposite direction to that identified for the first mass loss event. Mass losses in the first phase have been attributed to the breakdown of relatively weak urethane bonds, leading primarily to the liberation of low molecular weight fragments such as short diol chain extenders present in the polyol blend. The observed trends could therefore indicate that with higher heating rates, the corresponding lower period of heat exposure and greater thermal lag results in less complete cleavage of urethane bonds during the first phase. As a result, the dissociation of urethanes may be spread over a wider temperature interval, with a greater degree of overlap between the two mass loss phases.

3.3.7 Isothermal Thermogravimetry

Isothermal thermogravimetry provides additional insight into the nature of thermal reactions to by allowing the progress of reactions to be monitored over time at a constant temperature. A series of isothermal analyses have been carried out using line-produced PIR foams under inert conditions. These foams were taken from the same line-produced foam core stock as previous line-produced foams analysed in this thesis and samples were prepared using the same method.

Foams were heated at 20 °C/min to the target temperature and then held under isothermal conditions for 1 hour.

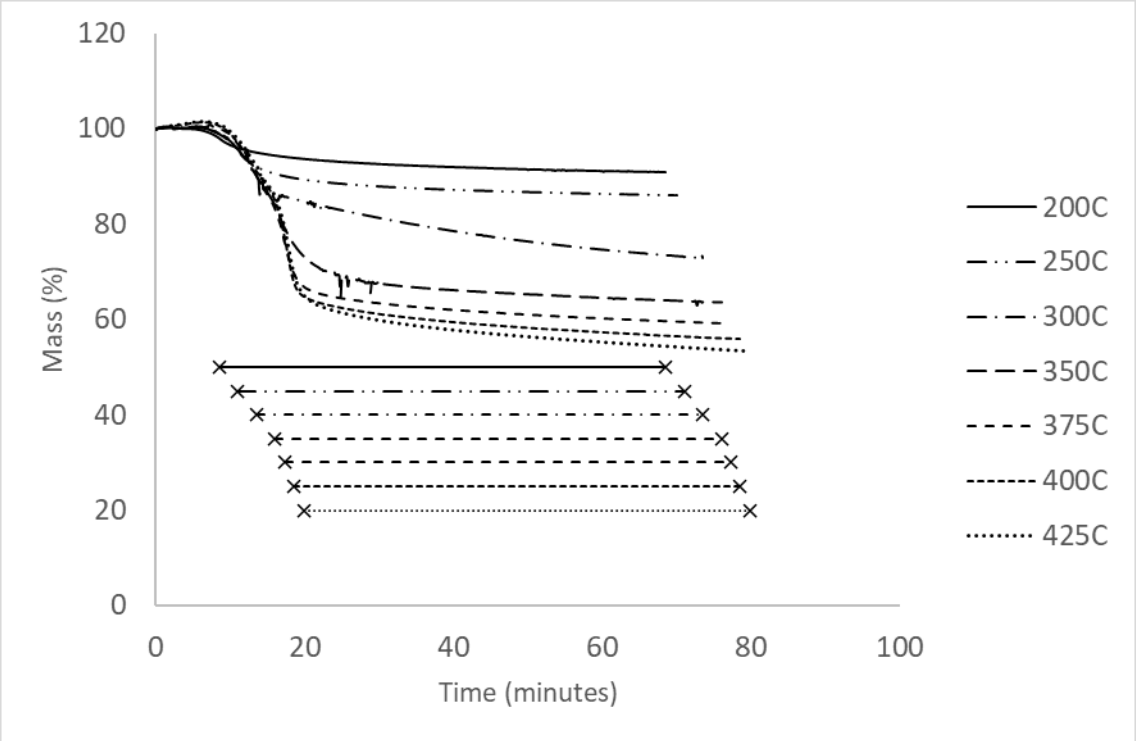

Figure 3.34. *TG thermograms for line-produced samples heated to listed temperatures at 20°C per minute under N_2 and held at temperature for one hour. Stacked lines beneath thermograms indicate isothermal temperature region of corresponding thermogram.*

At each temperature, mass loss during the ramp phase closely follows that observed during previous dynamic thermogravimetric experiments. Continued mass loss is observed throughout the isothermal region.

At a heating rate of 20°C per minute, the start point of the isotherm occurs at the following times for each isothermal temperature:

Temperature at Isotherm	**Time at Start of Isotherm (minutes)**
200 °C	8.5
250 °C	11
300 °C	13.5
350 °C	16
375 °C	17.3
400 °C	18.5
425 °C	19.8

At 200 °C, the recorded mass at the start of the isothermal region is 98.1 %, with a further mass loss of 7.1 % occurring over the next 60 minutes (91.0 %). Of this additional mass loss, 50 % occurs in the first 7 minutes of the isotherm, and 75 % occurs within 20 minutes. For the 250 °C sample, mass at the start of the isotherm is 95.9 %, with a further mass loss of 10.0 % over the next 60 minutes (85.9 %). In this case, 50 % of the additional mass loss occurs within 4.5 minutes and 75 % occurs within 14 minutes. While both isotherms fall well within the temperature range established for the first mass loss event, the total mass loss does not appear to trend towards a common value. Due to the small mass and volume of these samples, it is likely that the temperature throughout the sample would have equalised during the isotherm. This provides further evidence for the occurrence of multiple temperature-dependent physical and chemical processes within the first mass loss event, rather than single process that is triggered at a distinct temperature threshold, where it would be expected that a similar amount of mass loss would occur with only the rate of that reaction dependent on the isothermal temperature.

For higher temperatures, the isothermal region starts to fall within the temperature regime above the transition point into the second mass loss event. At 300 °C, a percentage mass of 90.1 % is recorded at the start of the isotherm. Over 1 hour at 300 °C, residual mass continues to decrease to a final value of 73.2 %, constituting an additional isothermal mass loss of 16.9 %. The TG curve appears to indicate a greater sustained mass loss rate at the end of this isotherm than for any of the other curves. Of the observed isothermal mass loss, 50 % occurred by t+16 and 75 % occurred by t+32. This contrast with the behaviour at 350 °C. At this temperature, mass at the start of the isotherm is 84.0 %, reaching 63.5 % after 1 hour, for a total isothermal mass loss of 20.5 %. While the total isothermal mass loss is greater than at 300 °C, much of the mass loss is occurs in the early stages of the isotherm. 50 % of the isothermal mass loss occurs within 4 minutes and 75 % within 8 minutes The difference in mass increased from 6.1 % at the start of isotherm to a maximum of 15 % after 9 minutes, decreasing to 9.4 % after 1 hour, with an apparent continuation of this trend.

Across the temperature range from 375-425 °C, mass loss at the beginning of the isotherm continued to increase, to 76.4 %, 68.4 %, and 65.3 % respectively. Endpoint masses are 59.1 %, 55.9 % and 53.4 %. This corresponds to a decrease in isothermal mass loss from 17.3 % at 375 °C, to 12.5 % at 400 °C and 11.9 % at 425 °C.

The obtained isothermal TG data, in combination with TG and dTG data obtained under dynamic experimental conditions, provide much insight into the thermal behaviour of PIR foams based on aromatic polyester polyols and 4,4-methylene diphenyl diisocyanate. Previous work reported in the literature on polyurethane foams have identified a pattern of behaviour in which increasing temperatures lead to the fragmentation of the polymer through the progressive cleavage of bonds of increasing stability(30). PIRs are closely related to polyurethanes, sharing as common structural features linear co-polymer segments consisting of diisocyanate and polyol moieties connected by urethane and, to a lesser extent, disubstituted urea linkages. It has been reported that urethanes may undergo thermal dissociation through several mechanisms at temperatures above 180 ^{o}C, primarily the depolymerisation of the urethane to reform the isocyanate and alcohol groups, and the cleavage of the urethane group forming a primary amine and an olefin with the evolution of CO_2 (10).

As seen from Figures 3.40 and 3.41, under both pyrolytic and oxidative conditions, the first mass loss event observed in PIR foams closely corresponds in temperature to the previously reported range for the cleavage of polyurethane bonds, and to the boiling point of diethylene glycol, which is likely to be one of the first low-molecular weight fragments resulting from the dissociation of these groups. It is also suspected that a significant leakage of pentane-based blowing agents occurs from the foam structure at this point. Release of the non-reactive fire retardant TEP is also to likely to occur in this temperature range, as this does not integrate into the polymer structure and has a boiling point of 215 ^{o}C (32), and accounts for 2 % of the total mass. Due to the complex nature of the material and the significant temperature overlap between these events, it is difficult if not impossible to deconvolute them based on thermogravimetric analysis. Attempts to subject the material to differential scanning calorimetry were abandoned as the highly insulating nature of the foams resulted in extremely poor thermal contact with the heating pan and produced no worthwhile data.

The high inherent thermal stability of PIR arises from the extensive network of cross-linkages produced by the trimerization of diisocyanates forming a trifunctional isocyanurate structure (11,13). The dissociation temperature of isocyanurates has been found to lie above 300 ^{o}C. This implies that the critical process involved in the thermolytic degradation of PIR foams is the breakdown of isocyanurate structures (Figure 3.9)

3.4 FT-IR Analysis of Virgin and Partially-pyrolyzed Polyisocyanurate Foams

Data obtained from thermogravimetric analyses of PIR foams has provided a clear picture of the temperature-dependent behaviour of these materials, but the nature of the underlying processes has thus far largely been inferred from previous work on related polyurethane-based materials.

These materials share key structural features, primarily the existence of linear polymer domains based on urethane linkages between 4,4-methylenediphenyldiisocyanate and the terminal hydroxyl groups of the phthalic anhydride-diethylene glycol polyester subunits and the diethylene glycol chain extender, with some interspersion from disubstituted urea linkages, originating from the hydrolysis of isocyanate to form primary amines, which are themselves reactive with isocyanate.

Attenuated total reflectance (ATR) FT-IR spectroscopy has been applied to both virgin and partially pyrolyzed foams to provide insight into the degradation processes occurring within the material, by monitoring the changes in the absorbance associated with key groups that are known to be present in the polymer structure.

Cuboidal sections of line-produced PIR foam with dimensions of 50 x 35 x 25 mm were subjected to heat treatment in an aerated ashing furnace for a period of one hour at temperatures ranging from 200-425 ^{o}C. Small sections of foam were then cut from the exposed surface of the treated foams, along with a sample taken from a piece of virgin polyiso foam. Spectra for each sample were then obtained as described in the methods section of this work. The FTIR spectrum for virgin PIR is shown in Figure 3.35.

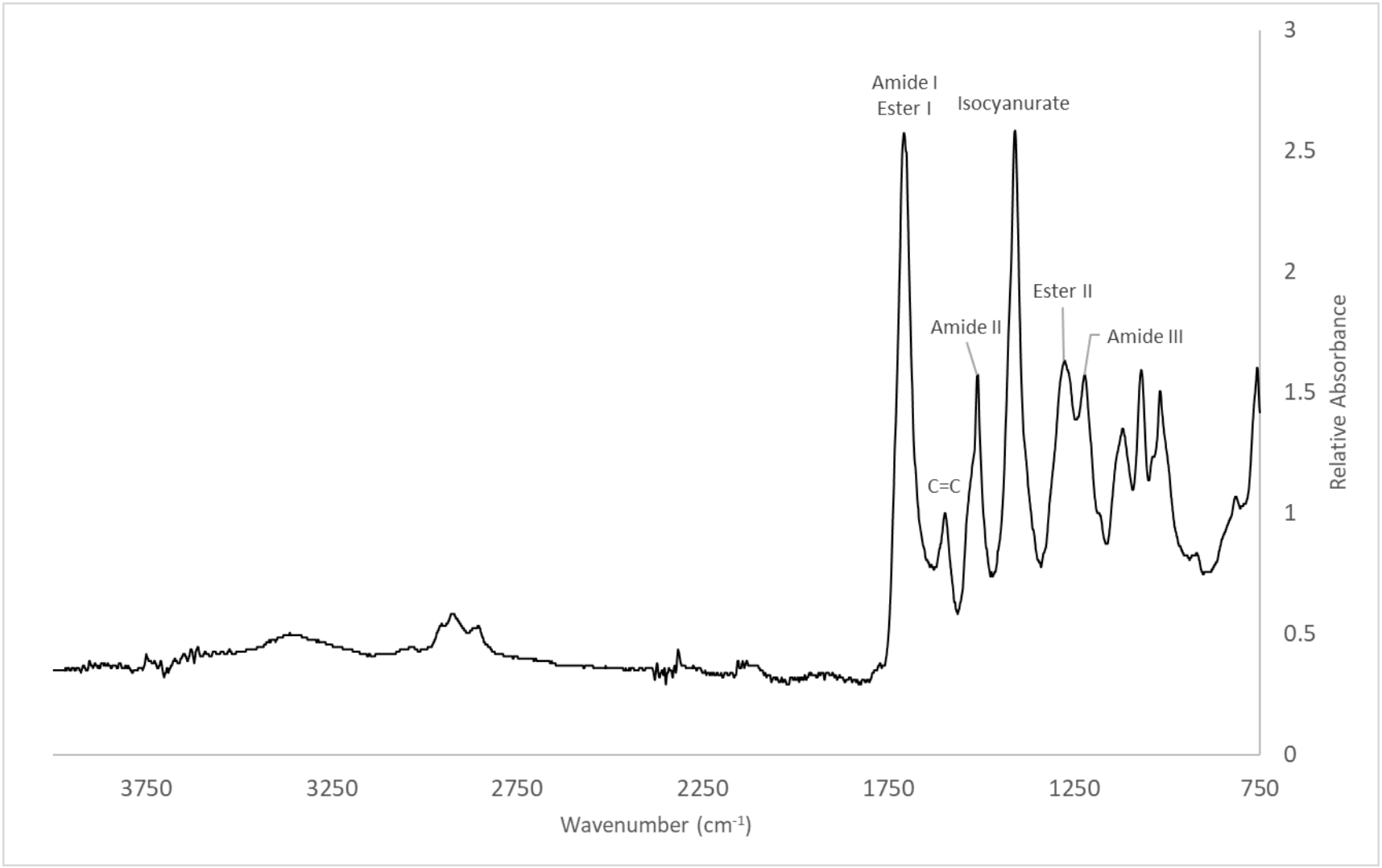

Figure 3.35. *ATR-FTIR spectrum of virgin polyisocyanurate foam*

From 3750-750 cm^{-1}, a total of 11 significant peaks are observed on the FTIR spectrum of virgin foam. The absorbance of these peaks was normalised relative to the intensity of the aromatic C=C peak at 1598 cm^{-1}, which is assigned an absorbance value of 1. The most likely assignments for these absorbances are given in the following table.

Several key groups with characteristic infrared absorptions have been identified.

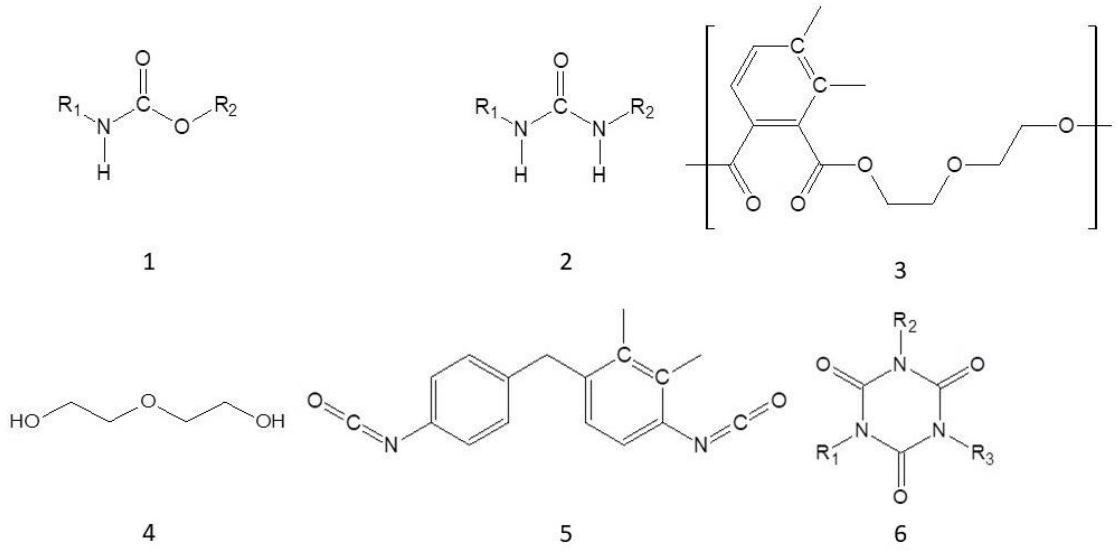

Figure 3.36. *Key groups and structures present in virgin polyisocyanurate foams: 1) urethane linkage; 2) disubstituted urea linkage; 3) diethylene glycol-phthalic anhydride polyester polyol subunit; 4) diethylene glycol; 5) 4,4-methylene diphenyl diisocyanate; 6) isocyanurate ring.*

The urethane linkage is associated with several absorption peaks, often referred to as amide bands. The amide A band occurs within the 3300-3500 cm^{-1} wavenumber range and corresponds and corresponds to the N-H stretching vibration. The amide I band corresponds primarily to the C=O stretch and is observed as an absorption at a wavenumber between 1600-1700 cm^{-1}, while the amide II band, at 1470-1570 cm^{-1} corresponds primarily to in-plane N-H bending with a significant C-N stretching contribution. An amide III band is also present in the 1200-1300 cm^{-1} range, with contributions from in-plane C=O and N-H bending and C-N stretching.

The disubstituted urea linkage bears similarities to the urethane group, differing in the substitution of the alkoxy group with a secondary amine. Similar characteristic peaks may therefore be expected to arise from this group, possibly with stronger activity to be expected at the amide A and amide II bands.

A number of groups functional groups are associated with the polyester polyol. These include the aromatic C=C stretch, typically ~1600 cm^{-1} in polyurethanes. This is an important group for normalisation of obtained spectra in these materials as it is present in the unpolymerized subunits of the polymer, and the abundance of this group is expected to be relatively unaffected by reactions occurring in the early stages of degradation. A characteristic FTIR feature of esters is a triad of peaks corresponding to the C=O, C-C-O and O-C-C stretches at around 1700, 1200, and 1100 cm^{-1} (33). An alkyl-alkyl ether peak arising from the diethylene glycol moiety should also be expected to appear in the region from 1070-1140 cm^{-1}, with the diethylene glycol chain extender also contributing to this signal(34)

4,4-methylene diphenyl diisocyanate also contributes to the aromatic C=C stretching peak while its isocyanate groups produce a potentially detectable peak at 2250-2275 cm^{-1}, depending on the degree of unreacted isocyanate present (34). A carbodiimide N=C=N peak may also appear in this region during degradation, typically in the region of 2100 cm^{-1}(35). These occur in a region of the IR spectrum that normally exhibits a paucity of peaks.

The extensive presence of isocyanurate ring structures throughout the polymer is the defining characteristic of PIR, producing a peak at around 1410 cm^{-1} (34) which is assigned to the C-N stretching within the ring.

Table 3.17 Peaks Appearing in the ATR-FTIR Spectrum of Virgin Polyisocyanurate Foam

Wavenumber (cm^{-1})	**Abs**	**Vibration**	**Assignment**
3363	0.51	νN-H	Amide A
2924	0.58	νC-H	Pentane
1709	2.57	νC=O	Amide I Ester I
1598	1	δC=C	4,4-methylene diphenyl diisocyanate Phthalic anhydride
1510	1.57	δN-H νC-N	Amide II
1410	2.58	νC-N	Isocyanurate
1276	1.63	νC-C-O δC=O δN-H νC-N	Ester II Amide III
1222	1.57		
1120	1.35	νO-C-C	Ester III
1070	1.59	νC-O-C	Ether
1019	1.51	νP-O-C	TEP/TCPP

The strongest absorbances are measured at 1709 cm^{-1}, corresponding to the C=O stretching vibration and at 1410 cm^{-1}, the isocyanurate C-N stretch. The amide II peak at 1510 cm^{-1} is likely to serve as a more distinctive indicator for urethane-related activity than the νC=O peak, because it is associated with bond vibrations that are present only in the urethane and disubstituted urea groups. Therefore, the ratio of these peaks may be indicative of the relative stability of the urethane/urea groups compared to the internal ester groups within the polyol, which are generally regarded as more thermally stable (36)(37). The ratio of the νC=O peak to the isocyanurate νC-N was 0.996:1.000, while the ratio of the amide II peak to the same was 0.609:1.000, respectively. The amide II to νC=O ratio was 0.611:1. As the absorbance of a peak is determined both by the abundance of a group and the change in dipole moment

associated with the specific modes of vibration, these ratios are not strictly quantitative, but can be tracked over a range of temperatures to provide an insight into changes in chemical composition occurring during the thermal degradation of the foam.

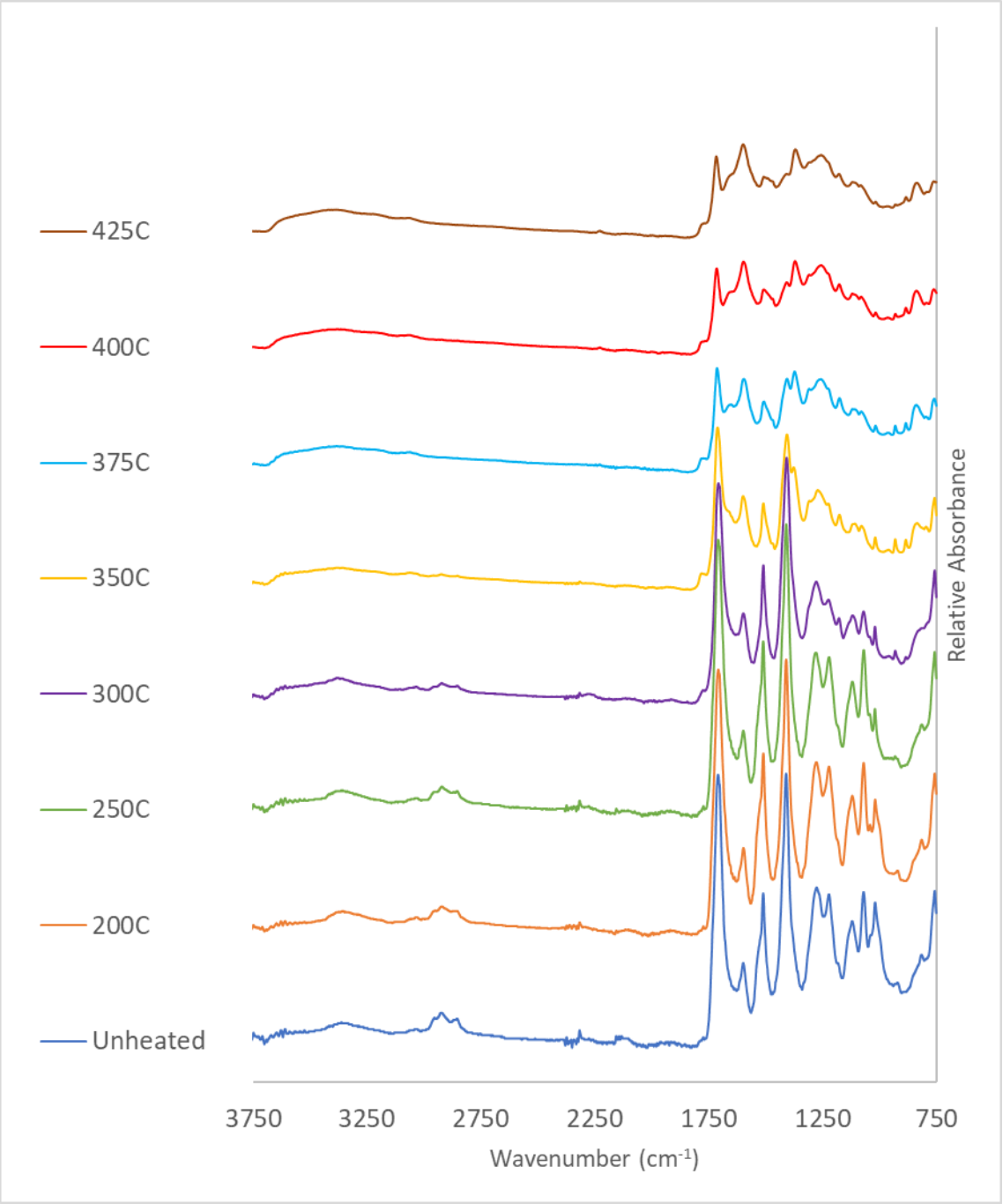

Figure 3.37. *Normalised ATR-FTIR spectra obtained for foam after heating to temperatures from 200-425°C for one hour. Data have been offset for better visualisation*

After one hour of heating at 200 °C, the ATR-FTIR spectrum obtained from partially degraded PIR foam exhibits modest changes when compared to that obtained for virgin foam. The

number and position of distinct peaks is largely unchanged, with the spectra appearing very similar on initial visual inspection. The following changes are noted. Relative absorbance at the alkane νC-H peak (~2920 cm^{-1}) decreases from 0.582 to 0.500. This reduction in absorbance supports the earlier proposition that some of the observed mass loss at lower temperatures is the result of the egress of pentane from the cellular structure. Absorbance at the νC=O peak is 2.52, a small decrease compared to the virgin foam (2.57), suggesting some cleavage of urethane bonds. Absorbance at the isocyanate νC-N peak is almost unchanged, resulting in a small decrease of the νC=O to isocyanurate νC-N ratio from 1.00:1.00 to 0.96:1.00 Notably, the amide II δN-H/νC-N peak increased significantly in absorbance to from 1.57 to 1.81. This is of a similar magnitude to the increase in relative absorbance observed throughout much of the spectrum but has the effect of increasing the amide II to νC=O ratio from 0.61:1.00 to 0.72:1.00 This ratio is higher in the foam samples heated to 200 ^{o}C than in any of the subsequent samples heated to higher temperatures and possibly indicates that during the early stage of degradation, cleaved urethane bonds often lead to the formation of new disubstituted urea linkages via the reaction of a carbodiimide product with depolymerised OH groups, a process that has been suggested elsewhere in the literature(38).

A decrease in absorbance from 1.51 to 1.41 occurred at the 1019 cm^{-1} peak. This peak proved difficult to definitively assign, with possible candidates being ν_aC-O-C of an alkyl-aryl ether and νP-O-C associated with organophosphates. Both diethylene glycol and TEP are expected to be released from the foam during the early stages of degradation, but the former appears less likely as the ether groups present in the PIR being analysed are of the aliphatic type, in which case the ν_aC-O-C peak is generally located in the 1140-1070 cm^{-1} range.

At 250 ^{o}C, further changes could be observed in the FTIR spectrum. Relative absorbance at the νC-H peak was almost unchanged, while the intensity of both the νC=O and isocyanurate νC-N peaks increased, although this increase was proportional, resulting in a further decrease of the νC=O/νC-N ratio to 0.95:1. Absorbance at the amide II peak decreased to 1.761, resulting in the ratio of amide II to isocyanurate decreasing to 0.64:1 while the amide II to νC=O ratio decreased to 0.67:1, consistent with the further dissociation of urethane and urea linkages. Additionally, there is a dramatic decrease in the absorbance at 1019 cm^{-1}, which is now presumptively assigned to P-O-C from fire retardants. The release of phosphate-based flame retardants from polymeric systems into the gas phase has previously been confirmed by FTIR(39) and GC/MS(40) studies, suggesting that at least some of this decrease is due to the

evaporation of the flame retardant, with some also likely to be consumed by reactions in the condensed phase(41).

The spectrum obtained after degradation at 300 °C exhibits far larger changes than are observed at lower temperatures. This is consistent with the data obtained from thermogravimetry, as 300 °C falls well within the second mass loss phase during which a rapid increase in mass loss occurred (section 3.3.1.2). It is therefore anticipated that this transition would mark a clear change in behaviour. This temperature marks the lowest ratio of both the νC=O and amide II δN-H/νC-N peaks to the isocyanate νC-N peak and appears therefore to represent a temperature at which there is relatively extensive breakdown of urethane and urea groups with a slower degradation of isocyanurates. The relative absorbance at all significant peaks is observed to decrease from 250 °C to 300 °C. The intensity of the νC=O peak decreases from 2.63 to 2.11, while the isocyanurate νC-N peak decreases from 2.76 to 2.33. A shift in wavenumber from 1709 cm^{-1} to 1711cm^{-1} is also observed in the case of νC=O. Such a broad decrease in relative absorbance is compatible with both the cleavage of previously identified linkages and likely an increase in the aromatic content through charring reactions, both of which are processes known to occur during the thermal degradation of the foam at these temperatures(30)(52)(53)

At degradation temperatures above 350 °C, marked changes are exhibited in the FTIR spectra. The general decrease in relative intensity across the entire spectrum continues from 350-425 °C. This is a strong indicator of increased conversion to aromatic structures occurring across this temperature range. While the relative absorbance of the aromatic C=C peak at around 1600 cm^{-1} peak has been set to 1.00 for the purpose of spectral normalisation, the actual absorbance at this peak shows a generally increasing value, further suggesting an increase in aromatic content which is likely indicative of char formation. This is partly responsible for the fire retardancy of the material, but likely also contributes to the high smoke production of PIR under fire conditions(12). The νC=O peak has a value of 1.585 at 350 °C at a wavenumber of 1713 cm^{-1}, declining to 0.897 at 425 °C with the peak shifting to 1717 cm^{-1}. The shifts of this peak towards a higher wavenumber with an increase in temperature indicates a change in relative abundance of different carbonyl-containing functional groups. The ester νC=O absorption typically occurs at a higher wavenumber than the amide νC=O, and the ratio of the νC=O peak to the νC-C-O and νO-C-C also decreases progressively at higher temperatures. A sharp decrease in the relative absorbance of the isocyanurate group is observed when increasing in temperature from 300 °C to 350 °C (2.328 to 1.526). This decrease continues from 350-425 °C to a final value 0.748. This result is consistent with the range of dissociation

temperatures reported for the isocyanurate group in the literature. The decline of the isocyanurate peak is accompanied by the emergence of a previously absent peak at 1370-1380 cm^{-1}. This absorption band appears to be most strongly associated with the symmetric ('umbrella') bending deformation of the $-CH_3$ methyl group.

The presented ATR-FTIR data are compatible with a decomposition mechanism in which the early stages of degradation of characterised by the release of blowing agent, cleavage of urethane bonds and reformation of the polymer structure to include increased amounts of urea and isocyanurate-like structures. This appear to be followed by the sequential loss of urea and isocyanurate groups and eventually a total degradation of the polymer structure to form a highly aromatic char.

3.5 Conclusions

Thermogravimetric data obtained from both line-produced and hand-mixed PIR foams containing tris(1-chloro-2-isopropyl) and TEP flame retardants, coupled with residual ATR-FTIR analysis corroborates previously suggested pyrolytic and thermo-oxidative degradation pathways for PIR. PIRs appear to be rather poorly studied materials when compared to related PUR and this application of FTIR analysis did not appear to have been carried out at this level of detail in the existing literature.

It has been found that chemical degradation begins at temperatures around 100^{o}C with near-negligible mass losses at lower temperatures being strongly inferred to result from the evaporation of adsorbed moisture and other volatiles. These values are in line with the determined moisture adsorption for these types of material.

Thermo-oxidative conditions appear to involve similar processes in the first degradation phase but show a smaller mass loss in the second phase. This finding was unexpected, as the *a priori* assumption was that oxygen would act exclusively to accelerate the decomposition of the foam. This finding was scarcely if at all mentioned in the literature and is here attributed to a combination of factors. Firstly, condensed-phase oxidation reactions converting diphenylmethane moieties to a benzophenone analogue as suggested by Servay *et al.*(27) which would both increase the molecular mass of the isocyanate moieties and the temperature required to volatilise fragmented material. Secondly, increased soft segment scission resulting in the formation of more stable polyol residues as per Marquis *et al.*(28). Furthermore, oxidative dehydrogenation of polyol residues may initially act to promote the formation of char through the production of carbon chains. This residue is almost entirely consumed by 600 ^{o}C,

with no persistent char. The decomposition of this highly unsaturated residue is likely the source of the large amounts of smoke generated during the decomposition of PIR.

The elucidation of the degradation pathway will form the basis for subsequent analysis in the following chapter of this work, where the influence of various formulation changed on stability will be studied using thermogravimetric analysis. This will be followed with metrological analysis of larger samples, to study bulk effects that are not readily apparent at the scale of thermogravimetry samples.

Chapter 3 Bibliography

1. Mullens MA, Arif M. Structural Insulated Panels: Impact on the Residential Construction Process. J Constr Eng Manag. 2006;132(7):786–94.

2. Mugahed Amran YH, El-Zeadani M, Huei Lee Y, Yong Lee Y, Murali G, Feduik R. Design innovation, efficiency and applications of structural insulated panels: A review. Structures. 2020;27(March):1358–79.

3. Gravit M, Kuleshin A, Khametgalieva E, Karakozova I. Technical characteristics of rigid sprayed PUR and PIR foams used in construction industry. IOP Conf Ser Earth Environ Sci. 2017;90(1).

4. Thomas G. Cleary JGQ. Flammability Characterization of Foam Plastics. 1991;

5. Burke SP, Schumann TEW. Diffusion Flames. Ind Eng Chem Res. 1928;20(10):998–1004.

6. ASTM International. ASTM E222-17(2017) Standard Test Methods for Hydroxyl Groups Using Acetic Anhydride Acetylation. 2017.

7. Jiricny J, Reese CB. THERMAL DECOMPOSITION OF ISOCYANURATES. British Polymer Journal. 1980;12(3).

8. Saadatkhah N, Carillo Garcia A, Ackermann S, Leclerc P, Latifi M, Samih S, et al. Experimental methods in chemical engineering: Thermogravimetric analysis—TGA. Canadian Journal of Chemical Engineering. 2020;98(1):34–43.

9. Dyer E, Newborn GE. Thermal Degradation of Carbamates of Methylenebis-(4-phenyl Isocyanate). J Am Chem Soc. 1958;80(20):5495–8.

10. Dyer E, Wright GC, Wright GC. Thermal Degradation of N-Alkyl Phenylcarbamates. J Am Chem Soc. 1958;81:2138–43.

11. Dick C, Dominguez-rosado E, Eling B, Liggat JJ, Lindsay CI, Martin SC. The Flammability of urethane-modified polyisocyanurates and its relationship to thermal degradation chemistry. Polymer (Guildf). 2001;42(3):913–23.

12. Chambers J, Jiricny J, Reese CB. The thermal decomposition of polyurethanes and polyisocyanurates. Fire Mater. 1981;

13. Dominguez-Rosado E, Liggat JJ, Snape CE, Eling B, Pichtel J. Thermal degradation of urethane modified polyisocyanurate foams based on aliphatic and aromatic polyester polyol. Polym Degrad Stab. 2002;78(1):1–5.

14. Xu D, Yu K, Qian K. Thermal degradation study of rigid polyurethane foams containing tris(1-chloro-2-propyl)phosphate and modified aramid fiber. Polym Test. 2018;67(October 2017):159–68.

15. Jiao L, Xiao H, Wang Q, Sun J. Thermal degradation characteristics of rigid polyurethane foam and the volatile products analysis with TG-FTIR-MS. Polym Degrad Stab. 2013;98(12):2687–96.

16. ASTM International. ASTM E681-09(2015) Standard Test Method for Concentration Limits of Flammability of Chemicals (Vapours and Gases). 2015.

17. Dušek K, Špirková M, Havliček I. Network formation of polyurethanes due to side reactions. Macromolecules. 1990;23(6):1774–81.

18. Lapprand A, Boisson F, Delolme F, Méchin F, Pascault JP. Reactivity of isocyanates with urethanes: Conditions for allophanate formation. Polym Degrad Stab. 2005;90(2 SPEC. ISS.):363–73.

19. Chuang FS, Tsi HY, Chow JD, Tsen WC, Shu YC, Jang SC. Thermal degradation of poly(siloxane-urethane) copolymers. Polym Degrad Stab. 2008;93(10):1753–61.

20. Kim B hyoun, Yoon K, Cheul D. Thermal degradation behavior of rigid and soft polyurethanes based on methylene diphenyl diisocyanate using evolved gas analysis- (gas chromatography)– mass spectrometry. J Anal Appl Pyrolysis. 2012;98:236–41.

21. He JJ, Jiang L, Sun JH, Lo S. Thermal degradation study of pure rigid polyurethane in oxidative and non-oxidative atmospheres. J Anal Appl Pyrolysis. 2016;120:269–83.

22. Goldstein H, Healy MJR. The Graphical Presentation of a Collection of Means. J R Stat Soc Ser A Stat Soc. 1995;158(1):175–7.

23. Welty JR, Wicks CE, Wilson RE, Rorrer GL. Fundamentals of Momentum, Heat and Mass Transfer. 2007.

24. Marin E. Thermal Physics Concepts: The Role of Thermal Effusivity. Phys Teach. 2006;44(7):432–4.

25. Salazar A. On thermal diffusivity. Eur J Phys. 2003;24(4):351–8.

26. Spearpoint M, Fleischmann C, Li KY. Thermophysical properties of polyurethane foams and their melts. 2014;(April 2017).

27. Servay T, Voelkel R, Schmiedberger H, Lehmann S. Thermal oxidation of the methylene diphenylene unit in MDI-TPU. 2000;41(June 1999):5247–56.

28. Marquis DM, Batiot B, Guillaume E, Rogaume T. Influence of reaction mechanism accuracy on the chemical reactivity prediction of complex charring material in fire condition. J Anal Appl Pyrolysis. 2016;118(June 2017):231–48.

29. Garrido MA, Font R. Pyrolysis and combustion study of flexible polyurethane foam. J Anal Appl Pyrolysis. 2015;113:202–15.

30. Chattopadhyay DK, Webster DC. Thermal stability and flame retardancy of polyurethanes. Progress in Polymer Science (Oxford). 2009;34(10):1068–133.

31. Bellucci F, Camino G, Frache A, Sarra A. Catalytic Charring-Volatilization Competition in Organoclay Composites. Polym Degrad Stab. 2007;92(3):425–36.

32. Haertel GH. Low-volatility polar organic solvents for sulfur dioxide, hydrogen sulfide, and carbonyl sulfide. J Chem Eng Data. 1985;30:57–61.

33. Smith BC. The C=O Bond, Part VI: Esters and the Rule of Three. Spectroscopy. 2018;33(7):20–3.

34. Reignier J, Méchin F, Sarbu A. Chemical gradients in PIR foams as probed by ATR-FTIR analysis and consequences on fire resistance. Polym Test. 2021;93(xxxx).

35. Hatchett DW, Kinyanjui JM, Sapochak L. FTIR analysis of chemical gradients in thermally processed molded polyurethane foam. Journal of Cellular Plastics. 2007;43(3):183–96.

36. Bautista Y, Gozalbo A, Mestre S, Sanz V. Thermal degradation mechanism of a thermostable polyester stabilized with an open-cage oligomeric silsesquioxane. Materials. 2017;11(1).

37. Zhang C, Feng S. Effect of glycols on the properties of polyester polyols and of room-temperature-curable casting polyurethanes. Polym Int. 2004;53(12):1936–40.

38. Duquesne S, Le Bras M, Bourbigot S, Delobel R, Camino G, Eling B, et al. Thermal degradation of polyurethane and polyurethane/expandable graphite coatings. Polym Degrad Stab. 2001;74(3):493–9.

39. Rabe S, Chuenban Y, Schartel B. Exploring the modes of action of phosphorus-based flame retardants in polymeric systems. Materials. 2017;10(5).

40. Mckenna ST, Birtles R, Dickens K, Walker RG, Spearpoint MJ, Stec AA, et al. Flame retardants in UK furniture increase smoke toxicity more than they reduce fire growth rate. Chemosphere. 2018;196:429–39.

41. Scharte B. Phosphorus-based flame retardancy mechanisms-old hat or a starting point for future development? Materials. 2010;3(10):4710–45.

42. Kordomenos PI, Kresta JE. Thermal Stability of Isocyanate-Based Polymers. 1. Kinetics of the Thermal Dissociation of Urethane, Oxazolidone, and Isocyanurate Groups. Macromolecules. 1981;14(5):1434–7.

43. Kordomenos PI, Kresta JE, Frisch KC. Thermal Stability of Isocyanate-Based Polymers. 2. Kinetics of the Thermal Dissociation of Model Urethane, Oxazolidone, and Isocyanurate Block Copolymers. Macromolecules. 1987;20(9):2077–83.

4 Effects of Modification on Thermal Behaviour of Polyisocyanurates

4.1 Introduction

Within the previous chapter of this work, thermogravimetric analysis and ATR-FTIR spectroscopy were used together to characterise the thermal behaviour of a typical commercial formulation of PIR foam. This characterisation was an essential first step in providing a baseline against which modified formulation could be compared. By comparison, this chapter looks at further application of these techniques to analyse the effects of modifications to the host PIR polymer material - focussing on the addition of fire retardants given the context of this work, and in particular to study alternative fire-retardant systems.

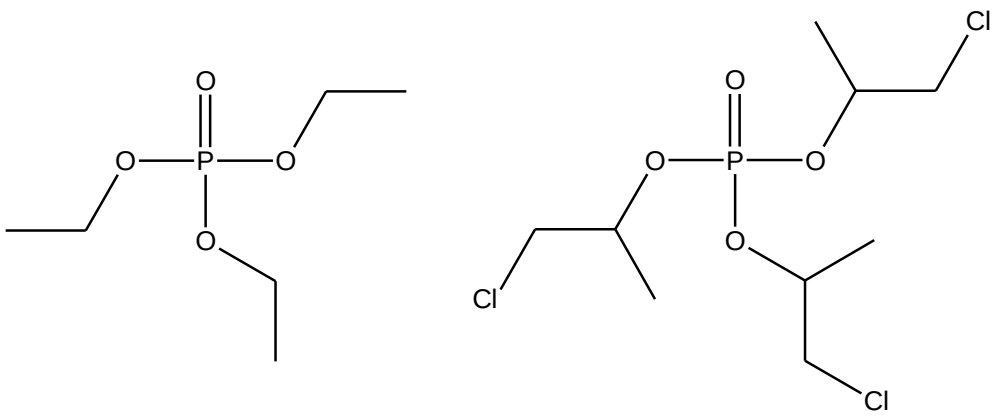

Figure 4.1. *Triethyl phosphate (left) and tris (1-chloro-2-propyl) phosphate (right) common fire retardants used in current commercial polyisocyanurate foams.*

The impetus to develop alternative fire-retardant systems has developed in response to increased public and legislative scrutiny (1) surrounding the fire safety of construction materials, and to increasing stringency of regulations regarding the environmental and health impact of chemical agents (2)(3)(4)(5). Many halogenated fire retardants, especially those containing bromine, have been largely phased out internationally, but some, in particular the so-called ‘chlorinated tris’ group consisting of tris(2-chloroethyl) phosphate, tris(1-chloro-2-isopropyl) phosphate and tris(1,3-dichloroisopropyl) phosphate are still in widespread use in construction materials and household furnishings. This is despite the strong evidence for their widespread release into the environment (5), ready absorption through dermal exposure and ingestion (6) and evidence of accumulation in human tissues (7)

At a minimum, any proposed replacement for these widely used fire-retardant systems must provide an equivalent degree of fire and smoke suppression. Meeting this standard would be sufficient to eliminate the potential environmental and health impacts associated with detailed above, without compromising current levels of fire safety.

4.2. Neat Polyisocyanurate (No Fire Retardant)

To understand the impact of replacement fire-retardant systems, it is necessary to understand the thermal stability of the existing system on its own. Two sets of 'bare' PIR foam samples were subjected to dynamic thermogravimetric analysis under pyrolytic (i.e. non-oxidative) conditions, identical to those used for analysis of the baseline control sets in the previous chapter. The first of these was a set of free-rise samples produced on-site at Swansea University. These samples were produced using the same method as the free rise (FR) sample sets analysed in the previous chapter. The second were a set of block-mould (BM) samples produced using the same method as the BM sample set from the previous chapter. These were supplied by the project industrial sponsor. In the case of the free-rise foams, it should be noted that the PS-2412 polyol blend did contain a small quantity of TCPP (5-10 %) so these samples were not truly free of all fire retardants, likely containing around 1% TCPP by weight. This is however a sixfold reduction in the proportion of TCPP compared to the "full" fire retardant loading tested in this chapter, and a complete removal of TEP. This was not the case for the block-mould samples, as these were produced using a TCPP-free polyol blend (PS-2602). This polyol blend was not available at the stage of the project in which the free-rise samples were produced. The PS-2602 polyol also differs somewhat in hydroxyl value compared to PS-2412 (270 mgKOH/g vs. 240mgKOH/g).

4.2.1. Free-rise Foams

Free-rise samples were produced with the same isocyanate to polyol ratio as the standard formulation and the quantity of catalysts was adjusted to maintain the same concentration. Free-rise samples were subjected to dynamic thermogravimetric analysis in an inert atmosphere of nitrogen using the standard experimental method previously described. These samples ranged in initial mass from 9.74 mg to 13.61 mg (mean mass 11.31 mg). Raw TG was processed using the previously described methods and TG/dTG thermograms were produced for each of three samples. These data were then used to construct mean TG/dTG curves (Figures 4.2 and 4.3).

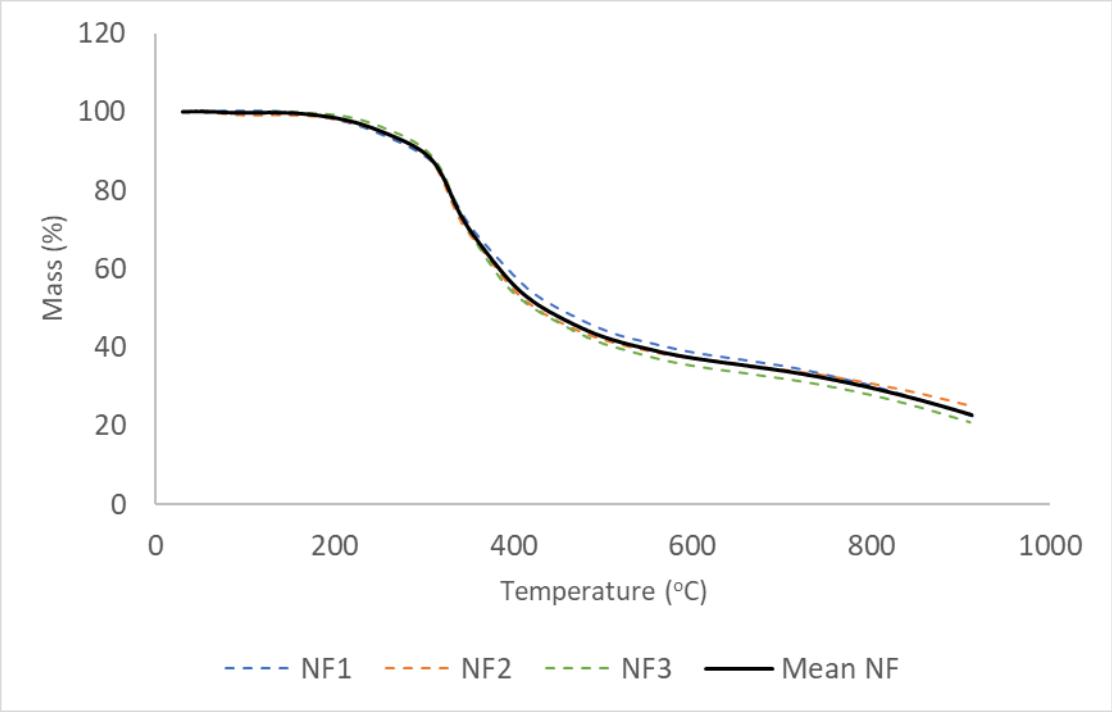

Figure 4.2. *TG thermograms for free-rise neat polyisocyanurate foams under inert atmosphere.*

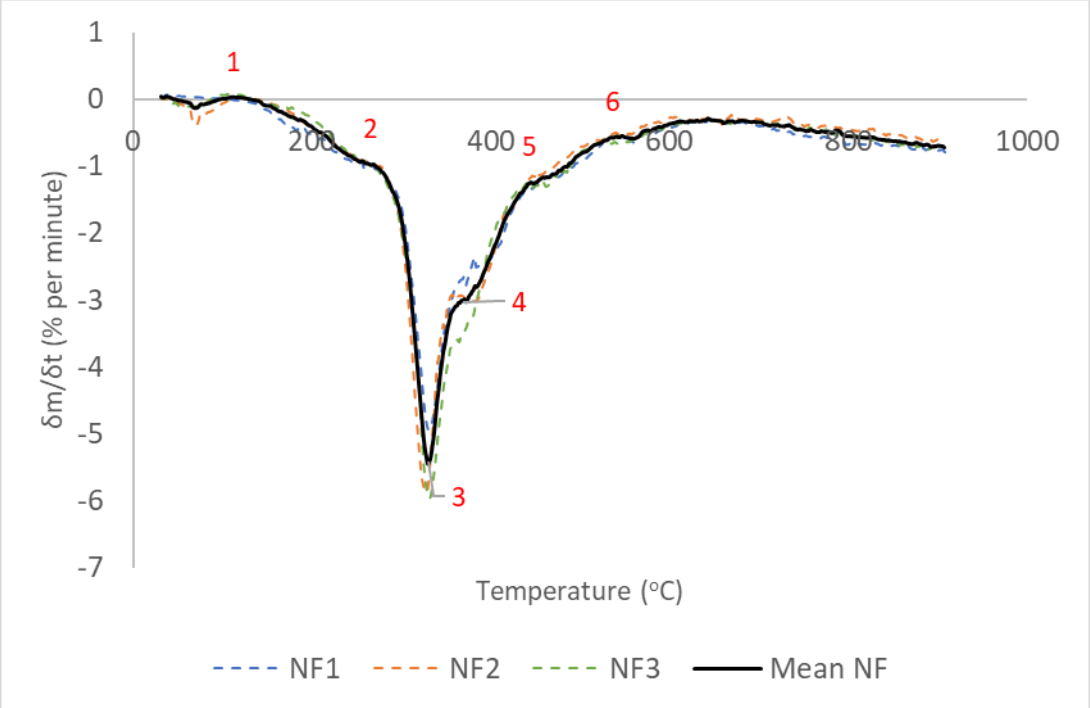

Figure 4.3. *dTG thermograms for free-rise neat polyisocyanurate foams under inert atmosphere. Significant features are numbered 1-6 for reference in text.*

TG thermograms (Figure 4.2) indicate largely consistent behaviour across all three samples, with negligible to very low mass loss recorded at temperatures up to 150 °C (0.0-0.8 %). Mass

loss exceeds 1% at 169-208 ºC, with a mean temperature of 186 ºC, and exceeded 2.5 % at 211-236 ºC with a mean of 220 ºC. These temperatures are clearly higher than those measured for the FR sample set analysed in the previous chapter. In that set, mass loss exceeded 1 % at a mean temperature of 140 ºC (range 136-146 ºC) and exceeded 2.5 % at a mean temperature of 166 ºC (range 160-171 ºC). There is no overlap in these temperature ranges for the no fire retardant (NF) and fire retardant (FR) sample sets, and Figure 4.4 shows that mean mass loss was lower for the NF sample set throughout the entire temperature range above 100 ºC, although there was no substantial difference in the retained char at the end of heating (NF; mean 22.8 %, range 20.9-25.0 % vs. FR; mean 20.6 %, range 20.2-21.1 %).

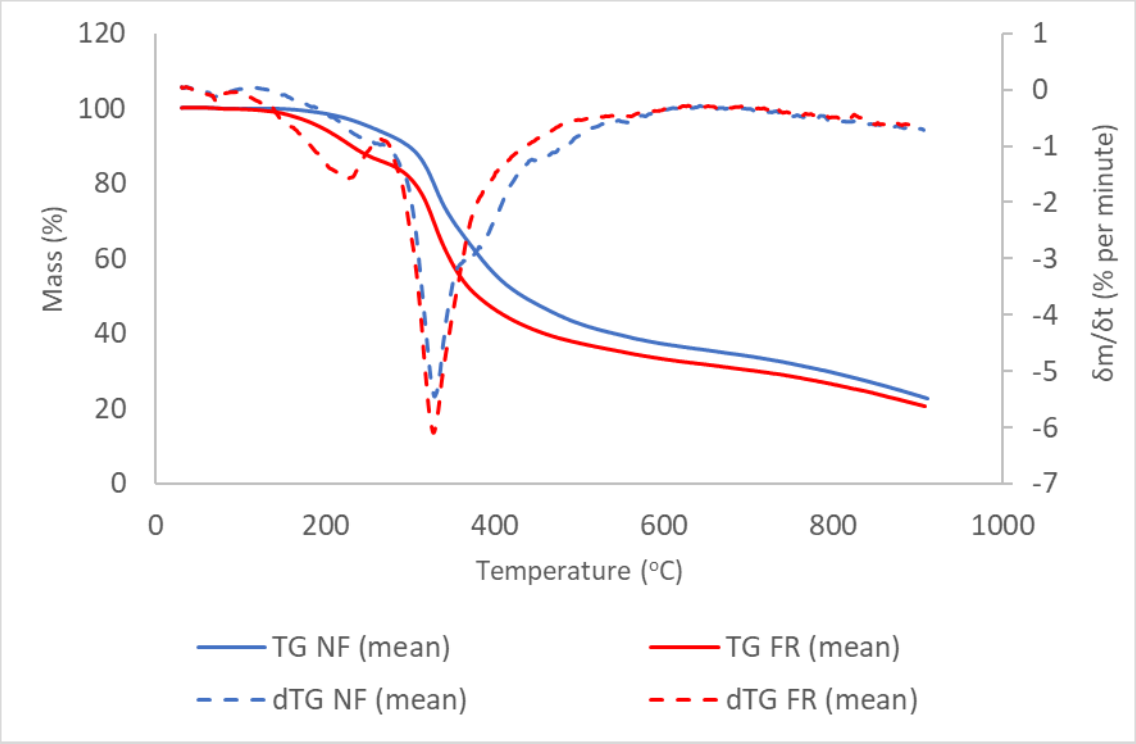

Figure 4.4. *Comparison of mean TG and dTG thermograms for NF and FR sample sets under inert atmosphere.*

The dTG thermograms further highlight some clear differences in the behaviour of the NF and FR sample sets. The mean curve for the NF samples (Figure 4.3) exhibits a region of minimal mass loss at temperatures up to 100 ºC, consistent with that observed in the FR samples [1]. This is followed by a region of gradually accelerating mass loss to an inflection point at 270 ºC [2]. Above this inflection point, the rate of mass loss more rapidly increases, reaching a maximum mean rate of 5.5 % per minute at 329 ºC [3]. The position of this peak is highly consistent between the three samples, falling within a range of 328-331 ºC, with a maximum rate of mass loss of 4.9-5.9 % per minute. To the right of the peak an initial rapid decrease in

the rate of mass loss from 270-370 ^{o}C [3-4] is followed by pronounced shoulder feature from 370-446 ^{o}C [4-5] and a further distinct region of mass loss from 446-537 ^{o}C [5-6]. Some variation can be seen between the three NF samples in this temperature regime.

Comparison of the dTG curves for the NF and FR sample sets (Figure 4.4) indicate clear differences between the two foams. The most noticeable difference is the absence from the NF samples of the lower temperature feature that is clearly visible at around 228 ^{o}C in the FR samples. It can also be seen that the temperature at which the highest rate of mass loss occurs is almost identical for the two samples sets but with a greater rate of mass loss in the FR samples. However, the rate of mass loss more rapidly decreases above the peak in the FR samples, with no shoulder regions as were observed for the NF samples.

In summary, while the total extent of mass loss is similar for both the NF and FR sample sets, the temperature regions in which this mass loss is concentrated differs substantially. The FR samples, which contain a fire-retardant system of tris-(1-chloro-2-isopropyl) phosphate and TEP exhibit greater mass loss at temperature up to the main peak, but lower mass loss at higher temperatures compared to the NF samples consisting of PIR alone. This suggests a possibility that lower temperature mass losses are associated with the decomposition or volatilisation of fire-retardant agents, but that these decompositions contribute to the formation of a more resilient char.

4.2.2. Block-mould samples

While early work in this thesis primarily focused on free-rise foams, much of the later analysis has been carried out on the block-moulded foams produced by Building Systems (Tata) UK. Due to the difference in production methods, block-mould foams are likely to exhibit behaviour more similar to that of manufactured PIR. For this reason, comparison of neat block-mould PIRs with those containing TCPP and TEP have also been carried out, as it was observed in the previous chapter that block-mould and free-rise foams exhibit appreciable differences.

The block-mould foams were subjected to identical experimental conditions to the free-rise samples. Each of the three replicate samples were taken from a separate batch of foam produced to an identical formulation based on Stepanpol™ PS-2602 aromatic polyester polyol. Like the PS-2412 blend used in the standard formulation, this blend is based on a phthalic anhydride-diethylene glycol co-polymer, with a diethylene glycol chain extender, but does not contain the 5-10 % pre-blended TCPP content. This samples set is here labelled BN, with the previous PS-2412 samples containing the fire retardants labelled BM. Smoothed TG and dTG thermograms

were produced for the BN samples using data processing methods outlined in the previous chapter (Figures 4.5 and 4.6).

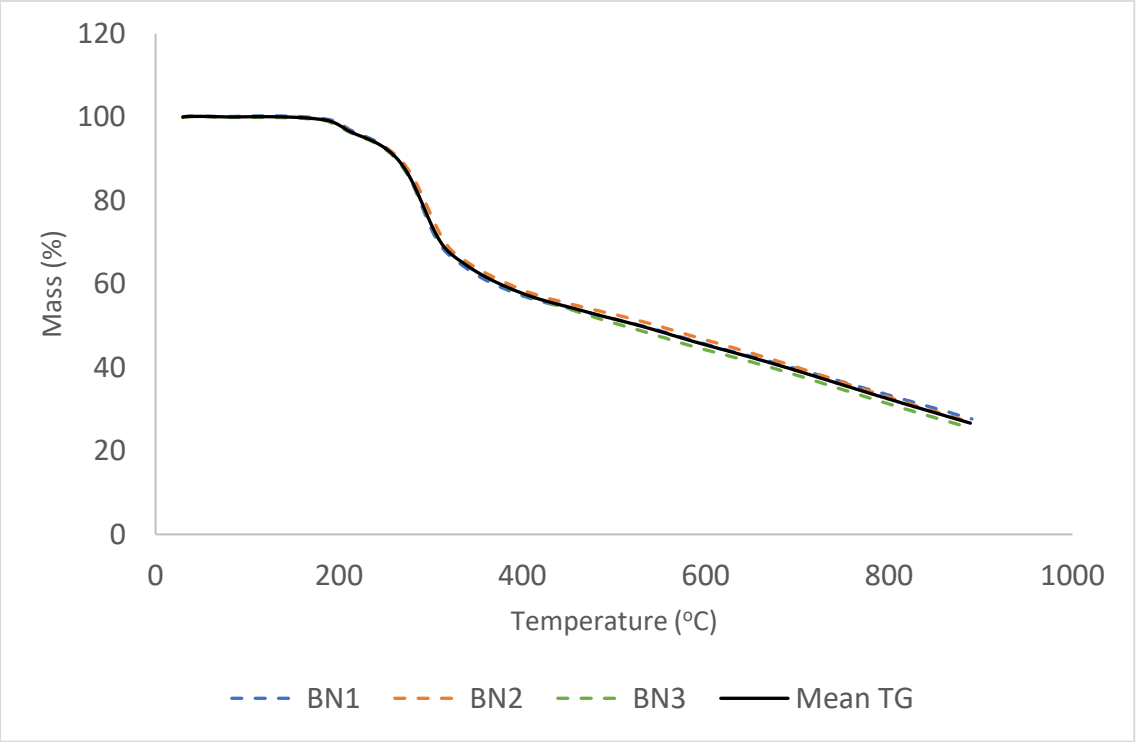

Figure 4.5. *TG thermograms for samples BN1, BN2, and BN3 and mean TG thermogram from 30-900°C at 10°C/min under* N_2.

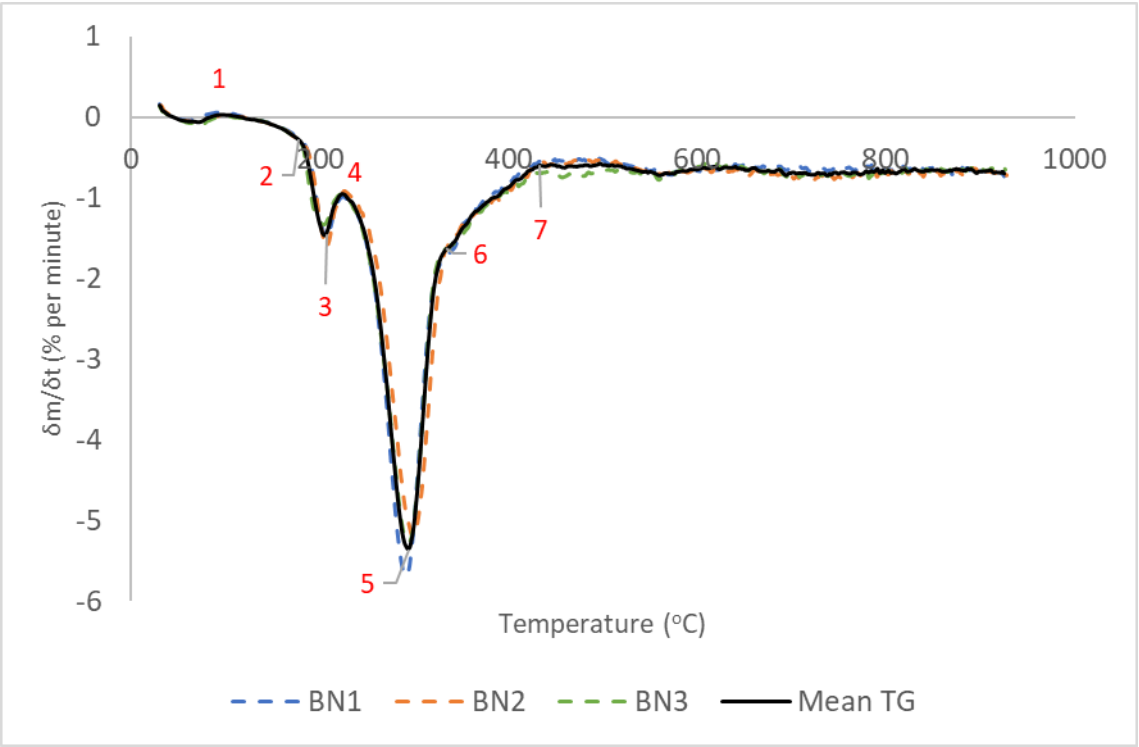

Figure 4.6. *dTG thermograms for samples BN1, BN2, and BN3 and mean TG thermogram from 30-900°C at 10°C/min under N_2. Significant features are labelled 1-7 and referenced in text.*

Highly consistent behaviour is observed across all three BN samples. Mean cumulative mass loss across the 30-95 °C temperature interval [1] is 0.35 % with a maximum rate of 0.11 % per minute at 72.8 °C. This appears as the small 'blip' at the beginning of the TG thermogram. This feature has been consistently observed in previous samples and has been attributed to the evaporation of water and other physisorbed volatiles. The highest observed mass loss rate for any of the three samples is 0.16 % per minute, observed in sample 3 at 72.5 °C. Mass loss approaches zero at the upper end of this interval (0.001 % per minute at 95.3 °C). This is followed by a gradual increase in mass loss rate from ~95-181 °C [1-2], reaching 0.34 % per minute.

Above 181 °C, there is a marked and rapid acceleration in mass loss with $\frac{dm}{dt}$ increasing to 1.5 % per minute at 205 °C [2-3], then decreasing to 1.0 % per minute at 225 °C [3-4]. This sharp peak is highly distinctive but of relatively small area compared to the low temperature peak observed in previous samples, accounting for a mass loss of 4.2 % and is consistent throughout the sample set, with maximum $\frac{dm}{dt}$ falling within a range of 1.3-1.6 % per minute, occurring at temperatures from 205-206 °C with total mass loss of 4.0-4.4 %. Above 225 °C, a

sharp increase in the rate of mass loss was again observed, reaching a maximum $\frac{dm}{dt}$ value of 5.4 % per minute (range 5.2-5.7 % per minute) at 294 °C (range 292-296 °C) [4-5]. Beyond this peak, mass loss rapidly decreases, with the appearance of a weakly-defined shoulder at around 338 °C [5-6], after which the decrease in the rate of mass loss tails off, stabilising at a quasi-constant rate above 436 °C [6-7]. Integrated mass loss in the pre-shoulder region of the primary mass loss peak is 30.8 %, with an additional 9.4 % in the shoulder region. Mean final mass at the end of heating is 23.4 % (range 22.4-24.4 %).

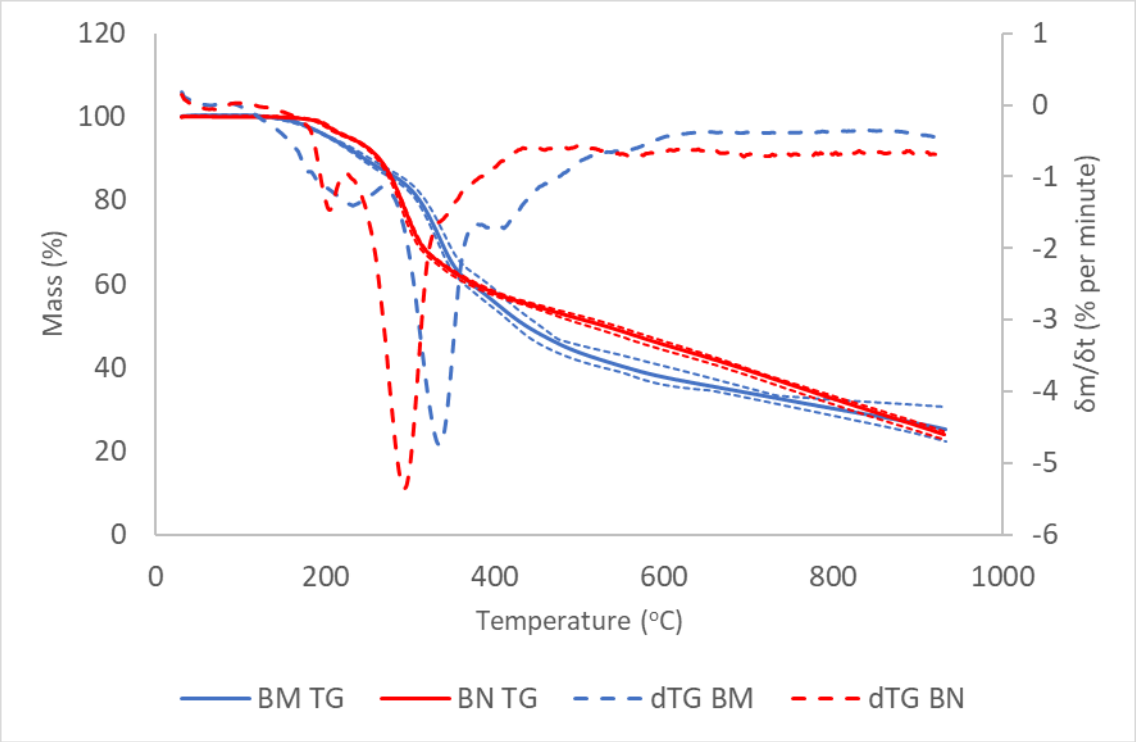

Figure 4.7*. Comparison of mean TG and dTG thermograms for BM and BN sample sets. Dotted lines around TG thermograms indicate range within sample set.*

The BN sample set exhibited significantly lower mass loss than the BM sample set over an approximate temperature interval of 145-265 °C and 440-775 °C (Figure 4.7) with this relationship being reversed from 285-340 °C. No significant difference is observed in retained char fraction at 900 °C. Within these temperature intervals there is no overlap in the retained mass range, indicated by the dotted lines around the TG thermograms.

While the first significant mass loss peak reaches a similar $\frac{dm}{dt}$ value in both the BM and BN sets, this peak occurs at a lower temperature in the BN samples (BM = 233 °C, BN = 204 °C) and the overall width and area of the peak is greatly reduced. In the BM sample set, this peak

spans a temperature interval from 87-271 ^{o}C with a total mass loss of 14.1 %, while the peak in the BN sample set spans a temperature interval of 95-225 ^{o}C with a mass loss of 4.2 %.

The temperature at which maximum mass loss is observed to occur is 40 ^{o}C lower in bare PIR than when TEP and TCPP are present (294 ^{o}C vs. 334 ^{o}C) with a greater maximum rate of mass loss also observed (5.4 % vs. 4.4 % per minute). These differences sharply contrast with the pattern observed in the free-rise samples, where there is minimal difference in the temperature at peak mass loss for neat PIR and PIR containing TEP and TCPP, and a slightly lower rate of peak mass loss in the neat PIR samples (Figure 4.4).

4.3. Comparison of Polyols PS-2412 and PS-2602

As discussed earlier in this chapter, the free-rise and block-moulded neat PIR differed from each other due to the use of the PS-2412 polyol for the free-rise samples and the PS-2602 polyol for the block-mould samples. The primary difference between these polyols was the addition of TCPP to PS-2412. However, the manufacturers technical specification gives different hydroxyl values for PS-2412 (240 mgKOH/g) and PS-2602 (270 mgKOH/g). A higher hydroxyl value may result in a greater prevalence of urethane groups for a given mass of polyol, as there more hydroxyl groups per unit weight able to undergo urethane-forming reactions with isocyanate.

Three block-mould samples of foams based on PS-2602 polyester polyol and containing the standard fire-retardant system of TEP and TCPP at approximate 2 % and 5 % respective loading were subjected to thermogravimetric analysis under an inert atmosphere of nitrogen at 20 cm^3 per minute, heating from 30-900 ^{o}C at a rate of 10 ^{o}C/min (Figs. 4.8 and 4.9). These samples are denoted the BP series in this chapter.

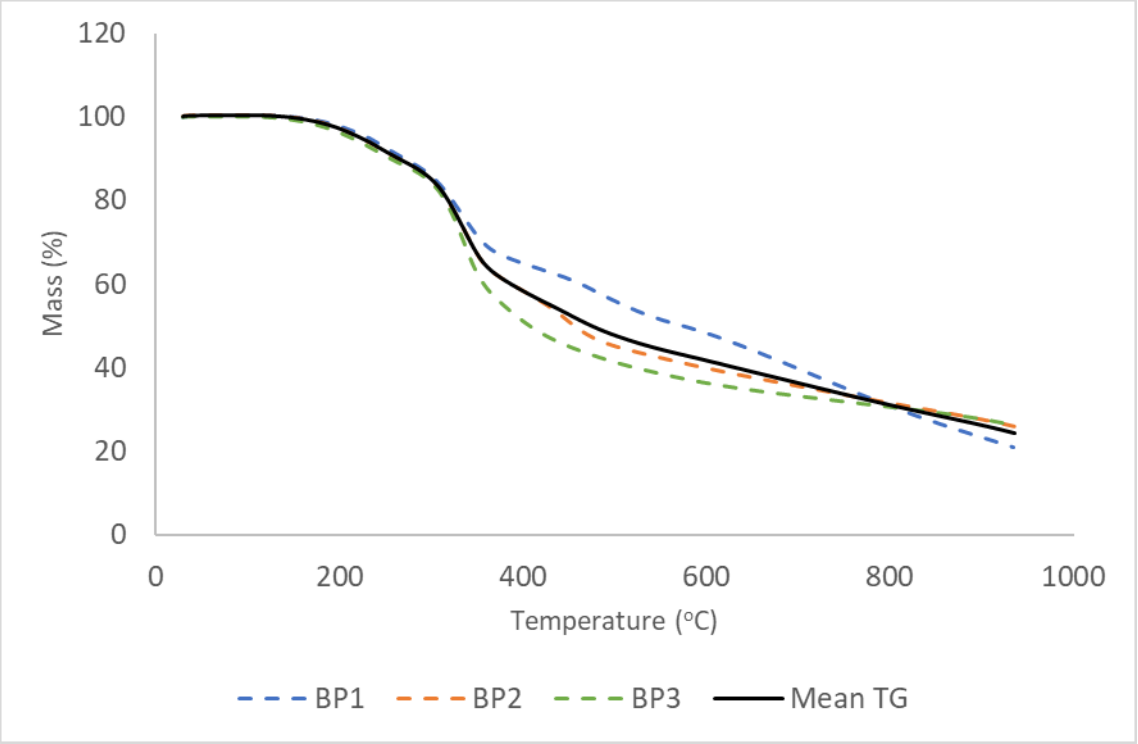

Figure 4.8.*TG thermograms for samples BP1-3 and mean TG thermogram from 30-900°C at 10°C/min under N_2.*

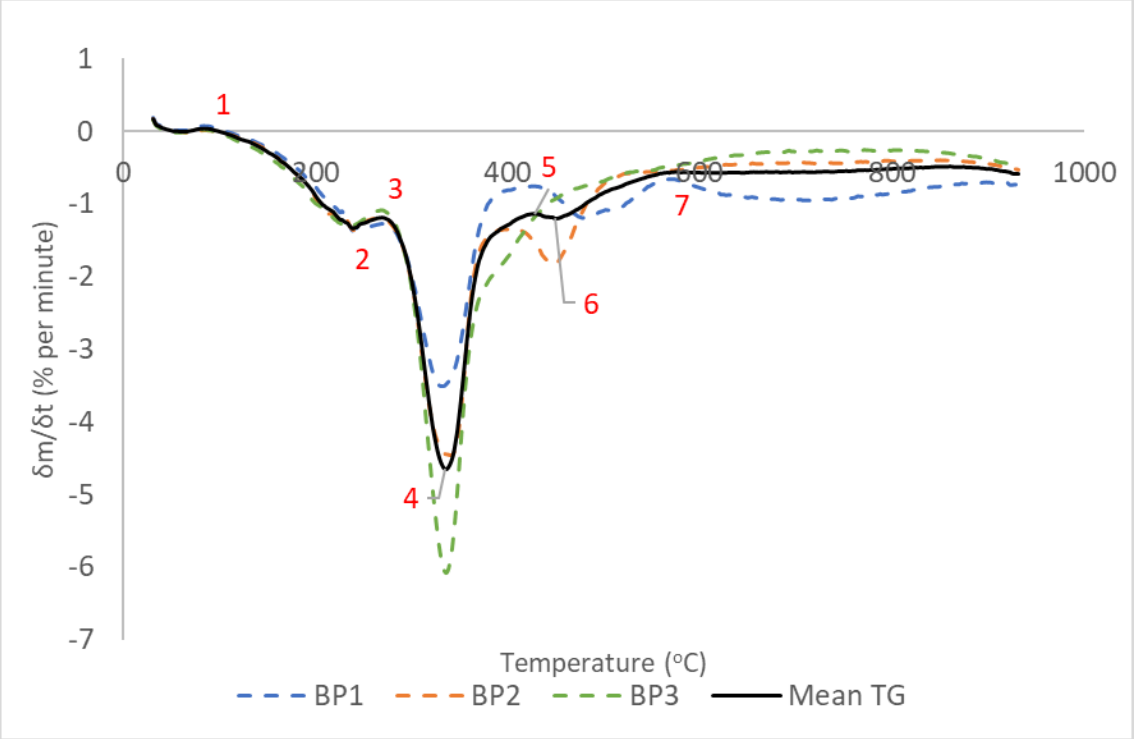

Figure 4.9. *dTG thermograms for samples BP1-3 and mean dTG thermogram from 30-900°C at 10°C/min under N_2. Key features are labelled 1-7 and referred to in text using square brackets.*

Table 4.1 Temperature at selected mass loss thresholds for samples BP1-3

Mass Loss	**BP1**	**BP2**	**BP3**	**Mean**
1%	179.5°C	169.6°C	159.2°C	171.2°C
2.5%	204.7°C	196.1°C	185.3°C	195.9°C
5%	232.7°C	221.6°C	214.3°C	223.4°C
10%	272.2°C	263.4°C	257.1°C	263.6°C
15%	305.3°C	299.3°C	296.4°C	301.5°C
20%	323.2°C	318.7°C	315.8°C	319.2°C
30%	357.4°C	343.9°C	335.7°C	342.7°C
40%	464.5°C	386.4°C	358.9°C	387.1°C
50%	575.4°C	456.2°C	408.2°C	474.1°C

As reflected in the TG and dTG thermograms (Figures 4.8 and 4.9), the behaviour of samples in the BP set is largely consistent at temperatures below 300 °C, but widely diverges at higher temperatures.

In common with previous samples, minimal activity is observed across the 30-92 °C temperature interval [1], with the dTG showing a small initial mass loss, which reaches a peak rate of 0.07 % per minute at 63 °C, attributed again the desorption of water and other light volatiles. The mean mass loss in this temperature range is 0.2 % (0.024 mg). Above 92 °C, an acceleration of mass loss occurs, with a peak rate of 1.3 % per minute at 238 °C [2]. This peak is highly consistent across the BP sample set in both temperature (238-242 °C) and the rate of mass loss (1.3-1.4 % per minute). This rate remains almost constant to 273 °C (1.3 % per minute) with a mass loss of 11.8 % occurring in this temperature range.

The mean maximum rate of mass loss of 4.7 % per minute occurs at 336 °C. The temperature at which this peak occurs is quite well-preserved throughout the BP set, falling within a range of 332-340 °C, but the rate of mass loss at this peak ranges from 3.5-6.1 % per minute. The mean rate of mass loss decelerates to 1.21 % per minute at 390 °C. Cumulative mass losses in this temperature range accounts for 25.8 % (3.20 mg) of the initial sample mass. This peak is immediately followed by another interval of near constant mass loss (1.21-1.24 %), continuing to 426 °C. with further mass loss of 4.3 %. Another peak occurs at 469 °C, with dm/dt = -1.9 % per minute. However, when the individual TG and dTG thermograms are inspected,

behaviour in this region is highly variable. BP1, which has the lowest rate of mass loss at the main peak, exhibits a broad third peak centred at 478 °C with a mass loss rate of 1.2 % per minute. BP2 also has a third peak, although this is centred at 448 °C with a mass loss rate of 1.9 % per minute. BP3, which exhibits the highest rate of mass loss at the main peak exhibits no significant third peak, with only a moderately pronounced shoulder in the region above the peak. The retained char fraction at 900 °C is 22.9 %, falling with a range of 21.0-26.0 %. The differences between the samples appears to be accounted for by an upward shifting in the temperature of mass loss for samples that exhibits lower rates of mass loss at the main peak.

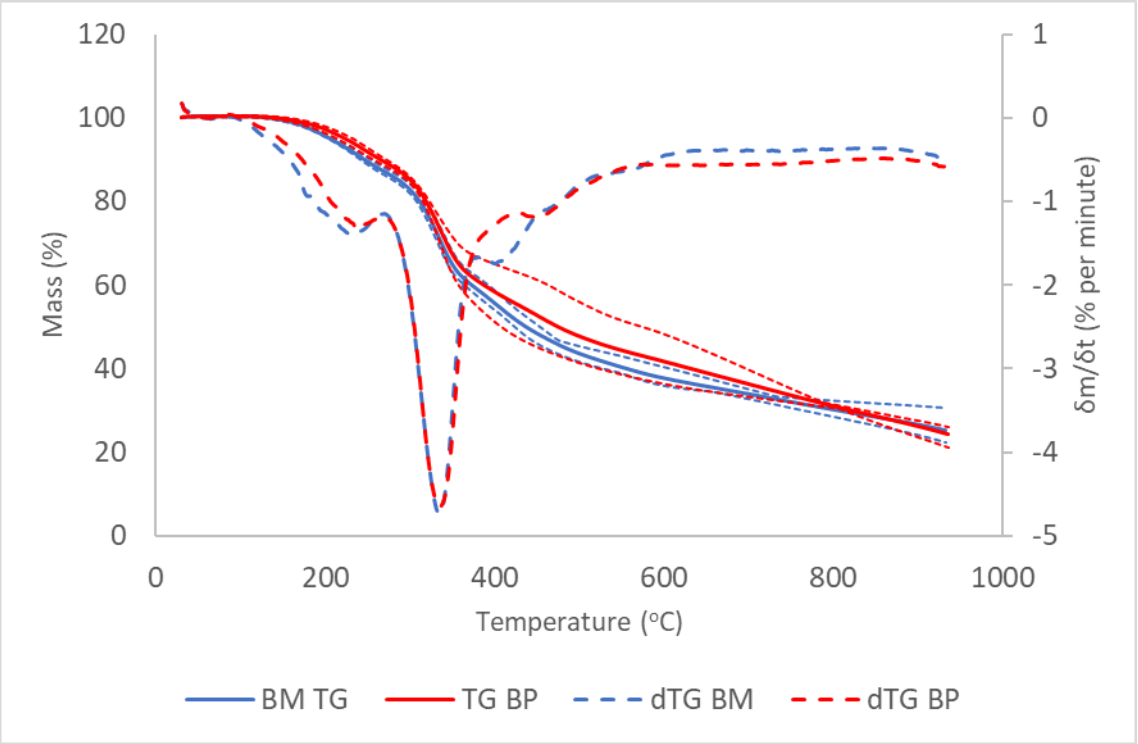

Figure 4.10. *Comparison of mean TG and dTG thermograms for BM and BP sample sets under N_2. Dotted lines around TG thermograms indicate upper and lower bounds of range between samples.*

Direct comparison of the mean TG thermograms shows that the PS2602-based BP foams exhibit on average lower mass loss across a temperature range from 150°C to around 775 °C than the PS-2412-based BM foams. However, due to the high degree of variation within the PS2602 samples, these differences are generally not found to be substantial, as indicated by extensive overlap between the ranges within each sample set, indicated by the dotted lines surrounding the TG thermograms (Figure 4.10*)*. Distinct separation of these ranges is only seen in the temperature interval from 185-300 °C, although the magnitude of the difference between the mean curves in this region is small, with retained mass in the BP samples being less than 2 % greater than that in the BM samples. Retained char at the end of heating is slightly higher on average for the BM samples (BM, 25.3 %; BP, 24.1 %) although there is again significant overlap when considering the sample sets as a whole.

The mean dTG thermograms show a slightly higher temperature for the first peak in the BP sample set than the BM sample set, with this occurring at 238 °C in the former and 233 °C in the latter. For BM samples, $\frac{dm}{dt}$ at this peak is -1.4 % per minute, compared to -1.3 % per minute for BP samples. Mass loss within the region of this peak is 13.2 % for the BM samples and 10.9 % for the BP samples. The second peak occurs at 335 °C in both BM and BP samples, with $\frac{dm}{dt}$ of -4.7 % per minute for both sample sets. In the case of the BM samples, a third peak occurs at 399 °C ($\frac{dm}{dt}$ = -1.7 % per minute) and in the BP samples at 450°C ($\frac{dm}{dt}$ = -1.2 % per minute).

Although there are some indications that mass loss in some of the BP samples is shifted to a higher temperature, the use of a TCPP-free polyol does not result in a substantial difference in overall thermal stability when comparing the BM and BP sample sets when taking into account the variability within each sample set. This suggests that the slightly greater loading of TCPP resulting from its presence within the polyol blend does not result in further improvement to thermal stability. The higher hydroxyl value of the PS-2602 polyol does not appear to have a detectable impact on isocyanate conversion or the prevalence of urethane bonds, as this would be expected to increase breakdown at lower temperatures, which is not observed.

4.4. Effects of Triethyl Phosphate and Tris(1-Chloro-2-Isopropyl) Phosphate

4.4.1. Triethyl Phosphate

As covered extensively throughout earlier sections of this thesis, the current commercial formulation of PIR foams relies on a two-component fire retardant system of TEP and TCPP. Analyses of block-moulded foam samples containing either TEP and TCPP in isolation have been carried out here to better understand the individual contributions of these flame retardants to the overall thermal stability of the PIRs.

Three samples of PIR foam based on PS2602 polyol and containing an approximate loading of 2 % TEP with no TCPP were subjected to thermogravimetric analysis under an inert atmosphere of dry nitrogen at a flow rate of 20 cm^3 per minute over a temperature range of 30-900 °C and constant heating rate of 10 °C/min. Samples ranged in mass from 12.21-12.96 mg, with a mean of 12.57 mg. This sample set has been assigned the identifier BQ, with the individual samples labelled BQ1, BQ2, and BQ3.

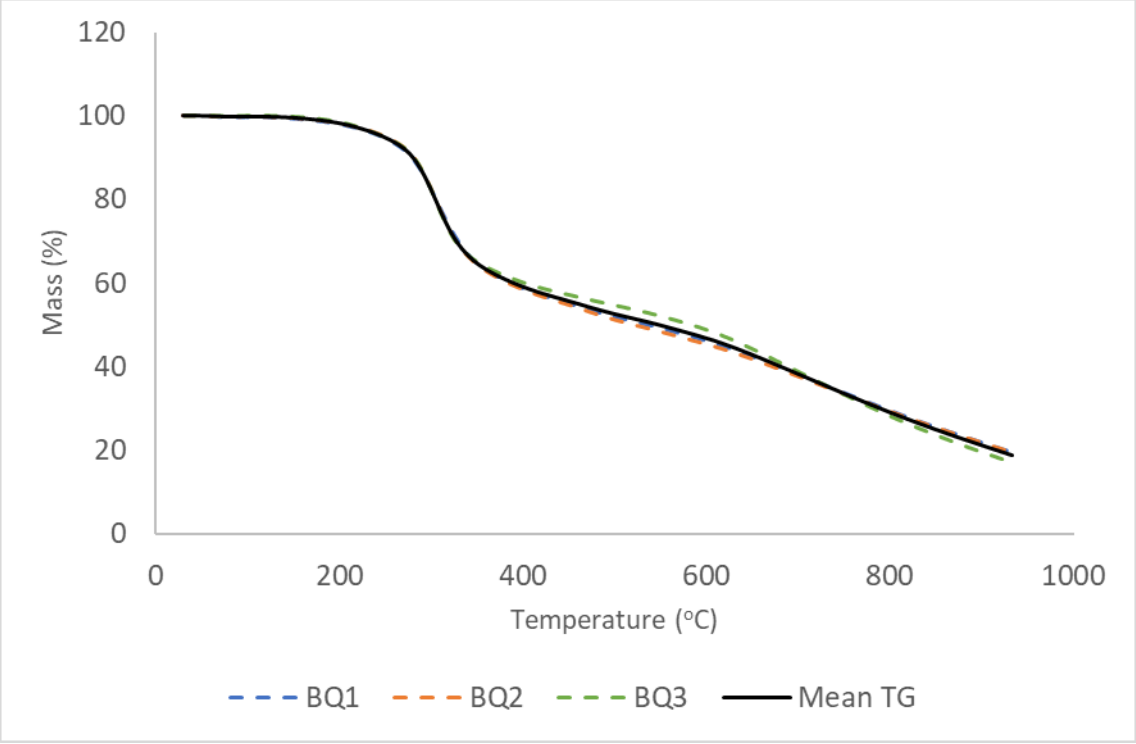

Figure 4.11. *TG thermograms of BQ1-3 and mean TG thermogram from 30-900°C at 10°C/min under N_2.*

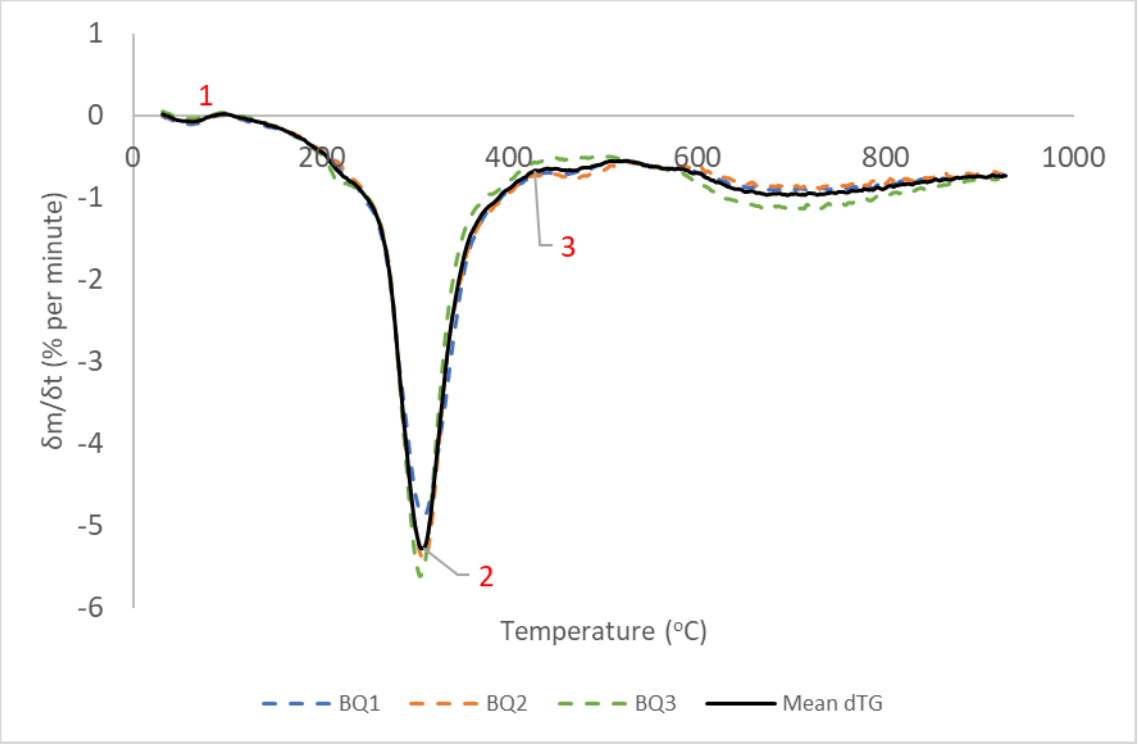

Figure 4.12. *dTG thermograms of BQ1-3 and mean dTG thermogram from 30-900°C at 10°C/min under N_2. Key features are labelled 1-3 and referenced in text using square brackets.*

The observed thermal behaviour is generally consistent across the three samples, contrasting with the large variations observed for the BP sample set. Presumed loss of adsorbed moisture is observed in all samples across an approximate 30-97 °C temperature range [1]. Across all samples, the maximum rate of mass loss in this region is 0.13 % per minute, with a mean total mass loss of 0.28 % (0.035 mg, range 0.15-0.42 %), consistent with previous sample sets.

Above this temperature, a gradual acceleration of mass loss is observed with a near continuous to maximum of 5.3 % per minute (range 4.9-5.6 % per minute) at 307 °C [2] (range 305-309°C). Conspicuously, there is no observable indication of a distinct lower temperature mass loss event to the left of the primary peak. Above the peak, mass loss decelerates to 0.9 % per minute at 447.6 °C [3]. Total mass loss across the 97-448 °C temperature range is 48.37 % (6.08 mg)

A small mass loss occurs across the temperature range from 448-535 °C, with a slight peak at 456.3 °C ($\frac{dm}{dt}$ = -0.96 % per minute). This event accounts for an additional 6.8 % (0.85 mg) mass loss. This event is less prominent in one of the samples, appearing as a region of shallower gradient with no distinct peak. Mean retained char fraction at the end of heating is 18.7 % within a range of 17.3-19.5 %.

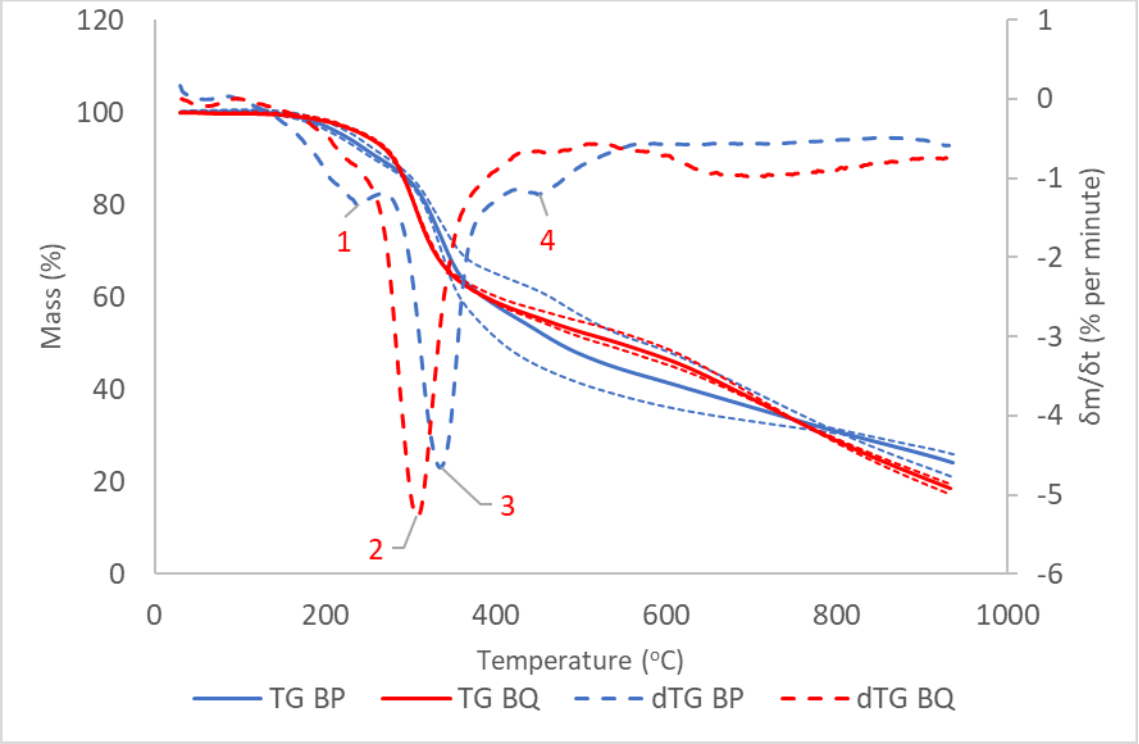

Figure 4.13. *Comparison of mean TG and dTG thermograms for BP and BQ sample sets under N_2. Dotted lines around TG thermograms indicated upper and lower bounds of range within sample set.*

When comparing (Figure 4.13) the BP foams (i.e., foams containing both TEP and tris (1-chloro-2-isopropyl) phosphate) to the BQ samples containing TEP alone the latter are found on average to undergo lower total mass loss in the relatively low temperature region between 150-290 °C (Figure 4.13*)*, and a lower rate of mass loss at temperatures below 255 °C, consistent with the absence of a distinct mass loss event below the main peak, contrasting with that present in the BP samples [1]. This relationship is reversed in the 295-345 °C interval, where retained mass is *lower* for BQ samples than BP samples. This correlates with a clear downward shift of the main peak [2,3]. In the BQ samples, a maximum rate of mass loss of 5.3 % per minute occurs at a temperature of 310 °C, compared to 4.7 % at 336 °C in the BP samples.

The minor mass loss event with its peak at 456 °C appears to closely correspond to the much larger third peak observed in a similar temperature region in the foams containing both TEP and tris(1-chloro-2-isopropyl phosphate) [4]. Residual char fraction is lower for foams containing TEP only compared to those containing both TCPP with no overlap in the ranges. This appears to suggest that the presence of TCPP is involved in the mass loss events that occurs around 250°C in samples containing this fire retardant, as this was also present in the

BM sample set. While TCPP appears to increase mass loss in the lower temperature regions, it appears obvious that it also increases the temperature at which the highest rate of mass loss occurs, compared to samples from which it is absent. This is an important observation, as it suggests that TCPP may raise the critical temperature at which rapid decomposition of the foam occurs and may therefore delay the onset of flaming combustion from the production of volatile fuel species.

4.4.2. Tris(1-chloro-2-isopropyl) Phosphate

Based on results from previous experiments detailed in this chapter, TCPP appears to have a greater impact on the temperature at which rapid PIR decomposition occurs than does TEP. To corroborate this, foams containing TCPP but no TEP were subjected to thermogravimetric analysis.

Three block-mould foam samples based on PS2602 aromatic polyester polyol and containing and approximate 5 % loading by mass of TCPP were subjected to thermogravimetric analysis using the same experimental procedure as previous samples. These samples were assigned the identification codes BR1, BR2 and BR3 and will be collectively referred to herein as the BR sample set. BR samples ranged in initial mass from 11.33 mg to 11.85 mg with a mean value of 11.74 mg. Results obtained from these analyses are presented below in Figures 4.14 and 4.15

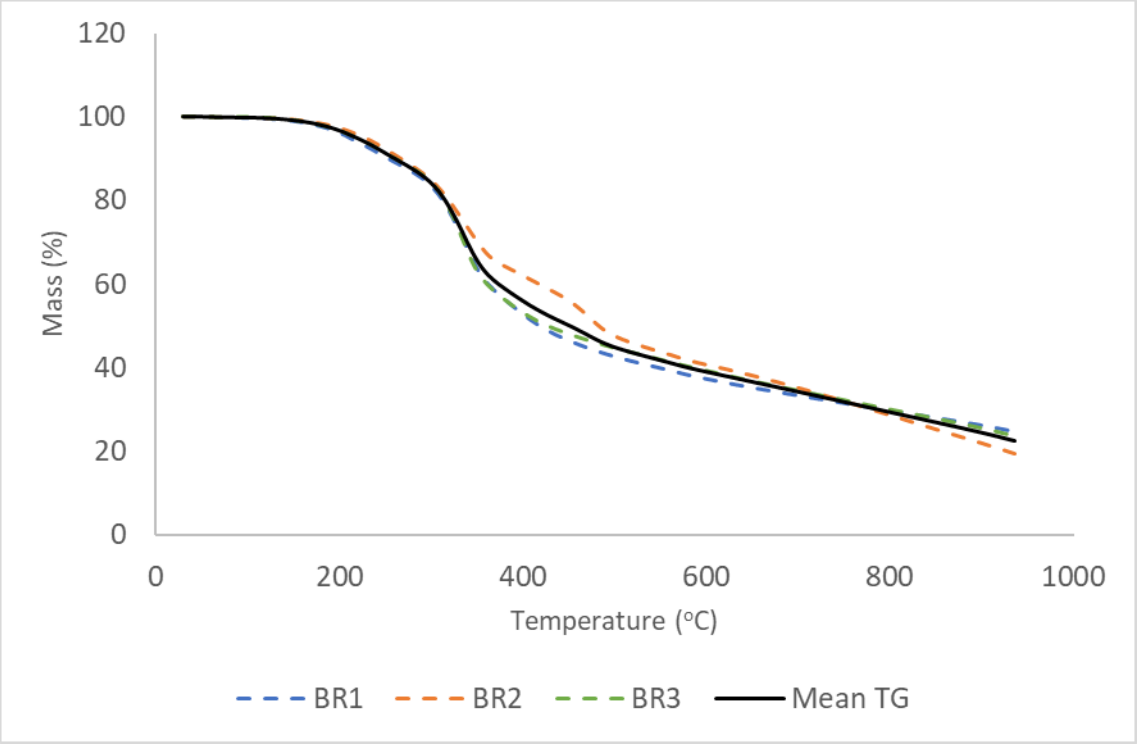

Figure 4.14. *TG thermograms of BR1-3 and mean TG thermogram from 30-900 °C at 10 °C/min under N_2.*

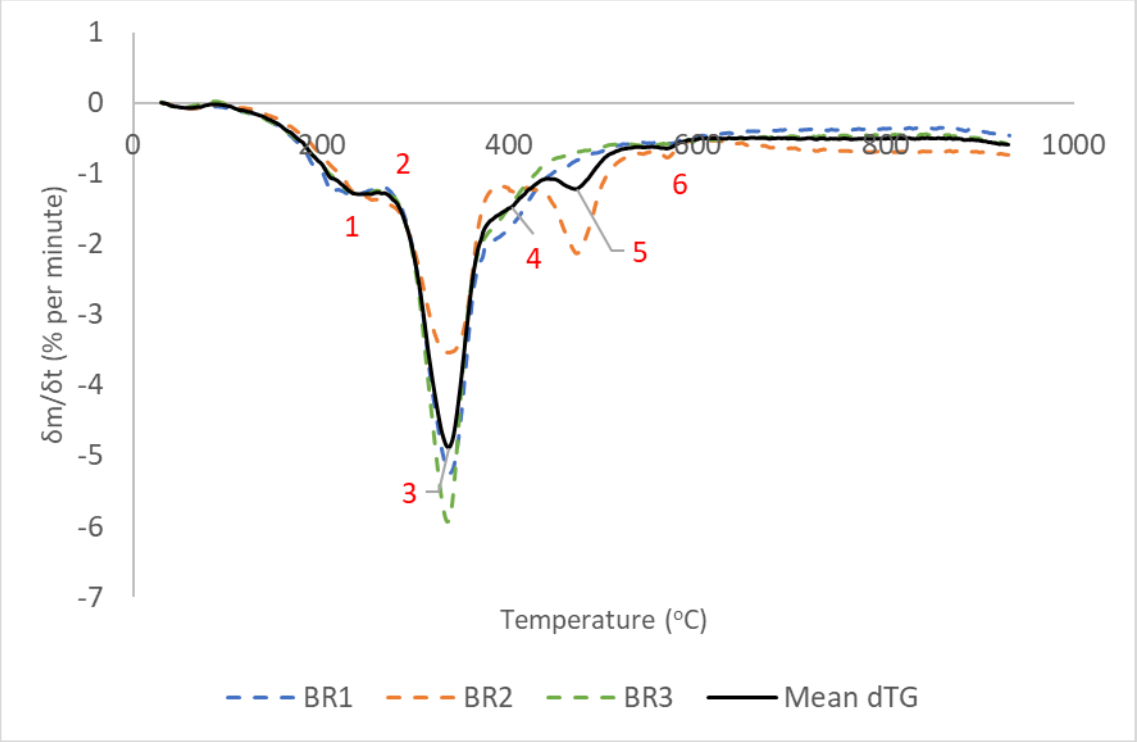

Figure 4.15*. dTG thermograms of BR1-3 and mean dTG thermogram from 30-900 °C at 10 °C/min under N_2. Key features are labelled 1-6 and referred to in text using square brackets.*

The TG and dTG thermograms again show that a presumed desorption of moisture occurred across an average temperature range of 30-90 ^{o}C, with $\frac{dm}{dt}$ = -0.07 % per minute at its highest rate, and a total of 0.2 % mass loss (0.02 mg). This feature has been consistent across all sample sets analysed in this thesis.

Within this set, there is a substantial degree of variation, with BR2 behaving quite differently to BR1 and BR3. In all cases, the initial putative desorption event is followed by an acceleration of mass loss. BR 1 and BR3 each exhibits a shallow peak at 238 ^{o}C and 241 ^{o}C respectively, with $\frac{dm}{dt}$ of -1.29 % per minute and -1.30 % per minute. The BR2 data lacks a distinct peak, instead exhibiting a weak shoulder terminating at 257 ^{o}C ($\frac{dm}{dt}$ = -1.37 % per minute). In aggregate, the mean dTG curve displays a broad, flattened mass loss peak centred around 243 ^{o}C [1], followed by a deceleration to an inflection point at 261 ^{o}C [2]. Mean cumulative mass loss during this phase was 9.8 % (1.15 mg) ranging from 9.0% (1.07mg) in sample 2 to 10.9% (1.30mg).

The position of the main peak in the temperature axis shows little variation between samples with a mean value of 335 ^{o}C [3] falling with a range of 334-337 ^{o}C. Much greater variation occurs in the value of $\frac{dm}{dt}$ at this peak, with mass loss rates of 3.5-5.9 % per minute and a mean value of 4.9 % per minute.

Above this peak, BR1 and BR3 exhibit a steady deceleration of mass loss into a small shoulder feature. By contrast, BR2 exhibits a gradually accelerating rate of mass loss from the inflexion point at 392 ^{o}C, then undergoes a more rapid acceleration, resulting in the appearance of a mass loss peak at 472 ^{o}C ($\frac{dm}{dt}$ = -2.13 % per minute) extending upwards in temperature to 557 ^{o}C, with another very small peak at 56.8 ^{o}C. Mass loss in the temperature range above the main peak is substantially greater (43.5 %, 5.15 mg) in sample 2 than in sample 1 (32.0 %, 3.86 mg) and sample 3 (32.7 %, 3.71 mg), equating to a mean mass loss of 36.4 % (4.27 mg). Mean retained char at the end of heating is 22.6 % (2.65 mg) with individual samples at 24.6 %, 19.5 %, and 23.7 %.

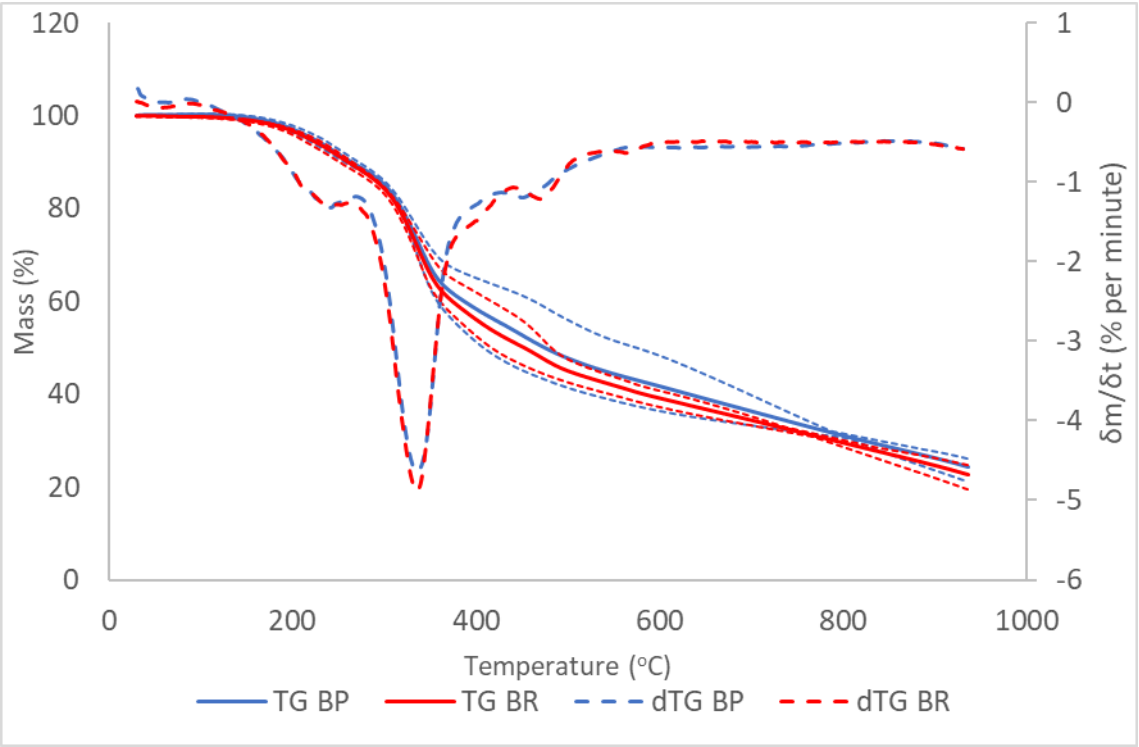

***Figure 4.16**. Comparison of mean TG and dTG thermograms for BP and BR sample sets under N_2. Dotted lines around TG thermograms indicated upper and lower bounds of range within sample set.*

Direct comparison of mean TG and dTG thermograms (Figure 4.16) shows very similar thermogravimetric behaviour across a large majority of the temperature range, differing by less than 0.5 % below 305 °C and above 610 °C. In the intervening range, mean stability is greater in the sample set containing both TEP and TCPP, with a maximum difference of 5.45 % at 417 °C. Mean retained char fraction is very similar for both sample sets at 22.9 % for samples containing TEP and TCPP and 22.6 % for sample containing TCPP alone. Owing to the high degree of inter-sample variability within each set and the extensive overlap of the ranges within each set, stability is not demonstrated to differ significantly between the BP and BR sample sets at any temperature within the 30-900 °C range.

Comparison of the dTG thermograms highlight only very subtle differences in behaviour. The two sample sets produces mean dTG curves that almost perfectly overlap in several key regions. The positions of both the first and second mass loss peaks are almost identical with respect to temperature with only a small difference in peak mass loss rate (4.7 % per minute for BP samples vs. 4.9 % per minute for BR samples). This comparison suggests that for the same polyol, the presence of TCPP in combination with TEP has little additional impact on thermal stability when compared to TCPP alone.

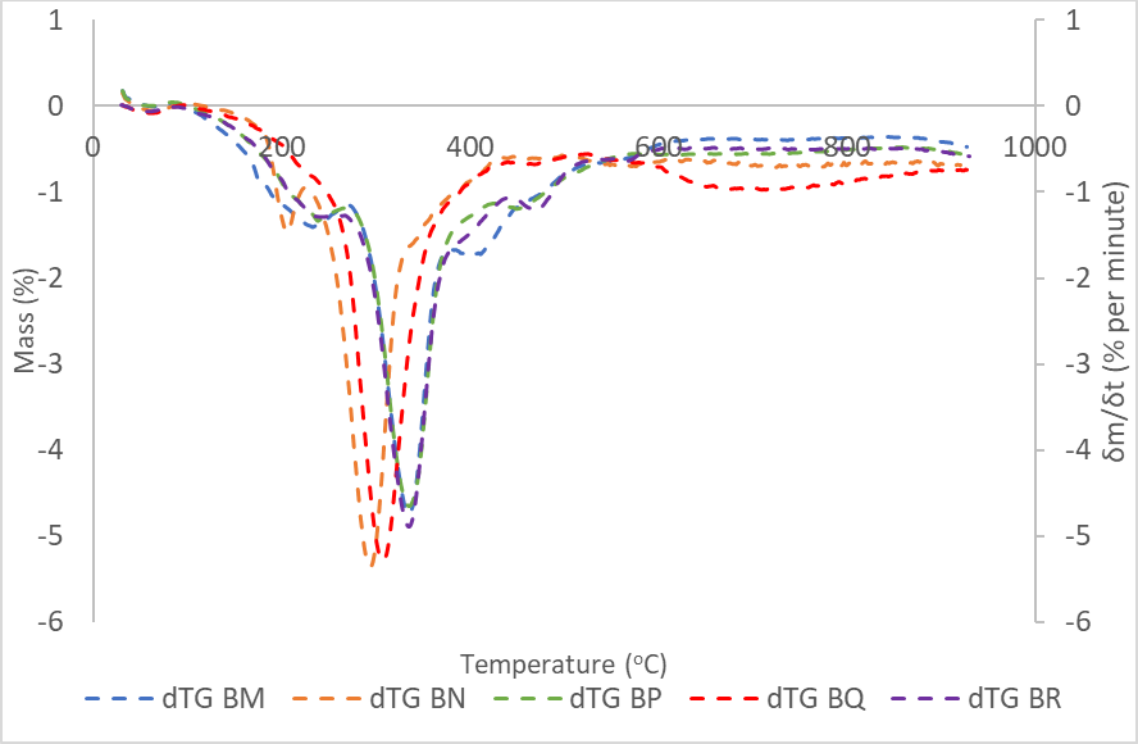

Figure 4.17. *Mean dTG curves of BM, BN, BP, BQ and BR sample sets from 30-900 °C at 10 °C/min under* N_2.

Figure 4.17 combines the dTG data for all five block-mould sample sets previously presented in this chapter. When all samples are compared simultaneously it can be clearly seen that the sample sets containing TCPP (BM, BP, BR) exhibit distinct dTG peaks in the 240-250 °C temperature range. These mass loss events accounted for 10-15 % mass loss. This event is absent from the BQ sample set, containing TEP alone, while the BN sample set containing no fire retardants exhibits a sharp peak at around 220 °C which accounts for only 4 % mass loss.

The BM, BP and BR sample sets also exhibit a near identical temperature of around 335 °C for the position of their largest mass loss peak. This temperature is around 41 °C higher than the corresponding event in the BN sample set with no fire retardants (294°C) and around 25 °C higher than the BQ sample set containing TEP alone (310 °C). Overall, there is a general pattern of behaviour in which the presence of TCPP appears to stimulate a certain degree of mass loss at low temperatures in exchange for shifting the major mass loss events to a higher temperature.

4.5. Effect of Low Hydroxyl-value Polyol

As discussed in the previous chapter, the physical properties of PIR foams are influenced to a large extent by the preponderance of isocyanurate ring structures within the polymer matrix (8). These structures are the product of trimerization reactions between the isocyanate groups of 4,4-MDI, and their relative abundance is influenced by the proportion of isocyanate groups consumed by reactions with hydroxyl groups present in water, diol chain-extenders, and the polyol component. Isocyanurate structures have previously been found(9,10) to exhibit a higher bond dissociation temperature than urethane groups, and therefore it was though that foams produced using such polyols may exhibit differences in their thermal stability characteristics.

A number of sample sets were produced using a lower hydroxyl value polyol, Terate HT2006, manufactured by Stepan. This polyol had a stated hydroxyl value of around 195 mgKOH/g, compared to values of 240 mgKOH/g and 270 mgKOH/g in the PS2412 and PS2602 polyols, respectively. A lower hydroxyl value means that per unit mass of the polyol blend, a smaller number of hydroxyl groups are present. Since isocyanate groups may react with either react with hydroxyl groups to form urethanes or undergo trimerization to form isocyanurates, a lower hydroxyl value will tend to favour the latter.

4.5.2.HT-2006 with Two-component Fire Retardant System

To isolate the effect of lowering the hydroxyl value of the polyol three samples of block-moulded PIR foam based on the HT2006 polyol (low hydroxyl value) with added TEP and TCPP, of mean mass 11.75mg, were subjected to non-oxidative thermal analysis using the previously described standard experimental method. These foams will be referred to hereafter as the LP sample set with individual samples labelled LP1, LP2 and LP3. These samples provide a direct comparison with the BP sample set, as the only parameter that was changed was the replacement of the PS-2602 polyol (hydroxyl value 240 mgKOH/g) with the HT-2006 polyol (hydroxyl value 195 mgKOH/g).

Individual sample and mean TG/dTG thermograms were produced using previously defined data processing methods and are displayed below.

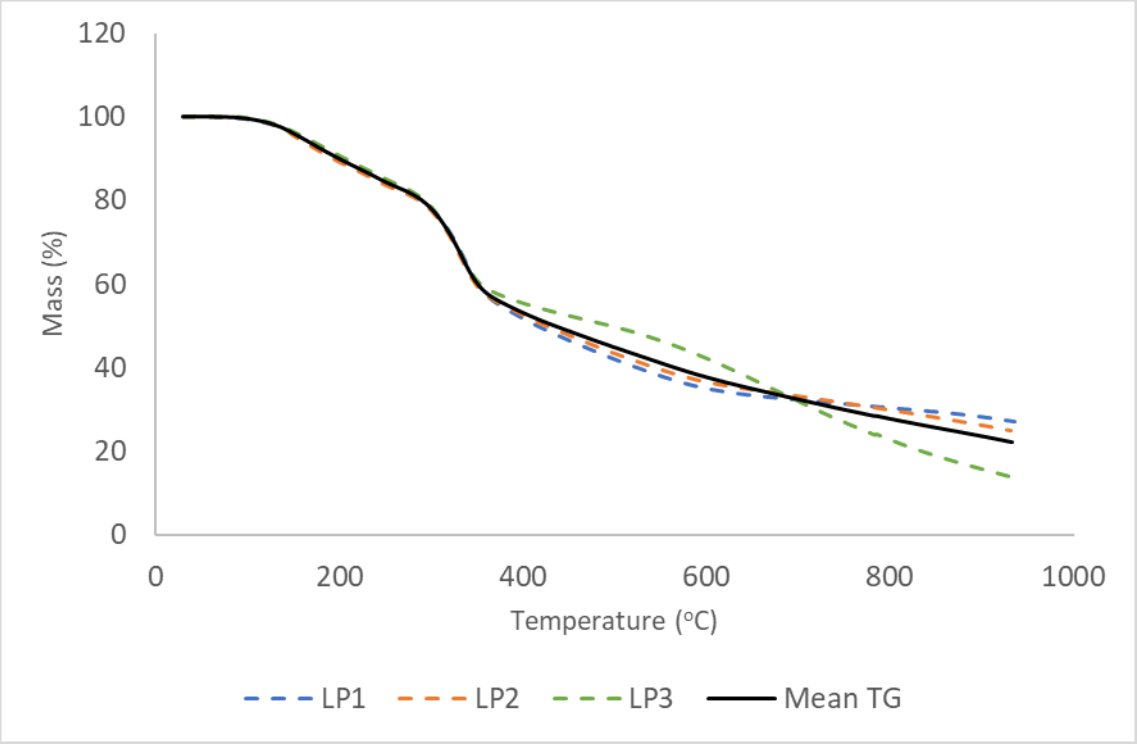

Figure 4.18. *TG thermograms of LP1-3 and mean TG thermogram from 30-900°C at 10°C/min under N_2.*

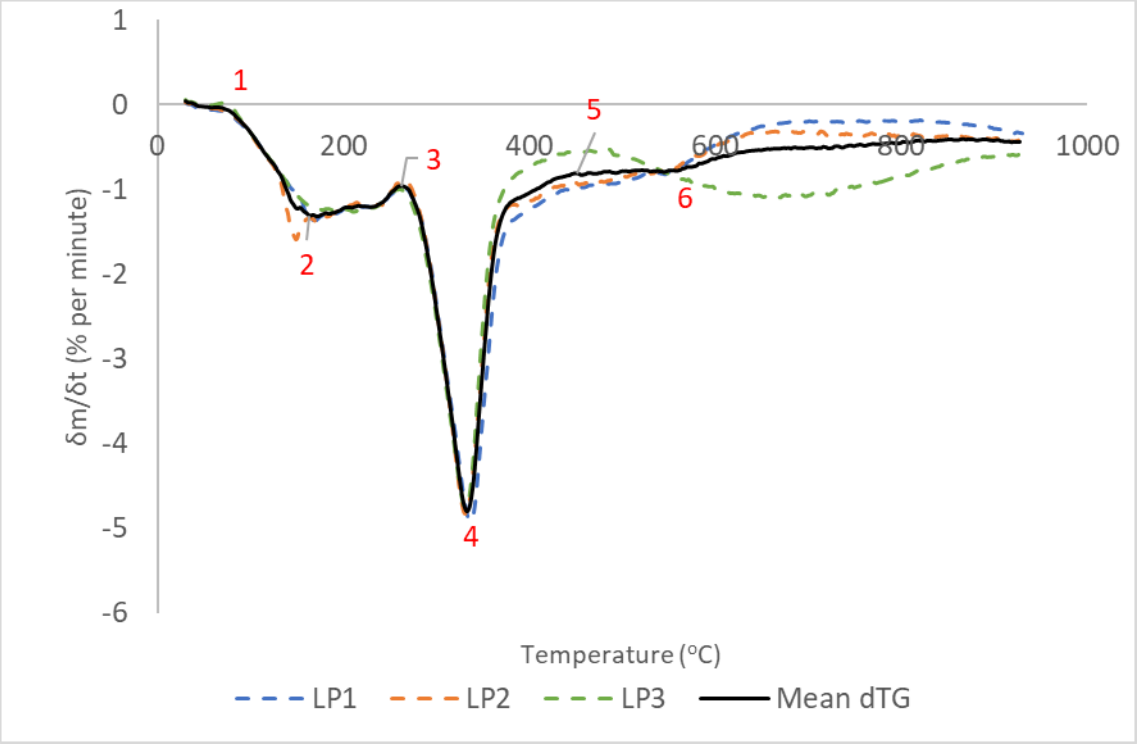

Figure 4.19. *dTG thermograms of LP1-3 and mean dTG thermogram from 30-900°C at 10°C/min under N_2. Key features are labelled 1-6 and referred to in text using square brackets.*

All three samples exhibit extremely consistent behaviour on the TG thermograms at temperatures below 350ºC, while some divergent behaviour was observed in LP3 in the temperature range above the main peak.

Mass loss exceeds 1 % at a mean temperature of 114 ºC (range 111-119 ºC) and exceeds 2.5 % at a mean temperature of 138 ºC (range 135-140 ºC). Mean retained mass at the end of heating is 22.2 % (range 13.7-27.0 %), with the large range reflecting the unusually low terminal stability of sample 3.

The dTG thermograms indicate a pattern of behaviour that is broadly similar to previous sample sets containing TCPP, but with some notable differences. The rate of mass loss remains very low at temperatures from 30-66 ºC [1]. dm/dt does not exceed 0.04 % per minute in this temperature range, and cumulative mass loss is around 0.14 %.

After this initial region, there is a gradual increase in dm/dt into a relatively broad first peak region. Even after smoothing, a noticeable degree of roughness is present in the dTG curve for the first mass loss event, with two of the samples exhibiting a small but sharp peak at the early stages of this event, occurring at 166 ºC (dm/dt = -1.39 % per minute) in LP1, and at 149 ºC (dm/dt = -1.6 % per minute) in LP2. LP3 exhibits a more rounded dTG profile in this region, with its peak occurring at 211 ºC (dm/dt = -1.27 % per minute). Averaged across the samples, the first mass loss event takes the form of a broad peak, with its maximum at 164 ºC [2] (dm/dt = -1.3 % per minute) and weak accessory peak at 230 ºC (dm/dt = -1.2 % per minute). This region extends upwards to a clear transition point at 263 ºC [3] (dm/dt = -1.0 % per minute), with mass loss across the 66-263 ºC range of 16.7% (1.96mg).

The primary mass loss event occurs across a mean temperature range of 263-376 ºC, with the maximum rate of mass loss occurring at 333 ºC [4] (range 332-337 ºC), with dm/dt = -4.8 % per minute (range -4.7-4.9 % per minute). Mass loss during this event is 27.5 % (3.23 mg).

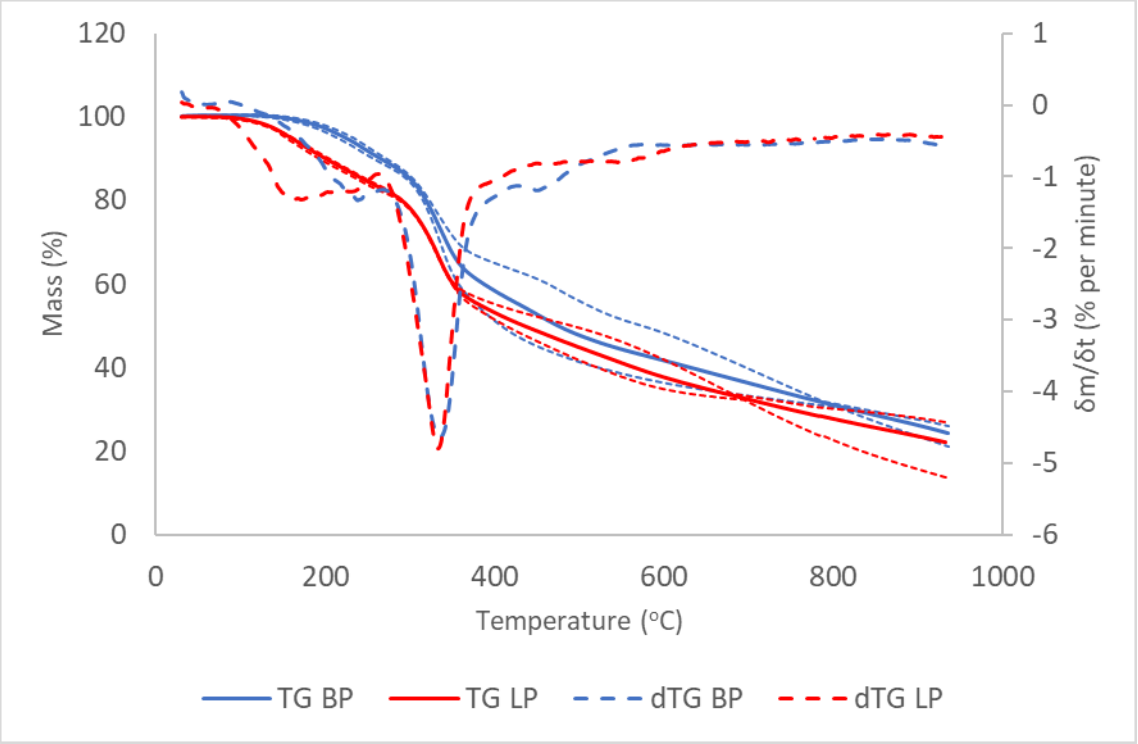

Figure 4.20. *Comparison of mean TG and dTG thermograms for BP and LP sample sets from 30-900 °C at 10 °C/min under N_2. Dotted lines around TG thermograms indicated upper and lower bounds of range within sample set.*

The HT-2006 formulation with TEP and TCPP is directly analogous to the PS-2602 formulation with the same flame retardant system, as these samples were produced using otherwise identical formulations. The TG and dTG data (compared in Figure 4.20) demonstrate that the HT2006-based formulation exhibits substantially greater cumulative mass loss across an approximate temperature range of 125-395 °C. Throughout the remainder of the temperature range, the mean TG curve for the LP sample set indicates lower retained mass on average than the BP sample set, but owing to the degree of variation in behaviour between samples within each set it cannot be definitively stated that these differences are significant.

These differences are reflected in the dTG curves. Here it is clear from visual inspection that a large degree of the additional mass loss occurs in the temperature interval below 270 °C, the region containing the first peak. This event accounts for a mass loss of 16.7 % in the LP sample set based on HT-2006, and just 11.6 % in the BP sample set. This peak is much broader in the LP sample set (66-263 °C) than the BP sample set (83-269 °C) and is shifted to the left (164 °C vs. 238 °C). By contrast, the dTG curves for the main mass loss peaks track very closely for both sample sets, with only a 2 °C leftward shift in the LP sample set where a peak mass loss rate of 4.8 % per minute occurs at 333 °C versus as peak mass loss rate of 4.7 % per minute at

335 ^{o}C in the BP sample set. In the region above the main peak, slightly higher mass loss occurs in the BP sample set, indicating a shift of mass loss to higher temperatures.

In combination with a fire-retardant system consisting of TCPP and TEP, the use of a low-hydroxyl value polyol does not appear to improve the overall thermal stability compared to the previous polyols, and results in a clear increase in mass loss at lower temperatures. While it is likely, based on the hydroxyl value of the HT-2006 polyol, that these foams contain a lower overall proportion of urethane linkages, it is also the case that this polyol blend contains a higher proportion of diethylene glycol chain extender, as well as a small amount of polyethylene glycol. This is likely to have decreased the thermal stability of some of the urethane bonds and increased the formation of volatile products resulting from urethane cleavage at these temperatures.

4.5.3. Neat HT-2006 Foam and One-component Fire Retardant Systems

In foams produced using the PS-2602 polyol blend, it has been demonstrated that the removal of one or both fire retardant agents has an observable impact on thermal stability. For the purpose of evaluating possible interactions between the fire-retardant system and the underlying polymer matrix, this process was replicated for foams based on HT-2006. By comparing the differences in thermal behaviour across and within each set, it could then be determined whether the choice of polyol exerts a significant impact upon the effectiveness of these fire retardants.

Two samples each of neat HT-2006 foam (LN1/2), HT2006 foam containing only TEP (LQ1/2) and foam containing only TCPP (LR1/2) were subjected to thermal analysis under identical conditions to the under the same conditions as the corresponding BN, BQ and BR sample sets.

TG and dTG thermograms for the LN sample sets are reproduced below in Figures 4.17 and 4.18.

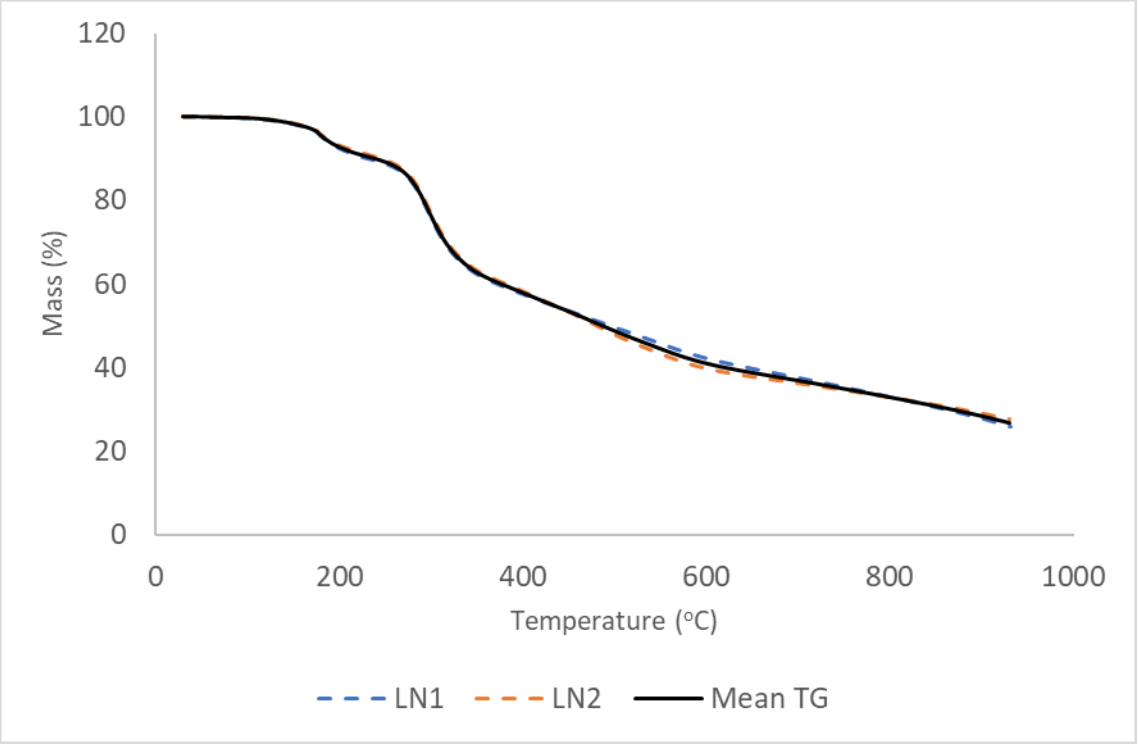

Figure 4.21. *TG thermograms for samples LN1-2 and mean TG thermogram from 30-900°C at 10°C/min under* N_2.

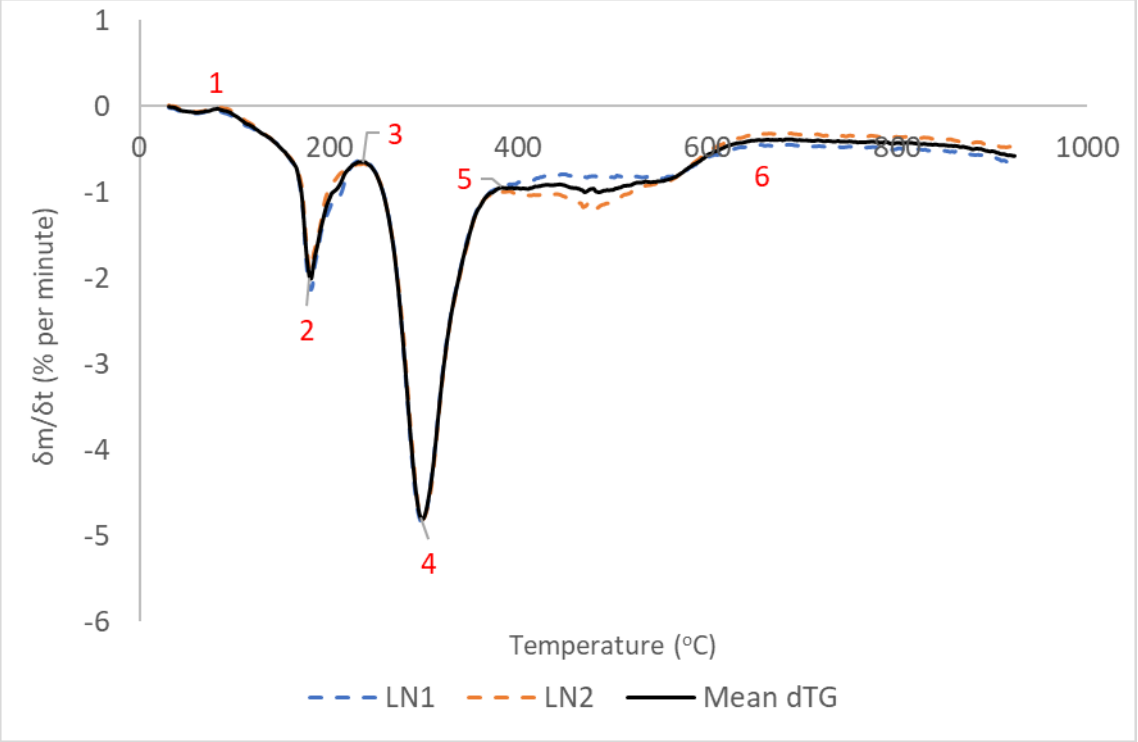

Figure 4.22. *dTG thermograms for samples LN1-2 and mean dTG thermogram from 30-900°C at 10°C/min under* N_2. *Key features are labelled 1-6 and referred to in text using square brackets.*

The LN samples exhibit a generally similar pattern of behaviour to that observed in the analogous PS2602 formulation. Mass loss exceeds 1 % at 113 °C and exceeds 2.5 % at 165 °C. Above 81 °C [1], $\frac{dm}{dt}$ increases at a relatively constant rate to 161.5 °C, then more rapidly, forming a narrow sharp peak at 181 °C [2], with the overall upper boundary of the peak at 233.7 °C. Mass loss across the entirety of this region is 9.6 % (0.73 mg).

A sharp transition into the primary mass loss event occurs above the local minimum, with $\frac{dm}{dt}$ = -4.8 % per minute at 298 °C. The end point of the peak is located at 380 °C, with a mass loss of 30.6 % (3.7 3mg) occurring from 233.7-380.1 °C. The data also show that $\frac{dm}{dt}$ remained relatively constant from 380 °C to around 481 °C, before decelerating to another relatively steady state above 650 °C. Retained char fraction at the end of heating is 26.7 %.

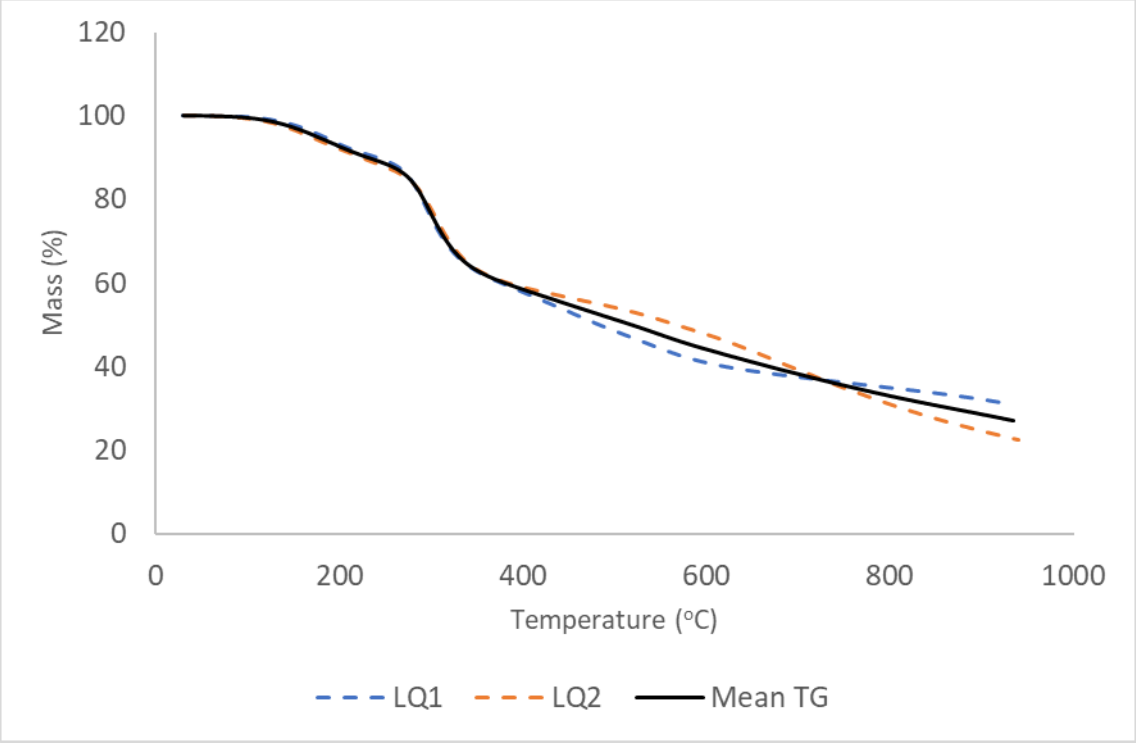

Figure 4.23. *TG thermograms for samples LQ1-2 and mean TG thermogram from 30-900 °C at 10 °C/min under N_2.*

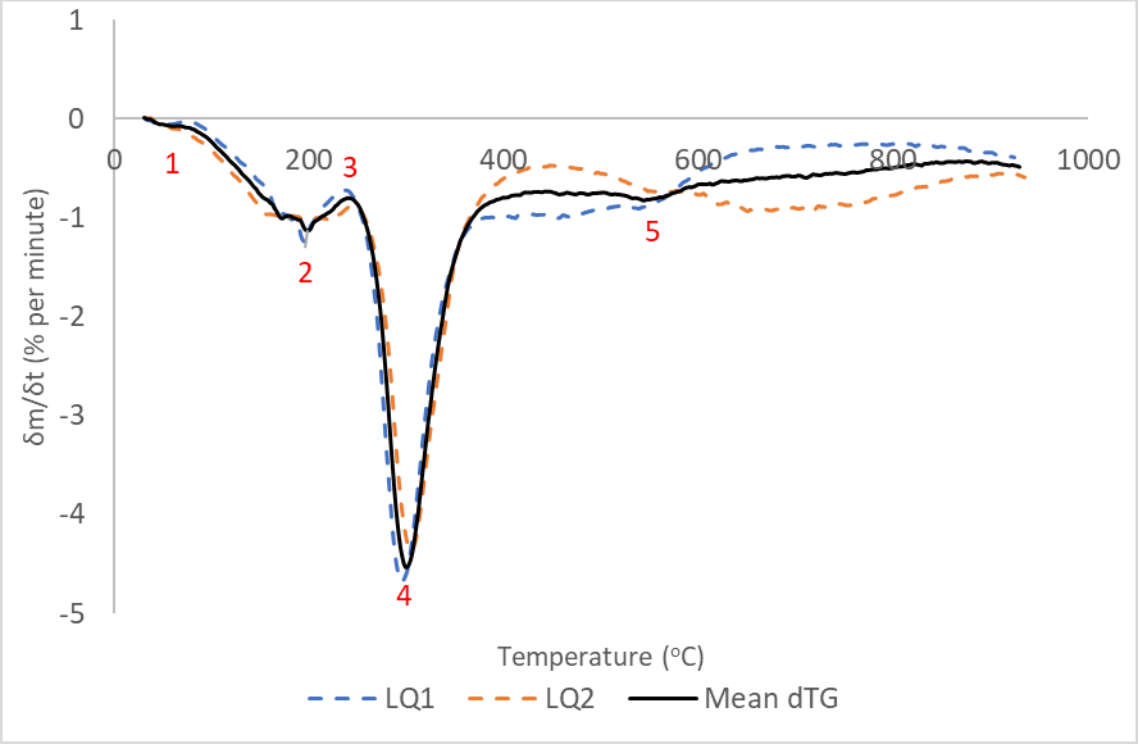

Figure 4.24. *dTG thermograms for samples LQ1-2 and mean dTG thermogram from 30-900 °C at 10 °C/min under N_2. Key features are labelled 1-5 and referred to in text using square brackets.*

The LQ sample set exhibits extremely consistent thermogravimetric behaviour at temperatures below approximately 275 °C. Mass loss exceeds 1 % at a mean temperature of 118 °C (LQ1 = 127 °C; LQ2 = 110 °C respectively) and 2.5 % at a mean temperature of 145.6 °C (LQ1 = 156 °C; LQ2 = 140 °C).

The first substantial mass loss event as observed on the dTG curve initiates at a temperature of 82 °C [1], with mass loss accelerating to a local maximum at 198 °C [2] (dm/dt = -1.1 % per minute) with this region extending upwards to 240 °C [3], incurring a mass loss of 10.4 % (1.30 mg).

Mass loss accelerates from 240°C to the primary mass loss peak located at 299 °C [4] (295 °C and 306 °C for LQ1/2) where dm/dt = -4.5 % per minute (LQ1 = -4.6 % per minute; LQ2 = -4.4 % per minute). Taking the upper boundary of this event as 390 °C, regional mass loss is 30.2 %, although substantial differences in behaviour between the two samples occurs in this region. Sample 1 undergoes a sharp transition into a region of more constant mass loss at around 375 °C with mass loss of 30.3 % occurring across 235-375 °C, while mass loss in LQ2 continues to decelerate smoothly up to 447 °C with mass loss of 30.6 % from 244-447 °C.

In LQ1, a relatively flat section of the dTG curve occurs in the 375-542 °C region, before gradually decelerating to around 700 °C. Mass loss in LQ2 increases from 447-548 °C, followed by a near flat section from 548-597 °C, before accelerating again to 673 °C before tailing off. Mean mass loss above beyond the main peak is 32.2 % with a final char fraction of 26.9 % (sample 1 = 30.9 %; sample 2 = 22.4 %).

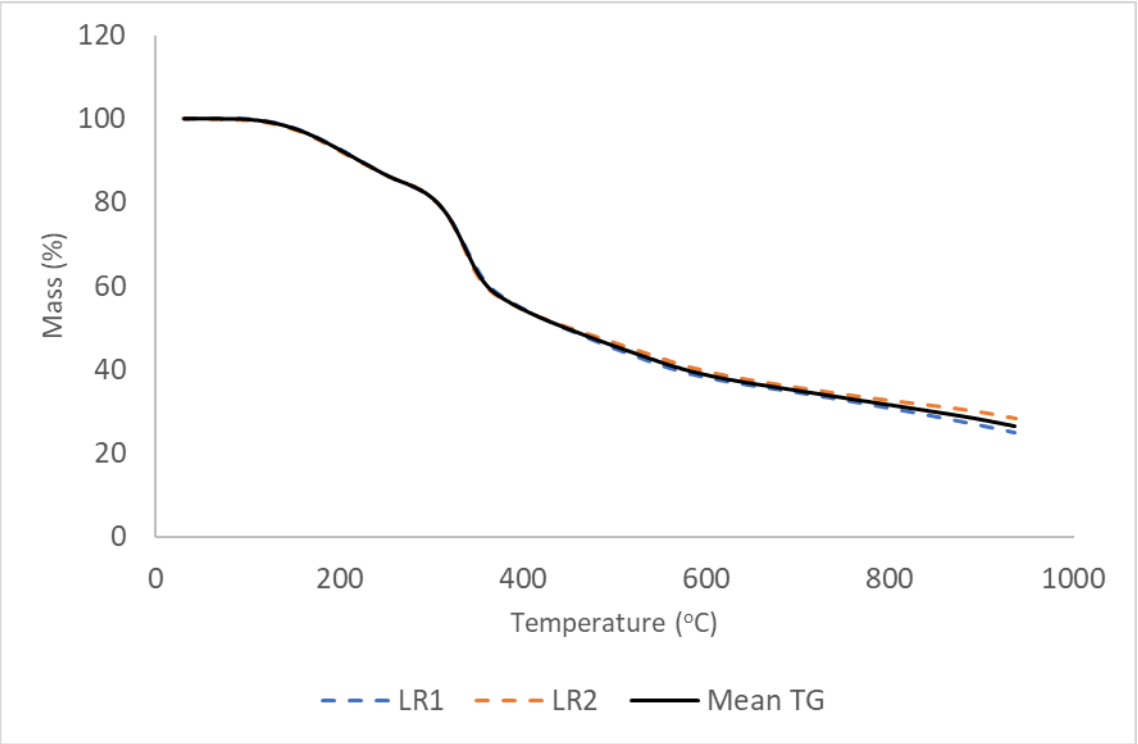

Figure 4.25. *TG thermograms for LR1-2 and mean TG thermogram from 30-900°C at 10°C/min under* N_2.

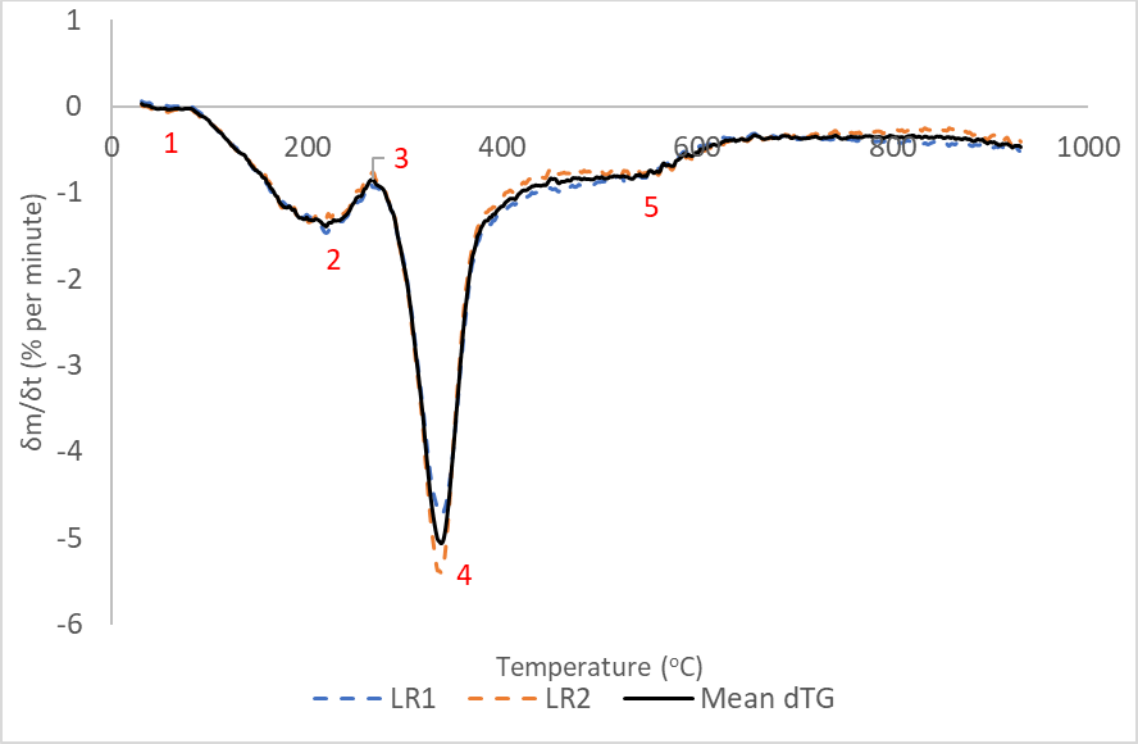

Figure 4.26. *dTG thermograms for LR1-2 and mean dTG thermogram from 30-900 °C at 10 °C/min under N_2. Key features are labelled 1-5 and referred to in text using square brackets.*

Thermogravimetric curves for the samples LR1 and LR2 (*Figures 4.21)* are highly consistent with a nearly perfect overlap throughout much of the temperature range. For a given temperature, mass loss differs by a maximum of 3.1 % with this difference occurring at the end of heating. Mean mass loss exceeds 1 % at 128 °C (LR1 = 133 °C; LR2 = 123 °C) and 2.5 % at 152 °C (LR1 = 154 °C; LR2 = 150 °C).

From the dTG curve (Figure 4.26), initiation of the first major mass loss event occurs at 80 °C [1], with mass loss accelerating into a rounded peak with a maximal mass loss rate at 220 °C [2] (dm/dt = -1.4 % per minute), then decelerating to a local minimum and transition point at 265 °C (dm/dt = -0.8 % per minute) [3], with mass loss of 14.6 % (1.83 mg).

Mass loss above the transition point accelerates to a maximum rate at 337 °C (dm/dt = -5.1 % per minute). This peak extends upwards to 389 °C, with mass loss of 29.7 % (3.72mg) occurring in this region.

The rate of mass loss slows from 389-444 °C, before stabilising at a relatively constant rate of 0.8 % per minute up to 533 °C, subsequently decelerating again and stabilising at 0.4 % per

minute above 627 °C. Final retained mass (mean) is 26.6 % (3.33mg) (sample 1 = 25.0 %, sample 2 = 28.1 %).

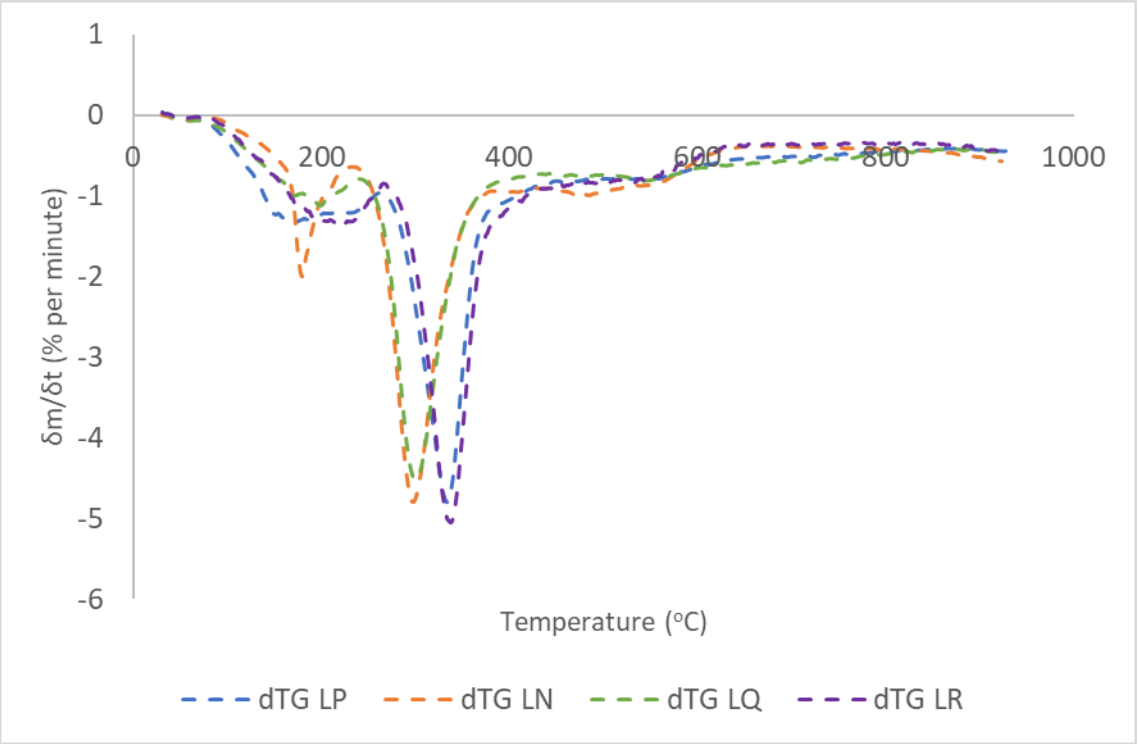

Figure 4.27. *Comparison of mean dTG curves for LP, LN, LQ and LR sample sets from 30-900 °C at 10 °C/min under* N_2

When all four sample sets based on HT-2006 are compared, it is noted that the LP and LR sample sets containing TCPP undergo their maximal rate of mass loss at substantially higher temperatures than those sample sets from which this is absent. The temperature at peak mass loss for these sample sets is 335 °C for LP and 337 °C for LR, compared against 298 °C for LN and 299 °C for LQ. For foams containing TCPP, this temperature is highly consistent regardless of whether the PS-2602 or HT-2006 polyol is used, falling within a range of 335-337 °C for the BP, BR, LP and LR sample sets. This is also the case for the sample sets containing neither fire retardants (BN and LN), where the maximum rate of mass loss occurs at 294 °C in the BN sample set and 298 °C in the LN sample set. However, in polyols based on PS-2602, the addition of TEP appears to substantially increase the temperature at the main mass loss peak, to 307 °C in the BQ sample set. This increase is not observed in foams based on HT-2006, with almost identical peak temperatures for the LN and LQ sample sets.

Furthermore, it was found that all sample sets containing HT-2006 exhibit greater mass loss during the first stage of mass loss than their corresponding PS-2602 based formulation.

Additionally, while the BQ sample set exhibits no distinct first peak, such a peak is observed in the LQ sample set, indicating a possible reduced effectiveness of TEP in improving low-temperature stability when used with this polyol.

4.6. Alternative Flame-retardant Agents in Block Mould Foams

Several halogen-free flame retardants have also been here analysed as potential alternatives to the current fire-retardant system, replacing either TEP or TCPP within the formulation. For block-mould foams, the trial substances are ammonium polyphosphate, macrocrystalline graphite, expandable graphite, and a proprietary phosphorus-rich reactive flame retardant, VeriQuel R100.

4.6.1. Ammonium Polyphosphate

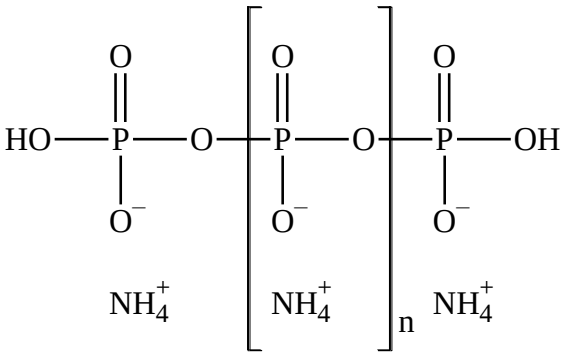

Ammonium polyphosphate is an inorganic salt of polyphosphoric acid and ammonia. Ammonium polyphosphate is used a flame retardant in various polymeric materials and is thought to exert its effects in the solid phase through intumescence. Upon heating to temperatures above 250 °C, the polyphosphate undergoes thermal decomposition to polyphosphoric acid, accompanied by the release of ammonia.

$$(NH_4PO_3)_n \rightarrow (HPO_3)_n + (NH_3)_n$$

The polyphosphoric acid formed by this process is able to react with free hydroxyl groups in the polymer, dehydrating these groups and enhancing the formation of char.

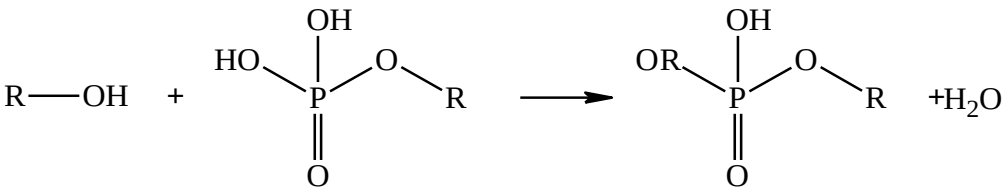

This reaction forms an unstable phosphate ester, the decomposition of which enhances the formation of char. The production of large quantities of gaseous ammonia increases decreases the density of this char through a blowing process, creating a surface layer that acts as an effective barrier to heat and oxygen, protecting the underlying material, while also reducing the flow of volatiles resulting from pyrolytic breakdown into the diffusion flame.

To determine the influence of ammonium polyphosphate on the thermal behaviour of PIR foam systems, three samples of PIR foam based on the PS-2602 polyol and containing ammonium polyphosphate and TEP (hereafter labelled AP1-3) were subjected to thermogravimetric analysis using the standard temperature program. These have then been compared against the BP and BQ sample sets. Thermogravimetric data from these analyses are shown in Figures 4.24 and 4.25 below.

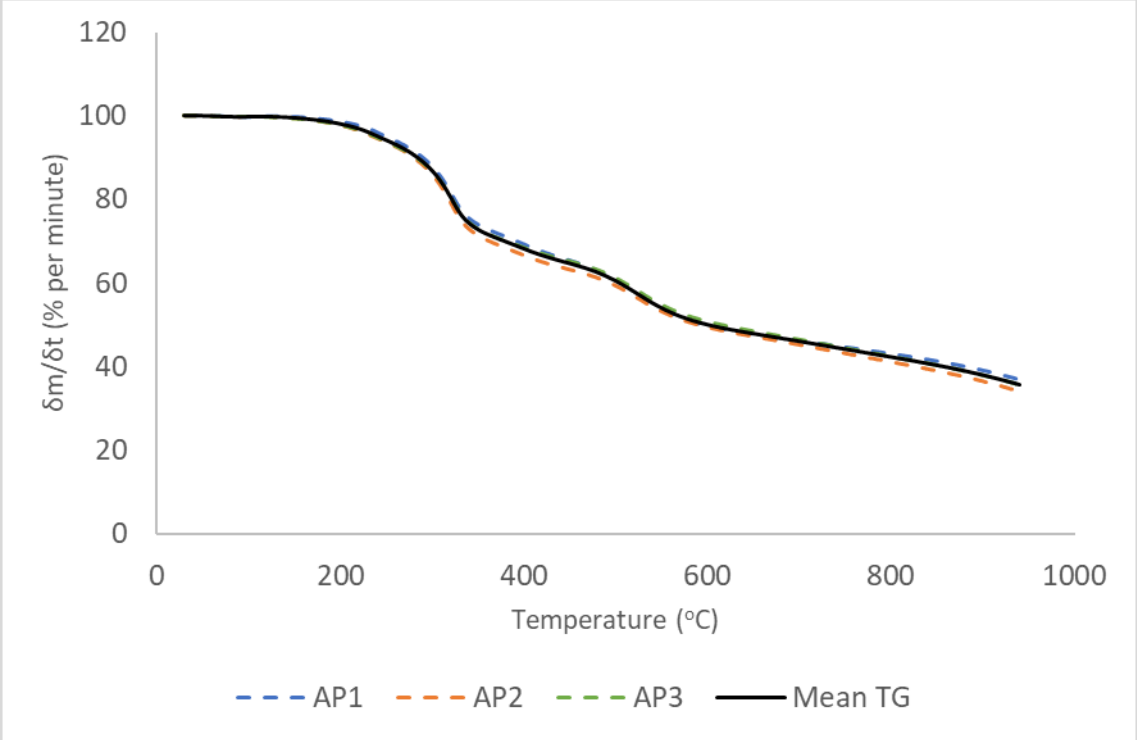

Figure 4.28. *TG thermograms for AP1-3 and mean TG thermogram from 30-900°C at 10°C/min under N_2.*

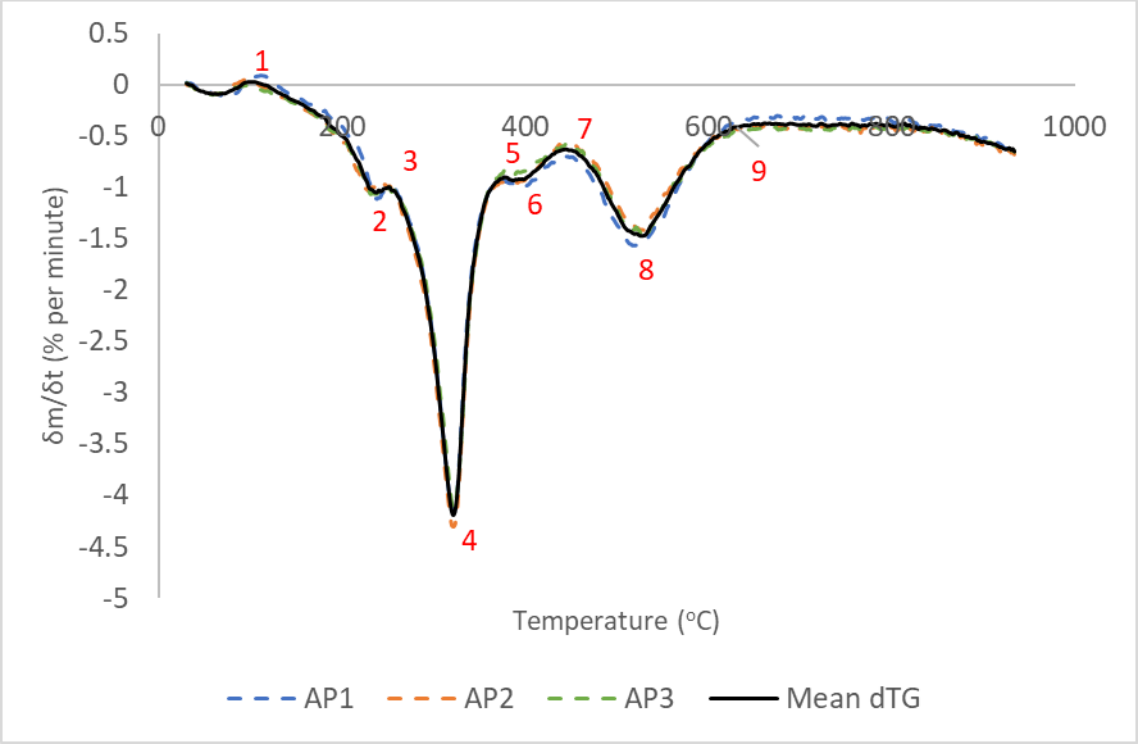

Figure 4.29. *dTG thermograms for AP1-3 and mean dTG thermogram from 30-900°C at 10°C/min under N_2. Key features are labelled 1-9 and referred to in text using square brackets.*

The observed behaviour is consistent across samples AP1-3, with TG curves (Figure 4.28) exhibiting a distinctive 'two-stepped' shape that differs from previous sample sets. Inspection of the dTG curves (Figure 4.29) shows that a minor mass loss event occurs in the temperature range from 30-98 °C [1], with a maximum rate of 0.1 % per minute at 64 °C. This phase accounts for total mass loss of 0.3 % (0.04 mg), similar to mass losses in this region for previously analysed sample sets. This is attributed to the desorption of moisture and other adsorbed volatiles.

This initial region is followed by an acceleration of mass loss, with increasing second derivative, reaching a local maximum with $\frac{dm}{dt}$ = -1.1 % per minute at 237 °C [2]. The endpoint of this phase occurs at 251 °C [3], $\frac{dm}{dt}$ = -1.0 % per minute. A mass loss of 5.6 % (0.66 mg) occurs from 98-251 °C.

Then mass loss accelerates to an absolute maximum at 322 °C [4], where $\frac{dm}{dt}$ = -4.2 % per minute. Deceleration follows across to the endpoint of the main mass loss event at 381 °C [5], with $\frac{dm}{dt}$ = -0.90% per minute, incurring a total mass loss across 251-381 °C of 24.3 % (2.87 mg). This is immediately followed by an additional small peak at 388 °C ($\frac{dm}{dt}$ = -0.9 %

per minute) [6], with mass loss then continuing to decelerate ($\frac{dm}{dt}$ = -0.6% per minute at 446 °C) [7]. This accounts for an additional mass loss of 5.0 % (0.59 mg).

All three samples exhibit a broad peak of moderately high amplitude in the region immediately following the main peak, with a mean local maximum at 528 °C [8], with $\frac{dm}{dt}$ = -1.5 % per minute. This event extends upwards to around 645 °C [9] ($\frac{dm}{dt}$ = -0.4 % per minute). Above this temperature, mass loss remains relatively low and constant, with a slight acceleration above 800 °C. Mass loss in the secondary peak, taken over 446-645 °C is 16.8 % (1.99 mg).

At the end of heating, the mean retained char fraction is 35.6 % (4.20 mg), with respective values of 36.9 % (4.50 mg), 34.3 % (3.81 mg), and 35.5 % (4.30 mg).

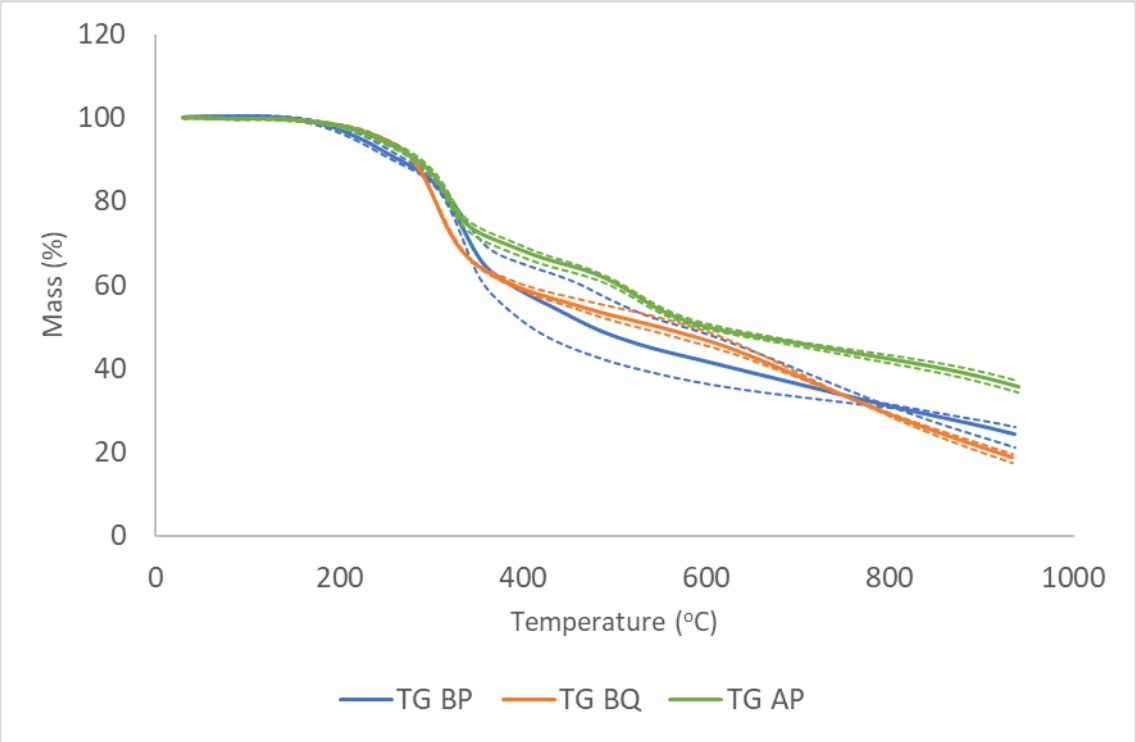

Figure 4.30. *Comparison of TG thermograms for BP, BQ and AP sample sets over 30-900 °C at 10 °C/min under N_2. Dotted lines around thermograms indicate range within sample set.*

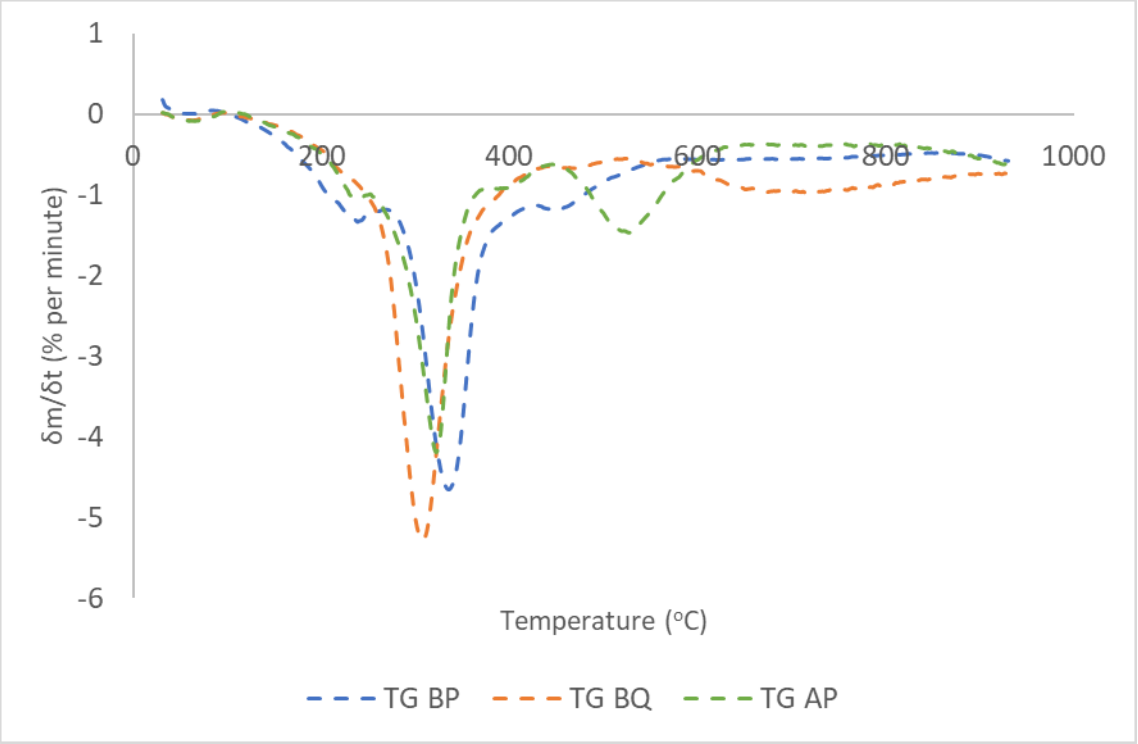

Figure 4.31. *Comparison of dTG thermograms for BP, BQ and AP sample sets over 30-900 °C at 10 °C/min under* N_2

TG and dTG data for the AP sample set are directly compared in Figures 4.30 and 4.31 alongside the BP and BQ sample sets. By visual inspection, it is apparent the AP foams exhibit equal or greater retained mass at all temperatures above 350°C than either of the other samples sets, with the lower end of the range within the sample set exceeding the upper end of the range for those sets.

Using the 1 % and 2.5 % thresholds for comparing the early stages of mass loss, these occur at 171 °C and 211 °C, respectively for the AP sample set versus 169 °C and 195 °C for the BP sample set and 174 °C and 216 °C for the BQ sample set. At the end of heating, a large increase in retained AP char is observed, with a final residual mass of 35.6 % (range 34.2-36.9 %), which is 11.4 % greater than the BP samples and 16.9 % greater than the BQ samples, supporting a mechanism in which ammonium polyphosphate promotes the formation of a thermally resilient char. This potentially implies that foams produced using this method would contribute less to fuel loading under fire conditions where the foams is exposed to intense indirect heat within a panel.

Inspection of the comparative dTG curves in Figure 4.31 exhibits reduced mass loss in the low temperature region compared for AP foams compared to BP foams, with a smaller mass loss

peak in the 200-270 °C temperature region, although in contrast to the BQ foams this peak is not entirely absent. The largest mass loss peak occurs at a temperature of 322 °C, intermediate to the BQ set (307 °C) and the BP set (335 °C). However, among these three peaks, the rate of mass loss for is lowest for the AP set ($\frac{dm}{dt}$ = -4.2 % per minute) with a smaller total area of the peak. The third peak centred at 528 °C is a substantial and distinctive feature of the AP sample set, implying the formation of a stabilised residue at an earlier stage of heating that undergoes decomposition in this temperature range.

Taken as whole these results suggest that ammonium polyphosphate results in greater overall thermal stability than TCPP but has a less potent effect on the temperature at which the highest rate of mass loss occurs. However, the lower rate of mass loss at this peak may reduce the ability of the foam to undergo sustained flaming combustion.

4.6.2. Expandable Graphite

Expandable graphite is a layered material produced by treating graphite with a strong oxidising agent, such as hydrogen peroxide H_2O_2, potassium permanganate $KMnO_4$, or potassium dichromate $K_2Cr_2O_7$. This has the effect of oxidising the edges of the graphite monolayers, and allowing the penetration of an intercalating agent, typically concentrated sulphuric acid H_2SO_4.

Heating, especially rapid heating, of the material, causes the expansion of the intercalating agent, with the production of a large volume of gas. This expansion forces the graphitic layers apart, leading to an increase in volume. In the context of a flame retardant activity, expandable graphite acts through an intumescent mode of action, facilitating the production of a low-density char carbonaceous char layer, forming a physical barrier to heat, fuel, and oxygen transport to and from the underlying material.

Two formulations of block-mould foam containing expandable graphite in combination with TEP were subjected to thermogravimetric analysis. The first set (hereafter referred to as the EG set consisting of samples EG1, EG2 and EG3) was based on the PS-2602 polyol, while the second set (hereafter referred to as the EH sample set, consisting of samples EH1, EH2 and EH3) was based on the HT-2006 polyol.

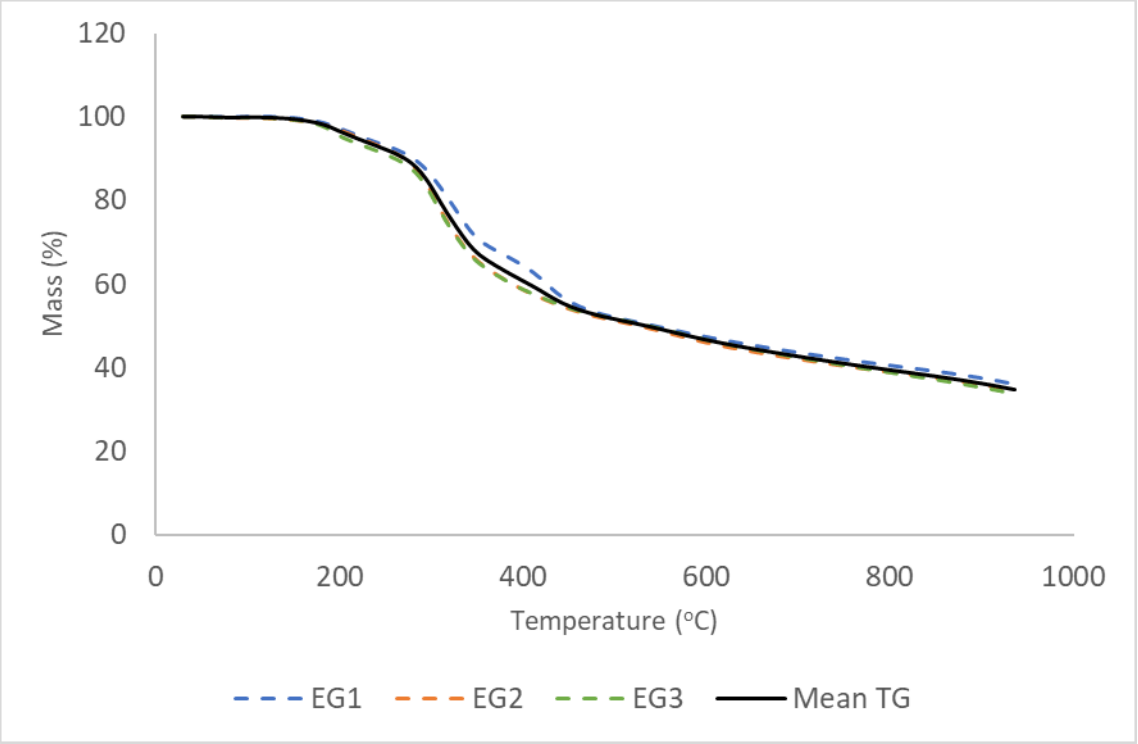

Figure 4.32. *TG thermograms for EG1-3 and mean TG thermogram from 30-900°C at 10°C/min under N_2.*

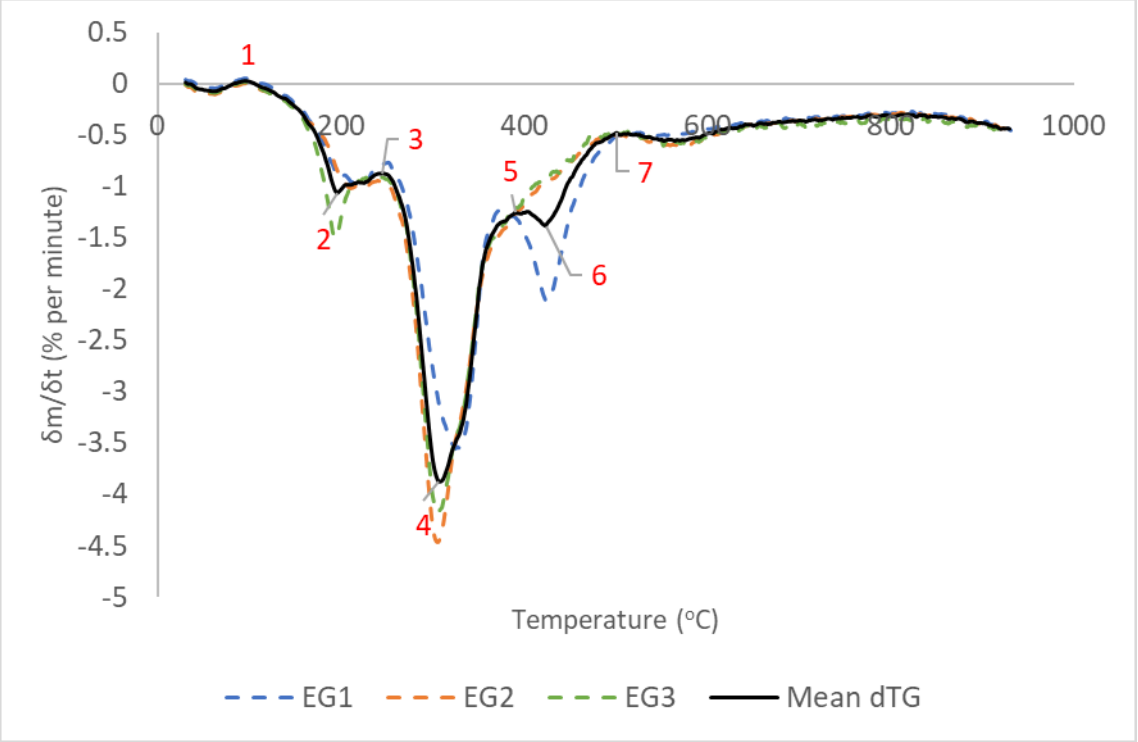

Figure 4.33. *dTG thermograms for EG1-3 and mean dTG thermogram from 30-900°C at 10°C/min under N_2. Key features are labelled 1-7 and referred to in text using square brackets.*

All three EG samples exhibit near identical behaviour at temperatures from 30-175 °C, with more divergent behaviour from 175-425 °C, in which region EG1 exhibits higher retained mass than the remaining samples. The initial desorption events reached its peak rate (dm/dt = -0.1 % per minute) at 62.0 °C, then decelerating to a local minimum at 94 °C. Mass loss exceeding 1 % is recorded at a mean temperature of 158 °C (range 158-162 °C) and exceeding 2.5 % at a mean temperature of 188 °C (range 184-193 °C).

Examination of the dTG curves after the initial desorption phase shows an acceleration of mass loss, with a negative second-order derivative, reaching a peak local mass loss with dm/dt = -1.1 % per minute at 197 °C. However, the position of this peak is influenced by unusual behaviour in sample 3, which exhibits a sharp peak (dm/dt = -1.5 % per minute) at 195 °C. By contrast, the first peak appears at 223 °C in sample 1 and at 211 °C in sample 2, with dm/dt = -1.1 % per minute and dm/dt = -1.0 % per minute respectively, with these peaks being more rounded in their form. This variance results in the jagged shape of the peak in the mean dTG thermogram. For the mean curve, mass loss decelerates to the endpoint of the peak at 249.5°C, with a total mass loss within the phase of 7.9 % (0.84 mg).

From the mean dTG curve, the maximum rate of mass loss occurs at 304.1 °C, with $\frac{dm}{dt}$ = -4.1 % per minute. For samples 1, 2, and 3, $T_{\Delta max}$ is recorded as 312.8 °C, 305.0 °C, and 306.6 °C respectively with dm/dt = -3.72, -4.46, and -4.18 % per minute. From the mean dTG curve, the main mass loss event appears to end at 364.4 °C, giving a total mass loss in the 249.5-364.4 °C interval of 28.0 % (2.95mg). This is then immediately followed by a third mass loss event. Examination of individual samples, however, shows no distinct mass loss event in samples 2 and 3. In both cases, mass loss decelerates continuously from the main peak, tailing off towards a minimum at 503.1 °C in samples 2 and 500.6 °C in sample 3. In contrast, in sample 1, the main peak is followed by a region of rapid fluctuations in the dTG curve, corresponding to a series of smaller fluctuations in the TG curve. The general shape of the TG curve suggests a third distinct mass loss event occurring in an approximate temperature interval of 350-500 °C, with a maximum recorded mass loss rate at 420.6 °C (dm/dt = -1.92 % per minute). Total mass loss in this range is 18.2 % (1.91 mg).

Retained mass loss at the end of mass loss has a mean value of 33.1 % (range = 31.2-34.3 %).

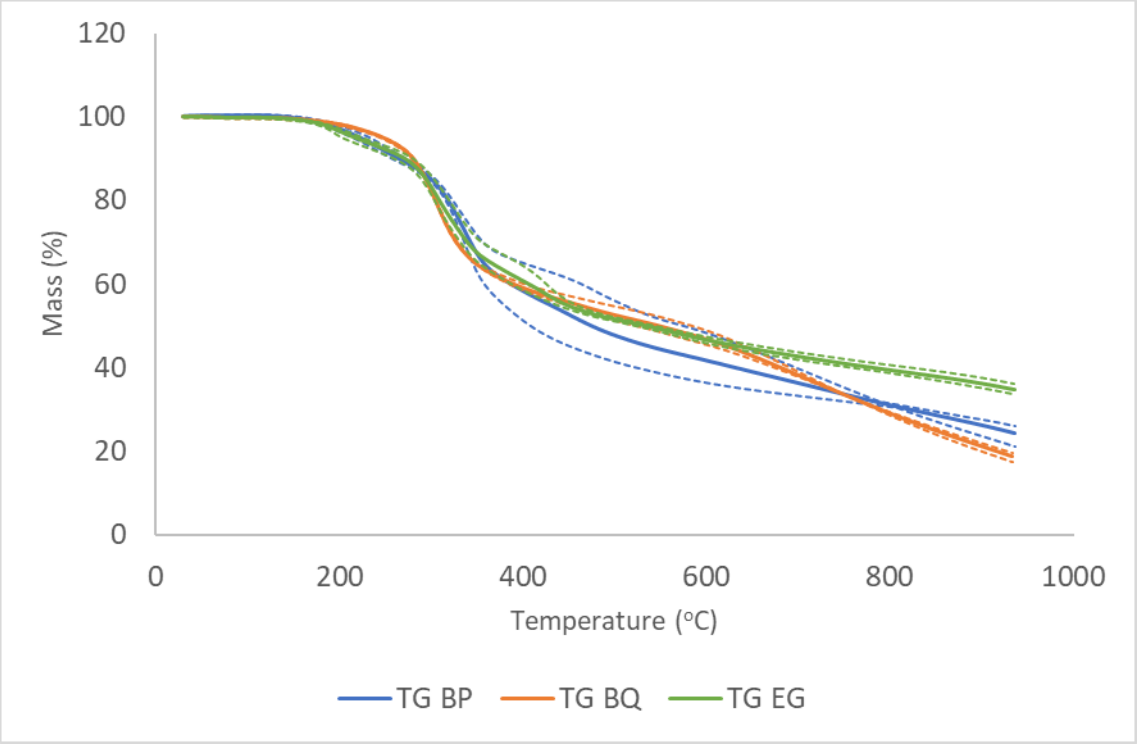

***Figure 4.34**. Comparison of mean TG thermograms for BP, BQ and EG sample sets over 30-900 °C at 10 °C/min under N_2. Dotted lines around thermograms indicate upper and lower bounds of range within sample set.*

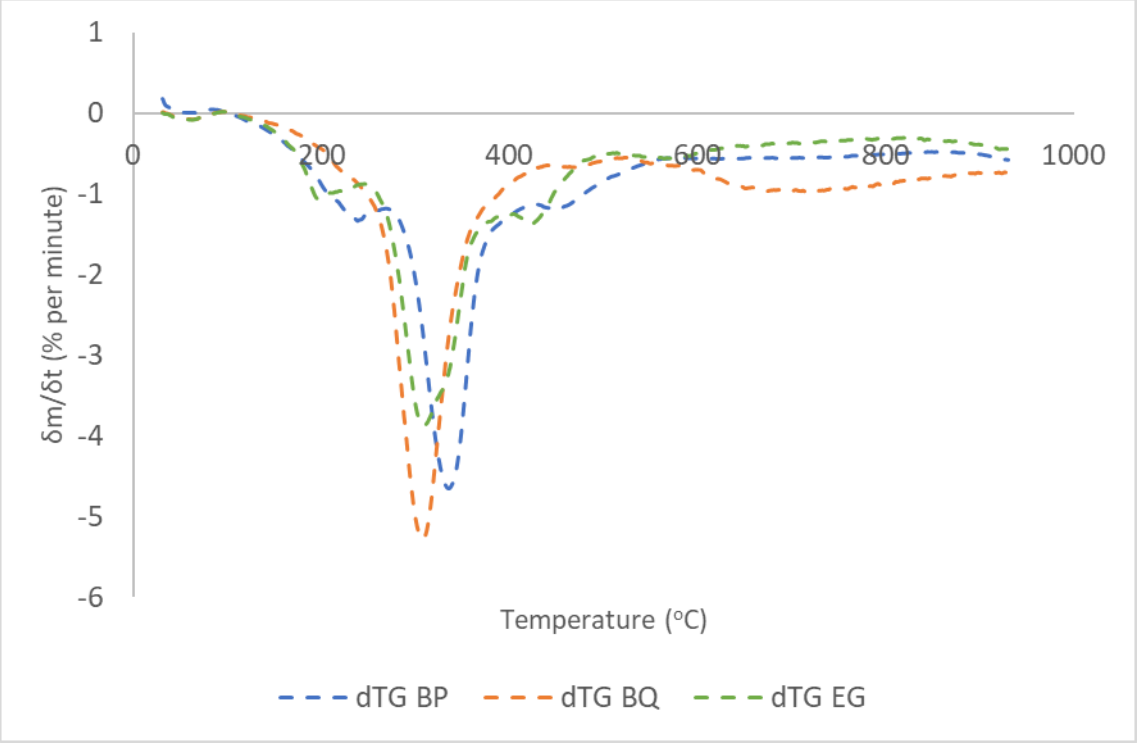

***Figure 4.35.** Comparison of dTG thermograms for BP, BQ and EG sample sets over 30-900 °C at 10 °C/min under N_2.*

In comparison to PS2602 foams containing TEP-TCPP, the expandable graphite foams exhibit similar stability at furnace temperatures from 30-250 ^{o}C, with the measured masses differing by less than 1 % across this temperature range. Above 258 ^{o}C, the formulation containing TCPP undergoes a period of greater relative stability, reaching a maximum difference of 4.9 % at 315 ^{o}C, with this relationship reversing above 448 ^{o}C, and continuously increasing to the endpoint of heating, where the final average retained char fraction in expandable graphite foams is 10.1 % greater than TCPP foams. Statistically significant differences are observed between 310-335 ^{o}C, with greater stability in TCPP foams, and above 725 ^{o}C, with greater stability in expandable graphite foams.

Differences in retained mass are generally smaller when comparing expandable graphite foams to those containing only TEP, nowhere exceeding 5 %. Retained was within ±1 % from 30-185 ^{o}C, with TEP foams initially exhibiting generally higher stability, reaching a maximum of 2.9 % at 230 ^{o}C. The stability of expandable graphite foams is greater by more than 1 % at temperatures above 295 ^{o}C, with a maximum difference of 4.9 % at 530 ^{o}C, stabilising to 4.0 % at the end of heating. These differences are found to be significant in favour of TEP foams from 190-270 ^{o}C (sample temperature) and in favour of expandable graphite-TEP from 390-815 ^{o}C.

Comparison of dTG curves shows clear difference in overall curve forms and identifies maximum mass loss rates occurring at 334.7 ^{o}C, 306.5 ^{o}C, and 304.1 ^{o}C for foams containing TEP-TCPP, TEP and expandable graphite-TEP respectively. This indicates that expandable graphite does not increase the maximal breakdown point compared to TEP alone. However, maximum negative values of dm/dt are found to be -3.9 % per minute, -5.2 % per minute, and -4.1 % per minute, demonstrating an improved mass stability for foams containing expandable graphite. Since mass loss reflects the release of breakdown products into the vapour phase. This may reduce the rate of heat release by slowing the release of flammable gaseous species into the diffusion flame front.

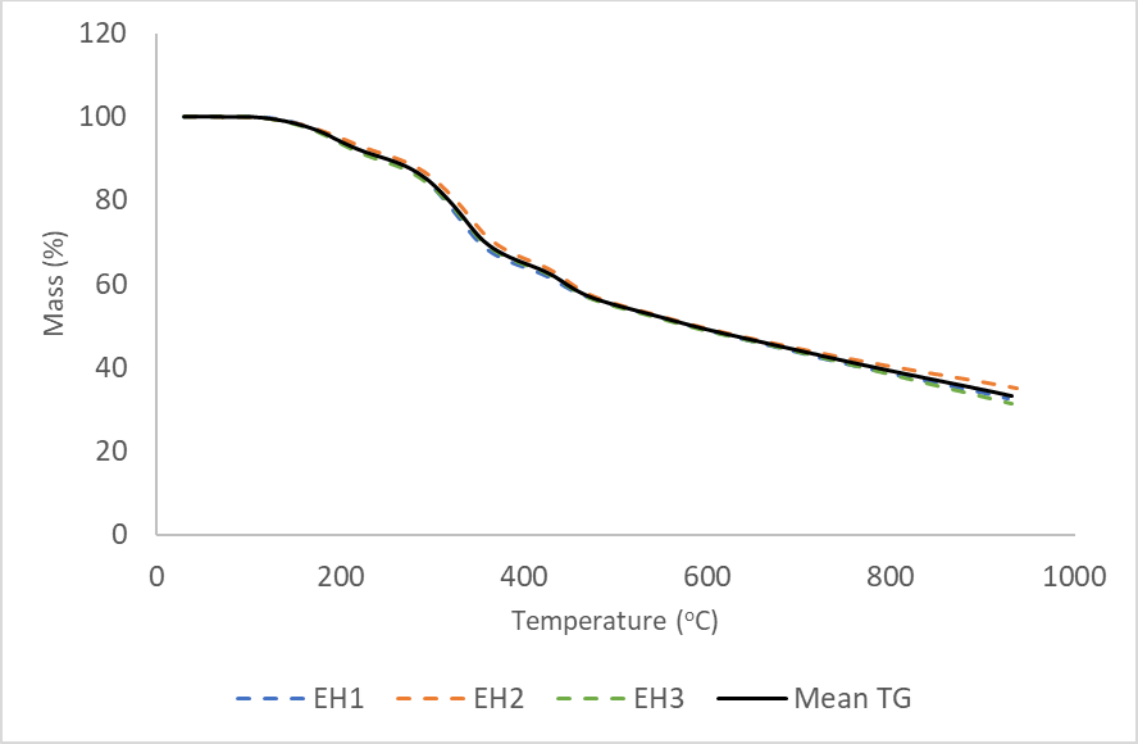

Figure 4.36. *TG thermograms from samples EH1 and mean TG thermogram from 30-900°C at 10°C/min under N_2.*

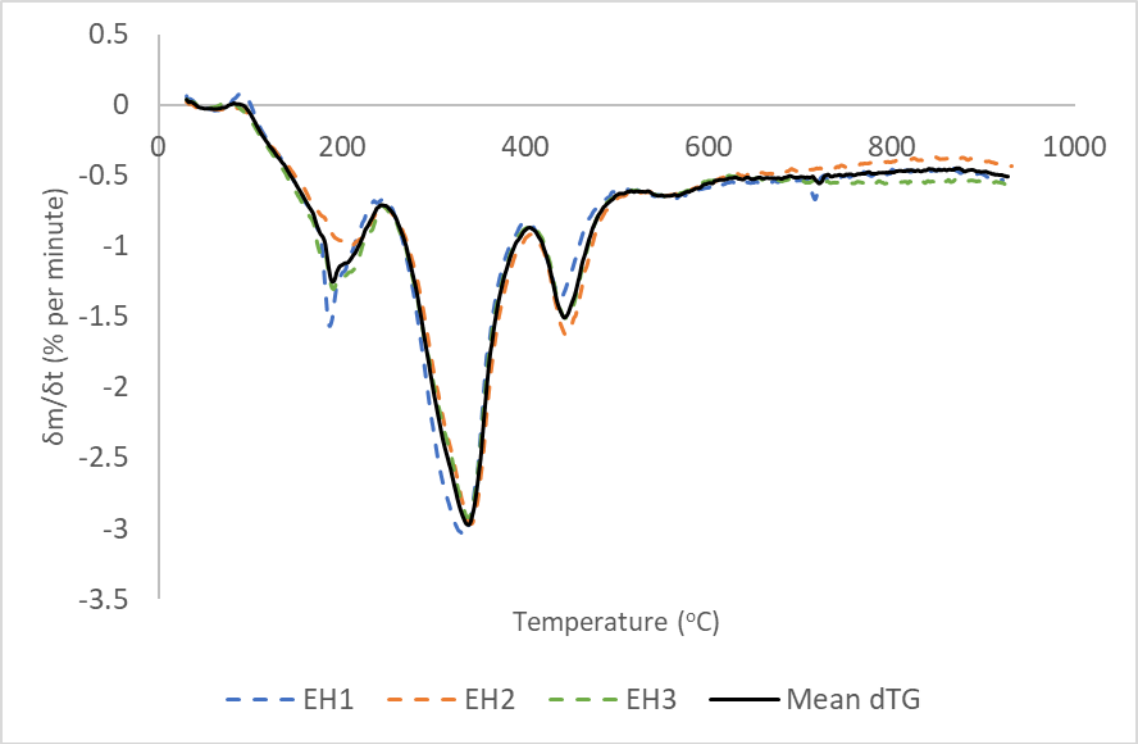

Figure 4.37. *dTG thermograms for samples EH1-3 and mean dTG thermogram from 30-900°C at 10°C/min under N_2.*

The EH sample set exhibits very consistent behaviour across all three samples. Following the initial desorption event from 30-82 °C, where a negligible mass loss of less than 0.1 % is observed. Mass loss exceeds 1 % at a mean temperature of 139 °C and exceeds 2.5 % at 166 °C. There is a relatively rapid acceleration of mass loss to a sharp peak at 191 °C (dm/dt = -1.25 % per minute). For individual samples the position of this peak is respectively 186 °C, 211 °C and 191 °C, with dm/dt = -1.0-1.6 % per minute. A total mass loss of 9.6 % is recorded from 82-243 °C, where dm/dt reaches a local minimum, dm/dt = -0.7 % per minute.

An acceleration of mass loss occurs from 243-339 °C where dm/dt = -3.0 % per minute, then decelerating to dm/dt = -0.9 % per minute from 339-404 °C. Mass loss from 243-404 °C is 25.8 %. The position of the peak ranges from 335-342 °C with dm/dt = -2.9-3.0 % per minute.

In all three samples, a prominent third peak is observed immediately after the main peak, with an acceleration across 404-442 °C to dm/dt = -1.5 % per minute, then decelerating to dm/dt = -0.6 % per minute at 502.8 °C. This temperature interval accounts for a mass loss of 9.9 %.

Residual char fraction at the end of heating averages 33.2 % with a range of 31.5-35.1 %.

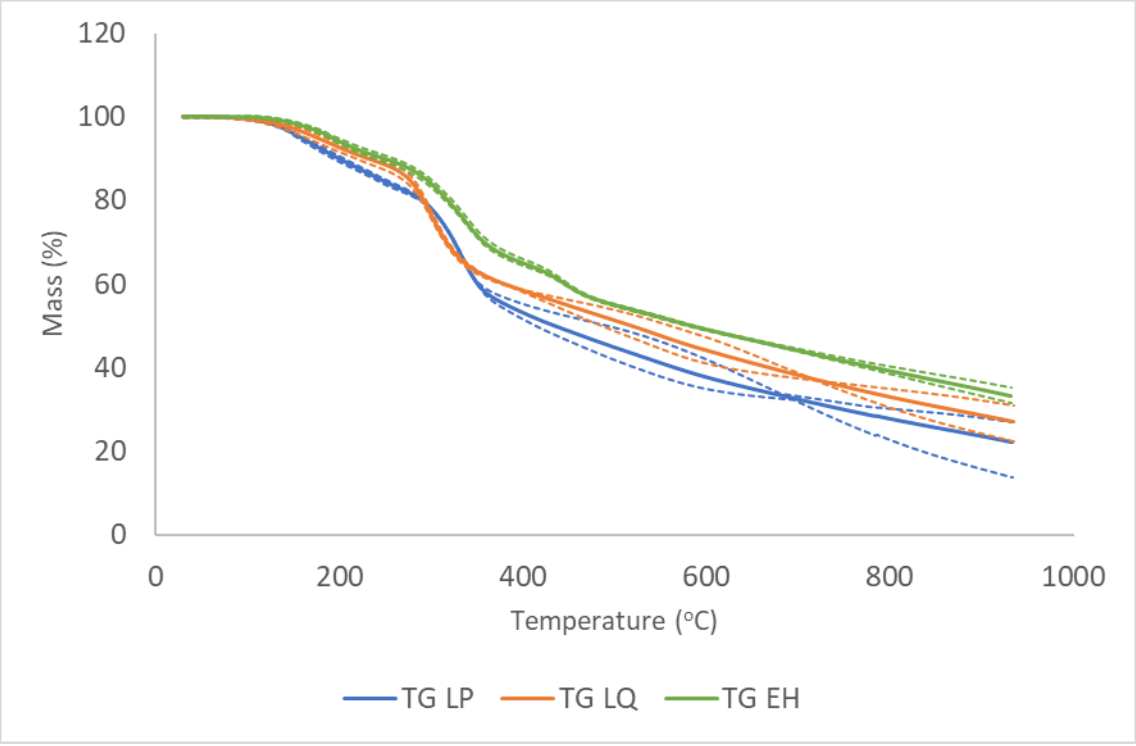

Figure 4.38. *Comparison of mean TG thermograms for LP, LQ and EH sample sets. Dotted lines around thermograms indicate upper and lower boundaries of range within sample set.*

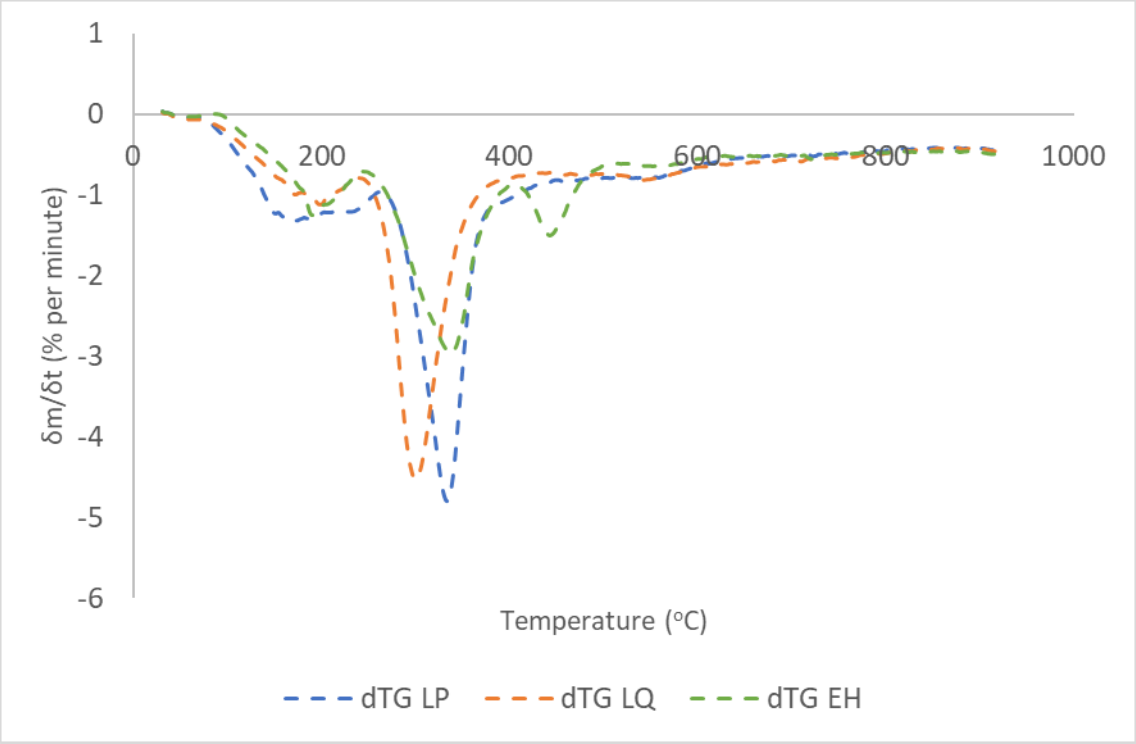

Figure 4.39. *Comparison of mean dTG thermograms for LP, LQ and EH sample sets.*

HT2006 foams containing expandable graphite and TEP exhibit consistently greater stability than foams containing either TEP and TCPP or TEP alone.

At all furnace temperatures above 123 °C, retained mass in expandable graphite foams is >1 % higher than for TEP-TCPP foams, with this difference generally increasing with temperature to a maximum of 12.2 % at a furnace temperature of 401 °C, with a final difference of 11.0 % at the end of heating. These differences were calculated to be significant at all temperatures in an approximate range from 105-830 °C.

In direct comparison to foams containing TEP only, expandable graphite foams also exhibit greater mass stability across the entire temperature range, exceeding 1 % at all temperatures above 136 °C, following a generally increasing trend to a maximum of 11.2 % at 316 °C, with a significant reduction in this difference, reaching 6.2 % at the end of heating.

Mean dTG curves exhibit clear differences in overall curve forms, with a substantially larger first mass loss event occurring in foams containing TEP and TCPP than in the other two samples sets. A distinct third mass loss peak is only observed in foams containing expandable graphite. The main mass loss peak is located at a significantly lower temperature in foams containing TEP only (299 °C) than either those containing TEP and TCPP (333 °C) or those containing TEP and expandable graphite (339 °C). This is a reversal of the behaviour seen in

PS2602 foams, where the presence of expandable graphite does not have a large positive effect on peak breakdown temperature compared to TEP alone. In addition, with peak dm/dt = -3.0 % per minute, the rate of breakdown is significantly reduced compared to TEP-TCPP or TEP alone.

The distinctive differences in the behaviour of expandable graphite in foams based on different polyols indicates a sensitivity to the physicochemical properties of the polymer matrix in the effectiveness of expandable graphite on modifying thermal stability. Expandable graphite increases the final char retention in combination with both polyol blends, with this increase being similar magnitude to that produced by ammonium polyphosphate. However, its inclusion only exerts a large impact on the critical breakdown temperature in combination with HT-2006 but not when used in combination with PS-2602.

4.6.3. VeriQuel R100

Veriquel R100 is a proprietary flame retardant described as a phosphorus rich reactive flame retardant. Reactive flame retardants differ from the previously examined additives, as they are directly integrated into the polymer structure during the polymerisation reaction. The chemical formula of VeriQuel R100 is not publicly available but, in common with other phosphorus-based flame retardants, it is likely that the primary mode of action is within the solid phase as a char-enhancing agent.

TG and dTG thermograms produced using the standard experimental method for three samples of PS2602-based foam containing VeriQuel R100 and TEP, referred to as VQ1-3, are reproduced below in Figures 4.35 and 4.36. The mean mass of the initial samples was 12.06mg.

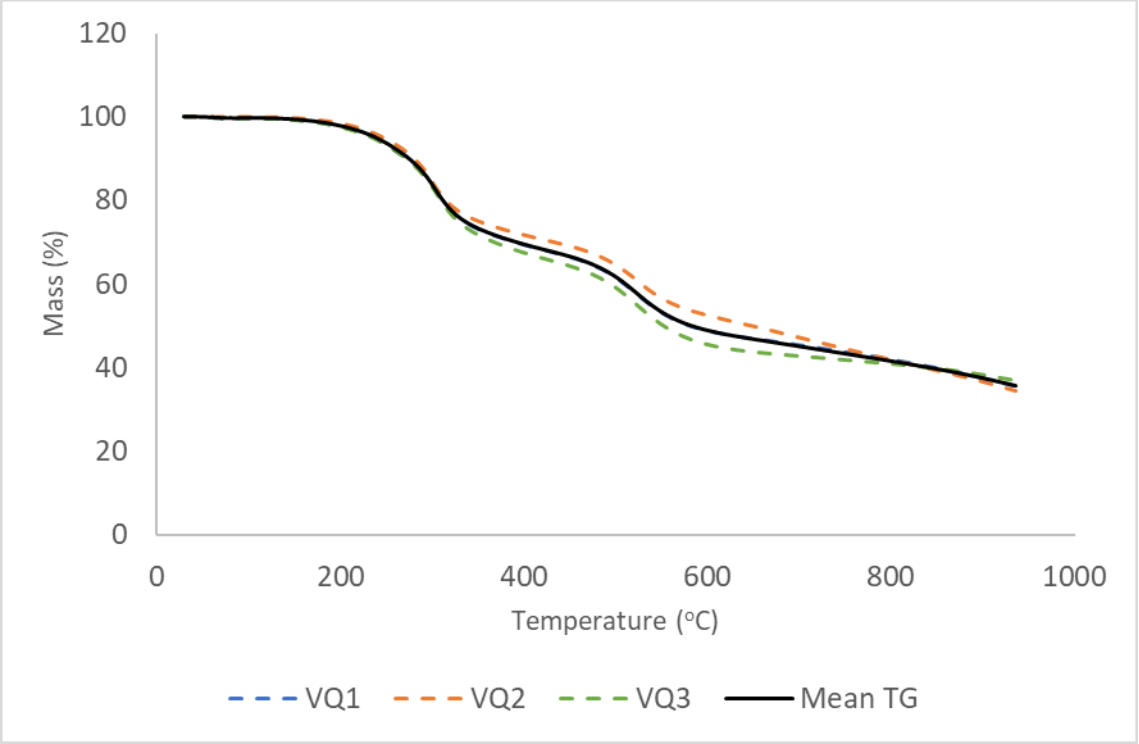

Figure 4.40. *TG thermograms for samples VQ1-3 and mean TG thermogram from 30-900 °C at 10 °C/min under N_2.*

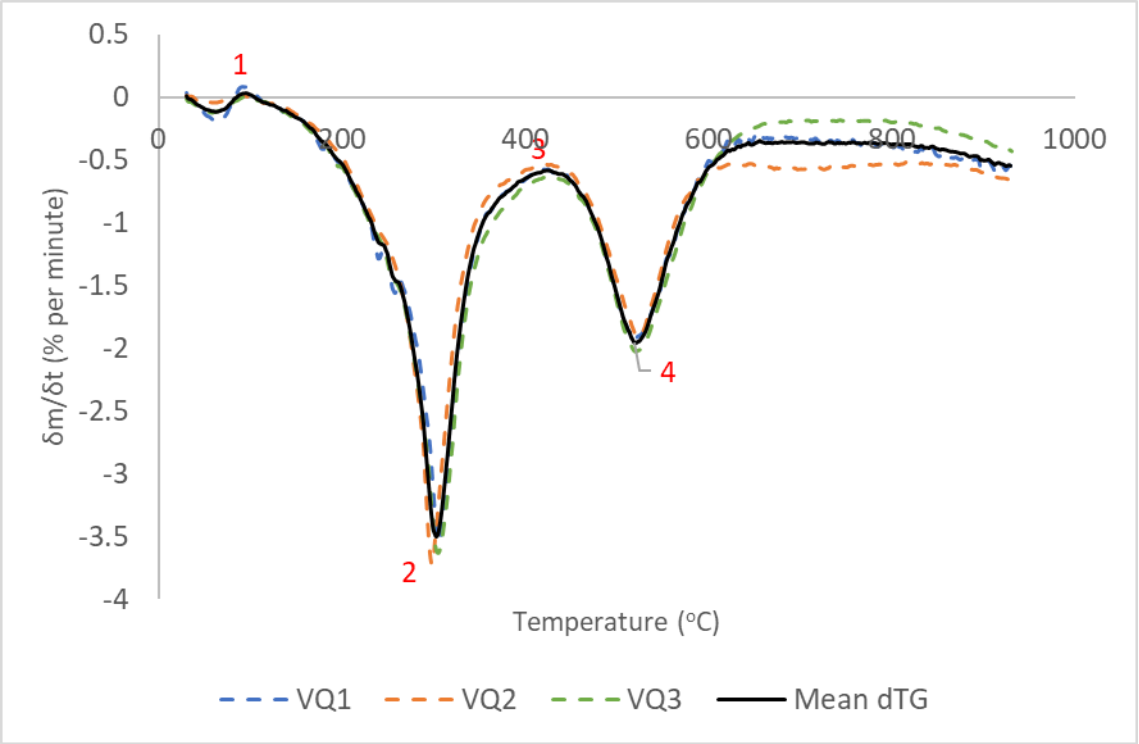

Figure 4.41. *dTG thermograms for samples VQ1-3 and mean dTG thermogram from 30-900 °C at 10 °C/min under N_2. Key features are labelled 1-3 and referred to in text using square brackets.*

Overall curve forms are broadly consistent between the members of the sample set, with a three-stepped shape to the TG curves and two large peaks on dTG. Behaviour is very similar at temperatures below up to 300 °C, with more substantial differences in retained mass developing in the middle of the temperature range. Mass loss exceeding 1 % is recorded at a mean temperature of 169.0 °C and exceeding 2.5 % at a mean temperature of 206.6 °C.

A small mass loss of 0.3 % occurs in the initial desorption phase from 30-95.4 °C, followed by an increasing acceleration of mass loss, reaching a maximum dm/dt = -3.5 % per minute at 303.3 °C. Across the sample set, the position of this peak occurs across a range from 298.1-305.5 °C (dm/dt = -3.5-3.7 % per minute). This is followed by a deceleration of mass loss, slowing toward a local minimum at 423.8 °C (dm/dt = 0.6 % per minute), with the position of this minimum being consistent across all samples. Mean mass loss across this temperature interval is 29.2 % (3.52 mg).

The second major mass loss peak occurs at 521.3 °C (dm/dt = -1.95 % per minute), with mass loss decelerating, approaching a relatively stable rate of terminal mass loss at 658.2 °C. The temperature range of this peak across the sample set is 518.8-523.3 °C (dm/dt = -1.9-2.0 % per minute). Mean mass loss across the second peak is 21.6 % (2.60 mg).

Residual char fraction at the end of heating averages 35.7 %, ranging from 34.4-36.9 %.

Three samples of PS2602-based foam containing VeriQuel R100 and TCPP in place of TEP were also subjected to thermogravimetric analysis, to compare the effect of TEP and TCPP in as a flame-retardant co-agent with VeriQuel R100. The TG and dTG thermograms obtained using the standard experimental method are reproduced below. These samples had a mean mass of 12.49 mg

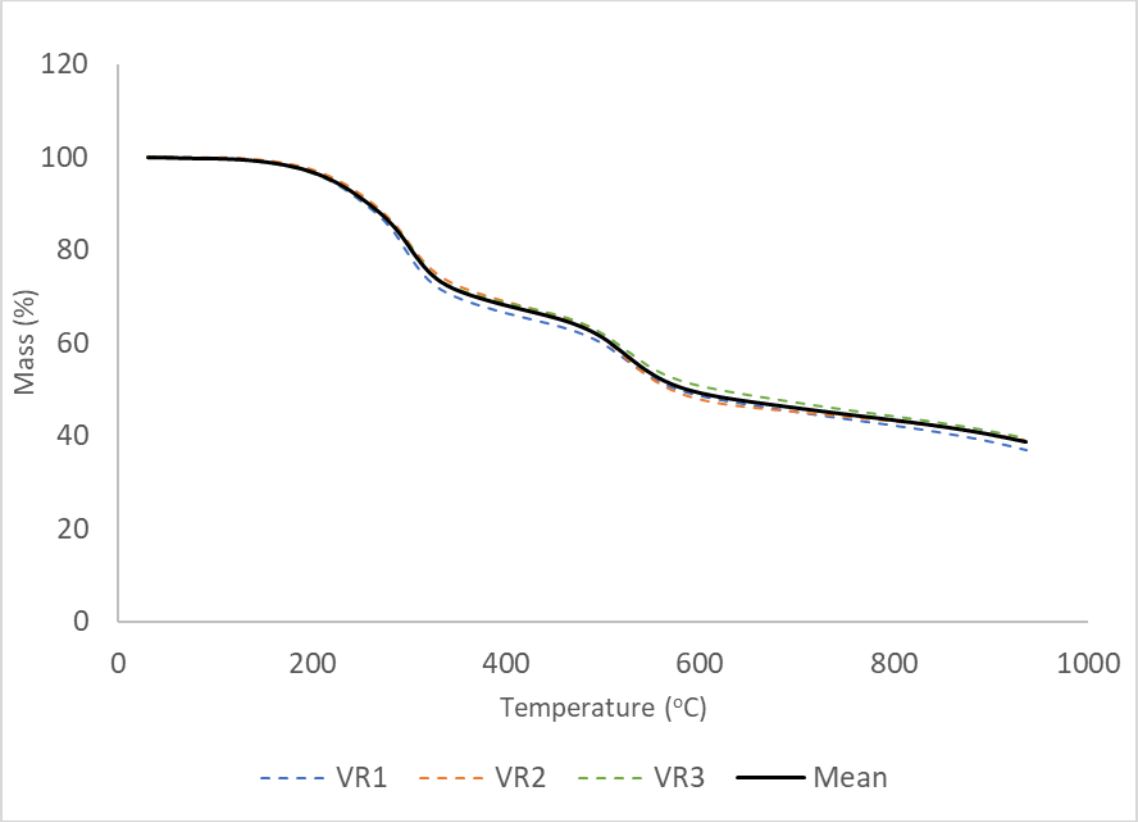

Figure 4.42. *TG thermograms for samples VR1-3 and mean TG thermogram from 30-900 °C at 10 °C/min under* N_2.

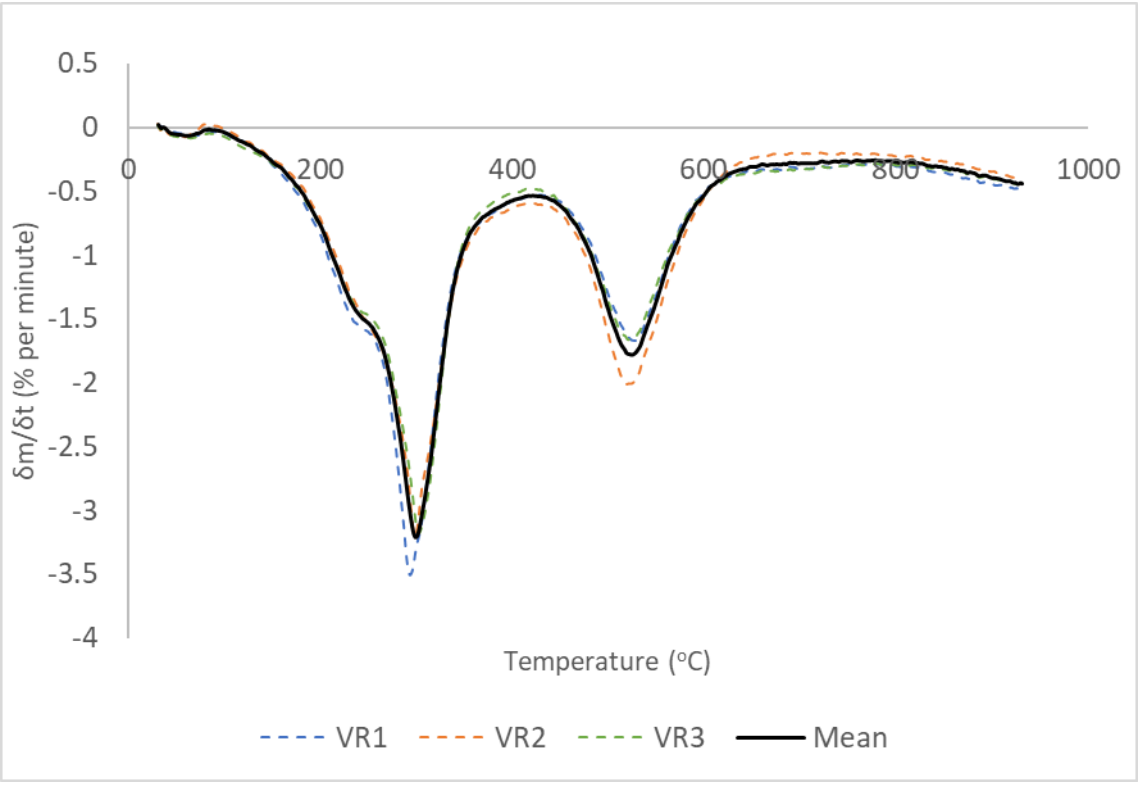

***Figure 4.43**. dTG thermograms for samples VR1-3 and mean TG thermogram from 30-900 °C at 10 °C/min under N_2.*

Curves exhibit a high degree of consistency across the samples set and are of a very similar form to those obtained for VeriQuel foams containing TEP, suggesting that the effects of VeriQuel on pyrolytic behaviour in PIR foams are dominant over the TEP and TCPP.

The initial desorption phase account for 0.2 % mass loss across 30-83.5 °C. Mass loss increases through a small shoulder around 246°C then continuing to a maximum rate of mass loss at 298.9 °C (dm/dt = -3.21 % per minute). The shoulder feature varies in intensity but appears to be consistently present across all three samples, being in a similar temperature range to the distinct first peak seen in previous formulations. This shoulder is absent in the VQ sample set, further suggesting that TCPP stimulates low temperature mass loss to an extent, and that this is conversely stabilised by TEP. The temperature at the main peak occupies a range from 293.6-302.8 °C (dm/dt = -3.2-3.5 % per minute). The deceleration of mass loss above the peak is initially rapid, tailing off towards a local minimum at 417.1 °C (dm/dt = -0.54 % per minute). Mean mass loss across this phase is 32.7 % (4.08 mg).

A large second mass loss peak occurs at a mean temperature of 524.3 °C (dm/dt = -1.8 % per minute), in a range from 519.7-526.0°C (dm/dt = -1.7-2.0% per minute), followed by a deceleration, decreasing in rate, towards 661.3 °C, with mass loss stabilising. Mass loss in the second phase is 20.2 % (2.52 mg).

At the end of heating, retained mass as char is 38.6 % (4.82 mg) on average (range is 36.9-39.5 %).

Direct comparisons of the BP, BQ, BR, VQ and VR sample sets have also been carried out, and these comparisons are shown in the Figures 4.39-4.42 below.

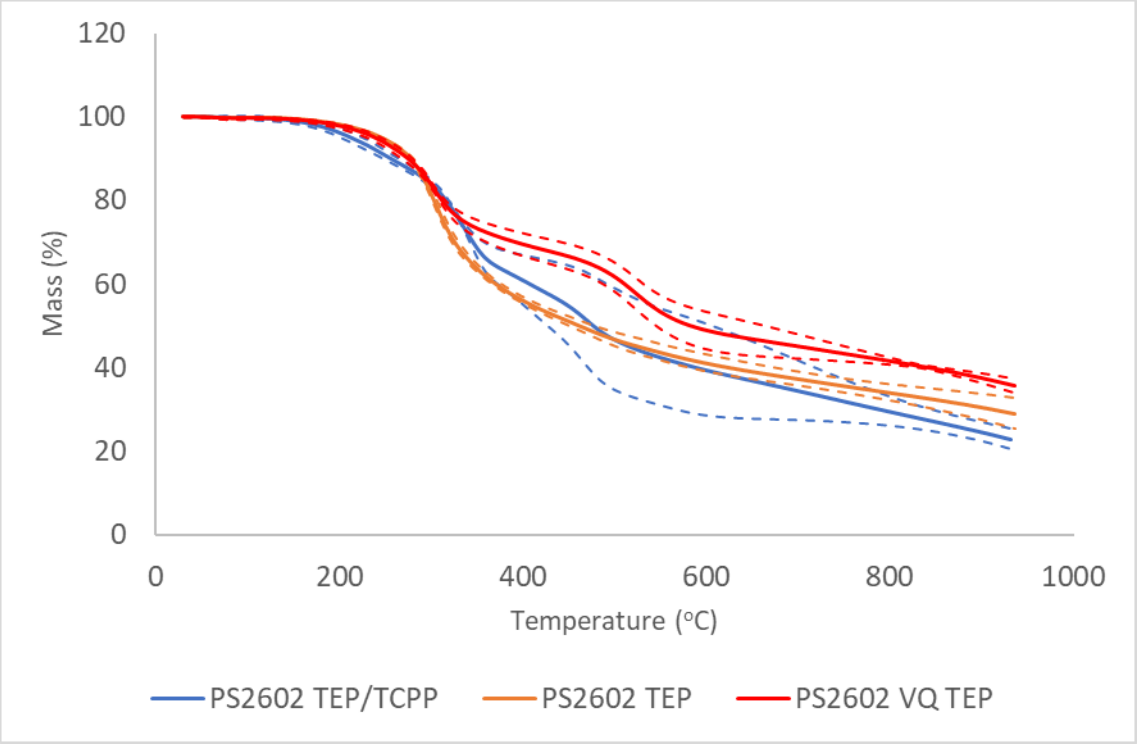

Figure 4.44. *Comparison of mean TG thermograms for BP, BQ and VQ sample sets over 30-900 °C at 10 °C/min under N_2. Dotted lines indicate upper and lower boundaries of ranges within sample sets.*

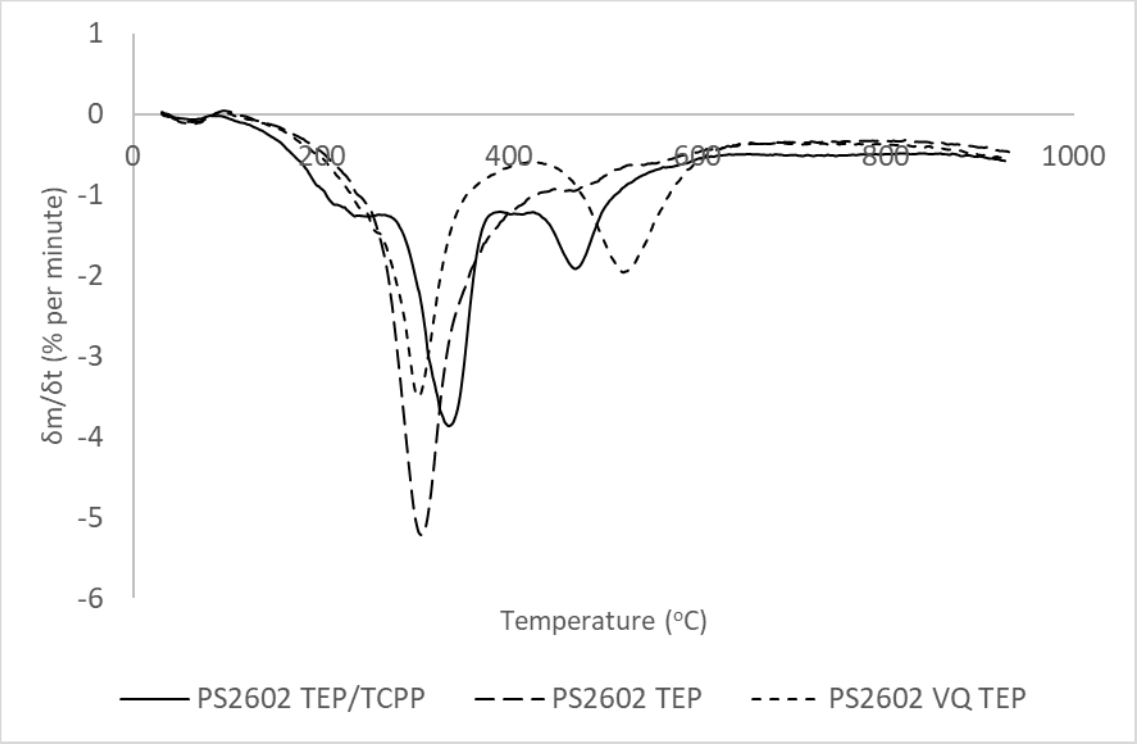

Figure 4.45. *Comparison of dTG thermograms for BP, BQ and VQ sample sets,*

In PS2602-based foams, samples containing a flame-retardant system of VeriQuel R100 with TEP exhibit generally greater mass retention than those containing either a combination of TEP and TCPP or those containing TEP alone. Side by side comparison matched for furnace temperature shows that, when compared to TEP/TCP foam, the VeriQuel-TEP formulation exhibits retained mass at least 1 % higher than TEP-TCPP in the 185-278.3 ^{o}C, 295-316.7 ^{o}C, and 328.3-900 ^{o}C temperature ranges, with a maximum difference of 14.7 % at 476.7 ^{o}C and a final difference in retained char of 12.7 %. TEP-TCPP exhibits greater retained mass in only a relatively narrow temperature range, 288.3-316.7 ^{o}C, with a maximum difference of 2.1 % at 306.7 ^{o}C.

These differences are found to be significant from 210-275 ^{o}C, 350-380 ^{o}C, and at temperatures exceeding 700 ^{o}C, in all cases exhibiting higher stability for the VeriQuel samples.

In comparison to TEP alone, VeriQuel foams exhibit slightly lower retained mass from 30-276.73 ^{o}C, with a maximum difference of 1.0 % at 253.3 ^{o}C. Retained mass is higher for VeriQuel foams at all temperatures above 278.3 ^{o}C, with a maximum difference of 15.8 % at 455 ^{o}C, and a final difference in retained char fraction of 6.6 %.

Comparison of dTG curves clearly demonstrates the lack of a significant elevation in the temperature at which the highest rate of mass loss occurs relative to TEP alone but indicates a dramatic reduction in the mass loss rate at this temperature, with VQ-TEP samples exhibiting a lower peak mass loss rate than either TEP-TCPP or TEP.

The second peak also occurs at a substantially higher temperature than the third peak observed in TEP-TCPP foams, which possibly indicates a char stabilising effect.

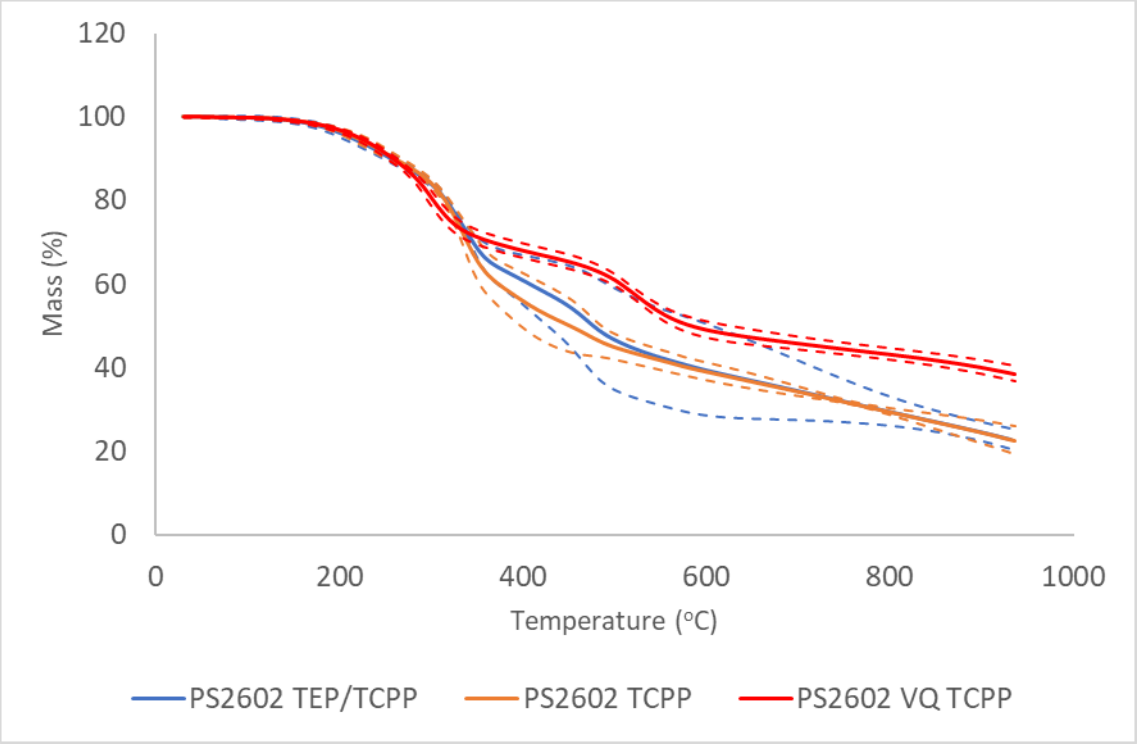

***Figure 4.46**. Comparison of mean TG thermograms for BP, BR and VR sample sets over 30-900 °C at 10 °C/min under N_2.*

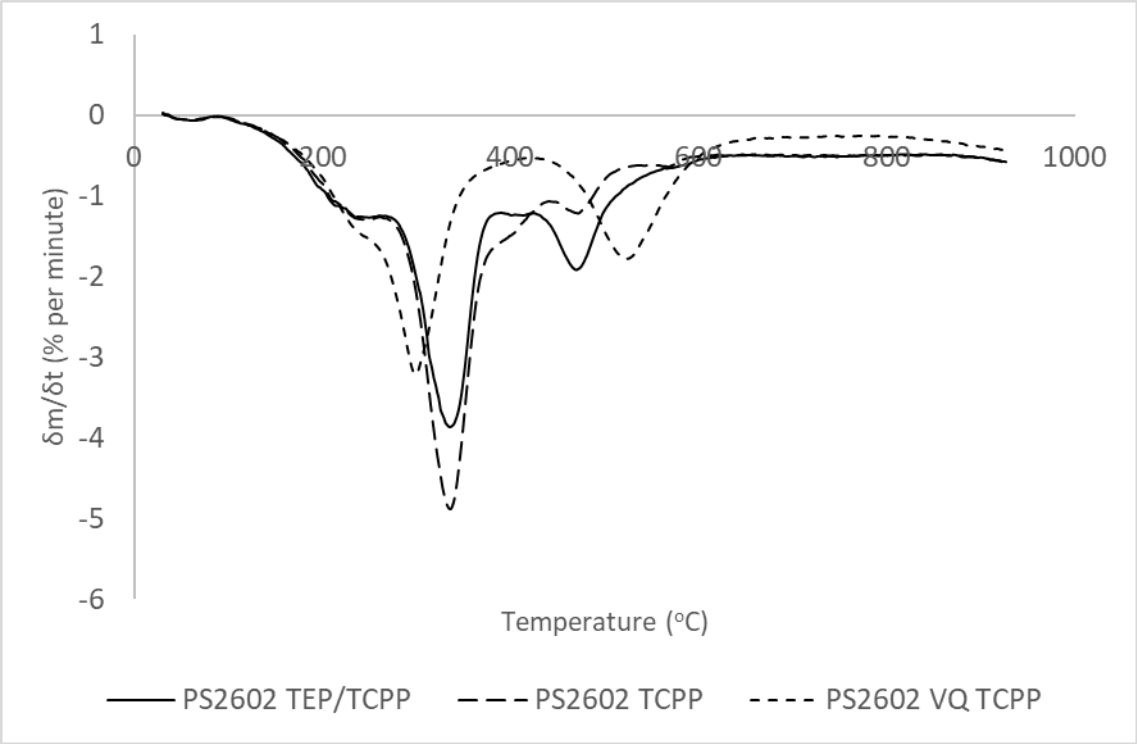

***Figure 4.47.** Comparison of mean dTG thermograms for BP, BR and VR sample sets.*

Comparison of foams containing VeriQuel R100 in combination with TCPP to those containing TEP-TCPP or TCPP alone show that, unlike the TEP set, VeriQuel samples exhibit generally lower mass retention in the early stages of heating. TEP-TCPP foams are more stable by at least +1 % from 266.7-328.3 ^{o}C, with a maximum difference of 5.1 % at 303.3 ^{o}C. This relationship is reversed at all temperatures above 336.7 ^{o}C, with a maximum and final difference in retained char fraction at the end of heating of 15.6 %

These differences are found to be significant from 295-325 ^{o}C, in favour of TEP-TCPP and from 480-515 ^{o}C and 660-900 ^{o}C in favour of VeriQuel-TCPP.

In comparison to TCPP alone, VQ-TCPP exhibits lower mass retention exceeding 1 % from 263.3-320 ^{o}C, with a maximum difference of 4.4 % at 300 ^{o}C. The opposite relationship is observed from 336.7-900 ^{o}C. The maximum observed difference in this direction is 16.1 % at 465 ^{o}C, with a final difference in retained char fraction of 16.0 %

Retained mass is significantly lower in VQ-TCPP foams from 295-315 ^{o}C and significantly higher at all temperatures above 355 ^{o}C.

Comparison of dTG curves shows very similar behaviour for all three samples sets across at temperatures up to 220 ^{o}C, but a significant reduction in the temperature at peak mass loss for VQ TCPP foams compared to either TEP-TCPP or TCPP alone. However, VQ-TCPP exhibits the lowest peak mass loss rate of any of the three formulations. The second mass loss peak again occurs at a higher temperature than the third peaks observed in the other samples sets, reaffirming the possibility of a char stabilising effect.

Table 4.1 Comparison of Key Data Points for Sample Sets Analysed in this Chapter												
	1% Mass Loss (°C)	2.5% Mass Loss (°C)	Mass at 200°C (%)	Mass at 250°C (%)	Mass at 300°C (%)	Mass at 350°C (%)	Mass at 400°C (%)	Mass at 500°C (%)	Mass at 600°C (%)	Final Mass (%)	Temp at Peak (°C)	δm/δt at Peak (% per minute)
BM	141.8	172.5	94.8	88.7	81.4	64.1	55.8	43.1	36.2	26.4	333.5	4.4
BP	149.7	182.6	96.1	90.6	83.8	68.4	60.9	46.7	39.4	22.9	334.3	3.9
BQ	175.5	213.6	98.1	94.4	81.0	63.6	56.1	46.7	41.1	29.1	306.5	5.2
BR	154.7	188.2	96.6	91.1	83.9	65.3	55.9	44.8	39.0	22.6	335.0	4.9
BN	173.9	200.9	97.3	91.6	73.4	62.0	56.8	50.7	44.5	23.4	293.8	5.4
LP	114.4	137.9	89.8	84.3	77.9	59.8	53.1	44.8	37.6	22.1	333.1	4.8
LQ	117.5	145.6	92.6	88.4	76.2	62.8	58.3	51.2	43.9	26.9	299.2	4.5
LR	127.9	152.1	92.4	86.6	80.9	63.3	54.3	45.6	38.8	26.6	337.4	5.1
LN	132.4	164.9	92.5	89.1	76.2	62.5	57.7	48.7	40.9	26.7	298.2	4.8
AP	173.1	210.8	97.9	93.9	86.8	72.7	68.1	60.3	49.9	35.6	321.6	4.2
EG	158.4	188.2	96.3	91.7	81.9	66.1	59.1	50.8	45.7	33.1	304.1	4.1
EH	140.4	166.1	94.0	89.9	83.8	71.4	64.9	54.9	49.0	33.2	338.7	3.0
VQ	169.0	206.6	97.8	93.7	83.3	73.1	69.4	61.7	48.9	35.6	303.3	3.5
VR	154.2	191.1	96.7	91.1	80.3	71.1	67.9	60.8	49.1	36.7	298.9	3.2

4.7 Conclusions

The analyses presented within this chapter provide a detailed picture of the effects of different fire-retardant additives and polyol components on the thermolytic behaviour of PIR foams.

Key data points for all the foam formulations analysed in this chapter are collated in Table 4.1 above, including indicators for onset of significant mass loss, retained mass at several selected temperature thresholds, and the temperature and mass loss rate at the main peak. In each column, the three highest and lowest values are highlighted.

For the 1 % mass loss marker, all three of the highest recorded temperatures occur in PS2602-based formulations containing expandable graphite-TCPP, TEP alone, and bare PIR. The lowest temperatures occur in HT2006-based formulations containing TEP-TCPP, TEP, and VeriQuel-TCPP.

A similar pattern is observed to occur at the 2.5 % mass loss threshold, with the three highest temperature values being recorded for high-hydroxyl value foams with flame retardant systems of TEP, ammonium polyphosphate-TEP, and VeriQuel-TEP, and the lowest temperatures occurring in three low-hydroxyl value foams.

Taken as a whole, high-hydroxyl value foams reach a higher temperature before the onset of significant mass loss than low-hydroxyl value foams. When formulations containing the same fire-retardant system but different polyols were directly compared, the high-HV formulation exhibited a greater temperature at the onset of mass loss than the corresponding low-HV formulation The average magnitude of this effect was 33.4 ^{o}C for the 1 % threshold and 40.6 ^{o}C for the 2.5 % threshold.

At the 200^{o}C reference temperature, which is generally taken to lie at the lower end of the urethane dissociation range, retained masses vary from 98.1 % to 89.8 %. The three highest values occur in formulations based on PS2602 with TEP, VeriQuel-TEP, and ammonium polyphosphate-TEP, while the three lowest values occur in HT2006-based formulations (HT2006 with TEP-TCPP, HT2004-TEP-TCPP, and HT2006-VeriQuel-TCPP

A very similar pattern is observed at the 250 ^{o}C reference temperature. Retained mass in this case ranges from 84.9-94.4 %, with the same formulation being the three most and three least stable. As is the case for onset of mass loss, PS2412/2602 formulations exhibits almost universally greater stability than the equivalent based on HT2004/2006, with a mean difference

of 4.5 % at 200 °C and 4.7 % at 250 °C. It is also apparent that the least stable formulations at these temperatures all contained TCPP. Comparisons of matched formulations containing either TEP or TCPP reveal a small difference of 0.9 % at 200 °C, and a somewhat larger difference of 2.2 % at 250 °C. This indicates that TCPP acts in some way to enhance the decomposition of the foam in the urethane dissociation range, and this is consistent with the previous observations of generally larger first mass loss events in TCPP-containing formulations in the TG and dTG thermograms.

Temperatures in the 300-350 °C range are expected to be associated with more rapid thermal breakdown of PIR through the de-trimerisation of isocyanurate ring structures back into isocyanates. This dissociation temperatures is widely reported in the literature and is supported by the location of the main mass loss peaks on the dTG thermograms collected here.

At 300 °C, retained mass ranges from 73.4-86.8 %, with the highest retained masses in PS2602-ammonium polyphosphate-TEP, PS2602-expandable graphite-TCPP, and PS2602-TCPP, and the lowest in bare PS2602, bare HT2006, and HT2006-VeriQuel-TCPP. By comparison, the lowest stability is observed in bare PS2602, HT2006 formulation are still generally less stable at this temperature, in a range of 76.0-83.8 % versus 73.4-86.8 %, with a mean difference of 2.7 % between matched formulations. The previously observed differences between matched formulation containing TEP and TCPP are here partially reversed, with the latter demonstrating greater retained mass except in formulations containing VeriQuel.

At 350 °C, formulations containing these alternative flame-retardant systems start to demonstrate superior stability when compared to foams containing only some combination of TEP and TCPP. Mass retention for these formulations ranges from 65.0-73.1 % versus 59.5-68.4 %, with the most stable formulations being PS2602-VeriQuel-TEP, PS2602-ammonium polyphosphate, and HT2006-expandable graphite-ammonium polyphosphate, while the least stable comprises HT2004-TEP-TCPP, HT2006-TEP-TCPP, and bare PS2602.

Final mass retention is markedly higher for the alternative fire-retardant systems as compared to those based on TEP and TCPP. In the former case, retained char fraction after heating to 900 °C is 33.1-38.6 %, compared against a range of 22.1-29.1 %.

The temperature at which peak mass loss occurs can be used to broadly divide the samples into two groups. Firstly, those for which this occurs around 300 °C (range = 293.8-306.5 °C), and those for which this occurs in around 335 °C (range = 332.2-338.7 °C). The PS2602-ammonium polyphosphate-TEP was a notable outlier here, with peak mass loss occurring at

321.6 ºC. The former group primarily consists of formulations without TCPP, although both VeriQuel formulations fall into this group, even in the presence of TCPP. All formulations in the latter group contain TCPP, except for HT2006-expandable graphite-TEP, which exhibits the highest temperature at peak mass loss among all formulations.

Based on this behaviour, it is found that unmodified PIRs reach a peak rate of mass loss at an average temperature of 296 ºC under inert atmosphere. This is substantially increased to an average of 336.2 ºC by the presence of TCPP when this is used alone. This effect was not conclusively demonstrated for TEP. When used with PS-2602, an increase was observed from 293.8 ºC to 306.5ºC, but there was almost no increase when HT-2006 was used. Of the alternative fire retardants, only ammonium polyphosphate exhibited this effect, and the presence of VeriQuel appeared to counteract the increase due to TCPP observed in other formulations.

While alternative fire retardants did not produce increases in the peak mass loss temperature on the same magnitude as TCPP, it was clear from examination of the data that peak mass loss rates were reduced in all cases when these were used. The observed patterns of mass retention indicate that all three alternative flame-retardant systems also reduce the volatilisation of polymer fragments across the entire temperature range, culminating in a substantially greater retained char fraction. This has implications for fire performance in terms of total available fuel load, as less material is ultimately released into the vapour phase to undergo combustion, and this also likely to be associated with a decrease in the quantity of toxic fire effluents released.

The following chapter of this thesis focuses on in situ analysis of foams during exposure to high-temperature conditions using through FT-IR and metrology of gram-scale foam samples, along with imaging and pyrolysis GC-MS analysis to gain a fuller understanding of the impacts of these fire retardant systems.

Chapter 4 Bibliography

1. UK. Fire Safety Act 2021. 2021.

2. Lindberg P, Sellstrom U, Haggberg L, de Wit C. Higher Brominated Diphenyl Ethers and Hexabromocyclododecane Found in Eggs of Peregrine Falcons (Falco peregrinus) Breeding in Sweden. Environ Sci Technol. 2004;38(1):93–6.

3. Shaw SD, Blum A, Weber R, Kannan K, Rich D, Lucas D, et al. Halogenated flame retardants: do the fire safety benefits justify the risks? Rev Environ Health. 2010;25(4):261–305.

4. Swedish Environmental Research Institute. Screening of Selected Metals and New Organic Contaminants. 2008.

5. van der Veen I, de Boer J. Phosphorus flame retardants: Properties, production, environmental occurrence, toxicity and analysis. Chemosphere. 2012;88(10):1119–53.

6. Minegishi K, Kurebayashi H, Nambaru S, Morimoto K, Takahashi T, Yamaha T. Comparative Studies on Absorption, Distribution and Excretion of Flame Retardant Halogenated Alkyl Phosphates in Rats. Eisei Kagaku. 1988;34(2):102–14.

7. LeBel GL, Williams DT, Berard D. Triaryl/alkyl Phosphate Residues in Human Adipose Autopsy Samples from Six Ontario Municipalities. Bull Environ Contam Toxicol. 89AD;43(2):225–30.

8. Park DH, Park GP, Kim SH, Kim WN. Effects of isocyanate index and environmentally-friendly blowing agents on the morphological, mechanical, and thermal insulating properties of polyisocyanurate-polyurethane foams. Macromol Res. 2013;21(8):852–9.

9. Kordomenos PI, Kresta JE. Thermal Stability of Isocyanate-Based Polymers. 1. Kinetics of the Thermal Dissociation of Urethane, Oxazolidone, and Isocyanurate Groups. Macromolecules. 1981;14(5):1434–7.

10. Kordomenos PI, Kresta JE, Frisch KC. Thermal Stability of Isocyanate-Based Polymers. 2. Kinetics of the Thermal Dissociation of Model Urethane, Oxazolidone, and Isocyanurate Block Copolymers. Macromolecules. 1987;20(9):2077–83.

5 In-situ Analysis of Polyisocyanurate Foam Degradation

5.1 Introduction

Chapters 3 and 4 of this thesis have focused primarily on the application of thermogravimetric analysis to PIR foams. In chapter 3, thermogravimetric analysis was used to characterise the behaviour of a typical commercial PIR foam formulation during heating. The data thus obtained was combined with ATR-FTIR spectra produced after exposure to a range of temperatures to propose a mechanism by which PIR undergo thermal decomposition. This analysis was extended in chapter 4 to evaluate the effects of changing a number of formulation parameters, and the impact upon thermal stability of alternative fire-retardant agents.

While thermogravimetric analysis is a powerful analytical technique, and the data in Chapters 3 and 4 demonstrates clear differences between the various formulations analysed, there are a number of salient limitations. Firstly, thermogravimetric analysis analyses samples with mass and volume of the order of 10-20 mg and 100-200 mm^3 respectively, and therefore may not account for phenomena related to bulk effects such as thermal conductivity, mass transfer and thermal expansion and deformation. Additionally, the majority of thermogravimetric analysis carried out has been conducted under inert atmospheres in pyrolytic conditions. This is valuable in characterising the pre-ignition behaviour and potential contribution to fuel load, but behaviour may differ under oxidative conditions.

This chapter will encompass the analysis of larger, gram-scale samples, primarily with direct physical measurements of such samples at various stages in heating to better understand the behaviour of PIR foams at macroscopic scales. In particular this will account for bulk heat transfer effects and allow dimensional stability to be compared. This is of importance for structural materials as a tendency to shrink and expand during heating or to become brittle may result in the loss of integrity of structural insulated panel systems. This may manifest itself in the opening of panel gaps, leading to flaring as flammable breakdown products are released into the fire compartment. It is therefore a desirable characteristic of foam formulation to exhibit a combination of high mass retention and relatively small dimensional changes.

ATR-FTIR spectroscopy has been applied to track spectral changes in the samples during thermal degradation to further elucidate the mechanism underlying the breakdown of foams and the results from pyrolysis-GC/MS will also be presented in this chapter in an effort to characterise volatile breakdown products.

5.2 Furnace Testing

All furnace testing was carried out using a Carbolite AAF1100 ashing furnace. In contrast to the thermogravimetric analyses, all furnace testing was carried out under freely-ventilated oxidative conditions. The purpose of this testing was to measure changes in the mass and volume of gram-scale foam samples during heating in a temperature range from 30-400 ^{o}C. This temperature range captures much of the pre-combustion temperature interval, below the autoignition temperature of the foam, and corresponds to the range of temperature under thermogravimetric analysis where two major mass loss peaks were generally observed.

5.2.1 PS-2412 Foam with Triethyl Phosphate and Tris(1-chloro-2-isopropyl) Phosphate

Baseline testing was conducted using block-mould foam samples matching the current commercial formulation. Several experimental parameters were investigated during this testing: sample volume and sample mass.

5.2.1.1 Effect of Sample Volume

Recalling the theoretical background provided in Chapter 3, it is known that the rate of transfer of thermal energy between a material and its surroundings is a function of that material's surface area (1). Meanwhile, the extensive heat capacity of a material is directly proportional to its mass, which is itself directly proportional to volume for a constant density (2). Furthermore, the rate of heat transfer between two isothermal planes is directly proportional to the linear distance between them (1). The geometric square-cube law states that for a given increase in the linear dimensions of the object, surface area will increase with the second power of the linear increase while volume will increase by the third power of the same as expressed below.

$$A_2 = A_1 \left(\frac{l_2}{l_1}\right)^2 \qquad (5.1)$$

$$V_2 = V_1 \left(\frac{l_2}{l_1}\right)^3$$

Therefore, the ratio of surface area to volume decreases as the linear dimensions of the object increase. To evaluate the impact of such changes on mass retention, three cubic samples of foam from the block mould (BM) sample set were prepared with the dimensions shown in Table 5.1. Foams from this sample set were previously analysed in Chapters 3 and 4 and consisted of PIR foam produced to a formulation matching that currently used by the industrial

sponsor. This formulation was based on the PS-2412 polyester polyol and contained TEP and TCPP

Table 5.1 *Dimensions of samples 1-3 from BM sample set.*

Sample	Length (cm)	Area (cm^2)	Volume (cm^3)	Area/Volume ($cm^{-1)}$	Mass (g)	Density (g cm^{-3})
1	1	6	1	6	0.051	0.051
2	2	24	8	3	0.407	0.051
3	4	96	64	1.5	2.996	0.047

The above samples were then placed on a steel tray and inserted into the bottom of a ventilated ashing furnace which had been preheated to 30 ^oC. The heating program consisted of a series of 10 $^oCmin^{-1}$ ramps to 200 ^oC, 250 ^oC, 300 ^oC, 350 ^oC, 400 ^oC and 450 ^oC and 500 ^oC. Upon reaching each ramp temperature, sample were allowed to dwell at the specified temperature for a period of five minutes. The program was then paused, and samples were removed, weighed, and put back into the furnace to heat to the next temperature in the series.

Table 5.2 *Retained mass of samples 1-3 at temperatures from 30-500 ^oC. The top table shows mass in (g) and the lower table shows the % mass retained*

Sample	30^{o}C	200^{o}C	250^{o}C	300^{o}C	350^{o}C	400^{o}C	450^{o}C	500^{o}C
1	0.051	0.046	0.043	0.036	0.033	0.032	0.027	0.019
2	0.407	0.373	0.349	0.286	0.276	0.263	0.236	0.185
3	2.996	2.832	2.663	2.186	2.106	2.033	1.783	1.338

Sample	30^{o}C	200^{o}C	250^{o}C	300^{o}C	350^{o}C	400^{o}C	450^{o}C	500^{o}C
1	100	90.0	84.0	69.7	65.2	62.4	52.6	44.7
2	100	91.7	85.6	70.3	67.8	64.6	58.0	45.4
3	100	94.5	88.9	73.0	70.3	67.9	59.5	37.4

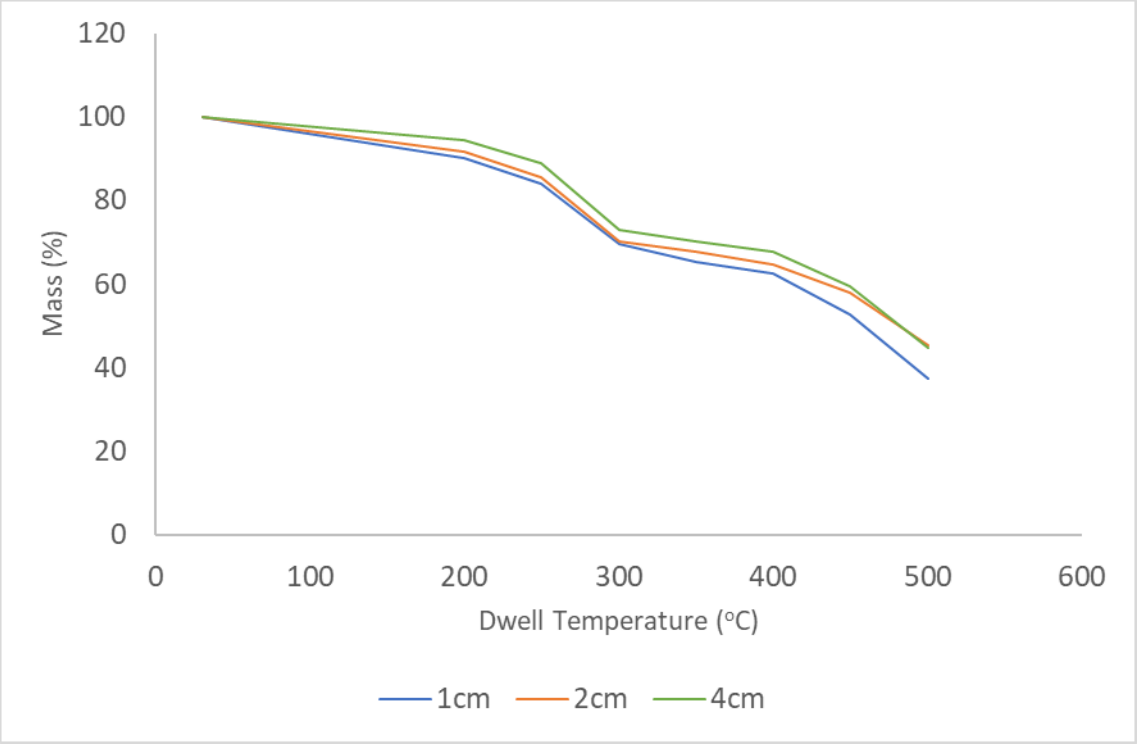

Figure 5.1 *Retained mass for 1 cm, 2 cm and 4 cm cubes of foam from block mould (BM) sample set at temperatures from 30-500 °C in ashing furnace.*

It can be seen (Figure 5.1) that at all elevated temperatures from 200-450 °C, retained mass is greatest for the 4 cm cube and lowest for the 1 cm cube, while at 500 °C, the 2 cm cube shows slightly greater retained mass than the 4 cm cube. These results demonstrate a relationship between sample size and mass loss that is likely the result of two related phenomena. Firstly, absorbed heat is producing a smaller overall temperature increase in the material due to the greater extensive heat capacity of the larger samples. Secondly, there is a more delayed redistribution of heat from the surface of the material throughout its bulk due to a combination of longer linear distance between isothermal planes and high thermal inertia.

5.2.1.2 Changes in Mass and Volume with Temperature

The use of larger samples also provides an important opportunity to study the physical effects of heating on PIR foams in greater detail. While changes in mass indicate decomposition of the material and possible production of volatile fuel species, dimensional changes under extreme heat may have important implications in fire scenarios. For example, pronounced expansion or shrinkage of foam within structural panels may lead to deformation, potentially forcing open gaps between panels and exacerbating the spread of fire by exposing flammable materials or releasing combustible breakdown products into the fire compartment.

To test this, eight blocks of PS-2412 foam containing TEP and TCPP were cut from a larger foam block. The approximate dimensions of these blocks were 3.5 cm x 2.5 cm x 2 cm. Exact measurements in each direction were taken using a set of digital Vernier callipers placed at the midline of opposite edges.

Table 5.3 *Experimental conditions for eight 3.5x2.5x2cm blocks of PS-2412 foam*

Block	**Conditions**
1	Unheated Control
2	Ramp to 200^{o}C at 10^{o}Cmin^{-1}
3	Ramp to 250^{o}C at 10^{o}Cmin^{-1}
4	Ramp to 300^{o}C at 10^{o}Cmin^{-1}
5	Ramp to 350^{o}C at 10^{o}Cmin^{-1}
6	Ramp to 400^{o}C at 10^{o}Cmin^{-1}
7	Flash heated at 500°C
8	Flash heated at 600^{o}C

The five samples that were to be exposed to ramped heating were placed together on a tray that was inserted into a furnace that was set to heat at a rate of 10 ^{o}Cmin^{-1} to 200 ^{o}C then hold a constant temperature for five minutes, then continuing this pattern of ramped heating and isothermal conditions at 50 ^{o}C increments to 400 ^{o}C. At the end of each isotherm, the program was briefly paused, to allow one sample to be removed for weighing and measurement of dimensions.

Table 5.4 *Initial dimensions of PS-2412 foam blocks*

Block	**Dimensions (cm)**			**Area (cm^{2})**	**Volume (cm^{3})**	**Area/Volume (cm^{-1})**	**Mass (g)**	**ρ (g cm^{-3})**
	x	**y**	**z**					
1	3.45	2.38	2.07	40.56	17.00	2.39	0.769	0.045
2	3.5	2.44	2.15	42.62	18.36	2.32	0.809	0.044
3	3.37	2.45	1.89	38.51	15.60	2.47	0.717	0.046
4	3.52	2.31	1.83	37.60	14.88	2.53	0.680	0.046
5	3.53	2.51	1.80	39.46	15.95	2.47	0.701	0.044
6	3.42	2.42	2.06	40.61	17.05	2.38	0.733	0.043

The surface area to volume ratio has been calculated within a range of 2.32-2.53 cm^{-1}, intermediate in value between the 2 cm and 4 cm cubic samples tested previously. Density for these samples was consistent, ranging from 0.430-0.046 gcm^{-3}.

Table 5.5 *Dimensions of PS-2412 foam blocks after heating.*

Block	**Dimensions (cm)**			**Area (cm^2)**	**Volume (cm^3)**	**Area/Volume (cm^{-1})**	**Mass (g)**	**ρ (g cm^{-3})**
	x	**y**	**z**					
1	3.45	2.38	2.07	40.56	17.00	2.39	0.769	0.045
2 (200^{o}C)	3.84	2.86	2.33	53.19	25.59	2.08	0.734	0.029
3 (250^{o}C)	4.05	3.06	2.3	57.49	28.50	2.02	0.589	0.021
4 (300^{o}C)	4.06	2.83	2.3	54.67	26.43	2.07	0.486	0.018
5 (350^{o}C)	4.03	2.88	2.02	51.13	23.44	2.18	0.496	0.021
6 (400^{o}C)	3.57	2.65	2.16	45.79	20.43	2.24	0.496	0.024

Table 5.6 *Proportional changes in dimension (%) of PS-2412 foam blocks after heating*

Block	**x (%)**	**y (%)**	**z (%)**	**Mean x,y,z (%)**	**Area (%)**	**Volume (%)**	**Retained mass (%)**
1	0	0	0	0	0	0	100
2 (200°C)	+9.7	+17.2	+8.3	+11.8	+24.8	+39.4	90.7
3 (250°C)	+20.2	+24.9	+21.7	+22.3	+49.3	+82.6	82.2
4 (300°C)	+15.3	+22.5	+25.7	+21.2	+45.4	+77.6	71.4
5 (350°C)	+14.1	+14.7	+12.2	+13.7	+29.6	+47.0	70.7
6 (400°C)	+4.4	+9.5	+4.9	+6.2	+12.7	+19.9	67.8

At temperatures up to 250 °C, an expansion of the foam is observed, with a mean linear expansion of 22.3 % averaged in the x, y, and z planes. This corresponds to a 49.3% increase in surface area and an 82.6 % increase in volume. At higher temperatures (from 250 °C to 300 °C), the foam appears to begin to shrink back towards its initial size, although this change is small within this temperature range. At 400 °C the linear expansion of the foam averages 6.2 % with 12.7 % greater surface area and 19.9 % greater volume. This expansion suggests a pyroplastic state where the cellular structure has been able to expand to accommodate the increasing volume of the intracellular gases. In turn, this must presumably also result in a thinning of the polymer cell walls which may result in gas egress. As the blowing agent is cyclopentane (flash point -37 °C), this will have important implications for potential fire ignition.

A mass loss of 9.3 % occurs during heating from 30-200 °C and over the duration of the subsequent five-minute dwell period. This is a greater mass loss than was recorded for same foam formulation at 200 °C under thermogravimetric analysis (4.5 %). This difference may be the result of further mass loss during the dwell period. This pattern continues at the 250 °C, 300 °C, and 350 °C temperature points, but retained mass at 400 °C is substantially higher for the furnace sample (67.8 %) than the results from thermogravimetry (54.0 %). In contrast to the thermogravimetric data, where the most rapid mass loss for this formulation occurs at 335 °C, this temperature interval from 300-350 °C is marked by only a small mass loss in the furnace sample (0.7 %). This may reflect differences in breakdown under oxidative conditions. Interestingly, it was noted in section 3.3.5 that the presence of oxygen appears to inhibit the large mass loss event from 300-350 °C with the main mass loss shifting to higher temperatures above 500 °C. These results therefore appear broadly consistent with the oxidative TGA data.

It can also be noted that, while a relatively large mass loss of around 10 % occurs between 250 ^{o}C and 300 ^{o}C, the volume of the foam remains relatively constant. This suggests either a continued expansion of the foam accompanied by ablation of the outer surface, or a thinning of the walls and struts within the foam which is sufficient to enable gas escape while the cellular structure remains sufficiently intact to maintain the overall foam dimensions.

The two remaining foam blocks were subjected to flash heating. This was performed by pre-heating the furnace to the target temperatures of 500 ^{o}C and 600 ^{o}C respectively and directly inserting the sample into the furnace at this temperature. Flash heating was carried out for a period of 30 seconds. The first flash heating sample had a mass before heating of 0.779 g. Upon inserting the sample into the furnace, a large quantity of yellow smoke was immediately observed from the which was rapidly followed by an autoignition event, producing a substantial quantity of dark smoke and visible particulates. The foam was undergoing flaming combustion when removed from the furnace but rapidly self-extinguished when extracted. The retained mass was 52.2 % with visible severe charring and cracking of the foam observed. Very similar behaviour occurred with the sample that was flash heated at 600 ^{o}C. The initial mass of this sample was 0.628 g and retained mass after 30 seconds was 34.6 %. Both flash heated samples were severely charred and were too fragile to carry out dimensional measurements. Sudden exposure to temperatures above 500 ^{o}C appears likely to induce rapid and violent autoignition, although the foam readily self-extinguishes on removal of the heat source.

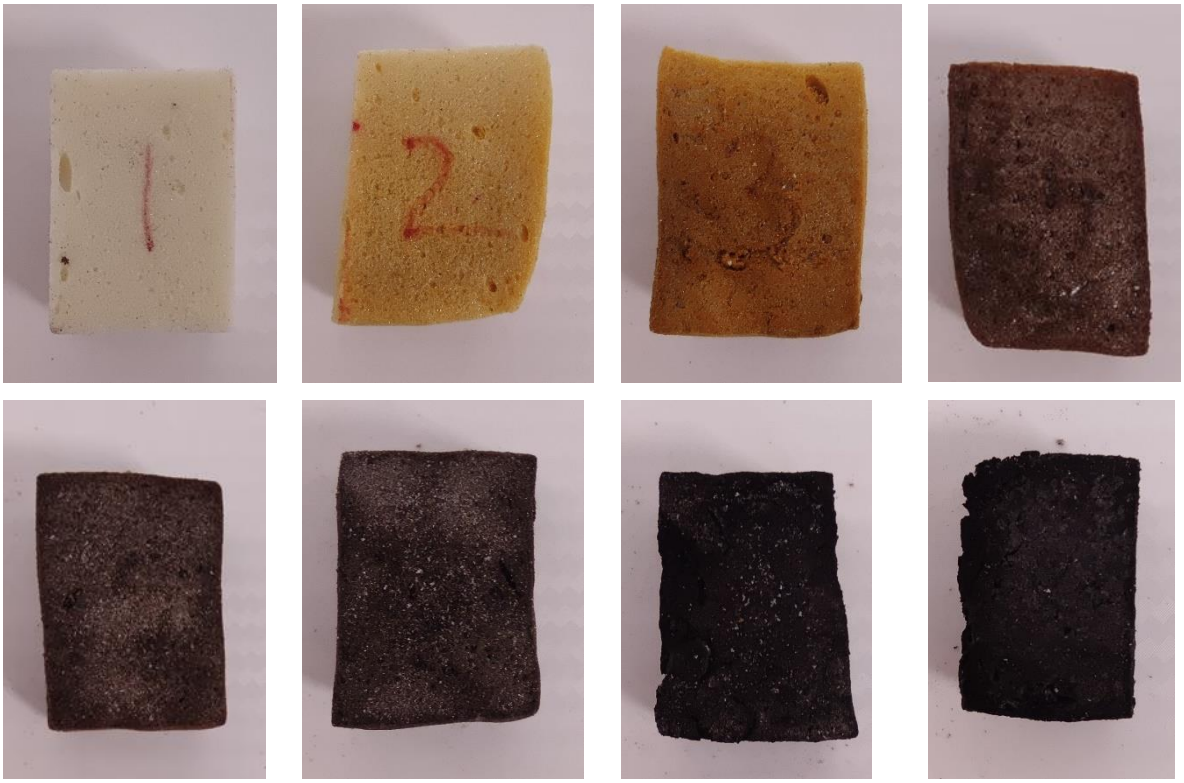

Figure 5.2 *Images of PS-2412 foam samples. Top row (left to right) unheated, 200°C, 250°C, 300°C; bottom row (left to right) 350°C, 400°C, 500°C flash, 600°C flash.*

Images of the foam blocks after heat exposure are shown in Figure 5.2 A progressive colour change from the off-white colour of the unheated foam to a dark brown was observed as the heating temperature increased. Ramp-heated samples appear to generally maintain their macroscopic structural integrity throughout heating. In contrast, the flash heated samples exhibit significant surface cracking and ablation. In particular, the sample that had been flash-heated at 600°C felt very fragile and powdery.

5.2.2 Time Series Heat Exposure Data

Results from isothermal TG were previously reported in section 3.3.7. Here, it was found that when foams are exposed to elevated temperatures under isothermal conditions, a substantial proportion of the observed mass loss occurs during the temperature ramp to the isothermal temperature. The rate of mass loss during the isothermal period then appears to decline asymptotically with the retained mass stabilising at a finite value. In the case of larger foam blocks, it is also likely to take a substantial period of time for temperature to equilibrate throughout the material, meaning that these processes will gradually propagate inwards from the surface. This analysis has been included to examine the rate at which the degradation of foams occurs in isothermal conditions at a range of temperatures.

In this section, three sets consisting of four blocks of PS-2412 foams containing TEP and TCPP fire retardants were directly introduced into furnaces preheated to temperatures of 200 ^{o}C, 250 ^{o}C and 300 ^{o}C. From each set, samples were removed after 1 minute, 5 minutes, 10 minutes or 30 minutes. As in section 5.2.1, samples were again measured for changes in mass and dimensions.

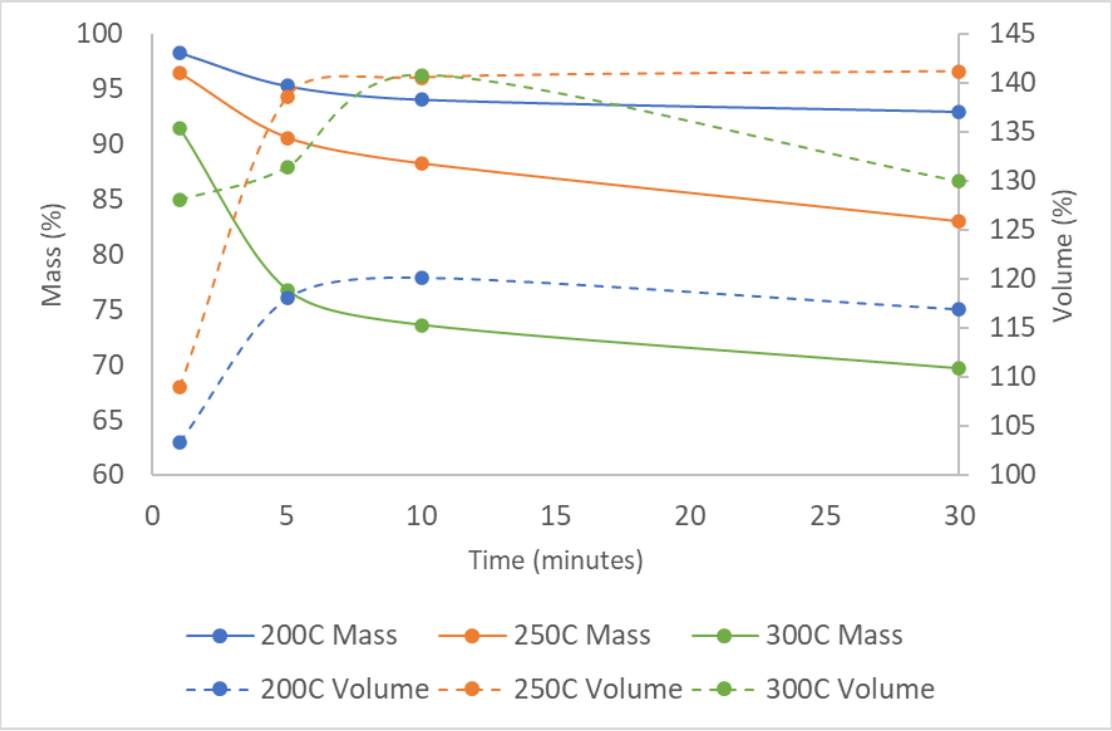

Figure 5.3 *% change in mass and volume for PS-2412 foam samples exposed to isothermal conditions at 200^{o}C, 250^{o}C and 300^{o}C.*

The date show that, at each time point, mass loss increases with temperature (Figure 5.3), and it is apparent that mass loss for each sample decelerates over time, with mass loss per minute decreasing for successive time intervals in all three sample sets (Figure 5.4).

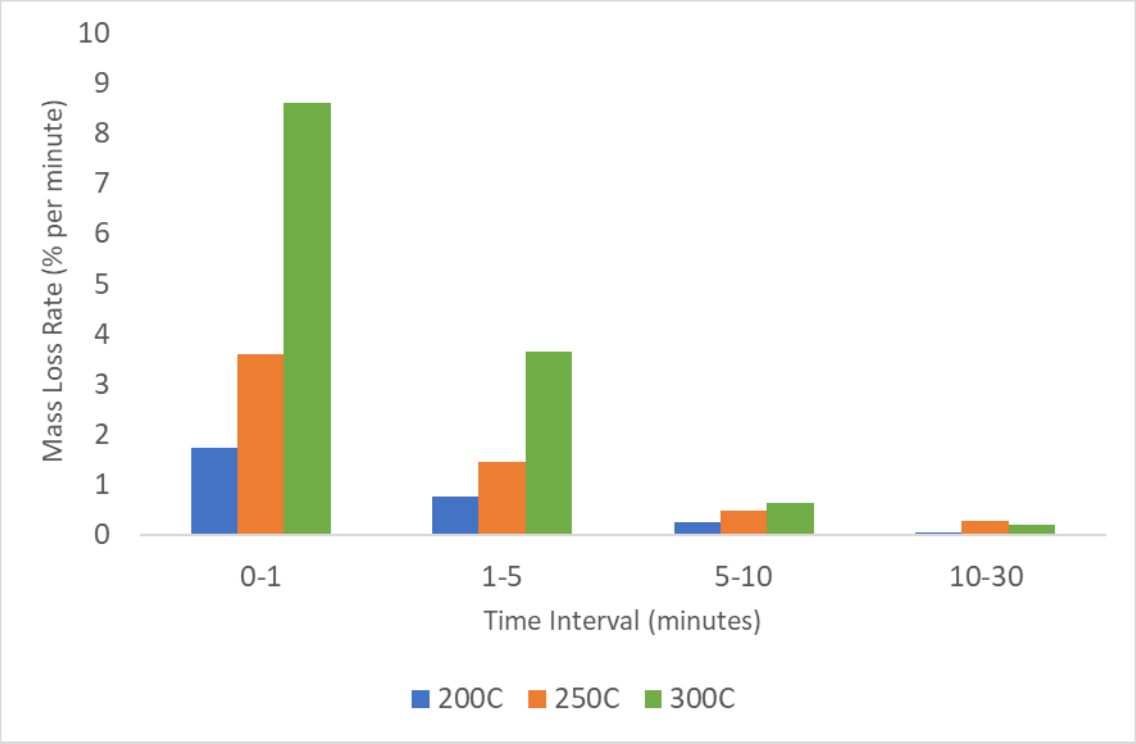

Figure 5.4 *Mass loss per minute (arithmetic mean) for each time interval at 200 °C, 250 °C and 300 °C*

Over the 0-1, 1-5 and 5-10 minute time intervals, the average rate of mass loss is greater for the higher temperature samples. However, this is not the case over the 10-30 minute interval, where the average mass loss is lower at 300°C. This indicates that the process of mass loss more rapidly reaches its endpoint at this temperature. This further suggests a mechanism whereby mass loss at a given temperature within this range is limited by the temperature-dependent processes that cannot occur below a critical temperature.

At 1 minute, volumetric expansion increases with temperature, with a 3.3 % increase at 200 °C, an 8.9 % increase at 250 °C, and a 28.0 % increase at 300 °C. At 200 °C, the foam samples continue to expand with longer dwell time, reaching 18.0 % after 5 minutes and 20.2 % after 10 minutes. Then they begin to contract falling to 16.9 % at 30 minutes. At 250 °C, expansion increases to 38.5 % at 5 minutes and continues to slowly increase to 40.5 % at 10 minutes and 41.1 % at 30 minutes. The pattern over time at 300 °C exhibits clearly distinct behaviour after the rapid initial expansion, reaching 31.3 % after 5 minutes, then more rapidly expanding to 40.7 % at 10 minutes and then contracting to 29.9 % at 30 minutes. Correlating with stability behaviour from the thermogravimetric analysis, it can be inferred the observed expansion is

primarily associated with the first mass loss event which is attributed to the breakdown of urethane bonds in the linear segments of the polymer (3,4). One chemical pathway for the degradation of these bonds involves the formation of carbon dioxide (5)(6), which may be a driver of expansion along with the thermal expansion of the blowing agent. Additionally, the cleavage of bonds may induce some degree of thermoplastic behaviour, allowing the matrix to expand. The contraction seen in the later stages of heating at 300 ^{o}C may indicate the widespread onset of isocyanurate degradation and the irregular shape of this curve (Figure 5.3) possibly indicating competing effects from these as they propagate through the foam.

5.3 Impact of Formulation Changes

In Chapter 4 of this thesis, extensive comparisons of thermogravimetric data were carried out to evaluate the effects of different polyols and fire-retardant systems upon the behaviour of PIR foams. This analysis has here been expanded to encompass the larger, gram-scale foam samples, under oxidative conditions. To this end, a range of foam formulations have been subjected to the same analysis covered in section 5.2.1.2, wherein foam samples were heated to temperatures between 200 ^{o}C and 400 ^{o}C with changes in mass and volume being recorded.

The formulations analysed encompassed the following range of fire-retardant systems.

Table 5.7 *Fire retardant systems included in analysed foams.*

Reference	**Flame Retardants**
FR0	None
FR1	Triethyl phosphate, tris(1-chloro-2-isopropyl phosphate)
FR2	Triethyl phosphate
FR3	Tris(1-chloro-2-isopropyl) phosphate
FR4	Ammonium polyphosphate, triethyl phosphate
FR5	Ammonium polyphosphate, tris(1-chloro-2-isopropyl) phosphate
FR6	Expandable graphite, triethyl phosphate
FR7	Expandable graphite, tris(1-chloro-2-isopropyl) phosphate
FR8	VeriQuel R100, triethyl phosphate
FR9	VeriQuel R100, tris(1-chloro-2-isopropyl) phosphate

For each of these fire-retardant systems, block-moulded foams were produced based on the PS-2602 and HT-2006 polyol, plus the reference formulation based on the PS-2412 polyol with

the FR1 fire-retardant system. Within this chapter, these samples will be prefixed with P for PS-2602 based foams and H for HT-2006 based foams, followed by the number of the fire-retardant system, e.g., P0 refers to the formulation consisting of PS-2602 based foam with no flame retardants. The reference formulation will be referred to as R1.

For some comparisons, samples have also been assigned to classes based on the presence of a particular components, shown in Table 5.8

Table 5.8 *Assignment of samples to classes based on presence of components.*

Class	**Samples**
PS2602	P0-P9
HT2006	H0-H9
Triethyl phosphate	P1*, P2, P4, P6, P8, H1*, H2, H4, H6, H8
Tris(1-chloro-2-isopropyl) phosphate	P1*, P3, P5, P7, P9, H1*, H3, H5, H7, H9
Ammonium polyphosphate	P4, P5, H4, H5
Expandable graphite	P6, P7, H6, H7
VeriQuel R100	P8, P9, H8, H9
**samples H1 and P1 have been excluded from direct comparisons of these sets due to their presence in both.*	

The data obtained from these sample sets are presented in Tables 5.9 and 5.10 below.

Table 5.9 *Mass retention (% of initial mass) for samples of various polyisocyanurate foam formulations at 200-400 °C. Maximum and minimum values in each column are highlighted in blue and red respectively.*

Formulation	Start	200°C	250°C	300°C	350°C	400°C
R1	100	90.7	82.3	71.4	70.7	67.8
P0	100	92.7	85.9	**69.6**	**67.3**	64.7
P1	100	93.6	86.3	75	72.3	68
P2	100	93.4	87.6	77.5	73.9	68.6
P3	100	**94.7**	**89.1**	76.1	71.4	68.1
P4	100	92.8	83.1	**78.2**	75.1	71.1
P5	100	93.9	82.6	77.6	**75.9**	**73.3**
P6	100	92.3	86.8	76.3	73.6	68.6
P7	100	91.6	84.7	75.8	73.4	69.5
P8	100	93.6	86.3	75	72.3	68
P9	100	90.8	84	73.8	67.6	**63.3**
H0	100	90.7	86.9	74.6	69.8	67.1
H1	100	**87.2**	79.8	73.3	68	65.7
H2	100	89.3	89	77.4	71.5	68.8
H3	100	90.2	85.2	76.7	68.7	65
H4	100	92.7	87.8	**78.2**	74.7	69.3
H5	100	88.5	84	73.6	68.6	64.5
H6	100	87.4	82.2	75	71.6	66.8
H7	100	89.6	80.4	72.1	69.4	64.8
H8	100	89.5	80.6	75.8	73.2	68.5
H9	100	92.3	**78.8**	77.1	**75.9**	70.9

Substantial variations in retained mass are observed across formulations throughout heating (Table 5.9). The highest retained mass values at each temperature are 94.7 % (P3) at 200 °C; 89.1 % (P3) at 250 °C; 78.2 % (P4, H4) at 300 °C; 75.9 % (P5, H9) at 350 °C and 73.3 % (P5) at 400 °C. The lowest retained mass values at each temperature are 87.2 % (H1) at 200 °C; 78.8 % (H9) at 250 °C; 69.6 % (P0) at 300 °C; 67.3 % (P0) at 350 °C and 63.3 % (P9) at 400 °C. Initial inspection suggests a generally greater mass stability across this temperature range for samples based on PS-2602 than those based on HT-2006.

Table 5.10 *% volume changes for samples of polyisocyanurate foam formulations at 200-400°C. Highest and lowest absolute changes in volume are highlighted in red and blue respectively.*

Foam	Start	200°C	250°C	300°C	350°C	400°C	Max (+/-)
R1	0	39.4	82.7	77.6	47.0	19.9	82.7
P0	0	19.2	5.7	-18.2	-20.3	-12.3	20.3
P1	0	38.6	54.6	51.5	53.5	44.8	54.6
P2	0	41.5	**109.1**	**92.7**	**84.9**	**78.9**	109.1
P3	0	31.7	63.5	70.6	39.8	31.2	70.6
P4	0	39.0	52.6	61.2	35.9	14.1	61.2
P5	0	20.5	17.1	15.1	29.2	29.1	29.2
P6	0	32.0	11.3	**1.7**	4.8	**-1.3**	32.0
P7	0	15.2	4.8	10.3	12	-4.5	15.2
P8	0	**63.3**	92.9	90.8	61.7	57.2	92.9
P9	0	14.8	43.4	48.9	39.4	42.4	48.9
H0	0	13.3	8.4	-15.0	-8.1	-19.4	19.4
H1	0	-4.0	-6.6	**-1.7**	-20.5	-20.9	20.9
H2	0	6.2	24.2	9.5	8.0	12.3	24.2
H3	0	4.3	1.2	-13.0	-13.4	-25.5	25.5
H4	0	11.9	**-0.4**	-2.2	**-2.7**	-11.0	11.9
H5	0	-8.1	-4.2	-15.1	-19.8	-18.9	19.8
H6	0	2.7	-8.4	-10.4	-14	-22.2	22.2
H7	0	**-0.5**	-10.4	-12.0	-16.5	-23.4	23.4
H8	0	60.3	46.5	18.8	19.9	14.3	60.3
H9	0	12.2	-14.7	35.3	5.8	-25.6	35.3

The degree of volumetric expansion varies widely between samples, with the highest recorded value being 109.1 % in P2 at 250 °C, a more than twofold increase in the volume of the sample and corresponding to a linear expansion of 27.8 %. For samples that undergo substantial expansion, this typically reaches a maximum extent at 250 °C or 300 °C and is followed by some degree of contraction. Several samples exhibit shrinkage throughout some, or all, of the temperature range, and it clearly appears that samples based on HT-2006 undergo less expansion and that most such samples shrink below their initial volume at 400 °C. H4 (HT-

2006, ammonium polyphosphate and TEP) exhibits the best overall dimensional stability, with a maximum volumetric change of 11.9 %, corresponding to a linear expansion of 3.8 %.

5.3.1 PS-2602 vs. HT-2006

Mass retention has also been compared for PS-2602 and HT-2006 based foams by taking the arithmetic means of values for P0-9 and H0-9 at each temperature. The relative positions of the two series in Figure 5.5 do indicate that samples based on PS-2602 exhibit, on average, greater stability than those based on HT-2006. However, these differences are generally quite small in absolute terms with the largest difference being 3.2 % at 200 °C, although it should be noted that range between the highest and lowest mass loss for any individual sample at this temperature is 7.5 % so this difference is relatively substantial. The difference in retained mass is smaller at 250 °C and the two sets have almost identical retained mass at 300 °C, differing by only 0.1 %. A difference of around 1 % is observed at 350 °C and 400 °C.

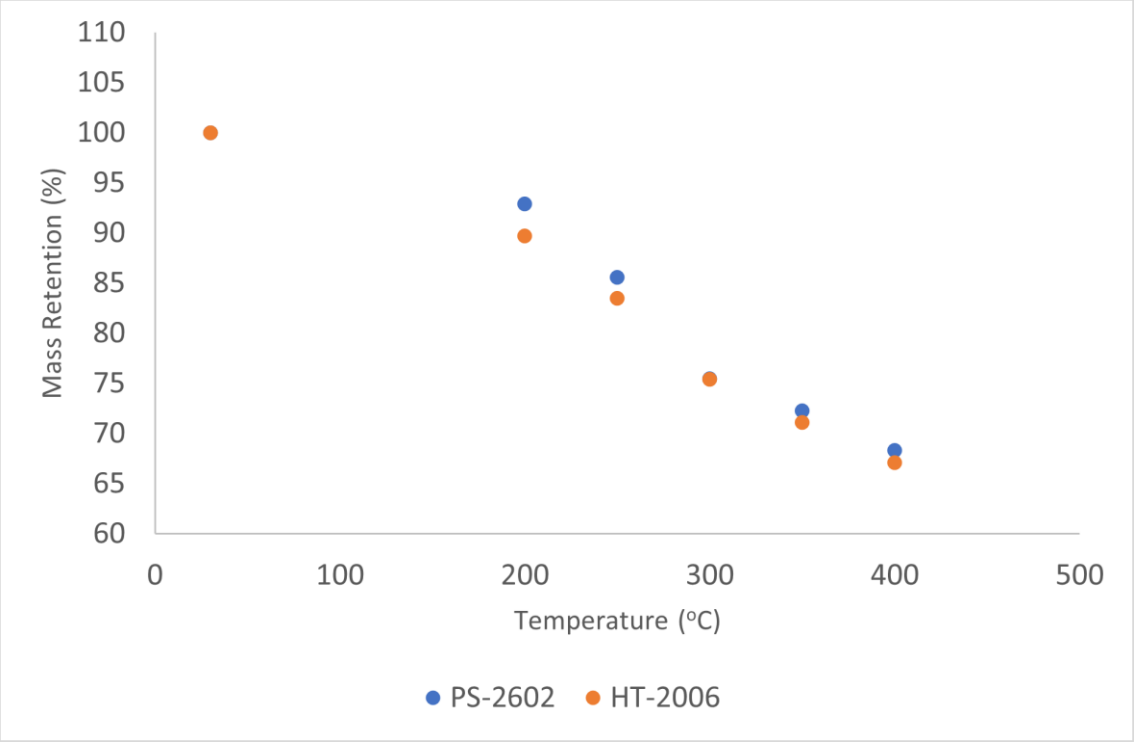

Figure 5.5 *Mean mass retention (%) versus temperature for PS-2602 (P0-9) and HT-2006 formulations (H0-9)*

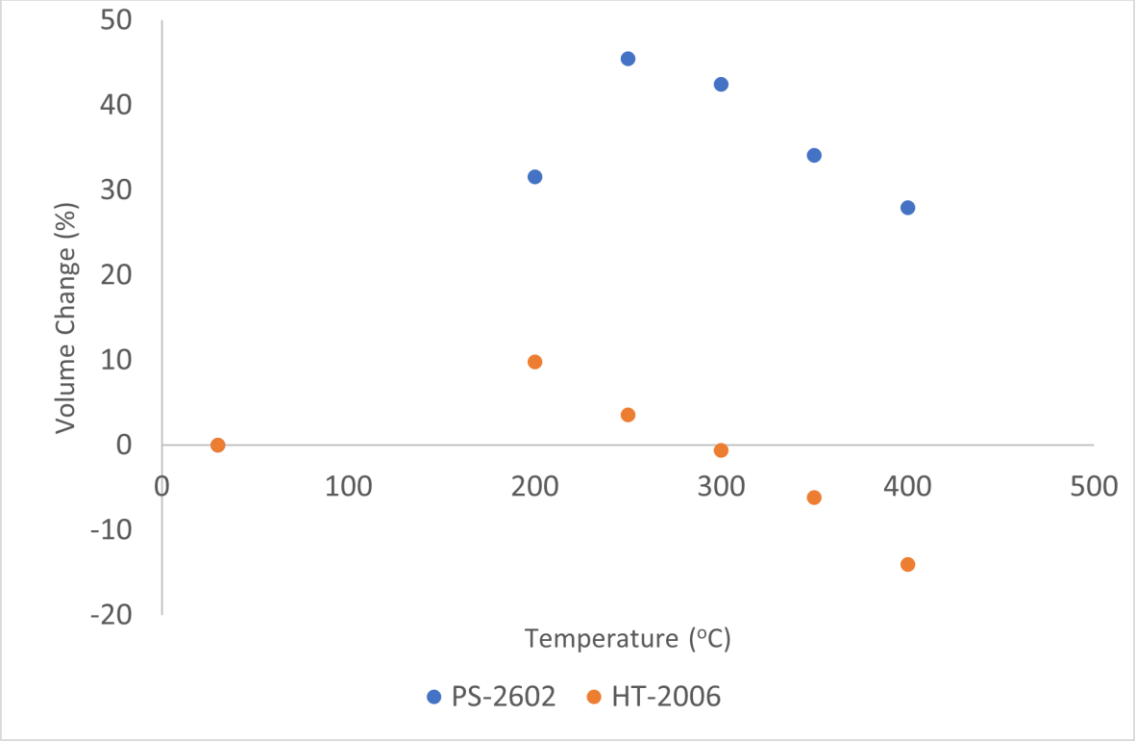

Figure 5.6 *Volume change (%) versus temperature for PS-2602 (P0-9) and HT-2006 (H0-9) formulations.*

In stark contrast to the relatively subtle differences observed in mass retention between the PS-2602 and HT-2006 samples, radical differences are observed in dimensional stability (Figure 5.6). At 200 °C, PS-2602 samples exhibit an average volumetric expansion of 31.6 % (linear = 9.6 %) compared to 9.8 % for HT-2006 (linear = 3.2 %). Furthermore, the mean expansion for PS-2602 samples further increases at 250 °C, reaching 45.5 % (linear = 13.3 %), while the HT-2006 samples generally began to contract, exhibiting a mean volume change of 3.6 % (linear = 1.2 %). For the temperature points above 250 °C, both sets of samples exhibit a progressive contraction with increasing temperature. In the case of HT-2006 samples, these exhibit on average as reduced volume compared to their initial dimensions, which reach a reduction of 14.0 % at 400 °C. This is not the case for PS-2602 samples. While the degree of expansion at 400 °C is lower than at 250 °C, the final average volume of PS-2602 samples is 28.0 % greater than their initial volume.

These data show that while foams based on HT-2006 tend to have somewhat lower mass retention than those based on PS-2602, they typically exhibit greater dimensional stability. This presumably reflects the influence of the different formulations on the pyro-plasticity of the polymer walls. So, the PS-2602 formulation retains a plasticizing effect while the polymer cell walls of the HT-2006 system remain more rigid.

5.3.2 Triethyl Phosphate vs. Tris(1-chloro-2-isopropyl) Phosphate

The objective of eliminating the use of halogenated fire retardants in construction materials has been a significant driving force behind this research. TCPP and closely-related materials have remained in use on the basis of demonstrable efficacy despite concerns over their environmental and health impacts (7)(8).

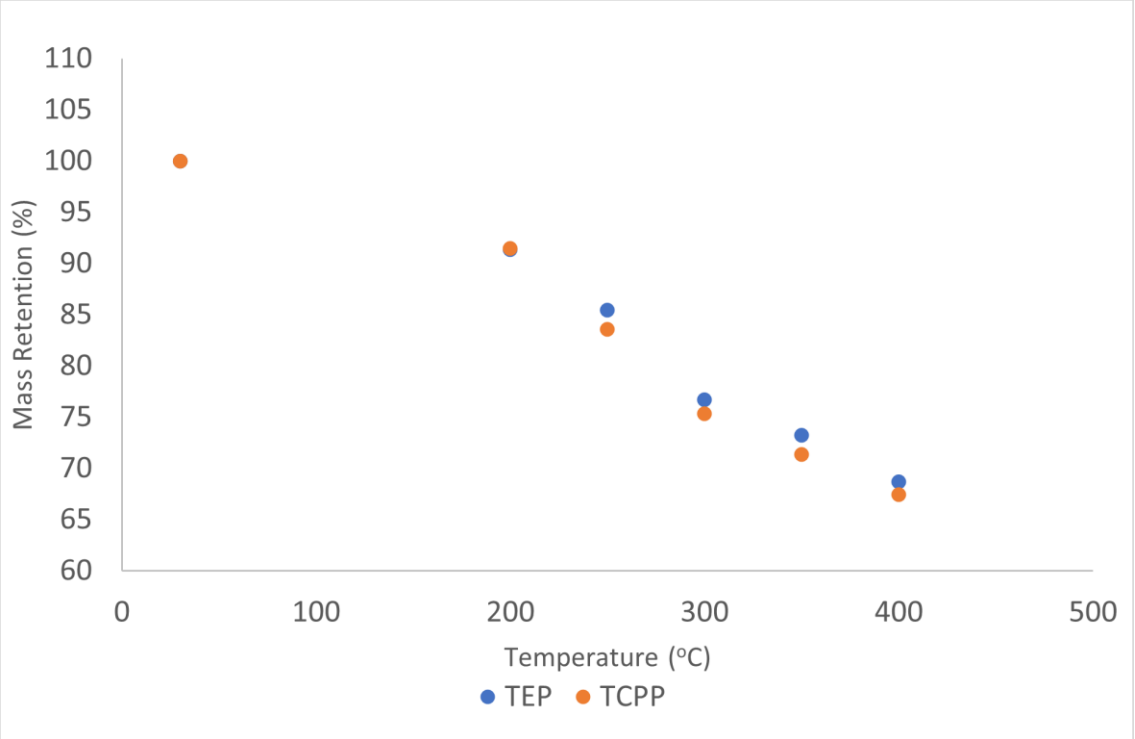

Figure 5.7 *Mass retention for triethyl phosphate (P/H2,4,6,8) and tris(1-chloro-2-isopropyl phosphate (P/H3,5,7,9) formulations*

The results obtained from furnace testing (Figure 5.7) demonstrate almost no difference in mass retention between the formulation containing TEP and that containing TCPP at temperatures of 200 °C and 250 °C, and slightly greater stability for the formulation containing TEP above this temperature. This pattern is also generally found to hold when comparing matched formulations which, in a majority of cases, indicate either negligible differences between TEP and TCPP, or slightly greater mass retention when TEP was present in the flame-retardant system compared to when TCPP is present.

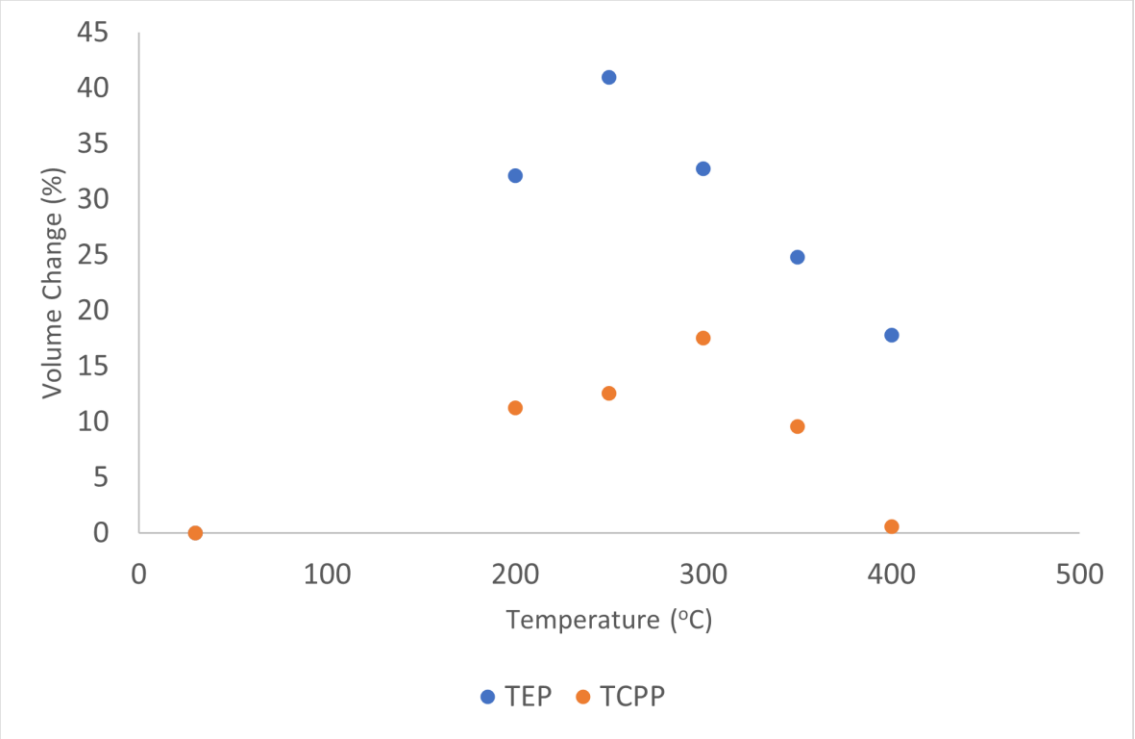

Figure 5.8 *Volume change for triethyl phosphate (P/H2,4,6,8) and tris(1-chloro-2-isopropyl) phosphate (P/H3,5,7,9) formulations.*

Comparison of dimensional stability for foams containing TEP with those containing TCPP reveals that this again differs to a far greater degree than did mass retention (Figure 5.8). Formulations containing TEP undergo, on average, a much greater degree of volumetric expansion than those containing TCPP. This is observed for the entirety of the temperature range, with the greatest difference occurring at 250 °C. At this temperature point, the mean expansion of formulation containing TEP is 41.0 %, compared to 12.6 % (linear 12.1 % vs. 4.0 %). For formulations containing TCPP, the maximum volumetric expansion is on average 17.5 % at 300 °C. For individual formulations, the largest volumetric expansion observed for a sample containing TCPP but not TEP is 70.7 % in P3.

The greater degree of expansion in the presence of TEP may be the result of its activity as a plasticiser (9) within the cell walls as the polymer matrix begins to degrade. Plasticisers increase the mobility of polymer chains enabling the polymer molecules to move relative to each other so that the material retains flexibility, and here may allow the polymer matrix to expand in response to increased pressure in the gaseous dispersed phase within the closed-cell structure.

5.3.3 Comparison of Alternative Fire Retardants

Three alternative, non-halogenated fire-retardant agents, ammonium polyphosphate, expandable graphite, and VeriQuel R100 were evaluated in Chapter 4 as possible replacements for the current fire-retardant system. Foams containing these agents have been tested here and have been found to exhibit greater final char retention than foams based on the FR1 and FR2 flame retardant systems, and most exhibit either similar or greater mass retention at earlier stages of heating. Results from furnace treatment for foams containing these fire retardants are here compared against the mean results for the R1, P1 and H1 formulations.

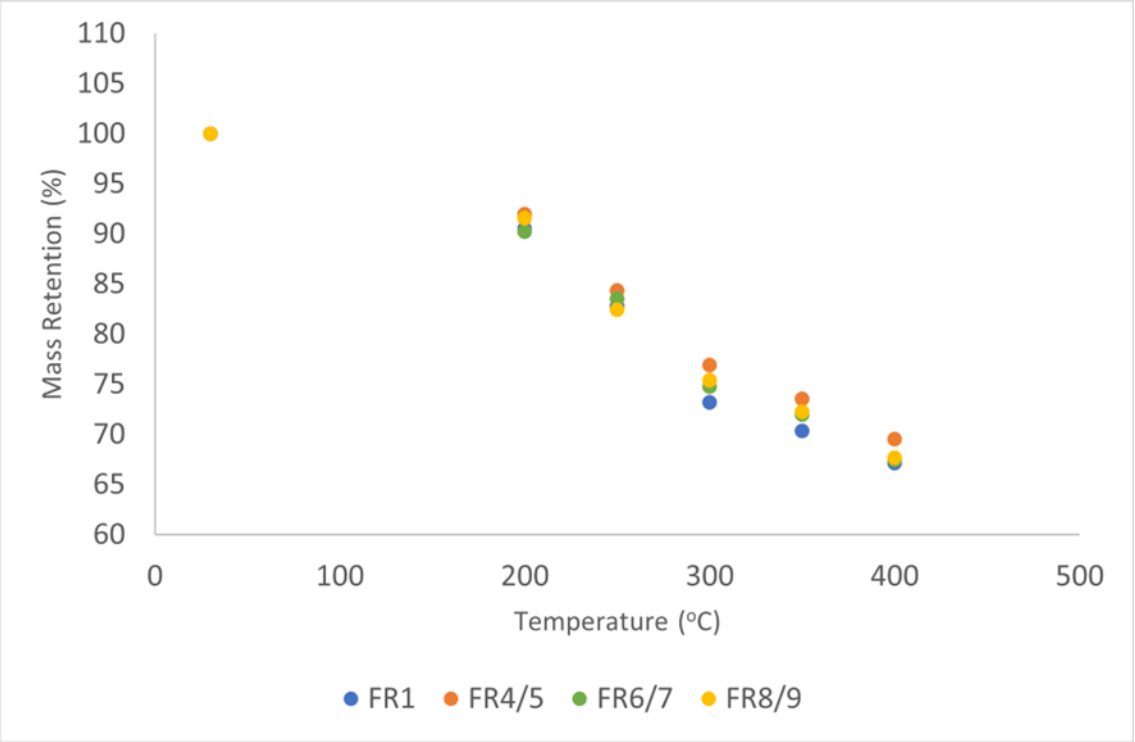

Figure 5.9 *Mass retention for foams containing alternative fire-retardant agents compared to standard fire-retardant system comprising triethyl phosphate and tris(1-chloro-2-isopropyl) phosphate.*

In aggregate, it can be seen that all three non-halogenated alternative fire-retardant agents exhibit increased mass retention at all temperatures from 300-400 °C, with foams containing ammonium polyphosphate having greater retained mass throughout (Figure 5.9).

Table 5.11 *Mean difference in retained mass (%) for alternative fire-retardant systems versus foams containing FR1 fire retardant system.*

	Fire retardant system	200°C	250°C	300°C	350°C	400°C
FR1	TEP+TCPP	1.0	1.0	1.0	1.0	1.0
FR4/5	TEP/TCPP + APP	1.5	1.6	3.7	3.2	2.4
FR6/7	TEP/TCPP + EG	-0.3	0.7	1.6	1.7	0.3
FR8/9	TEP/TCPP + VQ	1.1	-0.4	2.2	1.9	0.5

From the data in Table 5.11, it can be seen that all three alternative flame-retardant systems exhibit either very similar or slightly greater mass retention at all temperatures, with only marginally lower stability observed at two data points for FR6/7 and FR8/9.

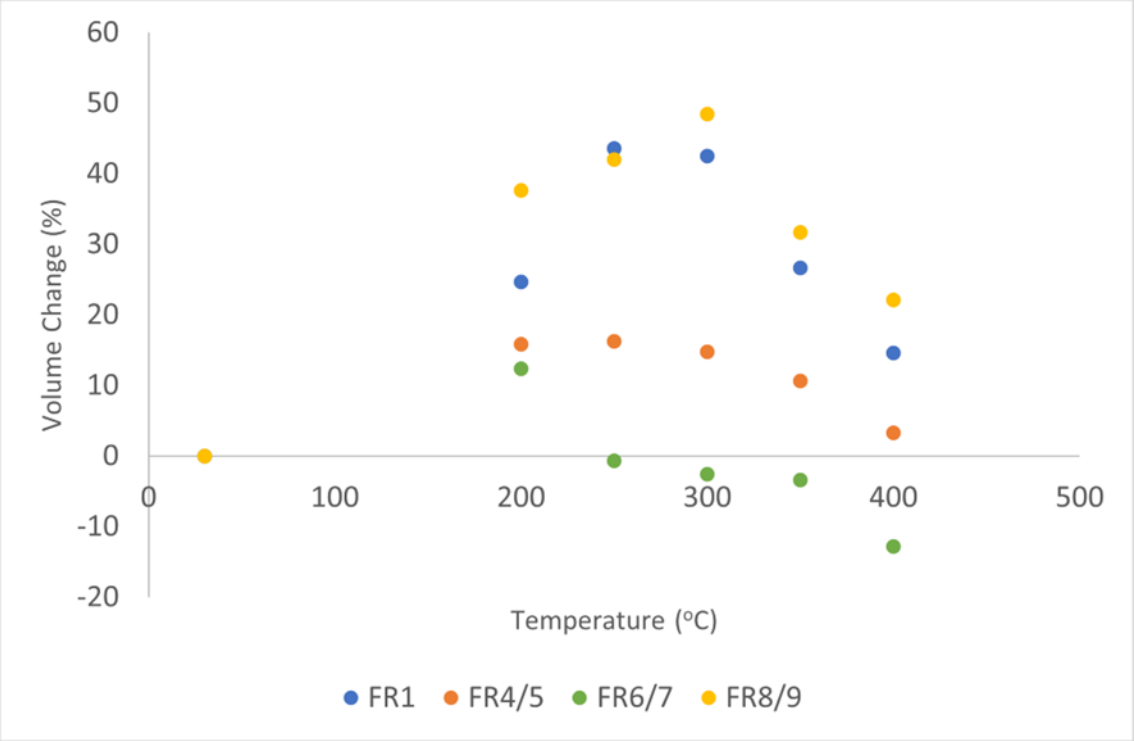

Figure 5.10 *Volume change for foams containing alternative fire-retardant agents compared to standard fire-retardant system comprising triethyl phosphate and tris(1-chloro-2-isopropyl) phosphate.*

The compared fire-retardant systems exhibit pronounced differences in dimensional stability (Figure 5.10), with FR1 and FR8/9 being associated with sustained volumetric expansion. This

expansion reaches a maximum of 42.1 % at 250 °C in the FR1 formulations and 48.5 % at 300°C in the FR8/9 formulations. At 200 °C, FR8/9 foams exhibit the largest expansion on average, with a 37.7 % increase in volume at this temperature compared to 24.7 % for FR1.

By contrast, a smaller expansion is observed for FR4/5, reaching a maximum of 16.3 % at 250 °C, falling back to just 3.3 % at 400 °C. FR6/7 exhibits volumetric expansion only at 200 °C (12.4 %) before shrinking below the initial volume, reaching a reduction of 12.9 % at 400 °C. In terms of absolute changes in volume, FR6/7 therefore demonstrates the greatest degree of dimensional stability.

The alternative fire-retardant agents integrated into these foams differ in their physical interaction with the foam matrix. Ammonium polyphosphate and expandable graphite are both additive flame retardants, which do not undergo reactions with 4,4-MDI and the polyol in the reaction mixture to become part of the polymer structure. However, ammonium polyphosphate does appear to exhibit some solubility in the reaction mixture, and homogenously disperses throughout the foam. In contrast, expandable graphite forms a visibly dispersed phase of macroscopic particles throughout the material. The presence of graphitic particles in and among the cell walls may increase their rigidity, and the rapid thermal expansion of the graphene monolayers at high temperature may disrupt the integrity of the cellular structure, limiting pressure-drive pyroplastic flow.

While the above comparisons indicate desirable performance for the alternative fire retardants, it is important to note that these comparisons include formulations containing these fire retardants in combination with the chlorinated fire-retardant TCPP. Therefore, a second comparison has been conducted, comparing the FR4, FR6 and FR8 fire-retardant systems alone against FR1.

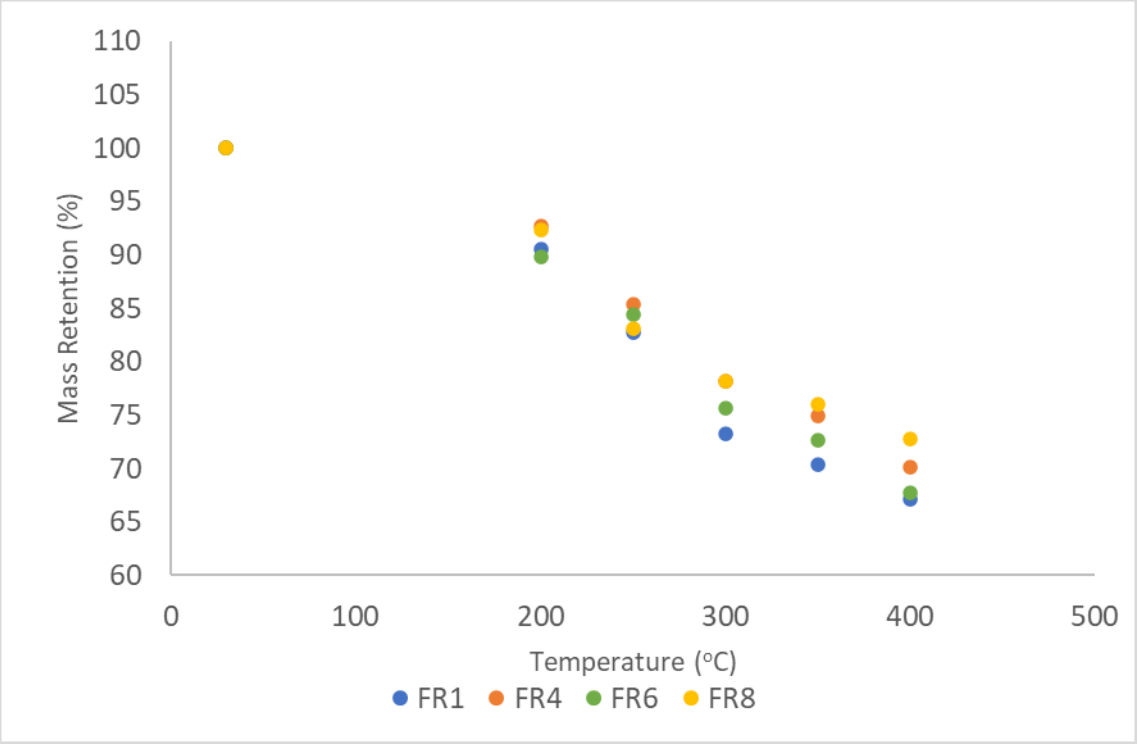

Figure 5.11 *Mass retention for foams containing alternative fire-retardant agents in combination with triethyl phosphate compared to standard fire-retardant system comprising triethyl phosphate and tris(1-chloro-2-isopropyl) phosphate.*

The omission of formulations containing FR5, FR7, and FR9 still demonstrates generally improved mass retention for formulations containing alternative fire retardant agents versus those containing FR1, with the exception of the slightly reduced stability of FR6 at 200 °C. When these formulations are included, those containing ammonium polyphosphate (FR4 and FR5) exhibit the highest stability throughout, but when considering FR4, FR6 and FR8 only, foams containing FR8 exhibit the highest stability at temperatures of 300 °C and above. This difference is most pronounced at 400 °C and this behaviour indicates a possible synergy between the reactive fire retardant VeriQuel R100 and TEP.

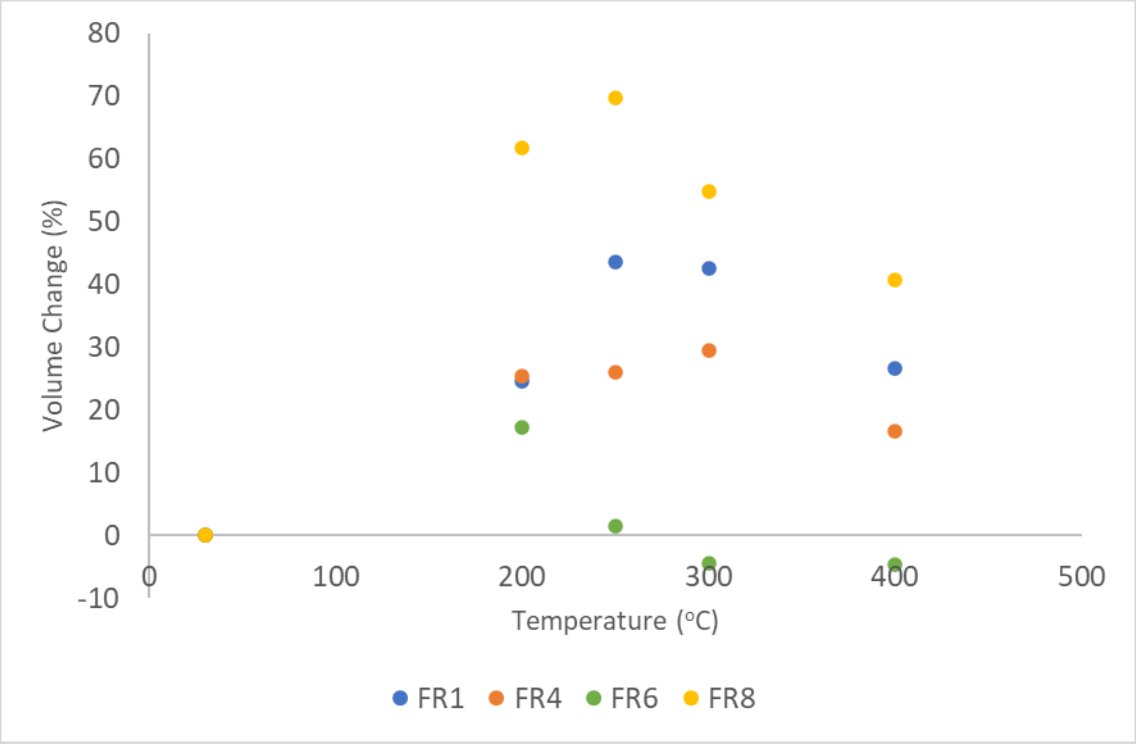

Figure 5.12 *Volume change for foams containing alternative fire-retardant agents in combination with triethyl phosphate compared to standard fire-retardant system comprising triethyl phosphate and tris(1-chloro-2-isopropyl) phosphate.*

Measured volumetric changes exhibit a similar pattern when omitting data for FR5, FR7 and FR9 (Figure 5.12). However, in this case, formulations containing FR8 exhibit substantially greater volumetric expansion than those containing FR1. The FR6 formulation, containing expandable graphite, again possesses the greatest dimensional stability, with a maximum expansion of 17.3 % at 200°C, decreasing to 1.4 % at 250 °C and a loss of volume of 4.4 % and 4.6 % at 350 °C and 400 °C, respectively. The formulation containing the FR4 fire retardant system shows an intermediate but relatively stable volumetric expansion between 16.6 % and 25.9 %.

Considered together, these results indicate an inverse relationship between dimensional stability and mass retention. Formulations containing VeriQuel exhibited the lowest mass loss values but underwent the highest degree of expansion. Conversely, expandable graphite exhibits only a small increase in mass retention compared to the standard fire-retardant system but has undergoes smaller dimensional changes than all other formulations, with a small *decrease* in volume observed above 300 °C. Ammonium polyphosphate was intermediate to

these formulations in both mass retention and dimensional stability, while performing better than the standard fire-retardant system in both measures.

These phenomena may be linked in an intumescent mechanism, whereby a combination of charring and gas production produces an expanded char layer on at the surface of the foam and inhibits transfer of heat to the interior of the material. However, this expansion may lead to deformation of structural members in the context of building panels during a fire. Such deformation may lead to loss of panel integrity or to the opening of gaps in panels allowing pyrolysis gases to escape into the fire compartment leading to flaring. There is therefore significant scope for future work investigating these effects *in situ* in larger scale fire tests using scaled-up model systems that were impracticable within the context of this thesis.

5.4 Chemical Changes in Foams by ATR-FTIR

Within this section, selected foam samples retained from furnace testing have been subjected to analysis using attenuated total reflectance-FTIR spectroscopy. This was intended to elucidate differences in spectral characteristics both before and during thermal degradation and to thereby gain a picture of the chemical changes induced in a range of foam formulations. This data has been used to correlate spectral changes with behaviour observed under heat treatment with a view to identifying key indicators associated with changes in mass.

The following formulations were selected for analysis:

- R1 (PS-2412, triethyl phosphate)
- P0 (PS-2602, no fire retardant)
- H0 (HT-2006, no fire retardant)
- P1 (PS-2602, triethyl phosphate, tris(1-chloro-2-isopropyl) phosphate)
- P2 (PS-2602, triethyl phosphate)
- P3 (PS-2602, tris(1-chloro-2-isopropyl) phosphate
- H1 (HT-2006, triethyl phosphate, tris(1-chloro-2-isopropyl) phosphate)
- P4 (PS-2602, triethyl phosphate, ammonium polyphosphate)
- P6 (PS-2602, triethyl phosphate, expandable graphite)

5.4.1 Spectral Comparisons of Unheated Foams

Firstly, a comparison for unheated foams has been carried out to characterise distinctive spectral features related to different polyols and flame-retardant systems using ATR-FTIR. The spectrum obtained for the R1 foam is presented in Figure 5.13 below.

In the 750-4000 cm^{-1} wavenumber range, a total of eleven significant peaks can be seen to be present. These peaks match closely with those previously observed in the spectrum obtained for line-produced foam of the same formulation (section 3.4, Figure 3.35). The spectrum is supplemented by Table 5.12, which gives the absorbance values and peak assignments for the peaks present in the spectrum.

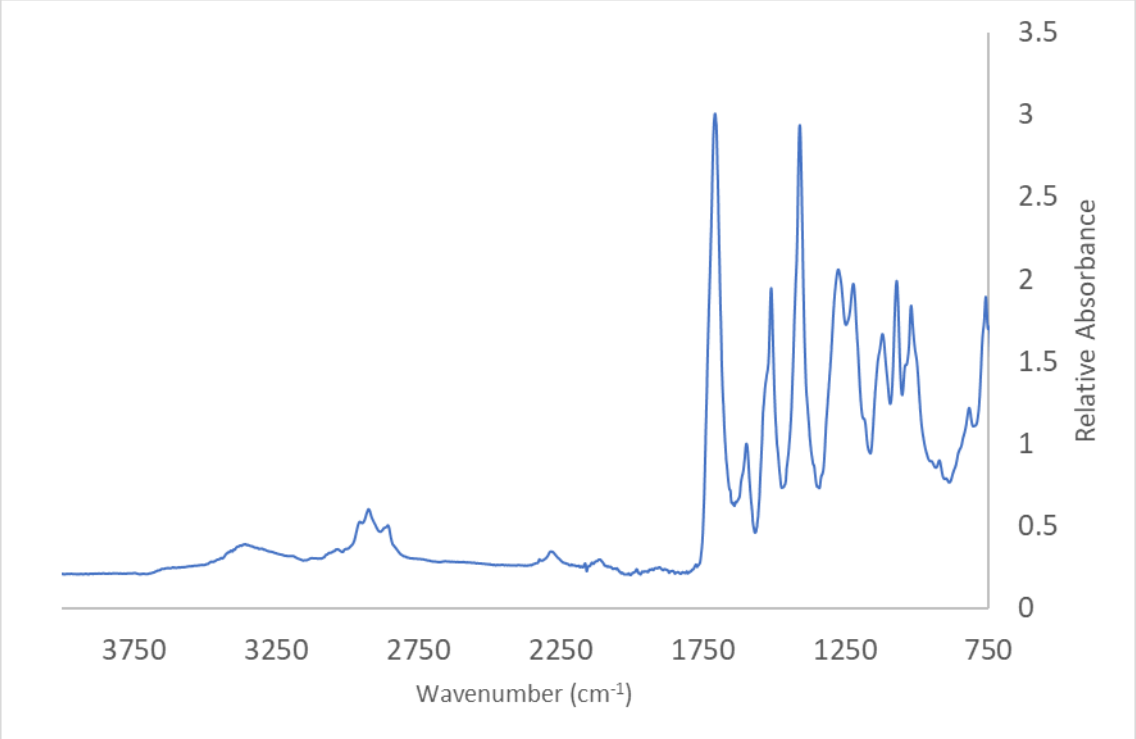

Figure 5.13 *ATR-FTIR spectrum of R1 foam from 4000-750cm^{-1}*

Table 5.12 *Peaks Appearing in the ATR-FTIR Spectrum of Virgin Polyisocyanurate Foam*

Wavenumber (cm^{-1})	**Abs**	**Vibration**	**Assignment**
3355	0.43	νN-H	Amide A
2956	0.54	νC-H	Pentane
1707	2.59	νC=O	Amide I Ester I
1597	1	δC=C	4,4-methylene diphenyl diisocyanate Phthalic anhydride
1510	1.72	δN-H νC-N	Amide II
1409	2.63	νC-N	Isocyanurate
1276	1.82	νC-C-O δC=O δN-H νC-N	Ester II Amide III
1222	1.76		
1119	1.51	νO-C-C	Ester III
1069	1.80	νC-O-C	Ether
1019	1.64	νP-O-C	TEP/TCPP

The two most prominent peaks are those assigned to νC=O, the carbonyl subgroup present within several key groups within the polymer structure, and νC-N, characteristic of the heterocyclic triazine ring within the isocyanurate group. The ratio of νC=O:νC-N peak intensities is 0.98, the amide II:νC-N ratio is 0.65 and the amide II:νC=O ratio is 0.66. These ratios are related to the relative abundance of urethane, disubstituted urea, and isocyanurate groups, within the polymer structure and changes in these ratios during thermal degradation are therefore indicative of the differing thermal stability of these groups.

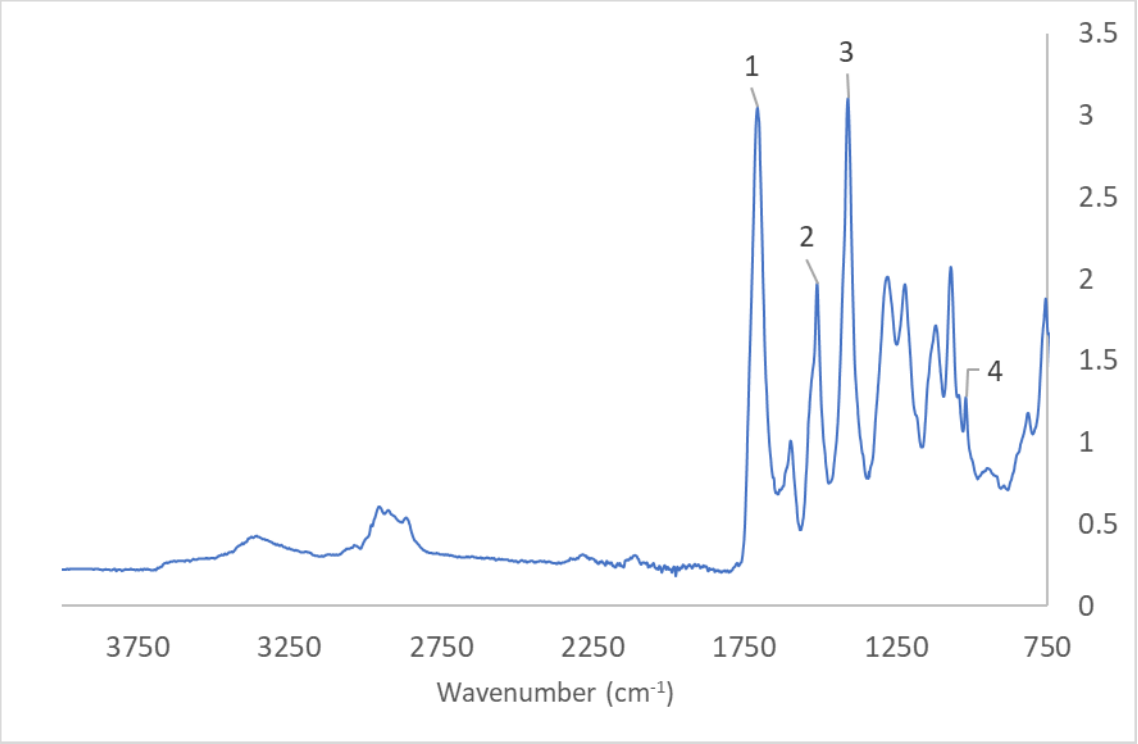

Figure 5.14 *ATR-FTIR spectrum of P0 foam from 4000-750cm^{-1}.*

The ATR-FTIR spectrum for P0 (Figure 5.14) appears to exhibit the same peaks as the R1 formulation. It is noted that the absorbance of the peak at 1020 cm^{-1} [4] is greatly reduced in comparison to the same peak in R1. This supports the assignment of this peak to the phosphoric ester associated with TEP and TCPP fire retardant which is absent from the P0 foam. The νC=O:νC-N [1:3] ratio is 0.99, the amide II:νC-N ratio [2:3] is 0.64 and the amide II:νC=O [2:1] ratio is 0.65. These ratios were generally very similar to those observed for R1, indicating strong similarities in relative abundance of the urethane, disubstituted urea, and isocyanurate groups within the polymer structure. This demonstrates that the addition of phosphorus-based fire retardants does not significantly influence the chemical composition of the polymer.

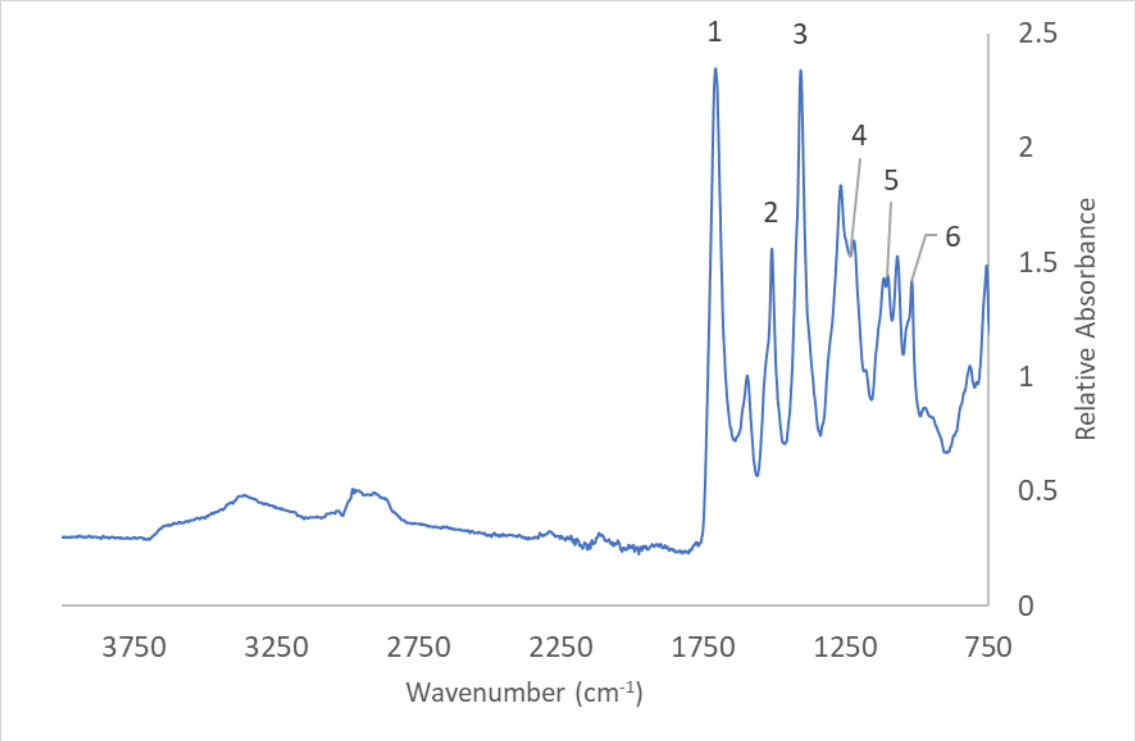

Figure 5.15 *ATR-FTIR spectrum for H0 foam from 4000-750cm^{-1}.*

The substitution of the PS-2602 polyol for HT-2006 produces some noticeable differences in the H0 infrared spectrum (Figure 5.15), notably in the region of wavenumber below 1300 cm^{-1}. The double peak in the 1220-1280 cm^{-1} range [4] associated with the ester II and amine III bands shows substantial asymmetry. The peak around 1120 cm^{-1} [5] is bifurcated at its tip, and the peak at 1020 cm^{-1} [6] is more intense. In the previous PS-2602 based formulations, this peak has been assigned to the phosphate ester of the fire retardants, as evidenced by its reduction upon their removal. Existing spectral data confirms the presence of a strong absorption at this wavenumber for TEP and TCPP phosphate. Its assignment in this case is uncertain, but this pattern appears to be characteristic of this polyol and may indicate the presence of some level of flame retardant in the polyol blend.

For H0 foams, the νC=O:νC-N [1:3] ratio is 1.00, the amide II:νC-N is 0.59 [2:3] and the amide II:νC=O [2:1] ratio is also 0.59. The latter two values are somewhat lower than those observed for R1 and P0 foams, possibly indicating a lower abundance of disubstituted urea groups.

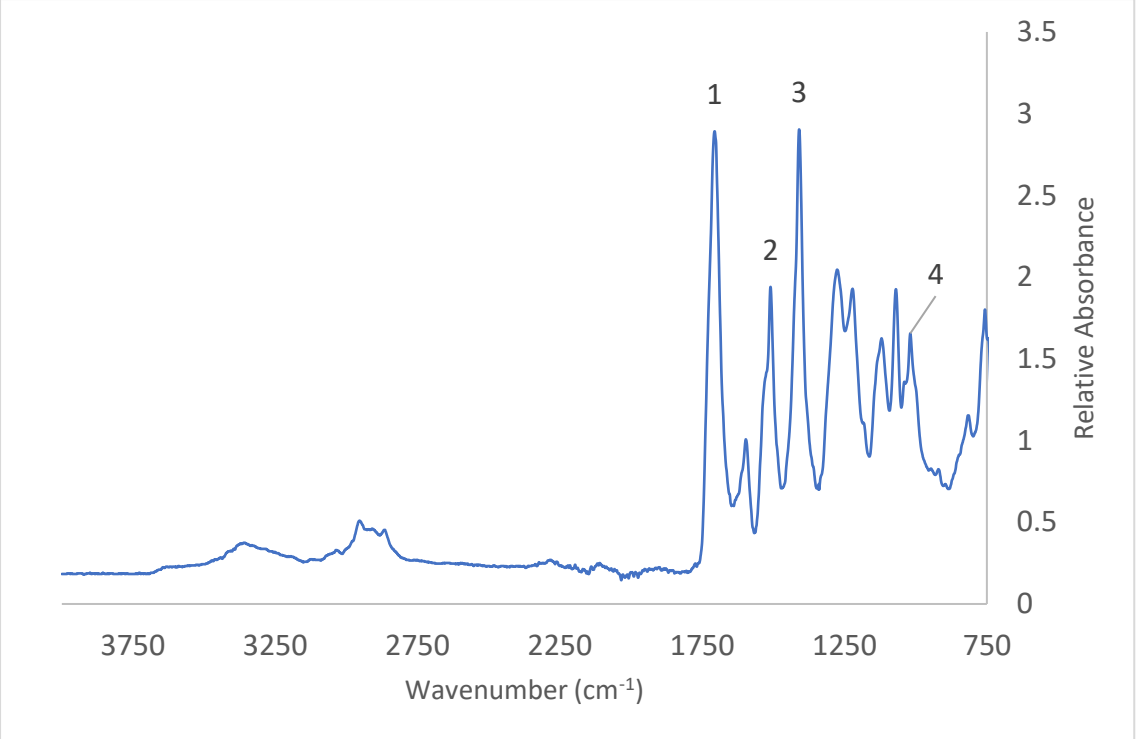

Figure 5.16 *ATR-FTIR spectrum for P1 foam from 4000-750cm^{-1}*

The P1 foam exhibits a very similar pattern of peaks to the R1 and P0 foams (Figure 5.16). The 1020 cm^{-1} peak [4] is somewhat smaller than that seen in R1, compatible with a lower loading of TCPP. The key peak ratios are 1.0, 0.67 and 0.67 for νC=O:νC=N [1:3], amide II:νC-N [2:3] and amide II:νC=O [2:1], respectively.

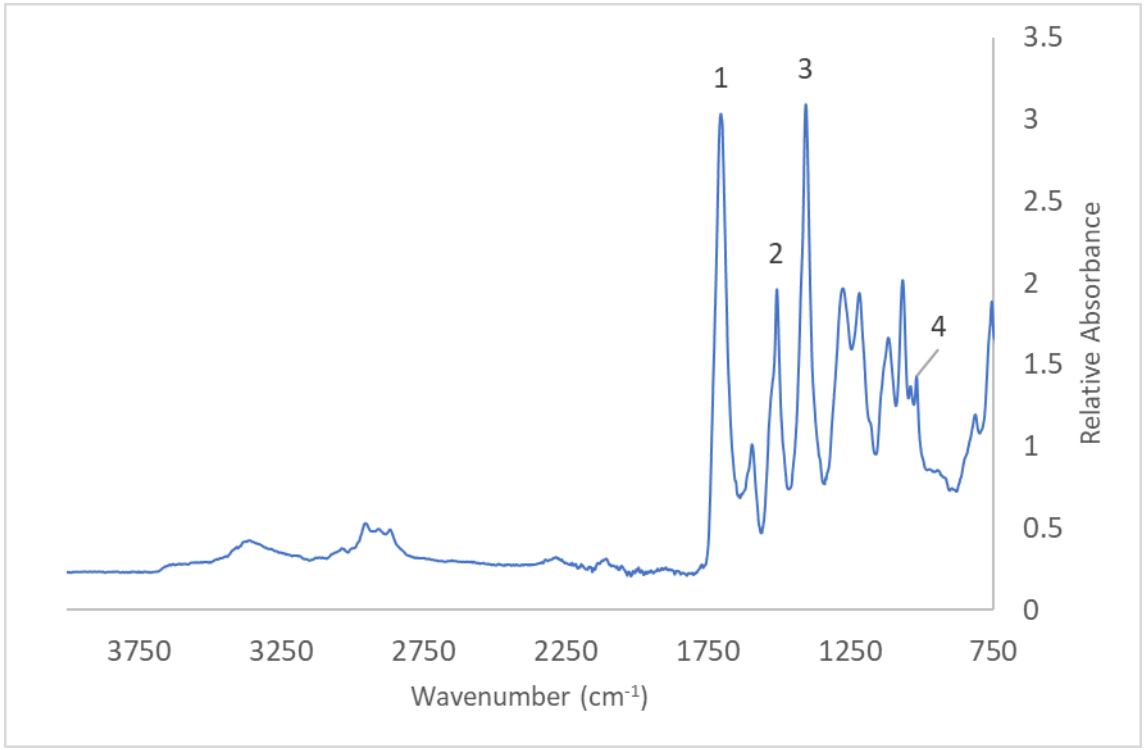

Figure 5.17 *ATR-FTIR spectrum for P2 foam from 4000-750cm^{-1}*

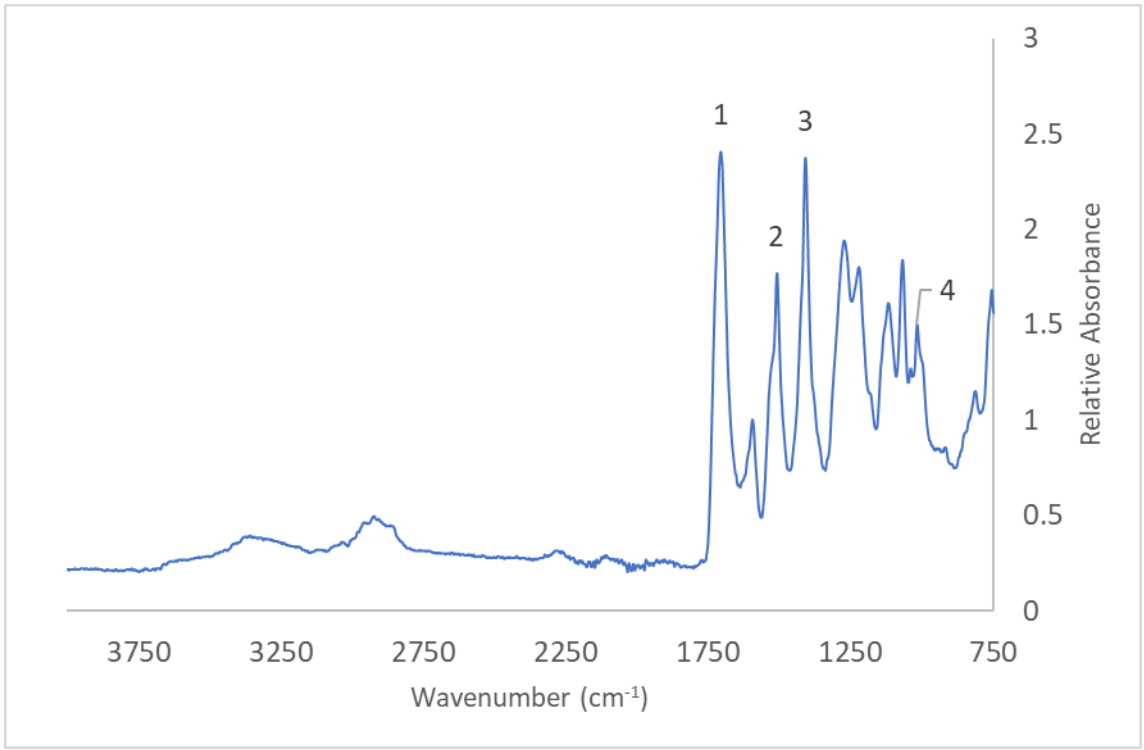

Figure 5.18 *ATR-FTIR spectrum for P3 foams from 4000-750^{o}C*

P2 and P3 foams (Figures 5.17, 5.18) are broadly consistent with previous PS-2602 foams. Peak intensities in the 1020 cm^{-1} band region [4] are intermediate between P0 and P1 and greater for P3 than P2, reflecting differences in the quantity of phosphates present from these fire-retardant systems.

The respective peak ratios for νC=O:νC-N [1:3], amide II:νC-N [2:3], and amide II:νC=O [2:1] are 0.98, 0.64 and 0.65 for P2 and 1.01, 0.65 and 0.64 for P3, respectively.

In totality, the spectral analysis of foams based around the currently employed fire retardants shows consistent spectral behaviour with the largest differences related to the choice of polyol. The following spectra have been obtained for foams containing ammonium polyphosphate, expandable graphite and VeriQuel R100.

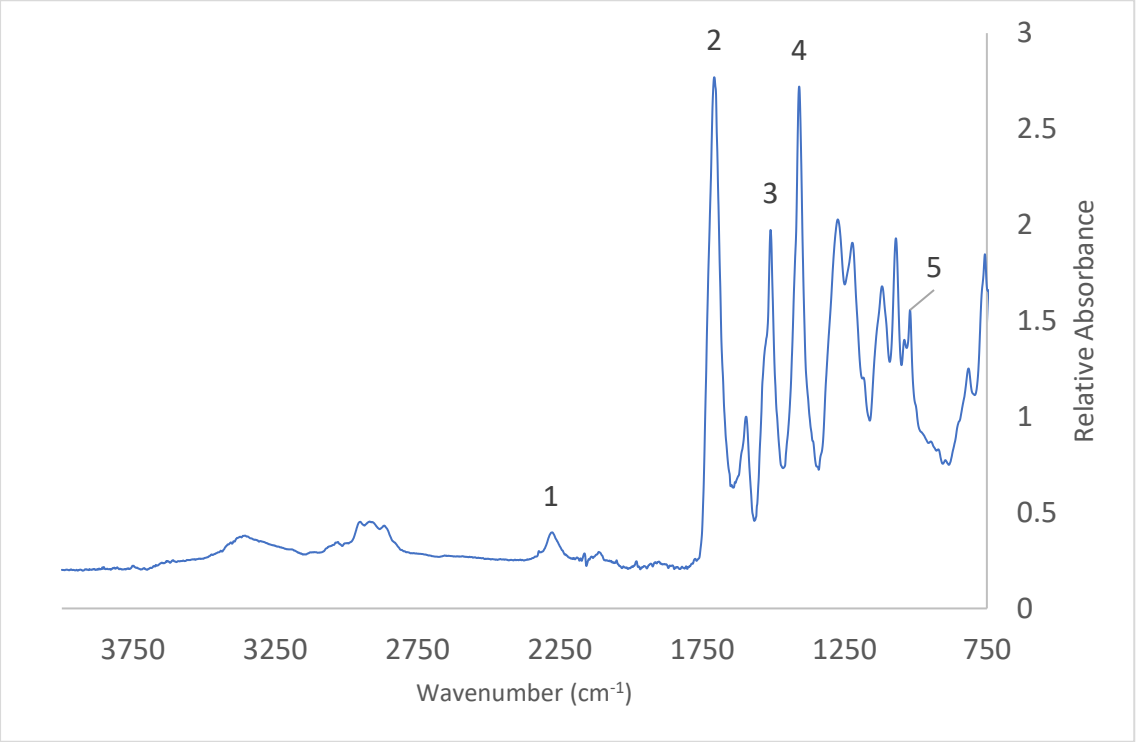

Figure 5.19 *ATR-FTIR spectrum for P4 foam from 4000-750cm^{-1}*

The obtained spectrum for the P4 foam containing ammonium polyphosphate (Figure 5.19) is generally similar to previous spectra in the range above 1750 cm^{-1}. A noted feature is the presence of a small, but distinctive peak at 2275 cm^{-1} [1]. This peak appears in a region of the spectrum which tends to exhibit a relative paucity of peaks and is characteristic of unreacted isocyanate (10). This is followed by a small peak at around 2115 cm^{-1} which possibly indicates the presence of carbodiimides (N=C=N) within the foam resulting from the reaction of

isocyanate groups. The phosphate peak at 1020 cm^{-1} [5] is relatively small. Ammonium polyphosphate, being an ionic compound, lacks the phosphate ester group that is deemed to be responsible for this peak, and therefore the peak represents only the TEP content of the polymer. The νC=O:νC-N [2:4], amide II:νC-N [3:4] and amide II:νC=O [3:2] ratios for this foam are 1.01, 0.69 and 0.68, respectively. These values are slightly higher than those obtained for conventional foams and suggest that the presence of ammonium polyphosphate during the foaming process may slightly increase the production of disubstituted ureas.

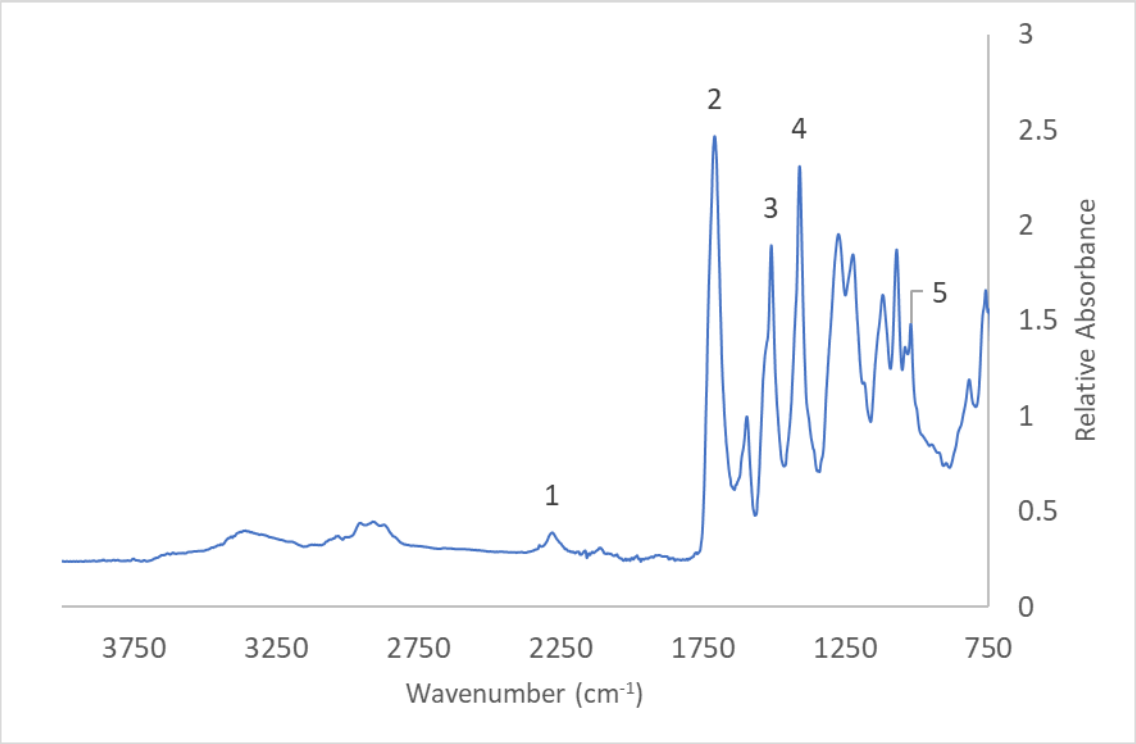

Figure 5.20 *ATR-FTIR spectrum for P6 foam.*

The addition of expandable graphite in the P6 foam (Figure 5.20) again results in the appearance of a distinctive isocyanate peak in the 2275 cm^{-1} band [1]. Also noted is a general reduction in relative absorbance versus the C=C reference peak at 1595 cm^{-1}. This has been confirmed on several repeat spectra. The νC=O:νC-N [2:4], amide II:νC-N [3:4], and amide II:νC=O [3:2] ratios are 1.03, 0.74 and 0.72, respectively. These values are highest among the formulations analysed here and are indicative of lower isocyanate conversion and a high relative abundance of disubstituted urea groups.

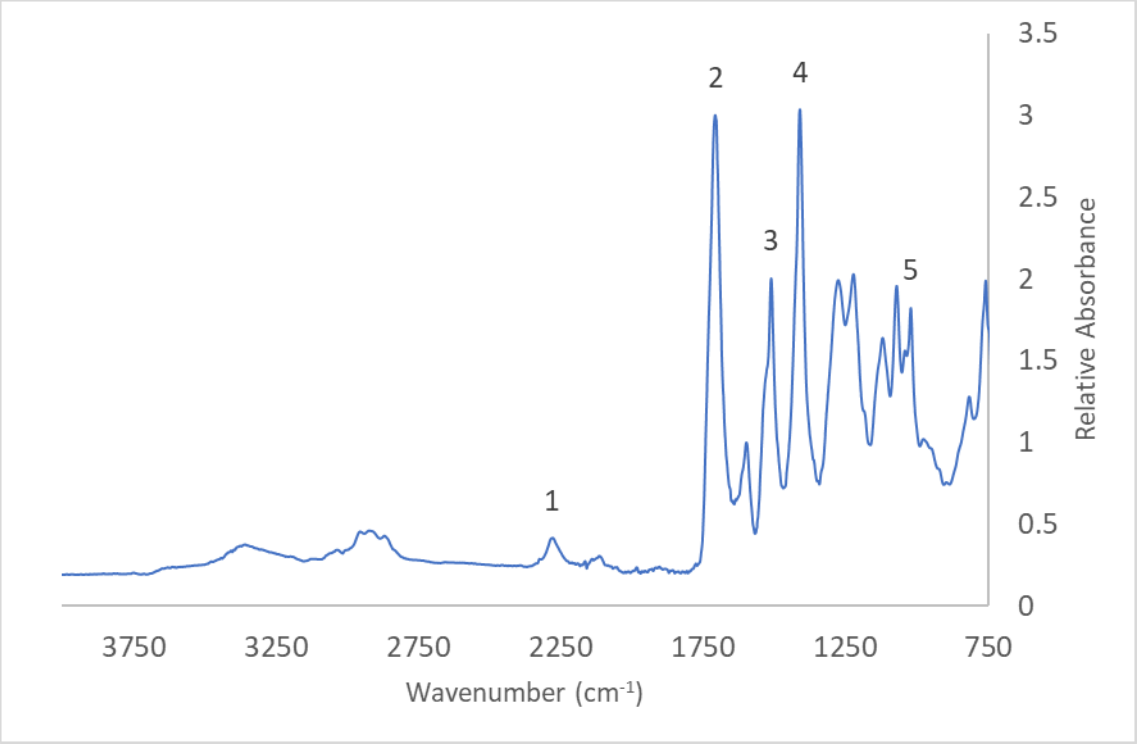

Figure 5.21 *ATR-FTIR spectrum for P8 foam*

In common with the F4 and F6 formulations, a prominent isocyanate peak is observed in the spectrum for F8 at 2275cm^{-1} [1]. The phosphate peak at 1020cm^{-1} [5] was larger here than for F4 and F6, likely reflecting the organic phosphate-rich nature of the VeriQuel R100 fire retardant. The νC=O:νC-N [2:4], amide II:νC-N [3:4], and amide II:νC=O [3:2] ratios are 0.99, 0.66 and 0.66, respectively. These ratios indicate a higher level of isocyanate conversion and lower disubstituted urea formation than the F4 and F6 formulations.

Looking across all these ATR-FTIR data, both ammonium polyphosphate and expandable graphite are solids of limited solubility, and their introduction to the reaction mix may physically interfere with the foaming and gelling processes involved in the production of PIR foams. Within the scope of this thesis, the influence of these additions on reaction characteristics has not been quantitatively characterised, and this provides significant scope for future work.

5.4.2 In-situ Characterisation of Thermal Polyisocyanurate Degradation by ATR-FTIR

Progressive changes in the ATR-FTIR spectra of PIR have previously been reported in the literature and replicated within this work (section 3.4, Figure 3.36). This is further expanded here by the application of this technique to a series of foam formulations, tracking the spectral changes throughout the course of thermal degradation. Each of the formulations tested in this

section were subjected to a heated programme wherein they were heated from ambient temperature to 400 ºC, with five-minute isothermal pauses at 200 ºC, 250 ºC, 300 ºC, 350 ºC, and 400 ºC. One sample was removed at the end of each isothermal pause and analysed using ATR-FTIR.

5.4.2.1 Polyisocyanurate P0

Spectra obtained for the P0 foam before heating and after heating to 200 ºC are reproduced below.

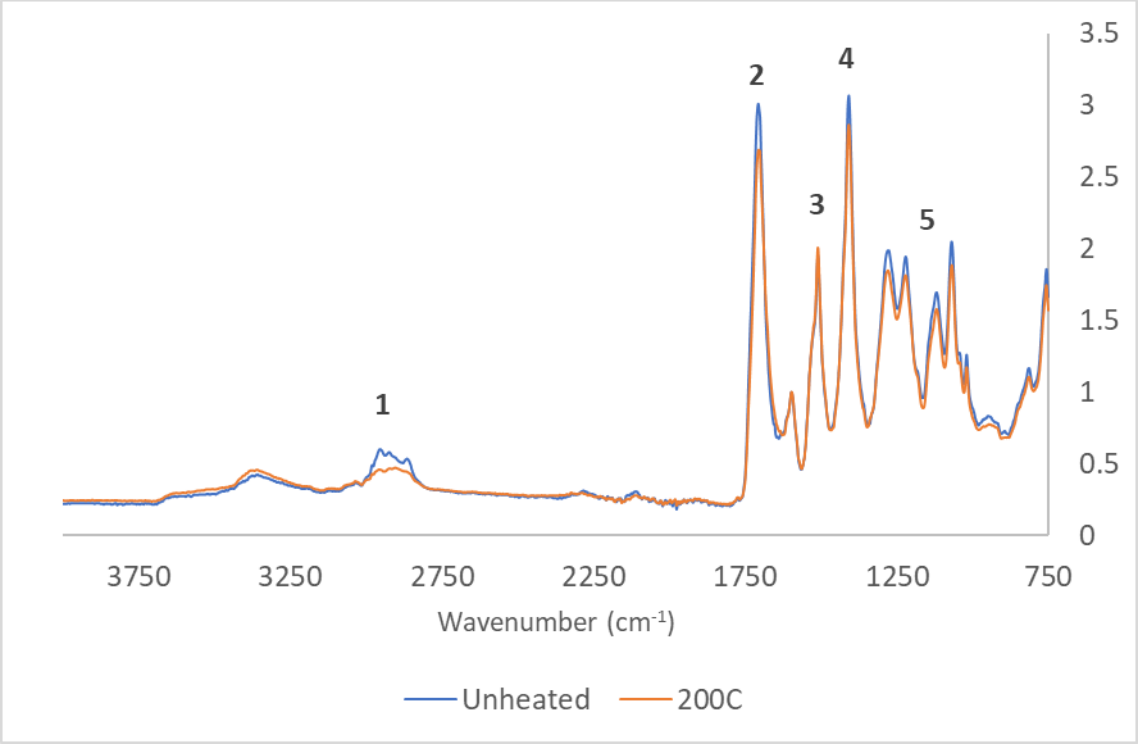

Figure 5.22. *Comparison of ATR-FTIR spectra obtained for unheated P0 foam and P0 foam after heating to 200 ºC.*

The positions of all major peaks were well preserved after heating to 200 ºC, although modest decreases in absorbance were apparent throughout. Moving right from the 4000 cm^{-1} end of the spectral range, the first substantial change was observed in the peak complex in the 3000-2850 cm^{-1} spectral band [1]. In the unheated foam, a maximum relative absorbance of 0.60 was seen at 2954 cm^{-1}. After heating to 200 ºC, this absorbance decreased to 0.47 at 2904 cm^{-1}. Absorbances in this region are characteristic of the C-H stretching vibration of alkanes. This decrease is therefore likely the result of an outgassing of pentane isomers from the foam.

In the 1750-1400 cm^{-1} range, the carbonyl C=O peak [2] decreased in absorbance from 3.00 in the unheated foam to 2.69 after heating to 200 ºC. The position of the peak underwent a small

shift from 1707cm^{-1} to 1706cm^{-1}. Similarly, the relative absorbance of the isocyanurate C-N peak [4] at 1408cm^{-1} decreased from 3.07 to 2.86. This resulted in a decrease of the νC=O:νC-N ratio from 1.00 to 0.94. Meanwhile, absorbance at the amide II peak [3] underwent a small increase from 1.95 to 2.01. As a result, a corresponding increase occurred in the amide II:νC=O ratio (0.65 to 0.74) and amide II:νC-N ratio (0.64 to 0.70). These changes are compatible with some dissociation of urethane bonds through the primary and secondary amine-forming pathways(11,12). This likely affects the polyurethane hard segments where the urethane bonds flank low molecular weight diol chain extenders and are more vulnerable to thermal degradation. At lower wavenumbers, a general and largely proportional reduction was noted in the remaining peaks [5].

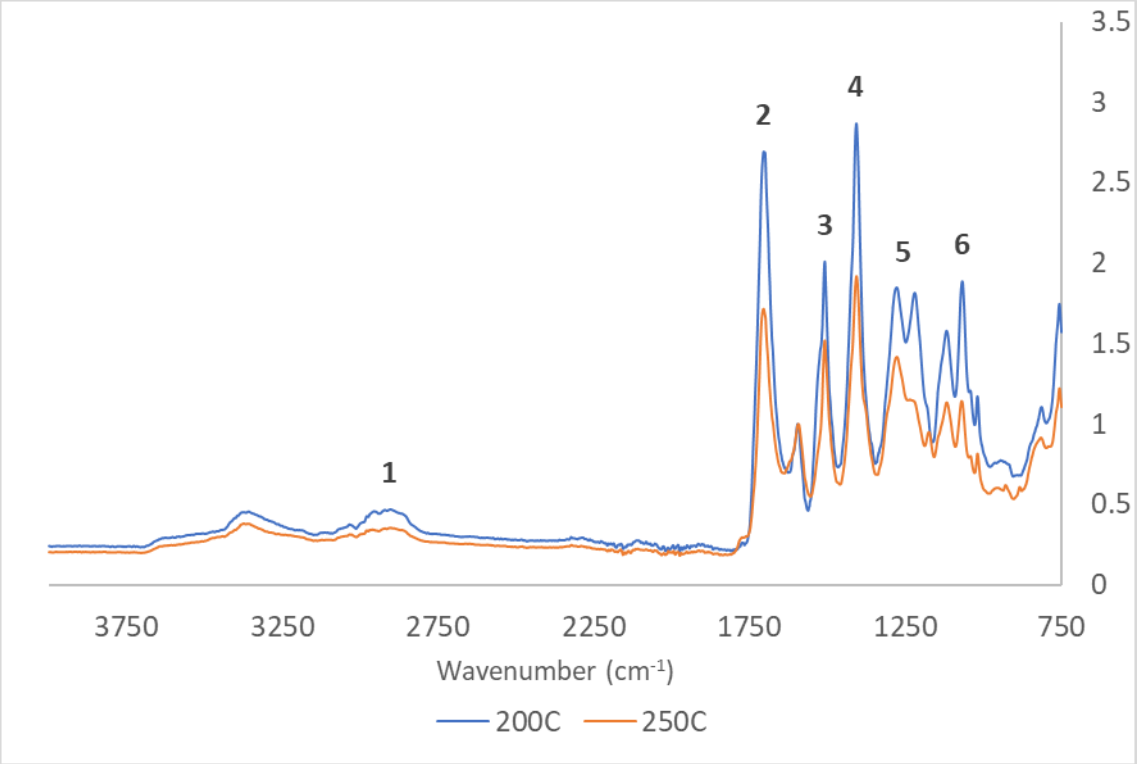

Figure 5.23 *Comparison of ATR-FTIR spectra obtained for P0 foam after heating to 200°C and 250°C.*

Larger changes were observed when comparing foams that had been heated to 200°C with those heated to 250°C (Figure 5.23). A further decrease in absorbance was observed in the alkane C-H peak complex [1], indicating continued loss of blowing agent. At wavenumbers below 1750 cm^{-1}, there was a general decrease in relative absorbance at all significant peaks except for the aromatic C=C reference peak. Absorbance at the 1706 cm^{-1} νC=O peak [2] decreased from 2.69 to 1.71, at the 1510 cm^{-1} amide II peak [3] from 2.01 to 1.52, and at the 1408cm^{-1} isocyanurate νC-N peak [4] from 2.86 to 1.92. νC=O:νC-N ratio decreased from 0.94 to 0.89 while amide II:νC=O ratio increased from 0.74 to 0.88 and amide II:νC-N ratio from 0.70 to 0.79.

The twinned peak in the 1300-1200 cm^{-1} [5] band underwent a substantial change in shape. Where this had consisted of two peaks of near equal intensity at 200 °C, there was a marked reduction at 250 °C in the lower wavenumber peak around 1220 cm^{-1}. This peak is part of the ester triad, corresponding to the C-C-O stretch. Its reduction here appears to be indicative of degradation occurring within the polyester polyol. Further evidence for this is provided by the reduction in other parts of the triad, both the νC=O peak and the O-C-C stretch at 1070cm^{-1}

[6]. There appears to be a general shift towards a structure more dominated by amide groups and aromatic structures at this temperature.

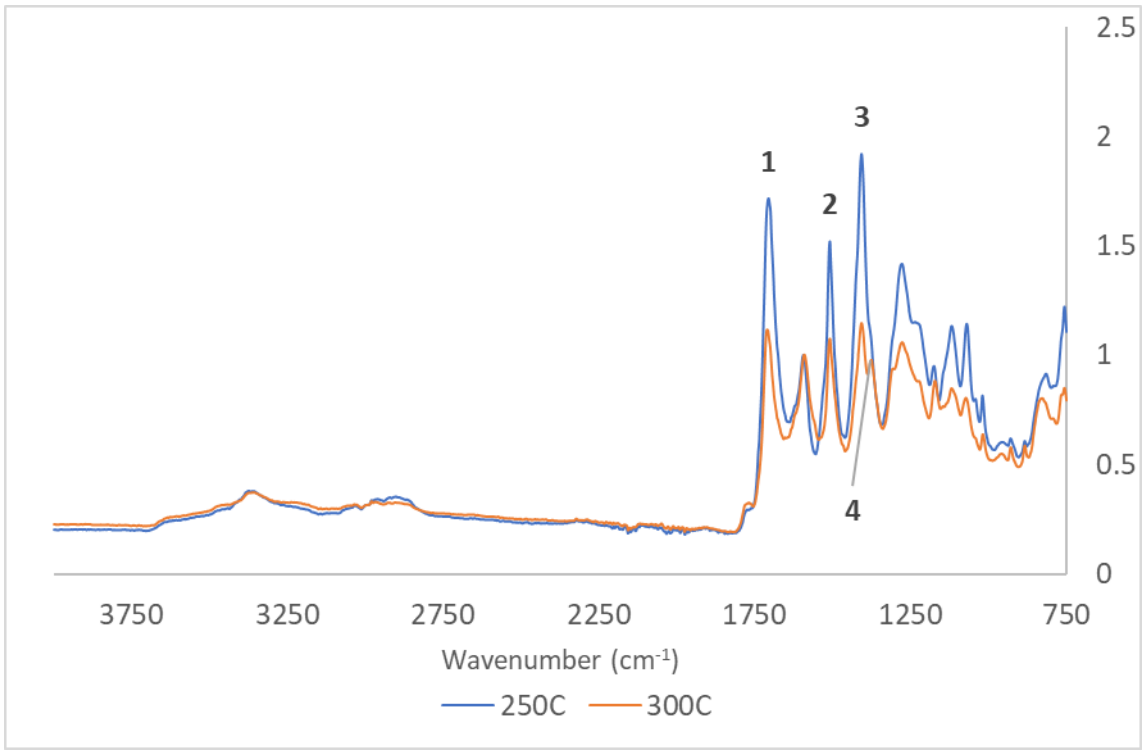

Figure 5.24 *Comparison of ATR-FTIR spectra obtained for P0 foam after heating to 250°C and 300°C.*

A continued global decrease in relative absorbance against the aromatic C=C peak was apparent when final heating temperature increased from 250 °C to 300 °C (Figure 5.24). Relative absorbance values at the νC=O [1], amide II [2], and νC-N [3] peaks were 1.11, 1.07 and 1.14 respectively, corresponding to a νC=O:νC-N ratio of 0.97, amide II:νC=O ratio of 0.96 and amide II:νC-N ratio of 0.94.

A notable feature of the absorption spectrum obtained at 300 °C was the emergence of a distinct peak just to the right of the 1408 cm^{-1} isocyanurate peak at 1375 cm^{-1} [4]. This peak is typically assigned to symmetric deformations of $-CH_2/-CH_3$ groups. The emergence of this peak is barely perceptible as a weak shoulder in the 250 °C spectrum. It is possible that this peak has become visible due to the diminution of the isocyanurate νC-N peak which had previously obscured other peaks in this spectral region.

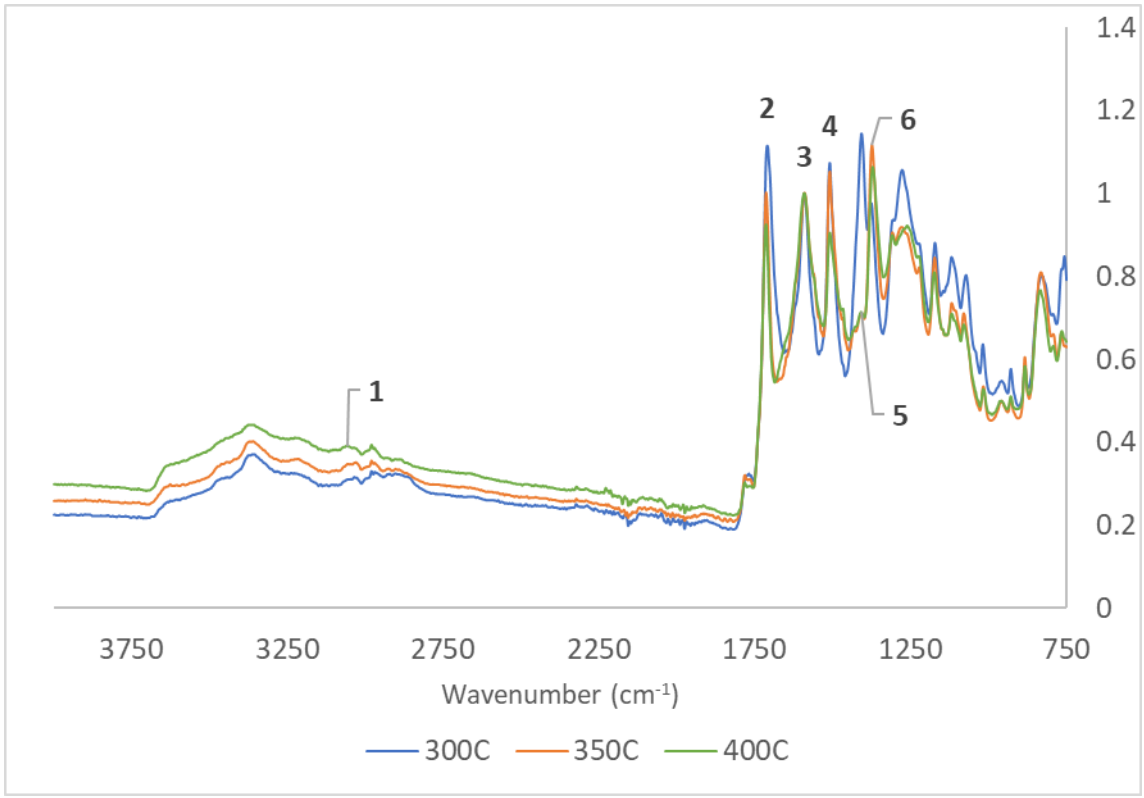

Figure 5.25 *Comparison of ATR-FTIR spectra obtained for P0 foam after heating to 300 °C, 350 °C and 400 °C.*

As the final heating temperature increased from 300 °C to 350 °C and 400 °C, comparative spectra (Figure 5.25) indicate a general enrichment of aromatic groups compared to other functional groups, evident from the decreased absorbance of peaks [2] and [4] relative to the aromatic reference peak [3]. In contrast to general patterns observed at lower temperatures, there was an apparent progressive increase in absorbance in the 'single-bond' region (4000-2500 cm^{-1}) of the spectral range [1]. O-H and N-H stretching may have increased due to the re-emergence of terminal hydroxyl and amine groups resulting from depolymerisation. Furthermore, the dissociation of urethanes to primary amines and the oxidation of C-C bonds also produces alkenes which produce a C-H stretching vibration around 3100-3000 cm^{-1}. Alkenes may also be formed due to the process such as dehydroxylation.

A prominent νC=O [2] peak remained visible throughout, but progressively decreased in absorbance (1.11 at 300 °C, 1.00 at 350 °C, and 0.93 at 400 °C). This peak also exhibited a gradual shift upward in wavenumber from 1711 cm^{-1} at 300 °C to 1714 cm^{-1} at 350 °C to 1715 cm^{-1} at 400 °C. The carbonyl group is a common to a range of functional groups and the position of the carbonyl νC=O peak is therefore dependent upon the prevalence of different

carbonyl-containing groups within the polymer. There was a continued decrease in absorbance at the amide II peak (1.07 at 300 ºC, 1.05 at 350 ºC, and 0.90 at 400 ºC).

At 350 ºC and above, there was a marked, almost complete disappearance of a distinct 1408 cm^{-1} isocyanurate νC-N peak [5]. Absorbance at this wavenumber was 0.71 at both 350 ºC and 400 ºC, but this appeared as a vestigial peak almost obscured by neighbouring features. Absorbance initially increased at 1375 cm^{-1} from 0.98 at 300 ºC to 1.12 at 350 ºC then decreasing to 1.06 at 400 ºC [6]. A possible source of this increase is the general decomposition of the residual material leading to the loss of functional groups such as hydroxyl and carboxyl groups and a resultant increase in terminal methyl groups.

In summary, these spectra indicate an overall pattern of behaviour in the P0 foam in which thermal degradation at temperatures up to 200 ºC consists largely of the physical loss of blowing agent from the foam, along with limited breakdown of urethane bonds. The stable absorption at the amide II peak suggests that cleaved urethanes undergo secondary reactions to form new disubstituted urea groups via a possible carbodiimide intermediate (13).

Larger changes occurred at higher temperatures starting at 250 ºC, with apparently extensive breakdown of both remaining urethane groups and subsequently formed substituted ureas. The decreased absorption at peaks in the ester triad also suggests that depolymerisation occurred at phthalic acid-diethylene glycol linkages within the polyurethane soft segments.

Above 300 ºC, the material exhibited clear signs of isocyanurate dissociation, which appeared to reach an endpoint at 350 ºC, as there was no further decrease in absorption at the 1408 cm^{-1} peak above this temperature.

5.4.2.2 Polyisocyanurate P1

In contrast to the P0 formulation, PIR P1 contains a standard fire-retardant system of system of TCPP and TEP at respective loadings of 5.5 % and 2 %. Comparative spectra for the unheated foam and following heating to 200 ºC are shown in Figure 5.26

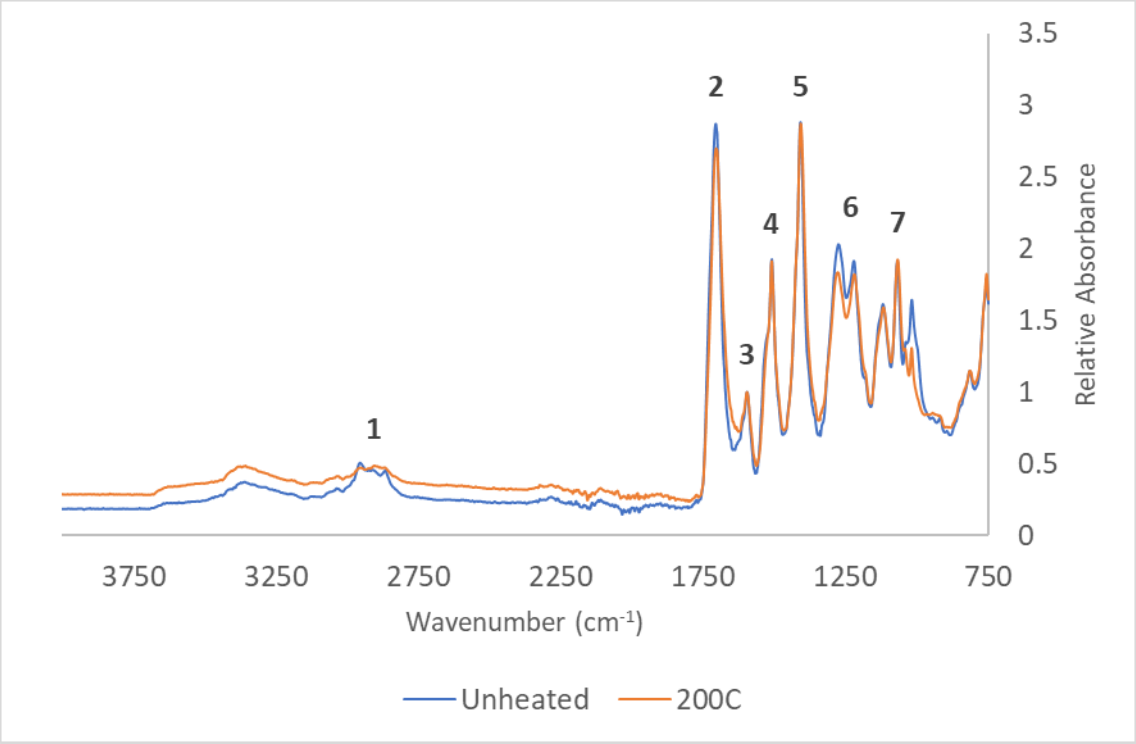

Figure 5.26 *Comparison of ATR-FTIR spectra obtained for unheated P1 foam and P1 foam after heating to 200 °C.*

After heating to 200 °C, spectral changes were generally modest throughout most of the spectral range. A generally increased absorbance was noted across the single-bond region (4000-2500 cm^{-1}) although the C-H peak complex appeared relatively less prominent [1].

The four peaks [2-5] in the 1800-1350 cm^{-1} band were generally well-preserved in position and absorbance after heating to 200 °C when compared to the unheated foam, with the most notable feature being a decrease in absorbance at the νC=O peak [2] from 2.87 to 2.70. Absorbance at the amide II peak [4] at 1510 cm^{-1} was almost unchanged with values of 1.93 and 1.91 in the unheated and 200°C samples, respectively. A similarly small change, from 2.88 to 2.87 was noted at the isocyanurate νC-N peak [5]. Taken together, these values produced a decrease in the νC=O:νC-N ratio of 1.00 to 0.94 and an increase in the amide II:νC=O ratio from 0.67 to 0.73. The amide II:νC-N ratio increased from 0.67 to 0.69. These changes are again suggestive of some degree of urethane degradation with secondary conversion to substituted ureas.

An asymmetric decrease was seen in twinned peak in the 1300-1200 cm^{-1} band [6], with a greater decrease at the left-hand peak (1277cm^{-1}) than at the right-hand peak (1222 cm^{-1}). The triple peak in the 1100-1000 cm^{-1} band [7] was unchanged for the leftmost and central peak,

but a sharp decrease occurred at the rightmost peak which has herein been associated primarily with the phosphate ester groups in the fire retardants.

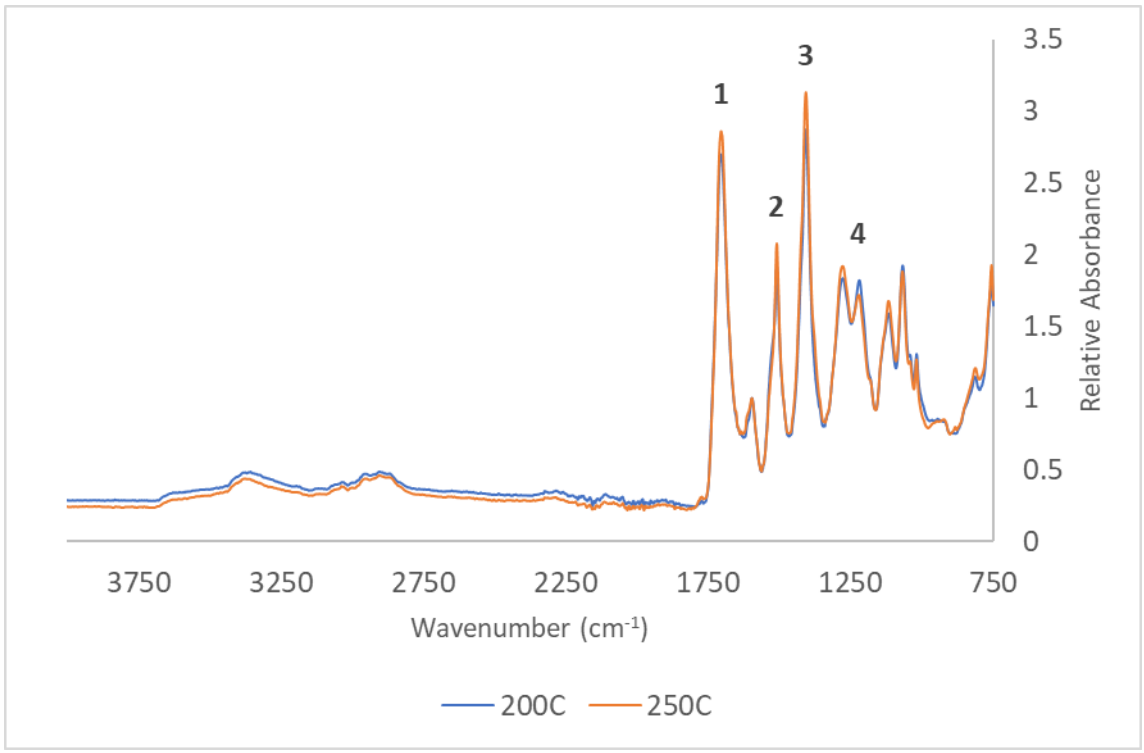

Figure 5.27 *Comparison of ATR-FTIR spectra obtained for P1 foam after heating to 200 °C and 250 °C.*

The FTIR spectrum obtained at 250 °C was generally similar to that obtained at 200 °C. This contrasts with the same temperature comparison carried out for P0 foams, where substantial changes occurred over the same increase in final heating temperature.

Notably, relative absorbance was seen to increase for the νC=O peak [1] (2.70 to 2.86), the amide II peak [2] (1.91 to 2.08), and at the isocyanurate νC-N peak [3] (2.87 to 3.13). Changes were calculated for the νC=O:νC-N ratio (0.94 to 0.91) and amide II:νC-N ratio (0.69 to 0.66), while the amide II:νC=O ratio was effectively unchanged. In spite of the general increase in relative absorbance of these three peaks, the changes in peak ratio still suggest a degradation of urethane and disubstituted urea groups with greater sparing of the isocyanurate structures.

In the 1300-1200 cm^{-1}, an asymmetric change occurred in the double peak [4], with an increase in absorbance at 1277 cm^{-1} and a decrease in absorbance at 1222 cm^{-1}, likely indicating an onset of soft segment degradation within the polyester polyol.

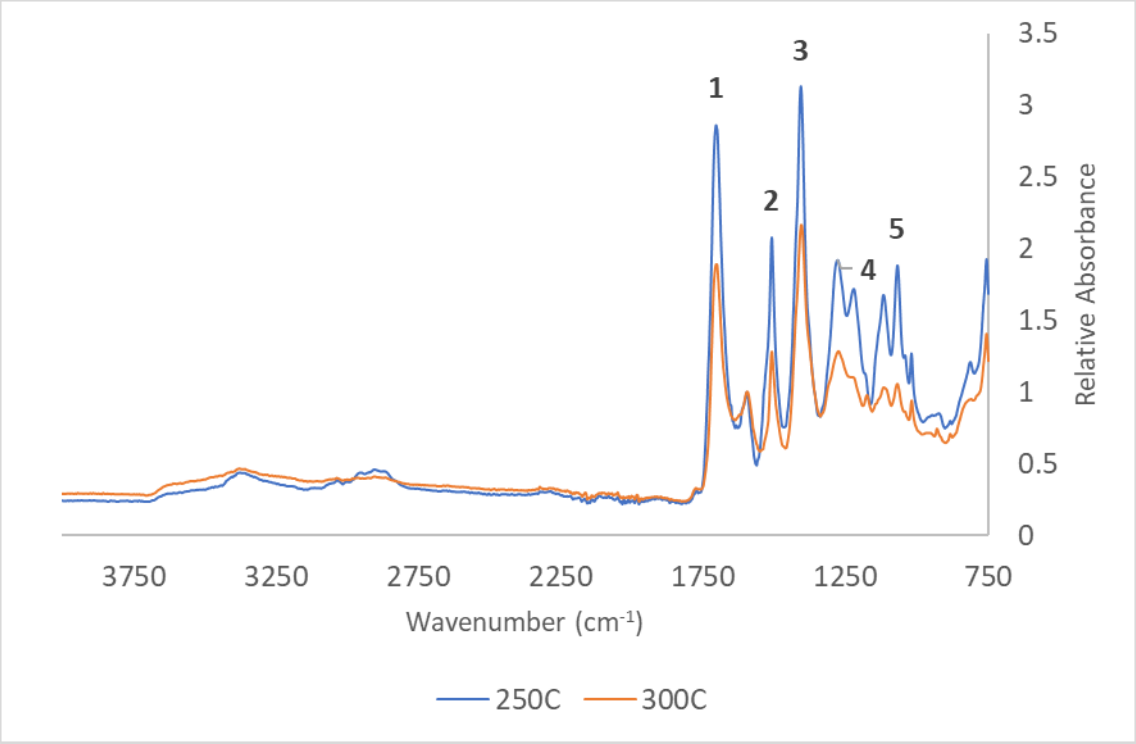

Figure 5.28 *Comparison of ATR-FTIR spectra obtained for P1 foam after heating to 250°C and 300°C*

As the final heating temperature increased from 250 °C to 300 °C, more substantial changes were observed in the obtained spectra (Figure 5.28). These changes are similar to those seen in the P0 foams across the 200 °C to 250 °C interval (Figure 5.23) but occur within a higher temperature range for the P1 sample. Aside from the fixed reference peak, absorbance decreased at all significant peaks in the region below 1800 cm^{-1}. A decrease from 2.86 to 1.89 was recorded for the νC=O peak [1], 2.08 to 1.28 at the amide II peak [2], and 3.13 to 2.16 at the isocyanurate νC-N peak [3].

As a result of the observed changes in absorbance, νC=O:νC-N ratio decreased from 0.91 to 0.86, while the amide II:νC=O ratio increased from 0.66 to 0.68. Amide II:νC-N ratio decreased substantially from 0.66 to 0.59.

At lower wavenumbers, obvious decreases occurred at the double peak in the 1300-1200 cm^{-1} band [4], with a larger decrease at the right-hand peak, and at the triple peak in the 1100-1000 cm^{-1} band [5].

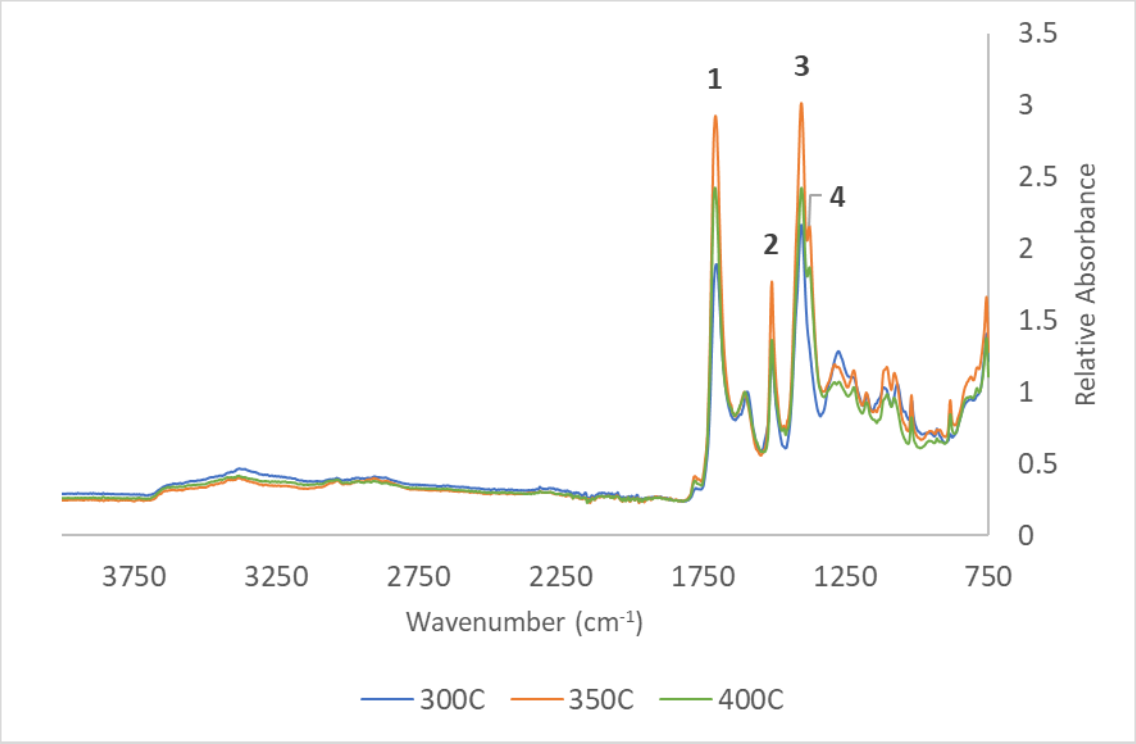

Figure 5.29 *Comparison of ATR-FTIR spectra obtained for P1 foam after heating to 300°C, 350°C and 400°C.*

At a final temperature of 350 °C, absorbance again increased at the key νC=O (1.88 to 2.93), amide II (1.28 to 1.78), and νC-N (2.16 to 3.01) peaks. These values correspond to a νC=O:νC-N ratio of 0.99, amide II:νC=O ratio of 0.61, and amide II:νC-N ratio of 0.59. These changes are compatible with a relatively greater degradation of amide and isocyanurate groups compared with carbonyl groups in the 300-350 °C temperature range. A shift in the position of the νC=O peak from 1704 to 1707 cm^{-1} may be attributed to the loss of amide groups, as the carbonyl substituent of these groups tends to absorb at a low wavenumber than that present in esters and carboxylic acids. As was the case for the P0 samples, a new peak emerged at 1378 cm^{-1} at 350 °C and remained present at 400 °C.

The increase from 350 °C to 400 °C was marked by another decrease in absorbance at the key peaks. A decrease from 2.93 to 2.43 occurred at the νC=O peak, accompanied by a further peak shift from 1707 cm^{-1} to 1709 cm^{-1}. Absorbance at the amide II peak decreased from 1.78 to 1.36 and at the νC-N peak from 3.01 to 2.43. νC=O:νC-N ratio was 1.00, while amide II:νC=O and amide II:νC-N ratios were both 0.56.

Taken in their entirety, the spectral data presented indicate and overall pattern of behaviour in which changes occurring during heating to 200 °C are again limited to the outgassing of

blowing agent, a small loss of carbonyl groups, likely through the degradation of less thermally stable urethane groups and what appeared to be some decomposition of the fire retardant.

Between 200 ^{o}C and 250 ^{o}C, spectral features were well preserved, but changes in peak ratio suggest a relative enrichment of isocyanurates within the structure as degradation is concentrated within the linear polyurethane domains.

Changes observed on increasing the heating temperature from 250 ^{o}C to 300 ^{o}C suggest more extensive thermolytic degradation, although peak absorbances were still generally higher than at the same temperature in the P0 foam, suggesting greater overall thermal stability under oxidative conditions when the dual-agent fire retardant system consisting of TCPP and TEP was present. These results are in agreement with the thermogravimetric data obtained under nitrogenous atmospheres, where it was found that bare PIR exhibited a maximum rate of mass loss at temperatures below 300 ^{o}C while those containing this fire-retardant system did not exhibit the same until an approximate temperature of 335 ^{o}C.

Of particular note was the preservation of a strong νC-N peak at all temperatures in the P1 foam, while this peak was almost entirely lost as a distinct spectral feature by 350 ^{o}C in the P0 foam. This demonstrated an ability of the fire-retardant system to significantly delay total degradation of isocyanurate groups.

Taken as points of comparison, the P0 and P1 ATR-FTIR data presented here provide reference points for the effectiveness of a fire-retardant system for modifying the thermal degradation of PIR foams. An extensive analysis of the data has been provided for this purpose. In the remainder of this section, data for other formulations will be presented in a more concise format, to highlight differences in the relative effectiveness of other fire-retardant systems, and therefore the viability of these as alternatives to the TCPP and TEP system.

5.4.2.3 Polyisocyanurate P2

PIR P2 was based on the PS-2602 polyester polyol and contained a single-agent fire-retardant system of TEP. Spectral data is presented in Figures 5.29-5.32 below, in the same comparative format as for sample sets P0 and P1.

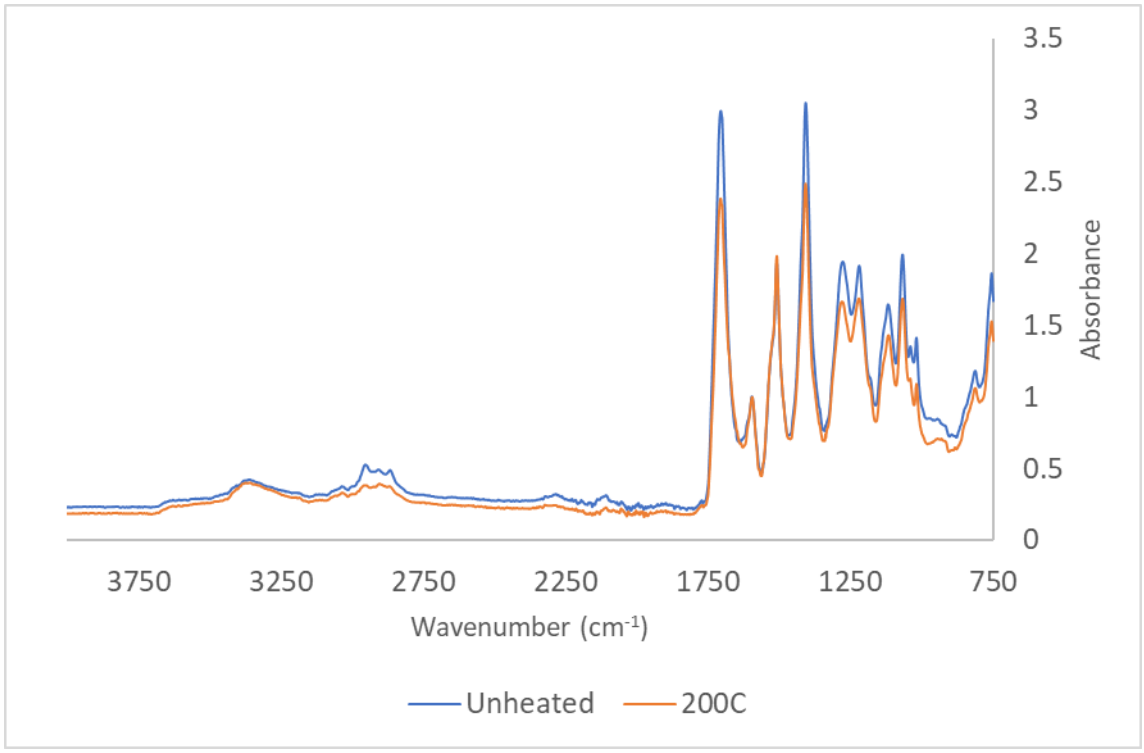

Figure 5.30 *Comparison of ATR-FTIR spectra obtained for unheated P2 foams and after heating to 200 °C.*

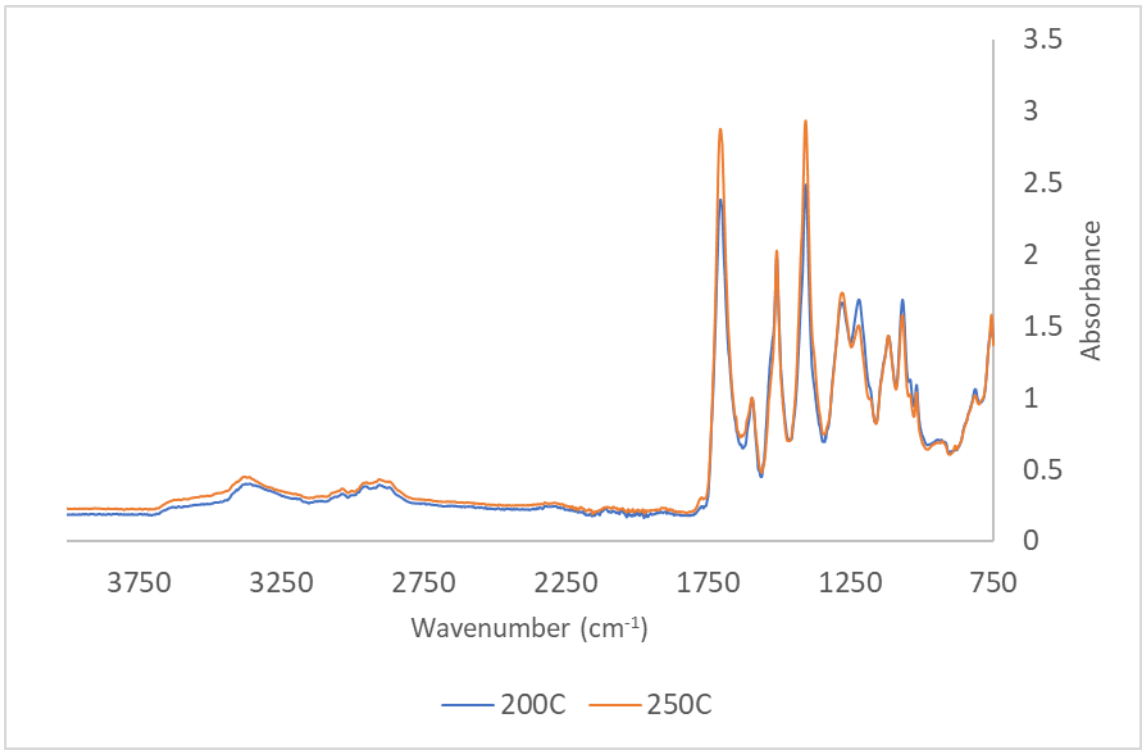

Figure 5.31 *Comparison of ATR-FTIR spectra obtained for P2 foam after heating to 200 °C and 250 °C.*

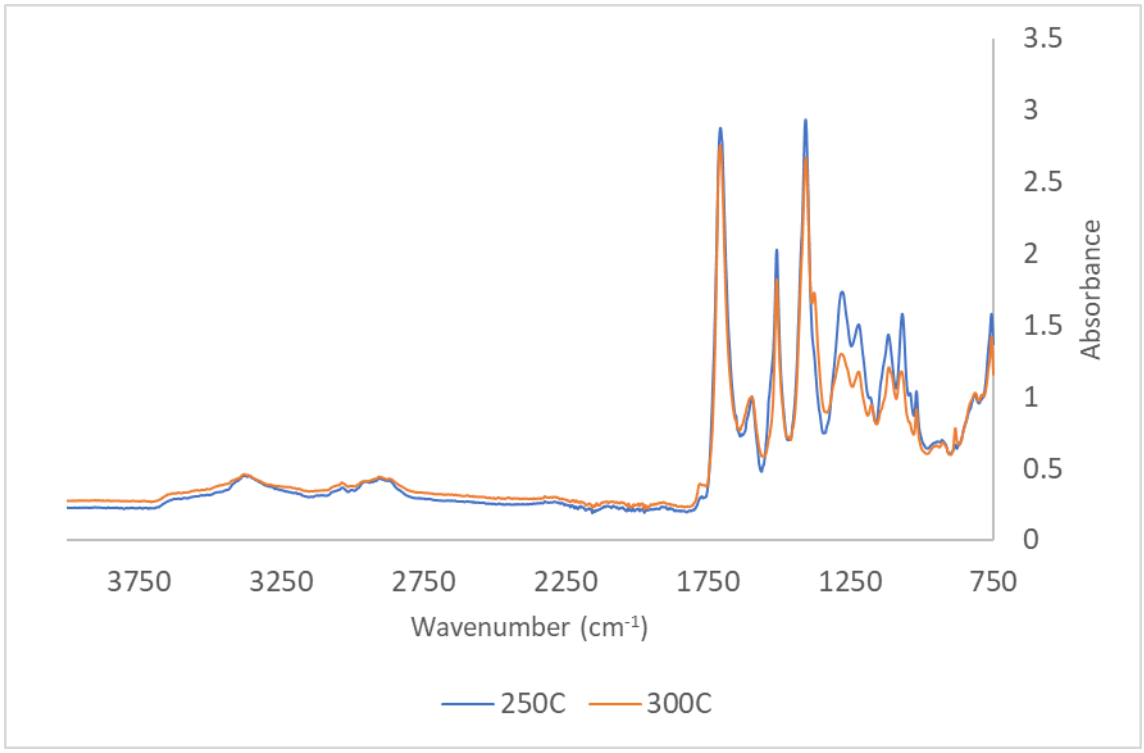

Figure 5.32 *Comparison of ATR-FTIR spectra obtained for P2 foam after heating to 250 °C and 300 °C.*

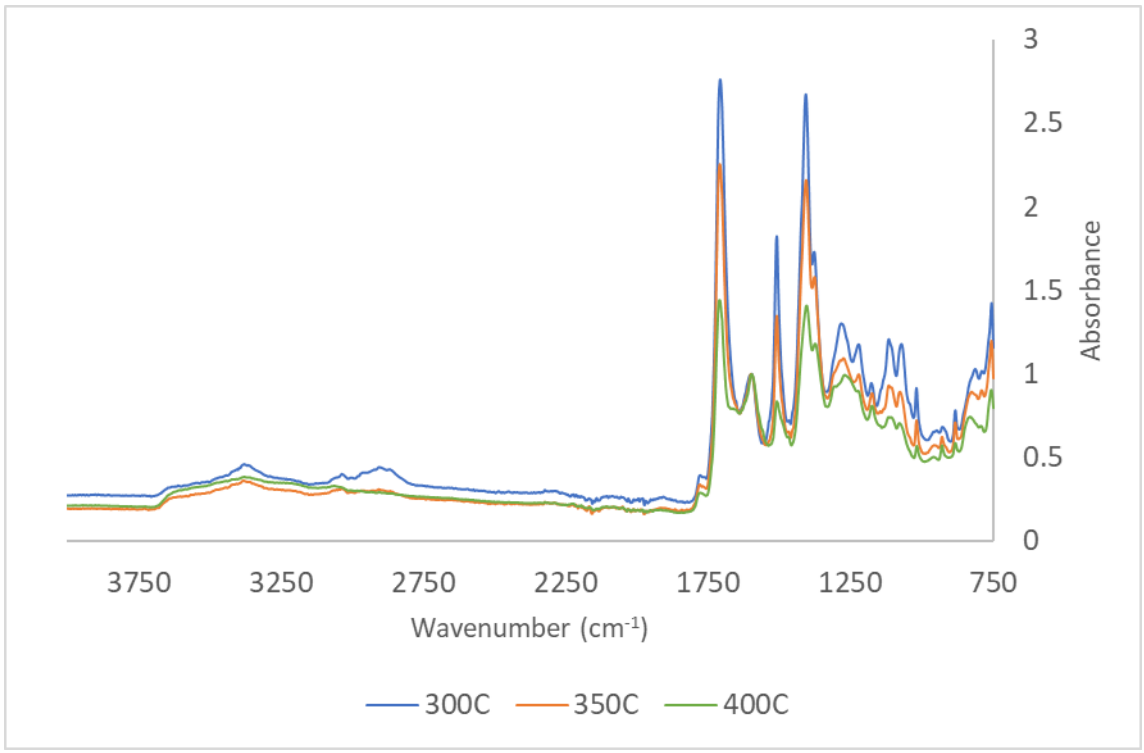

Figure 5.33 *Comparison of ATR-FTIR spectra obtained for P2 foam after heating to 300 °C, 350 °C and 400 °C.*

Key data for the above spectra are tabulated below in direct comparison with the P0 and P1 samples.

Table 5.13 Relative absorbance and wavenumber ($\bar{\upsilon}$) of νC=O peaks for P0, P1 and P2 polyisocyanurates at temperatures from ambient to 400ºC

	P0 Abs	**P0 $\bar{\upsilon}$**	**P1 Abs**	**P1 $\bar{\upsilon}$**	**P2 Abs**	**P2 $\bar{\upsilon}$**
Unheated	3.01	1707	2.87	1707	3.00	1707
200ºC	2.69	1706	2.70	1705	2.38	1707
250ºC	1.71	1707	2.86	1705	2.87	1708
300ºC	1.11	1711	1.89	1704	2.76	1709
350ºC	1.00	1714	2.93	1708	2.25	1710
400ºC	0.93	1715	2.43	1709	1.44	1712

Table 5.14 Relative absorbance and wavenumber ($\bar{\upsilon}$) of amide II peaks for P0, P1 and P2 polyisocyanurates at temperatures from ambient to 400 ºC

	P0 Abs	**P0 $\bar{\upsilon}$**	**P1 Abs**	**P1 $\bar{\upsilon}$**	**P2 Abs**	**P2 $\bar{\upsilon}$**
Unheated	1.95	1510	1.93	1510	1.94	1510
200	2.01	1510	1.91	1510	1.98	1510
250	1.52	1510	2.08	1510	2.02	1510
300	1.07	1510	1.28	1510	1.82	1510
350	1.05	1510	1.77	1510	1.35	1510
400	0.90	1510	1.36	1510	0.83	1510

Table 5.15 Relative absorbance and wavenumber ($\bar{\upsilon}$) of isocyanurate νC-N peaks for P0, P1 and P2 polyisocyanurates at temperatures from ambient to 400 ºC

	P0 Abs	**P0 $\bar{\upsilon}$**	**P1 Abs**	**P1 $\bar{\upsilon}$**	**P2 Abs**	**P2 $\bar{\upsilon}$**
Unheated	3.07	1408	2.88	1409	3.05	1409
200	2.86	1409	2.87	1408	2.49	1409
250	1.92	1408	3.13	1408	2.93	1409
300	1.14	1408	2.16	1407	2.67	1408
350	0.71	1409	3.01	1406	2.16	1407

400	0.71	1409	2.43	1406	1.41	1406

Unheated P0 and P2 PIR exhibited very similar key spectral features, with near identical absorbance values at the νC=O, amide II and νC-N peaks. By contrast, P1 PIR exhibited appreciably lower absorbance at the νC=O and νC-N peaks, but a similar absorbance at the amide II peak. P1 therefore differed in an apparently greater proportion of disubstituted urea groups and a slightly lower initial prevalence of isocyanurate groups.

At 200 ^{o}C, the P2 foam exhibited a greater decrease in absorbance at the νC=O and νC-N peaks than either P0 or P1 foams. Absorbance at the amide II peak increased, which was also observed in the P0 foam, while a decrease occurred in the P1 foam. As a consequence, the amide II:νC=O and amide II:νC-N ratios for the P2 foam were the highest among the three formulations at this temperature.

At 250 ^{o}C, absorbances at the νC=O and νC-N peaks had increased in the P2 foam and were similar to those in the P1 foam, as was the absorbance at the amide II peak which remained relatively stable. This contrasted with a substantial decrease at the νC=O and νC-N peaks observed in the P0 foam and is indicative of improved thermal stability when TEP alone was present compared to foam with no fire retardant. The similarity in spectral features between P1 and P2 foams suggests a similar composition of the residual material, although the νC=O:νC-N ratio of the P2 foam was substantially higher.

Fluctuations in relative peak intensity present some difficult in quantifying the degree of degradation of carbonyl, amide and isocyanurate groups, but at 250 ^{o}C and above it was observed that the νC=O:νC-N and amide II:νC-N ratio for P2 foam was generally higher than that for P1 foam, while amide II:νC=O ratios were generally more similar. This is likely indicative of more extensive isocyanurate degradation in the P2 foam and therefore corroborates thermogravimetric data which indicated reduced thermal stability in the absence of TCPP. The continued prominence of the νC-N peak at all temperature up to 400 ^{o}C clearly indicates that TEP alone does prevent more extensive degradation of isocyanurates below this temperature, but to a clearly lesser degree than the dual-agent system used in P1, as evidenced by a sharp decrease in absorbance at the νC-N peak from 350-400 ^{o}C.

It is also noted that the progressive upward shift in the wavenumber of the νC=O peak observed in the P0 foam was less pronounced in P2 foam but greater than that observed in the P1 foam.

This suggests a difference in the proportion of different groups containing a carbonyl substituent within the residues and is a potential avenue for future study.

5.4.2.4 Polyisocyanurate P3

PIR P3 was based on the PS-2602 polyester polyol and contained a single-agent fire retardant system of TCPP. Spectral data are presented in Figures 5.33-5.35 below, in the same comparative format as for sample sets P0 and P1.

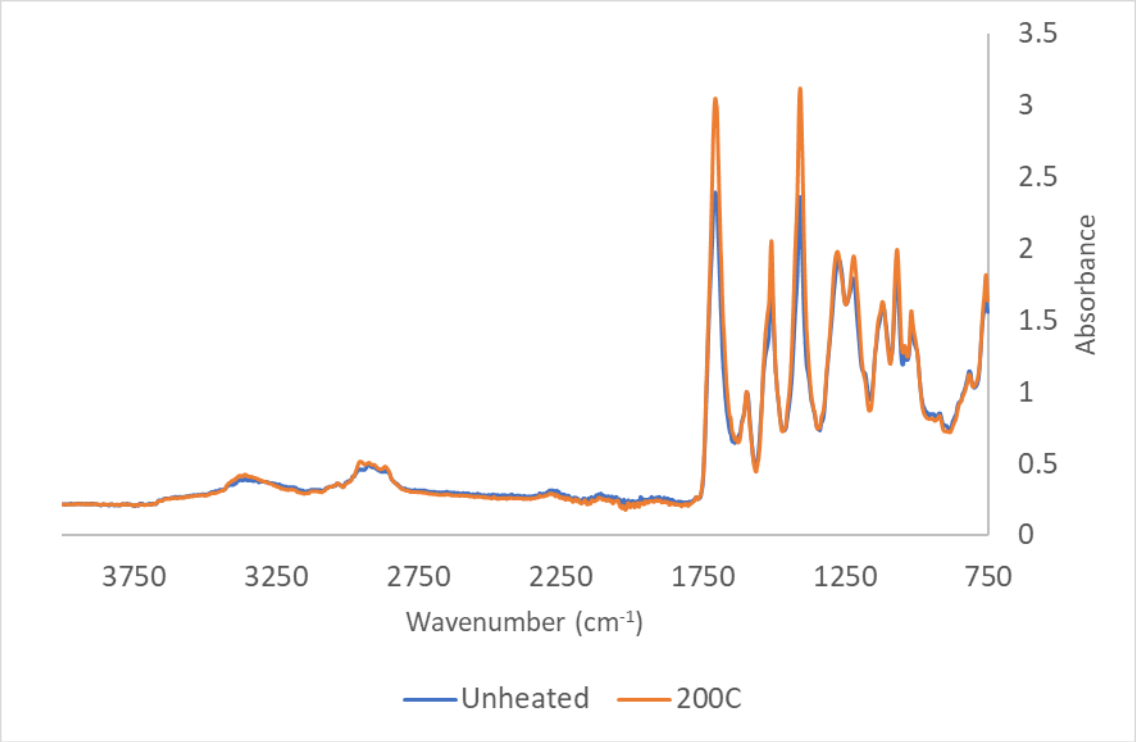

Figure 5.34 *Comparison of ATR-FTIR spectra obtained for unheated P3 foams and after heating to 200 °C.*

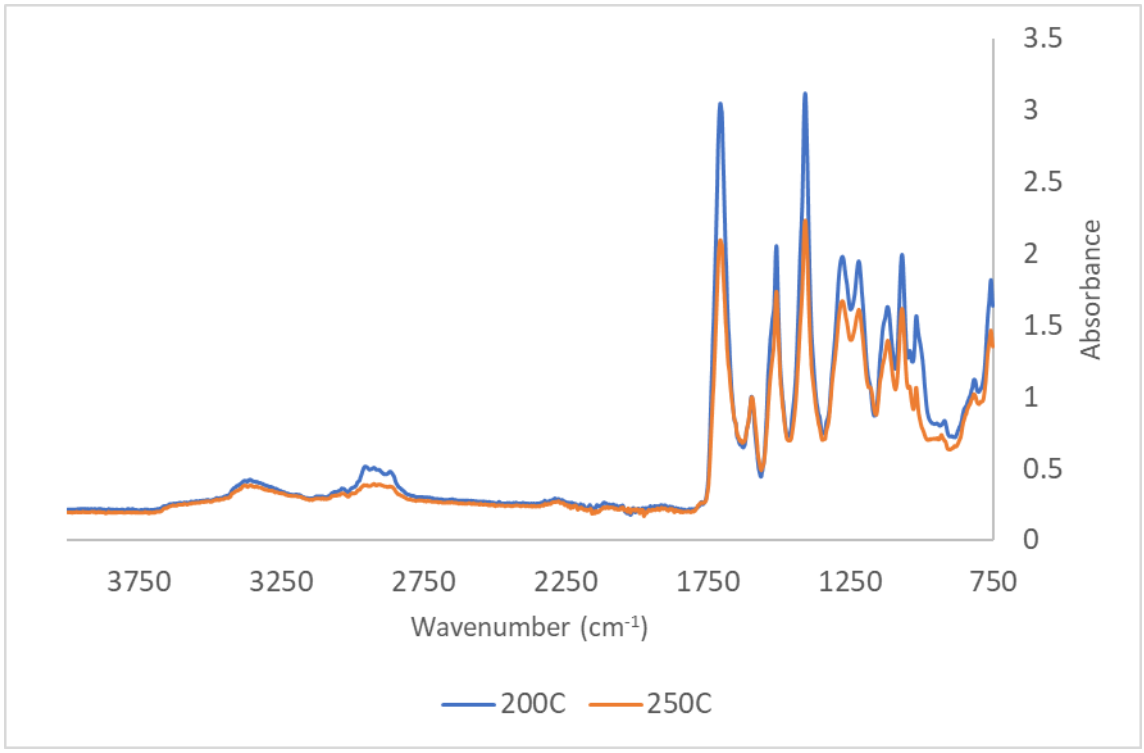

Figure 5.35 *Comparison of ATR-FTIR spectra obtained for P3 foam after heating to 200 °C and 250 °C.*

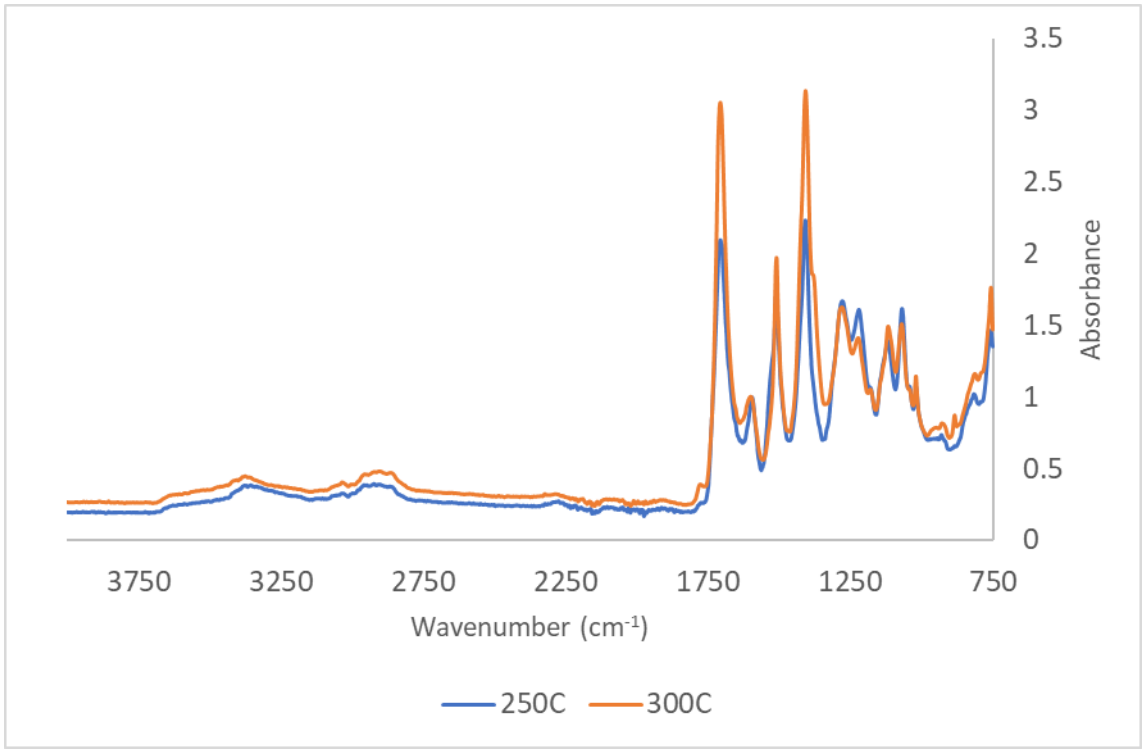

Figure 5.36 *Comparison of ATR-FTIR spectra obtained for P3 foam after heating to 250 °C and 300 °C.*

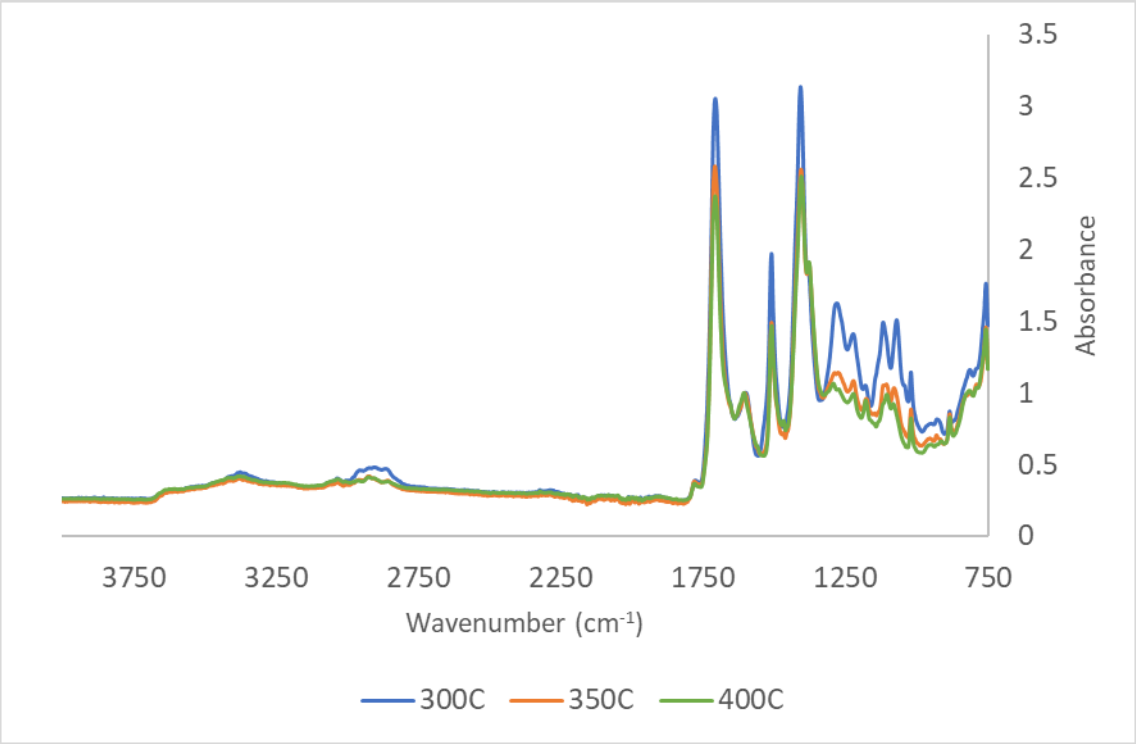

Figure 5.37 *Comparison of ATR-FTIR spectra obtained for P3 foam after heating to 300 ºC, 350 ºC and 400 ºC.*

Key data are again tabulated below to be directly compared to P0 and P1 foams.

Table 5.16 Relative absorbance and wavenumber ($\bar{\upsilon}$) of νC=O peaks for P0, P1 and P3 polyisocyanurates at temperatures from ambient to 400 ºC

	P0 Abs	**P0 $\bar{\upsilon}$**	**P1 Abs**	**P1 $\bar{\upsilon}$**	**P3 Abs**	**P3 $\bar{\upsilon}$**
Unheated	3.01	1707	2.87	1707	2.39	1707
200	2.69	1706	2.70	1705	3.04	1707
250	1.71	1707	2.86	1705	2.10	1707
300	1.11	1711	1.88	1704	3.05	1707
350	1.00	1714	2.93	1708	2.58	1709
400	0.93	1715	2.43	1709	2.37	1708

Table 5.17 Relative absorbance and wavenumber ($\bar{\upsilon}$) of amide II peaks for P0, P1 and P3 polyisocyanurates at temperatures from ambient to 400 ^{o}C

	P0 Abs	**P0 $\bar{\upsilon}$**	**P1 Abs**	**P1 $\bar{\upsilon}$**	**P3 Abs**	**P3 $\bar{\upsilon}$**
Unheated	1.95	1510	1.93	1510	1.76	1510
200	2.01	1510	1.91	1510	2.05	1510
250	1.52	1510	2.08	1510	1.74	1510
300	1.07	1510	1.28	1510	1.97	1510
350	1.05	1510	1.77	1510	1.49	1510
400	0.90	1510	1.36	1510	1.47	1510

Table 5.18 Relative absorbance and wavenumber ($\bar{\upsilon}$) of νC-N peaks for P0, P1 and P3 polyisocyanurates at temperatures from ambient to 400 ^{o}C

	P0 Abs	**P0 $\bar{\upsilon}$**	**P1 Abs**	**P1 $\bar{\upsilon}$**	**P3 Abs**	**P3 $\bar{\upsilon}$**
Unheated	3.07	1408	2.88	1409	2.36	1410
200	2.86	1409	2.87	1408	3.11	1409
250	1.92	1408	3.13	1408	2.23	1409
300	1.14	1408	2.16	1407	3.13	1408
350	0.71	1409	3.01	1406	2.55	1406
400	0.71	1409	2.43	1406	2.51	1405

The peak absorbance data for PIR P3 exhibited substantial fluctuations across the temperature range from ambient temperatures to 300^{o}C. In particular, the overall intensity of the νC=O, amide II and isocyanurate νC-N peaks were all markedly higher at 300^{o}C than for previous samples. These fluctuations are similar to those seen across the 250-350^{o}C range for P1. These fluctuations may arise from variations in absorbance at the C=C reference peak and are difficult to account for in terms of purely chemical processes. Analysis of peak ratios may therefore be more useful given this observation.

Calculation of peak ratios found that P3 PIR had a similar νC=O:νC-N peak ratio (1.01) to P0 and P1 PIRs, but had higher amide II:νC=O and amide II:νC-N ratios, suggesting that a greater proportion of disubstituted urea groups. This increase in amide II activity was also observed, to a lesser extent, for the P1 PIR compared to P0. The persistence of a prominent νC-N peak through the entirety of the temperature interval to 400 ^{o}C is again noted, indicating that

isocyanurate groups remain present in substantial quantities within this temperature range when TCPP and TEP are present either singularly or in combination.

This higher relative amide II activity was not present after heating to 200 °C, and in fact amide II:νC=O and amide II:νC-N ratios were lower for P3 than for either P0 or P1 foams. P3 foams had a higher νC=O:νC-N ratio at 200 °C than P0 and P1 foams, which may indicate *less* low temperature degradation of urethanes than for either of these foams and less subsequent reformation to disubstituted ureas. It was also noted from Figure 5.34 that the C-H peak attributed to pentane at around 2800 cm^{-1} remained and did not undergo the same loss of absorbance seen for P0 or P1 foams.

From 250-350 °C, P3 foam exhibited a higher νC=O:νC-N and amide II:νC-N ratio, which is taken as an plausible indication of greater degradation of isocyanurates. The amide II:νC=O ratio at 250 °C was higher than for P1 suggesting an increase in urethane degradation in the absence of TEP.

Comparison of peak ratios at 400 °C exhibited higher amide II:νC=O and amide II:νC-N ratios for P3 than P1 but lower than P0, while νC=O:νC-N ratio was higher for in P3 than either P0 or P1.

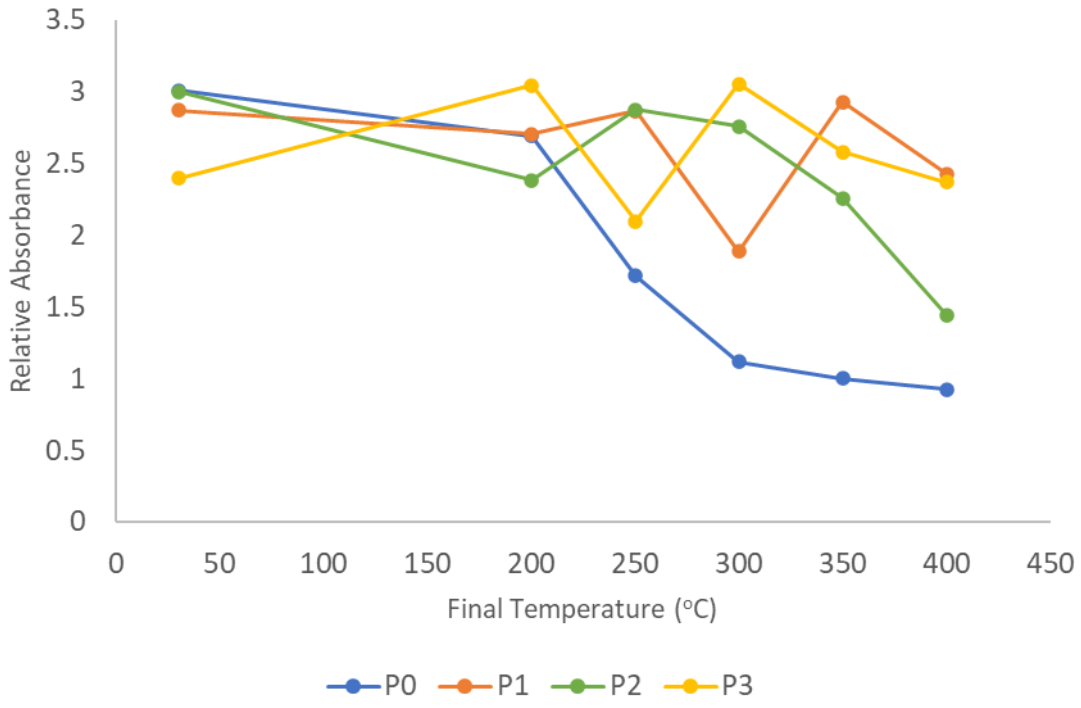

Figure 5.38 *Relative absorbance at νC=O peak at final temperatures from 30 °C to 400 °C for polyisocyanurates P0-P3.*

When considering absorbance at the νC=O peak for samples P0-P3 together, there appeared to be no consistent trend across these four formulations. In P0 (bare PIR) νC=O absorbance decreased at each successive temperature point, with the largest decrease occurring across the 200-250 °C and 250-300 °C temperature intervals. P1, containing both TEP and TCPP exhibited and alternating pattern of increasing and decreasing absorbance at this peak, with the highest absorbance occurring at 350 °C. A similar alternating pattern was also seen in P3, containing TCPP alone with the highest absorbance recorded at 300 °C. P2, containing TEP alone initially decreased in the sample heated to 200 °C, before increasing to a maximum value at 250 °C, and then decreasing at successive temperature points.

Above 350 °C, it was noted that the formulations containing TCPP (P1, P3) retained a higher absorbance at this peak than those containing either TEP alone (P2) or no flame retardants (P0), and that P0 exhibited the lowest absorbance at this peak at all temperature above and including 250 °C.

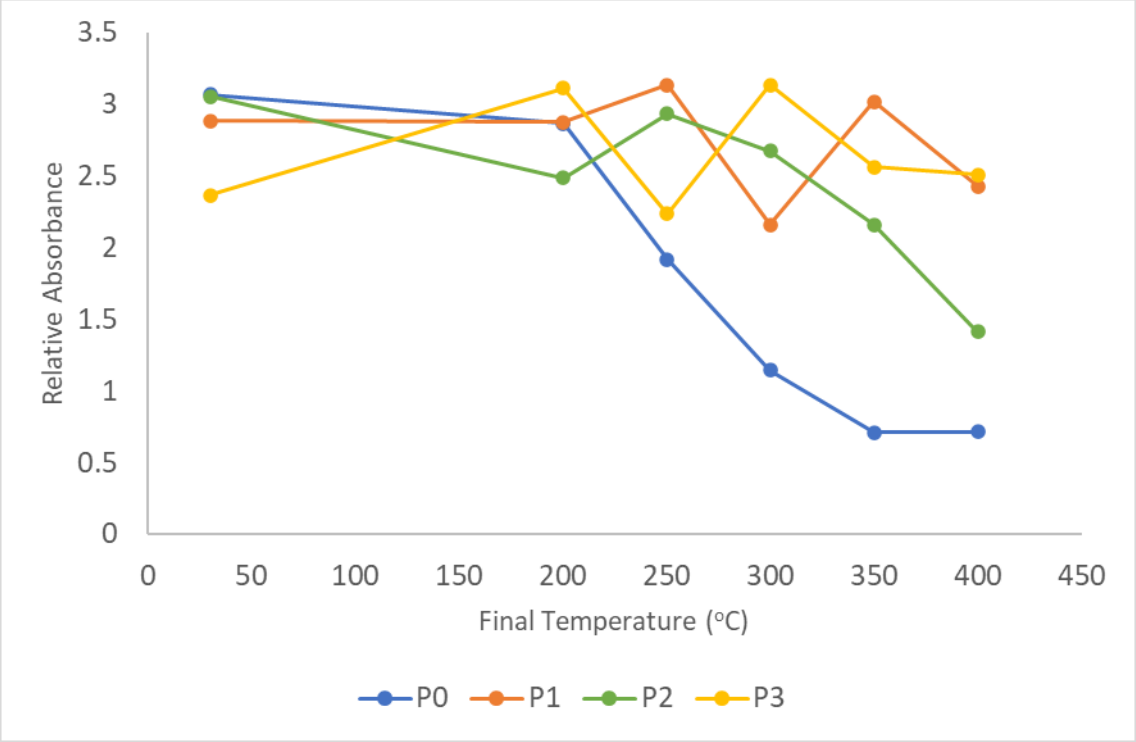

Figure 5.39 *Relative absorbance at νC-N peak at final temperatures from 30 °C to 400 °C for polyisocyanurates P0-P3.*

A very similar pattern of behaviour was observed for absorbance at the isocyanurate νC-N peak, suggesting that both TEP and TCPP are associated with reduced dissociation of both

urethane/urea bonds and isocyanurate ring structures, at least at temperatures ≥250 °C and that this effect is stronger for TCPP at temperatures ≥350 °C, although it is unclear to what extent these effects of these agents were additive or synergistic, as P1 did not clearly demonstrate greater stability throughout as compared to P3. These data correlate reasonably well with the temperatures at which the highest rate of mass loss occurred under thermogravimetry, where formulations containing TCPP appeared to be more stable by this metric than those containing TEP alone, which were in turn more stable than those containing no flame retardants. However, these differences in stability did not appear to strongly correlate with the mass retention measured for the furnace heated samples themselves. Although P0 underwent significantly increased mass loss in comparison to the other three samples, P2, containing TEP alone exhibited marginally higher mass retention than either P1 or P3.

The same correlation was not observed for samples the analogous set of formulations H0-H3, containing the same fire-retardant systems but based on the HT-2006 polyol.

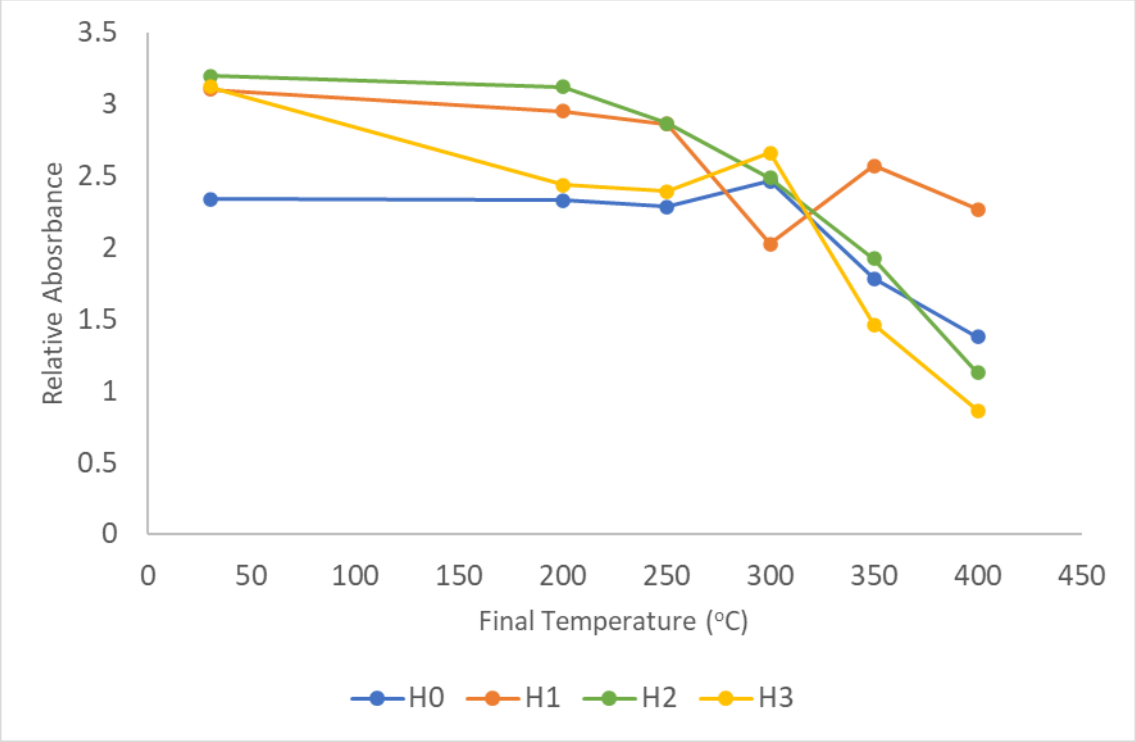

Figure 5.40 *Relative absorbance at vC=O peak at final temperatures from 30 °C to 400 °C for polyisocyanurates H0-H3*

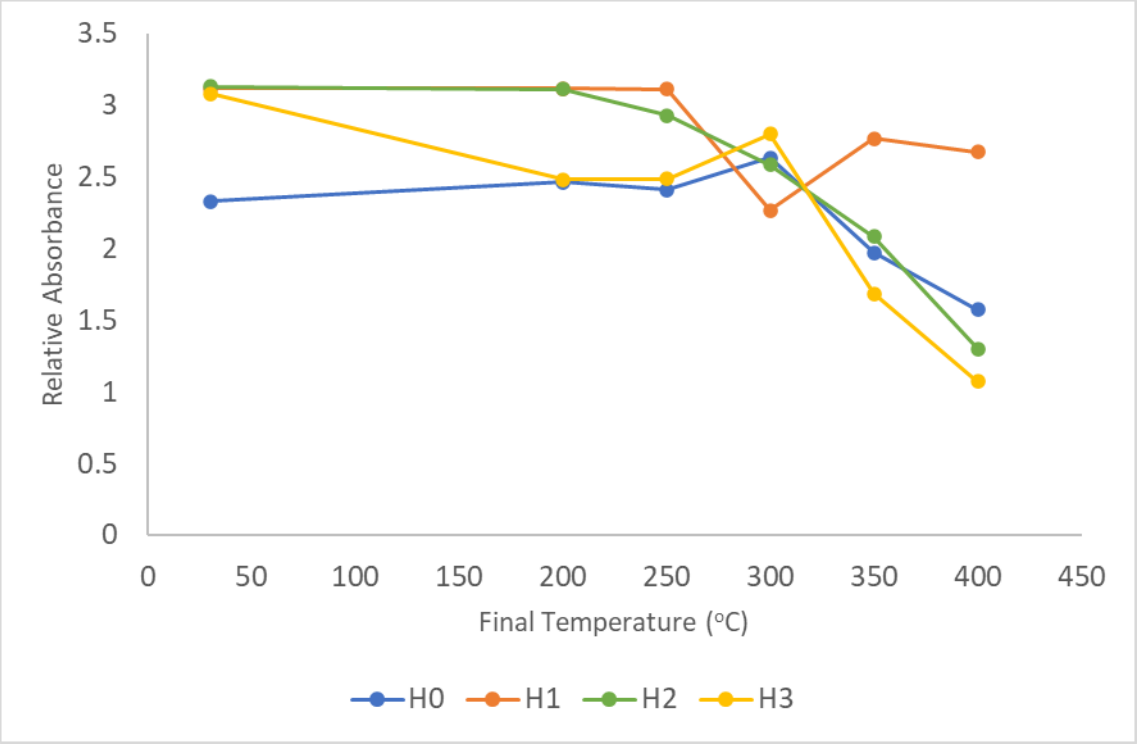

Figure 5.41 *Relative absorbance at νC-N peak at final temperatures from 30 °C to 400 °C for polyisocyanurates H0-H3*

Thermogravimetric data for foams based on HT-2006 followed a similar pattern to those for foams based on PS-2602 in regard to the temperature at which the maximum rate of mass loss occurred. Formulations containing no fire retardants were less stable than those containing TEP alone, which were themselves significantly less stable than those containing TCPP. Despite this, the temperature-resolved spectral features for formulations H0-3 (Figures 5.39,5.40) do not follow a similar pattern to those for formulations P0-3. Furthermore, there is again little apparent correlation with mass retention for the furnace heated samples.

On this basis, absorbance at the νC=O and νC-N peaks does not appear to be a generally strong indicator of thermal stability using this method.

Comparison of peak ratios across an extended data set including P0-P3, H0-H3 and the P4 formulation containing ammonium polyphosphate and TEP did reveal several possible correlations between spectral features and stability.

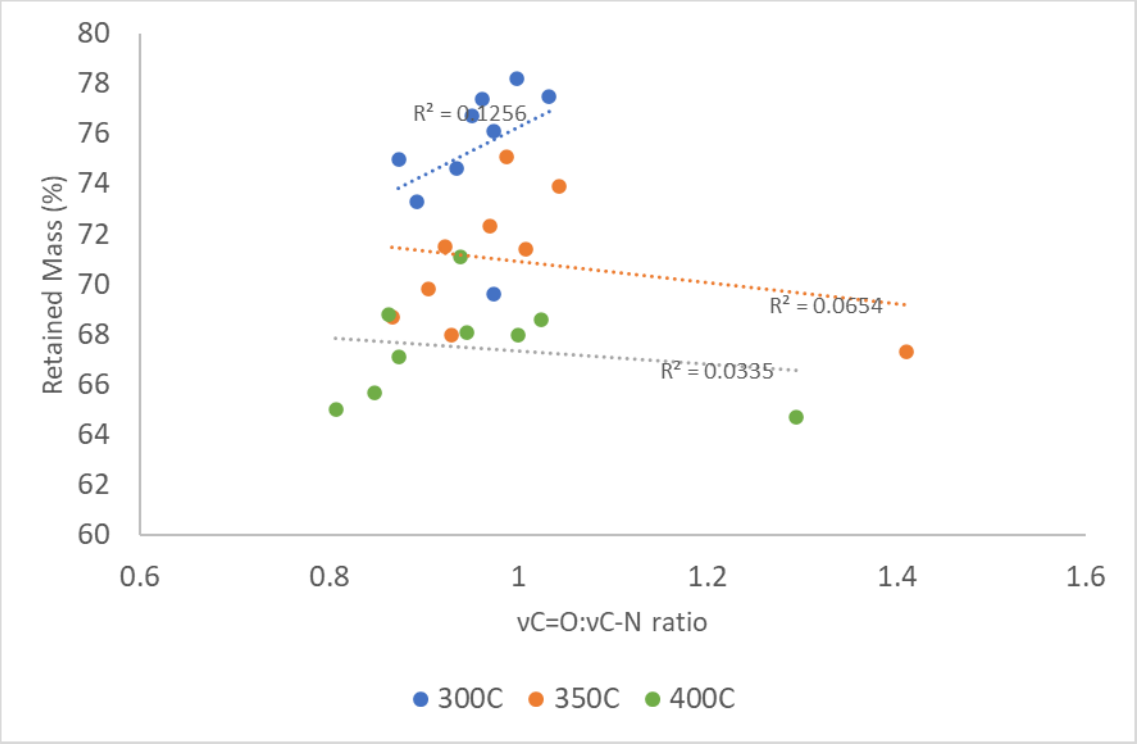

Figure 5.42 *νC=O:νC-N ratio for foam formulations P0-4 and H0-3 against retained mass at 300 °C, 350 °C and 400 °C. Outlying data points obtained from sample P0 can are clearly seen at 350 °C and 400 °C.*

In Figure 5.42, the νC=O:νC-N ratios of PIR formulations are plotted against retained mass at 300 °C, 350 °C and 400 °C. This initial plotting shows little apparent correlation between this peak ratio and retained mass, but it was noted that values obtained for P0 form significant outlying data points, due to very large decrease in absorbance at the νC-N peak which was not observed for any other formulation. In Figure 5.42 these are clearly seen lying far to the right of the main clusters of points in the 350°C and 400°C data series. These data are replotted in figure 5.43 below excluding these data points. When these values are excluded there appears to be a reasonably strong positive correlation between νC=O:νC-N ratio and retained mass at all three temperature points, with the R^2 value decreasing with temperature.

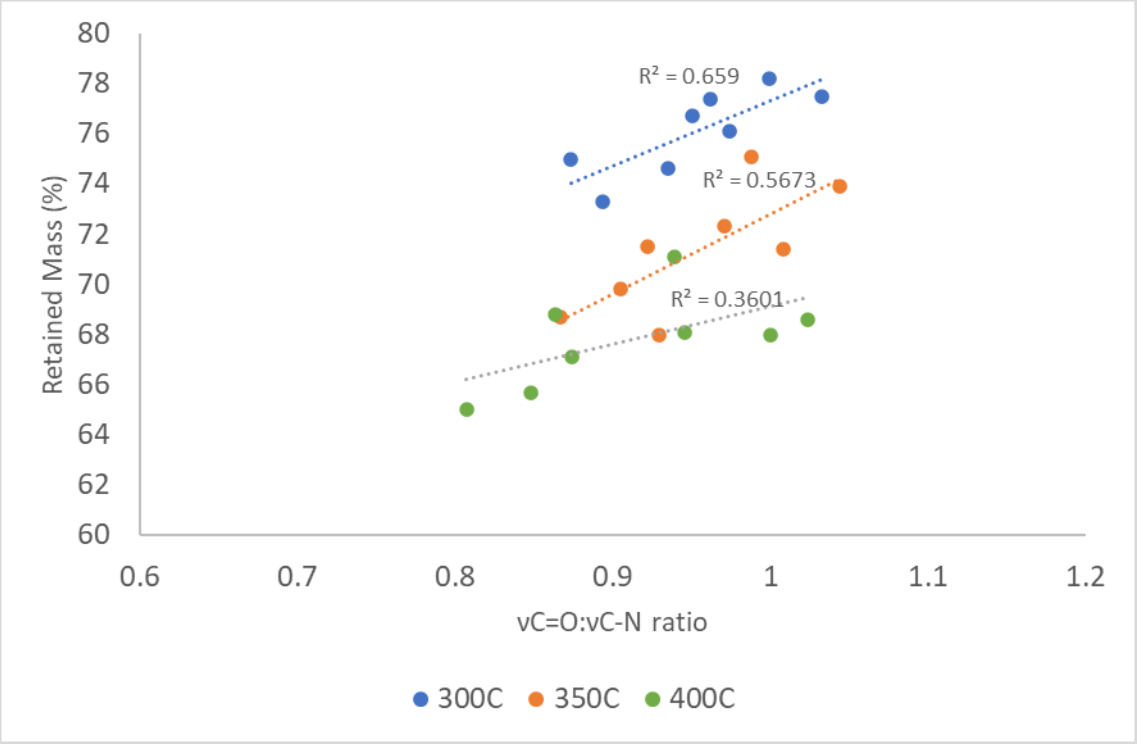

Figure 5.43 *vC=O:vC-N ratio for foam formulations P1-4 and H0-3 against retained mass at 300 °C, 350 °C and 400 °C*

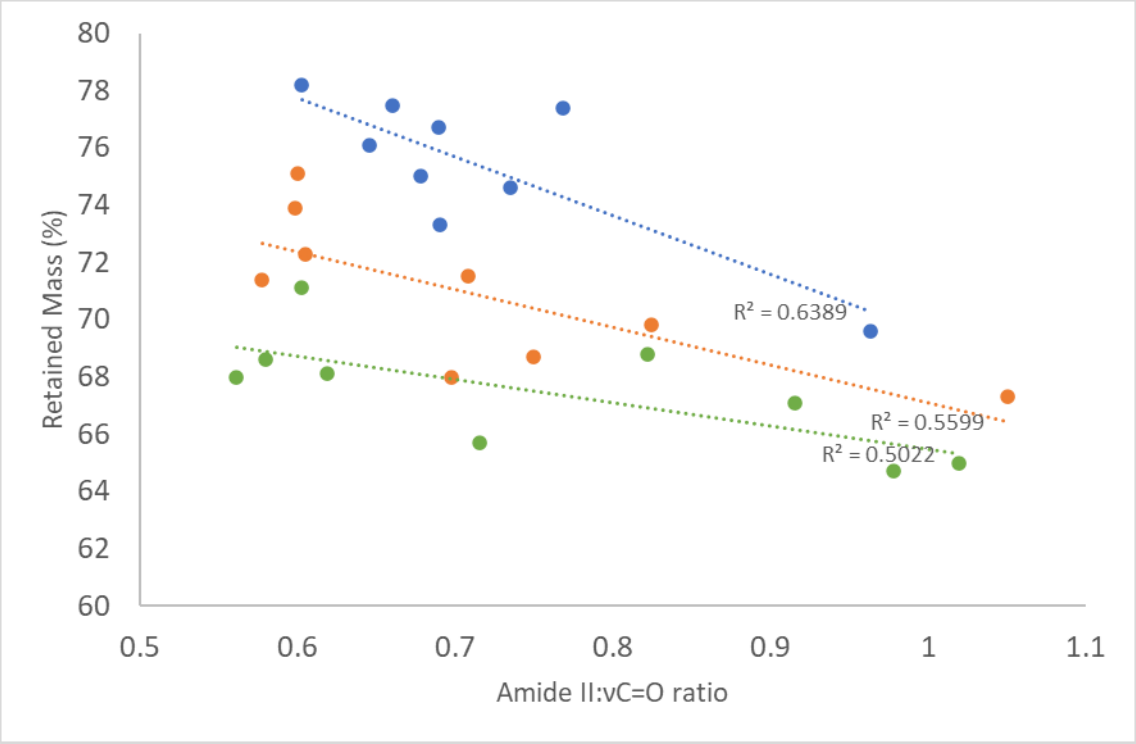

Figure 5.44 *Amide II:νC=O ratio for foam formulations P0-4 and H0-3 against retained mass at 300 °C, 350 °C and 400 °C*

Figure 5.44 indicates a negative correlation between retained mass and amide II:νC=O ratio existing within the 300-400 °C temperature range. These data indicate that stability is associated with a higher retention of νC=O groups, particularly when associated with lower formation of disubstituted ureas. Greater mass retention is associated with a lower contribution to fire load, as less volatilised material enters the vapour phase to undergo combustion. While these results are based on a relatively small sample set due to time constraints within the scope of this thesis, this finding suggests that these FTIR peak ratios provide an indicative measure of thermal stability in PIR foams and could be of practical utility in the screening of formulations for improved fire performance. There is scope for further work utilising larger data sets and expanded analysis methods to confirm the value of this technique.

5.5 Pyrolysis GC-MS Analysis of Foam Degradation

Analysis of solid residues from heated foams provides a partial picture of degradation processes occurring during thermal degradation but this is incomplete without characterisation of the volatilised species escaping into the gas phase. This is essential to understanding both the flammability of PIRs, since flaming combustion occurs entirely in the gaseous phase, and the toxicity of these effluents.

In pyrolysis-GC/MS, the material to be analysed is heated at an extremely high rate to a tightly controlled temperature with the resulting volatile fraction being transferred to a GC/MS for characterisation of its chemical constituents. In this thesis, a time-of-flight mass spectrometer was used, which separates ionic species on the basis of their travel time through a drift region, which is dependent upon their mass-to-charge (m/Q) ratio.

A sample of line-produced PIR based on PS-2412 polyester polyol with a fire-retardant system of TEP and TCPP was subjected to flash pyrolysis up to 800 ^{o}C. At this temperature, a total volatilization of the sample was achieved, producing a complex array of peaks as shown in the total ion current chromatogram displayed in Figure 5.45 below.

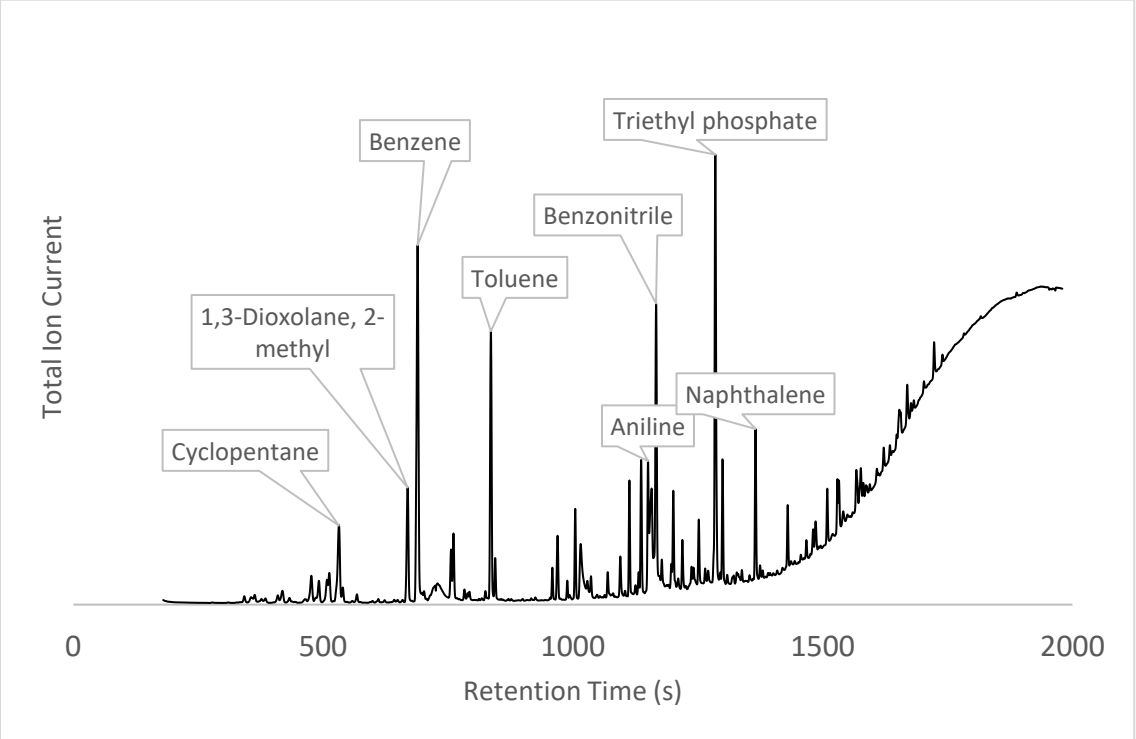

Figure 5.45 *Total ion current chromatogram for line foam pyrolyzed at 800^{o}C.*

A total of 349 peaks were detected, with many of these being of very small area. To restrict analysis to a manageable number of peak, those peaks with an area below 5 % of the area of the largest peak were excluded, reducing the number of peaks to 48. A further 12 peaks were excluded due to being either duplicate results, peaks that failed to produce a match with the NIST mass spectral library, or siloxane-derived compounds resulting from column bleed. The remaining 32 species are tabulated below, ordered by peak area.

Table 5.18 Prominent gas chromatogram peaks obtained from pyrolysis of line-produced polyisocyanurate foam at 800 ºC

Species	Base Mass	Peak Area
Benzene	77.98	7.91E+09
Diethylene glycol	74.95	4.9E+09
Semioxamazide	103.05	4.87E+09
1,3-Dioxolane, 2-methyl-	72.91	4.73E+09
Toluene	91.06	4.65E+09
Benzonitrile	103.03	4.57E+09
Naphthalene	128.05	3.28E+09
Triethyl phosphate	98.96	2.94E+09
Aniline	93.06	2.67E+09
Cyclopentane	54.92	2.11E+09
1,4-Dioxane	88.06	1.57E+09
Ethanol, 2-(2-chloroethoxy)-	62.85	1.53E+09
Quinoline	129.05	1.22E+09
Indene	115.05	1.16E+09
Bicyclo[4.2.0]octa-1,3,5-triene	104.06	1.13E+09
p-Xylene	91.06	1.1E+09
Allyl chloride	75.92	1.07E+09
Indole	117.05	1.03E+09
Quinoline, 2,7-dimethyl-	157.08	9.67E+08
Biphenyl	154.07	9.67E+08
Ethanone, 2-(formyloxy)-1-phenyl-	105.03	8.79E+08
Benzene, isocyanato-	119.03	8.44E+08
1-Propene, 1-chloro-	75.92	8.22E+08
Benzonitrile, 2-methyl-	117.05	8.08E+08
Fluorene	166.05	7.92E+08
Quinoline, 6-methyl-	143.06	7.61E+08
Benzene, 1-isocyanato-4-methyl-	133.05	7.49E+08
1,3-Cyclopentadiene	65.9	6.58E+08
Propane, 1,2-dichloro-	62.85	6.04E+08
Ethylbenzene	91.06	5.65E+08
Butane, 2-methyl-	56.94	5.52E+08
Phenol	94.05	5.34E+08
1,2-Benzenedicarbonitrile	128.03	5.17E+08
Acenaphthylene	152.05	5.03E+08
Benzonitrile, m-amino-	118.05	4.79E+08
Quinoline, 2-methyl-	143.07	4.43E+08

These degradation products comprise a mixture of the blowing agents from the foam (cyclopentane and 2-methylbutane); the fire retardant TEP; diethylene glycol, the chain

extender and polyester monomer; several dioxane-related compounds, which are likely to be secondary reaction products from the chain extender; and an array of aromatic hydrocarbons, a number of which are either heterocyclic or include nitrogenous side groups. In addition, there are a number of chlorinated compounds, which almost certainly arise from reactions involving TCPP as there is no other source of chlorine present in the isocyanurate. These chlorinated compounds may be the result of the fire-retardant action when the chlorine atoms combine with radicals formed during combustion. The high abundance of relatively small molecular species demonstrates that the PIR underwent rapid and extensive fragmentation at this temperature.

Many of these compounds will readily ignite in air and have lower explosive limits of 1-2 %. In addition, a number of these compounds are toxic, presenting an immediate danger to those exposed to fumes produced by the breakdown of the material. The presence of chlorinated compounds suggests a high likelihood that hydrogen chloride will be present in the fire effluent, which due to its caustic properties is a potential incapacitant.

In the early stages of a fire, it is unlikely that the bulk of the foam would be instantaneously exposed to temperatures of 800 ^{o}C, and this temperature is far above the critical breakdown temperature of PIR foams. To characterize the progression of thermal degradation, a sample of line foam was pyrolyzed in three stages, at 250 ^{o}C, 350 ^{o}C, and 450 ^{o}C.

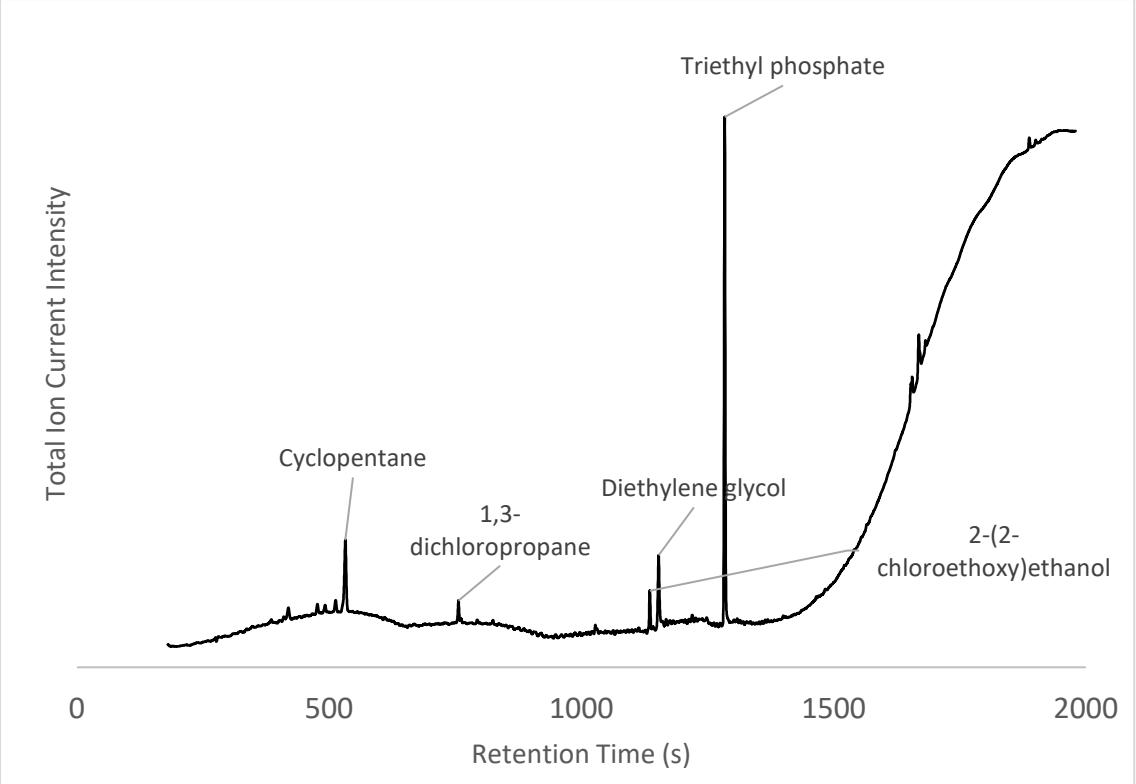

Figure 5.46 *Total ion current chromatogram for line foam pyrolyzed at 250ºC.*

The total ion current chromatogram obtained at 250 ºC displayed a far smaller number of highly prominent peaks and was dominated by a single very prominent peak at a retention time of around 21 minutes. A total of 82 peaks were detected but this was reduced to just 7 peaks when applying the same exclusion criteria used previously.

Table 5.19. Prominent gas chromatogram peaks obtained from pyrolysis of line-produced polyisocyanurate foam at 250 ºC, ranked by peak area.

	Peak Area	**R.T. (mins)**
Triethyl phosphate	2.16E+09	21.40
Cyclopentane	1.58E+09	8.87
Diethylene glycol	1.21E+09	19.22
Butane, 2-methyl-	2.47E+08	6.98
1-Propene, 1-chloro-	2.25E+08	8.55
Ethanol, 2-(2-chloroethoxy)-	2.02E+08	18.93
Propane, 1,2-dichloro-	1.45E+08	12.61

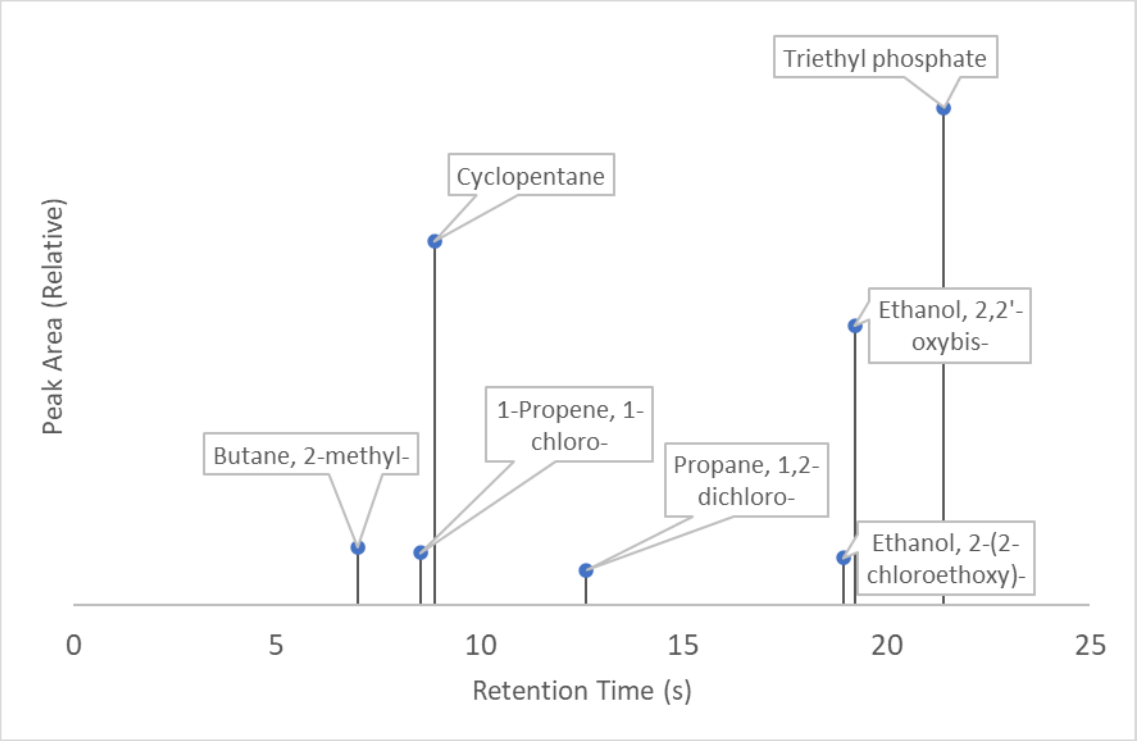

Figure 5.47 *Prominent chromatogram peaks obtained at 250 ^{o}C*

The very prominent peak corresponds to TEP while two of these peaks correspond to the blowing agents, cyclopentane and 2-methylbutane, and there is a significant detection of diethylene glycol. This effectively confirms that the primary sources of mass loss in the first phase of mass loss is due to the off-gassing of blowing agent and the volatilization of low-molecular weight chain extenders due to urethane bond cleavage. It is also shown that there is a significant loss of TEP to the gas phase at relatively low temperatures. Furthermore, the detection of three chlorinated compounds indicates the activity of TCPP, and suggests that hydrogen chloride release, while not detectable using this instrument, is possible at these temperatures. While the peaks were slightly below threshold, there was also a detection of TCPP and one of its isomers in the gas phase.

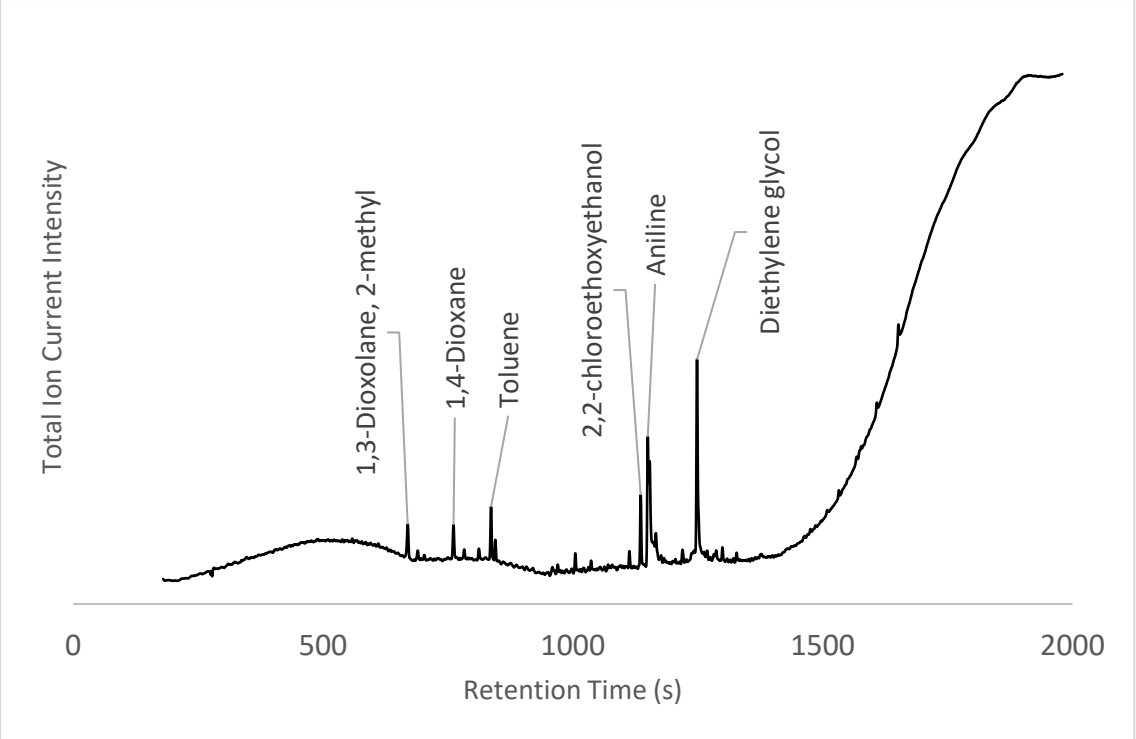

Figure 5.48 *Total ion current chromatogram for line foam pyrolyzed at 350 ºC.*

The total ion current thermogram obtained on the second pyrolysis at 350 ºC again produced a relatively small number of prominent peaks, with nine falling within the criteria for inclusion.

Table 5.20 Prominent gas chromatogram peaks obtained from pyrolysis of line-produced polyisocyanurate foam at 350 °C

	Area	R.T. (min)
p-Aminotoluene	2.7E+09	20.80833
Diethylene glycol	1.69E+09	19.22733
Aniline	1.54E+09	19.16567
1,3-Dioxolane, 2-methyl-	6.81E+08	11.15733
Toluene	5.51E+08	13.93753
1,4-Dioxane	4.26E+08	12.68435
Ethanol, 2-(2-chloroethoxy)-	4.13E+08	18.93
Benzonitrile	2.09E+08	19.436
Phthalimide	1.69E+08	27.5245

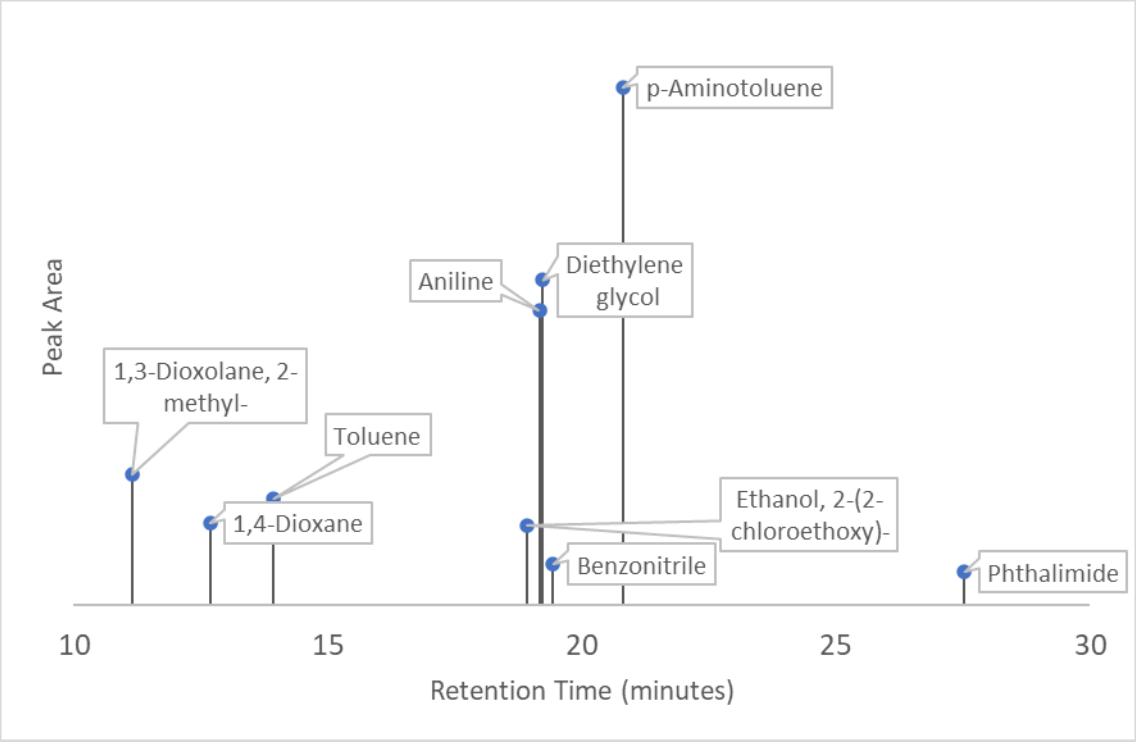

Figure 5.49 *Prominent mass peaks obtained on pyrolysis of line-produced polyisocyanurate foam at 350 °C.*

As observed at 250 °C, there was a prominent diethylene glycol peak. At this temperature, it is likely that some of the diethylene glycol was released due to cleavage of the internal bonds of the polyester polyol, especially in light of the presence of phthalimide, which is most likely to

have been derived from the phthalic anhydride unit of the polyol. Other compounds bearing a close structural relationship to phthalic anhydride, including 2-(hydromethyl) benzoic acid, were detected among the smaller peaks. 2-(2-chlorethoxy)ethanol was most likely a derivative of diethylene glycol resulting from reactions with tris(1-chloro-2-isopropyl)phosphate. A number of aromatic compounds, largely nitrogenous, are most likely to have arisen as secondary breakdown products of 4,4-methylene diphenyl diisocyanate, which was not itself detected. Among the smaller peaks, a number of species consistent with this, and with cleavage in the vicinity of urethane and disubstituted urea units were detected.

It is clear that a substantially different set of degradation processes dominate at 350 ^{o}C, which appear to primarily relate to the breakdown of urethane soft segments, both through urethane bond degradation flanking the polyester polyol but also with significant internal cleavage of the polyol units. Furthermore, there is evidence of the breakdown of secondarily formed disubstituted ureas and of 4,4-methylene diphenyl diisocyanate, with some larger and more complex fragments being produced by random scission within chains, as many minor species appear to contain moieties associated with more than one of the starting subunits from the polymer.

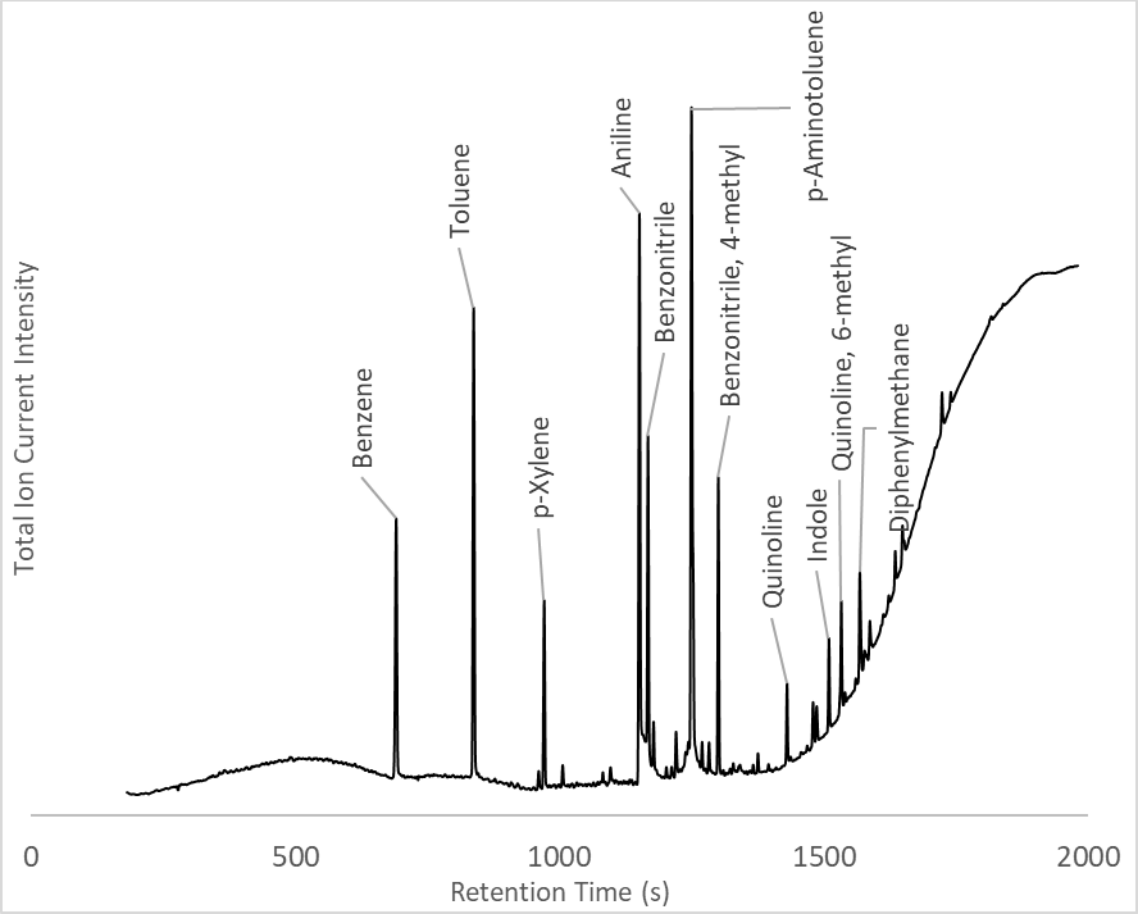

Figure 5.50 *Total ion current chromatogram for line foam pyrolyzed at 450 °C.*

At 450 °C, the total ion current chromatogram displays a higher number of prominent peaks than at 250 °C or 350 °C, with a total of 16 peaks meeting the criteria for inclusion. These peaks were identified to entirely consist of aromatic species, the majority of which were either heterocyclic nitrogen compounds or included amine or nitrile functional groups. This was also found to be the case for almost all of the peaks which fell below the 5 % of largest peak area threshold (Table 5.20).

The largest peak was that corresponding to p-aminotoluene, which along with diphenylmethane are predicted breakdown products of 4,4-methylene diphenyl diisocyanate, in the former case through the cleavage of this compound at the methylene group, and in the latter through the loss of its isocyanate groups. The abundance of nitrile compounds suggests that hydrogen cyanide is also likely to be present in significant quantities in the gaseous products produced at this temperature, corroborated by previous analyses (14). The absence of chlorinated compounds suggest that the TCPP does not undergo reactions with species entering the gas phase at this temperature and it is likely that the flame-retardant effects have been exhausted,

either through consumption or the loss of the flame retardant into the gas phase at lower temperatures.

Table 5.20 Prominent gas chromatogram peaks obtained from pyrolysis of line-produced polyisocyanurate foam at 450 °C

	Area	R.T. (s)
p-Aminotoluene	5.53E+09	1248.24
Toluene	3.79E+09	836.162
Benzene	3.6E+09	689.413
Aniline	3.59E+09	1149.98
Benzonitrile	2.93E+09	1166.1
Benzonitrile, 4-methyl-	1.73E+09	1299.24
p-Xylene	1.44E+09	969.837
Quinoline, 6-methyl-	7.94E+08	1531.95
Indole	7.34E+08	1508.64
Quinoline	6.47E+08	1429.26
Benzonitrile, 2-methyl-	4.9E+08	1251.69
1,2-Benzenedicarbonitrile	4.31E+08	1478.4
Fluorene	3.92E+08	1722.53
Phenol	3.79E+08	1176.74
Diphenylmethane	3.74E+08	1566.81
1H-Indole, 7-methyl-	3.66E+08	1586.02

5.6 Conclusions

Drawing together data from ATR-FTIR analysis of solid foam residues and characterisation of evolved gases from pyrolysis GC-MS a detailed picture has been built up of the degradation of PIRs that has previously been under-reported in the literature.

Degradation of PIRs proceeds similarly to that of the chemically similar polyurethane foams, wherein the early stages of degradation are characterized by a loss of blowing agent into the surroundings and the cleavage of urethane bonds leading to the volatilisation of low-molecular weight chain extenders such as diethylene glycol. Concentration of such compounds may provide a fuel-rich environment that is prone to sudden deflagration where ignition sources are present. TEP is likely to be most active during the early stages of degradation, and significant quantities of this agent escape from the foam during low temperature degradation, with this process being essentially complete when the material is heated to 250 °C. TEP appears to be

associated with volumetric expansion of the foam under heating, as it was consistently observed that this was greater in formulations where it was present, and that this effect was generally most pronounced at temperatures below 300 ^{o}C. Furthermore, there is evidence of significant activity of TCPP phosphate at temperatures up to 350 ^{o}C, in the form of chlorinated volatile species. This may account for the differences in stability when TCPP is present compared to TEP alone and it seems likely that these flame retardants are most effective at different stages in the degradation process. It is also likely that TCPP phosphate promotes the formation of hydrogen chloride as a fixed gas, which is likely to be the most significant noxious product at lower temperatures.

Degradation of foams at temperatures in excess of 300 ^{o}C appears to be associated with an increasingly nitrogenous residual composition, with these compounds being released during the final stages of decomposition at 450 ^{o}C. It is likely that at these temperatures, nitrogenous compounds, particularly hydrogen cyanide, could pose a significant hazard. At 450 ^{o}C, there is essentially no evidence of fire-retardant effects in the gas phase, and a widespread fragmentation of the polymer into low molecular weight aromatic species appears to occur.

It was however noted that PIR foams generally show good thermal resistance when slowly heated to temperatures up to 400 ^{o}C in oxidative conditions, and this appears to be largely the result of charring. This char is most likely formed primarily from the carbonisation of the polyester polyol, as species related to this component of the polymer are relatively less abundant in the volatile degradation products. Conversely, while isocyanurates are generally regarded as being responsible for the generally improved thermal stability of PIRs compared to polyurethanes, these parts of the polymer structure are ultimately released into the gas phase at temperature above 350 ^{o}C.

Autoignition has generally been observed in foams suddenly exposed to temperatures in excess of 500 ^{o}C, but even in such cases, these materials tend to rapidly self-extinguish when the source of heat is removed.

While PIRs do show generally good thermal stability and heat resistance in some regards, a continued reliance on chlorinated flame retardants is clearly undesirable due to the substantial evidence for potential environmental harms, and their likely contribution to the production of toxic combustion products, for which further evidence has been found here.

Chapter 5 Bibliography

1. Welty JR, Wicks CE, Wilson RE, Rorrer GL. Fundamentals of Momentum, Heat and Mass Transfer. 2007.

2. Halliday D, Resnick R, Walker J. Fundamentals of Physics (10th Ed.). 2014. 524 p.

3. Dominguez Rosado E, Liggat JJ, Snape CE, Eling B, Pichtel J. Thermal degradation of urethane modified polyisocyanurate foams based on aliphatic and aromatic polyester polyol. Polym Degrad Stab. 2002;78(1):1–5.

4. Dick C, Dominguez-rosado E, Eling B, Liggat JJ, Lindsay CI, Martin SC. The Flammability of urethane-modified polyisocyanurates and its relationship to thermal degradation chemistry. Polymer (Guildf). 2001;42(3):913–23.

5. Chambers J, Jiricny J, Reese CB. The thermal decomposition of polyurethanes and polyisocyanurates. Fire Mater. 1981;

6. Ketata N, Sanglar C, Waton H, Alamercery S, Delolme F, Raffin G, et al. Thermal degradation of polyurethane bicomponent systems in controlled atmospheres. Polymers and Polymer Composites. 2005;13(1):1–26.

7. Lindberg P, Sellstrom U, Haggberg L, de Wit C. Higher Brominated Diphenyl Ethers and Hexabromocyclododecane Found in Eggs of Peregrine Falcons (Falco peregrinus) Breeding in Sweden. Environ Sci Technol. 2004;38(1):93–6.

8. Watanabe I, Kashimoto T, Tatsukawa R. Polybrominated diphenyl ethers in marine fish, shellfish and river sediments in Japan. Chemosphere. 1987;16(10–12):2389–96.

9. Modesti M, Lorenzetti A, Simioni F, Camino G. Expandable graphite as an intumescent flame retardant in polyisocyanurate-polyurethane foams. Polym Degrad Stab. 2002;77(2):195–202.

10. Badri KBH, Sien WC, Shahrom MSBR, Hao LC, Baderuliksan NY, Norzali NR ‘Adawiyah. Ftir Spectroscopy Analysis of the Prepolymerization of Palm-Base Polyurethane. Solid State Science and Technology. 2010;18(2):1–8.

11. Chattopadhyay DK, Webster DC. Thermal stability and flame retardancy of polyurethanes. Progress in Polymer Science (Oxford). 2009;34(10):1068–133.

12. Chattopadhyay DK, Sreedhar B, Raju KVSN. Influence of varying hard segments on the properties of chemically crosslinked moisture-cured polyurethane-urea. J Polym Sci B Polym Phys. 2006;44(1):102–18.

13. Berta M, Lindsay C, Pans G, Camino G. Effect of chemical structure on combustion and thermal behaviour of polyurethane elastomer layered silicate nanocomposites. Polym Degrad Stab. 2006;91(5):1179–91.

14. Jiricny J, Reese CB. THERMAL DECOMPOSITION OF ISOCYANURATES. British Polymer Journal. 1980;12(3).

6 Conclusions and Future Work

6.1 Degradation Mechanisms of Polyisocyanurate Foams

With the potential benefits and hazards of PIR-based insulation materials in mind, the experimental research carried out in this thesis has sought to answer several questions regarding the fire behaviour of PIR foams. In the first instance, it was necessary to characterise the typical behaviour of commercial PIR under pyrolytic conditions. These conditions replicate the preheating phase of combustion, during which solid materials exposed to high temperatures undergo physical and chemical processes prior to, but setting the conditions for, the initiation of flaming combustion. The data in this thesis suggest that this phase is characterized by the heating of the material resulting leading to the evaporation of volatile extractives, the breakdown of larger molecular structures into fragmentary products capable of being vaporized, and in the case of blown foams the off gassing of blowing agents.

This characterization was the focus of Chapter 3 of this thesis, in which foams were subjected to thermogravimetric analysis under an inert atmosphere of N_2. Because oxygen was excluded, the processes observed were purely thermolytic in nature, and a characteristic pattern of behaviour was seen. Mass loss was found to be effectively negligible for line-produced foams at temperatures below 100^{o}C. What small mass losses were observed in this temperature regime were attributable to the loss of adsorbed moisture and as such would not be expected to produce a flammable or explosive atmosphere.

The first substantial mass loss event in line-produced foams occurred over a temperature range of 100-275 ^{o}C with the highest rate of mass loss at around 240 ^{o}C. This temperature corresponded to that reported in the literature for the breakdown of urethane bonds and for which two mechanisms are proposed; simple depolymerisation to reform the starting polyol and diisocyanate monomers and an alternate mechanism in which the ester portion of the urethane group is released as CO_2 forming an amine and an olefin. The species observed in the gas phase under pyrolysis-GC-MS in Chapter 5 indicate the co-occurrence of both mechanisms. The detection of diethylene glycol results from the depolymerisation pathway while cyclization products of diethylene glycol arose from the latter.

The deceleration of this mass loss from 240-275 ^{o}C indicates that the dissociation of urethanes approaches completion by the upper end of this temperature range. The degree of mass loss associated with this event is compatible with that resulting primarily from the loss of blowing agent, liberated diethylene glycol and the evaporation of flame retardants, which together

account for 15% of the total mass of the foam and this is confirmed by the gaseous products detected by Py-GCMS at 250 ^{o}C.

The second and largest mass loss event occurred over the approximate temperature range of 275-450 ^{o}C, with the peak falling at 335-340 ^{o}C and corresponding closely to that reported in the literature for the dissociation of isocyanurates (1). The substantial decrease in absorbance at the isocyanurate νC-N peak at 300 ^{o}C and 350 ^{o}C compared to the relative sparing of this peak at lower temperatures supports the attribution of this event to the degradation of isocyanurates. A number of aromatic compounds with nitrogenous side-groups were detected by pyrolysis-GC/MS which are probable fragmentary products of 4,4-methylene diphenyl diisocyanate and its aniline derivatives. Additionally, the presence of diethylene glycol and phthalimide suggest that this mass loss event also involves the breakdown of the polyester polyol at its internal ester bonds. Further evidence for this is presented by the loss of the peaks at 1200 cm^{-1} and 1100 cm^{-1}, associated with the C-C-O and O-C-C ester vibrations.

The results reported in this thesis provide a clear picture of the degradation mechanism occurring during the pyrolytic degradation of foam which tends to precede flaming combustion, but there is still significant scope for future work in this area. One potential avenue of research is the application of time resolved FTIR coupled to thermogravimetric analysis. In this method, the gaseous products liberated during the thermolytic degradation of the foam are transferred to a gas cell in the IR spectrometer and analysed in near real-time using a method similar to that reported by Williams *et al.* (2). This may be used to build a picture of the changes in gaseous products with respect to temperature and provide greater differentiation of distinct processes occurring during prolonged mass loss events.

Other approaches to be considered are the adsorption of volatile products produced during thermogravimetry onto packed tubes for subsequent analysis by GC/MS, allowing multiple samples to be captured corresponding to narrow temperature ranges under slow pyrolytic conditions. Solvent trapping could also be employed to dissolve gaseous products for analysis by GC/LC-MS. More sensitive methods such as GCxGC or GC/MS/MS could also improve characterization of complex mixtures of analytes arising from the degradation of foams.

One gap in this analysis, owing to time constraints, was the characterization of fixed gases. This analysis would be desirable to provide a full characterization of gaseous products such as $C_{1\text{-}3}$ hydrocarbons, CO/CO_2, nitrogen oxides and HCN.

6.2 Effects of Triethyl Phosphate and Tris(1-Chloro-2-Isopropyl) Phosphate

The second question that this thesis has sought to answer is that of the influence of flame retardants on the degradation of foams. In particular, the thesis has sought to answer whether, and if so how, these agents affect the behaviour of foams in the pre-ignition phase.

Foams based on both high and low hydroxyl-value polyols exhibited generally similar patterns of behaviour under non-oxidative thermogravimetry when TEP and TCPP were either present or absent from the formulation. When both flame retardants were present, the following key findings were observed:

- The first major mass loss event occurred over a higher temperature range in the PS-2602-based formulation (92-273 ^{o}C) than in the corresponding HT-2006 based formulation (66-263 ^{o}C).
- The first major peak occurred at a substantially higher temperature (238 ^{o}C) in the PS-2602-based formulation than in the corresponding HT-2006 based formulation (164 ^{o}C).
- Mass loss during the first major event was greater in the HT-2006-based formulation (16.7 %) than in the PS-2602-based formulation (11.8 %).
- The position and intensity of the second mass loss peak was almost identical for both polyols.
- Retained mass at the end of heating was similar for both polyols, being slightly higher (24.1 %) for the PS-2602-based formulation than for the HT-2006-based formulation (22.2 %).

The removal of both fire retardants produced the following changes:

- The first mass loss event occurred over a narrower temperature range of 95-225 ^{o}C in PS-2602-based foams and 81-234 ^{o}C in HT-2006-based foams.
- The position of the first mass loss peak shifted downwards to 205 ^{o}C (-35 ^{o}C) in PS-2602-based foams but increased to 181 ^{o}C (+17 ^{o}C) in HT-2006-based foam.
- There was a substantial reduction in overall mass loss during the first event in PS-2602-based foams (-12.0 %) but only a relatively small reduction in HT-2006-based foams (-2.2 %).

- Large downwards temperature shifts of similar magnitude were observed for the second mass loss peak to 294 ^{o}C in PS-2602-based foam (-41 ^{o}C) and 298 ^{o}C in HT-2006-based foam (-37 ^{o}C). The rate of mass loss at this peak was substantially greater in PS-2602-based foam but not in HT-2006-based foam.
- The absence of fire retardants did not significantly affect retained char fraction.

Based on these findings it is concluded that the most significant effect of the fire-retardant system consisting of TCPP and TEP on pyrolytic degradation is a substantial increase in the temperature at which the second mass loss peak occurs. This fire-retardant system was, however, associated with increased mass loss during the first mass loss event.

Formulations containing only TEP produced changes to the obtained results from thermogravimetric analysis that are indicative of this agent primarily acting over the temperature range in which the first mass loss event was observed in other formulations. This conclusion is based on the following observations:

- Absence or large reduction in area of the first mass loss peak compared to both formulations containing no fire retardants and those containing TCPP.
- Increase in position of largest mass loss peak compared to formulation containing no fire retardant was either smaller than that produced by combination of TEP and TCPP when used with PS-2602 or close to zero when used with HT-2006.
- Small to absent effect on retained char fraction.

This is consistent with the apparent loss of this fire retardant to the vapour phase during the early stages as suggested by ATR-FTIR findings and directly detected on Py-GC/MS.

When TCPP was used in isolation, the following key finding were observed:

- Position of the largest mass loss peak was identical or slightly higher than for corresponding formulations using both TCPP and TEP.
- Peak mass loss rate was slightly higher than when TEP was also present.
- Presence of TCPP increases mass loss during first mass loss event.
- TCPP does not exert a significant positive or negative effect on retained char fraction.

Considering these findings in their totality, both TEP and TCPP exert substantive effects on the pyrolytic degradation of PIR foams. Their combined effect appears to be dominated by that of TCPP, as the TG and dTG thermograms of the combined system were very similar to those of this agent alone, and the effects observed for TEP in the temperature range <270 ^{o}C appeared

to be largely absent in the combination. The presence of TEP does however appear to reduce the peak rate of mass loss compared to when TCPP is used alone.

These results demonstrate the effectiveness of the current fire retardant system in delaying the pyrolytic breakdown of the foam to a higher temperature and in the case of the PS-2602 base polyol, in reducing the peak rate of mass loss.

The establishment of a dose-response relationship between these fire retardants and thermal stability did not fall within the scope of this thesis and this is a possible avenue for future work and deeper understanding of the activity of these agents. A particular question here could be what is the lowest loading which exerts an effect, what is the highest loading which no longer exerts any further positive effect and why?

6.3 Effects and Efficacy of Alternative Fire Retardants

Three alternative non-chlorinated fire retardants were also evaluated within this thesis for their effects on thermal stability in the pyrolytic phase. These were ammonium polyphosphate, expandable graphite, and a proprietary flame retardant VeriQuel R100. The composition of the latter of these was not publicly available but it is described as an 'all-phosphorus reactive flame retardant' and is known to be non-halogenated.

- All of the alternative fire retardants tested produced an unambiguous increase in retained char fraction when compared to the standard fire-retardant system of TEP and TCPP, with an effect size of between 8.9% and 11.5%, when used in conjunction with TEP.
- Ammonium polyphosphate substantially reduced both the intensity of the urethane degradation peak and total mass loss in the temperature range below 250^{o}C when compared to the standard fire-retardant system consisting of TEP and TCPP.
- Ammonium polyphosphate increased the temperature at which the main mass loss peak occurred by when compared to foams with no fire retardants or those containing TEP alone, but this effect was smaller than that induced by TCPP. Neither expandable graphite nor VeriQuel R100 induced a significant increase in this temperature.
- All three alternative fire retardant substantially reduced the mass loss rate at the main peak, which may limit the ability of foams treated with these agents to sustain flaming combustion.

- Both ammonium polyphosphate and VeriQuel R100 exhibited a third significant mass loss event in the region between 425 ^{o}C and 650 ^{o}C which indicates the possible presence of a secondary stabilised structure that decomposes at a higher temperature. Further work could focus on characterisation of this mechanism, and the use of ammonium polyphosphate in an intumescent charring system including pentaerythritol and melamine(3).

In summary, this set of non-chlorinated fire retardants all demonstrated an ability to substantially decrease total mass loss at high temperatures and reduce the peak rate of mass loss. In the context of the potential fire hazards associated with PIR-based insulation material, this suggests that these agents may be effective in reducing the contribution of such materials to fire load and the production of noxious fire effluents. The removal of chlorinated agents from the flame retardant would almost entirely eliminate insulation materials as a source of HCl, which is identified as a dangerous incapacitant.

There remains a large set of fire retardants whose effects on PIR have not been evaluated in detail. Several such agents, including ammonium pentaborate, hydrotalcite, zinc hydroxystannate, and red phosphorus were screened during the work carried out in this thesis, but their results were outside the scope of this narrative. Further investigation to elucidate fire retardance mechanism using analysis of residues and evolved gases should be carried out to provide deeper insights that will enable the identification of more optimised fire-retardant systems, likely involving combinations of compatible and synergistic agents.

6.4 Gram-scale Foam Samples

The analysis of gram-scale samples under oxidative conditions allowed measurements to be taken of dimensional changes in the foam during heating along with mass loss. Aggregated over a set of formulations, those based on the PS-2602 polyol exhibited slightly greater mass stability but lower dimensional stability at temperatures up to 450 ^{o}C than those based on HT-2006. The effects of direct modification of the polymer have not been extensively appraised within the scope of this thesis, and this should be an avenue for further work. In particular, the effects of different polyols and chain extenders, and other modifications such as the incorporation of carbodiimide groups.

Comparison of formulations containing TEP and TCPP either in isolation of as part of a fire-retardant system containing ammonium polyphosphate, expandable graphite, or VeriQuel R100 found that TEP formulations retained slightly more mass at temperatures above 250 ^{o}C but underwent a greater degree of expansion during heating. This may be due to the plasticizing activity of TEP allowing the polymer to 'flow' as it undergoes thermal degradation.

Formulations containing alternative fire retardants tended to result in increased mass retention at temperatures above 300 ^{o}C, while both ammonium polyphosphate and expandable graphite resulted in greater dimensional stability while the results for VeriQuel formulations were similar to the reference formulation containing TEP and TCPP. This further supports other findings within this thesis, suggesting that these agents could reduce the contribution to fire load resulting from PIR-based insulation materials. Improved dimensional stability may further reduce fire risks by enhancing the ability of PIR-filled structural insulated panels to maintain structural integrity during fire, preventing or limiting the release of flammable pyrolysis products into the fire compartment.

6.5 Closing Statements and Recommendations for Future Work

These results suggest that the alternative fire retardants evaluated in this thesis are promising possible replacements for TCPP. This is especially the case for ammonium polyphosphate, which has been shown herein to both substantially reduce the overall volatilisation of PIR foam under pyrolytic conditions and increase the critical breakdown temperature while improving dimensional stability of the foam.

The combination of testing methodologies employed in this thesis represent a robust and systematic approach to the characterisation and analysis of both new and existing PIR foam formulations, particularly with a focus on fire performance and evaluating the efficacy of fire-retardant systems. This system is also applicable to investigating the fire performance of other polymeric insulation materials and represents possibly the most significant contribution of this thesis to its field.

It is recommended that further research is carried out to evaluate the non-halogenated fire retardants considered herein in larger-scale testing systems such as mass loss and cone calorimetry, and that the characterisation of ignition events is conducted. In particular, a fuller understanding of the quantity and toxicity of smoke produced during the degradation of foam will be essential to improving the fire safety profile. A combination of modifications to the polymer, including polysiloxane-polyurethane hybrids, and multi-component fire retardant

systems exploiting condensed phase mechanisms such as intumescence and glass-forming may have the potential to significantly improve the fire performance of PIR-based materials. This thesis makes a significant contribution to the understanding of the thermal degradation mechanisms of PIR and has in addition to the positive results obtained for alternative fire-retardant agents, has highlighted several promising avenues for future research into safer PIR foams. However, it is unlikely that PIR, or any other carbon-based polymeric foam, can ever be made completely non-combustible. Therefore, in addition to improving the fire performance of existing materials there is also an impetus for research into alternative classes of insulation materials such as polysiloxane or other non-combustible foams, which may be capable of producing similar benefits to conventional carbon-based polymer foams but with a greatly improved fire safety profile.

Chapter 6 Bibliography

1. Chattopadhyay DK, Webster DC. Thermal stability and flame retardancy of polyurethanes. Progress in Polymer Science (Oxford). 2009;34(10):1068–133.

2. Williams AE, Holliman PJ, Carnie MJ, Davies ML, Worsley DA, Watson TM. Perovskite processing for photovoltaics: A spectro-thermal evaluation. J Mater Chem A Mater. 2014;2(45):19338–46.

3. Wang J, Chen Y. Flame-retardant mechanism resulting from an intumescent system. J Fire Sci. 2005;